

**ADVERTIMENT.** La consulta d'aquesta tesi queda condicionada a l'acceptació de les següents condicions d'ús: La difusió d'aquesta tesi per mitjà del servei TDX ([www.tesisenxarxa.net](http://www.tesisenxarxa.net)) ha estat autoritzada pels titulars dels drets de propietat intel·lectual únicament per a usos privats emmarcats en activitats d'investigació i docència. No s'autoritza la seva reproducció amb finalitats de lucre ni la seva difusió i posada a disposició des d'un lloc aliè al servei TDX. No s'autoritza la presentació del seu contingut en una finestra o marc aliè a TDX (framing). Aquesta reserva de drets afecta tant al resum de presentació de la tesi com als seus continguts. En la utilització o cita de parts de la tesi és obligat indicar el nom de la persona autora.

**ADVERTENCIA.** La consulta de esta tesis queda condicionada a la aceptación de las siguientes condiciones de uso: La difusión de esta tesis por medio del servicio TDR ([www.tesisenred.net](http://www.tesisenred.net)) ha sido autorizada por los titulares de los derechos de propiedad intelectual únicamente para usos privados enmarcados en actividades de investigación y docencia. No se autoriza su reproducción con finalidades de lucro ni su difusión y puesta a disposición desde un sitio ajeno al servicio TDR. No se autoriza la presentación de su contenido en una ventana o marco ajeno a TDR (framing). Esta reserva de derechos afecta tanto al resumen de presentación de la tesis como a sus contenidos. En la utilización o cita de partes de la tesis es obligado indicar el nombre de la persona autora.

**WARNING.** On having consulted this thesis you're accepting the following use conditions: Spreading this thesis by the TDX ([www.tesisenxarxa.net](http://www.tesisenxarxa.net)) service has been authorized by the titular of the intellectual property rights only for private uses placed in investigation and teaching activities. Reproduction with lucrative aims is not authorized neither its spreading and availability from a site foreign to the TDX service. Introducing its content in a window or frame foreign to the TDX service is not authorized (framing). This rights affect to the presentation summary of the thesis as well as to its contents. In the using or citation of parts of the thesis it's obliged to indicate the name of the author



Septiembre 2015

tesis doctoral realizada por Marta Sarmiento-Comesías

Structural Behaviour and Design Criteria of  
Spatial Arch Bridges.

# Structural Behaviour and Design Criteria of Spatial Arch Bridges.

Volume 1 of 2

tesis doctoral realizada por:  
Marta Sarmiento-Comesías

dirigida por:  
Ángel C. Aparicio Bengoechea  
Ana M<sup>a</sup> Ruiz Terán

Barcelona, Septiembre 2015

Universitat Politècnica de Catalunya  
Departament d'Enginyeria de la Construcció

# TESIS DOCTORAL

# **CONTENTS**

# **TABLE OF CONTENTS**

## **VOLUME 1**

### **ACKNOWLEDGEMENTS**

I.	INTRODUCTION.....	1
II.	OBJECTIVES.....	13
III.	STATE-OF-THE-ART.....	19
	A) STATE-OF-THE-ART OF SPATIAL ARCH BRIDGES.....	21
	B) STATE-OF-THE-ART OF THE ANALYSIS METHODS AND BENCHMARKS.....	49
IV.	ELASTIC STRUCTURAL BEHAVIOUR OF INFERIOR DECK SPATIAL ARCH BRIDGES WITH IMPOSED CURVATURE.....	67
V.	SPATIAL ARCH BRIDGES WITH A SUPERIOR DECK.....	109
	A) GEOMETRY AND BEARING CONDITIONS STUDY OF SPATIAL ARCH BRIDGES WITH A SUPERIOR DECK.....	111
	B) PARAMETRICAL STUDY OF SPATIAL ARCH BRIDGES WITH A CURVED SUPERIOR DECK AND A PLANAR VERTICAL ARCH.....	131
VI.	STABILITY ANALYSES OF SPATIAL ARCH BRIDGES WITH A CURVED DECK.....	259
	A) BASIS OF STABILITY ANALYSES FOR ARCH BRIDGES.....	261
	B) BUCKLING ANALYSES OF SPATIAL ARCH BRIDGES WITH A CURVED DECK.....	279
	C) GEOMETRICALLY NON-LINEAR ANALYSES OF SPATIAL ARCH BRIDGES WITH A CURVED SUPERIOR DECK AND A PLANAR VERTICAL ARCH.....	333
VII.	DYNAMIC ANALYSIS OF SPATIAL ARCH BRIDGES WITH A CURVED SUPERIOR DECK AND A PLANAR VERTICAL ARCH.....	355
VIII.	CONCLUSIONS.....	395
IX.	DESIGN CRITERIA RECOMMENDATIONS.....	411
X.	FUTURE LINES OF STUDY.....	415
	REFERENCES.....	423

## **VOLUME 2**

### **ANNEXES**

N1. ANNEX RELATIVE TO III. A: DESIGNED EXAMPLES OF SABs

N2. ANNEXES RELATIVE TO IV:

N2.1. ARCH/STRUTS AND DECK/STRUTS JOINT STUDY

N2.2. SIMPLIFIED MODEL OF A PINNED HANGER WITH SPRINGS MODELLING THE STIFFNESS OF THE ARCH

N3. ANNEX RELATIVE TO V. A:

FIGURES OF THE STRUCTURAL BEHAVIOUR OF THE GEOMETRY AND BEARING CONDITIONS STUDY OF SPATIAL ARCH BRIDGES WITH A SUPERIOR DECK

## ACKNOWLEDGEMENTS

I would like to start thanking my supervisor, Prof Ángel C. Aparicio. He has not only been my thesis supervisor. He has been my adviser, my counselor, and my support in the most difficult moments. His experience and his way of understanding the research world in bridge design are key elements for this thesis. I am happy that he was my teacher and my supervisor, but I am mostly proud that I can count on him as my friend. I would like to stop referring to him as my supervisor but to use the German term which so good describes his role in my thesis: Doktorvater, father of my PhD. These words in Spanish are for him:

*Mi más sincero agradecimiento, Ángel. He disfrutado mucho trabajando contigo. La lista de cosas a agradecerte es larga:*

*En primer lugar, gracias por tu desinteresada dedicación, a cualquier hora, sacando tiempo de donde fuese.*

*Gracias por todas tus aportaciones como, tomando tus propias palabras, “guía espiritual” de la tesis.*

*Gracias por indicarme el camino a seguir, donde ahondar el estudio y donde no, qué temas escoger y cuáles descartar, y cómo enfocarlos.*

*Gracias por ofrecerme todas las aclaraciones que he necesitado.*

*Gracias por los ánimos y por las risas.*

*Gracias por brindarme la libertad de escoger ideas que hacen de este trabajo más personal, por dejarme imprimir una pequeña parte de mí en las decisiones y por animarme a tomarlas.*

*Gracias también por ofrecerme y comprender los paréntesis en el estudio, cuando necesitaba la energía de ver también investigaciones y trabajos distintos para retomar la tesis con energías renovadas.*

*Gracias por ser un gran profesor, que sabe ver en cada alumno su forma de entender y pensar, y ofrecernos la explicación a cada uno desde el punto de vista que mejor comprendemos.*

*Gracias por atenderme como doctoranda y por querer conocerme y comprenderme como persona.*

*En definitiva, no sólo gracias por tu ayuda y dedicación a nivel profesional, sino también a nivel personal. No hubiese podido escoger mejor “guía espiritual” y “Doktorvater” para esta tesis.*

Many special thanks to my supervisor Dr Ana Ruiz-Teran in Imperial College. The accuracy of the published papers would not be the same without her help. Thanks for the many ideas and reference suggestions. These grateful words in Spanish are for her:

*Muchas gracias, Ana, por tus consejos, correcciones y el tiempo que has dedicado a la revisión de artículos y que has conseguido sacar de forma impresionante. Pero, sobre todo, gracias por tus mensajes de ánimos. Durante estos años has sido para mí un gran ejemplo de organización, capacidad y rigor.*

The present thesis was developed mostly in Barcelona in the Construction Engineering Department (DEC) and I did an internship of six months in TU Berlin in the Massivbau Department. The last part of the thesis was written parallel to my work in LAP in Stuttgart. Therefore, I have been surrounded of the help of many different people in different moments.

Most of this study took place under the companionship of what I consider my UPC family, in the DEC. Hence, I would like to thank all my colleagues in Barcelona who shared with me the everyday work these last years. The following grateful words in Catalan are for them:

*Un molt especial gràcies als meus companys de despatx: l'Ana, l'altra Ana, l'Astrid, el Carlos, l'Eduardo, el Giorgio, la Míriam i el Matías; i també a les meves companyes de doctorat: l'Anna, la Catalina i la Mar. Tots ells no són només companys d'estudis o lloc de feina, sinó que són també els meus amics, amb qui durant tots aquests anys he compartit les reflexions a l'hora de dinar, les preocupacions tant de la tesi com personals i també el temps lliure de desconnexió. No hagués pogut trobar uns millors companys i amics.*

*Gràcies gran família del DEC per fer d'aquests últims anys a la universitat una experiència acollidora i positiva. Ha estat un temps de treball dur i gran aprenentatge, però també de germanor, d'intercanvi d'opinions i d'experiències, de recolzament en compartir preocupacions i dubtes i també d'alegria pels èxits d'uns i altres.*

*Gràcies a les nostres secretàries per aclarir dubtes sobre la documentació i organitzar els pica-piques que ens feien veure'ns una mica més enllà de la feina del dia a dia.*

*Gràcies a consergeria també per aclarir dubtes i dir amb un somriure el primer bon dia durant tants anys.*

*Gràcies als professors del DEC i als companys dels diferents grups de recerca per tenir sempre la porta oberta si buscava consells o aclariments. En especial al Dr Rolando Chacón, que m'ha atès en tots els dubtes d'ABAQUS i alguns aspectes de la no linearitat de les estructures metàl·liques.*

I would like to thank Mike Schlaich for welcoming me into his Department during my Internship in TU Berlin. Special thanks to Arndt Goldack, who supervised my work during the stay there. Thanks and most kind regards to my TU Berlin colleagues, who made me feel at home. Special thanks to Bernd for his help with Sofistik. I would also like to thank the help with photos, informatics and German, which I received from Ayham, Christian, Sherif, Hella and Inka.

This thesis contains a great amount of photographs which have come to me from all around the world and also many which I myself took in the visit to several bridges, with the unforgettable company of several friends and my family. Thanks for all the unconditional collaboration.

A special thanks to Astrid Montes for helping me in the Galindo Bridge photography adventure in Bilbao.

The last writing period parallel to work was an especially hard one. Thanks all the friends who kept encouraging me to finish my thesis. Special thanks to Thomas Lehman and Martin Romberg of LAP for the information of the Dreländerbrücke and the Nijmegenbrücke, respectively.

I would like to thank the support received by the FPU Scholarships of the Spanish Government, the AGAUR Scholarships of the Catalan Generalitat, the UPC Scholarships of the Technical University of Catalonia and the Scholarships of the Catalan Institution of Civil Engineers.

Last but not least, this thesis would not exist without the help and encouragement of my family. For them my whole gratefulness which can hardly be expressed in words:

*Gràcies per animar-me a començar el doctorat i, sobretot, gràcies per animar-me a acabar-lo.*

*Gràcies pel vostre recolzament i fe incondicional.*

*Gràcies per transmetre'm la força necessària per tornar-me a aixecar quan caic.*

*Gràcies per ser exigents i transmetre'm la importància de la constància i el rigor, però també per ser comprensius amb els meus errors.*

*Gràcies per compartir i entendre les meves il·lusions, per no jutjar, comprendre i recolzar les meves decisions.*

*Gràcies per ser sempre al meu costat.*

*Per tot això, gràcies. Sou el cor i els fonaments d'aquesta tesi.*

Finally, I apologise if I left out some names. The many years I spent working in this research have found the support of many people in many direct and indirect ways. To all those who helped me in some way: thank you.



# **I. INTRODUCTION**

## I. INTRODUCTION

## I. INTRODUCTION

*“A bridge incorporates the creativity of the visual arts and the discipline of physical science”*

D. P. Billington

*(Robert Maillart’s Bridges. The art of Engineering, p100).*

Bridges in urban areas have in recent times acquired a new function. In addition to simply providing a physical connection between two points, they are also expected to create a landmark, as a symbol of originality, innovation and progress.

New geometries for bridges have been devised: arches wind, twist and incline; cables are no longer mere structural elements but have become part of the game, suggesting ruled surfaces which frame the space; and the asymmetry, structurally astounding, finally overcomes the structure in the search for the sculpture (Figure 1).

Spatial arch bridges (SABs) have appeared in response to this social demand, but no compact definition and detailed classification have been given. In spite of the significant number of built spatial arch bridges, not enough systematic research studies focused on their structural behaviour have been developed.

These new geometries are most often used in the “bridge laboratory”<sup>1</sup> of footbridges and present a challenge for the accurate structural behaviour understanding.

The present doctoral thesis focuses on understanding the structural behaviour of SABs and on giving design criteria. Its aim is to fill part of the aforementioned research gap in this bridge type.

For a deck curved in plan, the structural solutions most commonly used employ bearings underneath the deck- continuous multi-span girders supported on piers-, or above it- stay-cable or hanging bridges usually with eccentric anchorages. Suspending or leaning a curved deck on an arch is a bridge type developed quite recently, apart from the first examples employed by Maillart. Different solutions have been developed.

The first approach of an engineer is to find the 3D antifunicular form of the arch for a certain loading, which works under compression with no bending moments. Such is the approach given in the few researches regarding this subject, namely the Ripshorst bridge and the in-depth research of Jorquera (2007). Once found the antifunicular form, the behaviour of such structures is already clear.

However, we are facing a bridge type that has a lot to do with a formal approach to bridges and urban landscapes, to architectural design and to solutions with geometries often fixed in competitions which did not always give the structural attention which

---

<sup>1</sup> I take the liberty of employing this term, which is very often used by my supervisor, Ángel C. Aparicio, based on a conference of J.A. Fernández-Ordóñez and S. Tarragó in the ETS Ing. de Caminos Barcelona (UPC)

## I. INTRODUCTION

they require. These determinants often allow no room for employing orthodox, antifunicular arch shapes of the loading.

Different solutions have been developed, some are clearly heterodox and others search for the structural orthodoxy, namely the Ripshorst bridge and the in-depth research of Jorquera (2007). For arches, structural orthodoxy implies finding the antifunicular form of the loading which works under compression with no bending moments. Once found, the behaviour of such structures is already clear. However, the structural behaviour is not that obvious, when considering more heterodox solutions. Hence, this work is devoted to the structural analysis of risky solutions and the proposal of design criteria, which without scarifying formal aspects, improve the structural behaviour.

Hence, the present work focuses on finding simple design criteria, available for all designers and based on deep structural understanding of heterodox solutions of this bridge type.





Figure 1: Examples of spatial arch bridges

The document is divided into chapters according to main subject blocks. Each chapter is divided into sections according to the different research studies which have been conducted. There is an index, objectives, conclusions, future lines of study and references for each of the main research studies. A compilation of the main objectives, conclusions and future lines of study references is presented, for the whole document, in *Chapters II, VIII* and *IX*, respectively.

The analysis method is described specifically for each chapter. For all research studies 3D frame models have been employed and analysed with SAP2000. For certain analysis SOFISTIK has also been employed.

A bookmark with the main geometry, load cases and parameters definition for Chapter V is also provided, to follow the analysis without having to search the definition given in the same chapter.

The methodology, employed for the different research studies developed in the thesis, is given at the beginning of each chapter.

## I. INTRODUCTION

To avoid confusion with chapters, annexes are numbered starting with “N”.

In the following lines the content of each chapter is summarised.

The objectives of this doctoral thesis are presented in *Chapter II*.

The state-of-the-art of this bridge type is presented in *Chapter III.A* and *Annex N1*. After several research studies which are explained, the SAB definition, variables and classification have been detailed, broadened and specified further.

SABs are defined as bridges in which vertical deck loads produce bending moments and shear forces not contained in the arch plane due to their geometrical and structural configuration. Moreover, the arch itself may not be contained in a plane.

A wide compilation of examples of this bridge type has been made (*Chapter III. A* and *Annex N1*) in chronological order according to their construction date, from Maillart’s first concrete spatial arch bridges to the latest designs and materials.

The aspects still to be studied are spotted.

Most SABs are steel footbridges. Hence the research has been focused on the structural behaviour of steel footbridges under self-weight, uniform loads and temperature and not those loads associated with road bridges. Although the structural behavior would be the same, some of the studied geometries could not be employed for road bridges, because of the loads larger value.

In order to decide which analysis methods and software should be employed for the present research, a state-of-the-art of the existing structural analysis software has been conducted in *Chapter III.B*. The advantages of each software for the needs of the present study have been evaluated and compared.

Different benchmarks have been developed to assure the validity of the analysis methods employed in the present research.

An in-depth study of planar and non-planar Inferior Deck Arch Bridges With Imposed Curvature (IDABWIC) has been carried out in *Chapter IV* and *Annex N2*. In this type of spatial arch bridges the arch and the deck centroid lines are both contained in the same vertical cylinder (Figure 2). The aim of the study is to propose the most appropriate design for controlling the out-of-plane response.

In order to understand the behaviour of these arches, different frame 3D models have been developed and analyzed with commercial software. The arch definition, the deck and arch plan curvature, the arch sag and cross-sections rigidity of arch, deck and hangers, as well as arch cross-section area and different hanger/deck and hanger/arch connection types, have been

## I. INTRODUCTION

studied as variables under both symmetrical and asymmetrical vertical loading. Both flexible and rigid hangers have been analysed.

An analytical formulation for a simplified hanger model has also been developed. This gives an intuitive point of view about the behaviour of this type of bridge and how it can be controlled by means of the different variables involved:

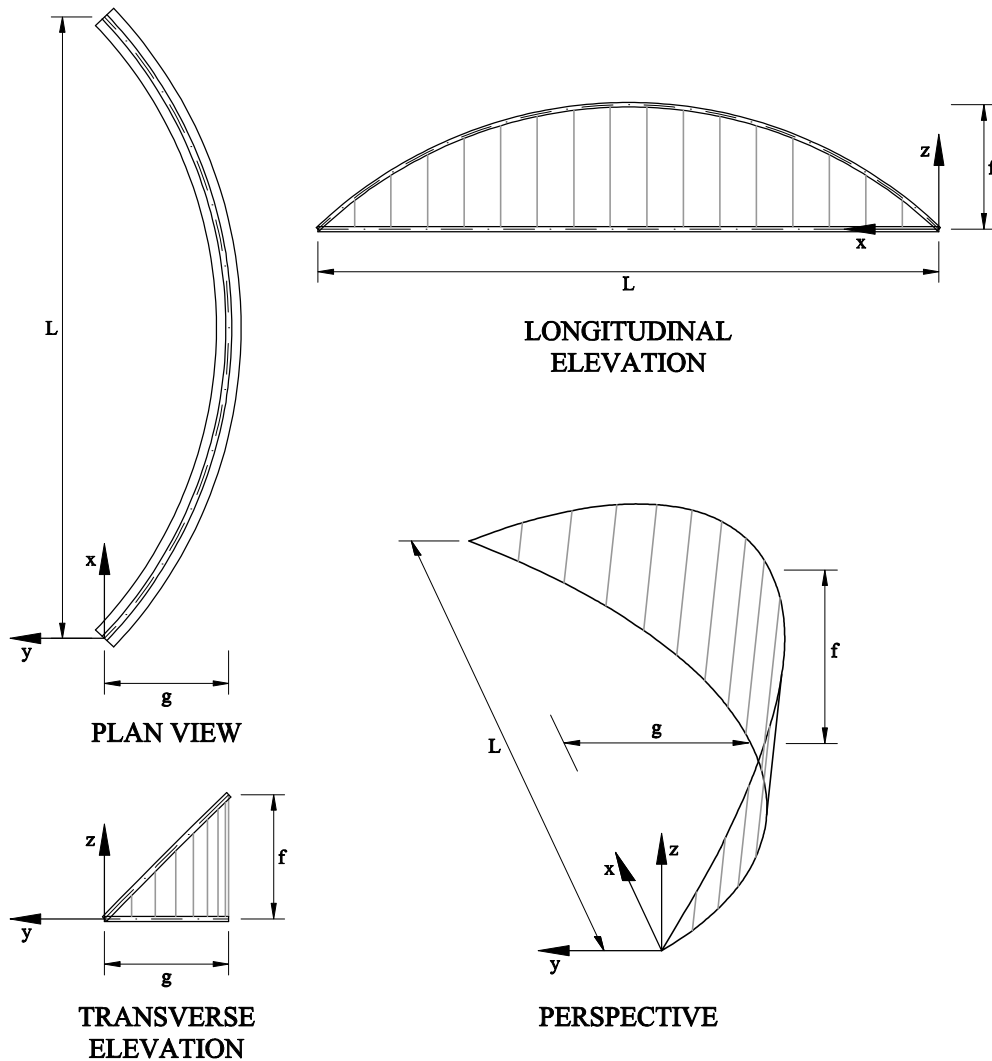


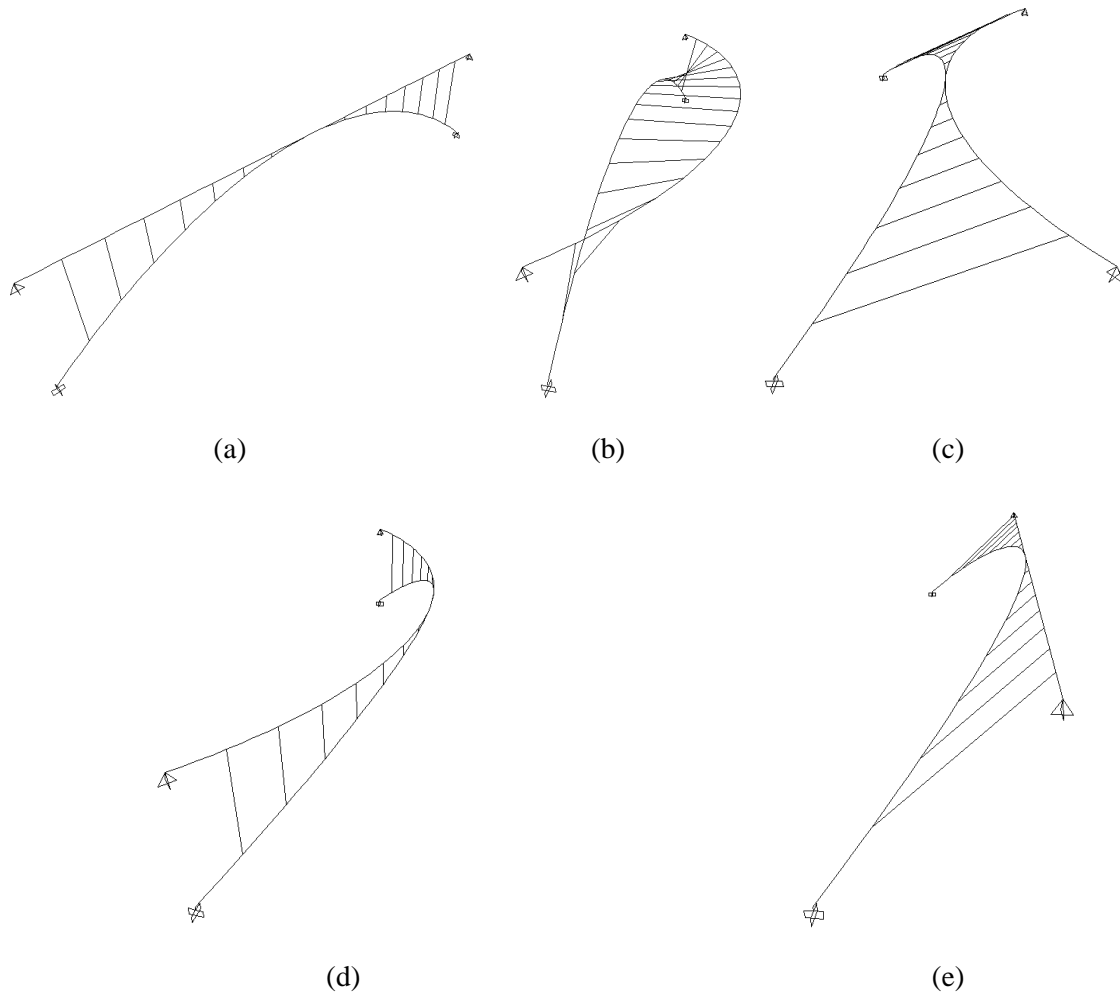
Figure 2: Inferior deck arch bridges with imposed curvature

A thorough study for different geometries of superior deck true SABs under vertical loading and temperature variation has been conducted in *Chapters V. A* and *B*.

The research study in *Chapter V.A* and *Annex N3* deals with the structural behaviour of spatial arches with superior deck. Their response under vertical loads and temperature increments is analysed and different geometrical configurations and boundary conditions at deck abutments are studied.

## I. INTRODUCTION

Superior deck arch bridges can suffer important temperature variations. If they are curved in plan the most efficient boundary conditions for seism or temperature might be different to the ones commonly employed for classical arch bridges.



**Figure 3: Studied bridge geometries.** (a) Vertical planar arch bridge with superior straight deck (reference model); (b) Vertical planar arch with superior curved deck; (c) Arch and deck with symmetrical curvature in plan; (d) Arch and deck with coincident curvature in plan (imposed curvature); (e) Arch curved in plan with superior straight deck (both contained in the same plane)

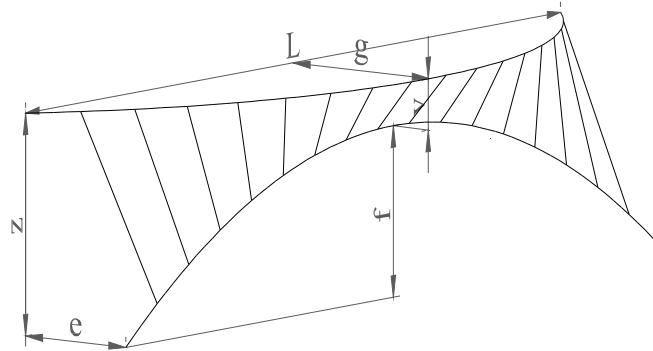
A priori, we can think that the curvature might diminish the longitudinal deformations and forces due to temperature compared to the straight deck geometries. In this case, it will be useful to take advantage of the plan curvature and fix the abutments in a similar way to the common practice for other bridge typologies in seismic areas. However, this also introduces other internal forces on the arch and it cannot be stated beforehand which boundary conditions are the most convenient. Therefore, a close study of the behaviour of the different bridge geometries for the different boundary conditions is required.

In order to analyse the behaviour of these arches, different linear frame 3D models have been developed and analysed with a commercial software (Figure 3).

The purpose of our study is to understand the structural behaviour of different geometries of this bridge type and to establish the best boundary conditions at abutments in each case.



Vertical planar arch bridges with a curved superior deck are spatial arch bridges (SABs) with a very characteristic structural behaviour and many interesting structural and aesthetic possibilities. This bridge type is studied in **Chapter V. B.**



**Figure 4: Vertical planar arch bridges with a curved superior deck. Parameters studied.**

A thorough parametric analysis has been conducted in order to establish efficient values of different parameters for this bridge type according to different criteria (Figure 4). The objective is to minimize the total amount of structural materials. It has also been studied whether different criteria proposed by the authors are appropriate to satisfy this objective. For such a purpose a piece of software has been developed.

The election of the value of these parameters highly influences the behaviour of this bridge type. It is demonstrated in this chapter that the position and connection of some key points of the arch and deck is essential in this bridge type in order to control the structural efficiency.

An appropriate range of values for the different parameters (arch/deck eccentricity, arch rise, arch/deck vertical distance, inclination of struts and the cross-section of the different elements) is given and it is established which parameters are key to the bridge behaviour. The changes in the structural behaviour according to the different parameters are explained.

In **Chapter VI** the stability of SABs with a curved deck is studied and compared with that of planar vertical arch bridges with a straight deck.

The basis of stability analysis of arch bridges is presented in **Part A** of this chapter, including several researches and the present codes for buckling and geometrically non-linear analysis.

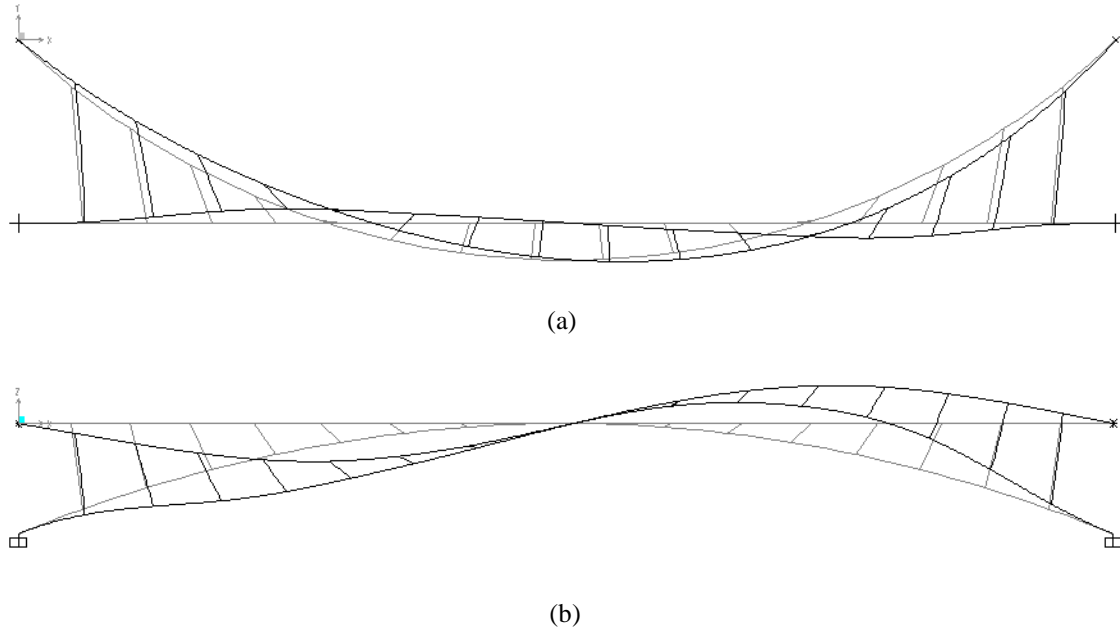
For different models of this bridge type a buckling study has been conducted in **Part B** of this chapter. Their behaviour has been compared with a classical planar vertical arch bridge with a superior straight deck.

A parametric analysis has also been developed, comparing the behaviour of the different SAB models. The buckling behaviour of this bridge type is completely different to that of a planar vertical arch bridge. Buckling takes place in both planes of the arch at the same time (Figure 5). This behaviour has been explained. It is difficult to calculate the out-of-plane buckling load for arch bridges and it is even more challenging for this bridge type.

## I. INTRODUCTION

Literature and code formulations for the buckling load of arch bridges have been compared with the numerical results for this bridge type.

Buckling loads have also been compared to design loads, assessing whether buckling can be disregarded as a main problem in this bridge type.



**Figure 5: SAB asymmetrical buckling shape in both planes for  $g=20m, f=10m$ , rlm and rtr, employing reference cross-sections (a) Plan view (b) Layout**

For different models of this bridge type geometrically non-linear analyses with and without imperfections have been conducted in **Chapter VI. B**.

The sensibility to imperfections has also been studied, considering the coded imperfections based on the behaviour of planar vertical arch bridges. The results of the analysis also show a high sensibility to the arch rise and this effect has been explained.

The geometrical non-linearities have a high influence on the bridge behaviour.

As already stated, most SABs are footbridges. Therefore, the dynamic behaviour of this bridge type is an important aspect to be considered. The dynamic behavior of this type of footbridges has been hence also conducted for a SAB example with curved superior deck in **Chapter VII**.

The thesis conclusions are drawn specifically for each chapter and finally summarised in **Chapter VIII**.

Future lines of study are suggested in **Chapter IX**.

At the present date, different publications have been derived of this research:

***Journal publications:***

Sarmiento-Comesías, M., Ruiz-Teran, A. and Aparicio, A. C.. “Structural Behaviour of Inferior-Deck Spatial Arch Bridges with Imposed Curvature” *Journal of Bridge Engineering*, 10.1061/(ASCE)BE.1943-5592.0000282 (29 June 2011). In paper Vol. 17, No. 4, pp. 682-690. 2012

Sarmiento-Comesías, M., Ruiz-Teran, A. and Aparicio, A. C.. Closure to “Structural behaviour of inferior-deck spatial arch bridges with imposed curvature” *Journal of Bridge Engineering*, Vol. 17, No. 4, pp. 682-690. DOI: 10.1061/(ASCE)BE.1943-5592.0000282). Closure 2013

Sarmiento-Comesías, M., Ruiz-Teran, A. and Aparicio, A. C.. “State-of-the-art of spatial arch bridges.” Special Issue on Arch bridge of the *Bridge Engineering Journal* of the Institution of Civil Engineering, Vol. 166, Issue 3, April 2013 pp163–176. Published on-line 2011. DOI: [10.1680/bren.11.00010](https://doi.org/10.1680/bren.11.00010)

***Symposium publications:***

Sarmiento, M., Ruiz-Teran, A. And Aparicio, A. C.. “Structural response of spatial arches with imposed Curvature.” *Proceedings of the 34th International. Symposium on Bridge and Structural Engineering, IABSE, Venice, Italy, 2010*, pp. 1-8 (CD-ROM)

Sarmiento-Comesías, M., Ruiz-Teran, A. and Aparicio, A. C.. “Superior deck spatial arch bridges.” *Proceedings of the 35th International. Symposium on Bridge and Structural Engineering, jointly organised by IABSE-IASS': 'Taller, Longer, Lighter'*, London, UK, September 20-23, 2011

Sarmiento-Comesías, M., Ruiz-Teran, A. and Aparicio, A. C.. “Puentes arco espaciales de tablero superior.” *Comunicaciones V Congreso de ACHE*, Barcelona, 25-27 Octubre, 2011, pp1-10 (CD-ROM)

Sarmiento-Comesías, M., Ruiz-Teran, A. and Aparicio, A. C.. “Spatial arch bridges with a curved deck: structural behaviour and design criteria” Presentation Future of Design, IABSE British Group, London, 2013

Sarmiento-Comesías, M., Ruiz-Teran, A. And Aparicio, A. C.. “Elastic behaviour of planar vertical arch bridges with a superior curved deck” *Proceedings of the 7th Conference on Arch Bridges “ARCH 2013”*, Split, Croatia, 2013, pp. 1-8

Sarmiento-Comesías, M., Ruiz-Teran, A. and Aparicio, A. C.. “Spatial arch rib with shell arch bridge design proposal”, *Footbridge 2014 - Past, Present & Future*. 5th International Conference, London, 2014

## I. INTRODUCTION

## **II. OBJECTIVES**

## II. OBJECTIVES

## II. OBJECTIVES

The main objectives of the present doctoral thesis, which deals mainly with Spatial Arch Bridges (SABs) as pedestrian footbridges are detailed in the following lines.

In general, the present doctoral thesis focuses on understanding the structural behaviour of SABs and on giving design criteria.

In relation to the different morphologies projected and/or constructed up to the present date, the aim of the thesis is to:

- Define what we understand by spatial arch bridges.
- Establish the different variables involved.
- Provide a classification for the different types of SAB.
- Summarise the present knowledge of this bridge type, giving a brief review about how the different examples have emerged.
- Explain the basic principles of behaviour and point out the research studies which have been carried out so far.

In relation the structural and morphologic bridge type of Inferior Deck Arch Bridges With Imposed Curvature (ID-ABWIC), it intends to:

- Define possible geometries for imposed curvature arch bridges.
- Study if non-planar geometries can be approximated by equivalent arches contained in an inclined plane.
- Establish which geometrical and mechanical variables influence the structural behaviour of these arch bridges.
- Find out which is the best way to control the arch behaviour, either with rigid arches or a rigid hanger-deck system.

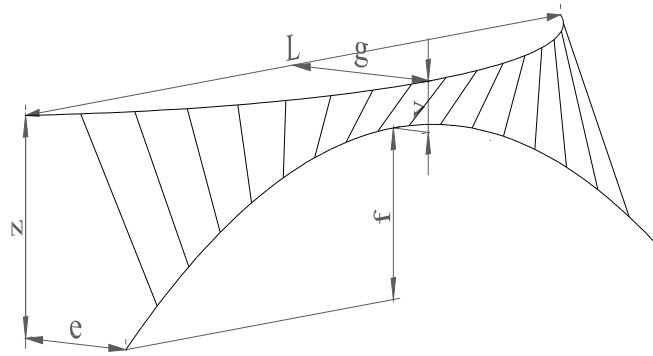
As far as the geometries of SABs with a superior deck concerns, the main objectives of the present doctoral thesis are to study:

- the global structural behaviour of different geometries of spatial arch bridges with superior deck under a vertical uniform loading and a temperature increment. The aim is to decide which bridge geometries help to improve the structural behaviour of these bridges.
- the suitability of different boundary conditions for the different bridge geometries under the considered loading cases.

## II. OBJECTIVES

When considering SABs with a superior curved deck, the objectives are to:

- understand the changes of the structural behaviour of this bridge type due to changes the different parameters ( $e, f, v, \beta^l, EI, GJ, z, g_A$ ) which have been previously described for different deck curvatures ( $g$ ) (**Figure 1**)
- establish a range of the best combination of the studied parameters in order to minimise the material employed for different spatial arch bridges
- study which will be the best indicator in order to minimise material
- assure whether the minimisation of bending moments is equivalent to the minimisation of stresses and if the latter corresponds to minimising the total mass of the bridge



**Figure 1: Nomenclature of variables.**

In relation to buckling analysis, the purpose of the study is:

- to analyse the influence of different parameters ( $f, \beta, EI$  and  $GJ$  of arch, struts and deck) on the buckling shape and loading of spatial arch bridges with a superior curved deck (SABWSCD) with a planar vertical arch with  $g=0$  and  $g=20\text{m}$  and  $e=16,57\text{m}$
- to analyse the buckling behaviour of IDABWIC with  $g=20\text{m}$  and  $f=20\text{m}$  and different cross-sections
- to compare the buckling shape and loading of SABs with that of equivalent (ie: with the same arch rise ( $f$ ) and span ( $L$ ) values) planar vertical arch bridges with a straight deck
- to evaluate the validity of different existing formulations for the determination of arch bridge buckling values
- to evaluate the worst live load distribution for SABs buckling

---

<sup>1</sup> the inclination of the struts in longitudinal view. See chapter V. B



## II. OBJECTIVES

Regarding the influence of geometrical non-linearities in the structural behaviour, the objectives are to:

- compare the effects of geometrical non-linearities on planar arch bridges with a straight deck and on SABs with a superior curved deck.
- compare the effects of geometrical non-linearities on SABs with a superior curved deck with different  $f$  values.
- evaluate the sensitivity of SABs with a superior curved deck to the values of imperfections stated in EC3
- evaluate whether the design cross-sections obtained from a linear analysis (LA) are still valid when considering geometrical non-linearities

Finally, regarding the dynamic behavior of footbridges of the studied structural type, it is pretended:

- to check the dynamic behavior of the geometry concluded in previous chapters as most efficient for SABWSCD with a planar vertical arch under design dynamic loads of one of the present codes or guidelines and also the behaviour under the dynamic load case of a single pedestrian and of a small group.
- to compare its dynamic behaviour with that of a planar vertical arch with straight deck with an equivalent span and rise.

Many research studies have already been conducted to develop different methodologies to obtain antifunicularity (eg: specifically for SABs: Jorquera, 2007, Todisco, 2014 and Lachauer, 2014). Developing a new methodology is hence not the point of interest of the present study.

The aim of this doctoral thesis is to clarify the structural behavior of SABs, establish design criteria and evaluate the importance of geometrical non-linearities and also check their dynamic behavior when employed as footbridges.

Once the main key parameters have been identified and design recommendations have been drawn, the most efficient solutions obtained in this thesis could be optimized employing the already developed techniques to obtain antifunicularity for a further research or for design.

## II. OBJECTIVES

## **III. STATE-OF-THE-ART**

### III. A) STATE-OF-THE-ART OF SPATIAL ARCH BRIDGES

# **III. A) STATE-OF-THE-ART OF SPATIAL ARCH BRIDGES**

### III. A) STATE-OF-THE-ART OF SPATIAL ARCH BRIDGES

## INDEX

1. INTRODUCTION .....	25
2. OBJECTIVES .....	26
3. DEFINITION .....	26
4. SPATIAL ARCH BRIDGE TYPES .....	27
4.1 Variables definition.....	27
4.2 Classification and examples.....	30
5. BRIEF HISTORICAL REVIEW. EXAMPLES AND EVOLUTION .....	37
6. RECENT STUDIES ON THE STRUCTURAL BEHAVIOUR OF SABS .....	41
7. CONCLUSIONS .....	43
REFERENCES .....	44
Notation .....	47

### III. A) STATE-OF-THE-ART OF SPATIAL ARCH BRIDGES



## 1. INTRODUCTION

This chapter is a broadened and further detailed version of the paper published in the *Bridge Engineering Journal* of the Institution of Civil Engineering in 2011 by the present author and her supervisors (Sarmiento-Comesías et al, 2011).

Bridges in urban areas have in recent times acquired a new function. In addition to simply providing a physical connection between two points, they are also expected to create a landmark, as a symbol of originality, innovation and progress.

New geometries for bridges have been devised: arches wind, twist and incline; cables are no longer mere structural elements but have become part of the game, suggesting ruled surfaces which frame the space; and the asymmetry, structurally astounding, finally overcomes the structure in the search for the sculpture (Figure 1-1).

Spatial arch bridges (SAB) have appeared in response to this social demand, but no compact definition and detailed classification have been given. The development of these new structural forms has not been underpinned by research either.

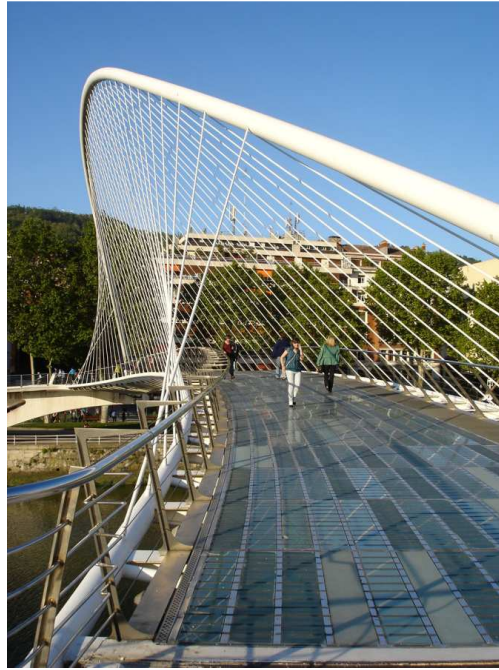
All of this is possible due to current technological development. Faster computers enable close to reality simulations and highly complicated analysis. New CAD/CAM technologies make buildable shapes that would otherwise be impossible to manufacture. These developments have broadened the design possibilities. However, the architectural and engineering characteristics must be in harmony in order to optimize the possibilities offered by both the new materials, and the drawing, calculation and construction methods.

However, the development of these new structural forms has not been underpinned by research. Few studies have been carried out so far on spatial arch bridges (Jorquera, 2007 and 2009). After six International Conferences on Arch Bridges, this bridge type has still not been considered, and only some examples have been presented. A deeper study is needed in order to clarify their behaviour and stability, to broaden and optimise the design possibilities and to establish design criteria. Before such a study is undertaken, it is essential to clearly define this bridge type and revise the state-of-the-art, including both the research studies and some of the examples which have been completed.

In the present chapter Spatial Arch Bridges are defined. The different variables and geometries that create such a structural configuration have been studied and classified.

A compilation of examples of this bridge type has been made in chronological order according to their construction date, from Maillart's first concrete spatial arch bridges to the latest designs and materials. A wider compilation of examples is also given in Annex N1 in Table format with the main data of each bridge.

This chapter is a broadened and further detailed version of the paper published in Special Issue on Arch bridge of the *Bridge Engineering Journal* of the Institution of Civil Engineering by the present author and her supervisors.



**Figure 1-1: Campo de Volantín footbridge in Bilbao** (see Annex N1 for further details)

## 2. OBJECTIVES

The objectives of this chapter are to:

- Define what we understand by spatial arch bridges.
- Establish the different variables involved.
- Provide a classification for the different types of SAB.
- Summarise the present knowledge of this bridge type, giving a brief review about how the different examples have emerged.
- Explain the basic principles of behaviour and point out the research studies which have been carried out so far.

## 3. DEFINITION

SABs are defined, for this document and all the papers from this document derived and published, as bridges in which vertical deck loads produce bending moments and shear forces not contained in the arch plane due to their geometrical and structural configuration. Moreover, the arch itself may not be contained in a plane.

Under the global concept of “spatial arch bridges” we understand both, bridges supported by arch ribs and by shells.

The previously given definition applies to SABs employing arch ribs. Their definition can be developed further: “true spatial arch rib bridges” are those in which vertical deck loads centred on the deck induce internal forces not contained in the arch plane, due to their geometrical and structural configuration (Figure 4-3). The spatial behaviour of the rest of spatial arch bridges is only activated by vertical loads which introduce torques also on the deck. From a geometrical standpoint, arch bridges which are longitudinally asymmetrical in plan are always true SABs (Figure 4-3 in section 4.2).

Non-true SABs are those arch bridges which are longitudinally symmetrical in plan (and therefore the arch and deck have a symmetrical cross-section) with more than one deck (eg: Figure 4-4c and d in section 4.2), more than one arch (inclined non-braced arches such as in the examples shown in Figure 4-4b in section 4.2) or more than one family of hangers (Figure 4-4b) or struts (eg: the arch bridge across high-speed road R52

### III. A) STATE-OF-THE-ART OF SPATIAL ARCH BRIDGES

near Bratic (Strasky and Husty, 1997)). The spatial behaviour of non-true SABs is only activated by the eccentricity of the vertical loads on the deck or the self-weight of the inclined arches.

Classical planar vertical arch bridges which have a spatial behaviour under wind loads are not considered SABs. Neither are those vertical planar arch bridges with a straight deck and one centred family of vertical rigid struts or hangers that introduce horizontal shear forces in the arch under eccentric vertical loads on deck.

Shell arch bridges have a completely different configuration and structural behaviour. In such bridges the main bearing element is an arch consisting of a shell with double curvature (Figure 4-5).

## 4. SPATIAL ARCH BRIDGE TYPES

Many variables are involved in the definition of a SAB. As a consequence of this, it is difficult to classify this bridge type because several criteria could be used.

Most SABs are footbridges in which either an aesthetical challenge is pursued or a curved deck is required due to accessibility criteria. For short and medium spans, arch bridges may be justified for aesthetical, environmental or clearance reasons, as the best alternative, allowing a potential SAB solution. For larger spans, under 600m, arches compete with cable-stayed and suspension bridges.

Most SABs have been built with steel and composite (steel and concrete) sections. The second most employed material is structural concrete. In some particular cases other materials have been used. Stainless steel was employed in the York Millenium bridge, UK, in 2001 (Firth, 2002), the Celtic Gateway bridge in Holyhead Town, UK, in 2005 and the stainless steel-GFRP pedestrian bridge in Sant Fruitós, Spain, in 2009. The Leonardo da Vinci bridge in Aas, Norway, was built in 2001 with timber (glulam curved beams) (von Buelow et al, 2010). Ultra-high performance concrete has also been used in the case of a research study for shell arch bridges (Strasky, 2008 and Terzijski, 2008).

### 4.1 Variables definition

There is a high number of variables that may be combined in many different ways. However, not all the combinations are structurally or geometrically possible. In addition, for some possible combinations, no bridges have been built yet.

The different variables can be observed in Figure 4-1 and are defined as follows:

- Type of arch members: ribs and shells
- Geometrical shape
  - Number of arches, decks, and sets of hangers (when the deck is beneath the arch) or struts (when the deck is over the arch)
  - Number of elements (hangers and/or struts) per set and spacing between them.
  - Arch and deck spans ( $L_A$  and  $L_D$  respectively), horizontal arch and deck sags ( $g_A$  and  $g_D$  respectively), arch rise ( $f_A$ ), geometric shape of the arch.
  - Angular tilt of the arch from the vertical plane ( $\omega$ )
  - Relative position between the arch and deck:
    - In elevation: it can be determined by the position of the deck in relation to the arch; the definition can be based on a relationship between the arch rise  $f_A$  and the height of

### III. A) STATE-OF-THE-ART OF SPATIAL ARCH BRIDGES

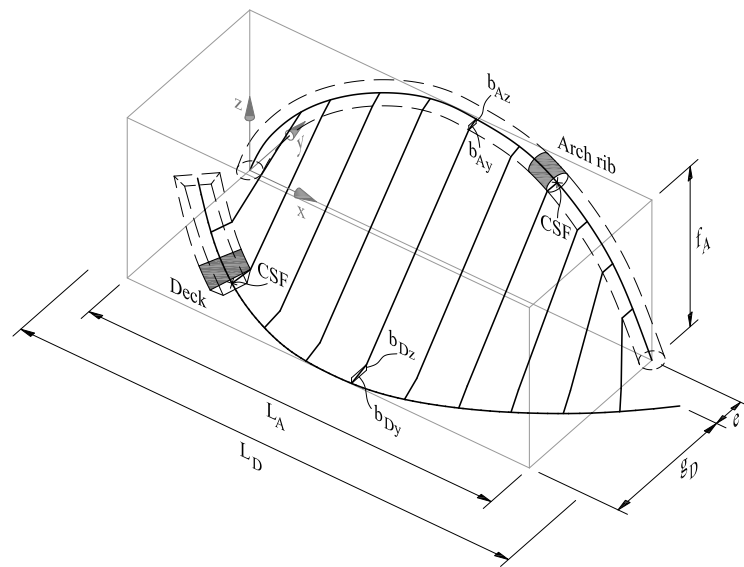
the deck measured from the arch springings  $z_D$  (Figure 4-1c). The bridge can have an ‘inferior-deck’ ( $z_D=0$ , i.e. a bridge with a spatial arch over the deck), a ‘superior-deck’ ( $z_D \geq f_A$ , i.e. a bridge with a spatial arch under the deck) or an ‘intermediate-deck’ ( $0 < z_D < f_A$ , i.e. a bridge with a spatial arch beneath and above the deck). For these definitions, inferior, superior, and intermediate only have a geometrical meaning, related to the position of the deck in relation to the arch.

- Plan eccentricity between the arch springings and the deck abutments ( $e$ )
  - Horizontal offset between the arch crown and the deck mid-span section ( $d$ )
  - Rotation of the arch in plan in relation to the alignment of the deck ( $\theta$ )
- Material
  - Support conditions for both the arch and the deck at the abutments
  - Deck-supporting members (hangers and struts):
    - Slope of the deck-supporting members (with or without a network configuration)
    - Distances from either the hanger anchorages or the strut connections to the shear centre of the cross-section of the arch ( $b_{Ay}$  horizontally and  $b_{Az}$  vertically) and the deck ( $b_{Dy}$  horizontally and  $b_{Dz}$  vertically)
    - Flexural stiffness of the deck-supporting members: rigid (mainly, either steel profiles for inferior-deck SAB or steel or concrete members for superior-deck SAB) or flexible (mainly stays and cables for inferior-deck SAB) members
    - The prestressing of the deck-supporting members: active (mainly post-tensioned hangers) or passive (non pre-stressed) members

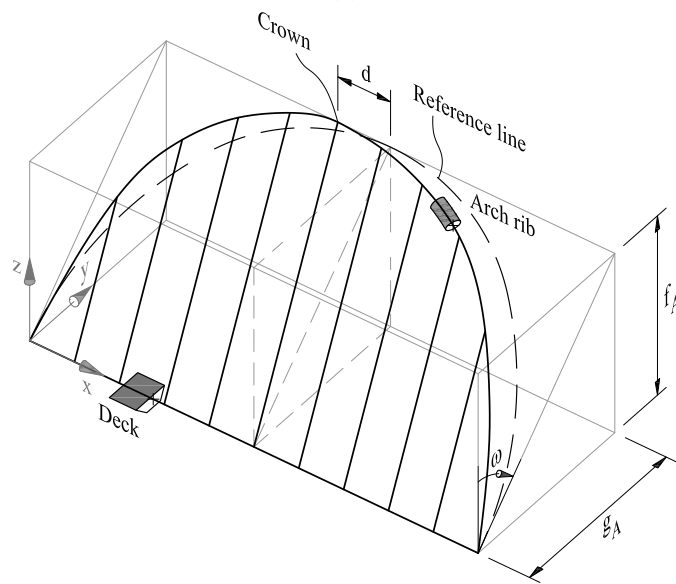
Geometrical variables are a clear way of classifying bridges. Nevertheless, from a structural standpoint, either geometrical or mechanical dimensionless ratios are more appropriate:

- Geometrical ratios:
  - Ratio between the distance from the deck shear centre to the axis joining the deck abutments and the span of the deck:  $(g_D \pm b_{Dy})/L_D$ . Similarly for the arch:  $(g_A \pm e \pm b_{Ay})/L_A$
  - Ratio between the arch depth and width ( $H_A/B_A$ ). This coefficient is required due to the relevance of the out-of-plane behaviour of the arch
  - The deck/span ratio:  $H_A/L_A$ ;  $H_D/L_D$
  - An appropriate relationship between  $f_A$ ,  $e$ ,  $g_D$  and  $g_A$  might be relevant for defining the spatial shape of the arch thrust line (i.e. the anti-funicular shape of the spatial arch)
- Mechanical ratios:
  - Arch/deck flexural rigidity ratio:  $(E_A \cdot I_A)/(E_D \cdot I_D)$
  - Flexural and torsional rigidity ratio (for both the arch and the deck):  $(E \cdot I)/(G \cdot J)$

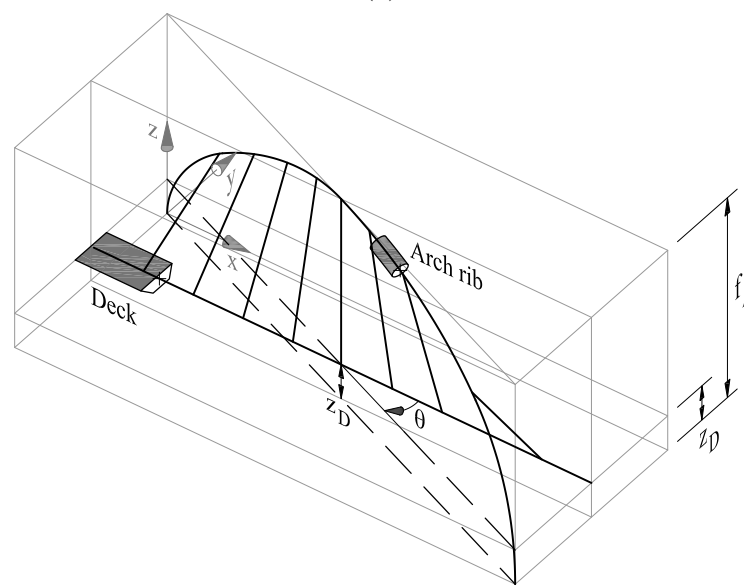
### III. A) STATE-OF-THE-ART OF SPATIAL ARCH BRIDGES



(a)



(b)



(c)

**Figure 4-1: Variables' nomenclature:** a) Vertical arch with curved inferior deck; b) Inclined arch with straight inferior deck; c) Rotated arch with intermediate deck

## 4.2 Classification and examples

Many types of classification can be made due to the high number of variables. Some variables defined in 4.1 appear also in classical vertical arches contained in a plane. Therefore, an interesting classification would be one that considers the variables intrinsic to SABs. Moreover, the classification criteria may either be morphological or structural. Morphological criteria will also lead to a good structural classification and they are visually clear.

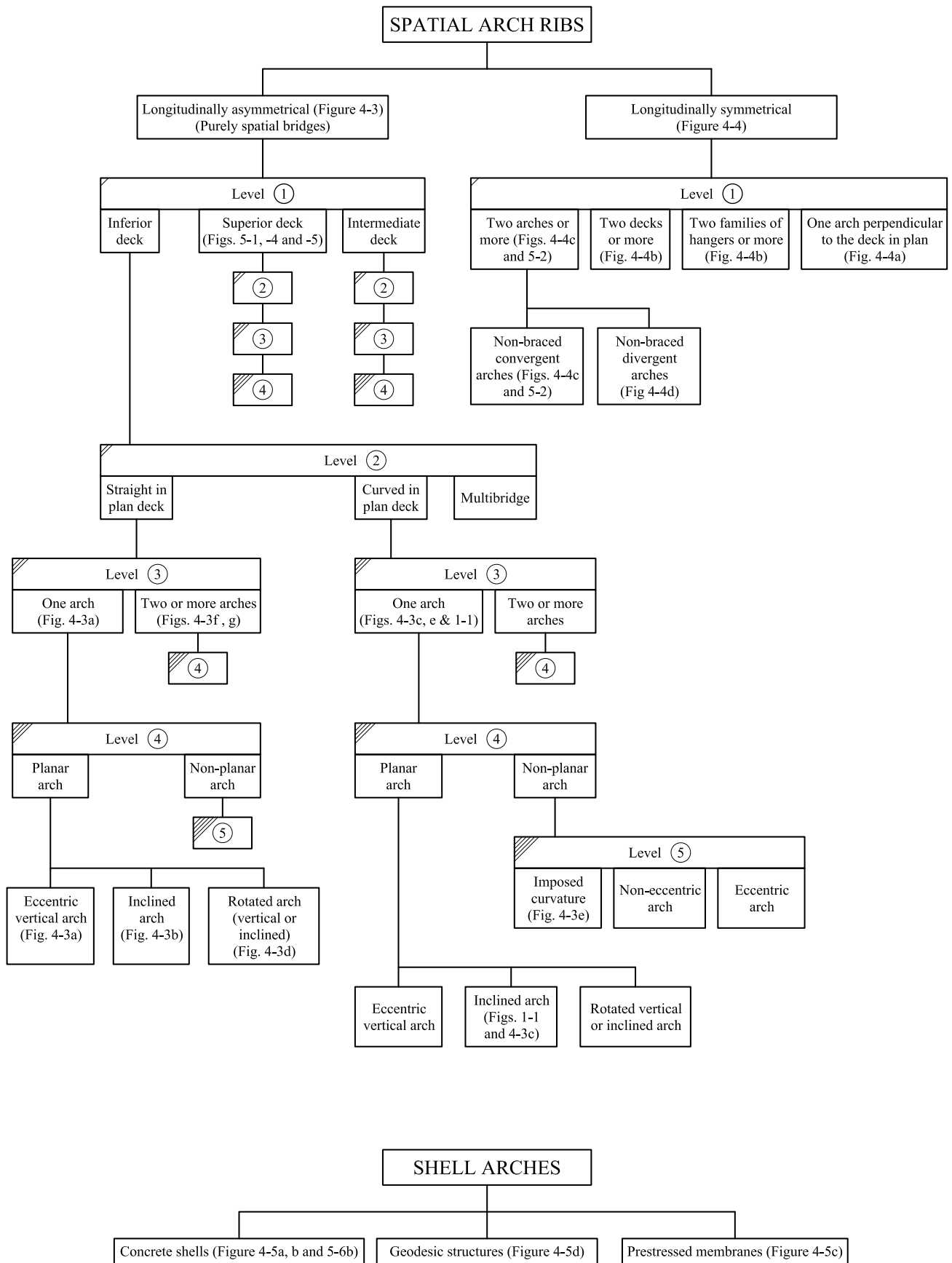
A scheme of a possible classification of SABs is shown in Figure 4-2. A set of different levels is considered. The levels in the flowchart have been numbered from 1 to 5 in order to avoid repetitions of the same information in the different branches.

Firstly, SABs can be divided into two large groups:

- Spatial arch ribs (Figure 4-3 and Figure 4-4): arches in which the cross-section of the arch has a width/span and depth/span ratios low enough for the arch to be accurately analysed with frame elements with 6 degrees of freedom per node.
- Shell arches (Figure 4-5) arches in which the cross-section of the arch has a width/depth and width/span ratios large enough for requiring an analysis with shell elements. The arch is a roof-like structure.

Spatial arch ribs can be classified into longitudinally asymmetrical (Figure 4-3) and symmetrical arches (Figure 4-4), which can in turn be sub-classified according to the relative vertical position between the arch and the deck (level 1), the deck curvature (level 2) and the number of arches (level 3). Finally, they are classified according to the shape of the arch and the deck and their relative position (levels 4 and d, Figure 5-2).

### III. A) STATE-OF-THE-ART OF SPATIAL ARCH BRIDGES



**Figure 4-2: Spatial arch ribs classification scheme**

Regarding spatial arch ribs, the following aspects should be clarified:

- Multi-bridges: these bridges have multiple (at least three) convergent decks, each of which may

### III. A) STATE-OF-THE-ART OF SPATIAL ARCH BRIDGES

be supported by, or on, an arch. The only already designed examples are tri-bridges, such as the Sanchinarro shopping-mall access bridge by J. J. Arenas in Madrid (J. J. Arenas, 2005) or the project of the Hacking Ferry bridge, also called Ribble Way, by Wilkinson Eyre, in Lancashire (Firth and Kassabian, 2001).

- Planar arches: these arches are contained in a vertical or inclined plane. This geometrical configuration allows the direct projection of the internal forces into two orthogonal planes, when employing arch cross-sections symmetrical on the arch plane.
- Non-planar arches: these are not contained in a plane. Even if a circular arch cross-section is employed, internal forces cannot be projected into two planes because internal forces are coupled.
- Arch bridges with imposed curvature (ABWIC). In these SABs, the arches are forced to have the same curvature in plan as the deck. Therefore, the arch and deck centroid lines are contained in the same vertical cylinder.
- They can have an inferior or superior deck (IDABWIC and SDABWIC). In IDABWIC, the deck is located under the arch and supported by vertical hangers which do not restrict the vertical clearance (Jorquera 2007). ABWIC can have either planar (inclined arch) or non-planar (Sarmiento-Comesías et al, 2010)
- A very scarce number of this kind of arches. Only a few bridges of this type have been built so far (see section 5).
- Arch bridges longitudinally symmetrical in plan with two or more braced arches do not have a spatial behaviour under vertical loads, whereas asymmetrical ones can be braced without losing the spatial behaviour that characterises SABs.
- Longitudinally symmetrical bridges with one arch perpendicular to the deck in plan. This takes place in the limit of an asymmetrical bridge with a rotated arch in plan in relation to the deck alignment. When it becomes symmetrical, with  $\theta \approx 90$ , it should not be considered an arch bridge, but a cable-stayed bridge with an arch-shaped pylon. Nevertheless, the arch would behave like a spatial arch.



(a)



(b)



### III. A) STATE-OF-THE-ART OF SPATIAL ARCH BRIDGES



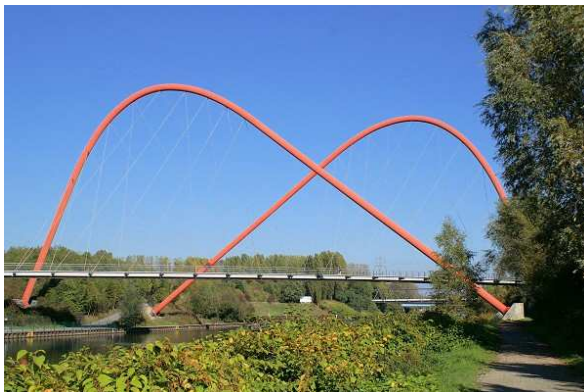
(c)



(d)



(e)



(f)

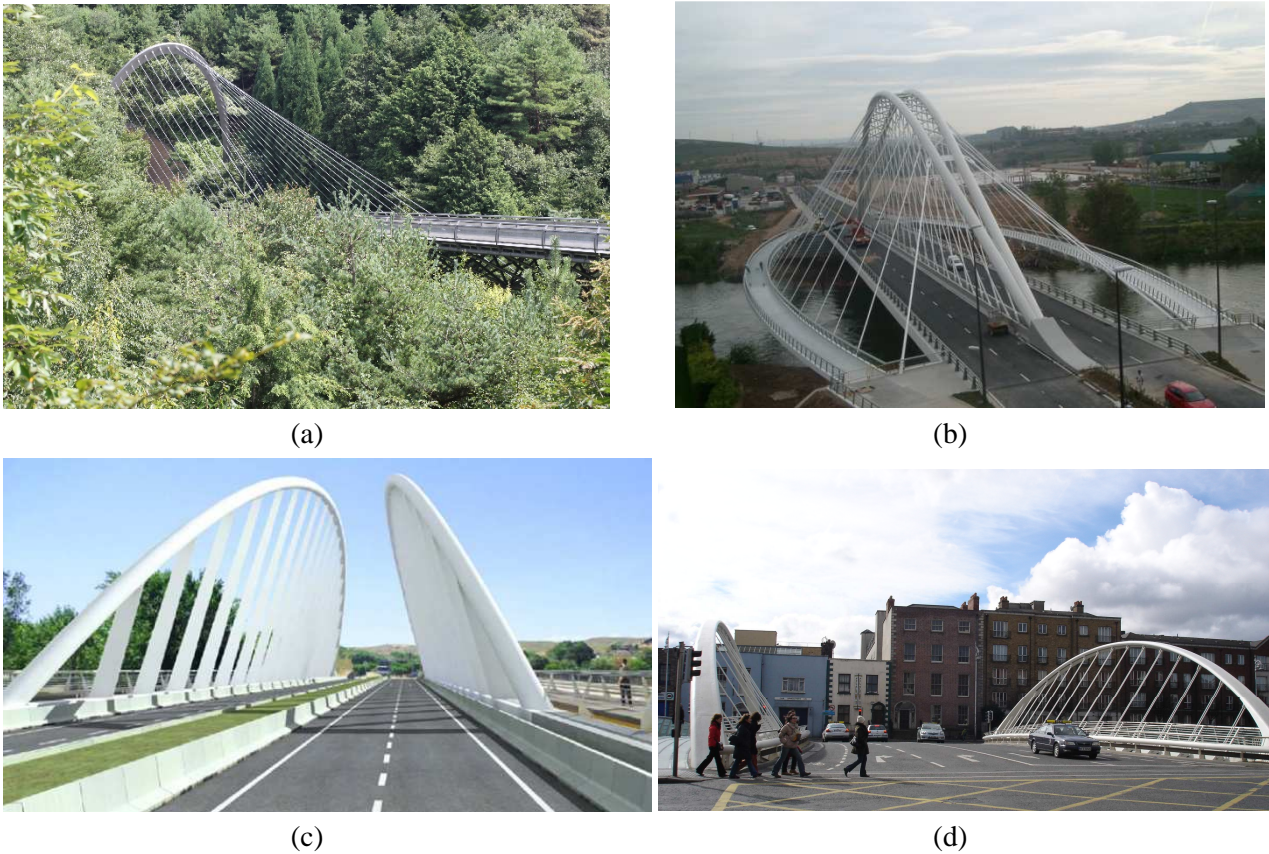


(g)

**Figure 4-3: Longitudinally asymmetrical inferior deck spatial arch bridges** (see Annex N1 for further details):

- One-arch bridges:
- (a) Eccentric vertical planar arch with rigid hangers: *Ondarroa Port bridge*;
  - (b) Inclined planar eccentric arch with straight deck: *La Alameda bridge* ;
  - (c) Inclined planar arch with curved deck: *Gateshead Millenium bridge* (Source: Gifford. company responsible for the structure of the bridge. Reproduced by kind permission of Nolan Mills);
  - (d) In-plan rotated arch: *Hulme arch bridge* (Source: Wilkinson Eyre);
  - (e) ID-ABWIC: *Galindo bridge*.
- Multiple-arch bridges:
- (f) displaced arch crown and rotated arches: *Nordsternpark bridge* (Source: Nicolas Janberg 2005. Reproduced by kind permission of Structurae (publisher)) (Source: Stefan Polónyi. Reproduced by kind permission of the author);
  - (g) convergent braced arches: *Dreiländer bridge* (Reproduced by kind permission of Hans-Peter Andrä).

### III. A) STATE-OF-THE-ART OF SPATIAL ARCH BRIDGES



**Figure 4-4: Longitudinally symmetrical inferior deck spatial arch bridges** (see Annex N1 for further details):

- One-arch bridges: (a) In-plan rotated arch: Miho Museum bridge (*Reproduced by kind permission of Massivbau, TU Berlin*).;
- (b) Two decks: Logroño bridge (*Reproduced by kind permission of Javier Manterola*).
- Multiple-arch bridges: (c) Two convergent arches: Peraleda bridge (*Source: AIA. Reproduced by kind permission of Ramón Sánchez de León*);
- (d) divergent arches: James Joyce bridge

Not all the arch bridges which look like a shell will behave like one structurally. A possible structural division is:

- Bridges in which the arch works like a shell and supports all the bridge loads (the deck can be either inferior or superior, Figure 4-5 (a) and (b)).
- Spatial arch rib bridges additionally loaded with a roof shell. Morphologically they look like shell arch bridges but the main loads are resisted by an arch rib.
- Bridges in which the deck works like an arch shell (Figure 4-5 (c)).
- Bridges with double-arch systems braced by a prestressed membrane acting like a roof (Figure 4-5 (e)). This bridge type has not yet been designed but it is a very interesting option.

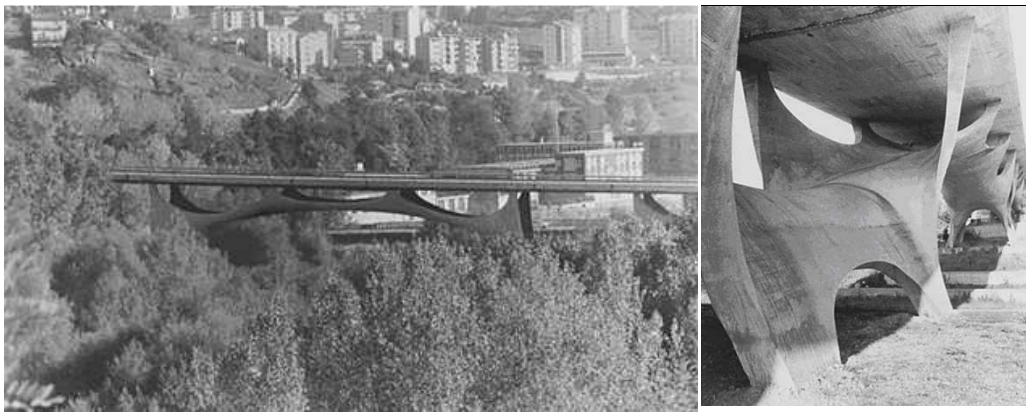
Very few shell arch bridges have been built so far (Nicoletti, 1999, DeLucchi, 2010 and Corres et al 2010 and 2011). Only a small number of projects and studies.

Structures of a bridge with a roof shell might be misleading, because the roof will support its own weight but not the bridge loads. These bridges are obviously not included in this classification type.

III. A) STATE-OF-THE-ART OF SPATIAL ARCH BRIDGES



(a)



(b)

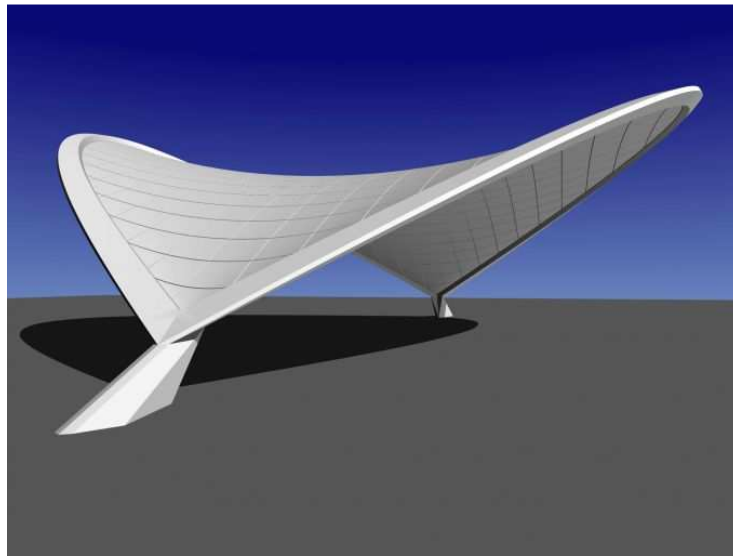


(c)

### III. A) STATE-OF-THE-ART OF SPATIAL ARCH BRIDGES



(d)



(e)

**Figure 4-5: Shell spatial arch bridges** (see Annex N1 for further details):

- (a) Inferior deck shell arch bridge: *Project of pedestrian bridge in StHelier (Reproduced by permission of Jiri Strasky)*
- (b) Superior deck shell arch bridge and arch used as pathway too: *Bridge over Basento river.*
- (c) Shell arch acting as pathway: *Leamouth (Reproduced by permission of Jiri Strasky).*
- (d) Geodesic shell arch: *Bridge of Peace (Reproduced by kind permission of Michelle De Lucchi)*
- (e) Studies of prestressed membranes (Reproduced by permission of Jiri Strasky)

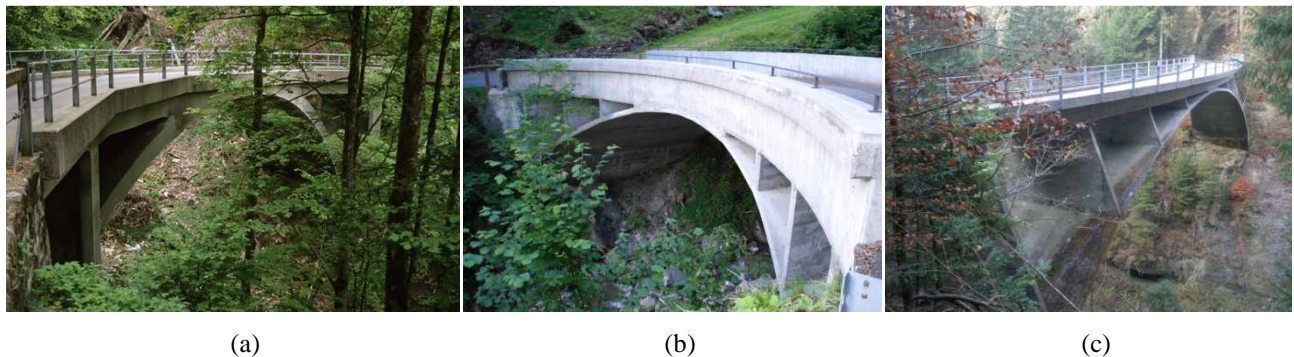
## 5. BRIEF HISTORICAL REVIEW. EXAMPLES AND EVOLUTION

Over 100 spatial arch bridges have been designed so far (Sarmiento-Comesías et al, 2009). In the present chapter, only some representative examples of the different types, mainly the first and latest ones, are referred to.

The concept of spatiality has appeared in some masonry arch bridges, such as skew arches, succession of arches which describe an angle in plan view, and tri-bridges. In all of them, the spatial thrust line is contained in the bridge cross-section. Leonardo da Vinci in 1502 had the foresight to design more slender masonry spatial arches, as his sketches for the Golden Horn bridge attest. His clear understanding and innovative thinking, significantly ahead of his time, led to the design of a true spatial rib arch bridge. His design was eventually built in 2001, in Aas, Norway, with timber rather than stone. It is called the Leonardo da Vinci bridge (Allied Arts Foundation 2001). However, spatial masonry arch bridges are not included in the definition of SABs considered in this document. Interest is focused on bridges built with materials which resist bending forces and in which live loads may cause the pressure line to fall out of the cross-section of the bridge.

The first true SABs were deck-stiffened arch concrete bridges designed by Robert Maillart (Billington, 1997), a pioneer of this bridge type. The Ziggenbach bridge (**Figure 5-1a**), was the first to be completed in 1924 in the central east side of Wägital lake in Schwyz, Switzerland (Billington, 1997). It comprises a straight-in-plan concrete arch bridge and a curved-in-plan superior deck. The demolished Landquart rail bridge also belongs to the same bridge type (Billington, 1979). The Bohlbach bridge (1932, **Figure 5-1b**), with a 14,4 m span, was the first one to have an arch with an axis curved in plan (Billington, 1997), whereas the Schwandbach bridge (1933, **Figure 5-1c**) was the first with an imposed curvature. It spans 38 m over the Schwandbach creek in Switzerland and consists of a polygonal-profile arch (defined as Stabbogen by Maillart) with a constant thickness of 0.2m, connected to the deck only for the central 2.8m of the span (a much lower length than the previous and shorter Bohlbach bridge). The arch splays out at the banks to meet the foundations (Billington, 1979).

All of these first spatial arch bridges are superior deck-stiffened arch concrete bridges that were designed by Robert Maillart (Laffranchi and Marti, 1997), not only pioneer of this bridge typology, but also an engineering genius.



**Figure 5-1: (a) Ziggenbach bridge** (Source: Yoshito Isono 1998. Reproduced by kind permission of *Structurae* (publisher)); (b) **Bohlbach Bridge**; (c) **Schwandbach Bridge**. See Annex N1 for further details.

At the same time many different examples of convergent braced symmetrical arches with inferior deck were built too.

### III. A) STATE-OF-THE-ART OF SPATIAL ARCH BRIDGES

It took over 30 years for the first shell arch bridge to appear. In 1969, Sergio Musmeci built what is believed to be the first and only concrete shell arch bridge with a superior deck. It is located in Potenza, Italy, and crosses the Basento river (Nicoletti, 1999).

In 1987 the construction of the Felipe II or Bac de Roda bridge, in Barcelona, Spain, which was designed by Santiago Calatrava (Figure 5-2) was completed. It is the first symmetrical double-arch non-true SAB. This bridge comprises two non-braced sets of arches, which are themselves asymmetrical braced double arches. Calatrava has designed the highest number of SABs since his first true spatial arch bridge design, the Gentil Footbridge in 1987. Most of them are inclined eccentric steel arches with either a curved or straight inferior deck. Examples are the Devesa footbridge in Ripoll and the Port of Ondarroa bridge (Figure 4-3 (a)), Spain, both built in 1989; la Alameda bridge (Figure 4-3 (b)) in Valencia, Spain, built in 1991; the Europe bridge, in Orléans, France, built in 2000 (Datry, 2001 and Hoeckman, 2001); the Observatory bridge in Liège, in Belgium, built in 2002 (Verlaine et al 2001); the Volantín footbridge (Flaga and Januszkiewicz, 2011); and the recent Reggio Emilia inclined and skew arch, in Italy, built in 2006. Inclined eccentric arches with inferior deck have also been widely used by other designers (some examples are described by Firth, 2001; Strasky, 2005 and Arenas, 2005).



**Figure 5-2: Bac de Roda bridge** (see Annex N1 for further details)

From the late 1980s, the use of bridges as city landmarks became widespread, and more examples of this bridge type are proposed. The search for a new millennium symbol enhanced the aesthetical power of spatial arch bridges and generated several examples.

In the 1990s a new concept was introduced: the arch rotated in plan in relation to the deck alignment. Some examples of this type are: Nordsternpark (Figure 4-3 (f)), built in 1996; the TZU footbridge, built in 1997; the Hulme arch bridge (Figure 4-3 (d)), built in 1997, which has become a symbol of Manchester (Hussain and Wilson, 1999); the Charvaux footbridge, and the impressive multiple-arch Juscelino Kubitschek bridge (Almeida et al, 2003), both built in 2002; and the more recent Te Rewa Rewa bridge, in New Plymouth, built in 2010.

In 1998, the construction of the Gateshead Millennium bridge over the Tyne was completed. It is the first and only spatial arch movable bridge (Figure 4-3c, Johnson and Curran, 2003, Curran, 2003 and Butterworth et al, 2003). One year later, the Ripshorst bridge (Figure 5-4) was completed (Schlaich and Moschner, 1999). It has a non-planar and anti-funicular arch (i.e. an arch in which the thrust line follows the arch centroid line, and therefore the arch works mainly under compression for a certain loading condition).

### III. A) STATE-OF-THE-ART OF SPATIAL ARCH BRIDGES



**Figure 5-3: Juscelino Kubitschek bridge in Brasilia, over the lake Paranoá, Brazil, 2000-2002.** Three arches rotated according to a vertical axis. (Reproduced by kind permission of Lukas Kohler). See Annex N1 for further details.



**Figure 5-4: Ripshorst bridge** (Reproduced by kind permission of Mike Schlaich). See Annex N1 for further details.

In the same period, the first divergent arches were employed: St James Garden footbridge in London, 1995; Butterfly bridge in Bedford, 1998 or Friends bridge in London, 1998. More recent examples include: the Churchill way footbridge in Hampshire, 2000-2003; the James Joyce bridge in Dublin, 2003 (Figure 4-4 (e)); and the Ponte della Musica in Rome, 2011 (Liaghat et al, 2011). There are fewer examples of asymmetrical divergent arches, such as the Celtic Gateway Bridge in Wales, 2003-2005, and the anti-funicular Nanning Butterfly tied-arch bridge in Guangxi, 2009 (Cheng et al, 2010).

Some examples of symmetrical arch bridges with several decks are the bridge over the Guadalentín river in Lorca, Spain, 2002 (Manterola et al, 2005) and the Father Bernatek's footbridge over the River Vistula in Cracow, Poland, 2010 (Flaga and Januszkiewicz, 2011), both with two decks, and the Logroño bridge (Figure 4-4b), Spain, 2003, with three decks (Manterola, 2001).

The structural schemes conceived by Maillart for his deck-stiffened SABs with imposed curvature were not subsequently used until Manterola designed the Endarlatsa bridge (Figure 5-5) and the Contreras bridges. Manterola contributed to the development of this structural type extrapolating Maillart's scheme from superior- to inferior-deck arch bridges. The bridge over the Galindo River, in Bilbao (Figure 4-3 (e), Spain

### III. A) STATE-OF-THE-ART OF SPATIAL ARCH BRIDGES

(Manterola et al, 2009 and 2011), is the first inferior-deck spatial arch bridge with imposed curvature, in which the arch has a double hanger system.



**Figure 5-5: Enderlatsa bridge** (Reproduced by permission of Javier Manterola). See Annex N1 for further details.

Musmeci's shell arch superior deck bridge has still not found a successor. Nevertheless, several studies, models and designs of shell arch bridges have been developed by Strasky (Figure 4-5 (a), (c) and (d)), although they have not been built yet (Strasky and Kalab, 2007, Strasky, 2008 and Strasky et al 2010). Matadero and Invernadero footbridges (Figure 5-6) are the first built shell arch bridges with an inferior-deck (Corres et al 2010 and 2011). In 2010 the first geodesic shell arch bridge, the bridge of Peace (Figure 4-5 d), was built in Tbilisi, Georgia (De Lucchi, 2010).



**Figure 5-6: Invernadero footbridge.** See Annex N1 for further details.

A great range of ideas and combinations of variables is still floating in the horizon, to be discovered, designed and constructed.



## 6. RECENT STUDIES ON THE STRUCTURAL BEHAVIOUR OF SABS

There are very few research studies on the behaviour of this bridge type.

A broad state-of-the-art review has been carried out, including the six international conferences on arch bridges held so far (1995, 1998, 2001, 2004, 2007 and 2010). Several papers briefly describe the arch behaviour for specific examples but very few tackle SABS as a bridge type. The research studies carried out so far are not wide enough to establish design criteria.

Non-linear behaviour of spatial arch bridges with superior deck and imposed curvature bridges have been very briefly studied (Verlaine et al, 2001; Liaghat et al, 2011 and Sarmiento-Comesías et al, 2011a). The effect of temperature on these bridges has only been studied for some specific subtypes (for example the Nanning bridge by Cheng et al, 2010; and a general research study of SABS with superior decks by Sarmiento-Comesías et al, 2011b). The recent analysis methods to obtain anti-funicular arches for SABS do not converge for some cases (Jorquera, 2007) and several variables still need to be studied. Many other formfinding software could be applied, for example employing graphic statics with a computer aided design software together with a parametric modelling plug-in and genetic algorithms (Lachauer, 2011). However, this approach neglects the material stiffness, the structural deformation, and the potential structural instability (buckling).

Jorquera (2007) conducted the first comprehensive research study of this bridge type, giving a first definition, variables and classification. Jorquera's research included the study of the linear behaviour of vertical planar arches with active flexible hangers and an inferior deck SAB with different deck curvatures. He also examined the effect of the arch/deck eccentricity in plan for a given curvature. For straight decks, he studied the behaviour of the arch when varying its inclination. The effect of hanger eccentricity with respect to the shear centre of the deck is also analysed. He coded a program to obtain anti-funicular arches for inferior- and superior-deck SABS with pinned hangers. Although Jorquera carried out a wide and interesting study for different variables, his research only partly clarifies the behaviour of spatial arch bridges. This research is not wide enough to establish design criteria. The effect of temperature on these bridges is not studied; non-linearity of spatial arch bridges with superior deck and imposed curvature bridges are only briefly studied; the antifunicularity program does still not converge for some cases and several variables are still to study.

Antifunicularity is now a theme in vogue, since new CAD/CAM technologies make buildable shapes that would otherwise be impossible to manufacture. There are several other studies employing different theories for finding anticunicularity for SABS, namely with static graphics (Lachauer, 2014) and with genetic algorithms (Todisco, 2014).

After several research studies which are explained in the present document, the SAB definition, variables and classification have been detailed, broadened and specified further in the present chapter.

Spatial arch bridges are subjected to important bending moments (as presented by specific case studies: Hussain and Wilson, 1999 and Johnson and Curran, 2003) and torsions (as presented by specific case studies: Manterola, 2001 and Verlain et al, 2001) and have low axial forces (Jorquera, 2007).

For vertical or inclined planar arches with a symmetric cross-section in relation to the arch plane, an intuitive way of understanding their behaviour is by means of uncoupling in-plane and out-of-plane behaviour. In-plane it works like an arch: axial forces and in-plan bending moments are coupled. Out-of-plane, it works as a so-called balcony-beam, i.e. a fully restrained curved beam with the loads acting perpendicular to the plane containing the beam centroid line. For the latter, the torsional moments and out-of-plane bending moments are

### III. A) STATE-OF-THE-ART OF SPATIAL ARCH BRIDGES

coupled. Depending on the relevant ratios between different variables, either the arch or the balcony-beam behaviour is enhanced.

When either the arch is not contained in a plane or the cross-section is not symmetrical in relation to the plane of the arch, this simple approach is no longer possible.

It can be intuitively understood that the higher either the arch plan curvature or the angle between the plane containing the arch and the hangers/struts, the higher the out-of-plane effects, i.e. the arch behaviour diminishes and the balcony-beam behaviour increases. It has been demonstrated that when employing mechanisms that increase the horizontal stiffness of the system, the behaviour improves (Laffranchi and Marti, 1997, Jorquera, 2007 and 2009, Manterola et al, 2009).

Nevertheless, even if it is possible to separate the behaviour into two planes, the behaviour is not always obvious and predictable, because the relationship between bending and torsional rigidities, the hanger/struts connection types and eccentricities, and the support conditions of the arch and deck at the abutments, play a fundamental role in the arch behaviour.

In conclusion, spatial arch bridges not only prove to be architecturally interesting, but also present reasonable structural behaviour when employing a geometry that enhances the arch/deck interaction and the adequate support conditions for both the deck and the arch at the abutments. Moreover, the deck curvature is advantageous in order to diminish the axial forces in the deck caused by temperature increments.

Considering the few references on the subject, the wide range of variables and the recent popularity of this bridge type, it is concluded that further research is necessary.

## 7. CONCLUSIONS

In this chapter spatial arch bridges have been fully defined and classified, and the variables that define both the geometrical and structural configuration have been presented.

- The spatial arch bridge type has its origins in some of Maillart's bridges built at the beginning of the 19th century, whose rationale was based on functional considerations. Its use has reached its peak in the 1990s, becoming increasingly popular in urban areas as a means of creating city landmarks.
- In spite of the significant number of built spatial arch bridges, not enough systematic research studies focused on their structural behaviour have been developed.
- Existing research studies demonstrate the relevance of the out-of-plane internal forces (i.e. the behaviour as balcony-beam) in spatial arch bridges.
- Many research studies have been conducted to develop different methodologies to obtain antifunicularity.
- Recent researches do not fully clarify the behaviour of spatial arch bridges yet
- No design criteria recommendations have been given yet.
- The effects of temperature, non-linearity, buckling and dynamic research studies have not been conducted yet.
- Many lines of research are currently open in this field in order to clarify linear and non-linear behaviour, to establish design criteria and to optimize the bridge behaviour.

## REFERENCES

- Allied Arts Foundation (2001). The Leonardo bridge project. Available at <http://www.leonardobridgeproject.org/> Accessed 19/02/2012
- Almeida, P. A. O., Stucchi, F.R., Rodrigues, J. F. S., Wainberg, M. and Berger, D. "Retronanalysis of the tests of the 3rd Bridge over the South Lake in Brasilia (Retroanálise dos ensaios na 3ª Ponte sobre o Lago Sul de Brasília)". *V Simpósio EPUSP sobre Estruturas de Concreto*, São Paulo, 2003 (in Portuguese)
- ARCH '07. Proceedings of the 5th International Arch Bridge Conference. Funchal, Madeira, Portugal, 12-14 September, 2007
- ARCH '10. Proceedings of the sixth International Arch Bridge Conference. Fuzhou, China. 11-13 October, 2010
- Arch Bridges IV. Advances in Assessment, Structural Design and Construction. Proceedings of the 4th International Conference on Arch Bridges. Barcelona, 17-19 November, 2004
- Arch bridges: proceedings of the First International Conference on Arch Bridges. Bolton, UK on 3-6 September 1995. 690p. ISBN 0-7277-2048-1
- Arenas de Pablo, J. J. "Quality in Engineering: Innovation and Maturity (Calidad en la ingeniería: innovación y madurez)". In: *AEC Proceedings 2005 (The life of bridges: Asociación Española de la Carretera. 2005)*. San Sebastián. 27-29 April 2005. p341 and 343 (in Spanish)
- Billington, D. P. "The Role of Science in Engineering." In *Robert Maillart's bridges. The art of engineering*. Princeton University Press. Princeton, New Jersey, 1979, pp. 94-105 and pp.111-112.
- Billington, D. P. *Robert Maillart. Builder, Designer, and Artist*. Cambridge University Press, 1997, pp. 146-149 and pp. 174-182.
- Butterworth, K., Carr D. and Kassabian, P. "Gateshead Millenium Bridge, UK: fabrication, assembly and erection". *Proceedings of ICE. Civil Engineering 156*. Paper 12826. March 2003, pp. 11-19
- Cheng, K. M., Ketchum, M. A., and Drouillard, F. "Nanning Butterfly Tied Arch Bridge over the Yong River in China", *Structural Engineering International*, 20 (3). 2010, pp. 308-311
- Corres Peiretti, H.; Sánchez Delgado, J. and Sanz Manzanedo, C.. "Pasarelas cáscara sobre el río Manzanares en Madrid". *Proceedings of V Congreso ACHE*. Barcelona, 2011 (in Spanish).
- Corres Peiretti, H.; Seijo Veiguela, C.; García Espinel, J.D.; Calvo Herrera, I.; Grávalos Moreno, J.; Chozas Ligeró, V.; Lampe Carreras, R. and Viñolo Albiolo, A.. "Aplicación de tecnologías avanzadas del hormigón en las pasarelas en cáscara sobre el río Manzanares para el proyecto de Madrid Río". *Revista Obras Públicas (ROP)*; 2010, nº 3.515, pp7-18. ISSN: 0034-8619 (in Spanish).
- Curran, P. "Gateshead Millenium Bridge, UK", *Structural Engineering International*, November 2003, 13 (4)
- Datry, J.-B.. "The Europe Bridge in Orléans (France): Lessons Learnt". *ARCH '01. Proceedings of the Third International Arch Bridge Conference*. Paris, 19-21 September 2001. pp735-743 (in French)

### III. A) STATE-OF-THE-ART OF SPATIAL ARCH BRIDGES

- De Lucchi, M.. “The bridge of peace. A monument to Tbilisi's different identities.” *Proceedings of the 34th International Symposium on Bridge and Structural Engineering, IABSE*, Venice, Italy, 2010, pp. 1-8 (CD-ROM)
- Firth, I. P. T. and Kassabian, P. E.. “The Ribble Way: Characteristics of a three-way arch”. *ARCH '01. Proceedings of the Third International Arch Bridge Conference*. Paris, 19-21. September 2001. Pp807-812
- Flaga, K., Januszkiewicz, K.. “On the aesthetics and technical efficiency of current arched footbridges”. *4th International Conference. Footbridge 2011*. Wrocław, 6-8 July, 2011
- Hoeckman, W.. “The Europe Bridge in Orléans (France): Construction Phases”. *ARCH '01. Proceedings of the Third International Arch Bridge Conference*. Paris, 19-21 September 2001. pp745-750
- Hussain, N.; Wilson, I.. “The Hulme Arch Bridge, Manchester”. *ICE Proceedings, Civil Engineering* 132. February 1999. pp 2–13
- Johnson, J. and Curran, P.. “Gateshead Millenium Bridge- an eye-opener for engineering”. *Proceedings of ICE. Civil Engineering* 156. Paper 12885. February 2003, pp. 16-24
- Jorquera, J. J. (2007). “Study of the structural behaviour of spatial arch bridges”, PhD Thesis. Supervised by Prof. Manterola, Technical University of Madrid (UPM), (in Spanish). See [http://oa.upm.es/812/1/JUAN\\_JOSE\\_JORQUERA\\_LUCERGA.pdf](http://oa.upm.es/812/1/JUAN_JOSE_JORQUERA_LUCERGA.pdf). Accessed 21/02/2011
- Jorquera, J. J.. “Structural behaviour of spatial arch bridges”, *Proceedings of the International Association for Shell and Spatial Structures (IASS) Symposium 2009, Evolution and Trends in Design, Analysis and Construction of Shell and Spatial Structures* (Domingo, A., and Lázaro, C. (Eds)), Valencia, 2009, pp. 2447-2457.
- Lachauer, L., Jungjohann, H. and Kotnik, T. “Interactive Parametric Tools for Structural Design” *Proceedings of the 35th International Symposium on Bridge and Structural Engineering, jointly organised by IABSE-IASS: ‘Taller, Longer, Lighter’*, London, UK, September 20-23, 2011, pp. 1-8 (CD-ROM)
- Laffranchi, M. and Marti, P.. “Robert’s Maillart’s concrete arch bridges”, *Journal of structural engineering*, 123(10), 1997, pp. 1280-1286.
- Liaghat, D., Powell-Williams, K. and Capasso, M.. “Ponte della Musica: An Urban Bridge in Rome”. *Footbridge 2011. Proceedings of the 4th International Conference Footbridge*. Wrocław, Poland 6 – 8 July 2011
- Manterola, J. “Composite arch bridges”. *ARCH '01. Proceedings of the Third International Arch Bridge Conference*. Paris, 19-21 September 2001. pp779-785
- Manterola, J., Gil, M. Á., and Muñoz-Rojas, J.. “Arch spatial Bridges over the Galindo and Bidasoa Rivers”, *Cauce 2000: Revista de ingeniería civil*, 147. 2009, pp. 20-29, (in Spanish).
- Manterola, J., Gil, M. Á., and Muñoz-Rojas, J.. “Arch spatial Bridges over the Galindo and Bidasoa Rivers”, *Structural Engineering International*, 21 (1). 2011, pp. 114-121
- Manterola, J., Muñoz-Rojas, J., López, A., Fernández, J.. “Guadalentin river and San Cristobal urban area Project in the city of Lorca (Actuación sobre el río Guadalentín y espacio urbano del barrio de San Cristóbal en la ciudad de Lorca)”. *ACHE Proceedings 2005 (Comunicaciones al III congreso ACHE de puentes y*

### III. A) STATE-OF-THE-ART OF SPATIAL ARCH BRIDGES

*estructuras*). Zaragoza. 2005. pp1802-1811 (in Spanish)

Michele De Lucchi Archive (aMDL). Ponte della Pace, Tbilisi (Georgia), 2009-2010. Available at: <http://www.archive.amdl.it/en/index.asp>. Last accessed 2<sup>nd</sup> April 2012

Nicoletti, M.. Sergio Musmeci: organicità di forme e forze nello spazio. Testo & Immagine, Torino, 1999

*Proceedings of the Second International Arch Bridge Conference*. (Venice, 6-9 Octubre 1998). [s.l.]: Taylor & Francis, 1998. 439p. ISBN 9058090124, 9789058090126.

Robertson, Leslie. "A life in Structural Engineering". In: Nordenson, Guy. *Seven Structural Engineers: The Felix Candela Lectures*. New York: The Museum of Modern Art, 2008. pp83-84

Sarmiento-Comesías, M., Ruiz-Teran, A. and Aparicio, A. C.. "State-of-the-art of spatial arch bridges." Special Issue on Arch bridge of the *Bridge Engineering Journal* of the Institution of Civil Engineering, Vol. 166, Issue 3, April 2013 pp163–176. Published on-line 2011. DOI: [10.1680/bren.11.00010](https://doi.org/10.1680/bren.11.00010)

Schlaich, J., and Moschner, T. (1999). "Die Ripshorster Brücke über den Rhein-Herne-Kanal, Oberhausen", *Bautechnik*, 6(76), pp. 459-462.

Stráský, J and Husty, I. "Arch bridge crossing the Brno-Vienna expressway". *Composite constructive – conventional and innovative. International conference*. Innsbrück, 16-18 September 1997. pp.870-871.

Stráský, J. "Bridges designed by Strasky, Husty & Partner". In: AEC Proceedings 2005 (The life of bridges: Asociación Española de la Carretera. 2005). San Sebastián. 27 -29 April 2005. p255-312

Strasky, J. and Kalab, P. "Model Test of the Prestressed Concrete Membrane". *IASS 2007 Conference - Shell and Spatial Structures. Structural Architecture - Towards the future looking to the past*, Venice, Italy, 2007, pp. 1-8 (CD-ROM)

Strasky, J., Kalab, P., Necas, R. and Terzijski, I. "Development of Membrane Roofs from Prestressed Concrete. Structural Concrete in the Czech Republic 2006-2009". *3rd fib Congress*, Washington, 2010.

Strasky, J.. "Bridges Utilizing High-strength concrete". *30<sup>th</sup> Conference of Slovenian Structural Engineers*. Bled, 2008, pp. 1-18.

Terzijski, I. "Optimization of UHPC for the Model of a Pedestrian Bridge in: Ultra High Performance Concrete (UHPC)". *Ultra high performance concrete (UHPC): proceedings of the Second International Symposium on Ultra High Performance Concrete*. (Fehling E., Schmidt, M. and Stürwald S. (eds)). Kassel, Germany, March 5-7, 2008, pp. 707-716

Thomas, G. E. "The Blythe Park Bridge". In: Martínez, J. (Dir y Ed). *Proceedings of Composite Bridges 2001*. Madrid: Ediciones del Colegio de Ingenieros de Caminos, CC y PP. 2001. Madrid, 22-26 January, 2001. pp 131-144 (in Spanish)

Verlain, D., Hardy, D., Schmit, C., Joris C., Duchêne, Y. and de Caters, P. "Bowstring bridge with curved deck". *ARCH '01. Proceedings of the Third International Arch Bridge Conference*. Paris, 19-21 September 2001. pp715-722 (in French)

Von Buelow, P., Falk, A. and Turrin, M. "Optimization of structural form using a genetic algorithm to search associative parametric geometry" *Proceedings of the International Conference on Structures & Architecture*

## Notation

$\alpha$  angle between the plane which contains the arch and the vertical hangers

$f$  arch vertical rise

$g_A, g_D$  horizontal sag of the arch and the deck, respectively

$L_A, L_D$  span of the arch and deck, respectively

$I_A, I_D$  balcony-beam flexural rigidity of the arch and the deck, respectively

$J_A, J_D$  torsional rigidity of arch and deck respectively

$E_A, E_D$  elastic moduli of the arch and the deck, respectively

$G$  shear modulus

$z_D$  height of the deck measured from the arch springings

$d$  horizontal offset between the arch crown and the deck mid-span section

$e$  plan eccentricity between the axis of the arch at the springings and the axis of the deck at the abutments

$B_A$  arch width

$H_A, H_D$  depth of the arch and the deck, respectively

$\theta$  rotation of the arch in plan in relation to the deck alignment

$\omega$  angular tilt of the arch from the vertical plane

$b_{Ay}, b_{Az}, b_{Dy}, b_{Dz}$  horizontal and vertical distances from the hangers anchorages to the shear centre of the cross-section of the arch and deck, respectively

## Acronyms

IDABWIC Inferior-Deck Arch Bridges with Imposed Curvature

SAB Spatial Arch Bridge

SDABWIC Superior-Deck Arch Bridges with Imposed Curvature

### III. A) STATE-OF-THE-ART OF SPATIAL ARCH BRIDGES



# III. B) STATE-OF-THE-ART OF THE ANALYSIS METHODS AND BENCHMARKS



# INDEX

1.	STATE-OF-THE-ART OF ANALYSES METHODS.....	53
1.1	FE models.....	53
1.2	Software comparison.....	54
2.	BENCHMARKS .....	54
2.1	INTRODUCTION.....	54
2.2	MATERIAL CHARACTERISTICS .....	55
2.3	STRAIGHT FRAME MODEL OF A CURVED STRUCTURE.....	55
2.4	BUCKLING AND NON-GEOMETRICAL ANALYSIS BENCHMARK: CANTILEVER WITH AN EXCENTRIC LOAD .....	58
2.5	PINNED BEAM WITH CODED IMPERFECTIONS. NUMERICAL FRAME MODEL VALUES COMPARED TO THE EUROPEAN BUCKLING CURVES .....	61
2.5.1	<b>Model description and objectives</b> .....	61
2.5.2	<b>Buckling hypothesis</b> .....	62
2.5.3	<b>Imperfections values</b> .....	62
2.5.4	<b>Analyses</b> .....	62
2.5.5	<b>Results</b> .....	63
3.	CONCLUSIONS .....	66
	REFERENCES .....	66



## **1. STATE-OF-THE-ART OF ANALYSES METHODS**

The state-of-the-art of analyses methods deals with different aspects. Some are specific for other studies and hence can be found in other chapters or annexes:

- The basis of analysis of approximate formulations for buckling, either coded or purposed in research studies, has been detailed and is exposed in chapter VI. A.
- The advantages and disadvantages of different FE modelling possibilities, with either frames or shells, have been considered and summarised in the present chapter (based on Sarmiento-Comesías, 2009)
- A comparison of different commercial software has been conducted in order to choose the most adequate one for the present research (summarised in the present chapter and based on Sarmiento-Comesías, 2009)

### **1.1 FE models**

Either frame or shell elements can be employed in a FE model. Each model type presents advantages and disadvantages which can be summarized as follows:

- Internal forces interpretation is easier when employing a frame model and the analysis is quicker.
- Non-linear material analysis gives good results with frame models when employing fibre hinges, in which the cross-section is divided into fibres and the stresses in each of them are controlled, the mechanical characteristics of the cross-section are modified as fibres plasticize. Softwares applying this analysis control material non-linearities without the need of employing shell models.
- Bending moments, shear forces and torsional moments interaction is not considered for obtaining stresses in frame models, whereas in shell models it is considered (eg: Von Mises for steel shell elements in SAP2000).
- Shell models allow obtaining local effects.

In conclusion, applying the aforementioned advantages and disadvantages to the present study:

- Spatial arch rib bridges global behaviour is best modelized by employing FE frame models.
- For shell spatial arch bridges it is best to employ shell FE models, since a frame model approximation is not good enough.
- In general, for the objectives of the present study, a frame 3D analysis is the most adequate, since it is the global behaviour of SABs what is considered and not the local effects.

## 1.2 Software comparison

A series of softwares have been compared (Sarmiento-Comesías, 2009). This comparison has led to the following conclusions for the present research:

The most adequate software to conduct a frame model either linear or geometrically and material non-linear analysis is SAP2000, since it employs fibre hinges for whatever material of which the constitutive equation can be introduced. This method allows for considering the formation of plastic hinges and it automatically iterates obtaining the new characteristics based on the fibres forming the hinges and obtaining the new internal forces until convergence is reached. SOFISTIK and ANSYS do not have this function automatically, a module should be programmed to obtain this analysis with plastic hinges.

However, the opposite happens with FE shell models: SOFISTIK and ANSYS are both adequate for non-linear shell analyses, but not SAP2000. SOFISTIK results output offers advantages over ANSYS. Moreover it has the possibility to implement precambers and antifunicularity, which offers advantages for design and future researches, and it is cheaper.

For the analysis of FE frame models with linear material but geometrically non-linear analysis SOFISTIK offers the advantage in front of SAP2000 of automatically introducing imperfections based on the buckling shape, whereas in SAP2000 this must be done by exporting and importing excel tables or programming a module.

Therefore, SAP2000 is concluded to be the best program for non-linear analysis of frame models and SOFISTIK for shells. Benchmarks will be developed for geometrically non-linear analyses with both software, SAP2000 and SOFISTIK.

## 2. BENCHMARKS

### 2.1 INTRODUCTION

With the objective to assure that the software employed for the present research study and the analyses methods can be considered valid, a broad state-of-the-art research has been conducted. On finding no specific results to approve the intended methodology specific benchmarks for this research study have been developed.

Three different benchmarks have been employed:

- The arch with the maximal curvature has been modeled with a different number of straight frames to measure the error committed by not employing curved frames according to the literature error calculation formulas for bending and torsional moments (Sawko in Manterola, 1977). This is necessary since SABs have to bear important out-of-plane forces also for vertical loading. To obtain the buckling error due to the same simplification the models have been compared to one with a high number of straight frames which can be considered to have a negligible error with curved frames.

This benchmark is presented in section 2.3 of the present chapter.

- A cantilever with an eccentric axial load has been analysed with two different softwares by means of a buckling analysis and geometrically non-linear analysis and compared with

Euler's buckling load and Timoschenko's (1957) analytical formula for the displacements in order to obtain the error committed by the FE element model.

This benchmark is presented in section 2.4 of the present chapter.

- A series of FE frame models of pinned beam of different lengths submitted to an axial load have been analysed with SAP2000 with a GNLA of P-delta+large displacements and also introducing material non-linearities. Eurocode 3 coded imperfections have been introduced to the beams employing the first mode buckling shape and the critical axial load values (Ncr) have been obtained in each case. A unitarian slenderness- Ncr diagram has been plotted with the results and compared to the European buckling curves. The objective is to assure that coded imperfections are conservative, since no European buckling curves exist for arch bridges.

This benchmark is presented in section 2.5 of the present chapter.

## 2.2 MATERIAL CHARACTERISTICS

The material employed for all the analyses of the benchmarks is steel with the following characteristics:

$$f_y=248,211\text{N/mm}^2$$

$$f_u=399,896\text{N/mm}^2$$

$$G=76903\text{N/mm}^2$$

For non-linear analyses the stress-strain diagram employed is the following (Figure 2-1):

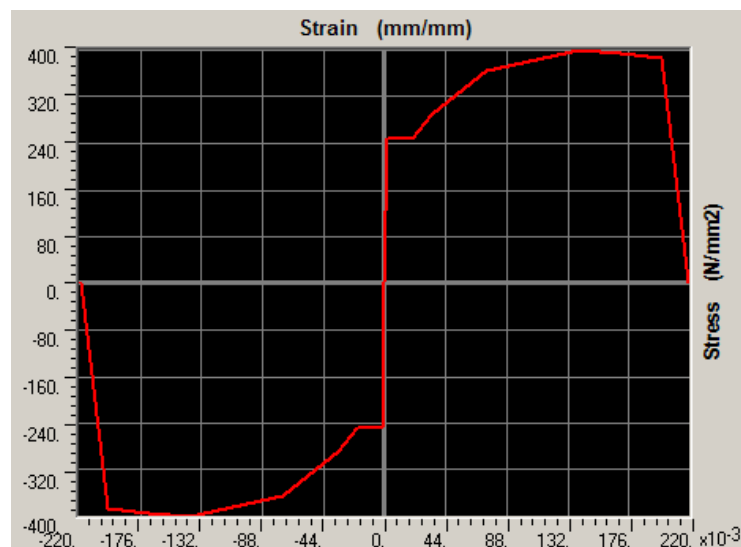
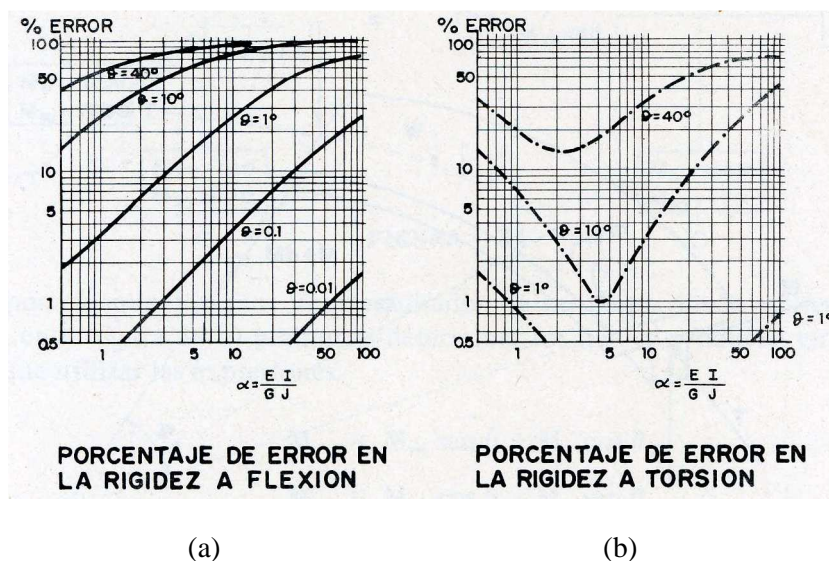


Figure 2-1: Employed steel stress-strain diagram

## 2.3 STRAIGHT FRAME MODEL OF A CURVED STRUCTURE

Employing straight frames to model curved beams neglects the curvature effects in each of the frames. The forces caused by the curvature will be concentrated on the joints between straight frames. The curvature effects in the case of SABs are important as in planar vertical arch bridges for the behavior in plane (axial forces and bending moments), but further more important for the

behavior out-of-plane as a balcony beam. In a curved girder or balcony-beam bending and torsional moments are coupled. The interaction between these internal forces is continuous along a curved beam. However, when using a model with straight frames the interaction between bending and torsional moments only takes place at the vertex of the polygonal line which the straight frames describe. The higher the number of frames, ie: lower angle between frames, the lower the internal forces deviation (Manterola, 1977). According to Manterola (1977) for bridges curved in plan when the angle between the frames is smaller than  $2^\circ$  a straight frame model can be employed with a negligible error. This is based on Sawko's method for a reasonable  $EI/GJ$  relationship. Employing Sawko's figures (Figure 2-2) and for the described arch cross-section values:  $EI/GJ=1,31$

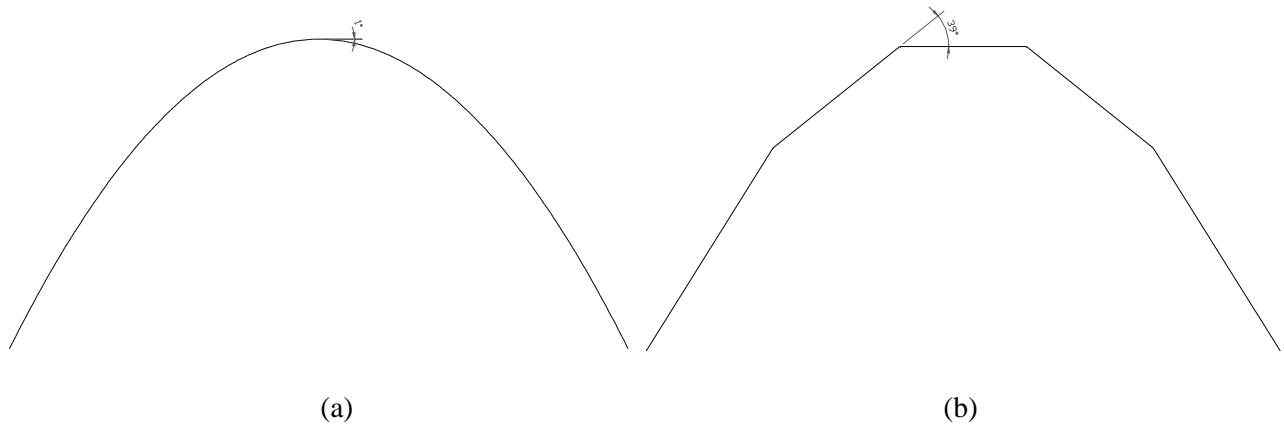


**Figure 2-2: Error defined by Sawko depending on the stiffness and the angle between frames (a) bending moments error (%) (b) torsional bending moments error (%). Figure obtained from Manterola (1977)**

If 68 frames are employed for each the arch and the deck, with the maximal rise  $f=50\text{m}$  for the arch and  $g=20\text{m}$  for the deck, the bending moments errors for the arch and deck, when compared with 200 frames for each the arch and the deck model, are below 5% and 4%, respectively, and for torsional bending moments below 0,75 and 0,6%. We consider these errors negligible. Most models employ the same arch rise and horizontal sag in plan  $f=g=20\text{m}$ , hence errors for the balcony-beam behaviour are in general below 4%

To make sure that this is also valid for buckling, a study has been conducted for a parabolic planar vertical arch with fixed bearings. The highest curvature value has been employed in the present study, corresponding to a  $f=50$  planar arch. Different models have been analysed varying the number of frames employed, from 200 (maximal angle between frames  $1^\circ$ , Figure 2-3a), considered the reference value supposing a 0 error, and diminishing it to 5 frames (maximal angle between frames  $39^\circ$ , Figure 2-3b). For the different models the values obtained for the buckling load and for the axial force at the arch springings under a vertical uniform loading on the whole arch span or only half its span have been compared.





**Figure 2-3 Arch frame models (a) 200 frames (b) 5 frames**

It has been proved that, when employing more than 6 elements (maximal angle between frames 37°) for the arch loaded with a vertical uniform loading on the whole span, the improvement of the results for buckling is negligible (the error is below 3%). Even less elements are need to obtain a good approximation of the axial forces at the arch springings. When loading the arch with a uniform loading on only half its span it is recommendable to employ more than 30 members (8°), since with this number the error for buckling is already above 3%.

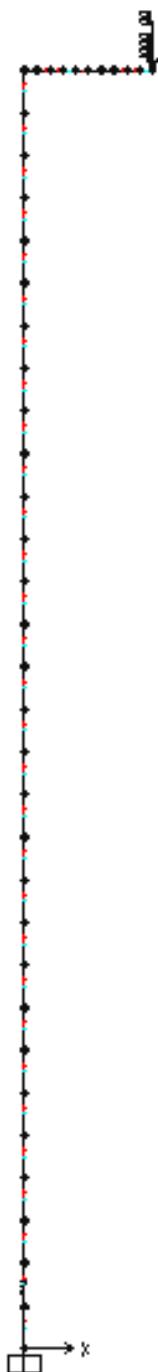
For all of the analytical studies the deck and arch will be divided into 68 straight frames as already stated, which gives an error below 1,2% (see Table 2-1). This fully guarantees the validity of the results in spite of not using curved frames.

Number of frames	qB (kN/m)	qB asym loading (kN/m)	Nspringing (kN) for q=5kN/m	Nspringing (kN) for q=10kN/m asym loading	error qB (%)	error qB asym (%)	error N (%)	error N asym (%)
200	11.698	22.777	400.114	626.467	0	0	0	0
68	11.696	22.506	399.994	625.883	0.0	1.2	0.0	0.1
50	11.694	22.360	-	625.548	0.0	1.8	-	0.1
30	-	21.995	-	624.649	-	3.4	-	0.3
25	11.680	21.803	399.600	624.300	0.2	4.3	0.1	0.3
10	11.583	-	398.178	-	1.0	100.0	0.5	-
6	11.362	18.543	395.770	611.062	2.9	18.6	1.1	2.5
5	11.206	-	394.223	-	4.2	100.0	1.5	-

*qB is the buckling loading value of a uniform vertical loading on the whole length of the arch for the 1<sup>st</sup> buckling mode  
qB asym is the buckling loading value of a uniform vertical loading on half the length of the arch for the 1<sup>st</sup> buckling mode  
Nspringing is the axial force at the arch springing for a vertical uniform loading q*

**Table 2-1: Axial force (N) and buckling load forces errors for dfferent number of frames arch model, considering 200 frames a good enough result with a theoretical error 0**

## 2.4 BUCKLING AND NON-GEOMETRICAL ANALYSIS BENCHMARK: CANTILEVER WITH AN EXCENTRIC LOAD



**Figure 2-4:**  
Cantilever FE model with an excentric load frame model. Height: 5m, load excentricity 0,5m

A step loading and geometrically non-linear analysis (GNLA) and an elastic buckling analysis have been developed for the 2D frame model shown in Figure 2-4 with SAP2000 v14. Various models with different number of FE have been analysed. An analysis with SOFISTIK has also been conducted.

The numerical results for the horizontal displacements at the top node ( $\delta$ ) of a column with height  $L=5\text{m}$  and an eccentricity at the top of  $e=0,5\text{m}$  have been compared with the analytical results according to Timoschenko (1957) (Eq 1).

$$\delta = \frac{e \cdot (1 - \cos pl)}{\cos pl} \quad \text{Eq 1}$$

The errors for the displacements in each loading step and the buckling load with respect to the analytical values have been calculated.

In Table 2-2 the analytical results and the numerical ones obtained for the Euler buckling axial load ( $N_b$ ) with SAP2000 and SOFISTIK employing 25 elements (15 in height and 10 horizontally) and buckling analysis are displayed, as well as the error committed employing the FE analysis (named “error Buckling” in the table). The error committed with both softwares is negligible. If this error is added to the one committed by employing straight frames to model the arch (section 2.3) the buckling error is still below 3%.

A summary of the results obtained with SAP2000 for the different cross-sections described in Table 2-3 is given in Table 2-4.

Analytical $N_b$ (kN)	4189,5		
Numerical $N_b$ SAP2000 (kN)	4119,0	error Buckling (%)	1,7
Numerical $N_b$ SOFISTIK (kN)	4161,0	error Buckling (%)	0,7

**Table 2-2: Euler analytical buckling axial load comparison with numerical buckling loads obtained with different softwares with buckling analysis**

In Table 2-4 “% $N_b$ ” is the percentage of the buckling load ( $N_b$ ) obtained with SAP with which the structure is loaded. For each loading value a displacement horizontal value at the top is obtained employing a GNLA with the P-delta+large displacements method. The displacement error with GNLA is the percentual difference of this value with respect to the analytical value obtained with Eq1. The nearer the loads to  $N_b$ , the larger the displacement error.

In Figure 2-5 and Figure 2-6 the analytical results and the numerical ones obtained with both softwares are compared.

The error does not depend on the bending stiffness of the cross-section, as results of sections from 1 to 3 attest (Table 2-4). The error is not caused by the analytical formula

neglecting shear stiffness, since, when neglecting shear stiffness, the displacement error for a same load value is larger.

According to this benchmark, the present study employing 3D frame models with SAP2000 v14 will consider results to be reliable only for loads under a 50% of the buckling load.

SOFISTIK gives a larger error (Figure 2-5 and Figure 2-6).

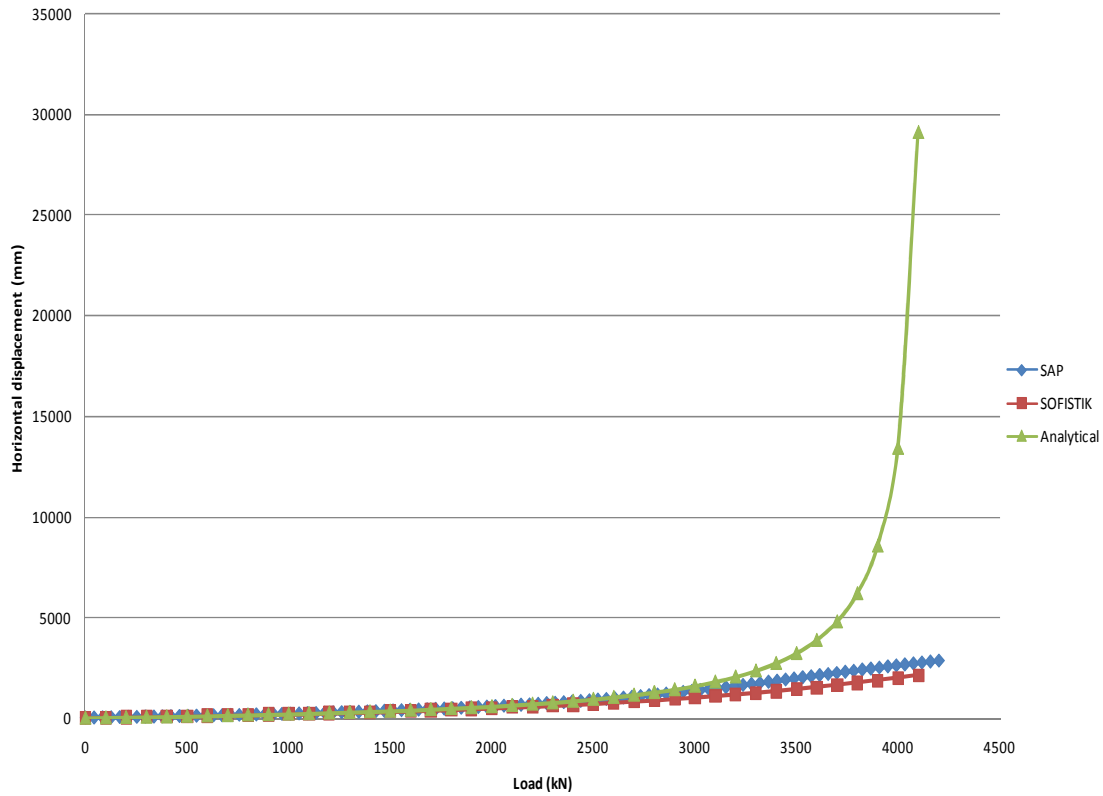
	Cross-section 1	Cross-section 2	Cross-section 3
Area (m <sup>2</sup> )	$6,645 \cdot 10^{-3}$	$6,645 \cdot 10^{-5}$	$6,645 \cdot 10^{-5}$
Moment of inertia (m <sup>4</sup> )	$2,123 \cdot 10^{-4}$	$2,123 \cdot 10^{-6}$	$2,123 \cdot 10^{-6}$
Torsional stiffness (m <sup>4</sup> )	$2,106 \cdot 10^{-7}$	$2,106 \cdot 10^{-7}$	$2,106 \cdot 10^{-7}$
Shear area (m <sup>2</sup> )	$3,426 \cdot 10^{-3}$	$3,426 \cdot 10^{-5}$	0

**Table 2-3: Frame cross-sections employed for 3 different models**

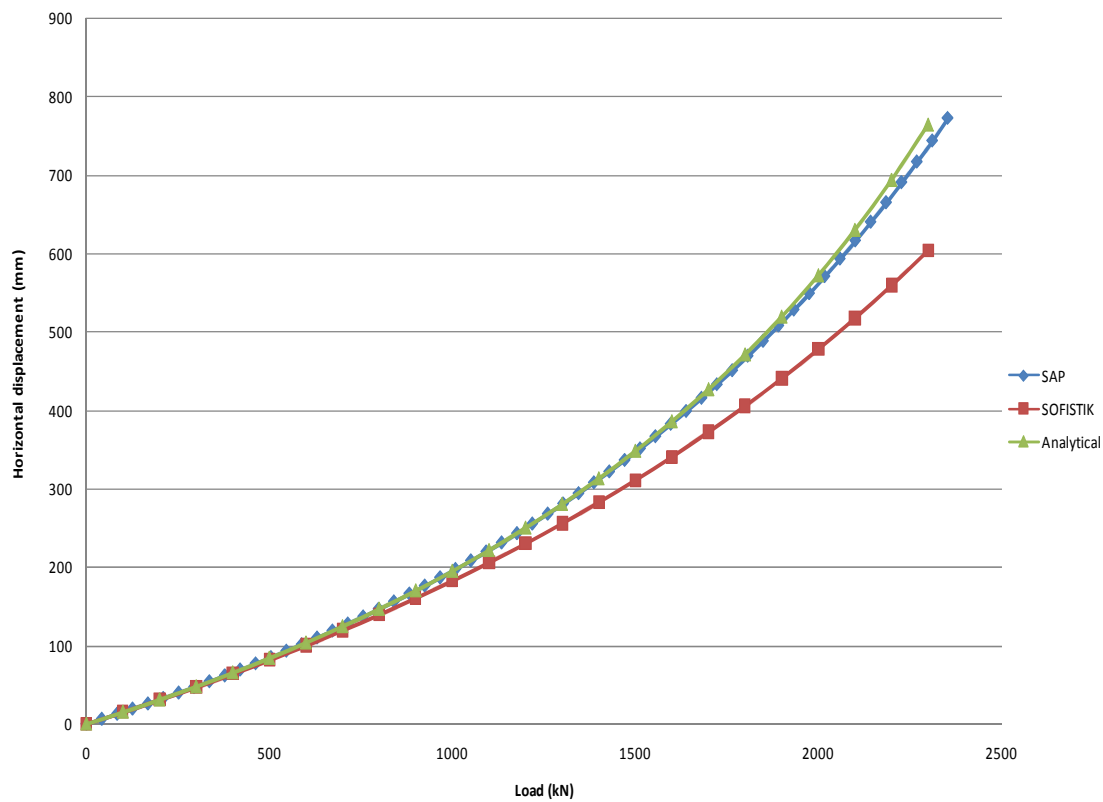
	Cross-section 1	Cross-section 2	Cross-section 3
Displacement error with GNLA(%)	%Nb SAP	%Nb SAP	%Nb SAP
3%	54	54	47
5%	59	59	54
10%	67	67	64

ERROR BUCKLING(%)	1,7	1,7	0,1

**Table 2-4: External loads correspondent to different displacement errors and SAP buckling load errors for different cross-section values shown in Table 2-3. The loads are given as a % of the SAP buckling load (Nb)**



**Figure 2-5: Axial load-horizontal displacement comparison of the analytical and numerical results until the analytical buckling load is reached**



**Figure 2-6: Axial load-horizontal displacement comparison of the analytical and numerical results until the error of the displacements reaches approximately 10% for SAP2000 and approximately 20% for SOFISTIK. Detail of Figure 2-5.**

## 2.5 PINNED BEAM WITH CODED IMPERFECTIONS. NUMERICAL FRAME MODEL VALUES COMPARED TO THE EUROPEAN BUCKLING CURVES

### 2.5.1 Model description and objectives

There are no equivalent European curves for arch bridges. Therefore, the coded imperfections will be employed following the first mode of buckling shape as stated in Eurocode 3 (EC3 Part 1.1, chapter 5.3.2). The specific values for arches in EC3 Annex D.3.5 and also EAE 22.3.4 will be employed for arches. This imperfection values are expected to be conservative, but it is convenient to confirm this with a benchmark for the program SAP2000 v14 which will be employed for the present research.

The frame model shown in Figure 2-7 has been analysed, employing the cross-section shown in Table 2-5, for different span lengths (L, Table 2-6). The aim is to compare the European buckling curves of the codes with the results obtained numerically introducing the coded eccentricities (EC 3) and conducting a GNLA with SAP2000 (with the P-delta + large displacements method, which has proved to give good results in section 2.4) and also a geometrically and material non-linear analysis (G and M NLA) with fibre hinges.

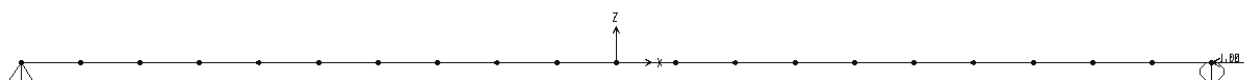


Figure 2-7: Beam FE model with an axial force

Area (m <sup>2</sup> )	$2,725 \cdot 10^{-3}$
Moment of inertia (m <sup>4</sup> )	$1,846 \cdot 10^{-5}$
Torsional stiffness (m <sup>4</sup> )	$4,926 \cdot 10^{-8}$
Shear area (m <sup>2</sup> )	$1,417 \cdot 10^{-3}$

Table 2-5: Mechanical characteristics of the cross-section employed for the model shown in Figure 2-7

L (mm)	Slenderness	Unitarian slenderness	e0= maximal imperfection value (mm)
200	2.4	0.027	$\lambda < 0,2$
500	6.1	0.068	$\lambda < 0,2$
1000	12.2	0.136	$\lambda < 0,2$
2000	24.3	0.273	1,24
4000	48.6	0.545	5,97
6000	72.9	0.818	11,06
8000	97.2	1.090	16,96
10000	121.5	1.363	23,81
16500	200.5	2.248	50,85

Table 2-6: Length, slenderness and imperfections for the different analysed models with the geometry shown in Figure 2-7

## 2.5.2 Buckling hypothesis

### Local buckling:

Enough thickness is given to the cross-section in order to avoid local buckling, according to the EC 3 classification.

### Plate buckling

Diaphragms and transverse bracings will control the buckling of the compressed plates and instabilities caused by shear forces.

### Global buckling

The aim of the present study is to analyze the global buckling of this bridge type.

## 2.5.3 Imperfections values

A frame model is employed and sectional effects are not modeled. Therefore residual stresses cannot be introduced

Residual stresses might cause the cross-section or a part of it to plasticize and this would lower the buckling load. This buckling load reduction is considered by means of an equivalent imperfection.

The imperfections stated in the codes comprise residual stresses, load eccentricities and geometrical imperfections.

Load eccentricities in the arch are caused, for example, by the gaps opened on the arch in order to pass gusset plates through. This can be considered in the bridge model.

Geometrical imperfections will not be larger than the tolerances and could be introduced with the buckling shape to be conservative.

In order to consider residual stress as recommended by the ECCS no 22 a sectional model must be developed (Manzanares and Hinojosa, 2011). Since studying cross-sectional behaviour is not our aim, we will be working with a 3D frame model as previously stated. Therefore, instead of introducing load eccentricities and residual stresses, the coded imperfections will be employed following the first mode of buckling shape as stated in EC3 (Part 1.1, chapter 5.3.2) and also in EAE 22.3.5. The imperfections for the different slenderness values of the analysed models are detailed in Table 2-6.

## 2.5.4 Analyses

A step loading geometrically non-linear analysis with the aforementioned imperfections has been conducted. The axial-bending moments at the mid-point have been plotted. The interaction diagram has also been plotted. The intersection of both diagrams shows the axial force and bending moment for which the first fiber plasticizes.

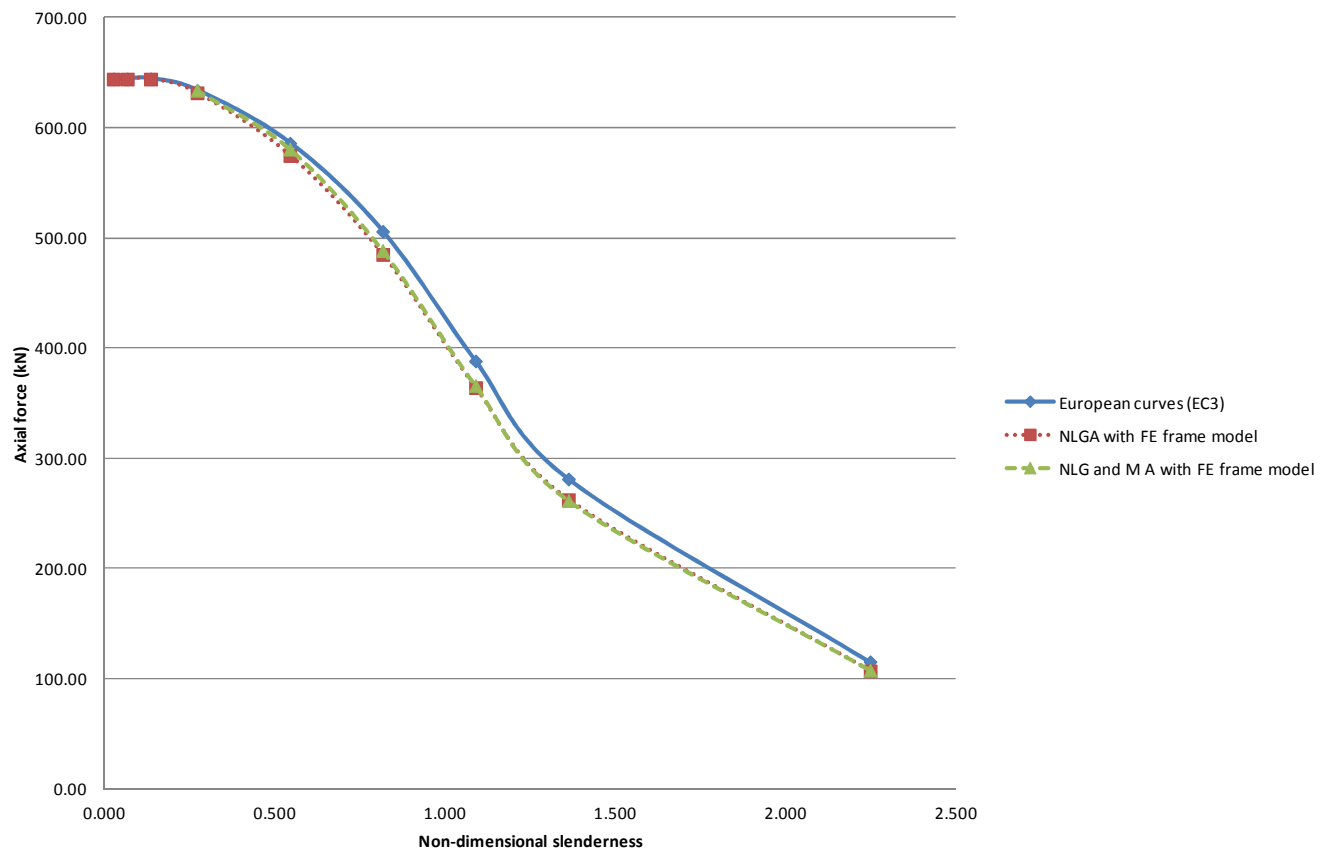
A geometrical and material non-linear analysis has also been developed, plotting the axial-bending moments at the mid-point. In order to do this analysis, two fiber hinges in the Newton

integration points of each frame have been employed. 80 fibers have been employed in order to accurately define the cross-section. The length of these hinges is half each frame. Frames with a large stiffness have been employed and the stiffness values have been given to those hinges. An equivalent analysis with only a hinge in the mid-point of each frame and with 160 fibers shows that the model is not improved further increasing the number of hinges or of fibers.

Displacement control has been employed.

### 2.5.5 Results

The results of the maximal axial force according to the european buckling curves (EC 3, Part 1.1, chapter 6.3.1.2), the plastification of the first fiber and the maximal axial force according to the geometrical and material non-linear analysis, have been compared (Figure 2-8).



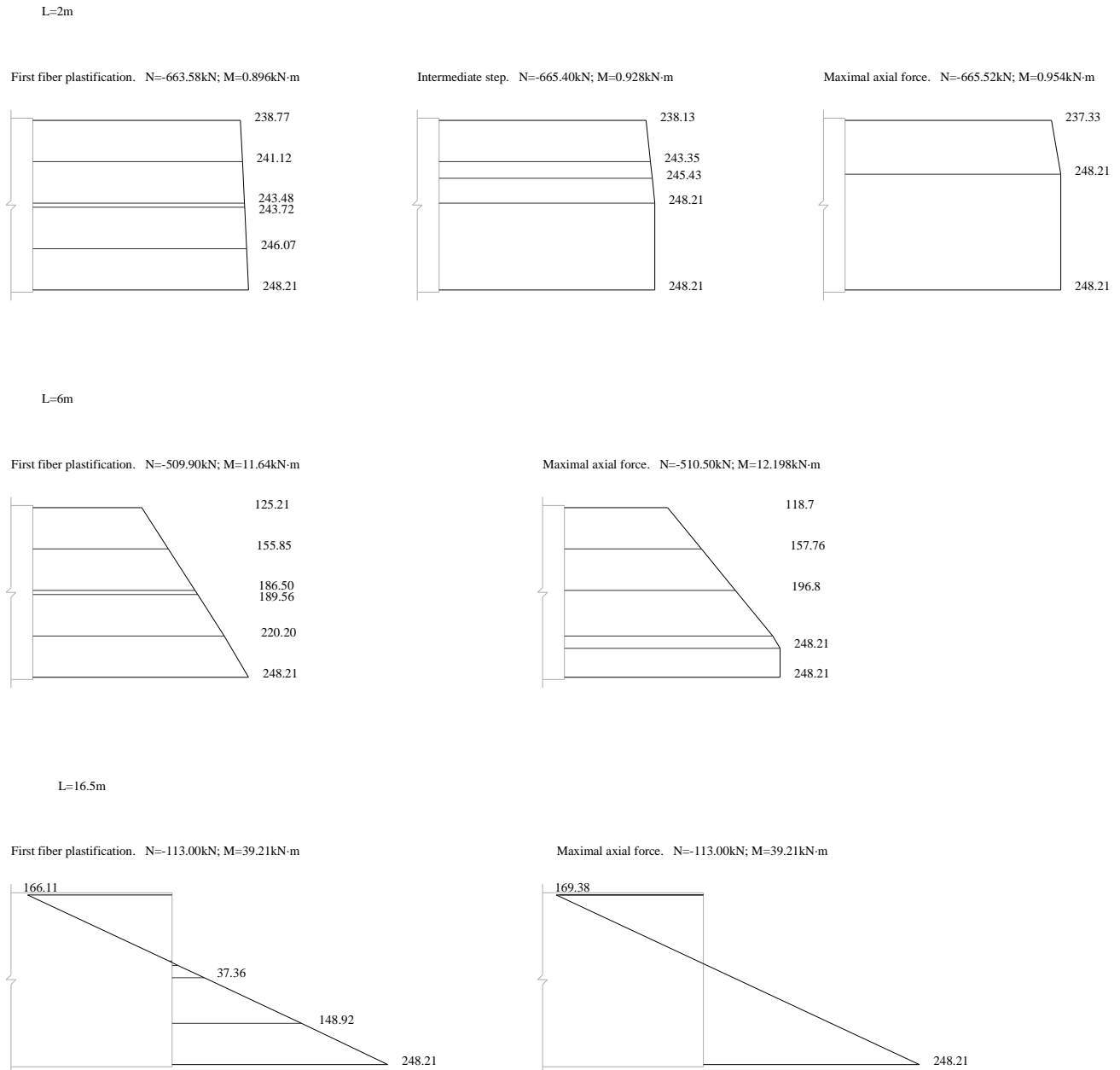
**Figure 2-8: Comparison of the unitarian slenderness-axial forces diagrams of the european buckling curves, the plastification of the first fiber and the maximal axial force according to the geometrical and material non-linear analysis**

The axial force difference between considering that the structure reaches its ultimate load when the first fiber plasticizes or when the maximal axial force forming a completely plasticized hinge<sup>1</sup> is reached is completely negligible (Figure 2-8). Therefore, it is equivalent to do a geometrically

<sup>1</sup> This leads to a mechanism, since the structure is isostatic.

non-linear analysis considering the interaction diagram and to consider both geometrical and material non-linearities. However, it must be borne in mind, that this model is isostatic.

Observing the evolution of the stresses in fibers, the cross-section stresses can be plotted as shown in Figure 2-9. After reaching the maximal axial load, axial forces will not increase anymore because bending moments increase very quickly (Figure 2-9), ie: the structure buckles due to important geometric effects, in spite of still being far from the Euler buckling load.



**Figure 2-9: Cross-sectional stress (MPa) diagrams for different lengths of the analysed beam and for different steps of loading in each case**



L (mm)	Ncr obtained from NLGA (kN)	Ncr obtained from the European buckling curves (kN)	Ncr obtained from G and M NLA (kN)	e1 (%)	e2 (%)
200	644,12	644,12	644,12	0	0
500	644,12	644,12	644,12	0	0
1000	644,12	644,12	644,12	0	0
2000	631,49	633,70	633,83	-0,37	0,0
4000	574,81	585,93	580,57	-0,99	-0,9
6000	484,89	505,94	488,57	-0,75	-3,4
8000	364,15	388,25	366,10	-0,53	-5,7
10000	262,55	281,23	261,74	0,31	-6,9
16500	107,24	115,44	107,80	-0,52	-6,6

*e1 is the error committed in the GNLA by neglecting material non-linearities*

*e2 is the error of the results obtained by the G and MNLA model with respect to European buckling curves*

**Table 2-7: Length, critical axial forces (Ncr) and errors for the different analysed models and employed methods**

- Considering the coded eccentricity is conservative, since axial forces are below the European buckling curves (Figure 2-8).
- Employing an eccentricity to model this effect has proved to commit a maximal error of 7% and minimal of 1% (Table 2-7)<sup>2</sup>. Developing buckling curves for arches equivalent to European curves, requires an accurate analysis in which residual stresses are introduced in a FE shell model. However, to obtain these curves is not the objective of the present study.
- Our aim is to understand this bridge type behaviour. Therefore, according to the present chapter results, SAP2000 is employed to model the SABs to study with 3D Frame models.
- These structures have a highly statically indeterminate. Hence, considering also material non-linearity is expected to give a higher bearing capacity to these structures.

<sup>2</sup> The slenderer the beam, the larger the error.

### 3. CONCLUSIONS

- Employing straight frames with an angle  $< 3^\circ$  to model a curved balcony-beam (as both the arch and the deck are, out-of-plane) gives bending moments error below 5% and a torsional bending moments below 0,75%. The buckling error is below 1,2%. Therefore, employing a straight frame model to model the arches and curved decks of the present study is considered valid if the angle between frames below  $3^\circ$
- SAP2000 gives good enough buckling results (error  $< 1,7\%$ ) and a geometrically non-linear analysis gives reliable displacements for loads inferior to a 60% of the buckling load (error  $< 5\%$ ).
- The coded imperfections, employing the first mode of buckling shape as stated in Eurocode 3 (EC3), are conservative in comparison with the European buckling curves. Therefore, this is the method which will be employed for the present research study.

### REFERENCES

ECCS No. 22. Manual on stability of steel structures; 1976.

ESPAÑA. MINISTERIO DE FOMENTO. *Documento 0 de Instrucción EAE de Acero Estructural*. Madrid: Ministerio de Fomento. Centro de Publicaciones, 2011. Artículos 22, 23, 24 y 35

Eurocode 3: Design of steel structures

Manterola, J. “Cálculo de tableros de puente por el método del emparrillado”, Hormigón y acero n122, pp93-149, ATEP, Madrid, 1977

MANZANARES JAPÓN, J. L. and HINOJOSA SÁNCHEZ-BARBUDO, I, “Non-linear plastic analysis of steel arches under lateral buckling”, *Journal of Constructional Steel Research*, n. 12 v. 67, December 2011, doi:10.1016/j.jcsr.2011.05.008, pp1850-1863

SARMIENTO-COMESÍAS M., “Non-linear behaviour and design criteria for spatial arch bridges” MPhil-PhD Transfer report. Jointly supervised by Prof. Aparicio (Director of studies) and Dr Ruiz-Teran, Technical University of Catalonia (UPC), Barcelona, 2009 (in Spanish).

TIMOSHENKO, S., *Resistencia de materiales. Primera Parte*, Espasa-Calpe S.A., Madrid 1957, p234 (in Spanish)

**IV. ELASTIC STRUCTURAL  
BEHAVIOUR OF INFERIOR-DECK  
SPATIAL ARCH BRIDGES WITH  
IMPOSED CURVATURE**

#### IV. STRUCTURAL BEHAVIOUR OF INFERIOR-DECK SPATIAL ARCH BRIDGES WITH IMPOSED CURVATURE

**INDEX**

1. INTRODUCTION ..... 71

    1.1 Definition ..... 71

    1.2 Research procedure and parameters considered ..... 72

2. BACKGROUND AND OBJECTIVES ..... 73

3. GEOMETRICAL DEFINITION OF INFERIOR-DECK ARCH BRIDGES WITH IMPOSED CURVATURE (ID-ABWIC) ..... 75

4. STRUCTURAL BEHAVIOUR OF IDABWIC ..... 78

    4.1 Understanding the effect of increasing the horizontal sag ..... 78

    4.2 General scope ..... 79

*Conceptual models* ..... 79

    4.3 Frame FE models of IDABWIC with rigid hangers ..... 84

        4.3.1 Study of the connections of rigid hangers with the arch and the deck ..... 84

        4.3.2 Structural behaviour under non-symmetrical vertical loading ..... 104

5. CONCLUSIONS ..... 106

6. FUTURE LINES OF STUDY ..... 107

REFERENCES ..... 107

Notation ..... 108

#### IV. STRUCTURAL BEHAVIOUR OF INFERIOR-DECK SPATIAL ARCH BRIDGES WITH IMPOSED CURVATURE

**1. INTRODUCTION**

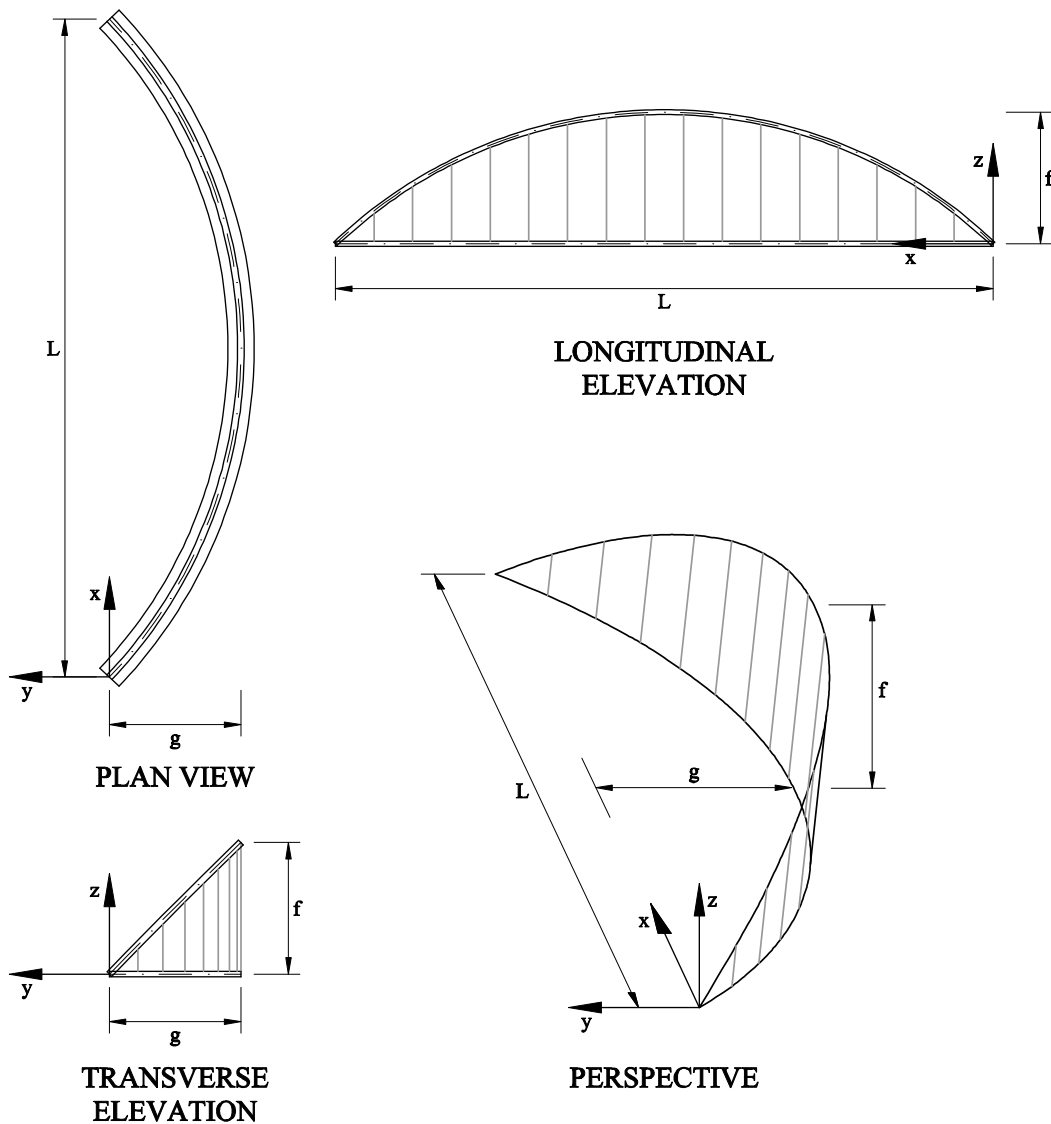
This chapter is a broadened and further detailed version of the paper published in ASCE Journal of Bridge Engineering in 2011 by the present author and her supervisors.

In the present chapter, arch bridges with imposed curvature (ABWIC) possible geometries and their linear structural behaviour are studied. The geometrical stability is addressed in chapter VI.

As a reminder, the definition of ABWIC already given in chapter III, is detailed in the following lines.

**1.1 Definition**

Arch bridges with imposed curvature (ABWIC) are those in which the arches are forced to have the same curvature in plan as the deck (Figure 1-1). Therefore, the arch and deck centroid lines are contained in the same vertical cylinder. In inferior deck ABWIC (ID-ABWIC), the deck is located under the arch and supported by vertical hangers which do not restrict the vertical clearance (Jorquera 2007; Sarmiento et al 2010).



**Figure 1-1: Nomenclature for the models that have been studied for inferior deck arch bridges with imposed curvature**

### 1.2 Research procedure and parameters considered

In order to understand the structural behaviour of these arch bridges, several 3D frame FE models have been developed and analyzed (using SAP2000 v14.2), as part of a set of thorough parametric analyses (Figure 1-1, model perspective). Several parameters, such as the arch geometrical definition, the deck and arch curvature in plan view (measured by means of the horizontal sag ( $g$ )), the arch rise ( $f$ ) (Figure 1-1), the cross-sectional area and the rigidities of the arch, have been considered. In addition, bearing in mind the relevance of the arch and deck interaction, the cross-sectional rigidities of the deck and the hangers, as well as the link connections between these structural members, are essential parameters to be investigated. One of the objectives of this study is to identify the set of these parameters for which the arch works mainly under compression (i.e. the arch tends to the anti-funicular of the loading).

For all the analyses presented in this paper, the following dimensions have been employed: span length  $L=100\text{m}$  and arch rise  $f=20\text{m}$ . Unless otherwise mentioned, the variable  $g$  is set equal to  $20\text{m}$ .

The arch-rise span ratio ( $f/L$ ) has been adopted equal to  $1/5$ , as usual in conventional arch bridges (O'Connor 1971). The plan curvature effects have been enhanced by making  $g=f$ .

All the arches included in these analyses are made of steel, as are most of the built spatial arch bridges. This material has an appropriate performance in this bridge type, since large bending moments occur due to its structural configuration (see section 4). The modulus of elasticity ( $E$ ) considered is equal to  $2,0 \cdot 10^8 \text{ kN/m}^2$ .

The studied arches in each of the studied models are fixed to the deck, which is itself fixed to the abutments.

The behaviour of this bridge type is studied under vertical uniformly distributed live loads ( $q=10\text{kN/m}$  on the whole deck, except for section 4.3.2). The dead loads and the pretension of the hangers counterbalance each other and need not be considered.



**2. BACKGROUND AND OBJECTIVES**

A considerable number of spatial arch bridges have already been built, but only a few of these have imposed curvature (see chapter III and Annex N1). Not much research has been done on spatial bridges so far, and even less on ID-ABWIC (Jorquera 2007). Therefore, there are hardly any references available.

The first spatial arch bridge to be built was Ziggenbach Bridge (1924, Figure 2-1a). It is a planar vertical arch with a curved superior deck (Billington 1979, Laffranchi and Marti 1997). The first bridge with an arch curved in plan was the Bohlbach Bridge (1932, Figure 2-1b) and the first bridge with imposed curvature was the Schwandwach Bridge (1933, Figure 2-1c). All these three bridges are deck-stiffened arch bridges designed by Robert Maillart in Switzerland (Billington 1979, Laffranchi and Marti 1997).



**Figure 2-1:** (a) Ziggenbach bridge (*Source: Yoshito Isono 1998. Reproduced by kind permission of Structurae (publisher)*); (b) Bohlbach Bridge; (c) Schwandwach Bridge (*Reproduced by kind permission of the author A. Ruiz-Teran*)

Bridge design did not revert to the first Maillart’s arch bridge with imposed curvature until Manterola used this typology in the Endarlatsa Bridge and the Contreras Bridge, and reconfigured it with inferior deck (ID-ABWIC) and a double hanger system in the bridge over the Galindo River in Bilbao (Figure 2-2; Manterola et al, 2009, 2011).



**Figure 2-2:** Bridge over Galindo river in Bilbao

This bridge type is subjected to large bending moments and torsions and the axial forces are smaller than expected. The higher the plan curvature, the stronger this effect. For a given arch vertical rise, the larger the curvature in plan, the larger the arch inclination, reducing the arch behaviour and enhancing the ‘balcony-

#### IV. STRUCTURAL BEHAVIOUR OF INFERIOR-DECK SPATIAL ARCH BRIDGES WITH IMPOSED CURVATURE

beam' behaviour (ie: out of plane behaviour of the arch, equivalent to a curved in plan beam with fixed supports loaded perpendicularly). The arch behaviour improves when employing mechanisms that increase the horizontal stiffness of the system (Laffranchi and Marti 1997, Jorquera 2007 and 2009, Manterola et al 2009). Until now, this effect has been justified by the presence of coupled horizontal forces (Jorquera 2007, Manterola et al 2009). According to these authors, a horizontal force outwards the plan curve is induced. This causes tension stresses that compensate part of the compression, diminishing the axial force in the arch. However, the different arch geometrical possibilities and the influence on the structural behaviour of the axial, flexural and torsional rigidities of the individual structural members have not been studied yet. In addition, both the appearance of these coupled horizontal forces and the bridge behaviour was not completely explained. Therefore, a deeper and wider research is required in order to establish efficient configurations and appropriate design criteria.

This paper focuses on ID-ABWIC and intends to:

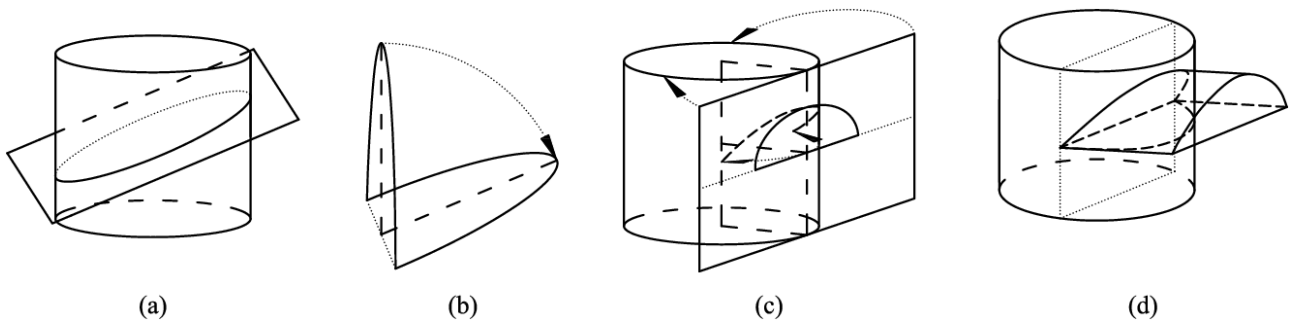
- Define possible geometries for imposed curvature arch bridges.
- Study if non-planar geometries can be approximated by equivalent arches contained in an inclined plane.
- Establish which geometrical and mechanical variables influence the structural behaviour of these arch bridges.
- Find out which is the best way to control the arch behaviour, either with rigid arches or a rigid hanger-deck system.
- Establish whether it is possible to define an anti-funicular configuration.

Therefore, the main original contributions of the present study with respect to the published literature are the following:

- Spatial arch bridges, using many different geometrical definitions, which have not been studied in the literature before, are defined, analyzed and compared.
- Clear conceptual models employing rigid hangers are theoretically and analytically described.
- Formulae for a simple analytical model with a single flexible hanger are derived. In addition, interesting conclusions have been drawn from the analysis of these formulae.
- The arch-deck interaction is enhanced by employing rigid hangers. The influence of the rigidities of the hangers, the deck and the arch is parametrically studied. The influence in the structural response of the connection type between the hangers and both the arch and the deck is also fully investigated (annex N2.1), and interesting and useful conclusions are drawn.

### 3. GEOMETRICAL DEFINITION OF INFERIOR-DECK ARCH BRIDGES WITH IMPOSED CURVATURE (ID-ABWIC)

Depending on how the arch for an ID-ABWIC is defined, it might be contained in a plane or not.



**Figure 3-1: Definition of (a) an elliptical planar arch bridge, (b) a parabolic planar arch bridge, (c) a bent parabolic arch bridge, (d) a cross vault ribbed arch bridge**

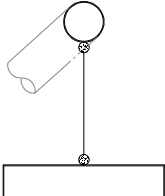
There are different ways of defining these arches, such as:

- *Elliptical planar arch bridges (Figure 3-1a)*: This planar arch bridge type arises when a vertical cylinder containing the deck center line is intersected by a plane.
- *Parabolic planar arch bridges (Figure 3-1b)*: This planar arch bridge type is obtained by rotating a parabolic vertical arch around the axis that joins its springings. The deck center line is obtained by projecting the rotated parabola. In such a case the arch would be imposing the plan alignment and not the opposite, which is the most usual case. Therefore, we have not included this geometrical case in our study, but the elliptical one as representative of a planar arch.
- *Bent parabolic arch bridges (Figure 3-1c)*: This type of arch bridge arises when a planar and vertical parabolic-shaped arch is bent or folded over a vertical cylinder that contains the deck center line. The bridge over the Galindo River (J. Manterola et al, 2011) is classified in this category. Using a parabolic-shape seems quite logical since this is the anti-funicular shape for a uniform distributed loading. However, this cannot be so easily stated once the parabola is bent, since the new curve is not planar anymore. This is the geometrical definition employed in all the studies presented in this article.
- *Cross vault ribbed arch bridges (Figure 3-1d)*: This type of bridge arises when a vertical cylinder containing the deck is intersected by a horizontal cylinder. The intersection is a non-planar shape unless both cylinders have the same diameter and coincident axes.
- Given a plan alignment for the deck, in a similar way as the example above, a non-planar arch with imposed curvature may be obtained by the intersection of a vertical cylinder containing the deck axis and a three-dimensional body, such as an ellipsoid, elliptic paraboloid, hyperbolic paraboloid, hyperboloid, cone or torus.

An initial parametric study ( $L=100\text{m}$ ,  $f=20\text{m}$  and  $g$  varying from 2 to 20m) to determine whether non-planar geometries can be approximated by an equivalent one contained in an inclined plane has been performed. This study is based on the comparison of the behaviour of the FE frame models of (1) an elliptical planar arch bridge, (2) a bent parabolic arch bridge, and (3) a cross vault ribbed arch bridge. The arch has a circular hollow section (CHS), with  $D=1000\text{mm}$  and  $t=30\text{mm}$ , the deck is a box girder  $4000\times 800\text{mm}$  and  $t=15\text{mm}$ , and the hangers are flexible stay cables (Table 3-1).

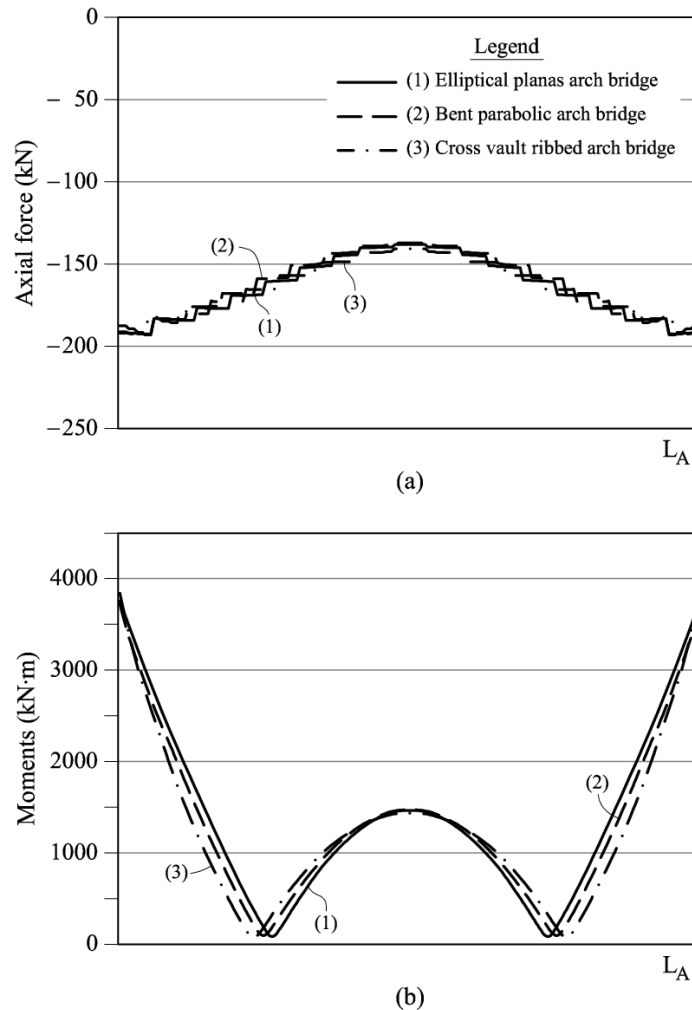
A brief geometrical study of arches is also conducted in Annex N2.1.

IV. STRUCTURAL BEHAVIOUR OF INFERIOR-DECK SPATIAL ARCH BRIDGES WITH IMPOSED CURVATURE

ARCH	CHS $D=1000mm$ ; $t=30mm$
DECK	BOX GIRDER $4000x800mm$ ; $t=15mm$
HANGERS	Flexible hangers: stay cables
HANGER JOINTS	Pinned
SYMBOL	

**Table 3-1: Cross-section values employed for the comparison of the behaviour of different arch geometry definitions for superior arch bridges with imposed curvature**

Non-planar arches with imposed curvature can be approximated by planar arches with imposed curvature, and identical rises, with differences in internal forces and displacements smaller than 1,75% for uniform distributed loading (Figure 3-2).

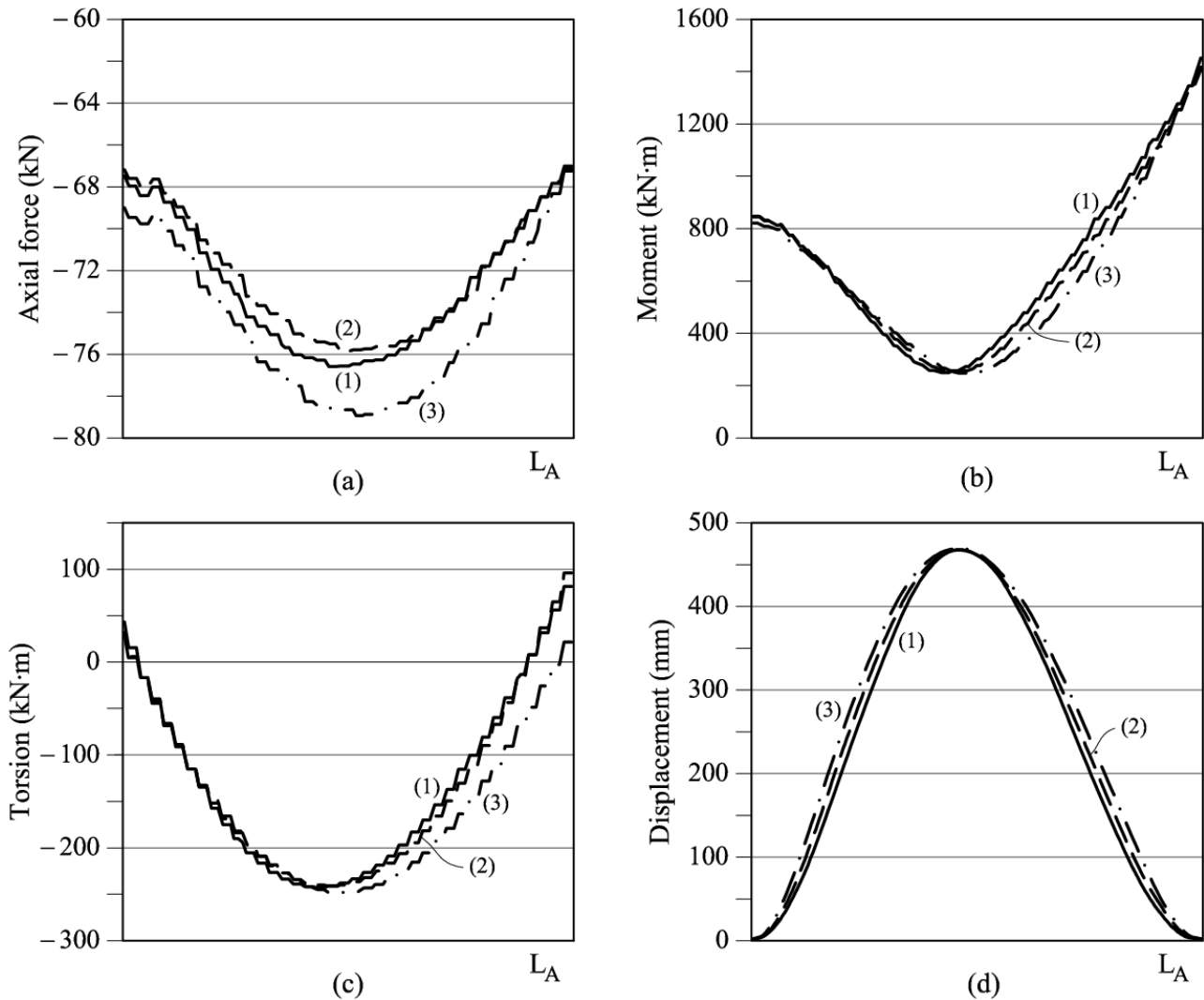


**Figure 3-2: Comparison of internal forces in the arch under uniform loading on the deck for different geometrical definition of the arch (a) Axial forces (b) Total bending moments**

Under asymmetrical loading, although the situation of the maximal point varies a bit when the arch is not

#### IV. STRUCTURAL BEHAVIOUR OF INFERIOR-DECK SPATIAL ARCH BRIDGES WITH IMPOSED CURVATURE

contained in a plane, this maximal value is the same or with a variation not superior to 2% for internal forces and displacements (Figure 3-3).



**Figure 3-3: Comparison of internal forces and displacements on the arch under asymmetrical loading on the deck for different geometrical definition of the arch (a) Axial forces (b) Total moment (c) Torsion (d) Total displacements**

Therefore, non-planar arches with imposed curvature can be approximated with negligible errors by inclined planar arches with imposed curvature with the same rise for  $g/f \leq 1$ . The larger the  $g/f$  ratio, the larger the errors.

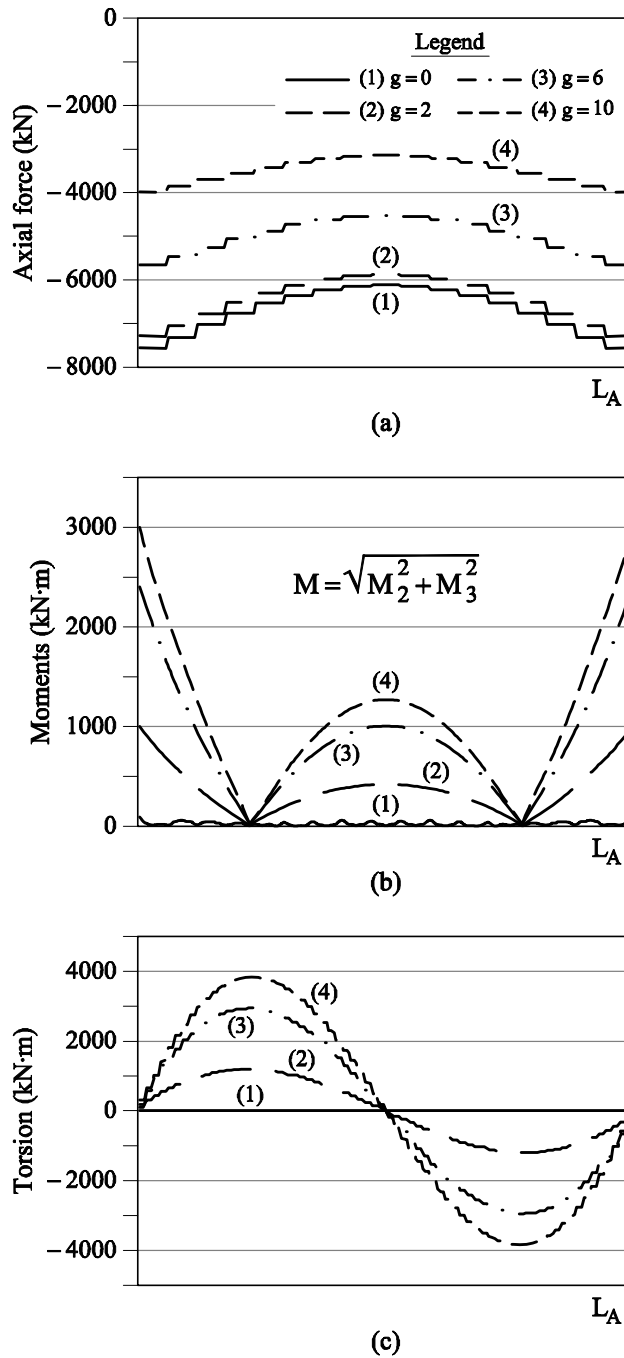
This conclusion is very powerful, allowing us to refer to in-plane and out-of-plane behaviour even for non-planar arches, when using symmetrical (with respect to the approximated arch plane) cross-sections, ie: loads can be projected into two orthogonal axes (one of them contained in the approximated arch plane).

### 4. STRUCTURAL BEHAVIOUR OF IDABWIC

#### 4.1 Understanding the effect of increasing the horizontal sag

The structural response of an arch bridge with imposed curvature,  $L=100\text{m}$ ,  $f=20\text{m}$ , and  $g$  varying from 0 to 10m is compared with a conventional vertical ( $g=0$ ) arch bridge having identical rise and span length. The comparison provides a first appropriate approach to this research. The mechanical properties are identical to those in the previous study (Table 3-1).

The results are displayed in Figure 4-1.



**Figure 4-1: Arch internal forces comparison for different deck curvatures (measured as g) (a) Arch axial forces (b) Arch total bending moments (c) Arch torsional moments**

For a given vertical rise, the analysis shows that a higher arch plan curvature leads to:

#### IV. STRUCTURAL BEHAVIOUR OF INFERIOR-DECK SPATIAL ARCH BRIDGES WITH IMPOSED CURVATURE

- smaller axial forces in the arch (see Figure 4-1(a))
- larger total bending moments in the arch (both in-plane and out of plane bending moments increase) (see Figure 4-1(b))
- larger in-plane and out of plane shear forces in the arch
- larger torsional moments in the arch (see Figure 4-1(c))

This had been observed also by Jorquera (2007).

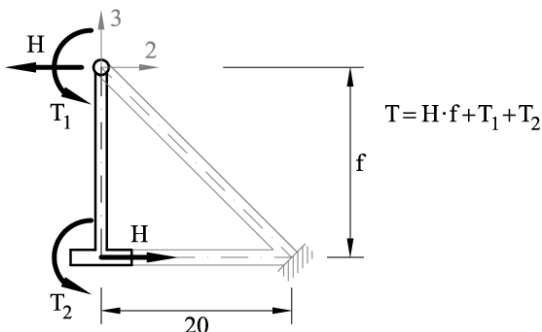
When the plan curvature is increased, the plane of the arch inclines. This causes the described changes in the internal forces of the arch, because the ‘arch behaviour’ in the plane of the arch decreases and the ‘balcony-beam behaviour’ of the arch is enhanced.

For these same studied cases it has been proved that the buckling critical load is higher when increasing  $g$ , since the axial forces are lower (chapter VI).

## 4.2 General scope

### Conceptual models

When employing rigid hangers (both in the longitudinal and transverse direction), fixed to both the arch and deck, in a first approach, the system may be considered a curved Vierendel truss, as it can be inferred from Manterola et al (2009). The larger the stiffness of the hangers, the higher the arch-deck interaction, and the higher the axial force in the deck (due to the fact that the abutments are fixed). Therefore, the axial force in the deck is a way to measure arch-deck interaction.



**Figure 4-2: Simplified conceptual model of the behaviour of an arch bridge with imposed curvature and rigid hangers (equivalent to a Vierendel curved truss cross-section)**

The structural response of this balcony beam under a vertical load leads to both bending and torsional moments. The resultant response torque will be resisted by the sum of St Venant torsion at both the arch and the deck (**Figure 4-2**,  $T_1$  and  $T_2$  respectively) and warping torsion (**Figure 4-2**,  $H \cdot f$ ). The distribution between the two torsion types depends on both the transverse flexural rigidity ( $I_{3-3}$ ) and the torsional rigidity ( $J_1$ ) of the arch, and on the transverse flexural rigidity and torsional rigidity of the deck ( $J_2$ ).

Horizontal forces,  $H$ , produce tension forces in the arch (in addition to the aforementioned compression in the deck), diminishing the axial compression in the arch. These  $H$  forces increase the out-of-plane forces in the arch too. Therefore, it is of interest to reduce them. To do so, we need to decrease the warping torsion. By increasing the torsional stiffness of the deck (high  $J_2$ ) and an arch with a low  $J_1$  and  $I_{3-3}$ , torques will be mainly resisted by the deck's St Venant torsional component. Therefore,  $H$  will tend to zero and no tensions will be introduced on the arch.

On the other hand, employing low  $J_1$  and  $J_2$  values, leads to  $T_1 \approx 0$ ;  $T_2 \approx 0$  and  $T = H \cdot f$ . Consequently, the axial compression forces in the arch diminish greatly.

This behaviour can be intuitively deduced, but the real behaviour is too complex to develop a simple analytical model. Consequently, we will study these cases with a FE analysis of full bridges.

#### IV. STRUCTURAL BEHAVIOUR OF INFERIOR-DECK SPATIAL ARCH BRIDGES WITH IMPOSED CURVATURE

This is analysed in detail in section 4.3.1.1.

If flexible or pinned hangers are employed, the curved Vierendel truss analogy is no longer possible. The system behaves like two balcony beams vertically connected by the hangers.

A simple analytical model of a single pinned hanger (Figure 4-3 and annex N2.2) of a bridge with an arch inclined an angle  $\alpha$  with respect to the hanger has been studied. The model has three springs:  $K_1$ , for the in-plane stiffness of the inclined arch;  $K_2$ , for the balcony-beam stiffness of the arch and  $K_3$ , for the balcony-beam stiffness of the deck.

The axial stiffness of the hanger is  $K_H = EA_H/L_H$ . The model leads to the following equations:

$$F_1 = \frac{Q}{\frac{1}{\cos\alpha} \cdot \left(1 + \frac{K_3}{K_2} \sin^2\alpha + \frac{K_3}{K_1} \cos^2\alpha + \frac{K_3}{K_H}\right)}$$

**Eq. 1: In-plane force acting on the arch**

$$F_2 = \frac{Q}{\frac{1}{\sin\alpha} \cdot \left(1 + \frac{K_3}{K_2} \sin^2\alpha + \frac{K_3}{K_1} \cos^2\alpha + \frac{K_3}{K_H}\right)}$$

**Eq. 2: Out-of-plane force acting on the arch**

$$F_3 = Q \cdot \left(1 - \frac{1}{1 + \frac{K_3}{K_2} \sin^2\alpha + \frac{K_3}{K_1} \cos^2\alpha + \frac{K_3}{K_H}}\right)$$

**Eq. 3: Vertical force acting on the deck**

$$F_H = \frac{Q}{1 + \frac{K_3}{K_2} \sin^2\alpha + \frac{K_3}{K_1} \cos^2\alpha + \frac{K_3}{K_H}}$$

**Eq. 4: Axial force in the hanger**

$$\delta_A = \frac{F_2}{K_2} \cdot \sin\alpha + \frac{F_1}{K_1} \cdot \cos\alpha = \frac{Q \cdot (K_1 \cdot \sin^2\alpha + K_2 \cdot \cos^2\alpha)}{\left(K_1 \cdot K_2 + K_1 \cdot K_3 \cdot \sin^2\alpha + K_2 \cdot K_3 \cdot \cos^2\alpha + \frac{K_1 \cdot K_2 \cdot K_3}{K_H}\right)}$$

**Eq. 5: Vertical deflection of the arch**



IV. STRUCTURAL BEHAVIOUR OF INFERIOR-DECK SPATIAL ARCH BRIDGES WITH IMPOSED CURVATURE

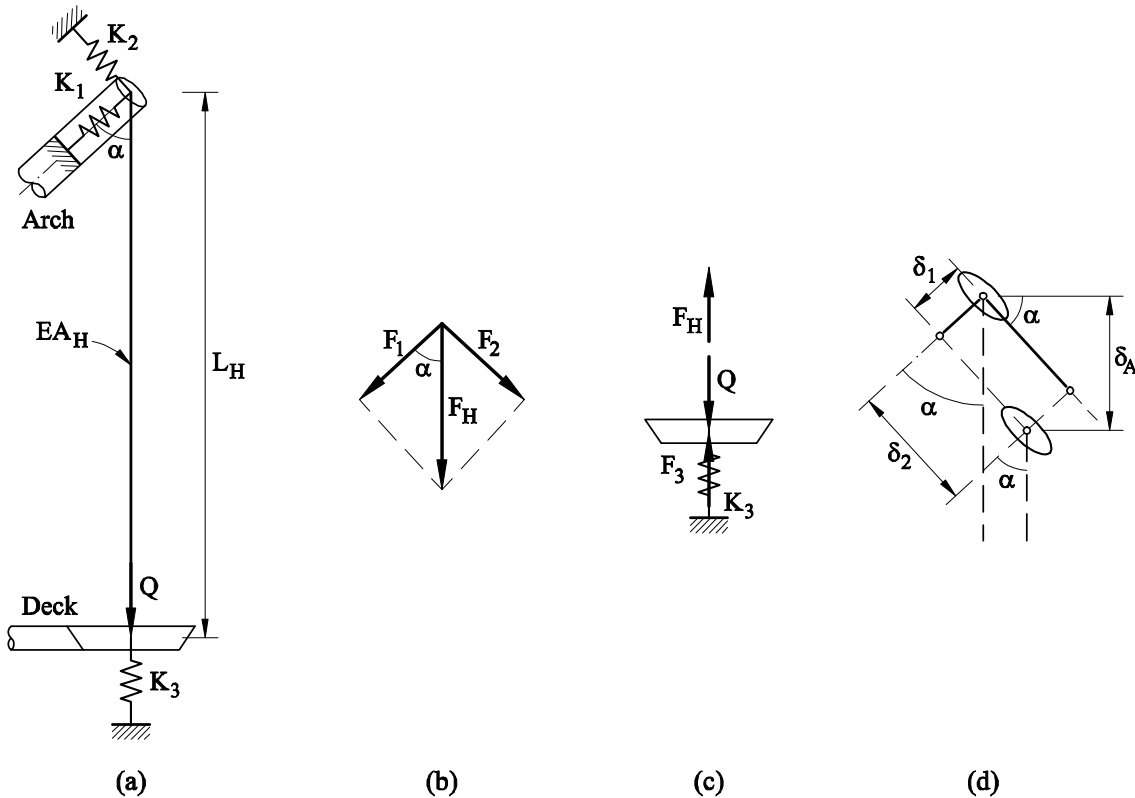


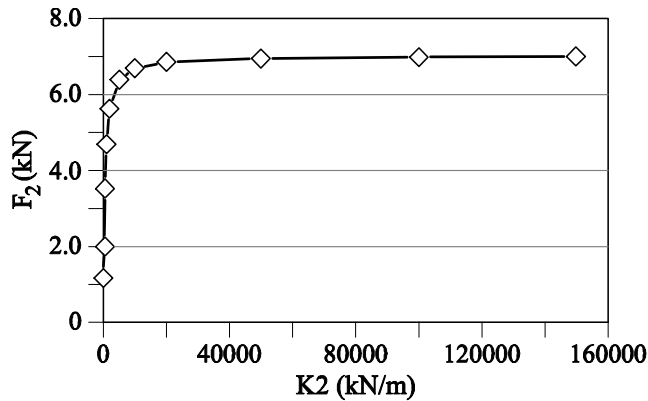
Figure 4-3: (a) Simplified model of a pinned hanger with springs modelling the stiffness of the arch (in its plane and out of it) and deck, submitted to a 10kN load (b) Reactions at arch (c) Reactions at deck and hangers (d) Arch deflection

Despite the simplicity of this analytical model, the conclusions that can be inferred from these equations are very useful, and they have served as a guide when addressing the complex FE models of the full bridge. Moreover, they have been confirmed by those complex FE models. The most relevant ones are the following:

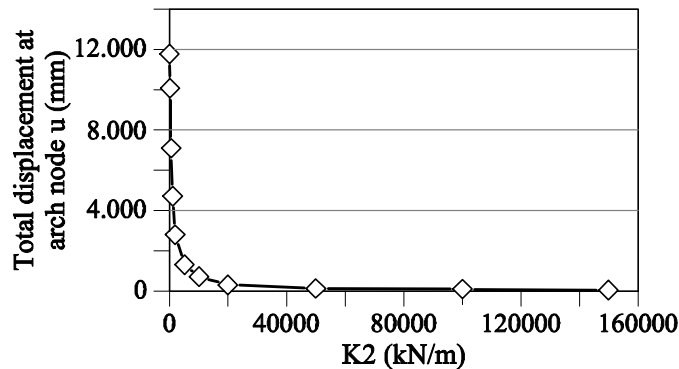
- The reaction to a vertical deck load in the directions associated to  $K_1$  and  $K_2$  with different stiffness ( $F_1$  and  $F_2$ ) only depends on the total equivalent stiffness, and is then projected in the different directions (Eq. 1 and Eq. 2).
- If  $F_2$  is represented as a function of the balcony beam stiffness of the arch ( $K_2$ ), for given values of  $\alpha$ ,  $K_3$ ,  $K_1$  and  $K_H$  (Figure 4-4), there is a bound for the balcony beam stiffness of the arch ( $K_2$ ) from which the contribution to the resistance of the arch ( $F_2$ ) does not increase. From this bound, the deflections of the arch ( $\delta_A$ ) do not decrease either (Figure 4-5).
- Increasing  $K_2$  enhances both the arch ( $F_1$ ) and the balcony beam ( $F_2$ ) mechanisms. Therefore, the arch behaviour can be enhanced, but a non-desirable balcony beam behaviour simultaneously occurs. On the opposite, if we reduce the balcony beam behaviour in the arch, we are simultaneously losing the benefits of the arch mechanism, the deflections increase and the deck balcony beam mechanism ( $F_3$ ) is enhanced.
- Obtaining an antifunicular arch, by modifying the stiffness of the different elements of the system, is impossible because  $F_2=0$  (no balcony-beam forces in the arch) implies  $F_1=0$  (no arch behaviour). Therefore, if we want to eliminate the bending moments we need to work with the hanger-arch and hanger-deck joint connections or to employ an additional external system (such as the stay cables in Galindo Bridge, Figure 2-2) which prevents out-of-plane displacements in the arch.

#### IV. STRUCTURAL BEHAVIOUR OF INFERIOR-DECK SPATIAL ARCH BRIDGES WITH IMPOSED CURVATURE

- The loads taken by the arch ( $F_1$  and  $F_2$ , see Eq. 1 and Eq. 2) will increase with increases of  $K_1$ ,  $K_2$  or  $K_H$  or with decreases of  $\alpha$  or  $K_3$ , but controlling certain parameters ( $K_3$ ) is more effective than others.



**Figure 4-4: Reaction at the superior node (representing the arch on a simplified model of a pinned rigid hanger with springs and  $\alpha=45^\circ$ ) function of the arch balcony beam stiffness ( $K_2$ ). The deck stiffness ( $K_3$ ) and the arch planar stiffness ( $K_1$ ) are constant.**



**Figure 4-5: Total displacements of the superior node (representing the arch on a simplified model of a pinned rigid hanger with springs and  $\alpha=45^\circ$ ) function of the arch balcony beam stiffness ( $K_2$ ). Deck stiffness  $K_3$  and arch planar stiffness  $K_1$  are constant.**

- The non-dimensional term  $(K_3/K_1) \cdot \cos^2 \alpha$  is much smaller than the rest, since the axial stiffness of the arch is significantly larger than the balcony beam stiffness of the arch. Therefore, the forces will not change significantly with variations of  $K_1$ , ie: the area of the arch is not a significant variable, although a closed area will be advisable because of torsional bending moments.

However, the higher the hangers' stiffness ( $K_H$ ) or the balcony beam stiffness of the arch ( $K_2$ ), the higher the influence of the axial stiffness of the arch ( $K_1$ ) on the balcony beam forces on the arch.

The higher the deck stiffness ( $K_3$ ), the axial stiffness of the arch ( $K_1$ ) or the curvature (measured as  $\alpha$ ), the lower the influence of the axial stiffness of the arch ( $K_1$ ) on the balcony beam forces on the arch. The  $K_1$ - $F_2$  relationship is of the type shown on Figure 4-6.

Given a high enough axial stiffness of the arch, the axial stiffness does not influence the balcony beam forces or displacements of the arch.

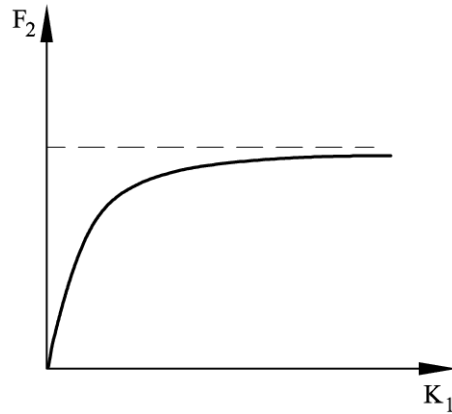


Figure 4-6: K1-F2 relationship

- It is interesting to employ a very rigid deck and flexible arch and hangers, in order to diminish the balcony beam force on the arch ( $F_2$ ). At the same time, this will diminish the arch axial force ( $F_1$ ) too, losing the arch behaviour effect (Eq. 4-2). Accordingly, in order to diminish the arch displacements, the most efficient way when employing pinned hangers according to this simple analysis is to increase the stiffness of the deck.
- If the force on deck ( $F_D$ ) is very important, it will be interesting to increase the hanger stiffness ( $K_H$ , see Eq. 3 and Eq. 4).

If we employ very rigid hangers and the curvature in plan is important, the forces taken by the arch mainly depend on its balcony beam stiffness and the stiffness of the deck:

$$\text{If } \begin{cases} K_1 \gg K_2 \\ K_H \gg K_3 \\ \alpha \gg 45^\circ \end{cases} \rightarrow \begin{cases} F_1 = \frac{Q \cdot \cos\alpha}{\left(1 + \frac{K_3}{K_2} \sin^2\alpha\right)} \\ F_2 = \frac{Q \cdot \sin\alpha}{\left(1 + \frac{K_3}{K_2} \sin^2\alpha\right)} \end{cases}$$

- For very rigid decks, it might be so that:  $\frac{\partial \delta_2}{\partial K_2} > 0$ . However, in general we can consider the  $K_2$ - $\delta_2$  relationship to be as shown on Figure 4-7.

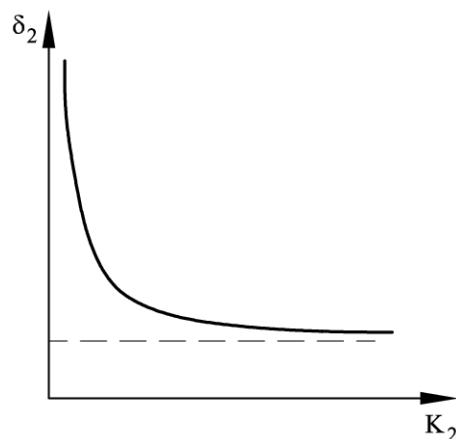


Figure 4-7: K2- $\delta_2$  relationship

- The derivative of  $\delta_2$  with respect to  $K_2$  is as follows:

$$\frac{\partial \delta_2}{\partial K_2} = \frac{Q \cdot \sin \alpha \cdot \left[ K_3 - K_2 \cdot \left( 1 + \frac{K_3}{K_2} \cdot \sin^2 \alpha + \frac{K_3}{K_1} \cos^2 \alpha + \frac{K_3}{K_H} \right) \right]}{K_2^3 \cdot \left( 1 + \frac{K_3}{K_2} \cdot \sin^2 \alpha + \frac{K_3}{K_1} \cos^2 \alpha + \frac{K_3}{K_H} \right)^2}$$

Eq. 6: Derivative of  $\delta_2$  with respect to  $K_2$

The higher the stiffness of the arch (both  $K_1$  and  $K_2$ ), the stiffness of the deck ( $K_3$ ) or the stiffness of the hangers ( $K_H$ ), the lower the influence of  $K_2$  on displacements (Eq. 6). This will be also observed in full bridge models with fixed hangers in section 4.3.1.1.

We can use fictional bearings to model a system which is infinitely stiff in a particular direction (that in which the displacements are restrained). This could be caused by either an infinitely large rigidity of the hanger-deck system or a second set of stay cables fixing the arch, as mentioned before. If there are bearings, the axial force on the arch depends on the component in the arch plane of the transmitted load projected in the direction in which the bearing prevents displacements (the studied case shown on Figure 4-8(c) is for the horizontal direction).

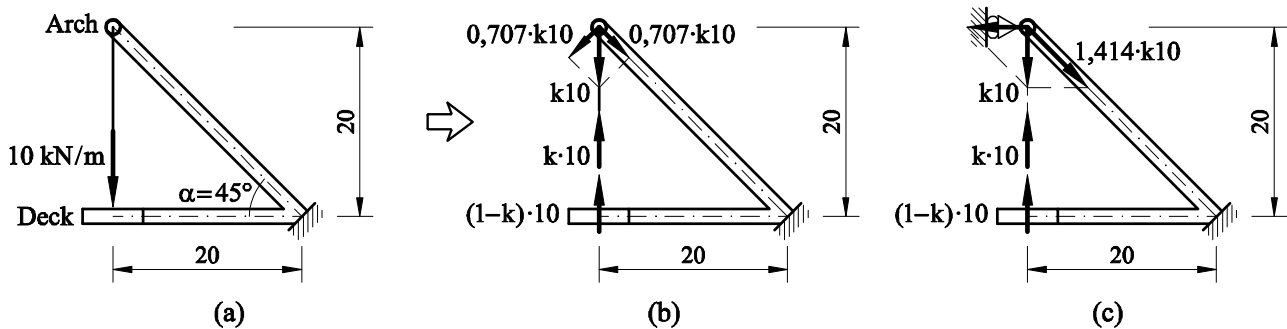


Figure 4-8: Simplified conceptual model of the behaviour of an imposed curvature bridge with flexible hangers for the particular case  $g=f$

The horizontal reactions on the bearings compensate the curved balcony beam behaviour and increase the arch in-plane component. This enhances the arch behaviour, resisting the deck loads mainly as an arch, in spite of being inclined. However, axial forces will also increase in comparison with a vertical planar arch.

In reality, the systems will not be as simple as these three models described here, since (1) the distribution of internal forces depends on the arch and deck individual behaviour (2) the hangers have different lengths and stiffness along the bridge and therefore transmit different axial forces, and (3) there will be no fixed bearings but elastic ones, function of the transverse rigidity of the system, that is different along the bridge (therefore, a single  $k$  (Figure 4-8) does not exist).

### 4.3 Frame FE models of IDABWIC with rigid hangers

We have done linear parametric analyses with a frame FE model of the whole arch bridge with  $L=100\text{m}$ ;  $f=20\text{m}$  and  $g=20\text{m}$ . The parameters studied are the rigidities of the deck, the arch and the hangers, and the connection types between the hangers and both the arch and the deck. The arch is fixed to the deck, which is itself fixed to the abutments.

#### 4.3.1 Study of the connections of rigid hangers with the arch and the deck

The possibilities of the connection between rigid hangers and arch and deck have been studied (Annex N2.1). On the following paragraphs the main results of this study are presented.

IV. STRUCTURAL BEHAVIOUR OF INFERIOR-DECK SPATIAL ARCH BRIDGES WITH IMPOSED CURVATURE

Fixed hangers transmit vertical loads, shear forces and bending moments to arch and deck. The value of the 6 internal forces they can transmit changes when releasing one of them.

The change of the bending moments transmitted by the hangers when they are either fixed or released, does not transmit axial forces neither to the arch nor the deck. What causes the variation of the axial forces is the change of the shear forces in the hanger.

Positive  $V_{3-3}$  values tension the deck and compress the arch and the opposite happens with  $V_{2-2}$  positive values (Figure 4-9).

Negative transverse shear forces values ( $V_{2-2}$ ) compensate out-of-plane bending moments ( $M_{2-2}$ ) and positive ones in-plane bending moments ( $M_{3-3}$ ).

The most interesting is to diminish out-of-plane bending moments and increase axial forces, to enhance the arch behaviour. Therefore, we will be interested in configurations of the hangers' connections which introduce negative  $V_{2-2}$ .

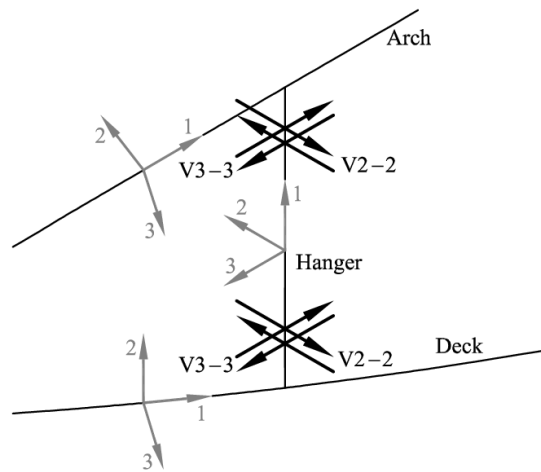


Figure 4-9: Positive shear forces in the hangers and their transmission to the arch and the deck

The definition of the bending moments in arch is the following:

- $M_{3-3}$  are in plane bending moments
- $M_{2-2}$  are out of plane bending moments

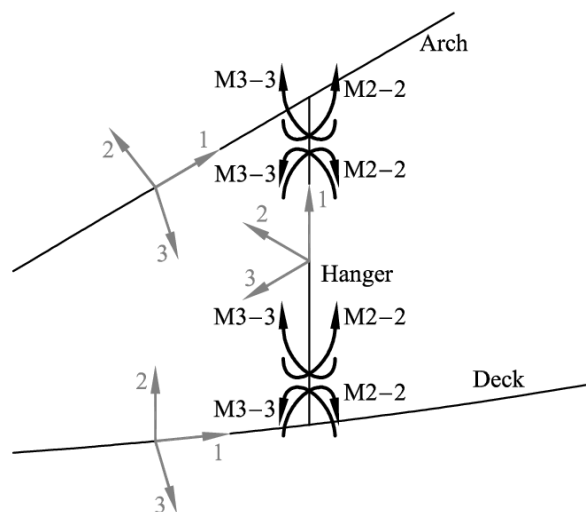


Figure 4-10: Positive bending moments in hangers and their transmission to the arch and the deck

#### IV. STRUCTURAL BEHAVIOUR OF INFERIOR-DECK SPATIAL ARCH BRIDGES WITH IMPOSED CURVATURE

According to the axis system in Figure 4-10:

- A positive  $M_{3-3}$  in a hanger causes a positive torsion in the arch and a negative one in the deck.
- A positive  $M_{2-2}$  in a hanger causes a positive  $M_{3-3}$  in the arch and a negative one in the deck.

It is interesting to introduce negative torques in the arch, to reduce in-plane bending moments ( $M_{3-3}$ ) and out-of-plane bending moments ( $M_{2-2}$ ) at the springings and positive torques to reduce  $M_{2-2}$  and  $M_{3-3}$  at the mid-span. According to this, it is favourable for the arch to have positive  $M_{3-3}$  in the hangers at the mid-span and negative ones at the springings.

Longitudinal bending moments transmitted by the hangers produce tension axial forces in the arch and compressions in the deck due to the change of shear forces (see Annex N2.1). This effect is particularly enhanced at the short extreme hangers, which have a higher stiffness, due to their smaller length.

When  $M_{2-2}$  is released at both ends of the hangers,  $V_{2-2}$  negative shear forces values increase, especially at the extreme stiffer (due to their shorter length) hangers. This increases axial tensions in the deck and compressions in the arch. Shear forces transmitted by hangers increase, tensioning the deck and compressing the arch. Longitudinal bending and torsions are diminished through the transmission of transverse bending moments.

Therefore, for every model, whatever the mechanical properties of the sections employed for deck and hangers, releasing  $M_{2-2}$  gives the maximal axial forces in the arch. However, when analysing the bending moments, we can observe that eliminating the longitudinal hanger/deck interaction is not the best solution to minimize them. This means that axial forces increase, but not because we are enhancing the antifunicular behaviour, but because we are increasing the horizontal rigidity of the system and, therefore, increasing the horizontal forces in the arch, which cause a decrease in the balcony beam forces, but lead also to an increase in the forces in the arch plane.

When employing what can be considered a deck with infinite torsional rigidity, the type of behaviour is divided into two big groups:  $M_{3-3}$  fixed and  $M_{3-3}$  released at the hanger/deck connection.

When  $M_{3-3}$  is fixed at the hanger/deck connection, the whole arch is under compression and the deck is tensioned. When released, the axial forces diminish and the behaviour at the abutments and springings changes completely. The arch is slightly tensioned at the springings.

As stated, the cases of fixed hangers or  $M_{3-3}$  released at hanger/arch joints give good results for decks with a large torsional stiffness. However, these configurations cause tensions when employing a deck with a small torsional stiffness.

IV. STRUCTURAL BEHAVIOUR OF INFERIOR-DECK SPATIAL ARCH BRIDGES WITH IMPOSED CURVATURE

Structural behaviour under a vertical uniform distributed loading applied on the whole deck

**4.3.1.1 Analogy with a curved Vierendel truss**

Six models with very rigid circular hangers and different cross-sections of arch and deck have been defined in order to prove the intuitive conceptual model described in section 4.2. The hangers have a fixed connection with both the arch and the deck. The values employed for the cross-sections are described in Table 4-1.

LEGEND NUMBER	ARCH	DECK	HANGERS	HANGER JOINTS	SYMBOL
<b>Model (0.1)</b>	<i>Reference arch</i> CHS D=1m; t=30mm A= 0,0914m <sup>2</sup> J= 0,0215m <sup>4</sup> I <sub>2</sub> = 0,0108m <sup>4</sup> I <sub>3</sub> = 0,0108m <sup>4</sup>	<i>Reference deck</i> CHS D=1m; t=30mm A= 0,0914m <sup>2</sup> J= 0,0215m <sup>4</sup> I <sub>2</sub> = 0,0108m <sup>4</sup> I <sub>3</sub> = 0,0108m <sup>4</sup>	<i>Rigid hangers</i> CHS 800x800mm; t=25mm A= 0,0609m <sup>2</sup> J= 9,149·10 <sup>-3</sup> m <sup>4</sup> I <sub>2</sub> = 4,575·10 <sup>-3</sup> m <sup>4</sup> I <sub>3</sub> = 4,575·10 <sup>-3</sup> m <sup>4</sup>	No releases	
<b>Model (0.2)</b>	<i>Arch with large torsional stiffness</i> A= 0,0914m <sup>2</sup> <b>J= 10m<sup>4</sup></b> I <sub>2</sub> = 0,0108m <sup>4</sup> I <sub>3</sub> = 0,0108m <sup>4</sup>	<i>Reference deck</i> CHS D=1m; t=30mm A= 0,0914m <sup>2</sup> J= 0,0215m <sup>4</sup> I <sub>2</sub> = 0,0108m <sup>4</sup> I <sub>3</sub> = 0,0108m <sup>4</sup>	<i>Rigid hangers</i> CHS 800x800mm; t=25mm A= 0,0609m <sup>2</sup> J= 9,149·10 <sup>-3</sup> m <sup>4</sup> I <sub>2</sub> = 4,575·10 <sup>-3</sup> m <sup>4</sup> I <sub>3</sub> = 4,575·10 <sup>-3</sup> m <sup>4</sup>	No releases	
<b>Model (0.3)</b>	<i>Arch with large torsional and balcony-beam flexural stiffness</i> A= 0,0914m <sup>2</sup> <b>J= 10m<sup>4</sup></b> <b>I<sub>2</sub>= 1m<sup>4</sup></b> I <sub>3</sub> = 0,0108m <sup>4</sup>	<i>Reference deck</i> CHS D=1m; t=30mm A= 0,0914m <sup>2</sup> J= 0,0215m <sup>4</sup> I <sub>2</sub> = 0,0108m <sup>4</sup> I <sub>3</sub> = 0,0108m <sup>4</sup>	<i>Rigid hangers</i> CHS 800x800mm; t=25mm A= 0,0609m <sup>2</sup> J= 9,149·10 <sup>-3</sup> m <sup>4</sup> I <sub>2</sub> = 4,575·10 <sup>-3</sup> m <sup>4</sup> I <sub>3</sub> = 4,575·10 <sup>-3</sup> m <sup>4</sup>	No releases	
<b>Model (0.4)</b>	<i>Reference arch</i> CHS D=1m; t=30mm A= 0,0914m <sup>2</sup> J= 0,0215m <sup>4</sup> I <sub>2</sub> = 0,0108m <sup>4</sup> I <sub>3</sub> = 0,0108m <sup>4</sup>	<i>Deck with large torsional stiffness</i> A= 0,0914m <sup>2</sup> <b>J= 10m<sup>4</sup></b> I <sub>2</sub> = 0,0108m <sup>4</sup> I <sub>3</sub> = 0,0108m <sup>4</sup>	<i>Rigid hangers</i> CHS 800x800mm; t=25mm A= 0,0609m <sup>2</sup> J= 9,149·10 <sup>-3</sup> m <sup>4</sup> I <sub>2</sub> = 4,575·10 <sup>-3</sup> m <sup>4</sup> I <sub>3</sub> = 4,575·10 <sup>-3</sup> m <sup>4</sup>	No releases	
<b>Model (0.5)</b>	<i>Reference arch</i> CHS D=1m; t=30mm A= 0,0914m <sup>2</sup> J= 0,0215m <sup>4</sup> I <sub>2</sub> = 0,0108m <sup>4</sup> I <sub>3</sub> = 0,0108m <sup>4</sup>	<i>Deck with large torsional and horizontal flexural stiffness</i> A= 0,0914m <sup>2</sup> <b>J= 10m<sup>4</sup></b> <b>I<sub>2</sub>= 1m<sup>4</sup></b> I <sub>3</sub> = 0,0108m <sup>4</sup>	<i>Rigid hangers</i> CHS 800x800mm; t=25mm A= 0,0609m <sup>2</sup> J= 9,149·10 <sup>-3</sup> m <sup>4</sup> I <sub>2</sub> = 4,575·10 <sup>-3</sup> m <sup>4</sup> I <sub>3</sub> = 4,575·10 <sup>-3</sup> m <sup>4</sup>	No releases	
<b>Model (0.6)</b>	<i>Reference arch</i> CHS D=1m; t=30mm A= 0,0914m <sup>2</sup> J= 0,0215m <sup>4</sup> I <sub>2</sub> = 0,0108m <sup>4</sup> I <sub>3</sub> = 0,0108m <sup>4</sup>	<i>Deck with large torsional and balcony-beam flexural stiffness</i> A= 0,0914m <sup>2</sup> <b>J= 10m<sup>4</sup></b> I <sub>2</sub> = 0,0108m <sup>4</sup> <b>I<sub>3</sub>= 1m<sup>4</sup></b>	<i>Rigid hangers</i> CHS 800x800mm; t=25mm A= 0,0609m <sup>2</sup> J= 9,149·10 <sup>-3</sup> m <sup>4</sup> I <sub>2</sub> = 4,575·10 <sup>-3</sup> m <sup>4</sup> I <sub>3</sub> = 4,575·10 <sup>-3</sup> m <sup>4</sup>	No releases	

**Table 4-1: Mechanical properties' values of the cross-sections employed on the study of the analogy of an IDABWIC with a curved Vierendel truss**

The axial forces results in arch and deck (Figure 4-11 and Figure 4-12) prove that H forces (Figure 4-2) are highest for the (0.1) model, as it had been theoretically described in section 4.2. Large H values cause tensions in the arch (Figure 4-11) and the highest compressions in the deck (Figure 4-12).

Increasing the balcony-beam flexural stiffness of either the deck or the arch leads to more uniform axial forces on both of them (models (0.3) and (0.6)). In these models axial forces in the deck decrease greatly due

IV. STRUCTURAL BEHAVIOUR OF INFERIOR-DECK SPATIAL ARCH BRIDGES WITH IMPOSED CURVATURE

to the decrease in H forces. Both torsional and balcony-beam flexural stiffness play an important role due to the coupling of torsional and balcony-beam bending moments.

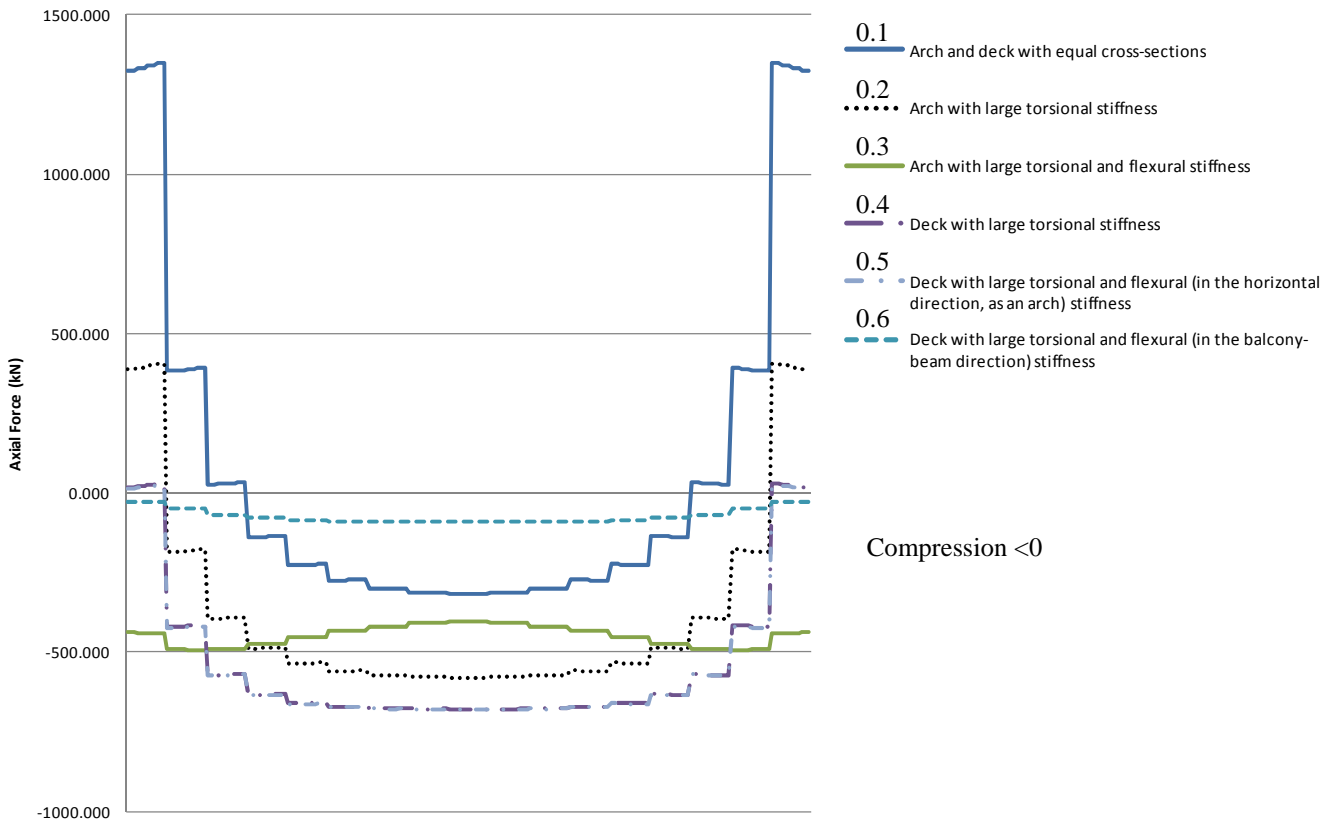
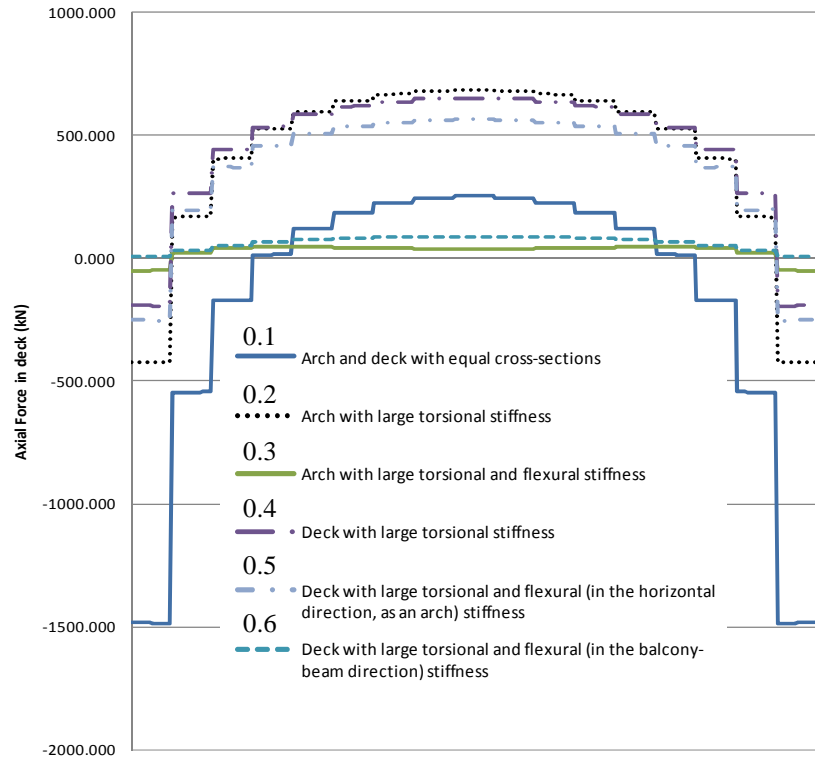


Figure 4-11: Arch axial forces comparison for different arch and deck sections in inferior deck arch bridges with 20m (L/5) rise. The abscissas are the arch length from 0 to  $L_A$  and the ordinates axial forces (kN)

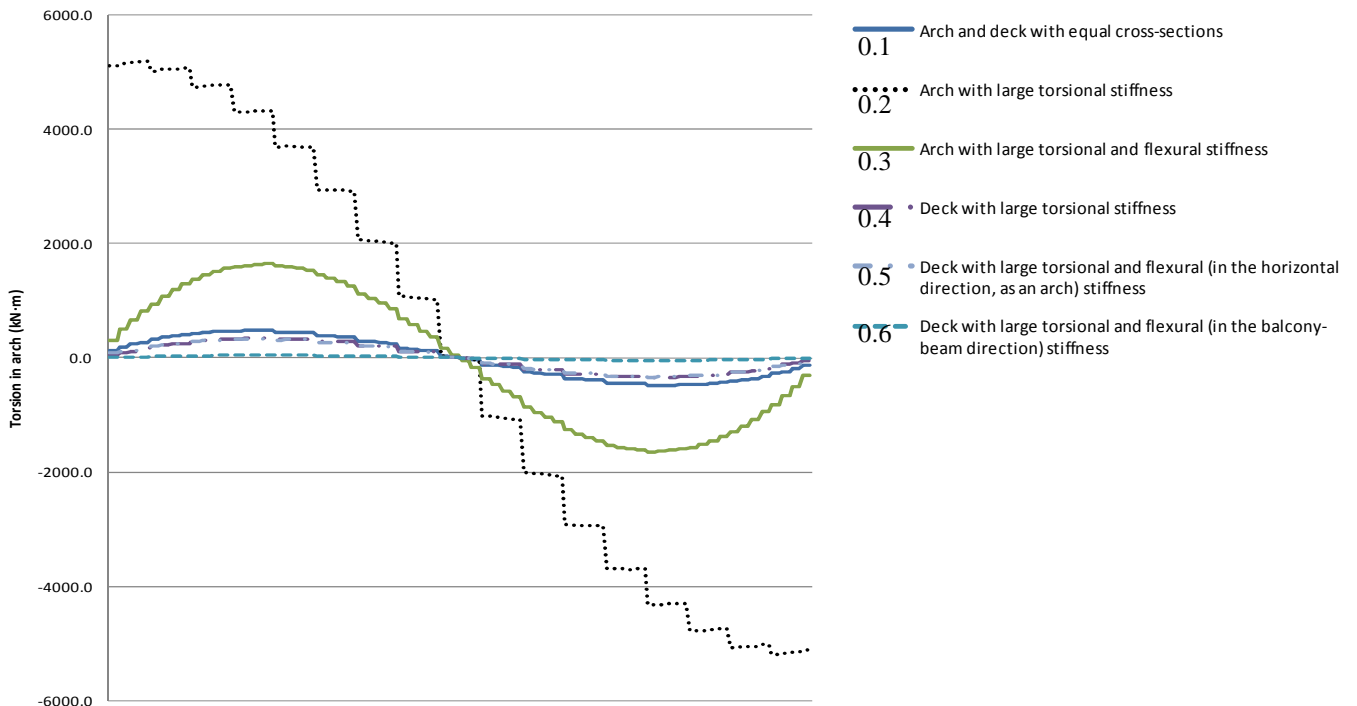


IV. STRUCTURAL BEHAVIOUR OF INFERIOR-DECK SPATIAL ARCH BRIDGES WITH IMPOSED CURVATURE



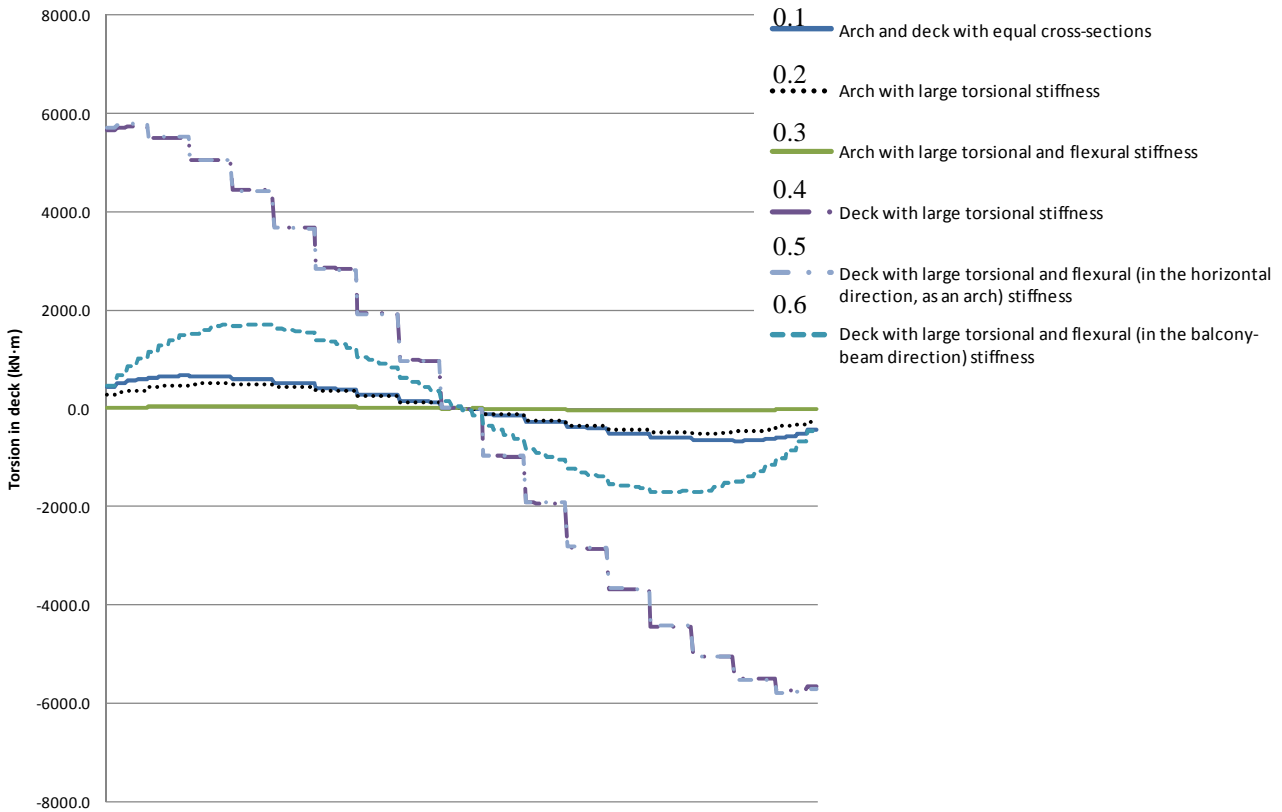
**Figure 4-12: Deck axial forces comparison for different arch and deck sections in inferior deck arch bridges with 20m (L/5) rise. The abscissas are the arch length from 0 to  $L_A$**

Minimal torsional moments in the arch (**Figure 4-13**) are achieved with a deck with both high torsional and flexural balcony-beam stiffness (0.6). However, the maximal torsional moments in the deck (**Figure 4-14**) are not achieved for this model but for (0.5) in which only the torsional stiffness is high. Vice-versa for the minimal torsional moments in the deck, achieved with model (0.3).



**Figure 4-13: Arch torsion comparison for different arch and deck sections in inferior deck arch bridges with 20m (L/5) rise. The abscissas are the arch length from 0 to  $L_A$**

IV. STRUCTURAL BEHAVIOUR OF INFERIOR-DECK SPATIAL ARCH BRIDGES WITH IMPOSED CURVATURE



**Figure 4-14: Deck torsion comparison for different arch and deck sections in inferior deck arch bridges with 20m (L/5) rise. The abscissas are the arch length from 0 to  $L_A$**

Local moments caused by the hangers in both arch and deck are minimized by increasing either the balcony-beam flexural stiffness of the arch or the deck (Figure 4-15 and Figure 4-16, models 0.3 and 0.6). The minimal torques achieved for these models imply very high balcony-beam moments (Figure 4-17 and Figure 4-18, models 0.3 and 0.6). To reduce these moments, the flexural stiffness must be maintained low. On the other hand, to maintain the arch in compression the torsional stiffness of either arch or deck must be high (models 0.2 and 0.5), paying high torsional costs (Figure 4-13 and Figure 4-14).

IV. STRUCTURAL BEHAVIOUR OF INFERIOR-DECK SPATIAL ARCH BRIDGES WITH IMPOSED CURVATURE

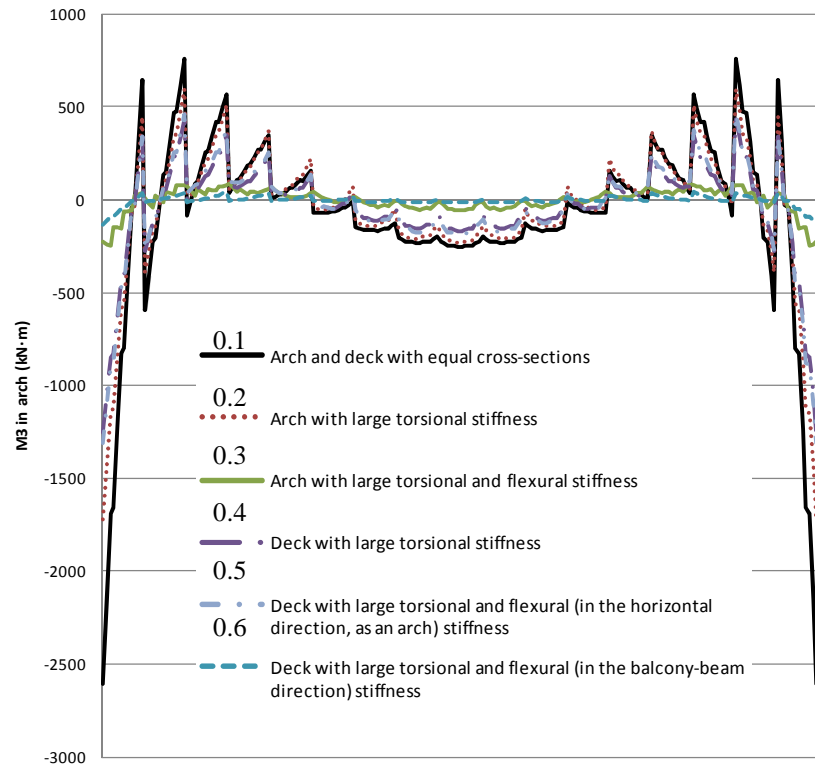


Figure 4-15: Arch in-plane bending moments comparison for different arch and deck sections in inferior deck arch bridges with 20m (L/5) rise. The abscissas are the arch length from 0 to  $L_A$

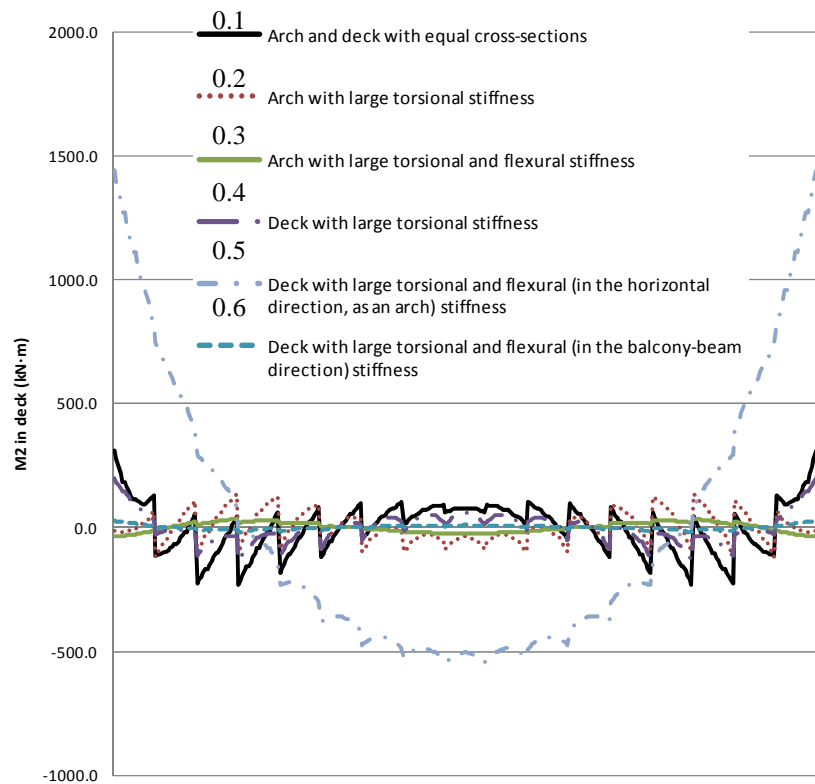


Figure 4-16: Deck horizontal bending moments (in the plane that contains the deck) comparison for different arch and deck sections in inferior deck arch bridges with 20m (L/5) rise. The abscissas are the deck length from 0 to  $L_D$

IV. STRUCTURAL BEHAVIOUR OF INFERIOR-DECK SPATIAL ARCH BRIDGES WITH IMPOSED CURVATURE

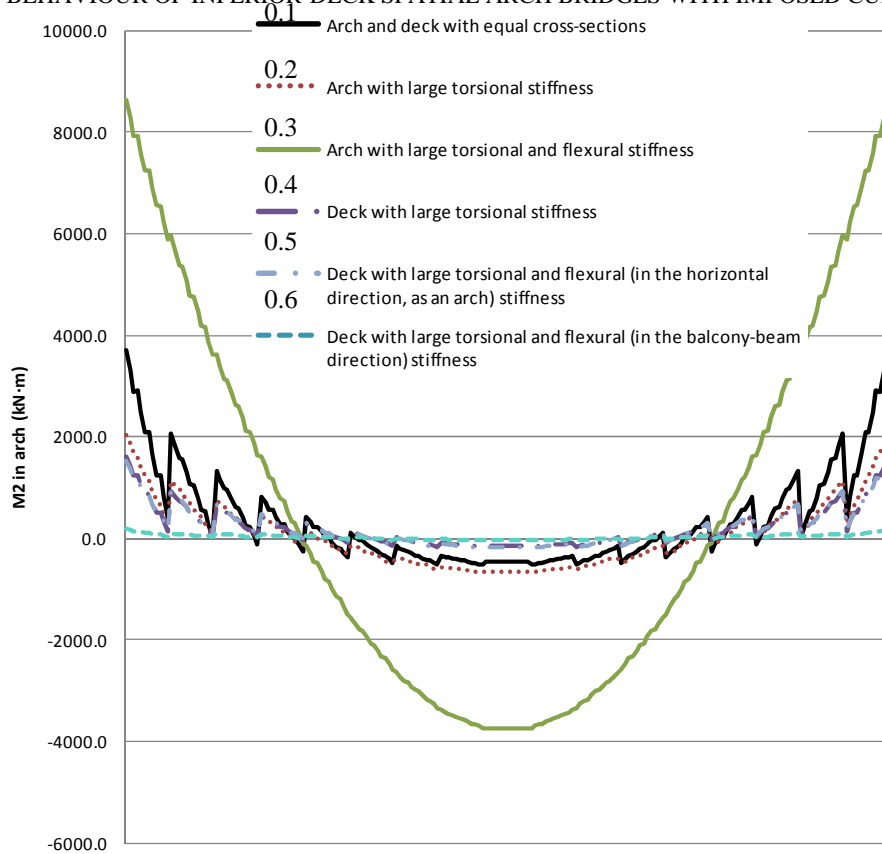


Figure 4-17: Arch balcony-beam bending moments comparison for different arch and deck sections in inferior deck arch bridges with 20m (L/5) rise. The abscissas are the arch length from 0 to  $L_A$

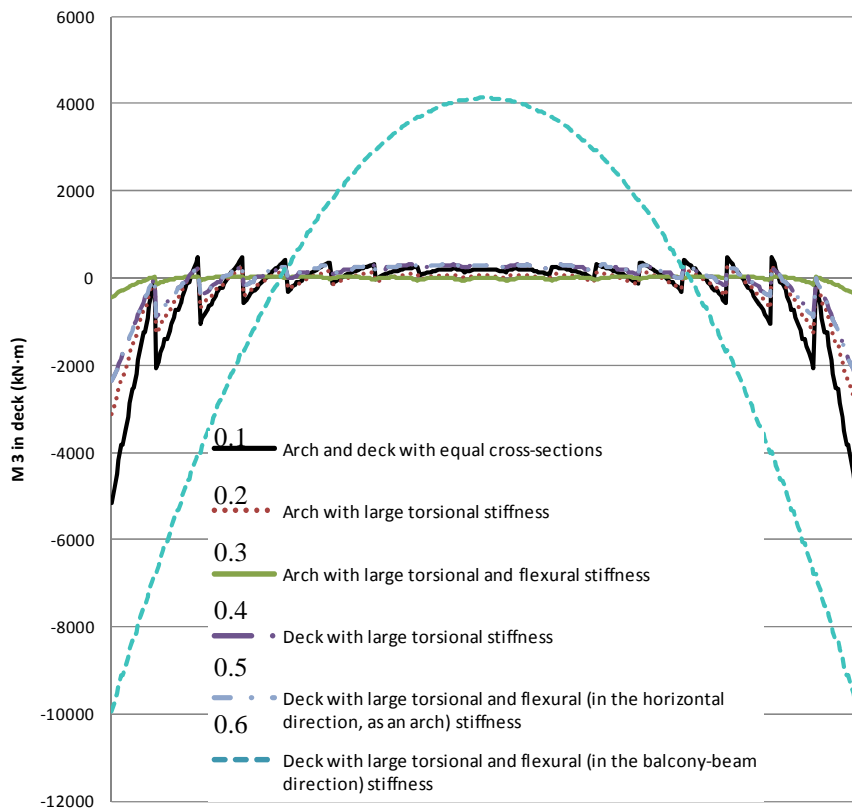
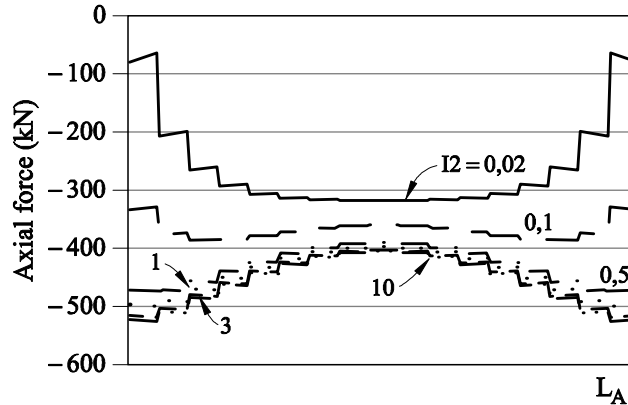


Figure 4-18: Deck balcony-beam bending moments comparison for different arch and deck sections in inferior deck arch bridges with 20m (L/5) rise. The abscissas are the deck length from 0 to  $L_D$

**4.3.1.2 Influence of the out-of-plane flexural rigidity of the arch**

The influence of the out-of plane flexural rigidity of the arch, i.e. the flexural rigidity for the balcony beam mechanism (with second moment of area  $\equiv I_2$ ) on the behaviour of arch bridges with imposed curvature under a vertical uniform distributed loading applied on the whole deck ( $q=10\text{kN/m}$ ), has been studied (Figure 4-19 and Figure 4-20). In this series of models, the hangers have a fixed connection with both the arch and the deck.

The values employed for the cross-sections are described in Table 4-2.



**Figure 4-19: Arch axial forces comparison for different arch sections (Table 4-2) in inferior deck arch bridges with 20m ( $L/5$ ) rise.**

When increasing the balcony beam flexural rigidity, the axial forces in the arch increase too and the increment is larger at the springings than at mid-span (Figure 4-19). For the set of fixed parameters, there is a certain  $I_2$  value above which:

- there is a change in the distribution of the axial forces along the arch. The forces in the springings become larger than those at mid-span somewhere in the range of  $I_2=0,1$  to  $0,5\text{m}^4$  (Figure 4-19). This is due to a stronger increase of the axial load in the hangers close to the abutments.
- the axial forces in the arch hardly vary (for  $I_2 \geq 3\text{m}^4$ , Figure 4-19)
- the bending moments in the arch hardly vary (for  $I_2 \geq 3\text{m}^4$ )
- the out-of-plane bending moments, i.e. the balcony-beam bending moments, remain steady (for  $I_2 \geq 3\text{m}^4$ )
- the arch displacements remain steady (Figure 4-20) (for  $I_2 \geq 3\text{m}^4$ ).

Therefore, there is no advantage in increasing  $I_2$  beyond  $I_2=3\text{m}^4$ .

To see the influence of the balcony beam rigidity of the arch on the total displacements, they have been measured at the arch span center deflection for each model described on Table 4-2 (Figure 4-20).

IV. STRUCTURAL BEHAVIOUR OF INFERIOR-DECK SPATIAL ARCH BRIDGES WITH IMPOSED CURVATURE

LEGEND NUMBER	ARCH	DECK	HANGERS	HANGER JOINTS	SYMBOL
<b>Model (1.1)</b>	Reference arch CHS D=1m; t=30mm A= 0,0914m <sup>2</sup> J= 0,0215m <sup>4</sup> I <sub>2</sub> = 0,0108m <sup>4</sup> I <sub>3</sub> = 0,0108m <sup>4</sup>	Reference deck BOX GIRDER 4000x800mm; t=15mm A= 0,1431m <sup>2</sup> J= 0,0615m <sup>4</sup> I <sub>2</sub> = 0,2517m <sup>4</sup> I <sub>3</sub> = 0,0196m <sup>4</sup>	Rigid hangers SHS 400x400mm; t=20mm A= 0,0304m <sup>2</sup> J= 1,097·10 <sup>-4</sup> m <sup>4</sup> I <sub>2</sub> = 7,337·10 <sup>-4</sup> m <sup>4</sup> I <sub>3</sub> = 7,337·10 <sup>-4</sup> m <sup>4</sup>	No releases	
<b>Model (1.2)</b>	Reference arch CHS D=1m; t=30mm A= 0,0914m <sup>2</sup> J= 0,0215m <sup>4</sup> I <sub>2</sub> = 0,0108m <sup>4</sup> I <sub>3</sub> = 0,0108m <sup>4</sup>	Rigid to torsion deck BOX GIRDER 4x0,8m; t=15mm A= 0,1431m <sup>2</sup> <b>J= 10m<sup>4</sup></b> I <sub>2</sub> = 0,2m <sup>4</sup> <b>I<sub>3</sub>= 0,02m<sup>4</sup></b>	Rigid hangers SHS 0,4x0,4m; t=20mm A= 0,0304m <sup>2</sup> J= 1,097·10 <sup>-4</sup> m <sup>4</sup> I <sub>2</sub> = 7,337·10 <sup>-4</sup> m <sup>4</sup> I <sub>3</sub> = 7,337·10 <sup>-4</sup> m <sup>4</sup>	No releases	
<b>Model (1.3)</b>	Reference arch CHS D=1m; t=30mm A= 0,0914m <sup>2</sup> J= 0,0215m <sup>4</sup> I <sub>2</sub> = 0,0108m <sup>4</sup> I <sub>3</sub> = 0,0108m <sup>4</sup>	Reference deck BOX GIRDER 4x0,8m; t=15mm A= 0,1431m <sup>2</sup> J= 0,0615m <sup>4</sup> I <sub>2</sub> = 0,2517m <sup>4</sup> I <sub>3</sub> = 0,0196m <sup>4</sup>	Rigid hangers High transverse bending rigidity A= 0,0304m <sup>2</sup> J= 1,097·10 <sup>-3</sup> m <sup>4</sup> I <sub>2</sub> = 7,34·10 <sup>-4</sup> m <sup>4</sup> <b>I<sub>3</sub>= 7,34·m<sup>4</sup></b>	No releases	
<b>Model (1.4)</b>	Reference arch CHS D=1m; t=30mm A= 0,0914m <sup>2</sup> J= 0,0215m <sup>4</sup> I <sub>2</sub> = 0,0108m <sup>4</sup> I <sub>3</sub> = 0,0108m <sup>4</sup>	Rigid to bending and torsion deck A= 0,1431m <sup>2</sup> <b>J= 10m<sup>4</sup></b> I <sub>2</sub> = 0,2m <sup>4</sup> <b>I<sub>3</sub>= 0,2m<sup>4</sup></b>	Rigid hangers SHS 0,4x0,4m; t=20mm A= 0,0304m <sup>2</sup> J= 1,097·10 <sup>-4</sup> m <sup>4</sup> I <sub>2</sub> = 7,337·10 <sup>-4</sup> m <sup>4</sup> I <sub>3</sub> = 7,337·10 <sup>-4</sup> m <sup>4</sup>	No releases	
<b>Model (1.5)</b>	Reference arch CHS D=1m; t=30mm A= 0,0914m <sup>2</sup> J= 0,0215m <sup>4</sup> I <sub>2</sub> = 0,0108m <sup>4</sup> I <sub>3</sub> = 0,0108m <sup>4</sup>	Rigid to bending and torsion deck A= 0,1431m <sup>2</sup> <b>J= 10m<sup>4</sup></b> I <sub>2</sub> = 0,2m <sup>4</sup> <b>I<sub>3</sub>= 0,2m<sup>4</sup></b>	Rigid hangers High transverse bending rigidity A= 0,0304m <sup>2</sup> J= 1,097·10 <sup>-3</sup> m <sup>4</sup> I <sub>2</sub> = 7,34·10 <sup>-4</sup> m <sup>4</sup> <b>I<sub>3</sub>= 7,34·m<sup>4</sup></b>	No releases	

Table 4-2: Mechanical properties' values of the cross-sections employed on the study of the influence of the arch cross-sectional balcony beam flexural rigidity

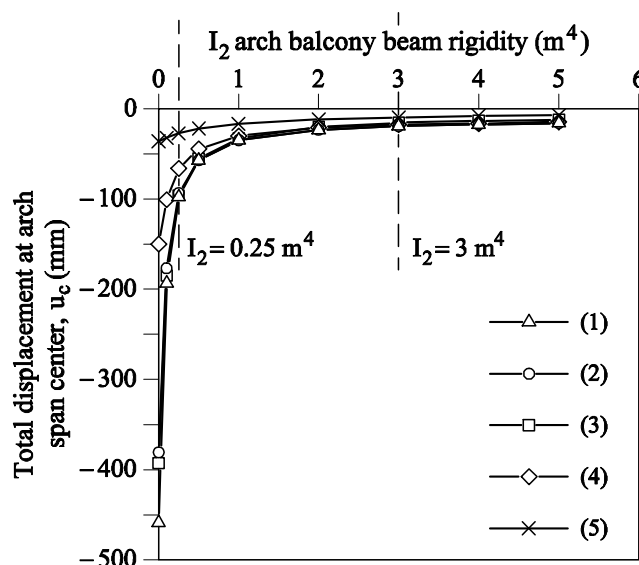


Figure 4-20: Total displacement of the arch at mid-span as a function of the out-of-plane arch stiffness (I<sub>2</sub>) for different models with hanger and deck cross-sections defined in Table 4-2. (1) corresponds to 1.1 in Table 4-2 and idem for the rest of models.

#### IV. STRUCTURAL BEHAVIOUR OF INFERIOR-DECK SPATIAL ARCH BRIDGES WITH IMPOSED CURVATURE

When employing both a large torsional ( $J$ ) and flexural ( $I_3$ ) rigidities for the deck (Table 4-2, models (1.4) and (1.5)), the arch displacements for small values of  $I_2$  significantly decrease (Figure 4-20, models (1.4) and (1.5)). This happens because, when the arch is very flexible, the only way to reduce the arch displacements is by reducing the deck deflections. When only one of these deck rigidities is large ( $J$ , model (1.2), Table 4-2), the arch deflections for small values of  $I_2$  do not decrease significantly (Figure 4-20, model (1.2)) as the vertical deflections in the deck are still large, due to the small value of the other deck rigidity ( $I_3$ , model (1.2), Table 4-2). For  $I_2 \geq 0,25\text{m}^4$  the differences in the arch deflections between models with the same torsional rigidity of the deck and different flexural rigidity of the deck are smaller than 3,4%. Furthermore, the value of  $I_2$  from which the arch displacement remains almost steady is independent of the rest of the parameters (Figure 4-20, all models).

When employing hangers with a large transverse rigidity (Table 4-2, models (1.3) and (1.5)), the arch displacements diminish considerably (Figure 4-20, compare (1.1) with (1.3) and (1.4) with (1.5)).

We can conclude that the out-of-plane flexural rigidity of the arch, i.e. the flexural rigidity for the balcony beam mechanism ( $I_2$ ), is the parameter that controls more efficiently the arch deflections. In fact, the arch deflections remain steady when  $I_2 \geq 3\text{m}^4$  (for our  $f=g=20\text{m}$  and  $L=100\text{m}$  model), regardless the value of the rest of the parameters. For low  $I_2$  values, arch deflections can be greatly improved by the hanger-deck system stiffness (Figure 4-20, Model 1.5).

##### ***4.3.1.3 Influence of the flexural rigidity of the arch versus the rigidity of the hanger-deck system***

Six different full bridge models (see Table 4-3) have been analyzed in order to determine, whether the behaviour can be more efficiently controlled by the rigidity of the arch or the hanger-deck system. In all of the models, the following parameters have been employed:  $f=g=20\text{m}$ ,  $L=100\text{m}$ , arch fixed to deck with encasted abutments, deck submitted to a uniform distributed loading of  $10\text{kN/m}$ .

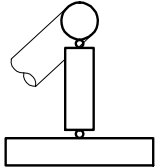
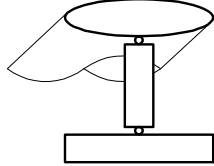
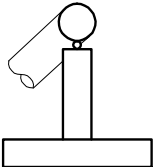
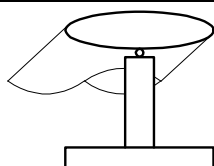
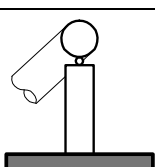
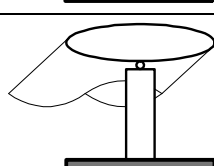
We have borne in mind the previous conclusions drawn in section 4.3.1 and the Annex N2.1.

- The minimal total bending moment in the arch, when employing a rigid to torsion cross-section, is obtained with M3-3 fixed at hanger/deck joints.
- The maximal total bending moment in the arch corresponds to hangers pinned at both ends.

The following figures (see from Figure 4-21 to Figure 4-26) demonstrate that to control arch moments and torsions, employing a rigid hanger-deck system and an arch with low rigidity is better than increasing the rigidity of the arch.

The models identified in **Table 4-3** as (2.1) and (2.2) have hangers with pinned connections to both the deck and the arch. Therefore, their behaviour can be directly compared to the analytical model described by Eqs 1 to 5. All the conclusions drawn from the analytical model about the effects of increasing the stiffness of the balcony beam are confirmed by these FE models of the full bridge.

IV. STRUCTURAL BEHAVIOUR OF INFERIOR-DECK SPATIAL ARCH BRIDGES WITH IMPOSED CURVATURE

LEGEND NUMBER	ARCH	DECK	HANGERS	HANGER JOINTS	SYMBOL
<b>Model (2.1)</b>	<i>Reference arch</i> CHS D=1m; t=30mm A= 0,0914m <sup>2</sup> J= 0,0215m <sup>4</sup> I2= 0,0108m <sup>4</sup> <b>I3= 0,0108m<sup>4</sup></b>	<i>Reference deck</i> BOX GIRDER 4x0,8m; t=15mm A= 0,1431m <sup>2</sup> J= 0,0615m <sup>4</sup> I2= 0,2517m <sup>4</sup> I3= 0,0196m <sup>4</sup>	A= 0,0304m <sup>2</sup> J= 1,097·10 <sup>-3</sup> m <sup>4</sup> I2= 7,34·10 <sup>-4</sup> m <sup>4</sup> <b>I3= 7,34·m<sup>4</sup></b>	Pinned hangers	
<b>Model (2.2)</b>	<i>Rigid arch</i> A= 0,25m <sup>2</sup> J= 0,18m <sup>4</sup> I2= 0,06m <sup>4</sup> <b>I3= 3,00m<sup>4</sup></b>	<i>Reference deck</i> BOX GIRDER 4x0,8m; t=15mm A= 0,1431m <sup>2</sup> J= 0,0615m <sup>4</sup> I2= 0,2517m <sup>4</sup> I3= 0,0196m <sup>4</sup>	A= 0,0304m <sup>2</sup> J= 1,097·10 <sup>-3</sup> m <sup>4</sup> I2= 7,34·10 <sup>-4</sup> m <sup>4</sup> <b>I3= 7,34·m<sup>4</sup></b>	Pinned hangers	
<b>Model (2.3)</b>	<i>Reference arch</i> CHS D=1m; t=30mm A= 0,0914m <sup>2</sup> J= 0,0215m <sup>4</sup> I2= 0,0108m <sup>4</sup> <b>I3= 0,0108m<sup>4</sup></b>	<i>Reference deck</i> BOX GIRDER 4x0,8m; t=15mm A= 0,1431m <sup>2</sup> J= 0,0615m <sup>4</sup> I2= 0,2517m <sup>4</sup> I3= 0,0196m <sup>4</sup>	A= 0,0304m <sup>2</sup> J= 1,097·10 <sup>-3</sup> m <sup>4</sup> I2= 7,34·10 <sup>-4</sup> m <sup>4</sup> <b>I3= 7,34·m<sup>4</sup></b>	Hangers fixed at deck and transversally pinned at arch (M3-3 released at arch) <sup>a</sup>	
<b>Model (2.4)</b>	<i>Rigid arch</i> A= 0,25m <sup>2</sup> J= 0,18m <sup>4</sup> I2= 0,06m <sup>4</sup> <b>I3= 3,00m<sup>4</sup></b>	<i>Reference deck</i> BOX GIRDER 4x0,8m; t=15mm A= 0,1431m <sup>2</sup> J= 0,0615m <sup>4</sup> I2= 0,2517m <sup>4</sup> I3= 0,0196m <sup>4</sup>	A= 0,0304m <sup>2</sup> J= 1,097·10 <sup>-3</sup> m <sup>4</sup> I2= 7,34·10 <sup>-4</sup> m <sup>4</sup> <b>I3= 7,34·m<sup>4</sup></b>	Hangers fixed at deck and transversally pinned at arch (M3-3 released at arch) <sup>a</sup>	
<b>Model (2.5)</b>	<i>Reference arch</i> CHS D=1m; t=30mm A= 0,0914m <sup>2</sup> J= 0,0215m <sup>4</sup> I2= 0,0108m <sup>4</sup> <b>I3= 0,0108m<sup>4</sup></b>	<i>Rigid deck</i> A= 0,1431m <sup>2</sup> <b>J= 10m<sup>4</sup></b> I2= 0,2m <sup>4</sup> <b>I3= 0,2m<sup>4</sup></b>	A= 0,0304m <sup>2</sup> J= 1,097·10 <sup>-3</sup> m <sup>4</sup> I2= 7,34·10 <sup>-4</sup> m <sup>4</sup> <b>I3= 7,34·m<sup>4</sup></b>	Hangers fixed at deck and transversally pinned at arch (M3-3 released at arch) <sup>a</sup>	
<b>Model (2.6)</b>	<i>Rigid arch</i> A= 0,25m <sup>2</sup> J= 0,18m <sup>4</sup> I2= 0,06m <sup>4</sup> <b>I3= 3,00m<sup>4</sup></b>	<i>Rigid deck</i> A= 0,1431m <sup>2</sup> <b>J= 10m<sup>4</sup></b> I2= 0,2m <sup>4</sup> <b>I3= 0,2m<sup>4</sup></b>	A= 0,0304m <sup>2</sup> J= 1,097·10 <sup>-3</sup> m <sup>4</sup> I2= 7,34·10 <sup>-4</sup> m <sup>4</sup> <b>I3= 7,34·m<sup>4</sup></b>	Hangers fixed at deck and transversally pinned at arch (M3-3 released at arch) <sup>a</sup>	

<sup>a</sup> Note: the longitudinal flexural rigidity of the hangers is low, so longitudinally they will tend to be pinned too.

**Table 4-3: Definition of the different cross-sections employed on the study of the influence of the flexural rigidity of the arch versus the rigidity of the hanger-deck system**



IV. STRUCTURAL BEHAVIOUR OF INFERIOR-DECK SPATIAL ARCH BRIDGES WITH IMPOSED CURVATURE

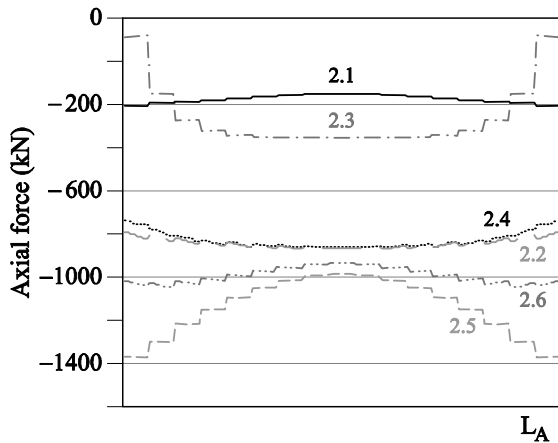


Figure 4-21: Arch axial forces comparison

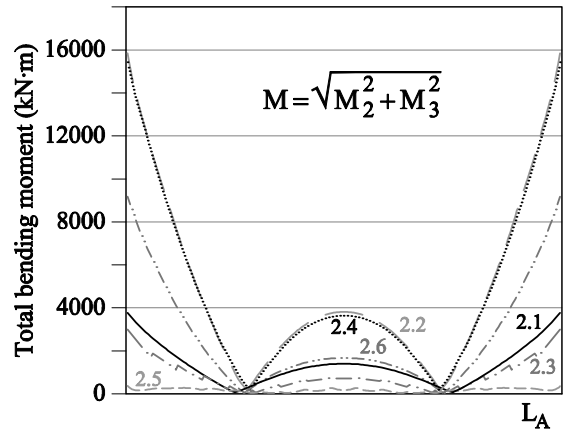


Figure 4-22: Arch moments comparison

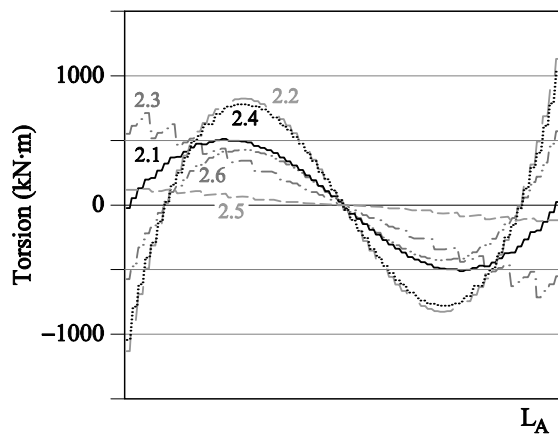


Figure 4-23: Arch torsion moments comparison

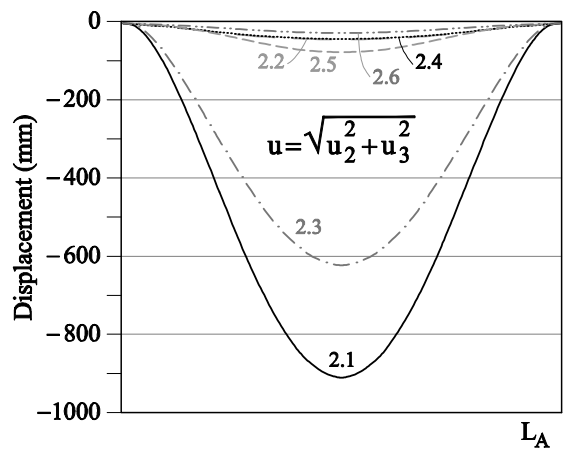


Figure 4-24: Arch displacements comparison

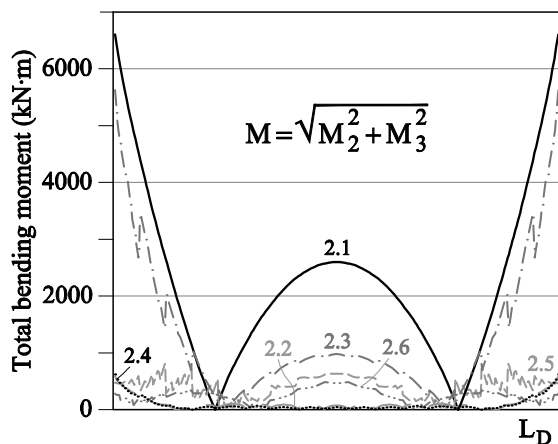


Figure 4-25: Deck moments comparison

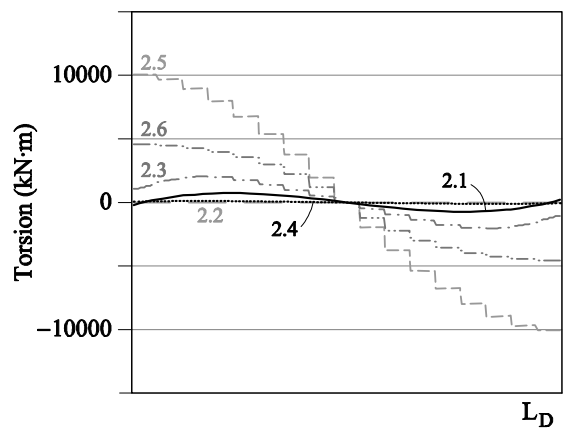


Figure 4-26: Deck torsion moments comparison

Regarding the displacements (Figure 4-24), it is very efficient to increase the flexural stiffness of the arch when the flexural stiffness of the deck is small (Figure 4-24, compare model (2.1) with (2.2)), and also to increase the flexural stiffness of the deck when the flexural stiffness of the arch is small (Figure 4-24, compare (2.3) with (2.5)). This is because the displacements are very sensitive to the only flexural stiffness that can control them, as the other one is small. It is also quite efficient to use fixed connections between the

#### IV. STRUCTURAL BEHAVIOUR OF INFERIOR-DECK SPATIAL ARCH BRIDGES WITH IMPOSED CURVATURE

hanger and the deck, but only when the flexural stiffness of both, the arch and the deck, are small (*Figure 4-24*, compare model (2.1) with (2.3)), because the shear forces in the hangers are the only mechanism to control the arch displacements. This mechanism is not efficient when the flexural stiffness of the arch is large, since there is more than one mechanism available to control the displacements in the arch (*Figure 4-24*, compare (2.2) with (2.4) and (2.6)).

Moreover, when the arch displacements are controlled (*Figure 4-24*, models (2.2), (2.4), (2.5) and (2.6)), the arch behaviour is enhanced (*Figure 4-21*, models (2.2), (2.4), (2.5) and (2.6)). However, when the displacements are controlled by means of the flexural stiffness of the arch (*Figure 4-24*, models (2.2), (2.4), and (2.6)), the bending moments in the arch are large (*Figure 4-22*, models (2.2), (2.4), and (2.6)). This effect is enhanced, when the flexural stiffness of the arch is the only parameter that is available to control the displacements in the arch (model (2.2) in *Figure 4-22* and *Figure 4-24*). Therefore, the arch displacements are best controlled by providing rigidity to the whole system. However, controlling the arch displacements while enhancing the arch behaviour, is achieved by providing rigidity only to the hanger-deck system (model (2.5), from *Figure 4-21* to *Figure 4-24*).

It is possible to define a set of parameters (Table 4-3, model (2.5)) for which the arch tends toward the antifunicular of the loading, i.e. enhancing the arch axial behaviour (*Figure 4-21*, model (2.5)) by cancelling the balcony-beam behaviour (*Figure 4-22* and *Figure 4-23*, model (2.5)). This behaviour is achieved when the hanger has a fixed connection to the deck in the transverse direction, the torsional rigidity of the deck is large, and the flexural rigidity of the arch is small. Therefore, opposite to what has been concluded in other studies (Jorquera 2007), antifunicular arches do exist for IDABWIC.

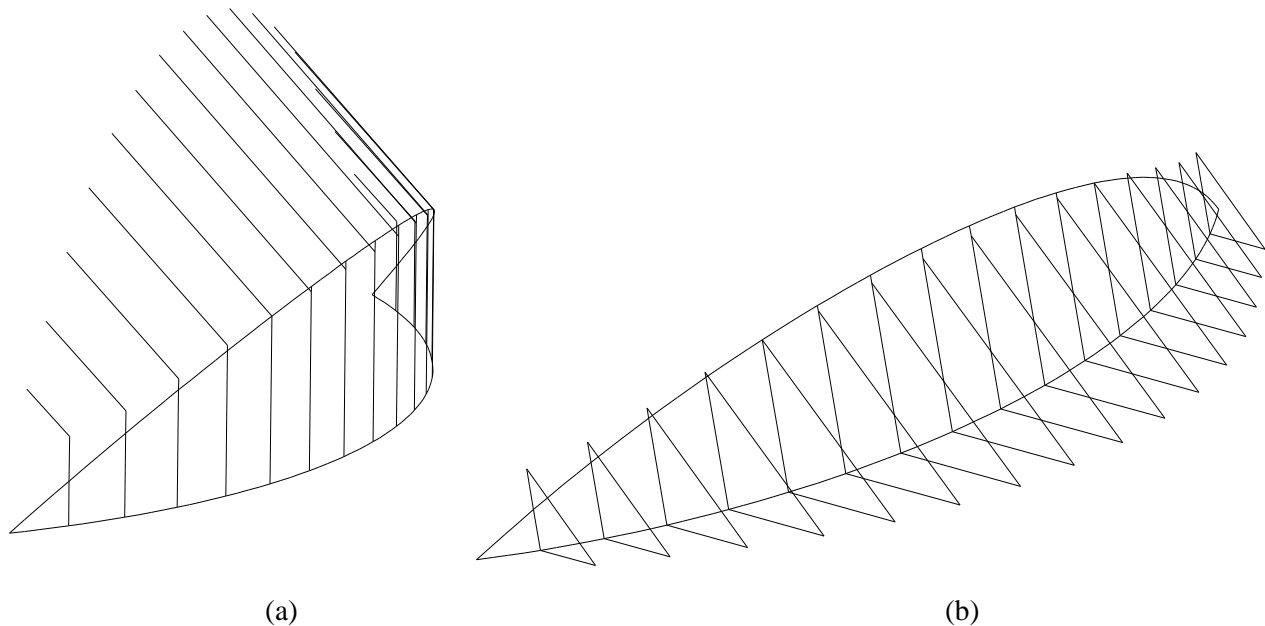
A geometrically non-linear analysis has been conducted in chapter VI.

The parameters proposed above in order to tend to an antifunicular IDABWIC are exactly the same as those that Robert Maillart used for his superior deck curved arch bridges, with a foresight that only a genius could have, although he did not prove it through calculations (Billington 1997, Laffranchi and Marti 1997).

**4.3.1.4 Secondary hanger systems**

The expected optimal configuration

In Annex N2.1 the forces needed to introduce in this bridge type in order to compensate internal forces are described. A solution in terms of the hanger/deck and hanger/arch connections and hanger-deck system stiffness is given and summarized in section 4.3.1.3 of the present chapter. However, this could also be achieved and more precisely controlled and visualised by employing a secondary hanger system. A scheme of such a system is shown in **Figure 4-27**. The vertical hangers will be in tension and the secondary system consists on rigid struts in compression which introduce compensatory torques in the arch.



**Figure 4-27: Secondary hanger system to compensate the internal forces in the arch caused by a uniform distributed load on the deck. (a) Initial reasoning: forces perpendicular to the plane of the arch are needed to resist the balcony-beam behavior. Eccentricities are introduced to compensate the bending moments. This secondary hanger system would work under tension, but geometrically it is not possible, it remains unconnected to the system at one end. (b) Strut system working under compression**

On the following figures a comparison of this geometry with  $g=f=20\text{m}$  and  $L=100\text{m}$  (model A) and an equivalent bridge without the secondary hanger system (model B) is presented (from **Figure 4-28** to **Figure 4-31**). The cross-sections employed for the arch, deck and vertical hangers in both models are the same ones as in Table 3-1. Struts with infinitely rigid cross-sections are employed to model the eccentricity of the secondary hanger system with the shear forces center of the arch and deck. The cross-sections employed for the secondary hanger system are CHS of 400mm diameter and 20mm of thickness.

Employing a compensatory hanger system with an adequate distribution:

- increases the axial forces compressions in the arch, because it increases the in-plane behaviour of the arch (Figure 4-28).
- diminishes the out-of-plane and total bending moments because it controls the out-of-plane behaviour of the arch (Figure 4-30).
- can be also employed to diminish in-plane bending moments in the arch (**Figure 4-29**).

IV. STRUCTURAL BEHAVIOUR OF INFERIOR-DECK SPATIAL ARCH BRIDGES WITH IMPOSED CURVATURE

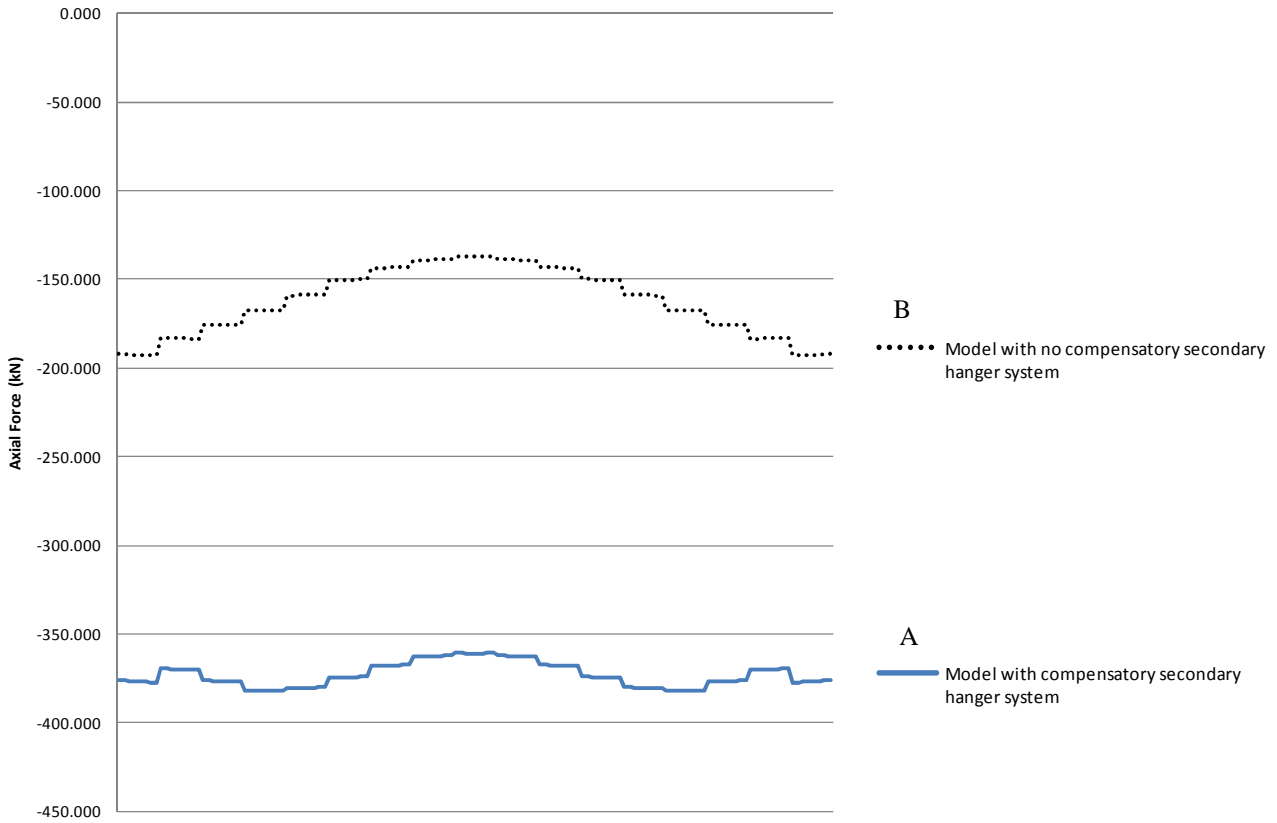
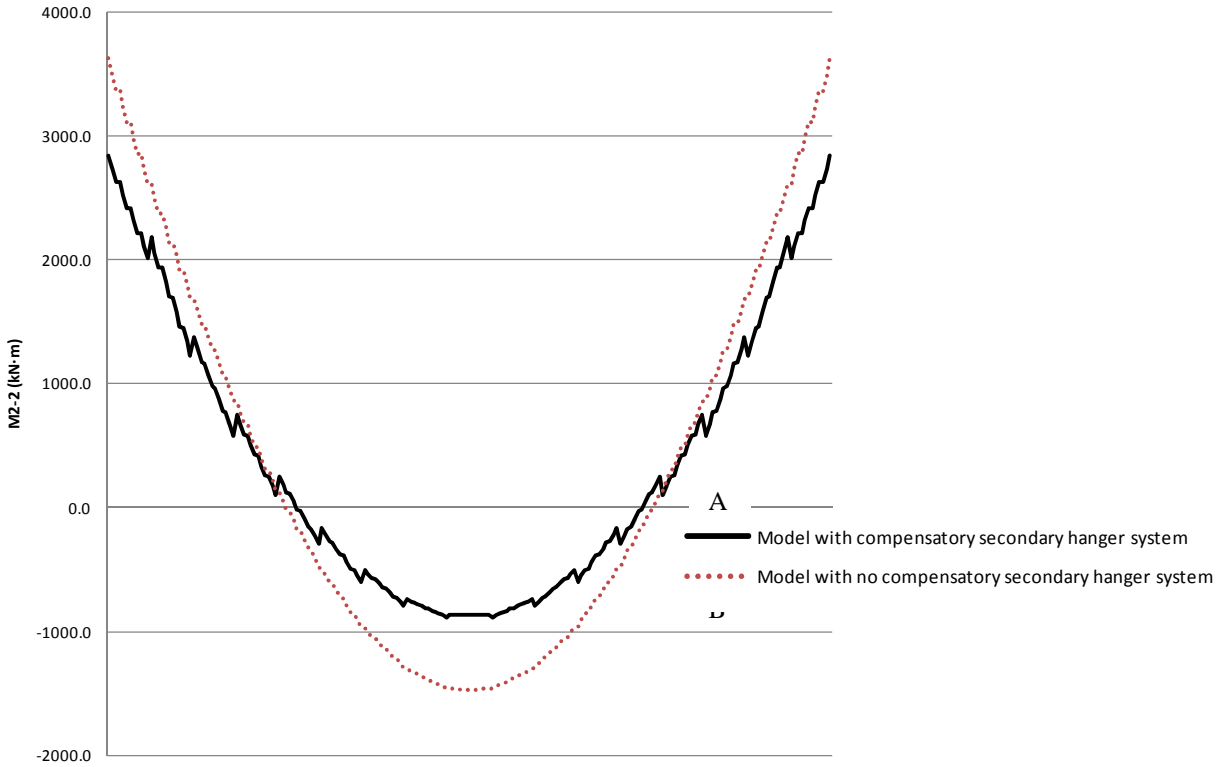


Figure 4-28: Arch axial forces comparison of models A and B with and without secondary hanger system. The abscissas are the arch length from 0 to  $L_A$

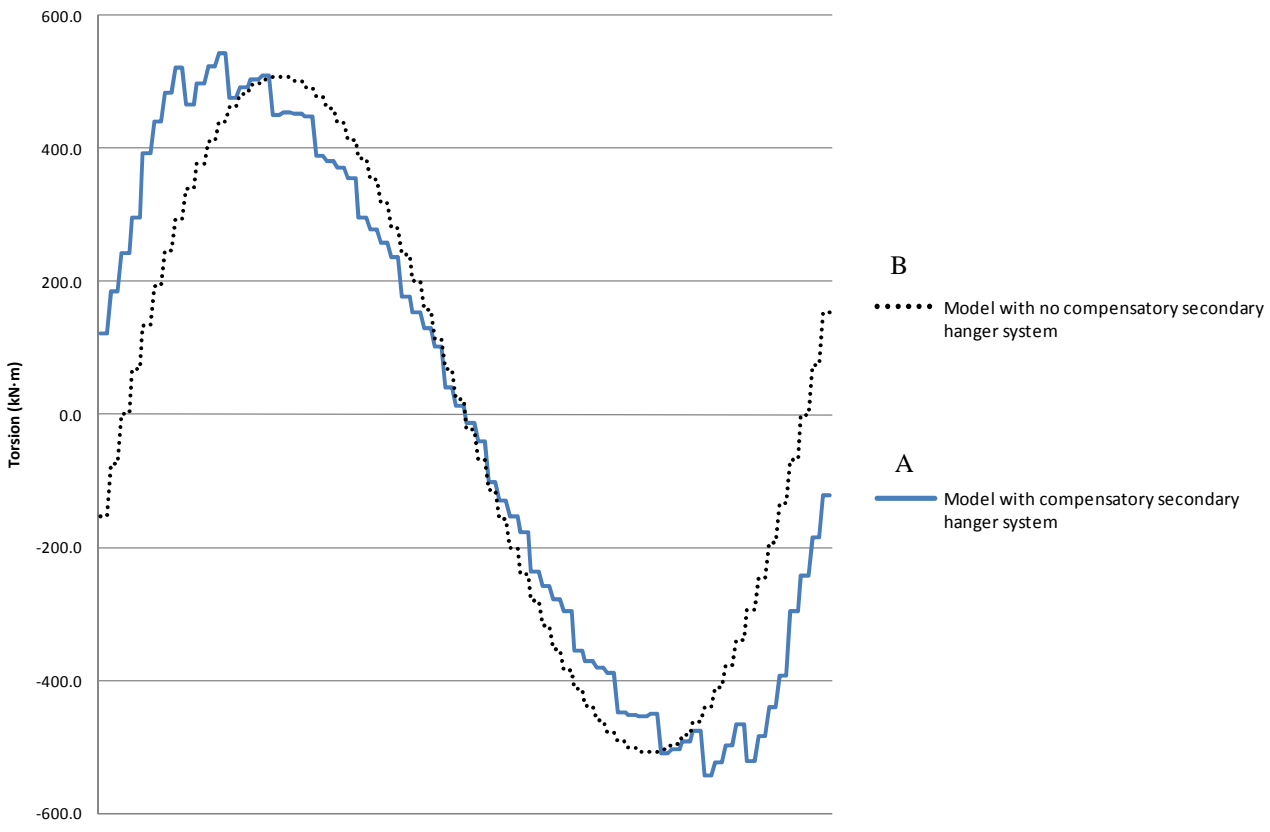


Figure 4-29: Arch in-plane bending moments comparison of models A and B with and without secondary hanger system. The abscissas are the arch length from 0 to  $L_A$

IV. STRUCTURAL BEHAVIOUR OF INFERIOR-DECK SPATIAL ARCH BRIDGES WITH IMPOSED CURVATURE



**Figure 4-30: Arch out-of-plane bending moments comparison of models A and B with and without secondary hanger system.** *The abscissas are the arch length from 0 to  $L_A$*



**Figure 4-31: Arch torsional moments comparison of models A and B with and without secondary hanger system.** *The abscissas are the arch length from 0 to  $L_A$*

#### IV. STRUCTURAL BEHAVIOUR OF INFERIOR-DECK SPATIAL ARCH BRIDGES WITH IMPOSED CURVATURE

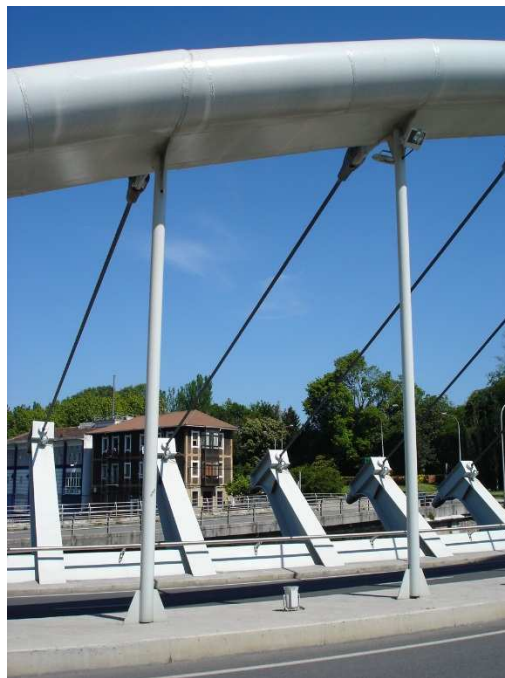
##### The particular case of the bridge over the Galindo river

The bridge over the Galindo river in the outskirts of Bilbao, designed by Javier Manterola, employs a compensatory cable system at the arch which is anchored in a series of struts connected to the deck (Figure 4-32).



**Figure 4-32: Bridge over Galindo river in Bilbao employing a secondary hanger system**

M3-3 transverse bending moments (Figure 4-10) are released at hanger/arch joints and longitudinal bending moments M2-2 are fixed. At hanger/deck joints M3-3 is fixed and M2-2 is released (Figure 4-33). If no compensatory cable system was employed, this would cause very low axial forces at both deck and arch, especially at arch springings and deck abutments, and high bending and maximal (compared to other joint configurations) torsional internal forces (see Annex N2.1).



**Figure 4-33: Detail of the hanger joints of the bridge over Galindo river in Bilbao**

The compensatory cables are at the inner side of the curve instead of the outer side as in the previous solution. At the extremes they tend to be more horizontal (Figure 4-32) and, therefore, with a higher

IV. STRUCTURAL BEHAVIOUR OF INFERIOR-DECK SPATIAL ARCH BRIDGES WITH IMPOSED CURVATURE

component perpendicular to the arch approximation plane<sup>1</sup> than the central cables. This means that lower axial forces will be introduced at extremes than at span center.

Since it is in the inner part of the curve, these “secondary” hangers work under tension.

This distribution is adequate to diminish the important bending moments at arch springings, but it will only slightly reduce bending at span center and increase the axial force which is already a compression force. It is not the distribution which helps to maximize the arch behaviour of the arch.

The cross-sections employed in the bridge over the Galindo river are detailed in Table 4-4. They have been approximated taking as a basis the ones described by Manterola (2011).

ARCH	A= m <sup>2</sup> J= m <sup>4</sup> I2= m <sup>4</sup> <b>I3= 0,0108m<sup>4</sup></b>
DECK	<i>Reference deck</i> BOX GIRDER 4000x800mm; t=15mm A= 0,1431m <sup>2</sup> J= 0,0615m <sup>4</sup> I2= 0,2517m <sup>4</sup> I3= 0,0196m <sup>4</sup>
HANGERS	<i>Flexible hangers</i> Stay cables A= 9,8·10 <sup>-4</sup> m <sup>2</sup> J= 0 m <sup>4</sup> I2= I3= 0 m <sup>4</sup>
HANGER JOINTS	M3-3 released at hanger/arch connection M2- released at hanger/deck connection
SECONDARY HANGER SYSTEM	<i>Flexible hangers</i> Stay cables A= 9,8·10 <sup>-4</sup> m <sup>2</sup> J= 0 m <sup>4</sup> I2= I3= 0 m <sup>4</sup>

**Table 4-4: Cross-section values employed for the bridge over the Galindo river**

<sup>1</sup> It is a bent parabolic arch according to the definition which has been developed for the present study in section 3. Hence, it is not contained in a plane. However, an approximation plane can be employed as demonstrated in section 3.

IV. STRUCTURAL BEHAVIOUR OF INFERIOR-DECK SPATIAL ARCH BRIDGES WITH IMPOSED CURVATURE

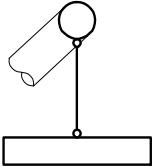
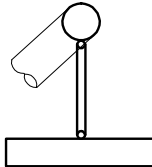
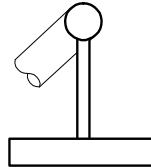
4.3.2 Structural behaviour under non-symmetrical vertical loading

For conventional vertical arch bridges ( $g=0$ ), the maximal arch shear forces, bending moments and deflections are significantly higher when the loading is applied on half the deck span (from the abutment to the mid-span,  $q'=10\text{kN/m}$ ), than on the whole deck span ( $q=10\text{kN/m}$ ). However, highest axial forces are obtained when the whole deck span is fully loaded ( $q=10\text{kN/m}$ ). This behaviour is shown in Figure 19.

In contrast, for IDABWIC (with a large  $g/f$  ratio), the critical load case, for both internal forces and displacements, is obtained when the uniform distributed loading is applied on the whole deck span (Figure 20).

A vertical uniform distributed loading applied on the exterior half of the deck's cross-section along the whole bridge span ( $q''=5\text{kN/m}$ ;  $t''=5\text{kN}\cdot\text{m/m}$ , ie: vertical loading and tipping torque) has also been analyzed, given the importance of torsional behaviour in this bridge type. For all the models, the internal forces proved to be mainly due to vertical loading.

All these conclusions are verified both for flexible and rigid hangers (see **Table 4-5**). Models 3.1 and 3.2 have very similar results, as expected.

LEGEND NUMBER	Model (1)	Model (2)	Model (3)
ARCH	<i>Reference arch</i> CHS D=1m; t=30mm A= 0,0914m <sup>2</sup> J= 0,0215m <sup>4</sup> I2= 0,0108m <sup>4</sup> <b>I3= 0,0108m<sup>4</sup></b>	<i>Reference arch</i> CHS D=1m; t=30mm A= 0,0914m <sup>2</sup> J= 0,0215m <sup>4</sup> I2= 0,0108m <sup>4</sup> <b>I3= 0,0108m<sup>4</sup></b>	<i>Reference arch</i> CHS D=1m; t=30mm A= 0,0914m <sup>2</sup> J= 0,0215m <sup>4</sup> I2= 0,0108m <sup>4</sup> <b>I3= 0,0108m<sup>4</sup></b>
DECK	<i>Reference deck</i> BOX GIRDER 4000x800mm; t=15mm A= 0,1431m <sup>2</sup> J= 0,0615m <sup>4</sup> I2= 0,2517m <sup>4</sup> I3= 0,0196m <sup>4</sup>	<i>Reference deck</i> BOX GIRDER 4000x800mm; t=15mm A= 0,1431m <sup>2</sup> J= 0,0615m <sup>4</sup> I2= 0,2517m <sup>4</sup> I3= 0,0196m <sup>4</sup>	<i>Reference deck</i> BOX GIRDER 4000x800mm; t=15mm A= 0,1431m <sup>2</sup> J= 0,0615m <sup>4</sup> I2= 0,2517m <sup>4</sup> I3= 0,0196m <sup>4</sup>
HANGERS	<i>Flexible hangers</i> Stay cables A= $9,8 \cdot 10^{-4} \text{ m}^2$ J= 0 m <sup>4</sup> I2= I3= 0 m <sup>4</sup>	CHS D=0,4m; t=20mm A= 0,0239m <sup>2</sup> J= $8,64 \cdot 10^{-4} \text{ m}^4$ I2= $4,32 \cdot 10^{-4} \text{ m}^4$ I3= $4,32 \cdot 10^{-4} \text{ m}^4$	CHS D=0,4m; t=20mm A= 0,0239m <sup>2</sup> J= $8,64 \cdot 10^{-4} \text{ m}^4$ I2= $4,32 \cdot 10^{-4} \text{ m}^4$ I3= $4,32 \cdot 10^{-4} \text{ m}^4$
HANGER JOINTS	Flexible hangers	Pinned hangers	Fixed hangers
SYMBOL			

**Table 4-5: Cross-section values employed for the study of the worse loading case for vertical planar arch bridges ( $g=0$ ) and IDABWIC with  $g=20$**



IV. STRUCTURAL BEHAVIOUR OF INFERIOR-DECK SPATIAL ARCH BRIDGES WITH IMPOSED CURVATURE

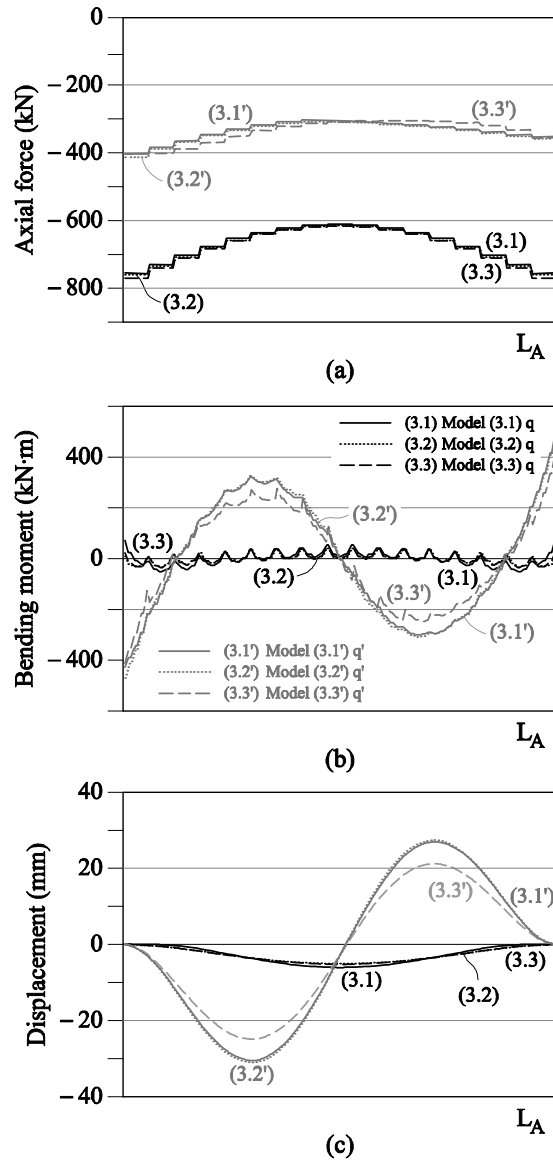


Figure 4-34: Internal forces and deflections along the arch length ( $L_A$ ) of a conventional vertical arch bridge ( $L=100$ ,  $f=20$ m and  $g=0$ ) for the different models defined in Table 4. Comparison between load cases  $q=10$ kN on the whole deck span and  $q'=10$ kN on half the deck span. (a) Axial forces (b) Total bending moments, (c) Deflections

#### IV. STRUCTURAL BEHAVIOUR OF INFERIOR-DECK SPATIAL ARCH BRIDGES WITH IMPOSED CURVATURE

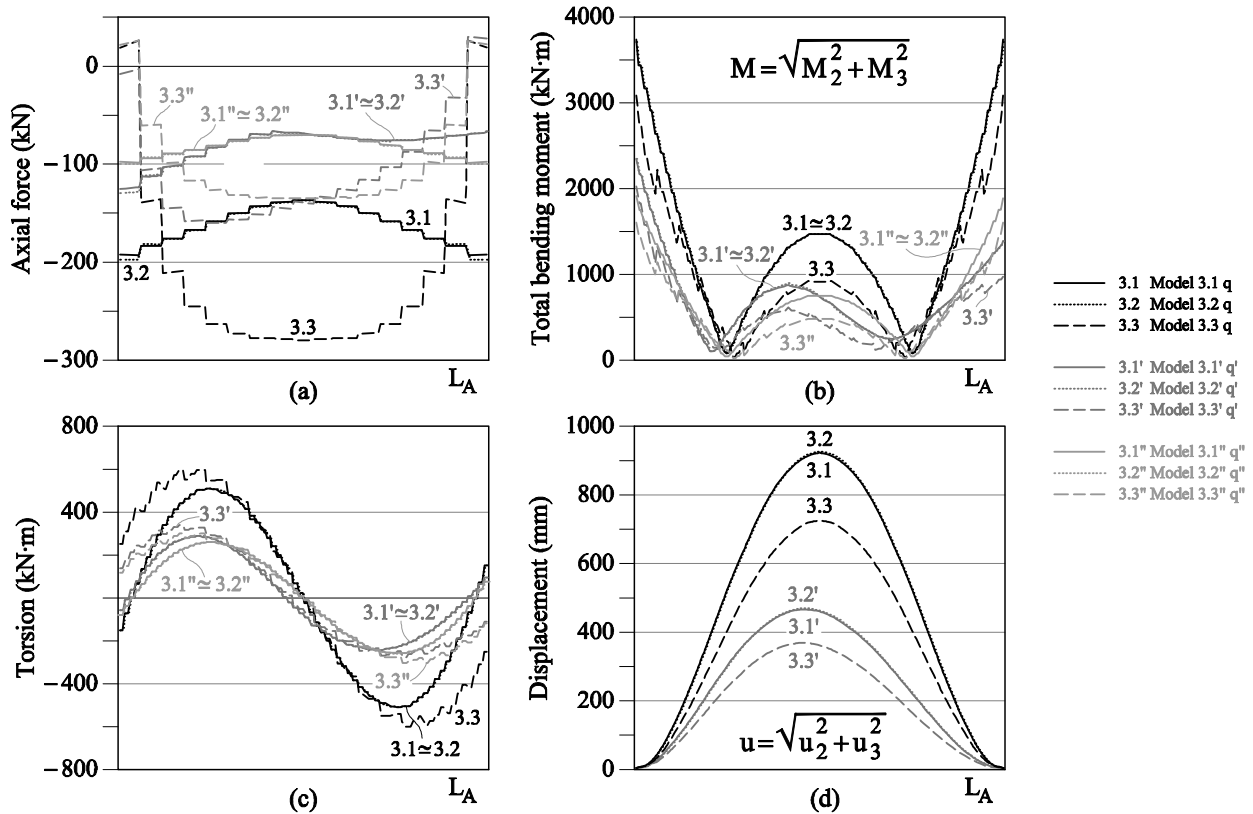


Figure 4-35: Internal forces and displacements along the arch length ( $L_A$ ) of an IDABWIC (with  $L=100$ ,  $f=20$ m and  $g=20$ m) for the different models defined in Table 4. Comparison between load cases:  $q=10$ kN on the whole deck span;  $q'=10$ kN on half the deck span and  $q''=5$ kN/m on the exterior half of the deck's cross-section along the whole bridge span. (a) Axial forces (b) Total bending moments (c) Torsional moments (d) Total displacements

#### 5. CONCLUSIONS

In the context of the present study, we can conclude:

- Non-planar arches with imposed curvature can be approximated by inclined planar arches with imposed curvature with the same rise, with an error for internal forces inferior to 1,3% for uniform distributed loading applied on the whole deck span and to 2% for uniform distributed loading applied on half the length of the deck span, in both cases for  $f/g \leq 1$ .
- There is a value for the out-of-plane arch rigidity for which the distribution of axial forces along the arch changes, tending to concentrate either at mid-span or at springings, and also a bound for which the internal forces and deflections converge. Increasing the balcony beam rigidity above this bound has no advantage at all.
- Given a vertical rise of the arch, and employing pinned hangers, the higher the plan curvature, the lower the axial forces and the higher the moments in the arch.
- To enhance the arch behaviour in an ID-ABWIC, employing a rigid hanger-deck system (a deck with high torsional rigidity and hangers with high transverse flexural rigidity) and an arch with low flexural rigidity is more efficient than increasing the rigidity of the arch. This 'ideal configuration' is the simplest way to make the arch tend toward its anti-funicular form.
- For ID-ABWIC with a large  $g/f$  ratio, the critical live load case is obtained when the uniform

#### IV. STRUCTURAL BEHAVIOUR OF INFERIOR-DECK SPATIAL ARCH BRIDGES WITH IMPOSED CURVATURE

distributed loading is applied on the whole deck span, whereas for a conventional vertical arch bridge ( $g=0$ ) the maximal arch shear forces, bending moments and deflections are higher for a uniform distributed loading applied on half the deck span.

- These conclusions are valid for a linear behaviour of ID-ABWIC.

#### 6. FUTURE LINES OF STUDY

- In a future research this study could be widened for more for more cross-sections, employing real cross-section values to quantify the improvement of increasing the stiffness.
- A parametrical relationship of the horizontal sag and the torsional and flexural stiffness of arch, hangers and deck could be found.
- The study of second hanger systems could be broadened. A comparison between model C and the bridge over the Galindo river would be interesting. In foresight of such a future study the same cross-sections as for the bridge over the Galindo have been employed.

#### REFERENCES

- BILLINGTON, D. P. "The Role of Science in Engineering." In *Robert Maillart's bridges. The art of engineering*. Princeton University Press. Princeton, New Jersey, 1979, pp. 94-105 and pp.111-112.
- BILLINGTON, D. P. *Robert Maillart. Builder, Designer, and Artist*. Cambridge University Press, 1997, pp. 146-149 and pp. 174-182.
- JORQUERA, J. J. (2007). "Study of the structural behaviour of spatial arch bridges", PhD Thesis. Supervised by Prof. Manterola, Technical University of Madrid (UPM), (in Spanish).
- JORQUERA, J. J. "Structural behaviour of spatial arch bridges", Proceedings of the International Association for Shell and Spatial Structures Symposium 2009, Evolution and Trends in Design, Analysis and Construction of Shell and Spatial Structures (Domingo, A., and Lázaro, C. (Eds)), Valencia, 2009, pp. 2447-2457.
- LAFFRANCHI, M. and MARTI, P. "Robert's Maillart's concrete arch bridges", *Journal of structural engineering*, 123(10), 1997. pp. 1280-1286.
- MANTEROLA, J., GIL, M. Á., and MUÑOZ-ROJAS, J., "Arch spatial Bridges over the Galindo and Bidasoa Rivers", *Structural Engineering International*, 21 (1). 2011, pp114-121
- O'CONNOR, C.. "Chapter 10: Arches." *Design of Bridges Superstructures*, John Wiley and Sons, New York, USA, 1971, pp88-544.
- SARMIENTO, M., RUIZ-TERAN, A. and APARICIO, A. C.. "Structural response of spatial arches with imposed Curvature." Proc., 34th Int. Symp. on Bridge and Structural Engineering, IABSE, Venice, Italy, 2010
- SARMIENTO-COMESÍAS, M., MPhil-PhD Transfer report. Jointly supervised by A. C. Aparicio and A. Ruiz-Teran, Technical University of Catalonia (UPC), Barcelona, Spain 2009 (in Spanish)
- SCHLAICH, J., and MOSCHNER, T.. "Die Ripshorster Brücke über den Rhein-Herne-Kanal, Oberhausen", *Bautechnik*, 6(76), 1999, pp459-462

**Notation**

$\alpha$  angle formed by the plane which contains the arch and the vertical hangers

$\delta_1$  arch displacement in the arch plane on a simplified hanger with springs model (direction of the model spring  $K_1$ )

$\delta_2$  arch displacement perpendicular to the arch plane on a simplified hanger with springs model (direction of the model spring  $K_2$ )

$\delta_A$  total arch displacement on a simplified hanger with springs model

$\delta_D$  vertical displacement of the deck on a simplified hanger with springs model

$f$  arch vertical rise

$F_1$  load taken by the arch as inclined arch on a simplified hanger with springs model

$F_2$  load taken by the arch as balcony beam on a simplified hanger with springs model

$F_3$  load taken by the deck on a simplified hanger with springs model

$F_H$  load taken by the hanger on a simplified hanger with springs model

$g$  horizontal sag of the arch and deck

$L$  span of the arch bridge (straight line measure between springings)

$L_A$  whole arch length

$L_D$  whole deck length

$K_1$  axial stiffness of the inclined arch on a simplified hanger with springs model

$K_2$  balcony beam stiffness of the arch on a simplified hanger with springs model

$K_3$  vertical stiffness of the deck on a simplified hanger with springs model

$I_2$  balcony beam rigidity

$u_2$  balcony beam displacements of the arch

$u_3$  axial shortage of the arch

$u$  total displacements of the arch  $\equiv u = \sqrt{u_2^2 + u_3^2}$

$u_C$  total displacements of the arch span centre

$M_{2,2}$  out of plane bending moments of the arch (balcony beam bending moments)

$M_{3,3}$  in plane bending moments of the arch

$M$  total bending moments of the arch

Abbreviations

ID-ABWIC inferior-deck arch bridges with imposed curvature

# V. SPATIAL ARCH BRIDGES WITH A SUPERIOR DECK



V. A) GEOMETRY AND BEARING  
CONDITIONS STUDY OF SPATIAL ARCH  
BRIDGES WITH A SUPERIOR DECK





## INDEX

1. INTRODUCTION.....	115
1.1 Objectives.....	115
1.2 Research procedure and values .....	116
1.3 Load cases and internal forces nomenclature.....	119
2. STRUCTURAL BEHAVIOUR. ANALYSIS OF RESULTS .....	119
2.1 Structural response. Internal forces.....	119
2.2 Efficiency of the system.....	127
3. CONCLUSIONS.....	129
REFERENCES.....	130



## 1. INTRODUCTION

This chapter is a broadened and further detailed version of the paper published in IABSE-IASS London Symposium in 2011 by the present author and her supervisors (Sarmiento-Comesías et al, 2011).

The main principles of behaviour studied for ID-ABWIC (inferior-deck arch bridges with imposed curvature; chapter IV) give a clear idea of how a SD-ABWIC (superior deck ABWIC) will behave. However, the imposed curvature idea in relationship with the minimum free height for users has lost its sense, since the arch is underneath and implies no determinants for users. For superior deck spatial arch bridges (SD-SAB) geometry is completely free as far as the use of the structure regards. Moreover, the struts will be necessarily rigid in this bridge type and their connection with the arch and deck will be very important for the bridge behaviour and the horizontal forces transmitted to the ground.

Different geometries of spatial arch bridges with superior deck are studied in the present chapter. Their response under vertical loads and temperature variations is analysed and different geometrical and bearing configurations at deck abutments are studied.

Extreme values for the curvature of the arch in plan have been adopted. They should not be regarded as realistic bridge designs but as theoretical examples, which have the objective to draw conclusions of the bridge behavior. This will be useful for the design of SABs within the range of the extreme geometries employed in this study.

The study of the deck's boundary conditions will prove to be essential. The main objective is to determine whether it is advisable to restrain the longitudinal movements or not. A priori, we might think that, on the one hand, restraining them will be the most suitable approach to resist seism, for instance. On the other hand, for conventional vertical planar arch bridges it is common knowledge that free longitudinal movements reduce internal forces due to temperature increments.

These studies have led to interesting conclusions for boundary conditions and have helped to gain a deeper understanding of the most adequate geometries for different cases.

### 1.1 Objectives

The main objectives of the present chapter are to study:

- the global structural behaviour of different geometries of spatial arch bridges with superior deck under a vertical uniform loading and a temperature increment. The aim is to decide which bridge geometries help to improve the structural behaviour of these bridges.
- the suitability of different boundary conditions for the different bridge geometries under the considered loading cases.

## 1.2 Research procedure and values

In order to understand the behaviour of these arches, different frame 3D models have been developed and analyzed, as part of a set of thorough parametric analyses (parameter nomenclature in Figure 1-1). A linear analysis of frame 3D FE models for each case study has been performed and analysed with SAP2000.

The different studied bridge geometries are defined in Figure 1-2. The values of the parameters (Figure 1-1) which have been employed are the following: a span ( $L$ ) of a 100m and a vertical rise of the arch:  $f = L/5 = 20\text{m}$  (usual value for arch bridges contained in a vertical plane (C. O'Connor 1971)).

The deck and arch plan curvature are measured as horizontal sag ( $g_D$  and  $g_A$ , respectively). Their value is 0 or 20m, as stated for each geometry.

The material employed is steel with a  $2,0 \cdot 10^8 \text{ kN/m}^2$  modulus of elasticity ( $E$ ).

In general, the struts are completely fixed to arch and deck.

In the figures the whole arch longitude will be named  $L_A$  and the deck's one  $L_D$ , whereas we should note that these values are different from the span so-called  $L$ .

On the following figures (Figure 1-2(a) to (e)) the different studied geometries are shown.

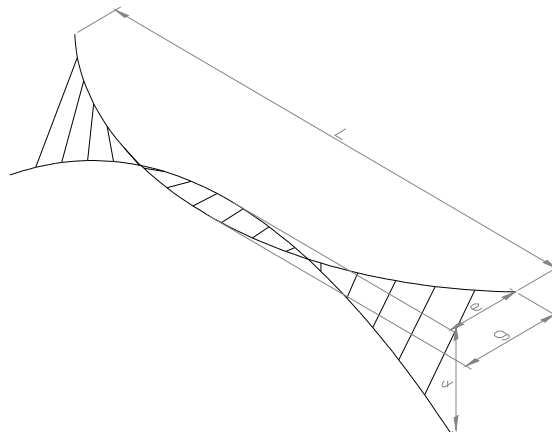
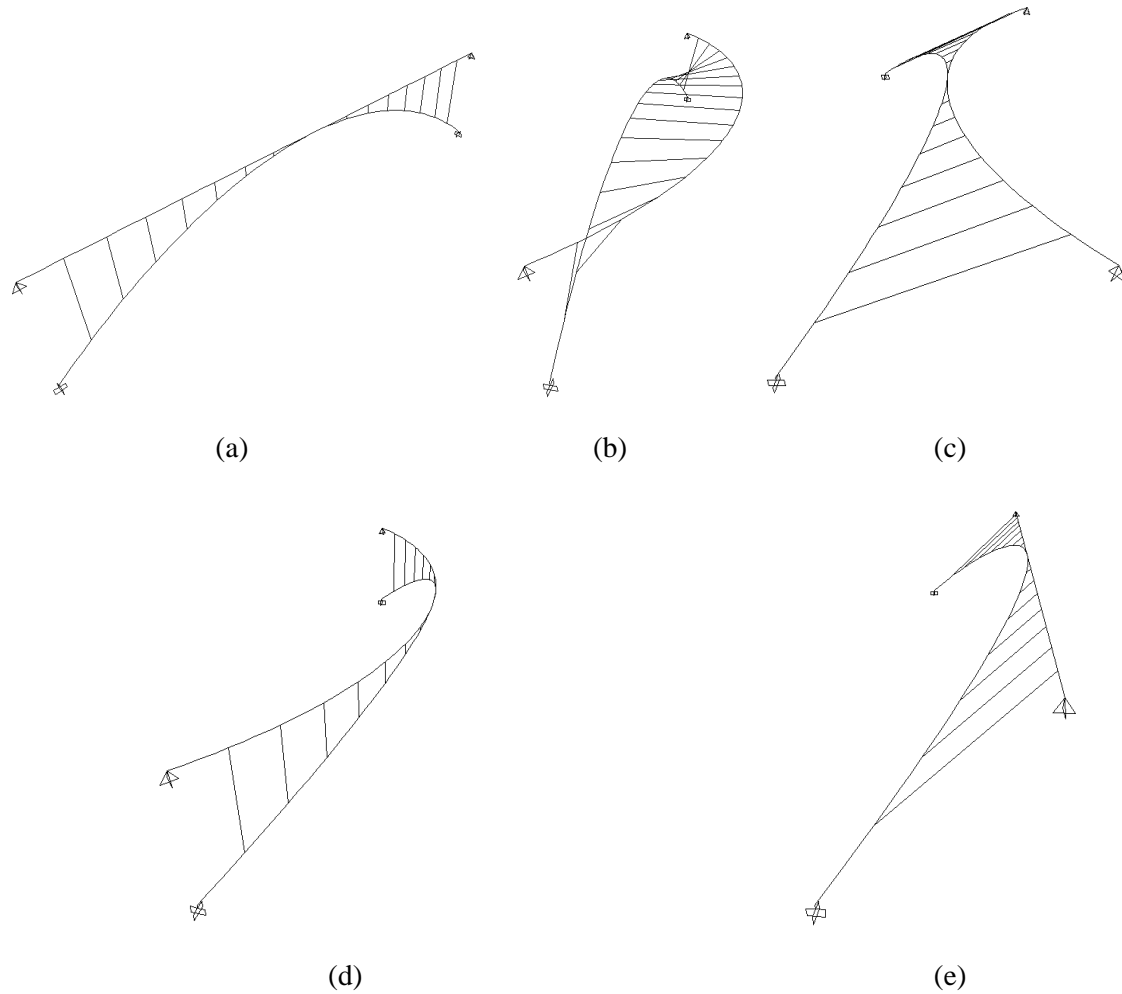


Figure 1-1: Variable Nomenclature



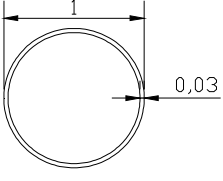
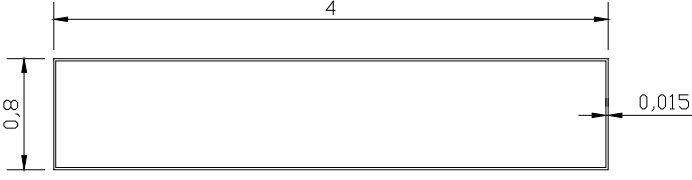
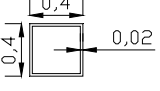
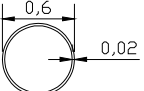
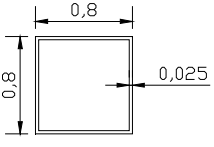
**Figure 1-2: Studied bridge geometries. (a) Vertical planar arch bridge with superior straight deck (reference model); (b) Vertical planar arch with superior curved deck; (c) Arch and deck with symmetrical curvature in plan; (d) Arch and deck with coincident curvature in plan (imposed curvature); (e) Arch curved in plan with superior straight deck (both contained in the same plane)**

Those bridge geometries have been studied for different hypothesis of the boundary conditions of the deck at its ends. The deck is pinned at abutments (ie: the bending moments at both support sections are released), the radial displacements are restrained and tangential longitudinal displacements might be free or restrained, as indicated for each case:

- Longitudinal displacements (ie: tangential to the curve in plan) may be free or restrained (*f.l.d.* or *r.l.d.*).
- The twisting rotation may be free or restrained (*f.t.r.* or *r.t.r.*).

In every case study the arch springings are fixed and the struts are fixed to both arch and deck.

The effect of the strut rigidity variation has been studied. The employed sections are displayed in Table 1-1:

	Model 1	Model 2	Model 3
ARCH			
DECK			
STRUTS			

**Table 1-1: Cross-sections for different models**

In the study for ID-ABWIC (chapter IV) we have concluded that the maximal axial force on the deck is reached for struts with the transverse moment ( $M_{2,2}$ ) released at arch. The minimal deck axial force values correspond to struts pinned at both ends. We can extend this conclusion to the strut joints of superior deck spatial arch bridges.

Fixed strut/deck and strut/arch joints have been employed. The different models are studied for both cases with its displacements fixed in all directions and allowing free longitudinal movements of the deck at abutments in two load cases: under a vertical uniform load on the deck and a temperature variation.

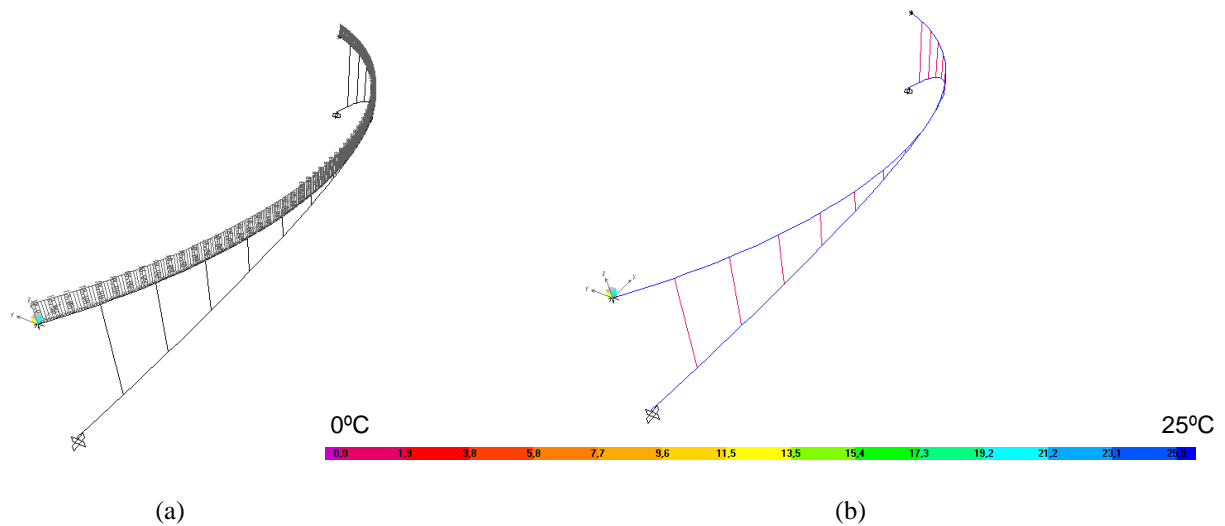
The arch is defined like a bent parabolic arch bridge (chapter IV). The spatial configuration has been considered with no simplifications for the frame model analysis. When analysing the results we will refer to in-plane and out-of-plane forces, although the arch is not contained in a plane, since, as concluded in chapter IV, non-planar arches can be approximated to inclined planar arches. The plane considered for analysing the results of its behaviour is an approximation plane given by three points: arch springings and arch span center.

### 1.3 Load cases and internal forces nomenclature

A linear analysis of frame 3D FE models for each case study has been performed and analysed with SAP2000.

The following loading cases have been studied:

- A vertical uniform loading on the whole deck span of 10kN/m (Figure 1-3a)
- A temperature increment of 25°C on arch, deck and both (Figure 1-3b)



**Figure 1-3: Analysed load cases. (a) vertical uniform loading on the whole deck span of 10kN/m (b) temperature increment of 25°C on both, arch and deck**

We will be referring to the bending moments M2-2 and M3-3 and the displacements  $u_1$ ,  $u_2$  y  $u_3$ , which, according to the employed local axes, are defined as the following:

- M2-2: bending moments with vertical axis in the deck and balcony-beam bending moments in the arch (ie: out of plane bending moments).
- M3-3: balcony-beam bending moments in the deck and in-plane bending moments in the arch.
- $u_1$  are the displacements which are tangential to the deck curve in plan,  $u_2$ , the radial ones and  $u_3$ , the vertical deflections.

## 2. STRUCTURAL BEHAVIOUR. ANALYSIS OF RESULTS

### 2.1 Structural response. Internal forces

In this section, figures of some of the diagrams of internal forces for model (c) are shown with the values for different deck boundary conditions (from Figure 2-1 to Figure 2-9), as a summary of the main results.

Next, comparative figures of the distribution of axial forces and total bending moments for the different bridge geometries and boundary conditions under the vertical uniform loading are shown (Figure 2-10 and Figure 2-11). Please refer to section 1.2 or employ the bookmark for the deck abutments boundary conditions nomenclature employed in the figures.

In the annex N3 all the figures of the structural behaviour of the models from (a) to (d) are detailed.

An extensive analysis of the internal forces and the influence of the struts is conducted in annex N3. This analysis has helped to understand the behavior of the different bridge geometries studied in this chapter. The main conclusions are summarized in section 3.

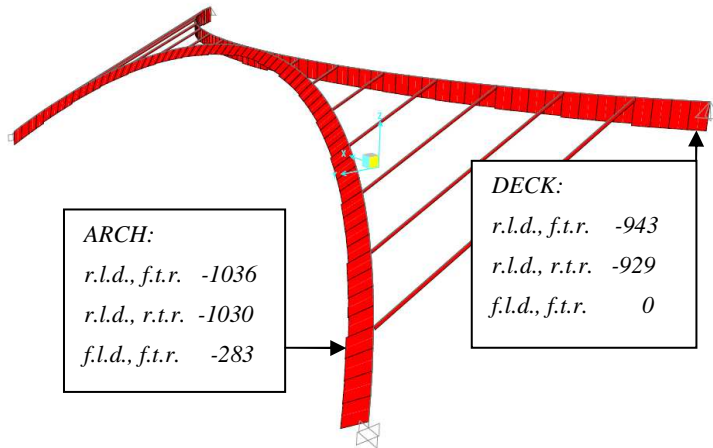


Figure 2-1: Axial forces (in kN, compressions  $N < 0$ ) of model (c) for different boundary conditions, under a vertical deck loading  $q=10\text{kN/m}$ . The diagram employed to show the values is the r.l.d. and f.t.r. case.

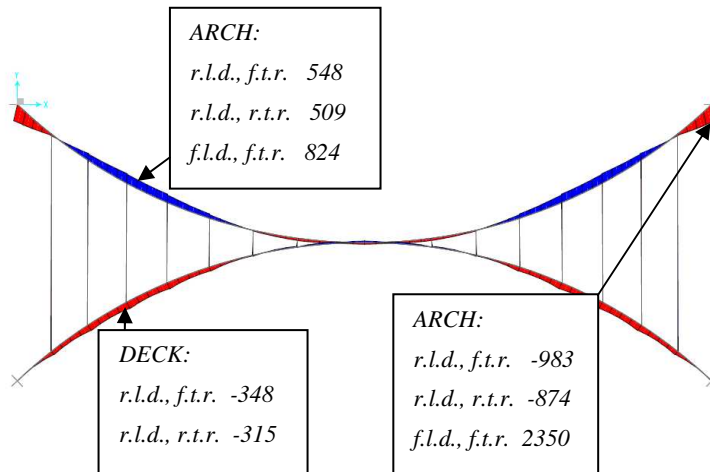


Figure 2-2: M2-2 bending moments (in  $\text{kN}\cdot\text{m}$ ) of model (c) for different boundary conditions of the deck abutments, under a vertical deck loading  $q=10\text{kN/m}$ . The diagram employed to show the values is plotted for the restrained longitudinal displacements (r.l.d.) and free twisting rotations (f.t.r.) case.



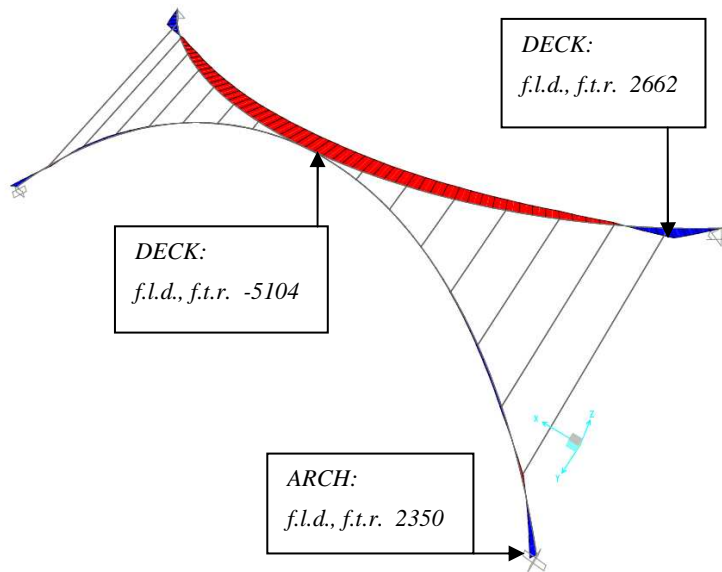


Figure 2-3: M2-2 bending moments (in kN·m) of model (c) for different boundary conditions of the deck abutments, under a vertical deck loading  $q=10\text{kN/m}$ . The diagram employed to show the values is plotted for the free longitudinal displacements (f.l.d.) and free twisting rotations (f.t.r.) case.

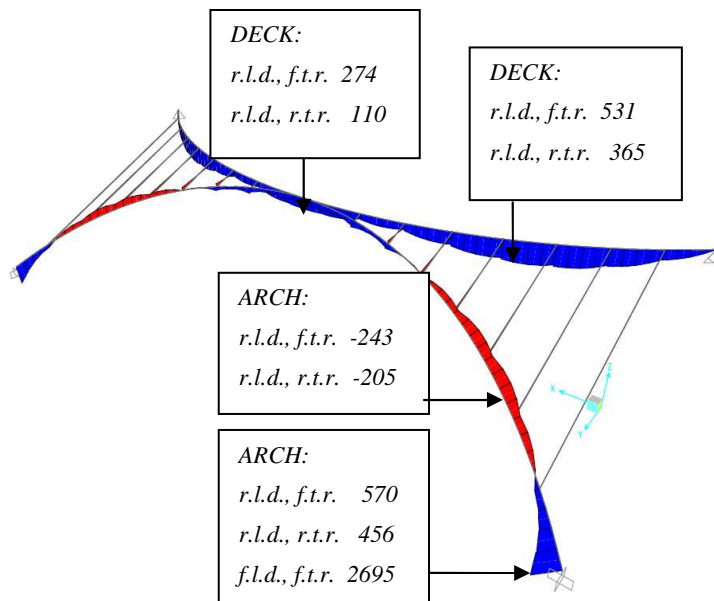


Figure 2-4: M3-3 bending moments (in kN·m) of model (c) for different boundary conditions of the deck abutments, under a vertical deck loading  $q=10\text{kN/m}$ . The diagram employed to show the values is the r.l.d. and f.t.r. case.

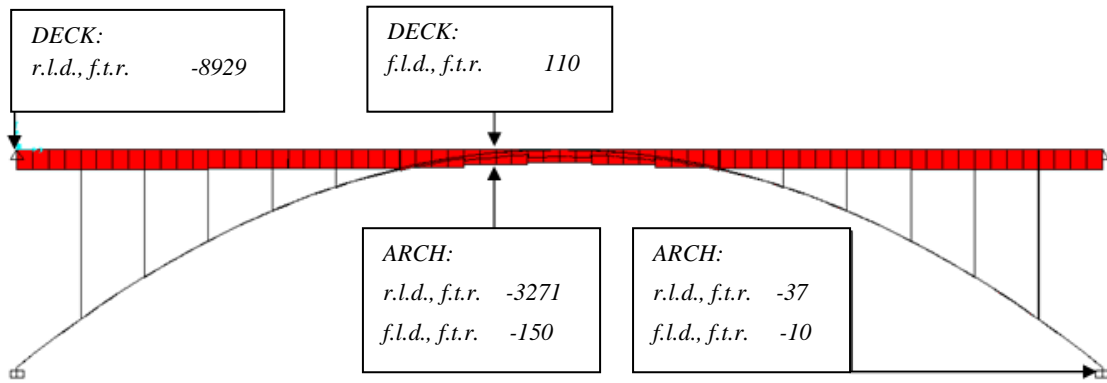


Figure 2-5: Axial forces (in kN, compressions  $N < 0$ ) of model (a) for different boundary conditions of the deck abutments, under a  $\Delta T = 25^\circ\text{C}$  at both arch and deck. The diagram employed to show the values is the r.l.d. and f.t.r. case.

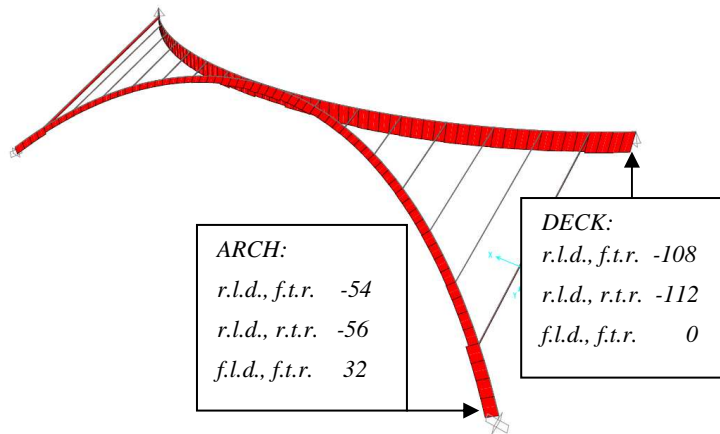


Figure 2-6: Axial forces (in kN, compressions  $N < 0$ ) of model (c) for different boundary conditions of the deck abutments, under a  $\Delta T = 25^\circ\text{C}$  at both arch and deck. The diagram employed to show the values is the r.l.d. and f.t.r. case. (As a reference value the axial force in the deck ends for model (a) with r.l.d. is -8927 kN)

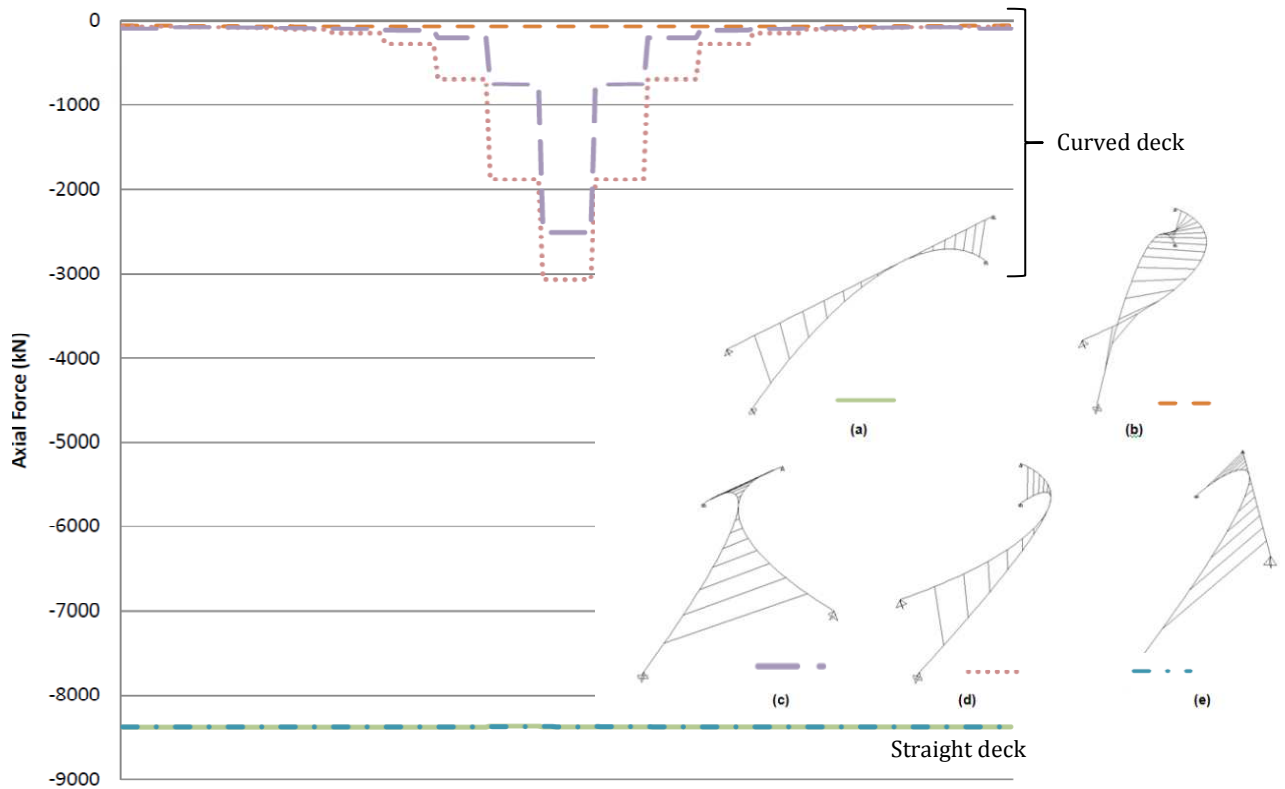


Figure 2-7: Arch axial forces comparison (in kN, compressions  $N < 0$ ) for the different models with restrained longitudinal displacements at the deck abutments, under a  $\Delta T = 25^\circ C$  at both arch and deck. The abscissas are the arch length from 0 to  $L_A$

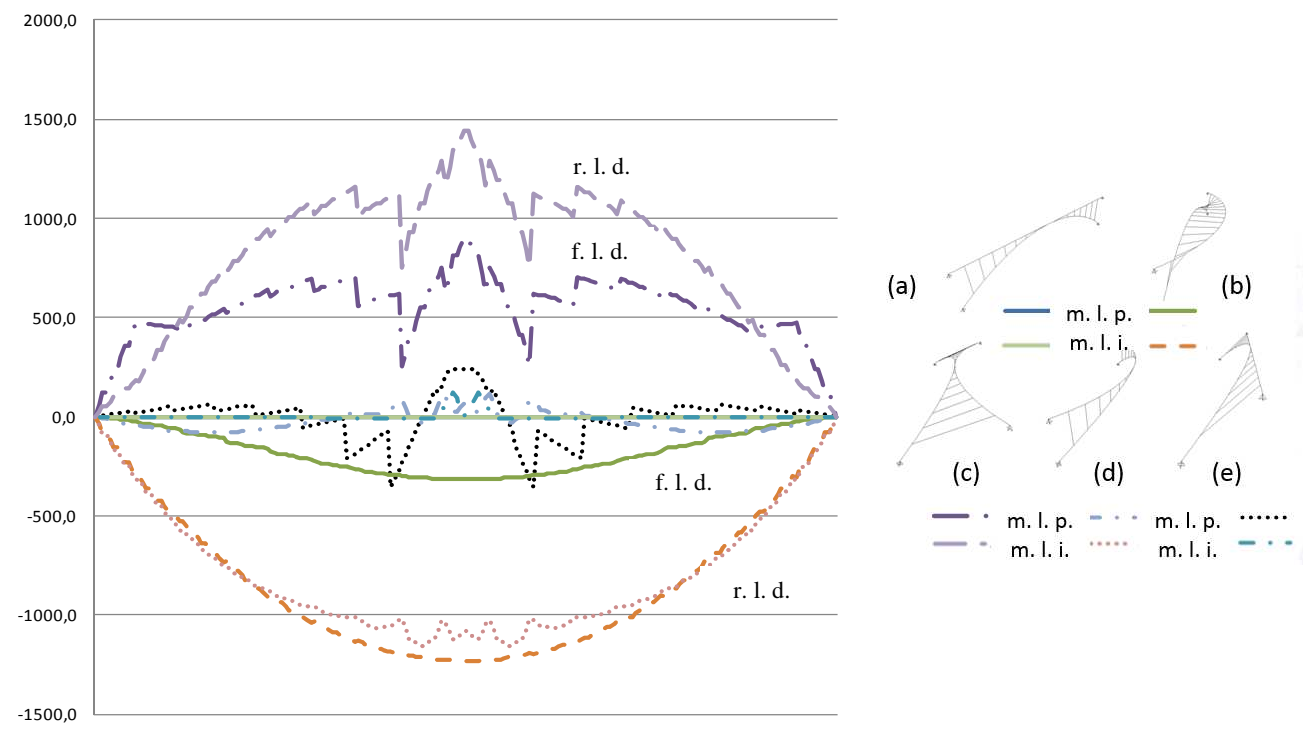


Figure 2-8: Arch M2-2 bending moments comparison (in  $kN \cdot m$ ) for the different models with restrained longitudinal displacements at the deck abutments, under a  $\Delta T = 25^\circ C$  at both arch and deck. The abscissas are the arch length from 0 to  $L_A$

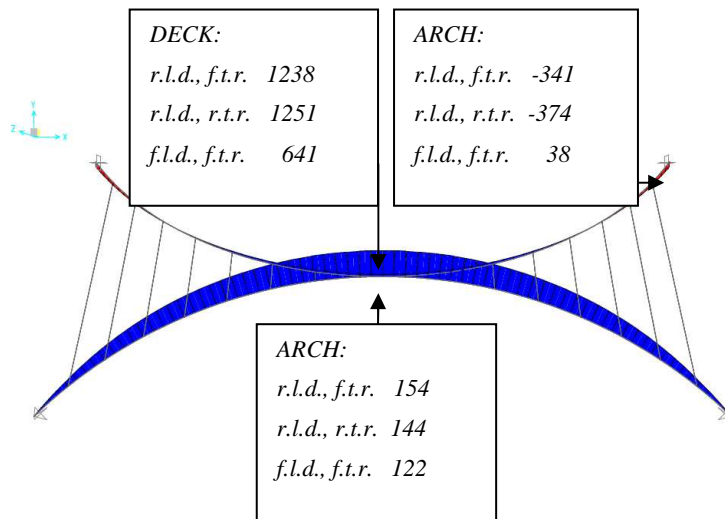


Figure 2-9: M2-2 bending moments (in kN·m) of model (c) for different boundary conditions of the deck abutments, under a  $\Delta T=25^{\circ}\text{C}$  at both arch and deck. The diagram employed to show the values is plotted for the restrained longitudinal displacements (r.l.d.) and free twisting rotations (f.t.r.) case.

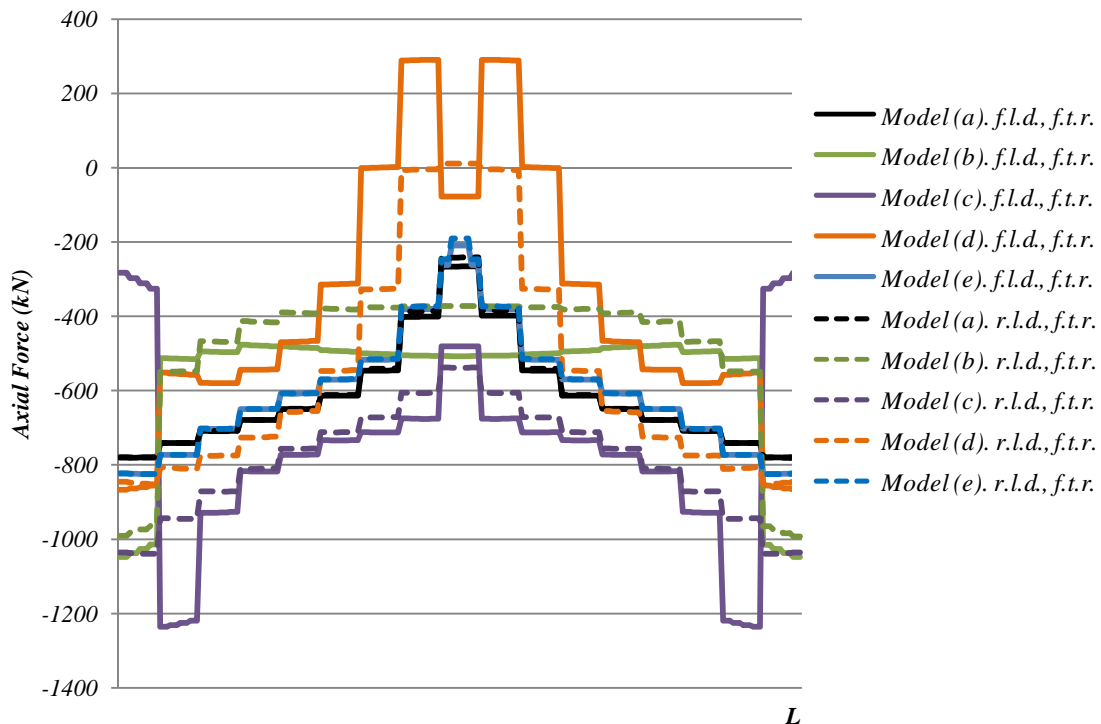


Figure 2-10: Comparative diagram of the arch axial forces (in kN, compressions  $N < 0$ ) of the different geometries and the different boundary conditions at the deck abutments, under a vertical deck loading  $q=10\text{kN/m}$ . The abscissas are the arch length from 0 to  $L_A$

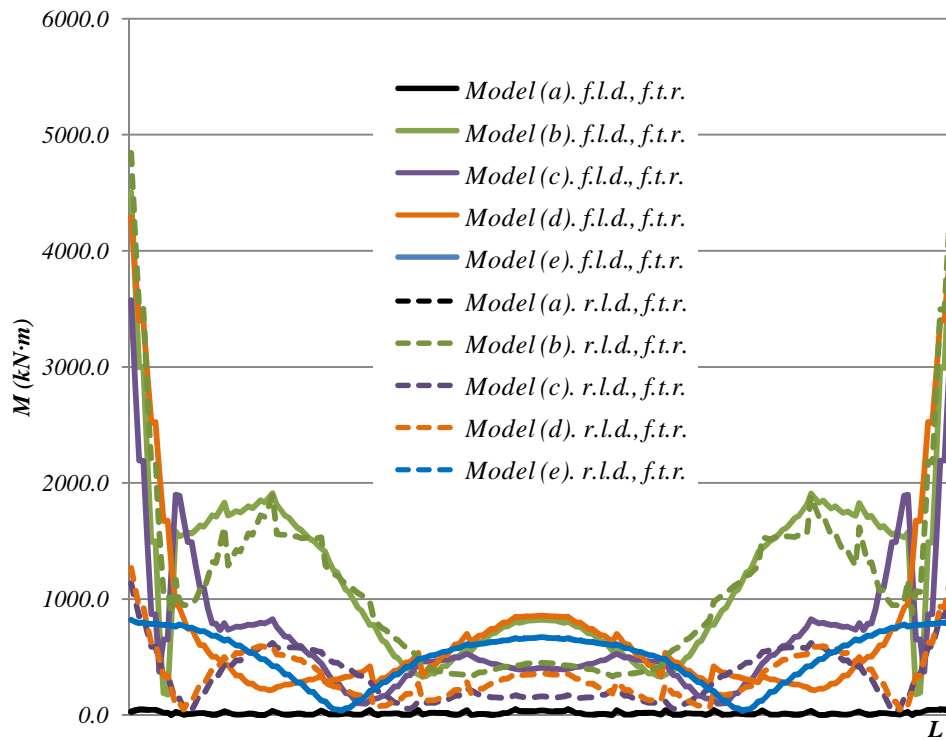


Figure 2-11: Comparative diagram of arch total bending moments ( $M = \sqrt{M_{22}^2 + M_{33}^2}$ , in kN·m) of the different bridge geometries and the different boundary conditions at the deck abutments, under a vertical deck loading  $q=10\text{kN/m}$ . The abscissas are the arch length from 0 to  $L_A$

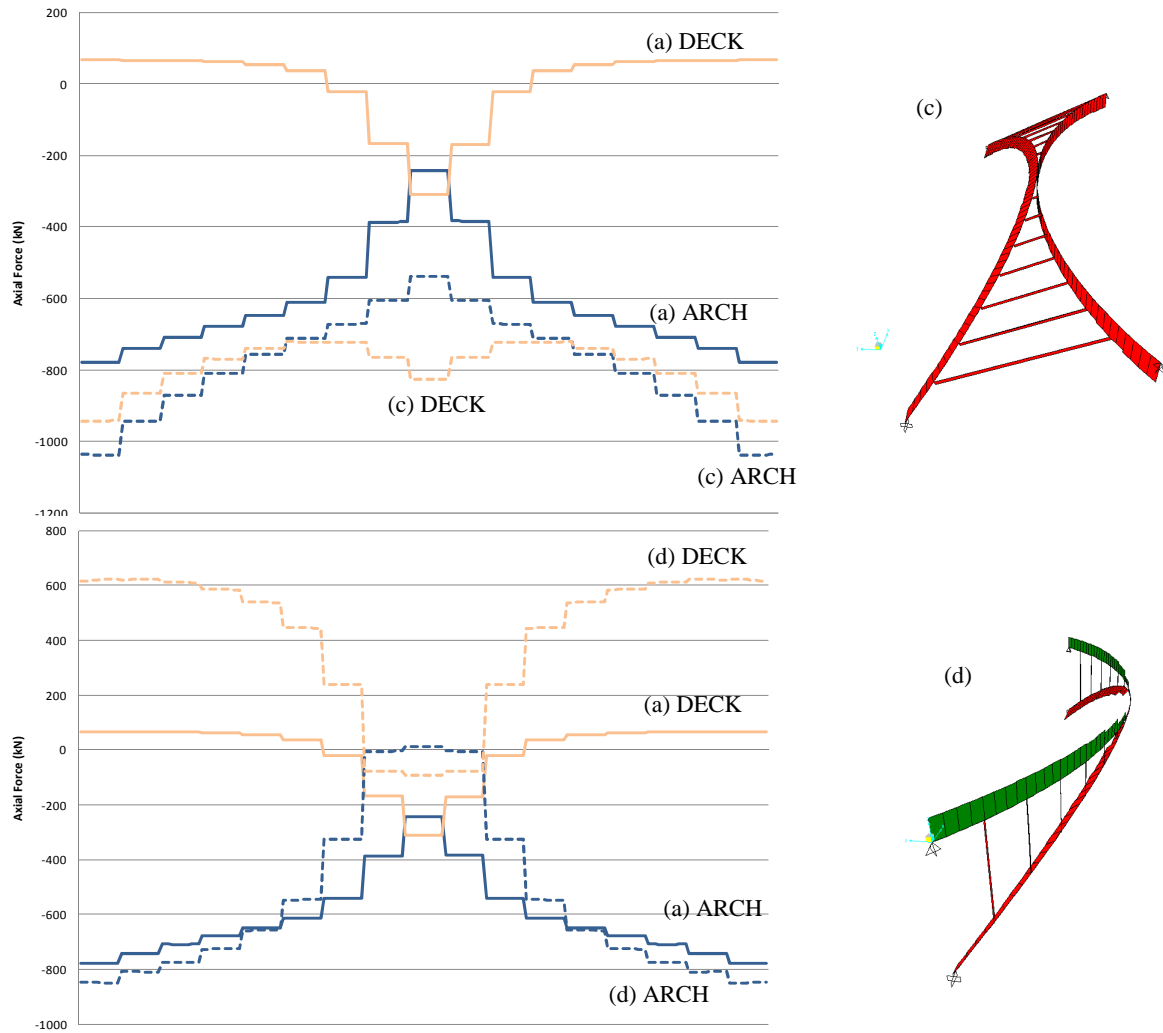


Figure 2-12: Comparative diagram of the axial forces (in kN, compressions  $N < 0$ ) of model (a) with models (c) and (d) with r.l.d. at the deck abutments, under a vertical deck loading  $q = 10 \text{ kN/m}$ . The abscissas are the bridge length from 0 to  $L$

Considering, on the one hand, the relevance of the arch and deck interaction when employing struts fixed to both arch and deck, and, on the other hand, the deck curvature, the structural behaviour of the studied bridges is characterized by the following facts:

- When the deck is curved in plan the axial forces caused by temperature increments diminish drastically (from Figure 2-5 to Figure 2-7) with respect to a conventional arch bridge with a straight deck.
- Significant bending moments with vertical axis appear in the deck (Figure 2-2, Figure 2-3, Figure 2-8 and Figure 2-9)
- The arch helps the deck to resist the balcony beam components of the forces.

## 2.2 Efficiency of the system

The quantification of the contribution of the arch with the deck to resist M3-3 bending moments, can be formulated as follows (Eqs. 1 to 4):

$$X = \frac{M_{DECK}}{M_{ISOST}} \quad (\text{Figure 2-13}) \quad (1)$$

$$\text{Total moment of the deck} \equiv M_{DECK} = \frac{-(M_{negleft} + M_{negright})}{2} + M_{pos} \quad (2)$$

$$\text{Isostatic moment} \equiv M_{ISOST} = \frac{q \cdot L_{DECK}^2}{8} \quad (3)$$

$$X' = 1 - X \quad (4)$$

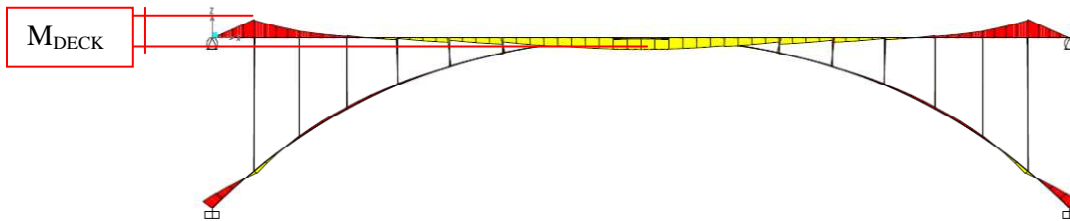


Figure 2-13:  $M_{DECK}$  definition

<i>Model</i>	<i>q</i> <i>kN/m</i>	<i>L<sub>DECK</sub></i> <i>m</i>	<i>M<sub>isost</sub></i> <i>kN·m</i>	<i>M<sub>neg</sub></i> <i>kN·m</i>	<i>M<sub>pos</sub></i> <i>kN·m</i>	<i>M<sub>syst</sub></i> <i>kN·m</i>	<i>X</i>	<i>X'</i>
(a) <i>r.l.d.</i>	10	100	12500	-51	61	112	0,009	0,99
(a) <i>f.l.d.</i>	10	100	12500	-49	59	108	0,009	0,99
(b) <i>r.l.d.</i>	10	110,4	15221	-3846	1817	5663	0,372	0,63
(b) <i>f.l.d.</i>	10	110,4	15221	-4522	1963	6485	0,426	0,57
(c) <i>r.l.d.</i>	10	110,4	15221	0	531	531	0,035	0,97
(c) <i>f.l.d.</i>	10	110,4	15221	0	2933	2933	0,193	0,81
(d) <i>r.l.d.</i>	10	110,4	15221	0	636	636	0,042	0,96
(d) <i>f.l.d.</i>	10	110,4	15221	-2133	1317	3449	0,227	0,77
(e) <i>r.l.d.</i>	10	100	12500	0	948	948	0,076	0,92
(e) <i>f.l.d.</i>	10	100	12500	0	947	948	0,076	0,92

**Table 2-1: System efficiency. Results for the vertical loading (q)**

The coefficient X (Eq 1) relates the sum of the maximal negative and maximal positive bending moments in the deck (Eq 2) with the isostatic moment that the same load would generate in a simply supported deck with an equivalent span (Eq 3).

The efficiency of the system is measured by X' (Eq 4). This value varies for the different bridge geometries and boundary conditions of the studied spatial arch bridges (Table 1) from 0,57 (model (b) with the longitudinal displacements released at the deck abutments (*f.l.d.*)) to 0,97 (model (c) with the longitudinal displacements restrained at the deck abutments (*r.l.d.*)).

The arch vertical efficiency index (X') leads to the following conclusions:

- The highest efficiency is obtained for decks with restrained longitudinal displacements at the deck abutments.
- The bridge geometries with a highest efficiency are (c) and (d).



### 3. CONCLUSIONS

From the analyses of the results of the studied cases, the following conclusions can be inferred:

- The highest total ( $M = \sqrt{M_{22}^2 + M_{33}^2}$ ) and out of plane (M2-2) bending moments in L/4 of the arch and in the arch springings under a vertical uniform loading are obtained for model (b). M3-3 bending moments are very high too (about fifty times larger than for model (a) in the deck and a hundred times in the arch).
- The highest total and out of plane bending moments in the mid-span of the arch under a vertical uniform loading are obtained for model (e).
- Models (c) and (d) show the best structural behaviour.
- Models (c) and (d) show a good structural behaviour only if the longitudinal displacements of the deck abutments are restrained (from Figure 2-1 to Figure 2-9).
- Model (b) is highly influenced by two parameters: (1) the arch/deck eccentricity in plan view (e) and (2) the vertical distance between the arch crown and the deck mid-span (v). A parametrical study of e and v has been done and the results will be commented in the following section V. B of the present chapter V.
- Spatial arch bridges have an improved structural behaviour under temperature increments with respect to conventional vertical arch bridges (model (a)) when restraining the longitudinal displacements of the deck abutments. Axial forces in the deck decrease, *e.g.*: for model (c) with r.l.d. the axial forces in the deck are nearly a hundred times smaller than those for model (a) (Figure 2-6). In exchange, significant M2-2 bending moments appear in the deck, but they are resisted by the deck's width, which is its highest dimension.
- For models with a curved deck (models (b), (c) and (d)), it is convenient to restrain longitudinal displacements of the deck abutments under both vertical loadings (Figure 2-10 and Figure 2-11) and temperature increments. This is a very important difference with conventional vertical arch bridges.
- For models with a straight deck (models (a) and (d)) it is obviously better to release longitudinal displacements of the deck abutments under temperature increments.
- In general, the restriction of the twisting rotations at the support sections on the abutments does not have a significant impact on the structural response

## REFERENCES

BILLINGTON D. P., “The Role of Science in Engineering.” *Robert Maillart’s Bridges. The Art of Engineering*. Princeton University Press. New Jersey, 1979, pp. 94-105 and 111-112.

JORQUERA J. J., *Study of the Structural Behaviour of Spatial Arch Bridges*, PhD Thesis. Supervised by Prof. Manterola, Technical University of Madrid (UPM), 2007 (in Spanish).

JORQUERA J. J., “Structural Behaviour of Spatial Arch Bridges”, *Proceedings of the IASS Symposium 2009, Evolution and Trends in Design, Analysis and Construction of Shell and Spatial Structures* (Domingo, A., and Lázaro, C. (Eds)), Valencia, 2009, pp. 2447-2457.

SARMIENTO-COMESÍAS, M., RUIZ-TERAN, A. AND APARICIO, A. C.. “Superior deck spatial arch bridges.” *Proceedings of the 35th International Symposium on Bridge and Structural Engineering, jointly organised by IABSE-IASS: ‘Taller, Longer, Lighter’*, London, UK, September 20-23, 2011

V. B) PARAMETRICAL STUDY OF  
SPATIAL ARCH BRIDGES WITH A  
CURVED SUPERIOR DECK AND A  
PLANAR VERTICAL ARCH



## INDEX

1. INTRODUCTION.....	137
1.1 PREVIOUS STUDIES .....	137
1.2 STUDIED PARAMETERS.....	138
1.3 TYPES AND SELECTION OF EFFICIENCY CRITERIA .....	139
1.4 OBJECTIVES .....	141
1.5 LOADING CASES AND COMBINATIONS .....	142
1.5.1 <b>Loading cases for analysing the structural behaviour</b> .....	142
1.5.2 <b>Loading cases for stresses in ULS and displacements in SLS</b> .....	142
1.5.3 <b>Loading combinations for stresses in ULS and displacements in SLS</b> .....	142
1.6 RESEARCH PROCEDURE AND VALUES .....	143
2. PARAMETRICAL STUDY OF THE ARCH/DECK ECCENTRICITY IN PLAN VIEW ( $e$ ) AND THE SYSTEM STIFFNESS DISTRIBUTION.....	146
2.1 DEFINITION AND EMPLOYED VALUES .....	146
2.2 STRUCTURAL RESPONSE UNDER A UNIFORMLY DISTRIBUTED VERTICAL LOAD 150	
2.2.1 <b>Structural response of varying <math>e</math> for different <math>g</math> values</b> .....	150
2.2.2 <b>Relationship between the value of <math>e</math> and the out-of-plane shape of the arch</b> .....	155
2.2.3 <b>Structural response of varying <math>e</math> for different <math>f</math> values</b> .....	155
2.2.4 <b>Relationship between the value of <math>e</math> and the distribution of stiffness in the system</b> 159	
2.3 STRESS BEHAVIOUR AND COMPARISON IN ULTIMATE LIMIT STATE....	162
2.4 EFFICIENCY CRITERIA.....	165
2.5 PARAMETER DISCUSSION .....	177
3. VERTICAL DISTANCE BETWEEN THE ARCH CROWN AND THE DECK MID-SPAN ( $v$ ) PARAMETRICAL STUDY .....	179
3.1 DEFINITION AND EMPLOYED VALUES .....	179
3.2 STRUCTURAL RESPONSE UNDER A UNIFORM VERTICAL LOAD ( $lu$ ) .....	179
3.3 STRESS BEHAVIOUR COMPARISON UNDER A UNIFORM LOADING $q$ AND DESIGN IN ULTIMATE LIMIT STATE .....	184
3.4 EFFICIENCY CRITERIA.....	187
3.5 PARAMETER DISCUSSION .....	190
4. ARCH RISE ( $f$ ) PARAMETRICAL STUDY .....	190
4.1 DEFINITION AND EMPLOYED VALUES .....	190
4.2 STRUCTURAL RESPONSE UNDER A UNIFORM VERTICAL LOAD ( $lu$ ) .....	191

4.3	STRESS BEHAVIOUR UNDER $q$ AND DESIGN AND COMPARISON IN ULTIMATE LIMIT STATE.....	202
4.4	EFFICIENCY CRITERIA .....	207
4.5	PARAMETER DISCUSSION.....	212
5.	INCLINATION OF STRUTS ( $\beta$ ) PARAMETRICAL STUDY.....	213
5.1	DEFINITION AND EMPLOYED VALUES.....	213
5.1.1	<b>Employed values</b> .....	213
5.1.2	<b>Previous studies</b> .....	214
5.2	STRUCTURAL RESPONSE UNDER A UNIFORM VERTICAL LOAD ( $lu$ ).....	214
5.3	STRESS BEHAVIOUR UNDER $q$ AND DESIGN AND COMPARISON IN ULTIMATE LIMIT STATE.....	219
5.4	EFFICIENCY CRITERIA .....	219
5.5	PARAMETER DISCUSSION.....	223
6.	DECK HEIGHT ( $z$ ) PARAMETRICAL STUDY .....	223
6.1	DEFINITION AND EMPLOYED VALUES.....	223
6.2	STRUCTURAL RESPONSE UNDER A UNIFORM VERTICAL LOAD ( $lu$ ).....	225
6.2.1	<b>Arch internal forces (Figure 6-3 to Figure 6-9)</b> .....	225
6.2.2	<b>Deck internal forces (Figure 6-10 to Figure 6-20)</b> .....	226
6.2.3	<b>Arch displacements (Figure 6-14 to Figure 6-16)</b> .....	226
6.2.4	<b>Deck displacements (Figure 6-17 to Figure 6-18)</b> .....	226
6.3	STRESS BEHAVIOUR UNDER $q$ AND DESIGN AND COMPARISON IN ULTIMATE LIMIT STATE.....	235
6.3.1	<b>Stresses behaviour under a uniform load <math>q=10\text{kN/m}</math></b> .....	235
6.3.2	<b>Critical loading combinations in ULS</b> .....	236
6.4	EFFICIENCY CRITERIA .....	237
6.5	PARAMETER DISCUSSION.....	239
7.	NON-VERTICAL ARCHES. ARCH IN PLAN SAG ( $g_A$ ) PARAMETRICAL STUDY.....	240
7.1	DEFINITION AND EMPLOYED VALUES.....	240
7.2	STRUCTURAL RESPONSE UNDER A UNIFORM VERTICAL LOAD ( $lu$ ).....	241
7.2.1	<b>Arch internal forces (Figure 7-2 to Figure 7-6)</b> .....	241
7.2.2	<b>Deck and struts internal forces (Figure 7-7 to Figure 7-10)</b> .....	241
7.2.3	<b>Arch displacements (Figure 7-11)</b> .....	241
7.3	STRESS BEHAVIOUR UNDER $q$ AND DESIGN AND COMPARISON IN ULTIMATE LIMIT STATE.....	247
7.3.1	<b>Stresses behaviour under a uniform load <math>q=10\text{kN/m}</math></b> .....	247
7.3.2	<b>Critical loading combinations in ULS</b> .....	247
7.4	EFFICIENCY CRITERIA .....	250

7.5	PARAMETER DISCUSSION .....	252
8.	CONCLUSIONS .....	253
8.1	Parameter conclusions .....	253
8.2	Efficiency criteria conclusions .....	255
8.3	Critical loading combinations conclusions.....	256
9.	FUTURE LINES OF STUDY .....	257
	REFERENCES .....	258





## 1. INTRODUCTION

A summary of the study presented in this chapter is in process of publication in Sarmiento-Comesías et al (2014) and a summary of the research study of one of the parameters was published in Sarmiento-Comesías et al (2013).

The thesis includes a bookmark which has the objective to help to read the present chapter by summarizing the different parameters and efficiency criteria employed in the present research and detailed in sections 0 and 1.6.

### 1.1 PREVIOUS STUDIES

According to the previous chapter V.A and the published paper Sarmiento-Comesías et al (2011) models with an arch curved in plan show the best structural behaviour to support a superior curved deck. However, it is suggested to study the improvement of this bridge type for the following reasons:

- The geometry is intermediate to the models that have shown the best behaviour, since the vertical plane is the symmetry plane for opposite sign curvatures arches. This leads to think that
- by studying how it is influenced by arch/deck eccentricity the behaviour could be greatly improved.
- The arch is vertical and planar. This simplifies project geometry and construction.

Previous studies:

- Laffranchi and Marti (1997) describe four projects of Robert Maillart which are spatial arch bridges with a curved superior deck (SABWCSD) and explain the relation with Ritter's theory of deck-stiffened arch and suspension bridges. Maillart's concepts are extended and equivalent frame bridges are analyzed. The similarity of a frame bridge to an equivalent arch bridge is proved in their study.
- Jorquera (2007) and Andrade (2010) prove that the structural behaviour of spatial arch bridges with a inferior curved deck (SABWCID) are highly dependent on the arch/deck eccentricity in plan view ( $e$ , Figure 1-1). This high influence has been explained by the proximity of the arch to the center of gravity ( $cg$ ) of the deck (Andrade 2010). Another way to explain the efficiency of  $e$  is to place the arch so that there are no resulting torsional moments due to permanent loads about the intersection line of the planes of arch and deck, as Laffranchi and Marti (1997, p1283) suggest in order to choose the  $e$  value for the case of spatial arch bridges with a superior curved deck (SABWCSD).
- Jorquera (2007) suggests that increasing the vertical distance between the arch crown and the deck will also improve the behaviour of SABWCSD.
- The rigidity of the hanger-deck system has proved to be a key parameter for inferior-deck arch bridges with imposed curvature (IDABWIC) (Sarmiento-Comesías et al, 2011). Therefore its influence is measured for different values and combinations of the

previously mentioned variables.

- The inclination of the struts planar vertical arch bridges with an inferior straight deck is studied by Bogaert (2010 and 2011).
- De Zotti et al (2007) compare network, fan and vertical arrangements of hangers for inferior straight deck vertical planar arch bridges. They conclude that vertical and fan arrangements lead to minimum values of hanger forces, but higher values of arch and lower chord bending moments.

Values employed in the aforementioned studies:

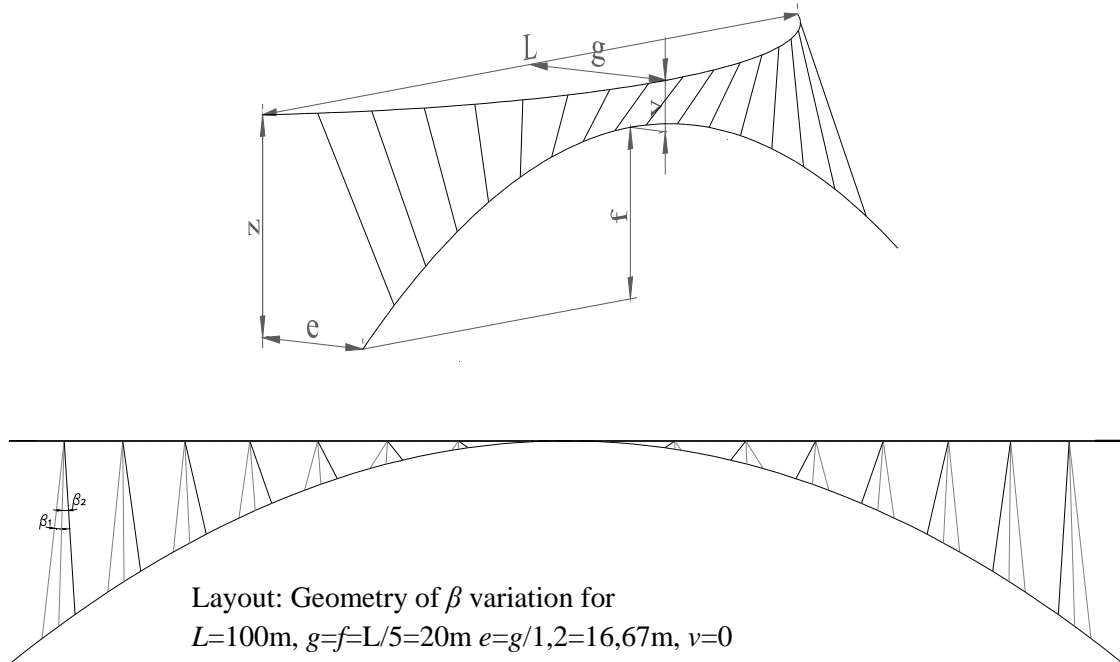
- In their studies, Jorquera (2007) and Andrade (2010) conduct a parametrical study of  $e$ , but only for specific cases with the same deck plan curvature and specific cross-sections and hanger distributions of SABWCID. Whereas for SABWCSD this parameter is highly conditioned by the clearance, in SABWCSD it does not interfere with it. The fact of the struts being fixed and the different distribution of the struts' length and thus the struts' stiffness compared to hangers', prevent the direct application of previous results of SABWCID for SABWCSD. Furthermore, a broader study for different deck plan curvatures and cross-sections is required and also an explanation of how the structure works and the reasons of the given  $e$  values as the most efficient parameters.
- The indicators employed by Jorquera (2007) for SABWCID aim to obtain antifunicularity and are the sum and quadratic sum of out-of-plane and total bending moments in the arch.
- In Jorquera's study of  $e$  for planar vertical arches with an inferior curved deck with pinned hangers, the reduction of out-of-plane bending moments has been considered a good indicator of the improvement of the structural behaviour. This can be understood as a reduction of the balcony-beam behaviour, enhancing the arch to actually behave like an arch.
- In Bogaert's 2010 study it is concluded that an optimum arrangement of sloping hangers with radial distribution (from the deck central zone and sloping radially to the arch) can be found. This is obtained by distributing the hanger nodes in an even manner and concentrating the nodes on the lower chord near to the center. This has also a stabilising effect for buckling in opposition to vertical hangers (Bogaert, 2010). A triangular arrangement of hangers requires less steel than a fan arrangement of hangers concurring at a centre above the arch top (Bogaert, 2011), but fan arrangement can be justified for aesthetical reasons.

## 1.2 STUDIED PARAMETERS

The high influence of  $e$  might also be thought to be highly related to the inclination and length of the struts, and thus their stiffness, for superior deck spatial arch bridges with a curved deck (SABWCSD) with fixed rigid struts and a planar vertical arch, as the ones concerning us in this section. Therefore, other parameters which influence the inclination of the struts are worth studying. A parametrical study of such variables has been conducted. These variables

are defined as follows (Figure 1-1):

- the arch/deck eccentricity in plan view ( $e$ ) (section 2)
- cross-section rigidity of deck, struts and arch ( $EI_D, GJ_D, EI_S, GJ_S, EI_A, GJ_A$ ) (section 2)
- the vertical distance between the arch crown and the deck mid-span ( $v$ ) (section 3)
- the rise of the arch ( $f$ ) (section 4)
- the inclination of the struts in longitudinal view ( $\beta$ ) (section 5)
- deck height ( $z$ ) (section 6)
- curvature of the arch in plan measured by its sag ( $g_A$ ) (section 7)



**Figure 1-1: Nomenclature of variables**

### 1.3 TYPES AND SELECTION OF EFFICIENCY CRITERIA

The minimisation of the total bending moments is an indicator of the spatial arch tending to the antifunicular form of the load. However, it has been observed that a decrease of bending moments is often linked to a very high increase of axial forces (Sarmiento-Comesías et al, 2012). Moreover, tending to the antifunicular of a uniformly distributed loading on the whole deck, is a priori no guarantee of an improvement in behaviour under asymmetric loadings on half the deck. Furthermore, the considered material for the present study is steel, which has a high tension bearing capacity in comparison with other materials and may suffer buckling under compression. Not only improving the behaviour of the arch is important, improvement should be regarded as minimisation of the material of the bridge system as a whole.

Therefore, in the present study it is considered that a design improvement is a minimisation of material and one of the aims of the study is to find an indicator as simple and quick to calculate as possible, which is equivalent to measure the total material of the bridge. This will be useful in order to make preliminary decisions for the initial geometry.

Firstly, improvements will be measured as a stress reduction of the whole bridge system for the stress envelope. However, this cannot be directly assured as a mass reduction, since the length of the structure might change with different parameters and, thus, stress reduction could mean a mass increase if the length is increased greatly. Therefore, this must be controlled and a parameter such as the stress multiplied by the length will be considered.

In order to be able to make quicker decisions simpler criteria have been employed, regarding simpler loading cases or controlling only one element. The arch is expected to be key to control the whole mass of the bridge. Finally, a simple criteria such as the maximal arch displacement, which has proved to be key on the structural behaviour of SABs (Sarmiento-Comesías et al, 2011 and 2013a) is expected to be a simple and good enough criteria.

Therefore, in the present study we have compared:

- the sum of stresses in all the cross-sections of the arch (in all the output stations), considering the envelope of the absolute values of the stresses in the arch for the worse loading case, considering self-weight, dead loads, temperature variations and/or live loads on the whole deck (uniform) or on half the deck span (asymmetrical) (A)
- the sum of stresses in all the cross-sections of the bridge, considering the envelope of the absolute values of the stresses in the arch for the worse loading case, considering self-weight, dead loads, temperature variations and/or live loads on the whole deck (uniform) or on half the deck span (asymmetrical) (B)<sup>1</sup>
- the sum of the total bending moments in all the cross-sections of the arch under self-weight and permanent loads (C)
- the sum of the stresses in all the cross-sections of the arch under a uniform loading on the deck (D)
- the sum of the stresses in all the cross-sections of the whole bridge under a uniform loading on the deck (E)
- the maximal stress in the arch for the worse loading case, considering self-weight, dead loads, temperature variations and/or uniform or asymmetrical live loads on the deck (F)
- the maximal stress in the arch under a uniform loading on the deck (G)
- maximal arch displacement under permanent loads (H)

---

<sup>1</sup> It depends on the number of elements of the model. In the analysed models, it has always been employed the same number of elements.

- the maximal sum of the absolute values of the stresses in the whole system (arch, deck and struts) for the worse loading case, considering self-weight, dead loads, temperature variations and/or uniform or asymmetrical live loads on the deck and multiplied by the length of the structural elements (both cases  $\frac{\sum_{i=1}^n \sigma_i}{n} \cdot \sum_{i=1}^n l_i$  and  $\frac{\sum_{i=1}^n \sigma_i \cdot l_i}{n}$  have been considered, where  $n$  is the number of output stations and  $\sigma_i$  and  $l_i$  are the stress and length of each output station respectively)
- total mass of the dimensioned bridge (the bridge is dimensioned for a first iteration of the linear analysis of the frame model).

The value of the maximal arch displacement will be also obtained as a control criteria. This will give an idea of the influence of second order effects, which is important in order to control the validity of the other criteria, since results are obtained with a linear analysis. If the geometry that shows a most efficient behaviour for the total mass indicator also gives the lowest displacements, the comparison employing a linear analysis is considered valid. If these indicators are not coincident, it means that a non-linear geometrical analysis (NLGA) study needs to be conducted in order to establish the most efficient geometry.

#### 1.4 OBJECTIVES

The purpose of our study is to:

- understand the changes of the structural behaviour of this bridge type due to changes the different parameters ( $e, f, v, \beta, EI, GJ, z, g_A$ ) which have been previously described for different deck curvatures ( $g$ ) (Figure 1-1)
- establish a range of the best combination of the studied parameters in order to minimise the material employed for different spatial arch bridges
- study which will be the best indicator in order to minimise material
- assure whether the minimisation of bending moments is equivalent to the minimisation of stresses and if the latter corresponds to minimising the total mass of the bridge

A linear analysis is conducted for the different models. A geometrically non-linear analysis is conducted in Chapter VI. C and structural behaviour is compared with the linear analyses.

## 1.5 LOADING CASES AND COMBINATIONS

### 1.5.1 Loading cases for analysing the structural behaviour

The global structural behaviour of all the models under a uniformly distributed load on the length of the whole deck of 10kN/m ( $q$ ) and on half the deck span ( $q_{asym}$ ) has been studied.

### 1.5.2 Loading cases for stresses in ULS and displacements in SLS

To obtain the different stress values considered, the following loading cases have been employed:

- Self-weight ( $w$ ), with a steel weight of 76,97kN/m<sup>3</sup>
- Permanent load ( $pl$ ) of 2,5kN/m<sup>2</sup>. Considering 4m width:  $pl=10$ kN/m
- Live loads ( $ll$ ) of 5kN/m<sup>2</sup> according to the spanish standards IAP2011 and Eurocode 1. Part 2: Traffic loads on bridges. Considering 3m of usage width, employing the rest of the width for the railings:  $ll=15$ kN/m. Two hypothesis have been considered:
  - A uniform loading on the whole length of the deck ( $lu$ , Figure 1-2a) and
  - An asymmetrical loading on half the length of the deck ( $la$ , Figure 1-2b)
  - A uniform loading on the central third of the deck ( $lc$ )
- Temperature variation of 25° on arch, struts and deck ( $\Delta T$ )

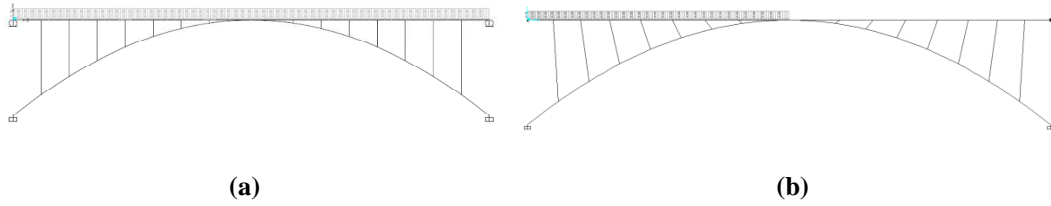
### 1.5.3 Loading combinations for stresses in ULS and displacements in SLS

The following load cases combinations have been considered for ULS:

- Combination A1:  $1,35 \cdot (w+pl) + 1,5 \cdot lu$
- Combination A2:  $1,35 \cdot (w+pl) + 1,5 \cdot la$
- Combination A3:  $1,35 \cdot (w+pl) + 1,5 \cdot lc$
- Combination B:  $1,35 \cdot (w+pl) + 1,5 \cdot \Delta T$
- Combination C1:  $1,35 \cdot (w+pl) + 1,5 \cdot (0,4 \cdot lu + 0,6 \cdot \Delta T)$
- Combination C2:  $1,35 \cdot (w+pl) + 1,5 \cdot (0,4 \cdot la + 0,6 \cdot \Delta T)$
- Combination C3:  $1,35 \cdot (w+pl) + 1,5 \cdot (0,4 \cdot lc + 0,6 \cdot \Delta T)$

and the service limit state response:

- Combination D1:  $1,0 \cdot (w+pl) + 1,0 \cdot lu$
- Combination D2:  $1,0 \cdot (w+pl) + 1,0 \cdot la$
- Combination E:  $1,0 \cdot (w+pl) + 1,0 \cdot \Delta T$
- Combination F1:  $1,0 \cdot (w+pl) + 1,0 \cdot (0,4 \cdot lu + 0,6 \cdot \Delta T)$
- Combination F2:  $1,0 \cdot (w+pl) + 1,0 \cdot (0,4 \cdot la + 0,6 \cdot \Delta T)$



**Figure 1-2: Loading (a) on the whole length of the deck ( $l_u$ ) and (b) on half the length of the deck ( $l_a$ )**

The stresses are obtained for the envelope of the aforementioned ULS combinations employing the reference cross-section values specified in section 1.6, Table 1-1. Hence, the stress values are very low in some cases. Afterwards they are redesigned for the material resistance.

## 1.6 RESEARCH PROCEDURE AND VALUES

In order to understand the behaviour of these arches, different frame 3D models have been developed and analyzed with commercial software, as part of a set of thorough parametric analyses (parameters described in section 1.2). A linear analysis has been employed.

The arch and deck plan curvature are measured as horizontal sag ( $g_A$  and  $g_D$  respectively), the arch rise is called  $f$ , the arch/deck eccentricity in plan view is  $e$ , the distance between arch and deck at span center is  $v$  and the arch and deck spans are  $L_{SA}$  and  $L_{SD}$  respectively and are considered equal ( $L$ ) in all models (Figure 1-1).

In all the models a vertical planar arch has been employed (Figure 1-1).

For all the studies presented, the following dimensions have been employed (Figure 1-1):

- $L_{SA}=L_{SD}=L=100\text{m}$ ;
- $g=20\text{m}$  when considered a fixed value and varying from 0 to 20m when expressed so specifically
- $e$  varying from  $g/2$  to  $g$ . When considered a fixed value  $e=g/1,2$
- $f=20$  when considered a fixed value and varying from  $L/10=10$  to  $L/2=50\text{m}$  when expressed so specifically and
- $v=0$  and varying from 0 to 6m when expressed so specifically
- $g_A$  is the sag of the arch in plan view and it is always 0, since it is a planar vertical arch, except for the case study of  $g_A$
- $z=f$  except for the case study of  $z$

The shape of the arch is always a parabola. 16 struts have been employed in all the models. The inclination of the struts is determined by the uniform division of the deck and the arch for all the models, except those in which the inclination of the struts in longitudinal view ( $\beta$ ) is studied.

The chosen arch rise ( $f=L/5$ ) is a usual value for arch bridges contained in a vertical plane. Usual values range from  $0,16*L$  (C. O'Connor 1971) and  $0,25*L$ .

Other fixed values for the other parameters of each parametrical study are adopted according to the results of the previous parametrical studies.

The material employed is steel S355 with a  $2,0 \cdot 10^8$  kN/m<sup>2</sup> modulus of elasticity (E) and resistance  $f_y=355$ MPa.

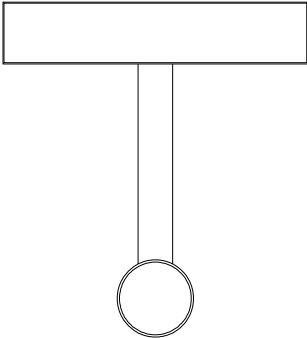
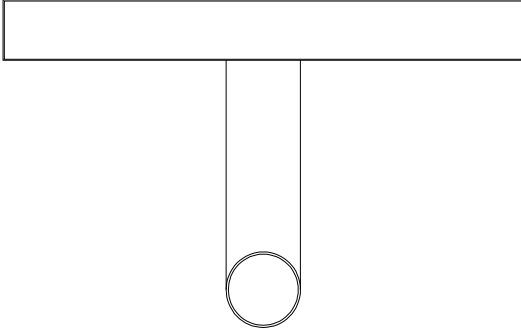
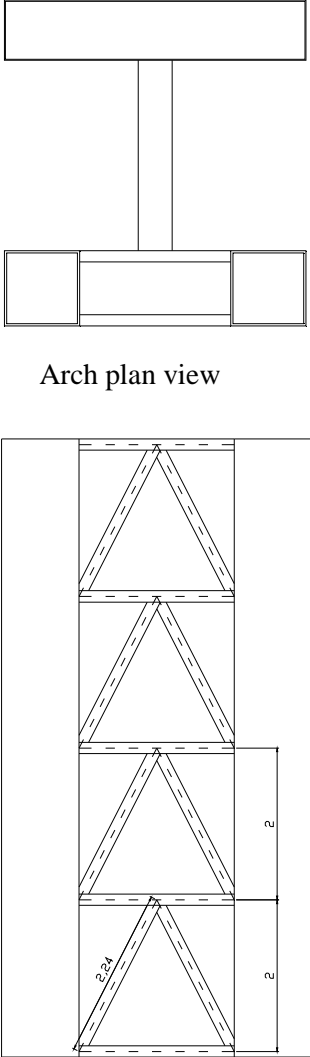
The studied arches in each of the considered models are fixed at the springings. The deck is pinned at abutments and tangential longitudinal displacements might be restrained for SABs and free for  $g=0$ , as recommended in Chapter V.A. The radial displacements are restrained.

The struts are completely fixed to both, arch and deck.

In the figures the whole arch length will be named  $L_A$  and the deck's one  $L_D$ , these values are different from the span so-called  $L$ .

For stresses and axial forces values  $>0$  are tensions and  $<0$ , compressions.



Reference model	Stiff strut-deck system (SSDS)	Horizontally stiff arch (HZSA)	
		 <p style="text-align: center;">Arch plan view</p>	
ARCH	CHS D=1m; t=30mm $A = 0,0914\text{m}^2$ $J = 0,0215\text{m}^4$ $I_2 = 0,0108\text{m}^4$ $I_3 = 0,0108\text{m}^4$	$A = 0,2328\text{m}^2$ $J = 0,0722\text{m}^4$ $I_2 = 0,5603\text{m}^4$ $I_3 = 0,0365\text{m}^4$ J calculated according to Kollbrunner and Basler (1969)	
DECK	BOX GIRDER 4000x800mm; t=15mm $A = 0,1431\text{m}^2$ $J = 0,0615\text{m}^4$ $I_2 = 0,2517\text{m}^4$ $I_3 = 0,0196\text{m}^4$	BOX GIRDER 7000x800mm; t=15mm $A = 0,2331\text{m}^2$ $J = 0,1161\text{m}^4$ $I_2 = 1,1393\text{m}^4$ $I_3 = 0,0335\text{m}^4$	BOX GIRDER 4000x800mm; t=15mm $A = 0,1431\text{m}^2$ $J = 0,0615\text{m}^4$ $I_2 = 0,2517\text{m}^4$ $I_3 = 0,0196\text{m}^4$
STRUTS	CHS D=451mm; t=22,6mm $A = 0,0304\text{m}^2$ $J = 0,0014\text{m}^4$ $I_2 = 0,0007\text{m}^4$ $I_3 = 0,0007\text{m}^4$	CHS D=1m; t=30mm $A = 0,0914\text{m}^2$ $J = 0,0215\text{m}^4$ $I_2 = 0,0108\text{m}^4$ $I_3 = 0,0108\text{m}^4$	CHS D=451mm; t=22,6mm $A = 0,0304\text{m}^2$ $J = 0,0014\text{m}^4$ $I_2 = 0,0007\text{m}^4$ $I_3 = 0,0007\text{m}^4$

**Table 1-1: Cross-sections for different models**

The cross-sections of arch and deck employed for the reference model are a circular hollow section (CHS), with D=1000mm and t=30mm, for the arch, a box girder 4000x800mm and t=15mm for the deck and CHSs with D=451mm and t=22,6mm for the struts (Table 1-1). These have equivalent area and stiffness to the HSSs employed in the previous studies in Chapters IV

and V.A. It is better to employ a CHS to avoid the axis orientation involved in square sections to influence the study.

The cross-sections employed by Jorquera for the arch and deck are equal to the reference ones of the present study in order to be able to compare the results. Other cross-sections have also been employed to ensure that the most efficient parameters do not depend on the stiffness of the elements (Table 1-1).

For the stiff strut/deck system (SSDS) models, a rigid to torsion deck according to the study for IDABWIC (Sarmiento-Comesías et al 2011) has been employed. For the struts a very rigid circular cross section has been employed (Table 1-1).

For the mass calculation each structure has been dimensioned with the stresses corresponding to the analysis of the reference model.

In each case study of the different parameters, the structural behaviour of the different models under  $q$  has been analysed and compared and the differences have been highlighted and explained. In most cases it is also explained what is expected before the structural analysis is carried out and why the studied parameter has been chosen. Then it is controlled whether the response is the expected one. There are so many variables involved that it is demonstrated that the response is not obvious a priori.

The same has been done for the stresses under the different ULS combinations described in section 0. When necessary according the efficiency criteria the envelope of stresses has also been obtained and the cross-sections of the different elements have been dimensioned in order to obtain the total mass of the bridge criteria. The different efficiency criteria described in 1.3 have been obtained for the studied models and compared. This has lead us to determine the most efficient parameters and to evaluate the validity of the different criteria which have been employed. Therefore, for each case study the following sections are provided:

- Structural response under a uniform vertical load
- Stress control and comparison in ultimate limit state
- Efficiency criteria

## **2. PARAMETRICAL STUDY OF THE ARCH/DECK ECCENTRICITY IN PLAN VIEW ( $e$ ) AND THE SYSTEM STIFFNESS DISTRIBUTION**

Part of the study presented in this section was published in Sarmiento-Comesías et al (2013).

### **2.1 DEFINITION AND EMPLOYED VALUES**

The values for the parametrical study of the  $e$  variable have been chosen on the basis of the  $e/g$  relationship (Figure 1-1). The proportion around which we expect to find good results and around which we have chosen the range of values to study is based on the  $e$  value obtained as the most efficient one in the study of Jorquera (2007) for SABWCID with flexible hangers for  $L=100$  and  $g=10$ . The value of the most efficient  $e$  in Jorquera's study for antifunicular arches with inferior-

deck with  $g=10\text{m}$  and pinned hangers is around  $7,35\text{m}$  (Jorquera 2007, p382) and for planar vertical arch bridges with inferior-deck with  $g=10\text{m}$  and pinned hangers  $8,32$  (Jorquera 2007, p159). According to the relationship in which we base our range of values for the present study the values obtained by Jorquera are  $e=g/1,36$  and  $e=g/1,2$  respectively. In our case, the in-plane bending moments and axial forces will change with  $e$ , since the struts are fixed. Results should also be different in comparison with SABWCID because the length of the struts changes and, therefore, the stiffness.

The Ripshorst bridge is a SABWSCD with an antifunicular arch and  $L=76,97\text{m}$  (Schlaich and Moschner, 1999). The dimensions we are studying have been approximately measured in the published figures. The arch has a double curvature, very low and with opposite sign to the deck near its springings and of the same sign as the deck at span center. Ripshorst bridge has a curved deck with  $g$  approximately  $g=14,5\text{m}$ . The  $g_A$  of the arch measured from the span center to its springings is  $g_A=1,66\text{m}$ ,  $e$  measured from abutments to springings is  $e_S=11,28$ ,  $e$  measured from the abutments to the point where the arch crosses the deck in plan view is  $e=11,21\text{m}=g/1,29$ . Around this value the struts which are employed in this footbridge are stiffer than in the rest of the length, since here V struts have been employed, whereas in the rest of length individual struts have been employed. This fact remarks the necessity of the structure of a larger stiffness in this length and, therefore, the most efficient  $e$  should be in the range of values which would intersect these stiffened struts. This built example confirms the proportion around which we expect to find the most efficient  $e$  value ( $e^*$ ) for SABWSCD. However, our study will be with a planar vertical arch and different  $g$  and  $f$  values and different system stiffness distribution in order to lead to more general conclusions for this bridge type, since this value could change. Therefore, we have chosen a broader range of values. Moreover, it is important to understand why an  $e$  value will be more efficient than another one and in which cases.

The efficiency criteria in the present study as well as the studied bridge types (SABWSCD with rigid struts) are different than for previous studies, as explained in section 1.

#### ***Parameter influence and values:***

The values employed in the present study are:

- $L=100\text{m}$ ;  $v=0$
- $g=5, 10$  and  $20\text{m}$
- $e$ : from  $0$  to  $g$ .

The proportions employed are  $e$  equal to:  $0, g/2, g/1,6, g/1,36, g/1,3, g/1,2$  and  $g/1$  (Figure 2-1, Table 2-1).  $g/1,1$  has also been added in some cases in order to see if a more accurate value was needed.

The study varying  $e$  has been conducted with the reference model cross-sections in Table 1-1 for the different  $g$  values and  $f=L/5=20\text{m}$ .

For the reference model cross-sections in Table 1-1 and  $g=20\text{m}$ , the study of  $e$  variation has been carried out for each of the following  $f$  values:  $f=10, 15, 20, 25$  and  $50\text{m}$ .

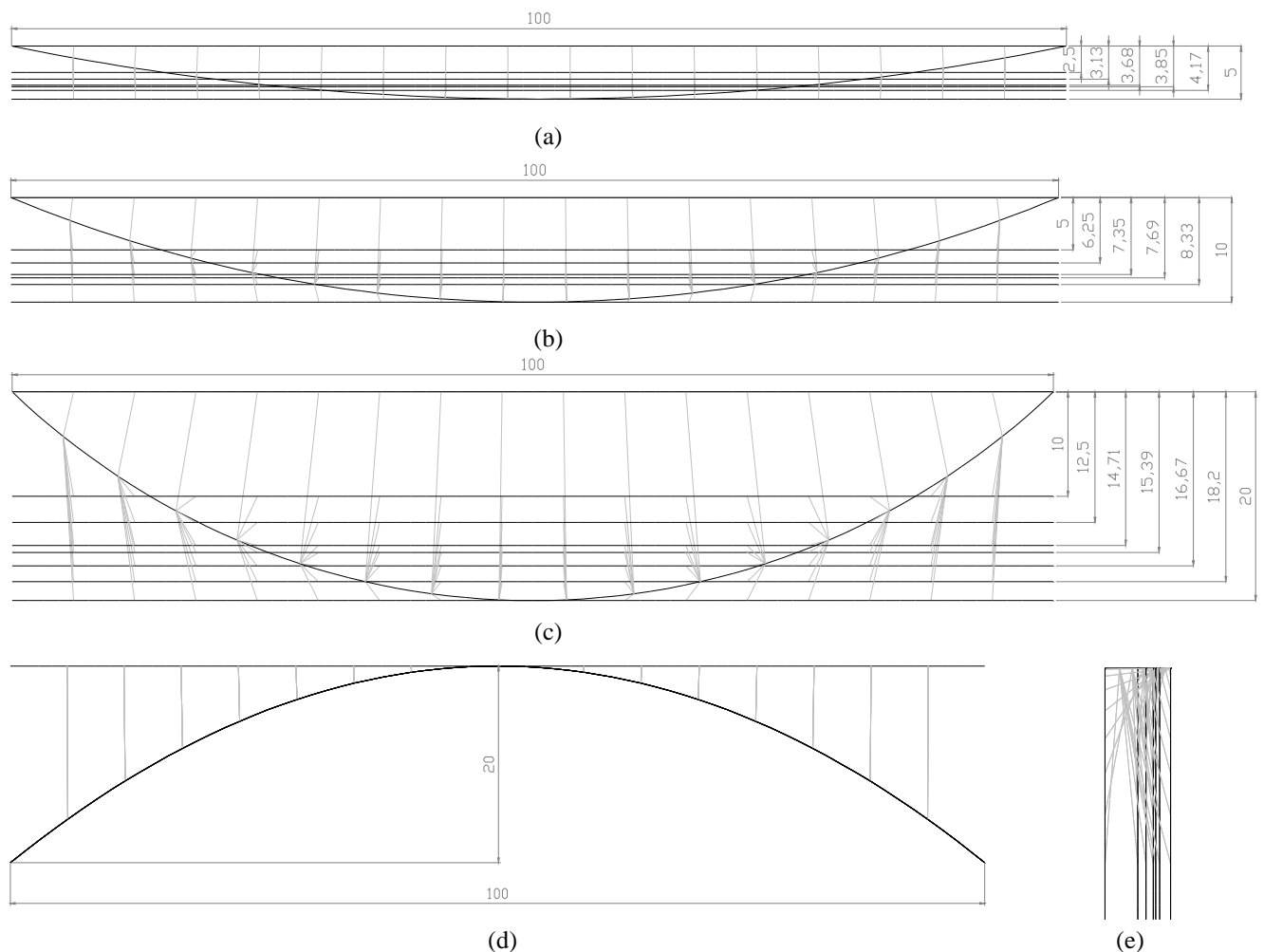
- $f$  varying from  $L/10$  to  $L/2$

If  $f$  increases the arch is expected to work better in plane and horizontal forces at springings would decrease, however the behaviour as balcony beam is also expected to increase. Geometrical changes in plan due to the  $e$  variation do not affect the longitudinal view of the bridge and viceversa, varying  $f$  does not affect the plan view. Therefore, geometrically the efficiency of  $f$  and  $e$  values is not expected to be coupled. However, the length and inclination of the hangers changes with  $e$  and  $f$  and hence its stiffness. Therefore, for different  $f$  values, it might be more interesting obtaining the largest rigidity in a point or another of the arch/deck connection by means of changing  $e$ . Thus the influence of this parameter must be studied.

- **Stiffness distribution variation: different cross-section values**

For  $g=20\text{m}$  and both cases,  $f=20\text{m}$  and  $f=25\text{m}$ , the study has been conducted for all the cross-sections in Table 1-1 in order to study the influence of different system stiffness distributions, which might lead to different  $e^*$  values.

The parametrical study of  $e$  for the other  $g$  values described in Table 2-1 have been done employing the reference values of the cross-sections described in Table 1-1.

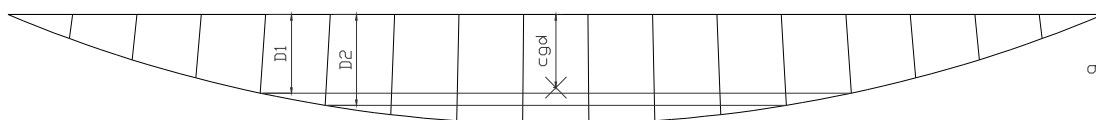


**Figure 2-1** Variation of  $e$  (a) Plan view for  $g=5$ . (b) Plan view for  $g=10$ . (c) Plan view for  $g=20$ . (d) Longitudinal view for  $g=20$ . (e) Side view for  $g=20$ .

<i>g</i>	<i>i</i>	$e=g/i$	<i>Cgd*</i>	<i>D**</i>	<i>g</i>	<i>i</i>	$e=g/i$	<i>Cgd*</i>	<i>D**</i>	<i>g</i>	<i>i</i>	$e=g/i$	<i>Cgd*</i>	<i>D**</i>
<b>5</b>	2,00	2.50	3,34= $g/1,50$	3,60-4,15 $g/1,39-g/1,20$	<b>10</b>	2,00	5.00	6,66= $g/1,50$	7,17-8,29 $g/1,53-g/1,21$	<b>20</b>	2,00	10.00	13,22= $g/1,51$	14,20-16,47 $g/1,41-g/1,21$
	1,60	3.13				1,60	6.25				1,60	12.50		
	1,36	3.68				1,36	7.35				1,36	14.71		
	1,30	3.85				1,30	7.69				1,30	15.38		
	1,20	4.17				1,20	8.33				1,20	16.67		
											1,10	18,20		
	1,00	5.00				1,00	10.00				1,00	20.00		

\**Cg* of the deck \*\*Interval of values of *e* with the same number of struts on each side: from *D1* to *D2* (see Figure 2-2)

**Table 2-1: Studied values. Relationship between *g* and *e*. Measured in meters**



**Figure 2-2: Plan view of a general bridge case study with  $e=0$ . Values for Table 2-1**

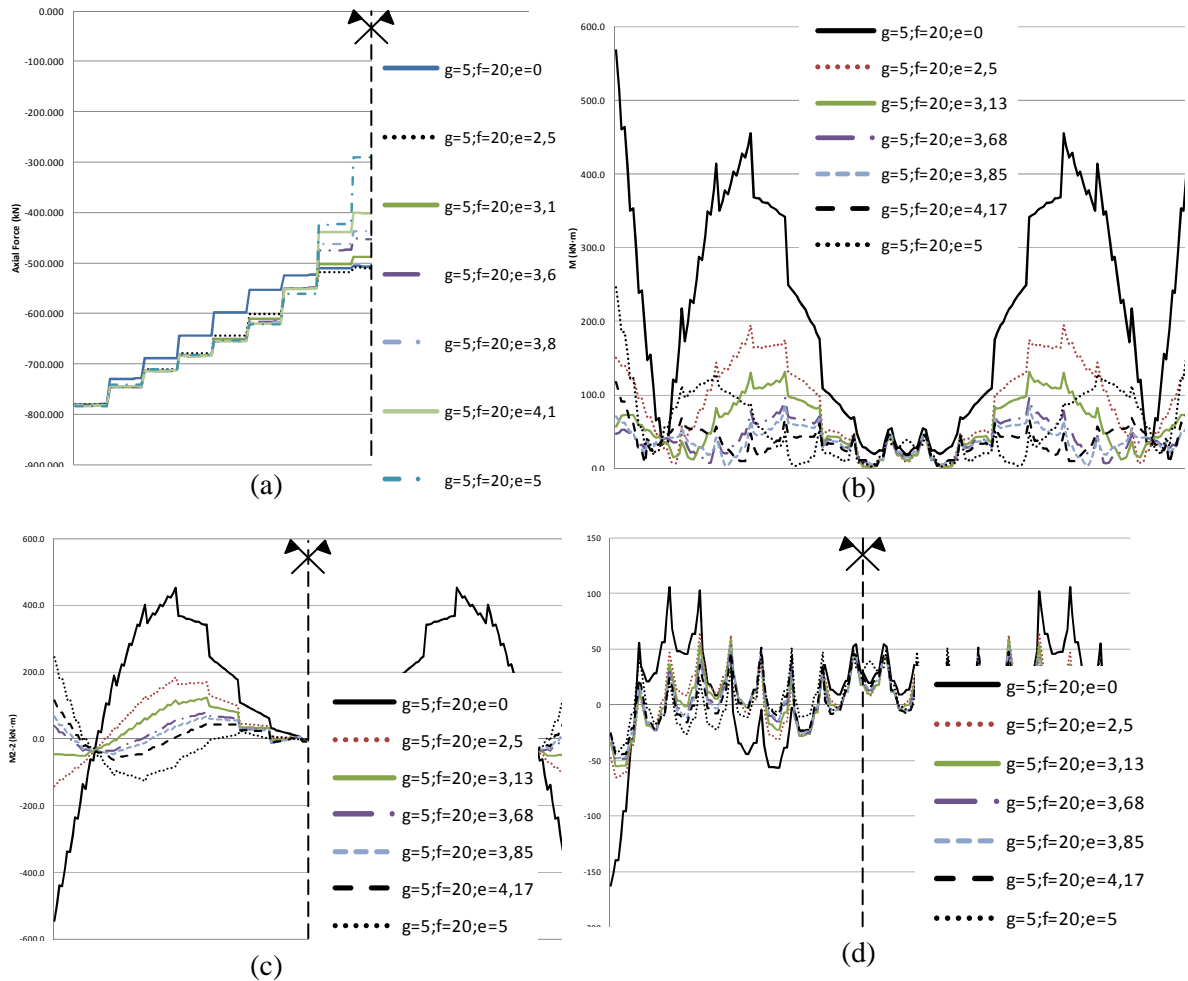
It is worth highlighting that whatever the value of *g* the *cg* of the deck and the maximal *e* for having the same number of struts on both sides of the arch keeps approximately the same proportion (Table 2-1).

## 2.2 STRUCTURAL RESPONSE UNDER A UNIFORMLY DISTRIBUTED VERTICAL LOAD

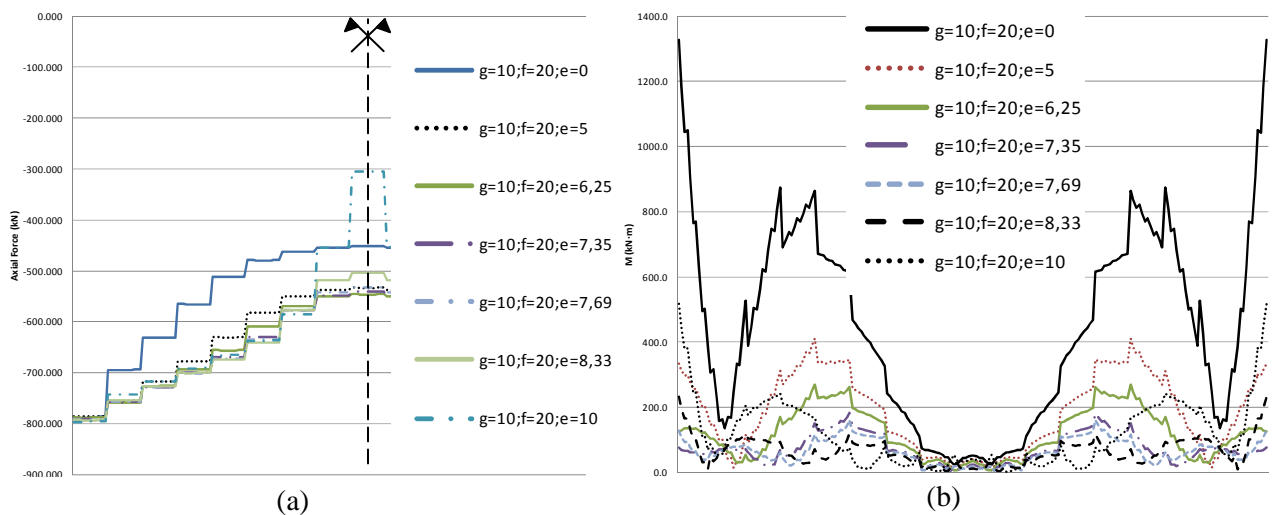
The structural behaviour has been studied for the different  $g$ ,  $f$  and cross-section values described above under a uniformly distributed load of 10kN/m on the whole deck and on half the deck ( $q$  and  $q_{asym}$ , respectively) for the described values of  $e$  in each case (Table 2-1 and Figure 2-1) and their structural response has been compared.

### 2.2.1 Structural response of varying $e$ for different $g$ values

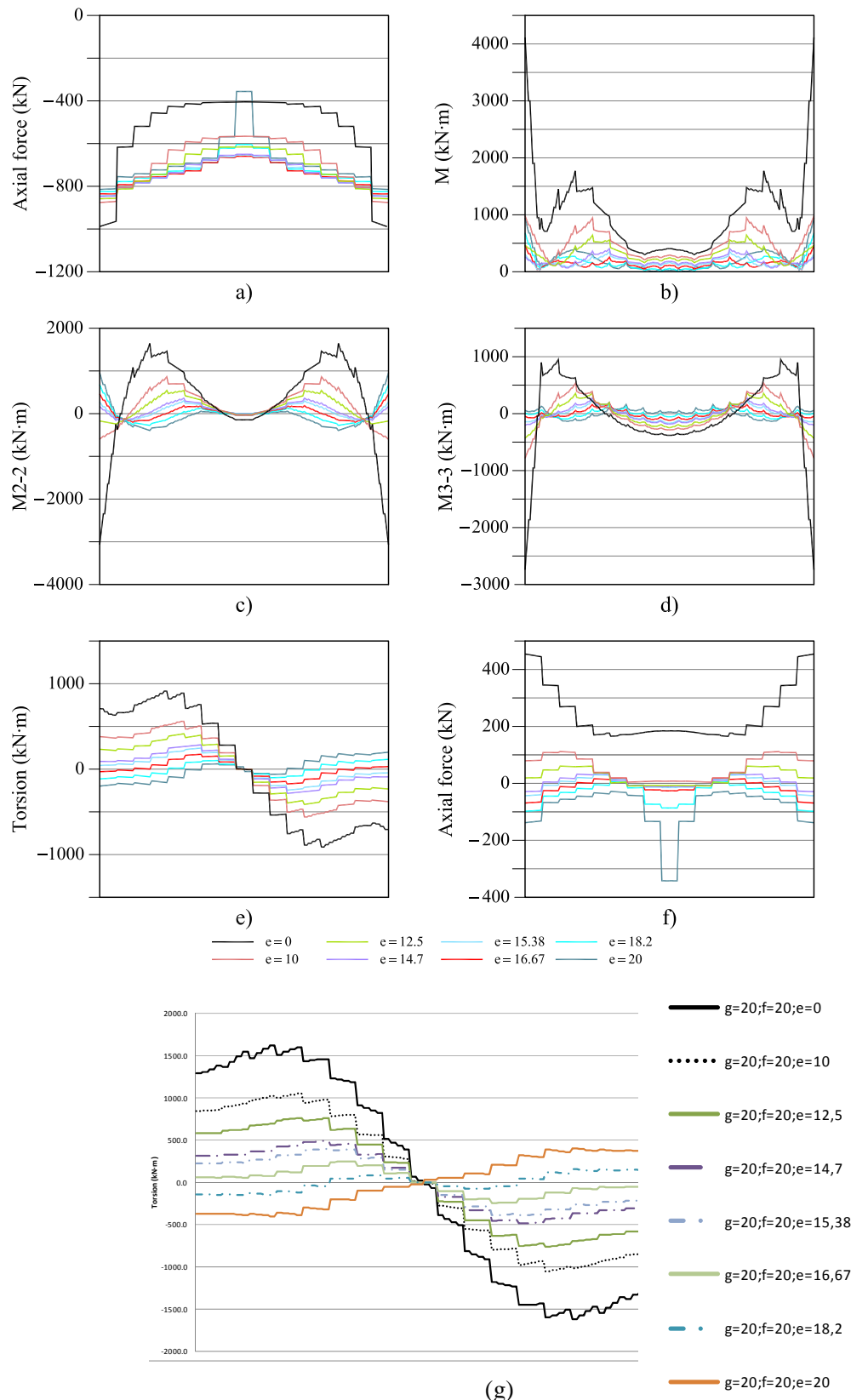
- For  $g=5$  and 10, the most uniform axial forces in the arch (Figure 2-3 (a) and Figure 2-4 (a)) are obtained for  $e=g/1,6$ , not far from the  $cg$  of the deck (Table 2-1). However, for  $g=20$  most uniform axial forces in the arch are obtained for  $e=g/1,2$  (Figure 2-5 (a)), far from the  $cg$  of the deck (Table 2-1). Total bending moments in the arch (Figure 2-5 (b)) and torsional moments (Figure 2-5 (e)) are also minimal around this value and  $e=g/1,1$ .
- Torsional moments are minimal for  $e=g/1,2$  whatever the value of  $g$  (Figure 2-3 (e), Figure 2-4 (e) and Figure 2-5 (e)). For  $g=20$ , this value also minimises the axial forces and the torsional moments of the deck. The total bending moments of the deck are minimal for  $e$  between  $g/1,30$  and  $g/1,36$  (Figure 2-5).
- For  $g=5$  and 10 under  $q$  or  $q_{asym}$ , bending moments do not have clear minimal values, but results are in the range of  $g/1,36 \leq e \leq 1,2$ , approximately in the range in which there is the same number of hangers at each side of the arch.
- For  $g=5$  out-of-plane bending moments in the arch are minimised at springings for  $e=g/1,36$ , at  $L_A/3$  for  $e=g/1,3$  and at the crown for  $e=g/1,2$  (Figure 2-3 (c)).
- The variation of in-plane bending moments in the whole arch (Figure 2-3 (d)) and of axial forces at springings (Figure 2-3 (a)) with  $e$  for  $g=5$  is very low.
- Under  $q_{asym}$  for  $g=20$ ,  $e=g/1,1$  in comparison with  $e=g/1,2$  works better at the crown of the arch and worse at springings, as far as out-of-plane bending moments are concerned.
- Regarding in-plane bending moments, the lowest ones for  $g=20m$ , under  $q_{asym}$ , are obtained for  $e=g$ .
- Until  $e=g/1,36$  the out-of-plane bending moments in the arch are so important that the variation of the in-plane bending moments of the arch will not have a high impact on the variation of the total bending moments. However, when out-of-plane and in-plane bending moments in the arch are the same order of magnitude, it is interesting to decrease both.



**Figure 2-3: Internal forces under  $q$  comparison for  $g=5$  and  $f=20$  for the parametrical study of  $e$ : (a) Arch axial forces; (b) Arch total bending moments; (c) Arch out of plane bending moments (M2-2); (d) Arch in-plane bending moments (M3-3) The abscissas are the arch length from 0 to  $L_A$  (or from 0 to  $L_A/2$  in cases a and c, the symmetry dashed line marks  $L_A/2$ )**



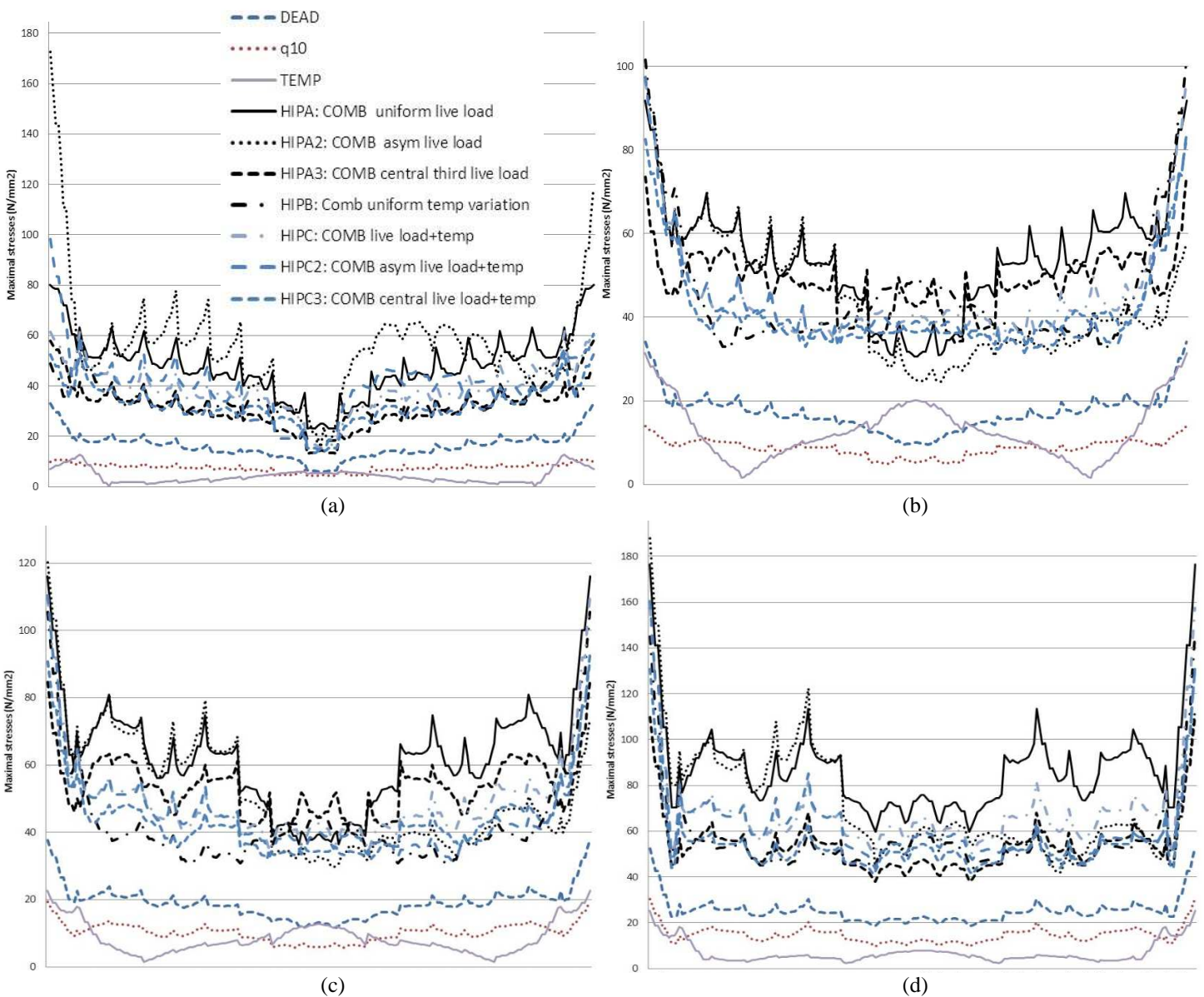
**Figure 2-4: Internal forces under  $q$  comparison for  $g=10$  and  $f=20$  for the parametrical study of  $e$ : (a) Arch axial forces; (b) Arch total bending moments. The abscissas are the arch length from 0 to  $L_A$  (or from 0 to  $L_A/2$  in cases a, the symmetry dashed line marks  $L_A/2$ )**



**Figure 2-5: Internal forces under  $q$  comparison for  $g=20$  and  $f=20$  for the parametrical study of  $e$ , employing the reference cross-sectional values shown in Table 1-1: (a) Arch axial forces; (b) Arch total bending moments; (c) Arch out of plane bending moments (M2-2); (d) Arch in-plane bending moments (M3-3); (e) Arch torsional moments; (f) Deck axial forces; (g) Deck torsional moments. The abscisses from (a) to (e) are the arch length from 0 to  $L_A$  and (f) and (g) are the length of the deck from 0 to  $L_D$**



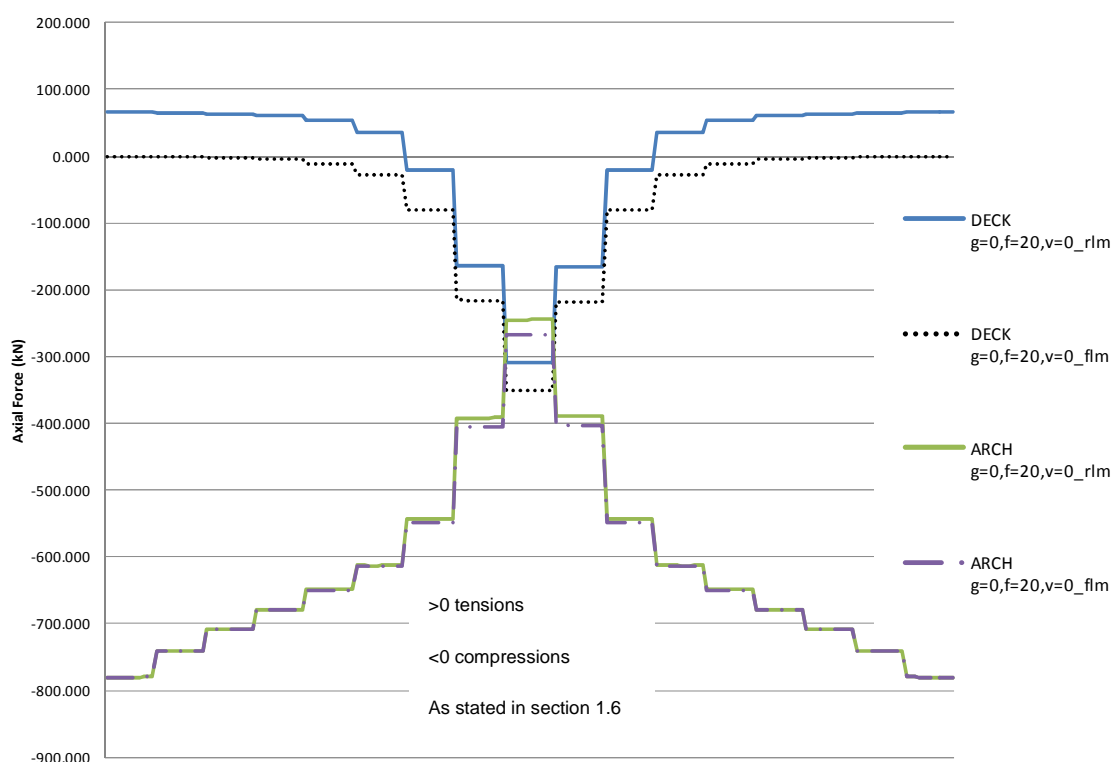
- For conventional vertical arch bridges ( $g=0$ ), the maximal arch shear forces, bending moments and deflections are significantly higher when the loading is applied on half the deck span ( $q_{\text{asym}}=10\text{kN/m}$ , Figure 1-2) than on the whole deck span ( $q=10\text{kN/m}$ ). However, the higher axial forces are obtained when the whole deck span is fully loaded ( $q=10\text{kN/m}$ ). It can be observed on the arch stresses that asymmetrical loading is the most unfavourable loading for most of the arch cross-sections (Figure 2-6a).
- On the contrary, for SABs with a superior curved deck, the critical load case, for both internal forces and displacements, is obtained when the uniform distributed loading is applied on the whole deck span. This had also been observed for other SABs types such as inferior-deck arch bridges with imposed curvature (Sarmiento-Comesías et al, 2012). It can be observed on the arch stresses that loading on the whole deck-span is the most unfavourable loading for most of the arch cross-sections in SABs (Figure 2-6b, c and d).



**Figure 2-6:** Stresses in the arch caused by different loading cases combination when employing the reference model cross-sections (Table 1-1). The abscissas are the arch length from 0 to  $L_A$ , (a) for  $g=e=0$  and  $f=20\text{m}$   $e=16,67\text{m}$ ; (b) for  $g=5\text{m}$ ,  $f=20\text{m}$  and  $e=g/1,2=4,17\text{m}$ ; (c) for  $g=10\text{m}$ ,  $f=20\text{m}$  and  $e=8,33\text{m}$ ; (d) for  $g=20\text{m}$ ,  $f=20\text{m}$  and  $e=16,67\text{m}$

**Axial forces in the deck**

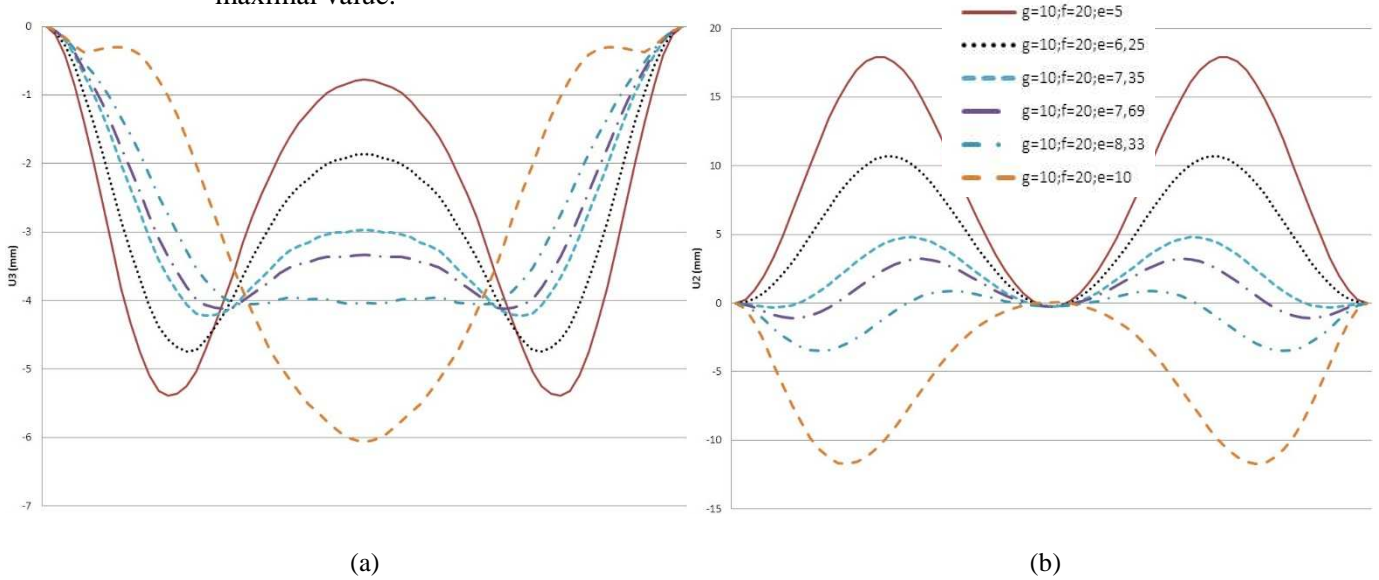
- For all  $g$  values, the deck is always completely tensioned for  $e=0$  (Figure 2-3 (f), Figure 2-4 (f) and Figure 2-5 (f)).
- As  $g$  increases, tensions in the deck increase.
- A planar vertical arch with a straight deck and  $g=e=0$  transmits compressions to a slightly tensioned deck, which is therefore compressed at the span center (Figure 2-7).
- For a curved deck, whatever the  $g$  values, the deck is always completely compressed for  $e=g$  (Figure 2-3 (f), Figure 2-4 (f) and Figure 2-5 (f)).
- For  $g=20$ , the deck is not under compression until  $e>g/1,6$ , whereas for  $g=5$  or  $10$  the deck is already under compression for  $e=g/1,6$ .
- For  $g=5$  or  $10$ , the deck is already **completely** under compression for  $e>g/1,3$ , whereas for  $g=20$  the deck is not completely under compression until  $e\geq g/1,1$ .
- When  $e=0$  the deck is held back by the arch and is tensioned.
- When  $e=g$  the deck is stopped by the arch and it is compressed.
- The higher the value of  $g$  for  $e=0$ , the higher the tensions in the deck, especially at the abutments.
- The difference of the axial forces at span center and springings increases with  $g$ . This effect is due to the curved shape of the deck and the increase of the distance from the arch.
- For  $e=g$  the compressions at the abutments also increase with  $g$ . However, at span center it is more difficult to transmit the arch horizontal forces which compress the deck as  $g$  increases.



**Figure 2-7- Axial forces in the arch and deck of a planar vertical arch bridge with straight deck under  $q$ . The abscisses are the arch length from 0 to  $L_A$  and the length of the deck from 0 to  $L_D$**

**Displacements**

- Largest displacements of the arch and deck take place between  $L_A/5$  and  $4 \cdot L_A/15$  respectively.
- The largest out-of-plane displacements in the arch take place between  $L_A/6$  and  $2 \cdot L_A/5$  and in-plane between  $L_A/6$  and  $L_A/2$ .
- The value of the maximal out-of-plane behaviour is larger in most cases but for  $e=g/1,2$  the out-of-plane displacement maximal value is equivalent to the in-plane displacement maximal value.



**Figure 2-8: Displacements under  $q$  comparison for  $g=20$  and  $f=20$  for the parametrical study of  $e$ , employing the reference cross-sectional values shown in Table 1-1: (a) Arch in-plane displacements; (b) Arch out-of-plane displacements. The abscisses are the arch length from 0 to  $L_A$**

**2.2.2 Relationship between the value of  $e$  and the out-of-plane shape of the arch**

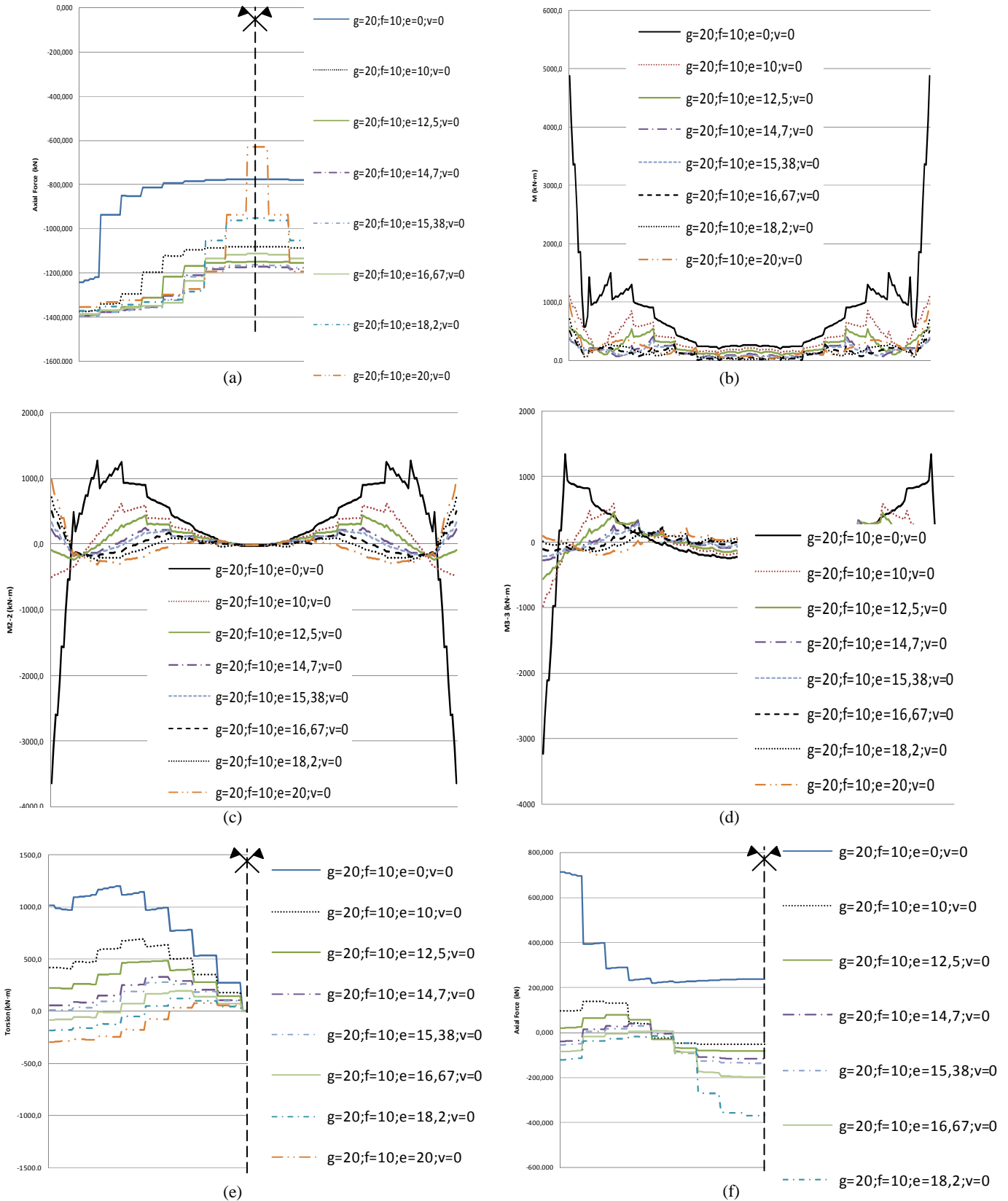
Regarding the out-of-plane shape of the arch, for low  $e$  values it is expected to be more convenient to tend to a geometry with the arch and deck with opposite curvature in plan view and for high  $e$  values, to one with the curvature in plan view in the same direction (section A of the present chapter). This is coincident with the results for inferior-deck arch bridges (Jorquera 2007).

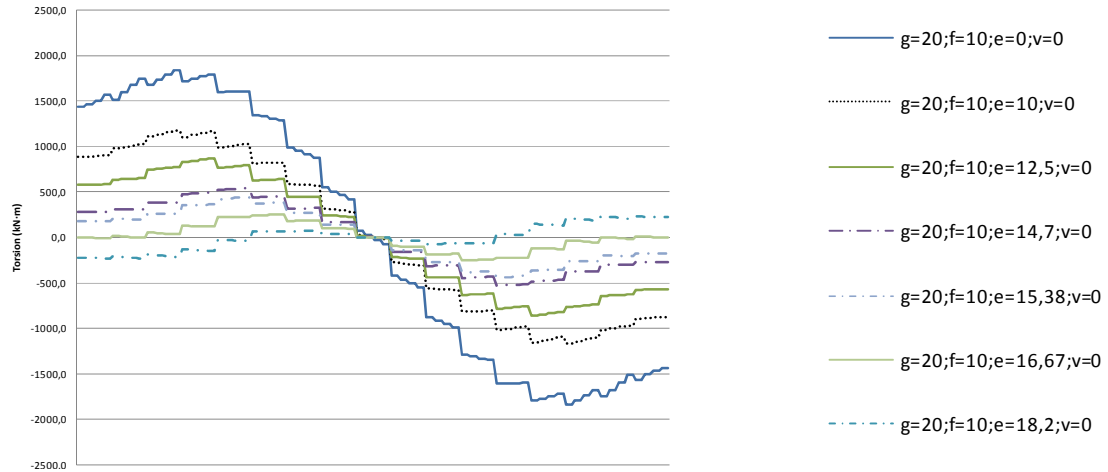
**2.2.3 Structural response of varying  $e$  for different  $f$  values**

The response when studying the effects of the variation of  $e$  for different  $f$  values (for  $g=20$ ,  $f=10$ , 15, 20, 25 and 50), is summarized in the following paragraphs. Results are shown for the extreme values  $f=10m$  and  $f=50m$  as examples (Figure 2-9 and Figure 2-10).

- For low  $f$  values, the variation of  $e$  has a higher influence on the axial forces in the deck (Figure 2-9f compared to Figure 2-10f).
- Given  $e=0$ , when increasing  $f$  the differences between the axial forces in the arch springings and crown increase (Figure 2-9a and Figure 2-10a).
- On increasing  $f$ , the total bending moments in the arch increase and the value of  $e$  acquires more influence (Figure 2-9b compared to Figure 2-10b)

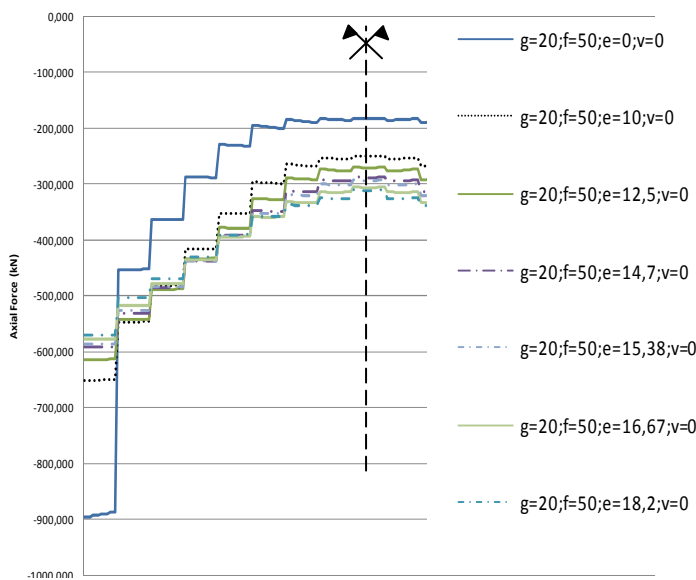
- On increasing  $f$ , the in-plane bending moments in the arch crown increase and in the arch springings they decrease. The value of  $e$  acquires more relative influence on in-plane bending moments in the arch (Figure 2-9d compared to Figure 2-10d)
- On decreasing  $f$  values, the variation of  $e$  has a higher influence on the torsional moments in the arch (Figure 2-9e compared to Figure 2-10e).



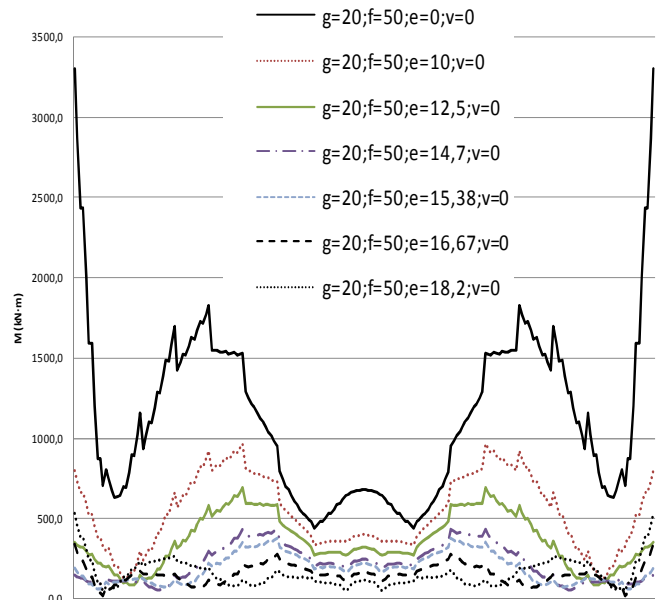


(g)

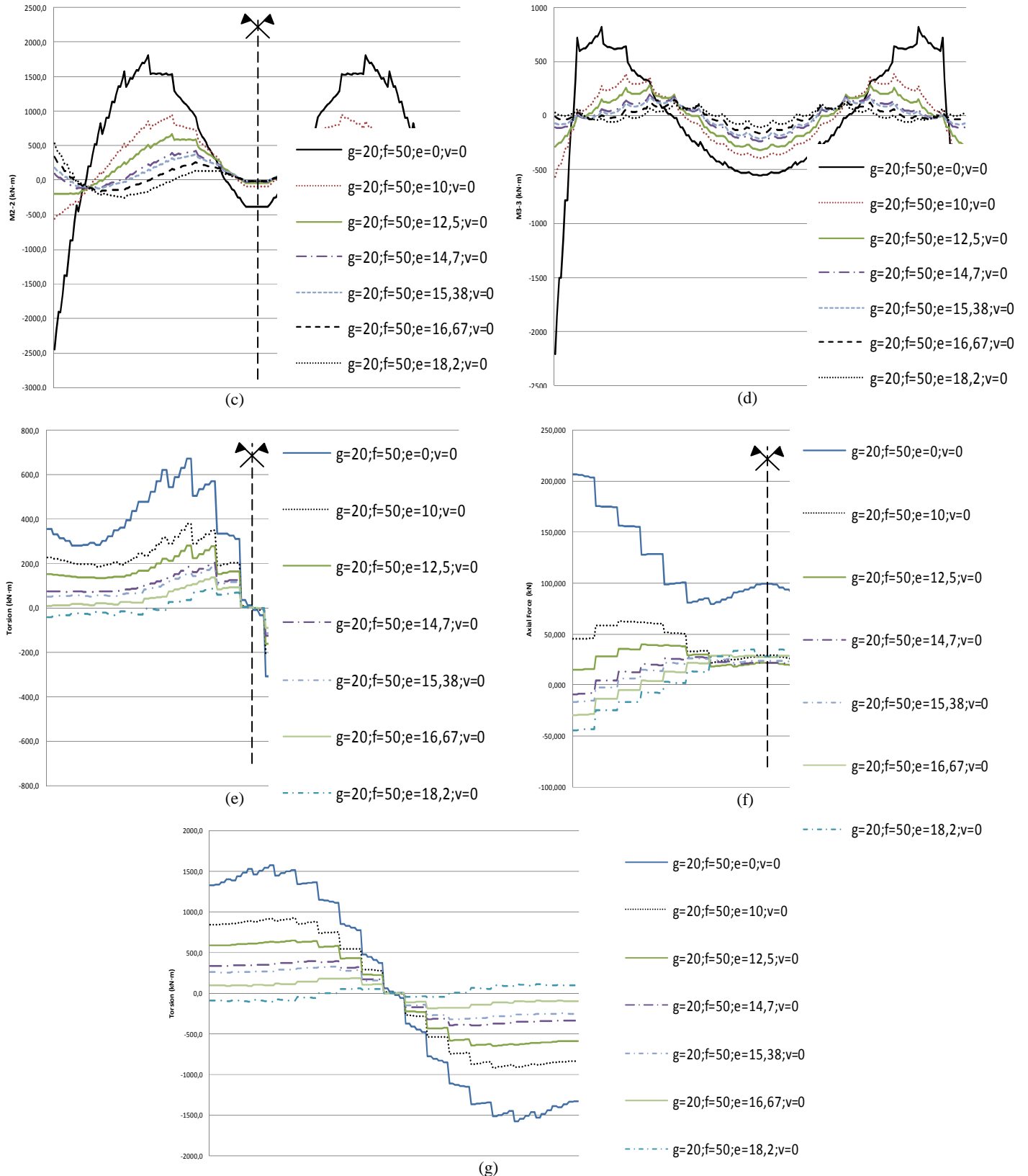
**Figure 2-9: Internal forces under q comparison for  $g=20$  and  $f=10$  for the parametrical study of  $e$ , employing the reference cross-sectional values shown in Table 1-1: (a) Arch axial forces; (b) Arch total bending moments; (c) Arch out of plane bending moments (M2-2); (d) Arch in-plane bending moments (M3-3); (e) Arch torsional moments; (f) Deck axial forces; (g) Deck torsional moments. The abscisses from (a) to (e) are the arch length from 0 to  $L_A$  and (f) and (g) are the length of the deck from 0 to  $L_D$**



(a)



(b)



**Figure 2-10: Internal forces under  $q$  comparison for  $g=20$  and  $f=50$  for the parametrical study of  $e$ , employing the reference cross-sectional values shown in Table 1-1: (a) Arch axial forces; (b) Arch total bending moments; (c) Arch out of plane bending moments (M2-2); (d) Arch in-plane bending moments (M3-3); (e) Arch torsional moments; (f) Deck axial forces; (g) Deck torsional moments. The abscissas for (a) to (e) are the arch length from 0 to  $L_A$  and for (f) and (g), the abscissas are the length of the deck from 0 to  $L_D$**

#### 2.2.4 Relationship between the value of $e$ and the distribution of stiffness in the system

- When employing a **Stiff Strut-Deck System (SSDS)**:
- The variation of  $e$  has a lower influence in the global behaviour of the arch (Figure 2-5 compared with Figure 2-11).
- A SSDS diminishes greatly the axial forces in the crown of the arch and increases the difference between the axial forces in the arch springings and the arch crown (Figure 2-11a). It also diminishes greatly the total bending moments in the springings of the arch (Figure 2-11b). However, axial forces and bending moments in the arch follow the same evolution with  $e$  whatever the  $f$  or cross-sectional values.
- For  $g=20$  and a SSDS, compressions in the deck start for  $e=g/2$  and the deck is completely compressed for  $e \geq g/1,2$  (Figure 2-11c), which are a lower values of  $e$  than for the reference model (Figure 2-5f).
- When the deck is completely compressed,  $e$  has a low influence on the axial forces in the arch (Figure 2-11c).
- The difference between the axial forces in the deck the abutments and span center increase for a SSDS (Figure 2-11c) in comparison with the reference model (Figure 2-5f).

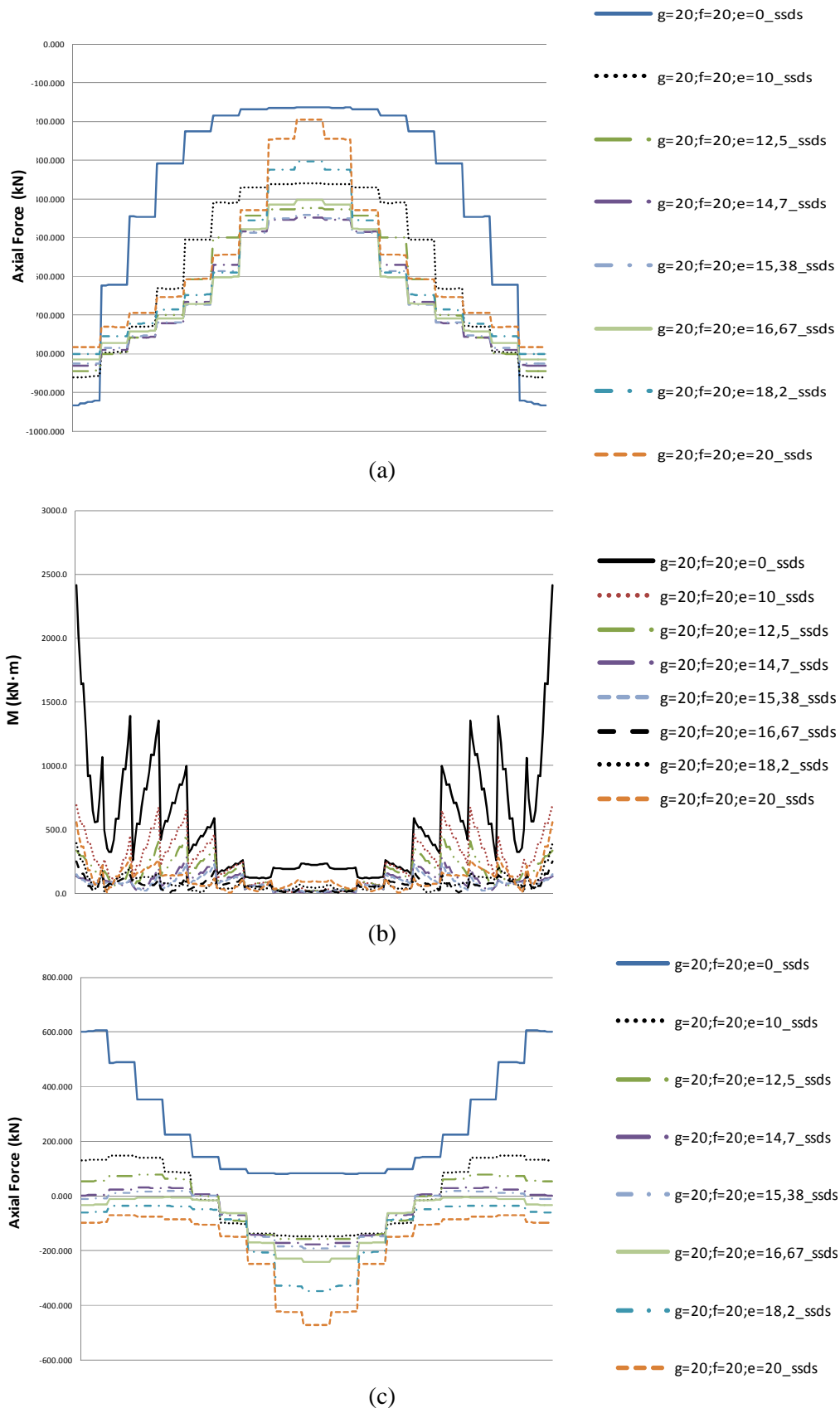
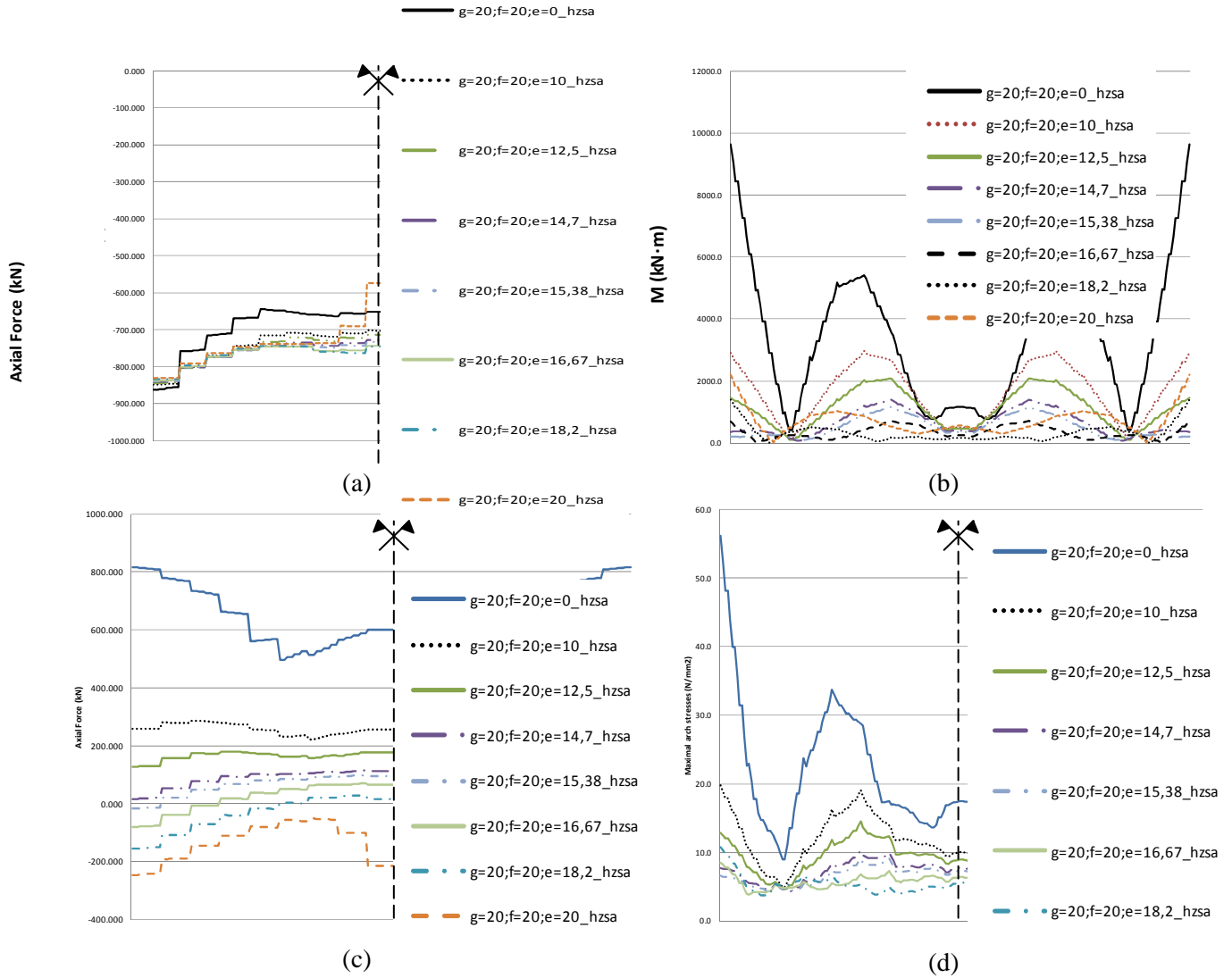


Figure 2-11: Internal forces under  $q$  comparison for  $g=20$  for the parametrical study of  $e$ , employing a stiff struts-deck system (cross-sectional values shown in Table 1-1): (a) Arch axial forces; (b) Arch total bending moments; (c) Deck axial. The abscissas of (a) and (b) are the arch length from 0 to  $L_A$  and for (c), the abscissas are the length of the deck from 0 to  $L_D$





**Figure 2-12: Internal forces under  $q$  comparison for  $g=20$  for the parametrical study of  $e$ , employing a horizontally stiff arch (cross-sectional values shown in Table 1-1): (a) Arch axial forces; (b) Arch total bending moments; (c) Deck axial forces. The abscissas for (a) to (c) are the arch length from 0 to  $L_A$  and for (d), the abscissas are the length of the deck from 0 to  $L_D$**

When employing a **HoriZontally Stiff Arch (HZSA)**:

- The axial forces in the arch become more homogeneous along the arch than for the reference model (Figure 2-5a).
- The variation of  $e$  does not influence the axial forces in the arch as much as in the reference model, especially at the arch springings (Figure 2-12a).
- The axial forces in the deck increase greatly (Figure 2-12c) in comparison with the reference model (Figure 2-5a).
- The total bending moments in the arch increase and the punctual influence of the struts is lower (Figure 2-12b).
- The deck axial forces become more homogeneous and the value of  $e$  gains influence (Figure 2-12c).

### 2.3 STRESS BEHAVIOUR AND COMPARISON IN ULTIMATE LIMIT STATE

In Figure 2-13 the comparison of the arch stresses behavior only under  $q=10\text{kN/m}$  for different  $e$  values, for  $g=20\text{m}$ ,  $f=20\text{m}$  and the reference model cross-sections (Table 1-1) is shown and in Figure 2-14, for SSDS (Table 1-1). The main aspects of the results for different models are analysed in this section.

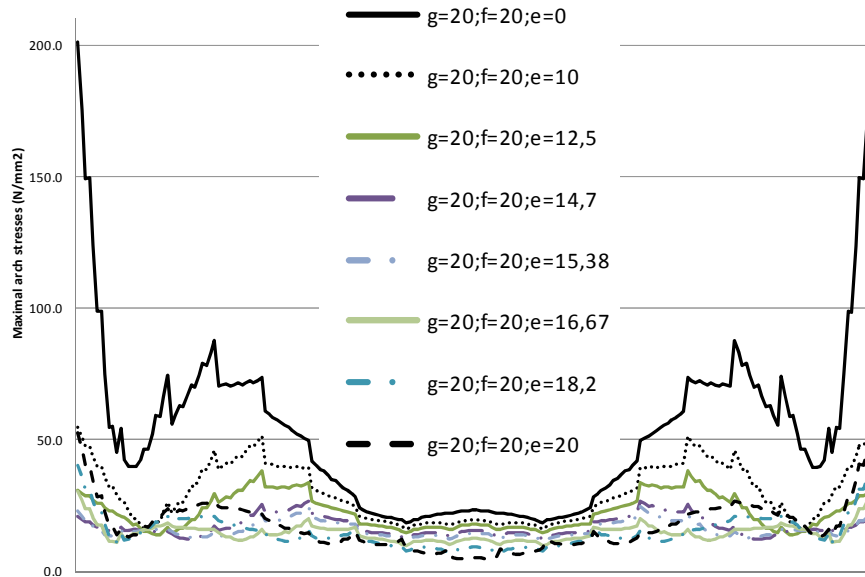


Figure 2-13: Arch stresses comparison under  $q$  for  $g=20$  and  $f=20\text{m}$  for the parametrical study of  $e$ , employing the reference cross-sections (Table 1-1). The abscissas are the arch length from 0 to  $L_A$

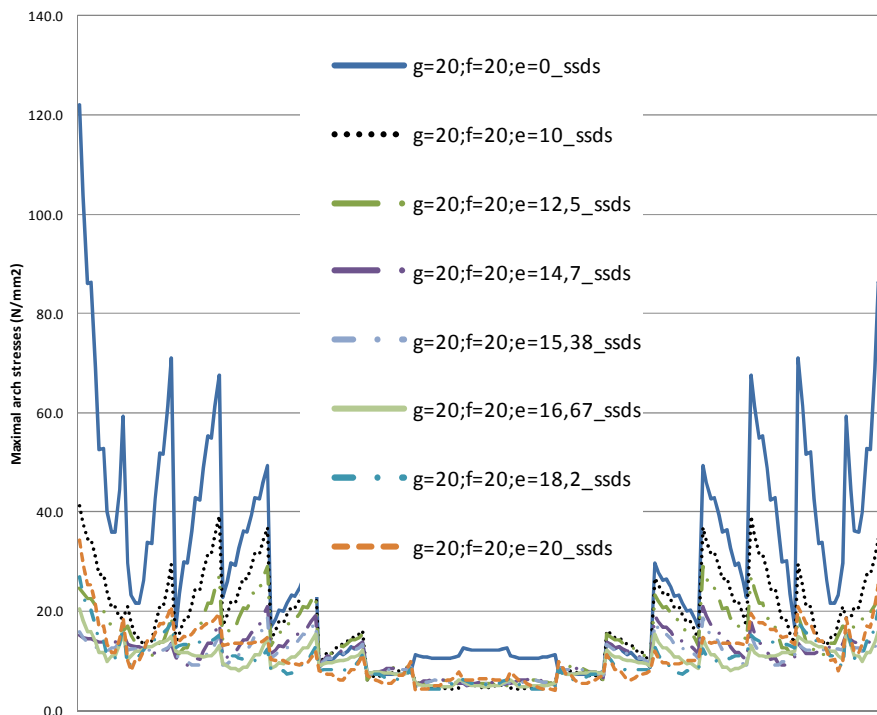


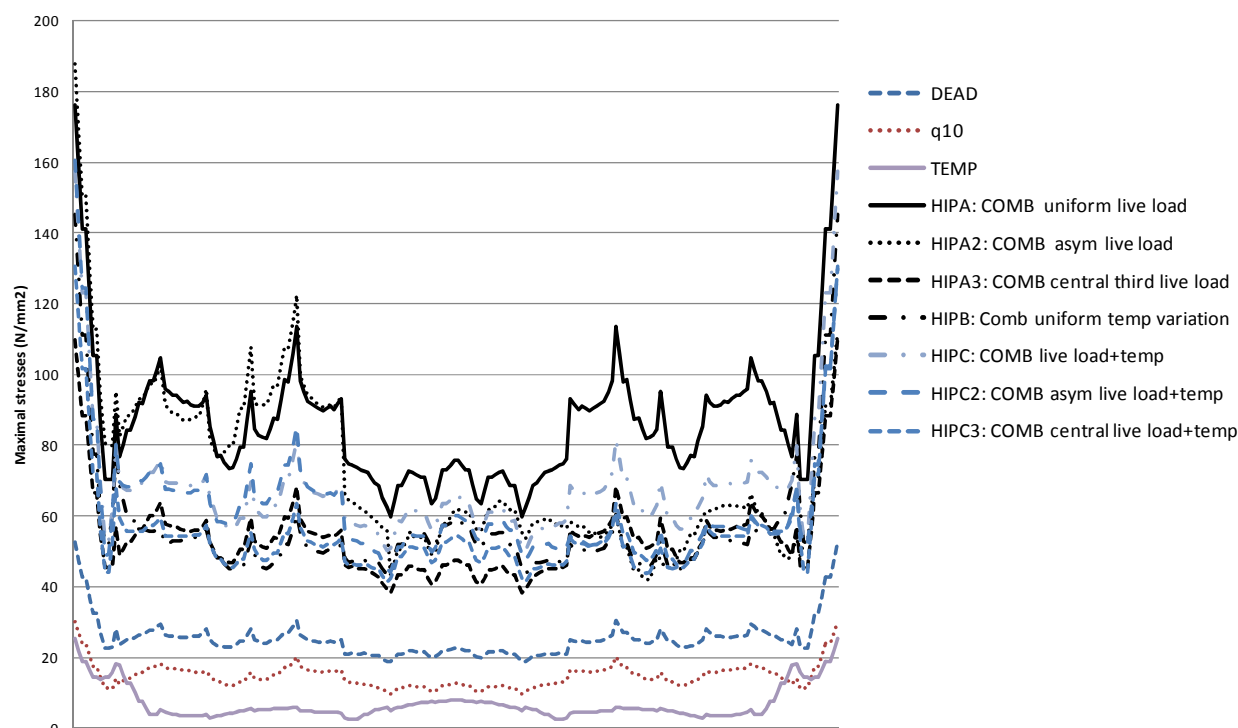
Figure 2-14: Arch stresses comparison under  $q$  for  $g=20$  and  $f=20\text{m}$  for the parametrical study of  $e$ , employing a stiff struts-deck system (cross-sectional values shown in Table 1-1). The abscissas are the arch length from 0 to  $L_A$

- Employing a SSDS lowers the stresses in the arch (Figure 2-13 and Figure 2-14).
- Whatever the  $g$  and  $f$  values, stresses in the arch for  $e \geq g/1,36$  are lower than for smaller  $e$  values (Figure 2-13 and Figure 2-14).

In Figure 2-15 the comparison between different loading cases and combination of the arch stresses is represented for the specific case  $e=16,67\text{m}$ ;  $g=20$  and  $f=20\text{m}$ . The worst loading combinations for the different models are commented in the following lines:

- For  $g=20\text{m}$ ,  $f=10$  to  $25\text{m}$  and  $e=16,67\text{m}$  when employing the reference model cross-sections (Table 1-1), the worst hypothesis for the arch is combination A1 except at springing and  $L_A/4$  where A2 is worse, determined by the loading case  $l_a$  (Figure 2-15).
- The importance of asymmetrical loading for stresses in the arch diminishes when increasing the value of  $f$  or the stiffness of the strut-deck system.
- The worst loading cases combination for  $g=20\text{m}$ ,  $f=50\text{m}$ ,  $e=g/1,2=16,67\text{m}$  for the reference model cross-sections and for  $g=20\text{m}$ ,  $f=20\text{m}$ ,  $e=16,67\text{m}$  for the SSDS model (Table 1-1) cross-sections is A1.
- When the structural behaviour of the arch is not under control ( $e=0$ ) A1 is the most critical loading combination for the arch, ie:  $lu$  is the worst live load for arch stresses, since the out-of-plane behaviour is predominant over the arch behaviour, whatever the cross-section.
- For the reference model cross-sections (Table 1-1) and  $e$  in the range of values  $g/1,36 \leq e < g/1,2$  A2 increases its influence on arch maximal stresses from the springings to  $L_A/4$ , in the rest of the arch length A1 is the worst loading combination.
- For  $g/1,2 \leq e < g$  stresses caused by A2 are maximal at springings and  $L_A/3$  but get closer to A1,  $la$  loses influence in front of  $lu$ .
- When employing a HZSA for  $e \geq g/1,6$  ,A2 increases its influence on arch maximal stresses from the springings to  $L_A/3$ .
- When employing a SSDS and  $e$  in the range of values  $g/1,6 \leq e < g/1,1$  A2 and A1 cause similar values of stresses at springings. Therefore, we can conclude that it is not necessary to consider  $la$  whatever the value of  $e$  when employing a SSDS.
- When employing a HZSA and a SSDS (Table 1-1), the influence of temperature variation on the arch stresses increases.
- When employing a HZSA and  $e$  in the range of values  $g/1,36 \leq e \leq g/1,1$ , B is the worst loading combination at approximately from  $L_A/25$  to  $L_A/6$  and for  $e = g/1,1$  also at the arch crown.
- For  $e > g/1,1$  the difference of the stresses caused by B, A2 and A1 decreases, but A1 is not as predominant as for the reference model or a SSDS.
- When employing a SSDS and  $e$  in the range of values  $g/2 \leq e < g/1,1$ , B is the worst loading combination at the arch crown.

- For  $e \geq g/1,1$  worst arch stresses at the arch crown are caused again by A1 and at springings for  $g/1,2 \leq e < g$  stresses caused by A1, A2 and B are very close.
- For  $e = g$  A1 causes the largest arch stresses in the whole length of the arch.



**Figure 2-15: Stresses in the arch caused by different loading cases combination for  $g=20\text{m}$ ,  $f=20\text{m}$  and  $e=16,67\text{m}$  when employing the reference model cross-sections (Table 1-1). The abscissas are the arch length from 0 to  $L_A$**

For  $g=20\text{m}$ ,  $f=20\text{m}$  and  $e=16,67\text{m}$ , the models with different stiffness distribution have been dimensioned. The following cross-sections for S 355 steel have been obtained employing a linear analysis:

- The arches are CHS of 750mm diameter and thickness ranging from 10mm at span center to 30mm at springings for the reference model, from 6mm at span center to 22mm at springings for the SSDS model and 2 steel tubes for the arch cross-section of dimensions: 1000x1000mm and 6mm thickness joint by K bracings for the HZSA model.
- The struts are CHS of 300mm diameter and thickness ranging from 15mm at extremes to 35mm at span center for the reference model and from 8mm at extremes to 45mm at span center for the HZSA model. For the SSDS model, CHS of 750mm diameter were employed, with thickness ranging from 6mm at extremes to 12mm at  $L/3$  approximately.
- The deck is a 4000x700≠10mm steel box girder for the reference model and for the HZSA model and 7000x700≠10mm for the SSDS model. It would be enough with 3mm to resist the stresses considering a compact cross-section. However, 10mm are considered for local bending moments, local instability of compressed plates and durability.

These design cross-sections are employed in the geometrically non-linear analysis in chapter VI.

## 2.4 EFFICIENCY CRITERIA

The results of the chosen criteria are shown for the different models which have been studied in tables from Table 2-2 to Table 2-11. In these tables the nomenclature already given in section 1.3 is employed. Please use the bookmark to comfortably interpret the tables, and note whether the length is considered or not, since the nomenclature and units of the criteria are modified. The following values are specifically employed for the tables in this section:

- $e^*$  is the value of  $e$  which minimizes each criteria and is measured in meters.
- $i$ =% of difference of B (bookmark and section 1.3) from the most efficient  $e$  value for B ( $e^*$ )

A different  $e^*$  is obtained for each criteria. The results of the efficiency criteria are commented in the following lines:

- For high  $g$  values, ie: when spatial behaviour increases, the influence of  $e$  is larger ( $i$  values in Table 2-2, Table 2-4 and Table 2-5).
- For  $g=5$  the relative difference between stresses when varying  $e$  in the range of  $g/1,36$  and  $g$  values is negligible ( $i$  value in Table 2-2). However, for  $g=20$ , the value of  $e$  has a high influence ( $i$  value in tables from Table 2-2 to Table 2-5).
- Whatever the value of  $g$ , minimising the value of the sum of the stresses of the whole system is equivalent to minimising the sum of stresses in the arch (Table 2-2, Table 2-4 and Table 2-5). However, for  $g=20$  when employing a stiff strut-deck system, the value of  $e$  which minimises the value of the sum of the stresses of the whole system and the one which minimises the sum of stresses in the arch and the bending moments are different (B, A and C respectively in Table 2-6). Nevertheless, the relative differences for  $e$  values in the range of  $g/1,36$  and  $g$  are negligible. Therefore, in order to determine the most efficient  $e$  value, the criteria referring to minimising the stresses along the arch or in the whole bridge can be considered equivalent.

Model	Criteria								i
	A	B	C	D	E	F	G	H	
$g=5;f=20;e=0$	20154	38140	99521	3441	5597	198	35	50	53,2
$g=5;f=20;e=2,5$	13992	28521	41985	2267	3145	108	16	21	14,5
$g=5;f=20;e=3,13$	12642	26547	30459	1988	2705	94	13	16	6,6
$g=5;f=20;e=3,68$	11815	25323	23387	1808	2469	91	12	12	1,7
$g=5;f=20;e=3,85$	11692	25108	22128	1780	2441	95	12	11	0,8
$g=5;f=20;e=4,17$	11613	24902	21307	1771	2457	101	14	11	0,0
$g=5;f=20;e=5$	12211	25619	28011	1960	2806	120	20	14	2,9
$e^*$	$e=4,17$	$e=4,17$	$e=4,17$	$e=4,17$	$e=3,85$	$e=3,68$	$e=3,68$	$e=4,17$	

**Table 2-2: Efficiency indicators for the case study employing  $g=5$  and  $f=20$**

Model	Criteria							
	A	B	C	D	E	F	G	H
e=0	6786157	12842146	33509786	1158468	1884508	66809	11735	16668
e=2,5	4422557	9014566	13270264	716522	994017	33979	5199	6783
e=3,13	3947664	8289779	9511342	620696	844677	29277	4209	4913
e=3,68	3658895	7841646	7242205	559966	764448	28185	3591	3751
e=3,85	3612591	7757648	6837005	550103	754118	29226	3653	3524
e=4,17	3576376	7669104	6561994	545451	756536	31258	4311	3268
e=5	3754652	7877122	8612656	602606	862845	36849	6138	4422
e*	e=4,17	e=4,17	e=4,17	e=4,17	e=3,85	e=3,68	e=3,68	e=4,17

**Table 2-3: Efficiency indicators for the case study employing  $g=5$  and  $f=20$  considering the length of the elements of the bridge**

Model	Criteria								
	A	B	C	D	E	F	G	H	i
g=10;f=20;e=0	31047	57970	208408	5430	10280	390	70	105	159,7
g=10;f=20;e=5	18637	31205	86062	3181	4929	151	26	43	39,8
g=10;f=20;e=6,25	15578	26272	57055	2586	3807	114	20	27	17,7
g=10;f=20;e=7,35	13482	23068	37610	2167	3054	102	16	17	3,3
g=10;f=20;e=7,69	13124	22548	34260	2105	2947	106	15	14	1,0
g=10;f=20;e=8,33	12899	22325	32396	2085	2970	120	19	12	0,0
g=10;f=20;e=10	14817	25892	49663	2501	3887	184	33	26	16,0
e*	e=8,33	e=8,33	e=8,33	e=8,33	e=7,69	e=7,35	e=7,69	e=8,33	

**Table 2-4: Efficiency indicators for the case study employing  $g=10$  and  $f=20$**

Models	Criteria							
	A (MPa)	B (MPa)	C (kN·m)	D (MPa)	E (MPa)	F (MPa)	G (mm)	i
e=0	60977	122328	497072	10636	21620	1123	233	307
e=10=g/2	34197	57339	225001	6047	10140	325	97	91
e=12,5=g/1,6	26565	42638	150783	4615	7262	220	60	42
e=14,7=g/1,36	20751	33170	95021	3487	5156	174	32	10
e=15,38=g/1,3	19462	31485	82797	3247	4786	173	26	5
e=16,67=g/1,2	17958	30026	69354	2999	4502	188	19	0
e=18,2=g/1,1	17919	31323	70866	3043	4801	227	29	4
e=20=g/1	19754	35904	90248	3463	5865	292	45	20
e*	e=18,2	e=16,67	e=16,67	e=16,67	e=16,67	e=15,38	e=16,67	

**Table 2-5: Efficiency indicators for the case study employing  $g=20$  and  $f=20$**

- For  $g=5$  and  $g=10$  the sum of stresses under a uniform load and the sum of maximal stresses in the arch show different most efficient  $e$  values, but again the relative differences for  $e$  values in the range of  $g/1,36$  and  $g$  are negligible (Table 2-2 and Table 2-4).
- Whatever the value of  $g$ ,  $f$  and the cross-sections employed, the value of  $e$  which minimises the maximal stress in the arch is lower than the one which minimises the sum of stresses in the whole length of the arch (Table 2-2, Table 2-4 and Table 2-5).
- The value of  $e$  which minimizes the sum of the maximal stresses in the whole bridge is independent of the stiffness of the strut-deck system or that of the arch and of the value of  $f$  and is equal to  $g/1,20$  (from Table 2-8 to Table 2-11, Table 2-6 and Table 2-7).

Model	Criteria								
	A	B	C	D	E	F	G	H	i
$g=20;f=20;e=0_{ssds}$	46690	79430	413586	5814	10154	910	122	178	242,1
$g=20;f=20;e=10_{ssds}$	26511	40498	165059	3528	5469	300	41	76	74,4
$g=20;f=20;e=12,5_{ssds}$	21824	31581	108454	2879	4145	201	29	49	36,0
$g=20;f=20;e=14,7_{ssds}$	17960	25726	68619	2319	3149	152	21	29	10,8
$g=20;f=20;e=15,38_{ssds}$	16971	24536	59250	2185	2937	150	19	23	5,7
$g=20;f=20;e=16,67_{ssds}$	15559	23216	47511	2043	2746	167	20	17	0,0
$g=20;f=20;e=18,2_{ssds}$	14988	23253	45969	2078	2864	194	27	16	0,2
$g=20;f=20;e=20_{ssds}$	15972	25329	60811	2329	3348	236	34	24	9,1
$e^*$	$e=18,2$	$e=16,67$	$e=18,2$	$e=16,67$	$e=16,67$	$e=15,38$	$e=15,38$	$e=18,2$	

**Table 2-6: Efficiency criteria for  $g=20, f=20$  and different  $e$  values employing the SSDS cross-sections defined in Table 1-1**

Model	Criteria								
	A	B	C	D	E	F	G	H	i
$g=20;f=20;e=0_{hzsa}$	26875	83942	1691104	4536	14927	321	56	46	364,1
$g=20;f=20;e=10_{hzsa}$	15109	36942	757311	2471	6485	138	20	18	104,2
$g=20;f=20;e=12,5_{hzsa}$	12366	27096	514620	1939	4568	106	14	13	49,8
$g=20;f=20;e=14,7_{hzsa}$	10291	20984	302923	1477	3136	82	10	11	16,0
$g=20;f=20;e=15,38_{hzsa}$	9763	19456	243948	1340	2785	76	9	10	7,6
$g=20;f=20;e=16,67_{hzsa}$	8973	18088	162000	1160	2381	74	8	10	0,0
$g=20;f=20;e=18,2_{hzsa}$	8819	18508	150274	1090	2378	83	11	10	2,3
$g=20;f=20;e=20_{hzsa}$	9968	21790	323507	1319	3120	95	14	11	20,5
$e^*$	$e=18,2$	$e=16,67$	$e=18,2$	$e=18,2$	$e=18,2$	$e=16,67$	$e=16,67$	$e=16,67$	

**Table 2-7: Efficiency criteria for  $g=20, f=20$  and different  $e$  values employing the HZSA cross-sections defined in Table 1-1**

In tables Table 2-8 to Table 2-11 the efficiency criteria when varying  $e$  for different  $f$  values are shown. The length of the different struts for the studied  $e$  values for  $f=20\text{m}$  is displayed in Table 2-12. The main conclusions of the analysis of the results of these tables are the following:

- For the reference model, the stress indicator is equivalent to the total mass indicator since the total length of the structures is lowest for the most efficient  $e$  value (Table 2-12). The results for the linear elastic analysis will not change with the consideration of geometrical non-linearities since displacements are lowest for the most efficient  $e$  value (Table 2-2, Table 2-4, Table 2-5, Table 2-6, Table 2-7 and from Table 2-8 to Table 2-11). Therefore, given a  $g$  value  $e=g/1,20$  is always recommendable, whatever the value of  $g$ ,  $f$  and the cross-section values.
- The higher the  $f$  value, the higher the importance of choosing an adequate  $e$  value (i values in Table 2-5 and from Table 2-8 to Table 2-11). Obtaining a higher stiffness in the key points  $g/1,2$  becomes more critical because: (i) the struts are longer and hence less stiff and (ii) the out-of-plane behaviour of the arch increases at approximately  $L_A/3$ , which is the key point range of values (section 4).
- For all  $g$  and  $f$  values and for all cross-sections, the value of  $e$  for which the sum of maximal total bending moments along the arch is minimal is the same as the one for which the sum of maximal stresses along the arch is minimal, ie:  $e=g/1,20$  (Table 2-6). For all  $g$  and  $f$  values and for all cross-sections, the relative differences for  $e$  values in the range of  $g/1,3$  and  $g/1,1$  are negligible (Table 2-2, Table 2-4, Table 2-5, Table 2-6, Table 2-7 and from Table 2-8 to Table 2-11). Therefore, employing the antifunicularity criteria for fixing an efficient  $e$  value for SABWCSD is a valid design procedure.

Model	Criteria								
	A	B	C	D	E	F	G	H	i
$g=20;f=10;e=0;v=0$	57202	128288	401278	9757	22487	1336	239	151	216,0
$g=20;f=10;e=10;v=0$	36180	63925	171735	6282	11199	389	66	72	57,5
$g=20;f=10;e=12,5;v=0$	30624	50524	115031	5244	8638	288	42	53	24,5
$g=20;f=10;e=14,7;v=0$	26491	41948	75572	4431	6798	243	34	42	3,3
$g=20;f=10;e=15,38;v=0$	25588	40810	67838	4255	6500	239	33	40	0,5
$g=20;f=10;e=16,67;v=0$	24666	40594	61499	4067	6317	244	39	38	0,0
$g=20;f=10;e=18,2;v=0$	24866	43041	68809	4145	6765	270	48	41	6,0
$g=20;f=10;e=20;v=0$	26913	47643	87079	4582	7800	332	60	48	17,4
$e^*$	$e=16,67$	$e=16,67$	$e=16,67$	$e=16,67$	$e=16,67$	$e=15,38$	$e=15,38$	$e=16,67$	

**Table 2-8: Efficiency indicators for the case study employing  $g=20$  and  $f=10$  and reference cross-section values**



Model	Criteria								
	A	B	C	D	E	F	G	H	i
$g=20;f=15;e=0;v=0$	59132	124675	459789	10252	21999	1205	216	192	271,3
$g=20;f=15;e=10;v=0$	34515	59234	203578	6078	10442	346	59	82	76,4
$g=20;f=15;e=12,5;v=0$	27633	44998	135364	4787	7667	242	39	54	34,0
$g=20;f=15;e=14,7;v=0$	22505	35976	85783	3783	5666	197	28	33	7,1
$g=20;f=15;e=15,38;v=0$	21401	34563	75513	3573	5319	196	27	28	2,9
$g=20;f=15;e=16,67;v=0$	20112	33580	65009	3356	5086	209	34	23	0,0
$g=20;f=15;e=18,2;v=0$	20101	35307	68360	3401	5451	246	44	26	5,1
$g=20;f=15;e=20;v=0$	22052	40084	88181	3833	6562	311	56	38	19,4
$e^*$	$e=18,2$	$e=16,67$	$e=16,67$	$e=16,67$	$e=16,67$	$e=15,38$	$e=15,38$	$e=16,67$	

**Table 2-9: Efficiency indicators for the case study employing  $g=20$  and  $f=15$ , for reference cross-section values**

Model	Criteria								
	A	B	C	D	E	F	G	H	i
$g=20;e=0;f=25;v=0$	157284	209853	1401235	27918	37466	1856	335	70	652,4
$g=20;e=10;f=25;v=0$	34235	56196	240291	6044	9937	311	52	113	101,5
$g=20;e=12,5;f=25;v=0$	26140	41277	162504	4529	7025	207	37	69	48,0
$g=20;e=14,7;f=25;v=0$	19859	31466	102769	3322	4883	160	27	35	12,8
$g=20;e=15,38;f=25;v=0$	18422	29650	89100	3059	4485	159	24	26	6,3
$g=20;e=16,67;f=25;v=0$	16724	27892	73114	2784	4148	174	28	21	0,0
$g=20;e=18,2;f=25;v=0$	16635	28824	72939	2825	4402	213	38	34	3,3
$g=20;e=20;f=25;v=0$	18477	33295	91957	3239	5419	276	50	53	19,4
$e^*$	$e=18,2$	$e=16,67$	$e=18,2$	$e=16,67$	$e=16,67$	$e=15,38$	$e=15,38$	$e=16,67$	

**Table 2-10: Efficiency indicators for the case study employing  $g=20$  and  $f=25$ , for reference cross-section values**

Model	Criteria								
	A	B	C	D	E	F	G	H	i
$g=20;f=50;e=0;v=0$	66346	115741	588436	11393	20211	942	163	556	370,2
$g=20;f=50;e=10;v=0$	35115	53551	282091	5960	9297	280	48	215	117,5
$g=20;f=50;e=12,5;v=0$	26205	38719	197912	4321	6451	202	36	129	57,3
$g=20;f=50;e=14,7;v=0$	19049	29064	130741	2998	4307	136	24	60	18,1
$g=20;f=50;e=15,38;v=0$	17272	26998	113582	2700	3884	135	21	41	9,7
$g=20;f=50;e=16,67;v=0$	14962	24616	89478	2367	3486	149	22	34	0,0
$g=20;f=50;e=18,2;v=0$	14462	24939	80704	2375	3658	183	31	63	1,3
$g=20;f=50;e=20;v=0$	16221	29006	96496	2778	4568	236	41	102	17,8
$e^*$	$e=18,2$	$e=16,67$	$e=18,2$	$e=16,67$	$e=16,67$	$e=15,38$	$e=15,38$	$e=16,67$	

**Table 2-11: Efficiency indicators for the case study employing  $g=20$  and  $f=50$ , for reference cross-section values**

Strut number	e=0	e=10	e=12,5	e=14,7	e=16,69	e=18,2	e=20
1 (nearest to springing)	16.17	16.62	17.64	18.78	19.93	20.92	22.16
2	14.29	11.96	12.61	13.55	14.61	15.56	16.79
3	14.26	8.70	8.66	9.21	10.08	10.96	12.17
4	15.39	7.27	6.17	5.96	6.43	7.16	8.30
5	16.91	7.51	5.51	4.21	3.82	4.19	5.20
6	18.33	8.49	6.11	4.13	2.69	2.21	2.86
7	19.38	9.41	6.93	4.77	2.89	1.58	1.27
8 (nearest to span center)	19.93	9.93	7.43	5.23	3.28	1.76	0.32
		nearest strut to arch deck intersection in plan view, ie: most vertical struts					
		shortest strut of the model					
		strut that is shortest in this model compared to the rest of models					

**Table 2-12. Length of struts comparison between models with L=100, g=20 and f=20**

The value of  $e^*$  concluded as the most efficient is proportional to  $g$  and has a constant relationship with  $L$  and  $f$ . This is shown in Figure 2-16 and Figure 2-17:

- It can be appreciated that the relationship between the intersection point deck/arch in plan and of the projection of this point on the arch rise in layout has the same value: approximately an 80% of their value, ie:  $e^*/g=0,8$  and  $f_{intersection}/f=0,8$  (Figure 2-16).
- The deck of the studied cases has a circular curvature and the arch a parabolic one. Since the aforementioned relationships have the same value, it can be stated that the variation of the key points to control their behavior depends on their sag or rise, but hardly depends on the shape.
- The value of  $e^*$  is independent of the  $f$  value, as suspected a priori, because the variation  $f$  does not affect the plan view geometry of the bridge when employing a planar vertical arch, ie: the key points where it is most favourable to increase the stiffness of the system do not change with  $f$ . Not only do these points have a constant relationship with  $g$  (which can still be considered constant with  $L$ ), but also with  $f$  (Figure 2-17).

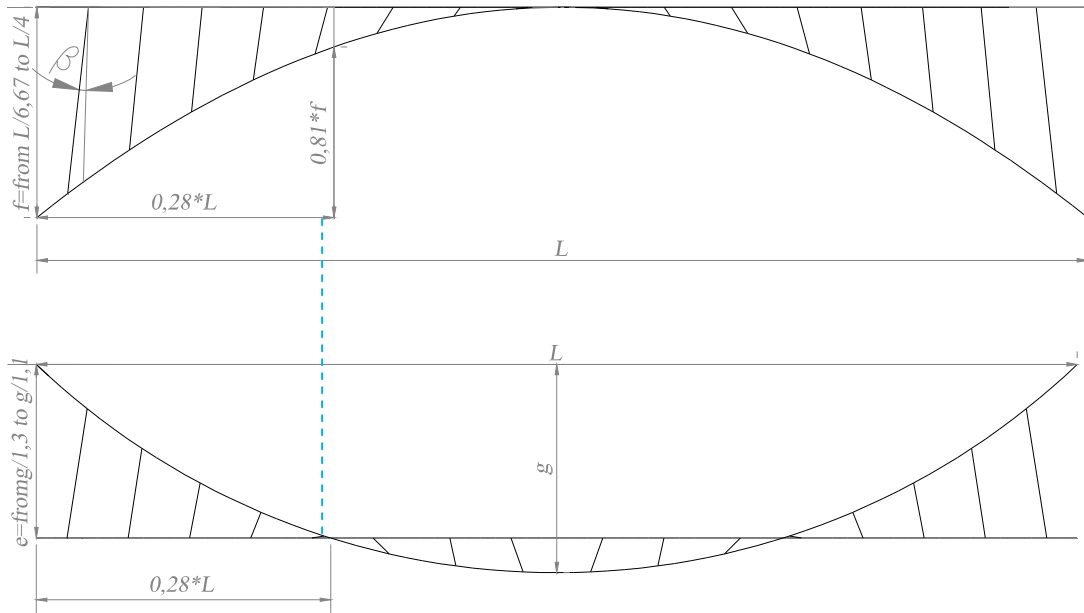


Figure 2-16: Relationships of the most efficient  $e$  value ( $e^*$ ) with  $L$  and  $f$

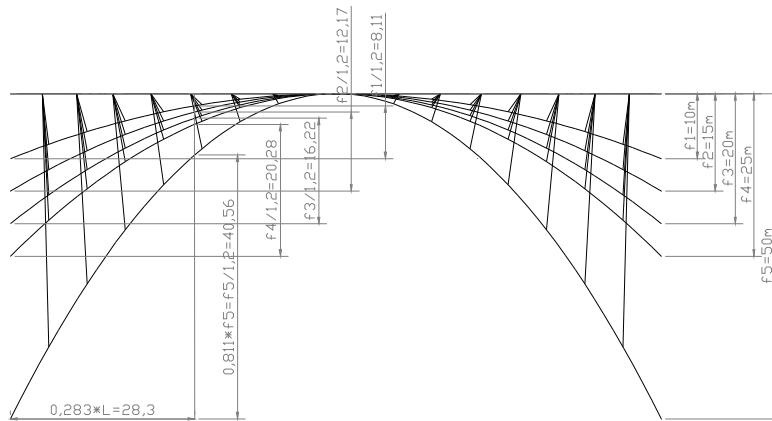


Figure 2-17: Relationships of the most efficient  $e$  with  $L$  and  $f$  for different  $f$  values

### Comparison of the different stiffness distributions

A comparison of the different stiffness distributions has been done for various criteria and is shown in tables from Table 2-13 to Table 2-21.

For  $g=20$  the following conclusions regarding the stiffness distribution can be drawn:

- Whatever the  $e$  value, employing a SSDS diminishes all the stresses in the arch, deck and struts, and also for the total bending moments in the arch (Table 2-13, Table 2-14 and Table 2-15), as it was the case for IDABWIC (Sarmiento-Comeías et al 2012).
- Regarding the stresses in the arch, employing a strut-deck system with a large transverse stiffness highly reduces the maximal stress in the arch, and has even more influence when considering the stresses along the whole arch (Table 2-13). The influence of employing a stiff strut-deck system is lower for values of  $e$  between  $g/1,30$  and  $g/1,20$ , ie: for those

values of  $e$  which give lower stresses in the arch, the strut-deck stiffness has a lower influence (Table 2-13 and Table 2-15). Nevertheless, the stiffness of the strut-deck system has still a high influence. Therefore, whatever the value of  $e$ , it is always worth controlling the stiffness strut-deck system.

- However, depending on the stiffness of the strut-deck system it might be worth or not adjusting the value of  $e$ . When employing the reference cross-sections, it is highly convenient to adjust the value of  $e$  in order to diminish the stresses along the whole bridge length (Table 2-2, Table 2-4, Table 2-5, from Table 2-8 to Table 2-11, Table 2-6 and Table 2-7).
- Employing a HZSA (Table 1-1) diminishes the arch and the total bridge stresses with respect to the reference model (Table 2-16 and Table 2-17) or with SSDS model (Table 2-18 and Table 2-19), especially the stresses in the arch are largely diminished when compared with the reference model (Table 2-16). However, the sum of bending moments in the arch increases greatly (Table 2-17 and Table 2-19).

	Maximal arch stress (MPa)*	Relative difference with respect to SSDS (%)	Sum of arch stresses (MPa)	Relative difference with respect to SSDS (%)
g=20;f=20;e=0_ssd	910.2	-23.36	46690.0	-30.60
g=20;f=20;e=0	1122.9		60976.5	
g=20;f=20;e=10_ssd	299.8	-8.35	26510.6	-28.99
g=20;f=20;e=10	324.9		34197.1	
g=20;f=20;e=12,5_ssd	201.1	-9.46	21823.5	-21.72
g=20;f=20;e=12,5	220.2		26564.5	
g=20;f=20;e=14,7_ssd	152.0	-14.44	17960.0	-15.54
g=20;f=20;e=14,7	174.0		20751.2	
g=20;f=20;e=15,38_ssd	150.0	-15.47	16970.6	-14.68
g=20;f=20;e=15,38	173.1		19462.4	
g=20;f=20;e=16,67_ssd	167.2	-12.31	15559.5	-15.42
g=20;f=20;e=16,67	187.8		17958.0	
g=20;f=20;e=18,2_ssd	194.3	-16.75	14987.7	-19.56
g=20;f=20;e=18,2	226.8		17919.5	
g=20;f=20;e=20_ssd	235.9	-23.63	15972.2	-23.67
g=20;f=20;e=20	291.6		19753.6	

**Table 2-13: Arch stresses comparison for the cross-sections of the reference model and SSDS model in Table 1-1, for  $g=20\text{m}$ ,  $f=20\text{m}$  and different  $e$  values**

	Maximal deck stress (MPa)*	Relative difference (%)	Sum of deck stresses (Mpa)	Relative difference (%)	Maximal strut stress (MPa)*	Relative difference (%)	Sum of strut stresses (MPa)	Relative difference (%)
g=20;f=20;e=0_ssds	257.254561		25545.45569		365.5994193		7194.421325	
g=20;f=20;e=0	399.1538378	-55.16	43497.17547	-70.27	682.424154	-86.66	17854.58018	-148.17
g=20;f=20;e=10_ssds	101.685032		10715.06099		153.7690157		3272.492246	
g=20;f=20;e=10	106.0514189	-4.29	12437.31597	-16.07	430.2468883	-179.80	10704.36536	-227.10
g=20;f=20;e=12,5_ssds	68.7159539		7257.031534		114.6038807		2500.914508	
g=20;f=20;e=12,5	76.214501	-10.91	7845.006215	-8.10	367.9891763	-221.10	8228.286573	-229.01
g=20;f=20;e=14,7_ssds	46.39222784		5731.559054		82.45936174		2034.816285	
g=20;f=20;e=14,7	59.81215962	-28.93	6193.103427	-8.05	286.5126532	-247.46	6226.063582	-205.98
g=20;f=20;e=15,38_ssds	42.33094027		5631.886908		73.57750118		1933.296465	
g=20;f=20;e=15,38	56.52194114	-33.52	6310.544533	-12.05	255.2760451	-246.95	5711.762286	-195.44
g=20;f=20;e=16,67_ssds	41.32020309		5809.903001		72.37950884		1846.260912	
g=20;f=20;e=16,67	65.516318	-58.56	7085.575567	-21.96	198.6148466	-174.41	4982.132218	-169.85
g=20;f=20;e=18,2_ssds	47.69462606		6319.953007		86.11823289		1945.323102	
g=20;f=20;e=18,2	84.63339386	-77.45	8583.820337	-35.82	213.9047494	-148.38	4819.90554	-147.77
g=20;f=20;e=20_ssds	56.10743357		7024.152009		104.3603745		2332.373063	
g=20;f=20;e=20	103.7177725	-84.86	10511.75533	-49.65	263.6731898	-152.66	5638.290372	-141.74

**Table 2-14: Deck stresses comparison for the cross-sections of the reference model and SSDS model in Table 1-1, for g=20m, f=20m and different e values**

	Sum of total stresses (Mpa)	Relative difference (%)	Sum of total bending moments in the arch (kN·m)	Relative difference (%)
g=20;f=20;e=0_ssds	79430		413586	
g=20;f=20;e=0	122328	-54.01	497072	-20.19
g=20;f=20;e=10_ssds	40498		165059	
g=20;f=20;e=10	57339	-41.58	225001	-36.32
g=20;f=20;e=12,5_ssds	31581		108454	
g=20;f=20;e=12,5	42638	-35.01	150783	-39.03
g=20;f=20;e=14,7_ssds	25726		68619	
g=20;f=20;e=14,7	33170	-28.94	95021	-38.48
g=20;f=20;e=15,38_ssds	24536		59250	
g=20;f=20;e=15,38	31485	-28.32	82797	-39.74
g=20;f=20;e=16,67_ssds	23216		47511	
g=20;f=20;e=16,67	30026	-29.33	69354	-45.98
g=20;f=20;e=18,2_ssds	23253		45969	
g=20;f=20;e=18,2	31323	-34.71	70866	-54.16
g=20;f=20;e=20_ssds	25329		60811	
g=20;f=20;e=20	35904	-41.75	90248	-48.41

**Table 2-15: Total bridge stresses comparison for the cross-sections of the reference model and SSDS model in Table 1-1, for g=20m, f=20m and different e values**

	Maximal arch stress (MPa)*	Relative difference with respect to HZSA (%)	Sum of arch stresses (MPa)	Relative difference with respect to HZSA (%)
g=20;f=20;e=0_hzsa	320,5255562	-250,32	26875,37847	-126,89
g=20;f=20;e=0	1122,865996		60976,53743	
g=20;f=20;e=10_hzsa	137,922457	-135,56	15109,30511	-126,33
g=20;f=20;e=10	324,8883673		34197,12571	
g=20;f=20;e=12,5_hzsa	106,134813	-107,45	12365,54911	-114,83
g=20;f=20;e=12,5	220,1730602		26564,50849	
g=20;f=20;e=14,7_hzsa	82,30941764	-111,35	10291,48298	-101,63
g=20;f=20;e=14,7	173,9573784		20751,2053	
g=20;f=20;e=15,38_hzsa	75,67933824	-128,76	9763,311221	-99,34
g=20;f=20;e=15,38	173,1245698		19462,41819	
g=20;f=20;e=16,67_hzsa	73,83371797	-154,38	8973,49481	-100,12
g=20;f=20;e=16,67	187,8189355		17957,98939	
g=20;f=20;e=18,2_hzsa	82,69372649	-174,26	8819,097361	-103,19
g=20;f=20;e=18,2	226,7923692		17919,49945	
g=20;f=20;e=20_hzsa	95,24298	-206,17	9968,458443	-98,16
g=20;f=20;e=20	291,6088625		19753,56572	

**Table 2-16: Arch stresses comparison for the cross-sections of the reference model and HZSA model in Table 1-1, for g=20m, f=20m and different e values**

	Sum of total stresses (Mpa)	Relative difference with respect to HZSA (%)	Sum of total bending moments in the arch (kN·m)	Relative difference with respect to HZSA (%)
g=20;f=20;e=0_hzsa	83942	-45,73	1691104	70,61
g=20;f=20;e=0	122328		497072	
g=20;f=20;e=10_hzsa	36942	-55,21	757311	70,29
g=20;f=20;e=10	57339		225001	
g=20;f=20;e=12,5_hzsa	27096	-57,36	514620	70,70
g=20;f=20;e=12,5	42638		150783	
g=20;f=20;e=14,7_hzsa	20984	-58,07	302923	68,63
g=20;f=20;e=14,7	33170		95021	
g=20;f=20;e=15,38_hzsa	19456	-61,83	243948	66,06
g=20;f=20;e=15,38	31485		82797	
g=20;f=20;e=16,67_hzsa	18088	-65,99	162000	57,19
g=20;f=20;e=16,67	30026		69354	
g=20;f=20;e=18,2_hzsa	18508	-69,24	150274	52,84
g=20;f=20;e=18,2	31323		70866	
g=20;f=20;e=20_hzsa	21790	-64,77	323507	72,10
g=20;f=20;e=20	35904		90248	

**Table 2-17: Total bridge stresses and arch bending moments comparison for the cross-sections of the reference model and HZSA model in Table 1-1, for g=20m, f=20m and different e values**

	Maximal arch stress (MPa)*	Relative difference with respect to SSDS (%)	Sum of arch stresses (Mpa)	Relative difference with respect to SSDS (%)
g=20;f=20;e=0_ssds	910,2	64,8	46690,0	42,4
g=20;f=20;e=0_hzsa	320,5		26875,4	
g=20;f=20;e=10_ssds	299,8	54,0	26510,6	43,0
g=20;f=20;e=10_hzsa	137,9		15109,3	
g=20;f=20;e=12,5_ssds	201,1	47,2	21823,5	43,3
g=20;f=20;e=12,5_hzsa	106,1		12365,5	
g=20;f=20;e=14,7_ssds	152,0	45,9	17960,0	42,7
g=20;f=20;e=14,7_hzsa	82,3		10291,5	
g=20;f=20;e=15,38_ssds	149,9	49,5	16970,6	42,5
g=20;f=20;e=15,38_hzsa	75,7		9763,3	
g=20;f=20;e=16,67_ssds	167,2	55,9	15559,5	42,3
g=20;f=20;e=16,67_hzsa	73,8		8973,5	
g=20;f=20;e=18,2_ssds	194,3	57,4	14987,7	41,2
g=20;f=20;e=18,2_hzsa	82,7		8819,1	
g=20;f=20;e=20_ssds	235,9	59,6	15972,2	37,6
g=20;f=20;e=20_hzsa	95,2		9968,5	

**Table 2-18: Arch stresses comparison for the cross-sections of the SSDS model and HZSA model in Table 1-1, for g=20m, f=20m and different e values**

	Sum of total stresses (MPa)	Relative difference with respect to SSDS (%)	Sum of total bending moments in the arch (kN·m)	Relative difference with respect to SSDS (%)
g=20;f=20;e=0_ssds	79429,9	-5,7	413585,7	-308,9
g=20;f=20;e=0_hzsa	83942,0		1691103,9	
g=20;f=20;e=10_ssds	40498,2	8,8	165058,7	-358,8
g=20;f=20;e=10_hzsa	36941,7		757310,7	
g=20;f=20;e=12,5_ssds	31581,5	14,2	108453,5	-374,5
g=20;f=20;e=12,5_hzsa	27095,9		514620,4	
g=20;f=20;e=14,7_ssds	25726,4	18,4	68618,9	-341,5
g=20;f=20;e=14,7_hzsa	20984,4		302923,4	
g=20;f=20;e=15,38_ssds	24535,7	20,7	59249,6	-311,7
g=20;f=20;e=15,38_hzsa	19455,6		243948,5	
g=20;f=20;e=16,67_ssds	23215,6	22,1	47510,7	-241,0
g=20;f=20;e=16,67_hzsa	18088,5		161999,6	
g=20;f=20;e=18,2_ssds	23253,0	20,4	45969,2	-226,9
g=20;f=20;e=18,2_hzsa	18508,2		150274,1	
g=20;f=20;e=20_ssds	25328,7	14,0	60811,0	-432,0
g=20;f=20;e=20_hzsa	21790,2		323507,0	

**Table 2-19: Total bridge stresses and arch bending moments comparison for the cross-sections of SSDS model and HZSA model in Table 1-1, for g=20m, f=20m and different e values**

In order to judge which stiffness distribution works better, the total mass of the bridge should be considered. As expected the antifunicularity criteria relies on the system stiffness distribution and to judge its validity or the stress criteria validity it is essential to calculate the mass. The results of the mass criteria and the stress criteria calculated in the different ways explained in section 1.3 are detailed in Table 2-20 and Table 2-21. The main highlights are commented in the following lines:

- The reference model is the stiffness distribution which needs the lower mass of steel for the total bridge (Table 2-20) when we dimension it according to the stress results of the first iteration (section 2.3).
- The HZSA model requires the same mass for the deck, since the stresses are widely resisted in all models but a minimal thickness is required in order to stand local bending moments, local instability of compressed plates and durability. A lower mass is needed for the struts, but a much larger one for the arch (Table 2-21).
- The SSDS model requires a slightly lower mass for the arch but much larger mass for the struts and deck (Table 2-21).
- When considering the stiffness distribution of a system, the only valid criteria to choose the most efficient distribution is calculating the total mass of the dimensioned system, a simpler criteria cannot be adopted.

Model	Mass of the bridge (kg)	% of mass of the bridge variation with respect to the lowest one	Criteria 0: Stress efficiency average of the bridge	Criteria 1: Stress efficiency average of the bridge*total length of the bridge (m)	Criteria 2: Sum of the stress efficiency in each output station*Length of each output station of the bridge (m)
g=20;e=16,67;f=20;v=0	130543,5	0,0	0,2	20,9	70,8
g=20;e=16,67;f=20;v=0 SSDS	182550,4	39,8	0,1	16,2	49,7
g=20;e=16,67;f=20;v=0 HZSA	134278,5	2,9	0,1	13,6	46,4
Minimal Mass (kg)	130543,5		0,1	13,6	46,4

**Table 2-20: Mass and stress criteria comparison for different system stiffness distribution values based on Table 1-1**

Model	Mass of the arch (kg)	Mass of the deck (kg)	Mass of the struts (kg)
g=20;e=16,67;f=20;v=0	29065,9	81076,6	20401,0
g=20;e=16,67;f=20;v=0 SSDS	25490,4	133048,7	24011,3
g=20;e=16,67;f=20;v=0 HZSA	41133,6	81076,6	12068,3
Minimal Mass (kg)	25490,4	81076,6	12068,3

**Table 2-21: Mass distribution of the different elements of the bridge for different system stiffness distribution values based on Table 1-1**



## 2.5 PARAMETER DISCUSSION

Whatever the deck curvature, the value of  $f$ , the stiffness of the strut-deck system or that of the arch:

- Results for all the different indicators are low enough in the range of  $g/1,3 \leq e \leq g/1,1$ , approximately in the range in which there is the same number of hangers at each side of the arch. This is not far from the range of values  $D$  described in Table 2-1 and Figure 2-2, in which there is the same number of struts at both sides of the deck, but the range of the most efficient  $e$  tends to be nearer to the outside of the deck curvature in plan, ie: nearer to the deck span center.
- Given a  $g$  value, in the range  $g/1,36 \leq e \leq g/1,2$  the internal forces in the whole bridge are reasonable.
- Whatever the value of  $g$ , minimising the value of the sum of the stresses of the whole system is equivalent to minimising the sum of stresses in the arch.
- In order to choose the most efficient  $e$  value, employing an indicator to minimise the total bending moments in the arch under permanent loads is equivalent to minimizing the stresses in the bridge for the worst loading case and to minimizing the total material employed for the bridge. A simpler indicator such as the maximal arch displacement can also be employed.
- Given a  $g$  value, the value  $e=g/1,2=0,83g$  is the most efficient value for the arch/eccentricity in plan view according to all of the studied efficiency indicators. For this value internal torsional moments in the arch and the deck under a uniform deck load are also minimal.
- For high  $g$  values, ie: when spatial behaviour increases, the influence of  $e$  is larger,
- The higher the  $f$  value, the higher the importance of choosing an adequate  $e$  value.
- Regarding the stresses in the arch, the influence of employing a stiff strut-deck system is lower for values of  $e$  between  $g/1,30$  and  $g/1,20$ .
- When considering the stiffness distribution of a system, the only valid criteria to choose the most efficient distribution is calculating the total mass of the dimensioned system, a simpler criterion cannot be adopted.

### *Proportions of the key point $e=g/1,2$ with the rest of parameters:*

The value  $e=g/1,2=0,83g$  is equivalent approximately to 1,25 times the distance of the  $cgd$  from the abutments. It is also the limit value in which there is the same number of struts on both sides of the arch, ie: for the 16 struts in the studied model there are 6 short and nearly vertical struts on one side of the arch in central area of the span (contained in the inner part of the deck curve), 2 vertical struts and 4+4 struts on the other side (contained in the outside part of the deck curve) at each of the ends of the span. Compared to the other  $e$  values it is the one which gives the shortest length for the 5th struts from the springings (Table 2-12), ie: it obtains the stiffest struts at a distance of approximately  $0,28L$  of the springings of the arch (Figure 2-1), whatever the  $g$  value. The relationship with  $f$  of the height of this point in the arch is also constant and has a value of  $0,81*f$ . This is a key point to control the arch behaviour. It increases the stiffness of the struts

around this key point, since it decreases their length, and also increases their verticality where controlling the out-of-plane behaviour is most critical. It is also significant that for this value, maximal in-plane and maximal out-of-plane displacements acquire the same value (section 2.2), which means that it is the value that best controls out-of-plane behaviour.

***Comparison with previous studies and evaluation of the results:***

- It can be appreciated that the value obtained for  $e^*$  for SABWCSD with a planar vertical arch is different than for SABWCID with a planar vertical arch with pinned hangers according to Jorquera's study (2007) for  $g=10\text{m}$  which according to other indicators gave a value for which we found the equivalency to  $e^*=g/1,36$ .
- The most efficient  $e$  for the present study is nearer to the value obtained by Jorquera (2007) for SABWCID with an antifunicular arch or the range of values where stiffened double struts are employed for the Ripshorster footbridge, which is a SABWCSD with an antifunicular arch.
- SABWCID with a planar vertical arch work better with a larger  $e$  value than SABWCSD with a planar vertical arch.
- This difference is due to:
  - The difference of the length of the struts distribution
  - In the study of SABWCID the hangers are pinned and in the present study for SABWCSD with a planar vertical arch the struts are fixed.
    - Since hangers are pinned it is more efficient to increase of the longest central hangers, for which a larger  $e$  value is needed.
    - For fixed struts, it is more efficient to increase their stiffness by reducing their length. Longest struts are nearer to the springing. Therefore, a lower  $e$  value is needed.
    - Antifunicularity allows for obtaining verticality of the struts with a lower  $e$  value, ie: an antifunicular arch has a lower  $e^*$  value than a planar vertical one because the struts tend to be more vertical.

### 3. VERTICAL DISTANCE BETWEEN THE ARCH CROWN AND THE DECK MID-SPAN ( $v$ ) PARAMETRICAL STUDY

#### 3.1 DEFINITION AND EMPLOYED VALUES

The vertical distance between the arch crown and the deck mid-span ( $v$ ) is a parameter which has still not been studied for SABs. The values for the parametrical study of the  $v$  variable have been chosen in order to increase the verticality of the struts. The studied models have the following values:  $L=100\text{m}$ ,  $g=20\text{m}$  and  $f=20\text{m}$ . For each of the cases with different  $e$  values  $e=0$ ; 14,7 and 16,67m, four different values of  $v$  have been employed  $v=0$ , 2, 4 and 6m.

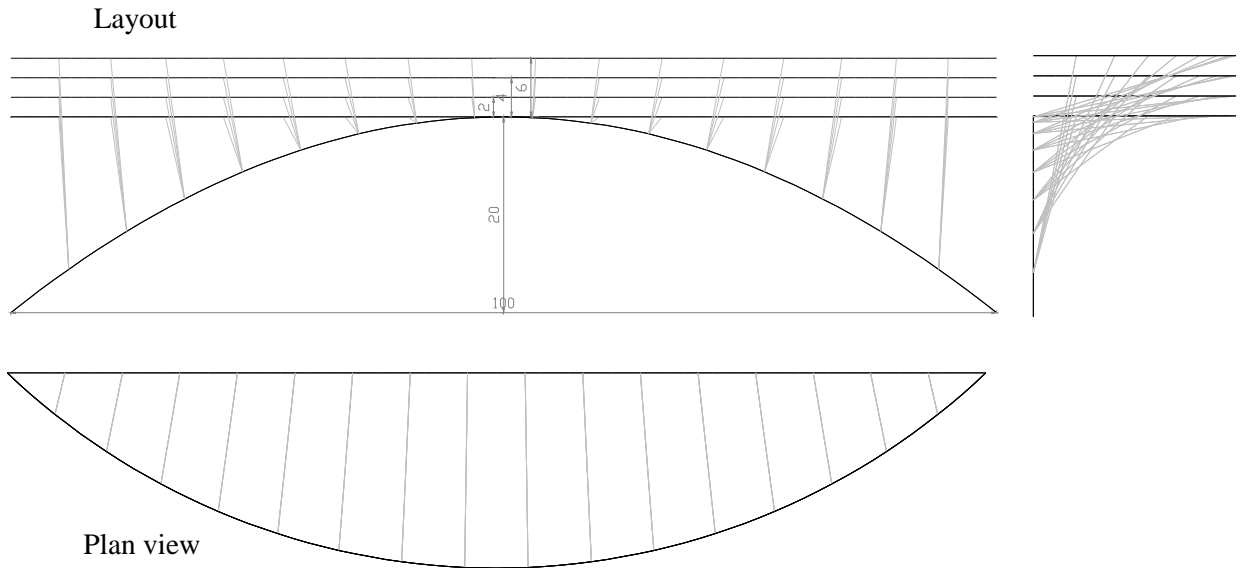


Figure 3-1: Geometry of  $v$  variation ( $v=0$ , 2, 4 and 6m) for  $L=100\text{m}$ ,  $g=20\text{m}$ ,  $f=20\text{m}$ ,  $e=0$

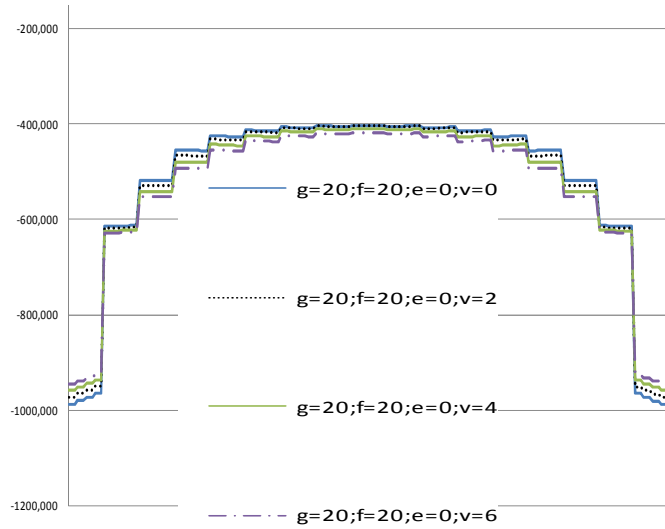
#### 3.2 STRUCTURAL RESPONSE UNDER A UNIFORM VERTICAL LOAD ( $lu$ )

The structural behaviour has been studied only under a uniform load of  $10\text{kN/m}$  on the whole deck<sup>2</sup> (Figure 1-2) for the described model with the different values of  $v$  and their structural response has been compared. The results are shown in Figure 3-3 and Figure 3-4 and they are commented in the following lines:

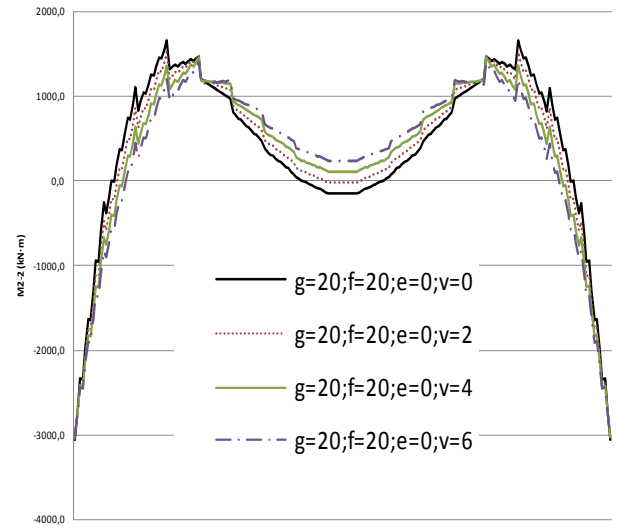
- A priori, we would have expected that increasing  $v$  improved the structural behaviour of this bridge type, since it increased the struts verticality. Struts at the central area of the bridge tend to be very horizontal for the chosen  $e$  values, so increasing their verticality would be expected to be more favourable (Jorquera 2007) in order to decrease the bending moments in the struts, increase the axial forces and decrease the out-of-plane forces introduced on the arch. The arch would then further help to support the deck and deflections would be expected to diminish.

<sup>2</sup> Without self-weight or permanent loads

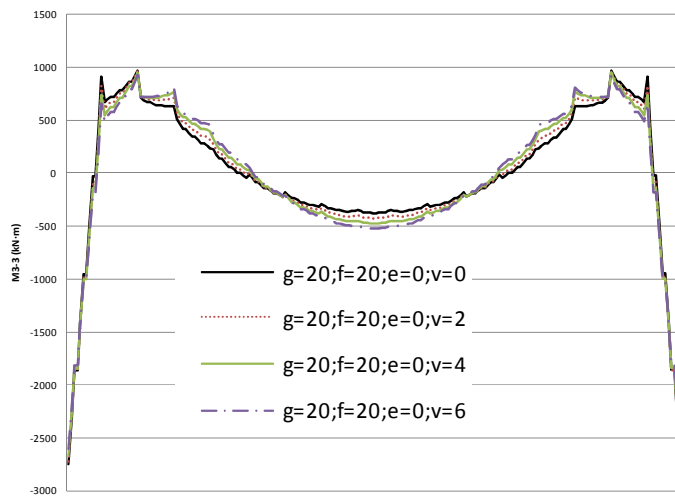
- For  $e=0$  the struts remain nearly horizontal in spite of increasing  $\nu$ . So, whatever the  $\nu$  value, there is a large difference of the arch axial forces at springings and in the rest of the arch's length (Figure 3-2a).
- However, for  $e=16,67$ , the axial forces in the arch are much lower at span center for  $\nu=0$  than for other  $\nu$  values which increase the verticality of the struts (Figure 3-3a). The axial forces at central struts increase with  $\nu$  as expected (Figure 3-4a).
- For  $\nu=0$  central struts do not transmit axial compressions to the arch (Figure 3-4a) but they are under large total bending moments (Figure 3-4b). Those introduce bending moments and torques on the arch.
- The lower the  $\nu$  value, the larger the stiffness of the struts, and therefore they are under larger bending moments.
- Torsional moments in the arch decrease with  $\nu$  (Figure 3-3b), so do balcony-beam bending moments at approximately  $L/3$ , which is logical since these internal forces are coupled. However, balcony-beam bending moments increase with  $\nu$  at span center (Figure 3-3c).
- Total bending moments decrease at span center (Figure 3-3d), highly influenced by out-of-plane bending moments.
- These effects are less important for  $e=0$  (Figure 3-2b, c and d).  $e$  is a key parameter, ie: most important is to control  $e$ . For a good  $e$  value,  $\nu$  has a non-negligible influence. However for values of  $e$  in which the structural behaviour of the bridge is not good, it is better to control the behaviour changing  $e$  than  $\nu$ .
- The out-of-plane behaviour of the arch is controlled by the deck, hence the deck tensions at the span centre for  $\nu=0$  (Figure 3-3e). However, for  $\nu>0$  the struts are more vertical and less stiff and the deck does not control the out-of-plane behavior of the arch as efficiently as for the case of  $\nu=0$ , with stiffer struts. The center of the span is more sensitive to this effect, since the relative variation of the length (and thus the stiffness) of the struts with  $\nu$  is greater.
- This is clearly observed with the horizontal displacements of the arch (Figure 3-3f).
- The deck vertical (Figure 3-3g) and horizontal displacements are also lower at span center for  $\nu=0$ , hence the arch-deck higher interaction due to stiffer hangers.
- The lowest total displacements for the arch are obtained for  $\nu=0$ , and for  $\nu=2$  for the deck (Table 3-1).



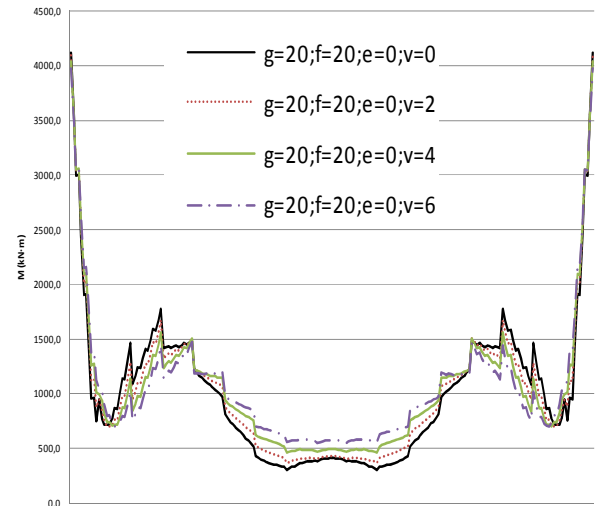
(a)



(b)



(c)

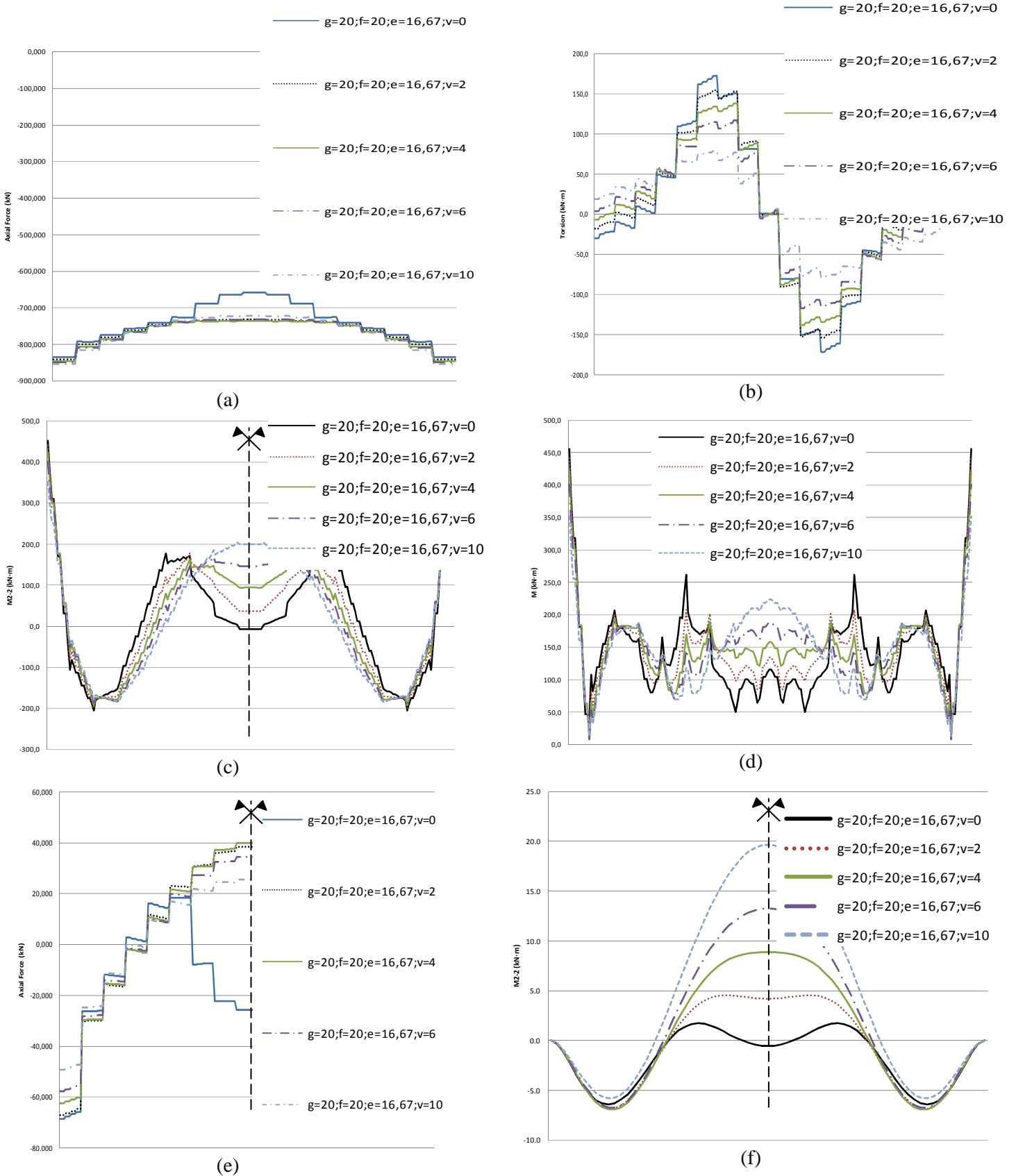


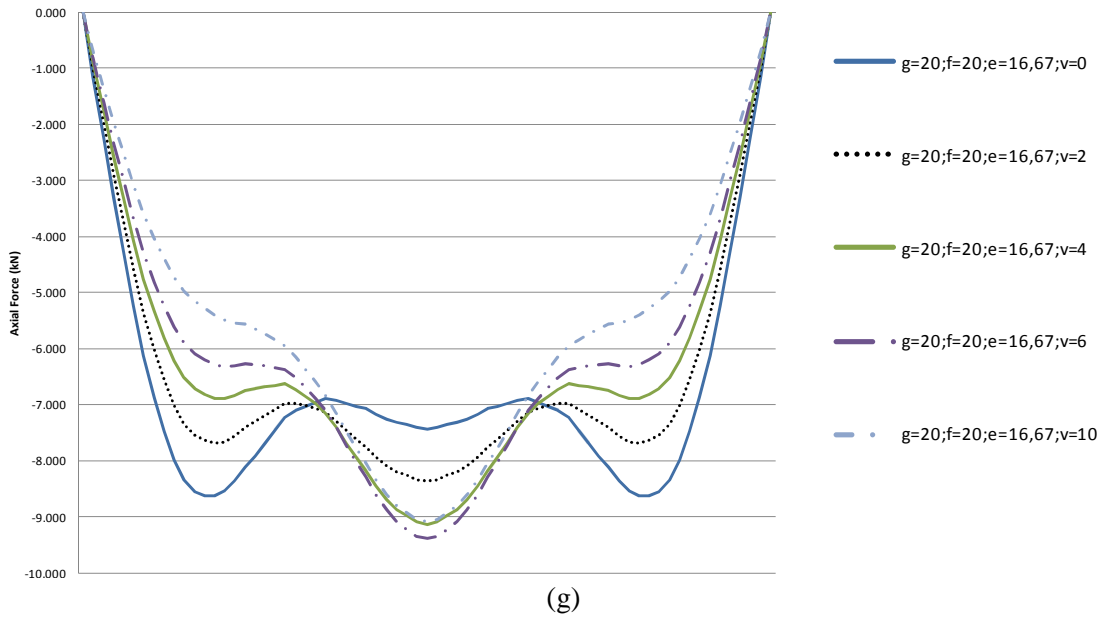
(d)

**Figure 3-2: Internal forces comparison for different  $v$  values and  $e=0$ . (a) Arch axial forces (b) Arch out-of-plane bending moments (c) Arch in-plane bending moments (d) Arch total bending moments.**

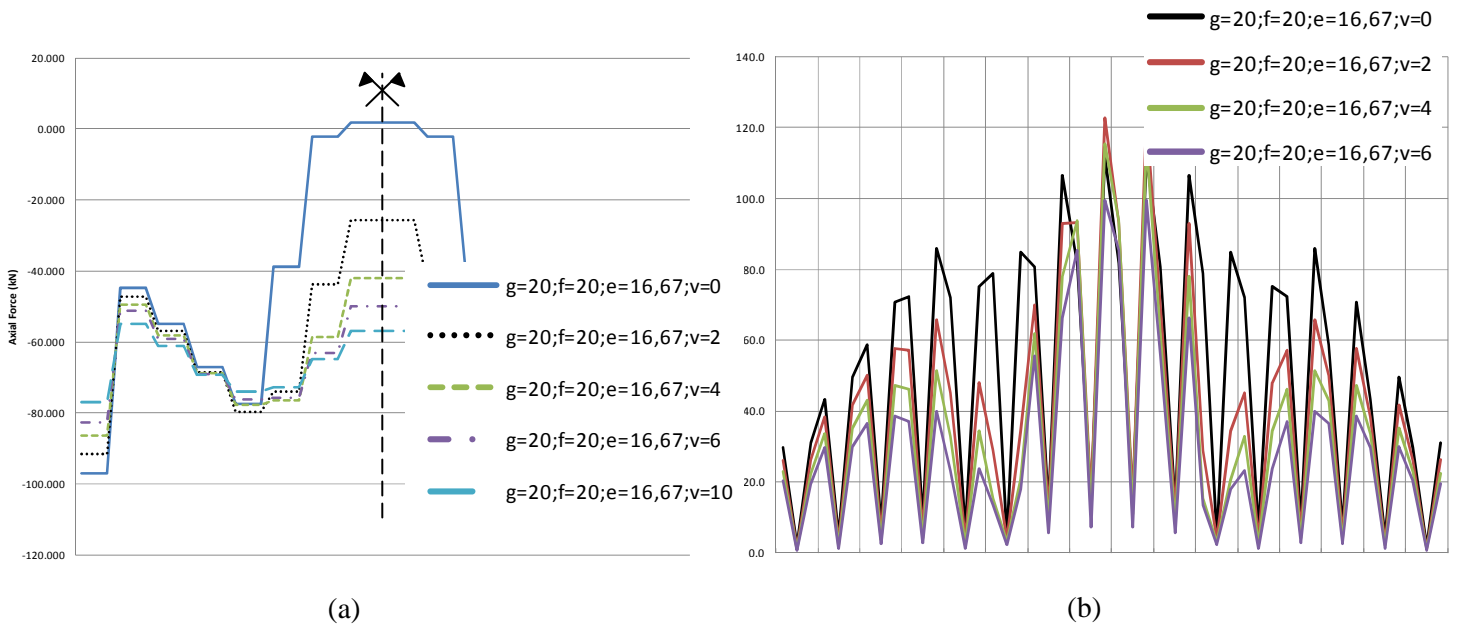
*The abscissas are the arch length from 0 to  $L_A$*

V. B) PARAMETRICAL STUDY OF SPATIAL ARCH BRIDGES WITH A CURVED SUPERIOR DECK AND A PLANAR VERTICAL ARCH





**Figure 3-3: Structural behaviour comparison for different  $v$  values and  $e=16,67$**  (a) Arch axial forces (b) Arch torsional bending moments (c) Arch out-of-plane bending moments comparison (d) Arch total bending moments (e) Deck axial forces (f) Arch horizontal (out-of-plane) displacements (g) Deck vertical displacements. *The abscissas for (a) to (d) and (f) are the arch length from 0 to  $L_A$ , for (e) and (g) they are the deck length from 0 to  $L_D$*



**Figure 3-4: Struts internal forces comparison for different  $v$  values and  $e=16,67m$**  (a) Axial forces (b) Total bending moments. *The abscissas are the output stations of the different struts (at the bottom, center and the top of their length)*

Model	Deck vertical maximal displacement under q10 (mm)	Deck horizontal maximal displacement under q10 (mm)	Deck maximal total displacement under q10 (mm)	Arch vertical maximal displacement under q10 (mm)	Arch horizontal maximal displacement under q10 (mm)	Arch maximal total displacement under q10 (mm)
g=20;f=20;e=16,67;v=0	-8.6	-0.6	8.6	-6.6	-6.4	7.1
g=20;f=20;e=16,67;v=2	-8.4	-0.4	8.4	-6.4	-6.8	7.4
g=20;f=20;e=16,67;v=4	-9.1	-0.5	9.1	-6.2	8.9	9.0
g=20;f=20;e=16,67;v=6	-9.4	-0.6	9.4	-6.0	13.3	13.3
g=20;f=20;e=16,67;v=10	-9.1	-0.7	9.1	-5.7	19.7	19.8
Minimal values	-8.4 for v=2	-0.4 for v=2	8.4 for v=2	-5.7 for v=10	-6.4 for v=0	7.1 for v=0

**Table 3-1: Maximal displacements comparison for different  $v$  values and  $e=16,67$**

### 3.3 STRESS BEHAVIOUR COMPARISON UNDER A UNIFORM LOADING $q$ AND DESIGN IN ULTIMATE LIMIT STATE

The stresses distributions in the struts, deck and arch only under  $q=10\text{kN/m}$  are shown in Figure 3-5, Figure 3-6 and Figure 3-7 for the reference cross-sections.

The stresses distribution under ULS is shown in Figure 3-8 as an example.

Afterwards, the different elements cross-sections are designed according to the ULS in EC1 Part2.

The results are explained in the following lines:

- The higher the  $v$  value, the lower the stresses in the struts (Figure 3-5) and the deck (Figure 3-6), but higher in the arch at span center (Figure 3-7).
- The envelope of the stresses has been employed in order to obtain the necessary cross-sections. This envelope is given mainly for the A1 hypothesis (with uniform loading) and A2 in the arch and struts and A2 and B for the deck
- Increasing  $v$ , increases the influence of  $la$ , ie.: the difference between A1 and A2, in the cross-sections where A2 is more critical, increases (Figure 3-8 compared to Figure 2-15).
- The different elements in the bridge have been dimensioned resulting in:
  - Whatever the  $v$  value the deck should be a  $4000 \times 700 \neq 10\text{mm}$  steel box girder. It would be enough with 3mm to resist the stresses considering a compact cross-section. However, 10mm are considered for local bending moments, local instability of compressed plates and durability.
  - The models with  $v=0, 2$ , and 4m have been dimensioned. The following cross-sections for S 355 steel have been obtained employing a linear analysis.
  - The arches are CHS of 750mm diameter and thickness ranging from 30mm at springings to 10mm at span center for  $v=0$  and for  $v=2\text{m}$ , and from 35mm at extremes to 15mm at span center for  $v=4\text{m}$ .
  - The struts are CHS of 300mm diameter and thickness ranging from 15mm at extremes to 35mm at span center for  $v=0$ , from 15mm at extremes to 30mm at  $L/3$  for  $v=2\text{m}$  and from 20mm at extremes to 45mm at span center for  $v=4\text{m}$ .



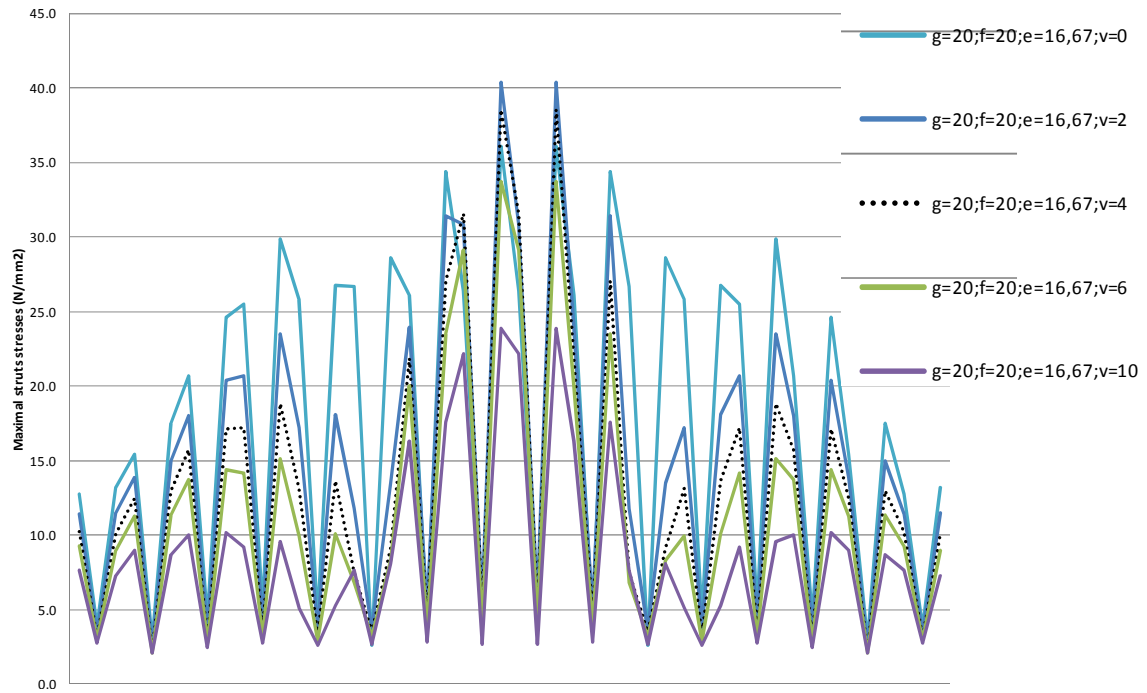


Figure 3-5: Struts stresses comparison under  $q_{10}$  for different  $v$  values,  $L=100m$ ,  $f=20$ ,  $g=20$  and  $e=16,67$ . The abscissas are the output stations of the different struts (at the bottom, center and the top of their length).

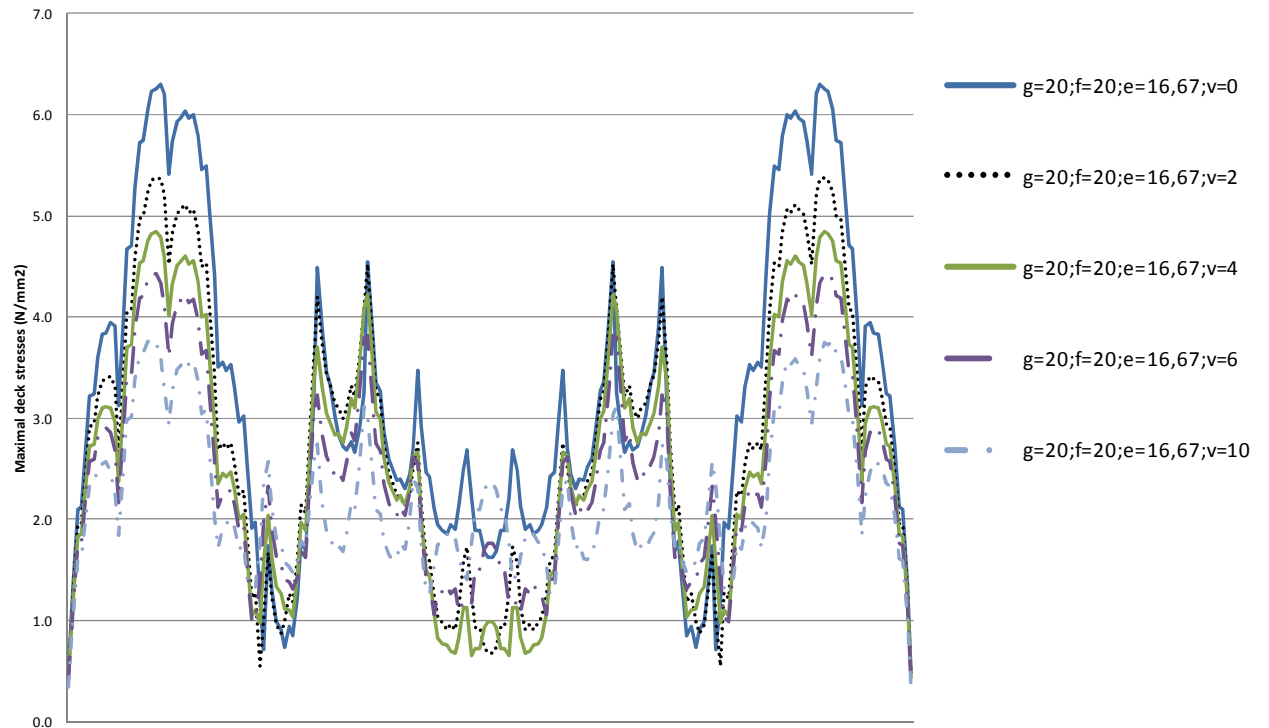


Figure 3-6: Deck stresses comparison under  $q_{10}$  for different  $v$  values,  $L=100m$ ,  $f=20$ ,  $g=20$  and  $e=16,67$ . The abscissas are the deck length from 0 to  $L_D$

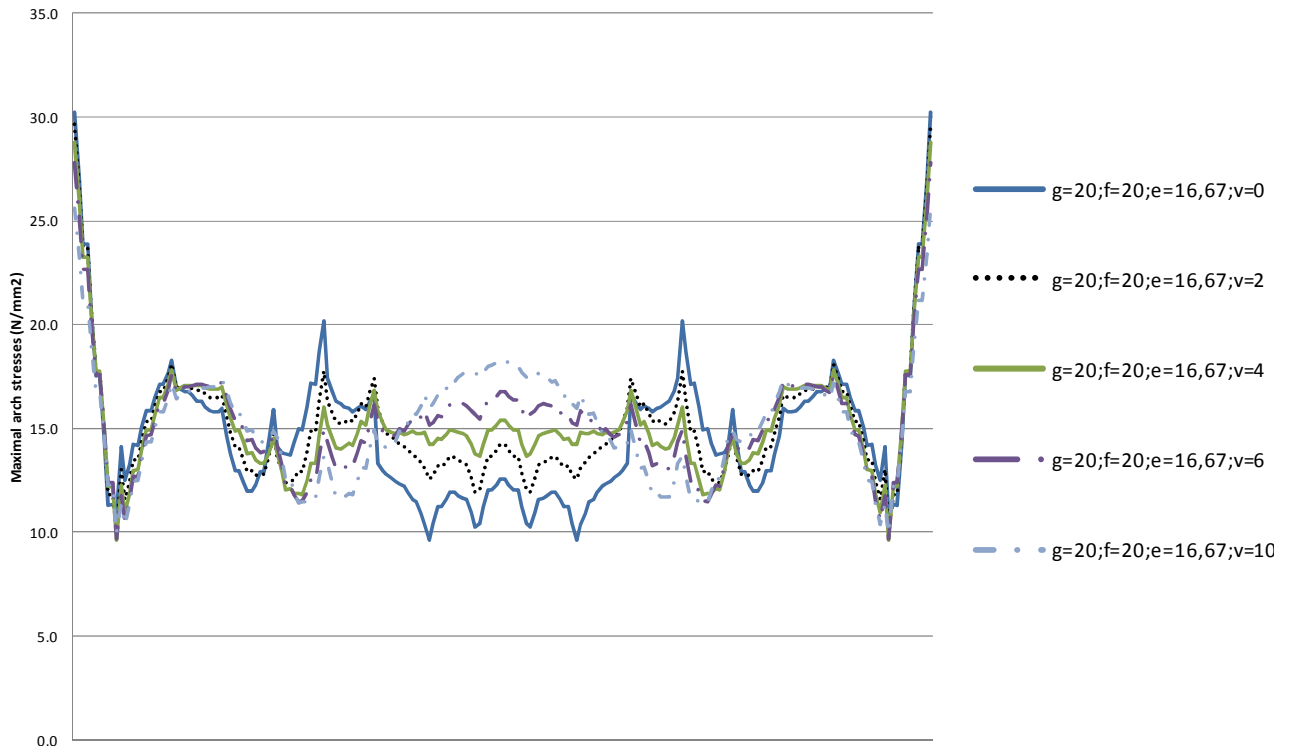


Figure 3-7: Arch stresses comparison under q10 for different  $v$  values,  $L=100m$ ,  $f=20,g=20$  and  $e=16,67$ . The abscissas are the arch length from 0 to  $L_A$

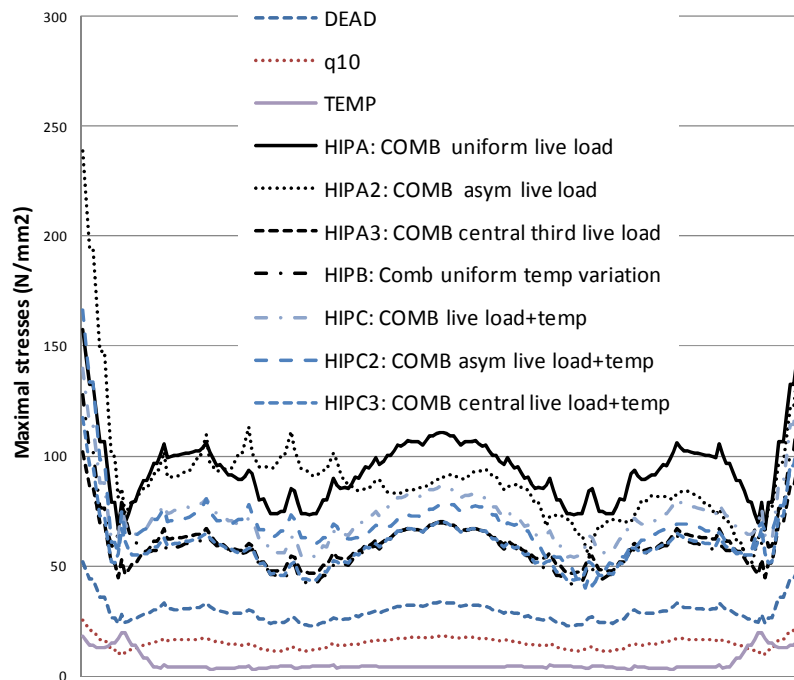


Figure 3-8: Stresses in the arch caused by different loading cases combination for  $g=20m$ ,  $f=20m$ ,  $e=16,67m$  and  $v=10m$  when employing the reference model cross-sections (Table 1-1). The abscissas are the arch length from 0 to  $L_A$

### 3.4 EFFICIENCY CRITERIA

The results of the chosen criteria are shown for the different models which have been studied in tables from Table 3-2 to Table 3-9. In these tables the nomenclature already given in section 1.3 is employed. Please use the bookmark to comfortably interpret the tables, and note whether the length is considered or not, since the nomenclature and units of the criteria are modified. The following values are specifically employed for the tables in this section:

- $v^*$  is the value of  $v$  which minimizes each criteria (m)
- $i = \%$  of difference of B from the most efficient  $v$  value for B ( $v^*$ )

A different  $v^*$  is obtained for each criteria. The results of the efficiency criteria are commented in the following lines:

- It is convenient to employ the lowest possible vertical distance between the arch and the deck in order to reduce the total material employed for the bridge.
- Whatever the  $e$  value, the maximal displacement under permanent loads is the simplest criteria to employ (Table 3-2 and Table 3-4), equivalent to consider the lowest mass of the bridge depending on  $v$  (Table 3-8), the lowest stresses considering the length of all the elements (Table 3-3 and Table 3-5) and the lowest sum of the total bending moments in the arch under permanent loads and arch stresses considering the total length of the bridge or not (Table 3-2, Table 3-3 and Table 3-4). This is so because, although the total stresses in the deck and struts decrease, the length of the struts increases (Table 3-6 and Table 3-7), causing the total mass to be larger (Table 3-8 and Table 3-9). The stresses in the arch and its mass increase when increasing  $v$  (Table 3-6 Table 3-7 and Table 3-9).
- The way in which the stress criteria is calculated (Criteria 1 and 2, Table 3-8) is not relevant, since they all lead to the same result.
- If the total length of the bridge is not considered, whatever the value of  $v$ , the sum of the total stresses of the bridge under  $q$  or the maximal arch stress under  $q$  are not valid criteria (Table 3-2 and Table 3-4).
- Varying  $v$  has a negligible influence for  $e=0$  ( $i$  value in Table 3-3), but for an adequate  $e$  value according to the study in section 2, varying the  $v$  value has a larger influence ( $i$  value Table 3-5 and Table 3-8), as expected from the internal forces in section 3.2.
- The fact that the displacement criteria gives the same results as the mass criteria confirms that a linear analysis is enough in order to determine which  $v$  value is the most efficient.

Model	Criteria							
	A	B	C	D	E	F	G	H
v=0	60977	122328	497072	10636	21620	1123	201	233
v=2	62229	120708	509617	10820	21284	1120	200	285
v=4	63633	119300	523593	11020	20965	1109	197	344
v=6	65227	118182	539225	11246	20681	1098	194	413
v*	v=0	v=6	v=0	v=0	v=6	v=6	v=6	v=0

Table 3-2: Efficiency criteria not considering the length of the elements for g=20m, f=20m, e=0 and v variable

Model	Criteria								
	A	B	C	D	E	F	G	H	i
v=0	29841917	59867467	243266960	5205368	10581038	549531	98441	114029	0
v=2	31301248	60715898	256337600	5442542	10705662	563258	100581	143442	1
v=4	33025469	61916715	271744978	5719386	10880976	575642	102362	178676	3
v=6	35040160	63487218	289671655	6041276	11109957	590037	104419	222049	6
v*	v=0	v=0	v=0	v=0	v=0	v=0	v=0	v=0	

Table 3-3: Efficiency criteria considering the length of the elements for g=20m, f=20m, e=0 and v variable

Model	Criteria							
	A	B	C	D	E	F	G	H
v=0	17958	30026	69354	2999	4502	188	30	19
v=2	18718	29750	70415	3071	4347	201	30	20
v=4	19181	29427	71092	3093	4228	216	29	20
v=6	19626	28947	72695	3115	4147	229	28	31
v=10	20161	28101	74316	3105	3955	239	26	47
v*	v=0	v=10	v=0	v=0	v=10	v=0	v=10	v=0

Table 3-4: Efficiency criteria not considering the length of the elements for g=20m, f=20m, e=16,67m and v variable

Model	Criteria								
	A	B	C	D	E	F	G	H	i
g=20;f=20;e=16,67;v=0	6241658	10436032	24105290	1042528	1564703	65280	10502	6753	0
g=20;f=20;e=16,67;v=2	6945346	11038889	26127478	1139590	1612974	74462	10995	7390	6
g=20;f=20;e=16,67;v=4	7643374	11726045	28328684	1232663	1684728	86167	11472	8066	12
v*	v=0	v=0	v=0	v=0	v=0	v=0	v=0	v=0	

Table 3-5: Efficiency criteria considering the length of the elements for g=20m, f=20m, e=16,67m and v variable

	Sum of maximal deck stresses (MPa)	Sum of maximal arch stresses (MPa)	Sum of maximal strut stresses (MPa)
g=20;f=20;e=0;v=0	43497.2	60976.5	17854.6
g=20;f=20;e=0;v=2	41014.2	62229.1	17464.2
g=20;f=20;e=0;v=4	38709.6	63632.9	16957.5
g=20;f=20;e=0;v=6	36598.1	65227.4	16356.2
v*	v=6	v=0	v=6

Table 3-6: Stresses in the different elements comparison for g=20m, f=20m, e=0 and v variable

	Sum of maximal deck stresses (MPa)	Sum of maximal arch stresses (MPa)	Sum of maximal strut stresses (MPa)
g=20;f=20;e=16,67;v=0m	7085.6	17958.0	4982.1
g=20;f=20;e=16,67;v=2m	6635.9	18718.1	4396.4
g=20;f=20;e=16,67;v=4m	6152.7	19181.3	4092.9
g=20;f=20;e=16,67;v=6m	5639.5	19626.0	3681.6
g=20;f=20;e=16,67;v=10m	5025.6	20160.6	2914.9
v*	v=10	v=0	v=10

Table 3-7: Stresses in the different elements comparison for g=20m, f=20m, e=16,67m and v variable

Model	Mass of the bridge (kg)	% of mass of the bridge variation with respect to the lowest one	Criteria 1: Stress efficiency average of the bridge*total length of the bridge (m)	Criteria 2: Sum of the stress efficiency in each output station*Length of each output station of the bridge (m)
g=20;e=16,67;f=20;v=0	130543	0.00	20.9	70.8
g=20;e=16,67;f=20;v=2	135712	3.96	21.3	73.5
g=20;e=16,67;f=20;v=4	140711	7.79	21.7	77.8
Minimal Mass (kg)	130543		20.9	70.8

Table 3-8: Efficiency criteria considering the length and the mass of the elements for g=20m, f=20m, e=16,67m and v variable

Model	Mass of the arch (kg)	Mass of the deck (kg)	Mass of the struts (kg)
g=20;e=16,67;f=20;v=0	29065.9	81076.6	20401.0
g=20;e=16,67;f=20;v=2	31345.6	81076.6	23289.7
g=20;e=16,67;f=20;v=4	32906.8	81076.6	26727.6
Minimal Mass (kg)	29065.9	81076.6	20401.0

Table 3-9: Comparison of the mass of the different elements for g=20m, f=20m, e=16,67m and v variable

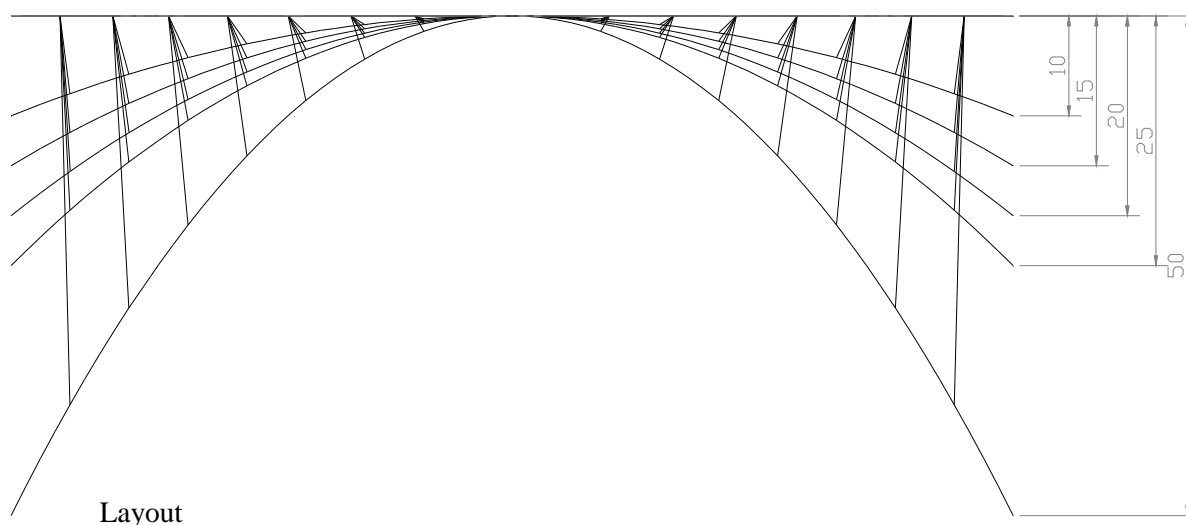
### 3.5 PARAMETER DISCUSSION

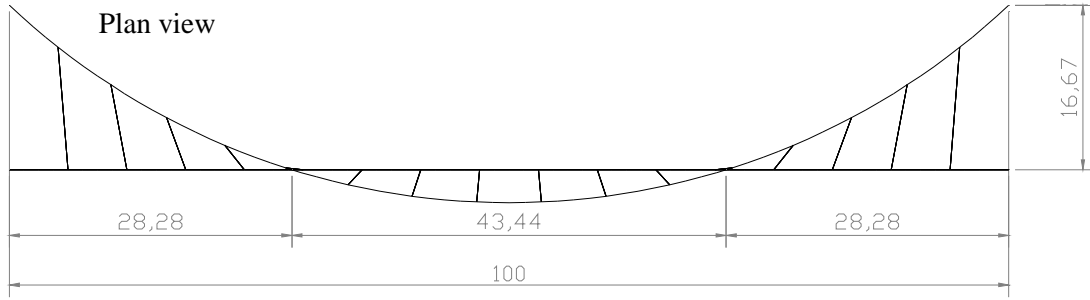
- Increasing the verticality of the struts by increasing the vertical distance between the arch crown and the deck mid-span ( $v$ ), decreases the efficiency of the system, since it increases the length of the struts and thus decreases their stiffness.
- For an efficient  $e$  value,  $v$  has a significant influence in the internal forces, stresses and mass of the bridge. However for values of  $e$  in which the structural behaviour of the bridge is not good, it is better to control the behaviour changing  $e$  than  $v$ .  $e$  is a key parameter, ie: most important is to control  $e$ .
- In order to choose the most efficient  $v$  value, employing an indicator to minimise the total bending moments in the arch under permanent loads is equivalent to minimizing the {stresses in the bridge}\*{total length of the bridge} under a uniform load and to minimizing the total material employed for the bridge (see indicators definition in bookmark or section 1.3). A simpler indicator such as the maximal arch displacement can also be employed.

## 4. ARCH RISE ( $f$ ) PARAMETRICAL STUDY

### 4.1 DEFINITION AND EMPLOYED VALUES

The rise of the arch ( $f$ ) is a parameter which has still not been studied for SABs. The values for the parametrical study of the  $f$  variable will influence on the verticality and length, hence the stiffness, of the struts and on the shape of the arch. For planar arch bridges with a superior straight deck values from  $0,16*L$  (O'Connor 1971) to  $0,25*L$  are the most usual ones for road bridges, but this range of values need not be the most efficient ones for pedestrian SABs with a curved superior deck. It might even change for different values of other parameters. However, we have studied the variation of  $f$  choosing the previously studied parameters and determined as the most efficient. The studied models have the following values:  $f=L/10=10m$ ;  $f=L/6,67=15m$ ;  $f=L/5=20m$ ;  $f=L/4=25m$  and  $f=L/2=50m$  for  $L=100m$ ,  $g=20m$ ,  $e=16,67m$  and  $v=0$  (Figure 4-1).





**Figure 4-1: Geometry of  $f$  variation ( $f=10, 15, 20, 25$  and  $50\text{m}$ ) for  $L=100\text{m}$ ,  $g=20\text{m}$ ,  $e=L/1,2=16,67\text{m}$ ,  $v=0$ . Measures in meters**

An equivalent study has been conducted for a planar arch with straight deck ( $L=100\text{m}$ ,  $g=0\text{m}$ ,  $e=0\text{m}$  and  $v=0$ ) in order to compare the results.

For conventional arch bridges each  $f$  value has an antifunicular arch for a given load, so, for this case study, the sum of bending moments might not make much sense as an efficiency criteria. None the less it is considered interesting to analyse the value.

#### 4.2 STRUCTURAL RESPONSE UNDER A UNIFORM VERTICAL LOAD ( $lu$ )

The structural behaviour has been studied for only under a uniform load of  $10\text{kN/m}$  on the whole deck<sup>3</sup> (Figure 1-2) for the described model with the different values of  $f$  ( $f=L/10=10\text{m}$ ;  $f=L/6,67=15\text{m}$ ;  $f=L/5=20\text{m}$ ;  $f=L/4=25\text{m}$  and  $f=L/2=50\text{m}$  for  $L=100\text{m}$ ,  $g=20\text{m}$ ,  $e=g/1,2\text{m}=16,67\text{m}$  and  $v=0$ , Figure 4-1, and  $f=10, 20$  and  $50\text{m}$  for  $L=100\text{m}$ ,  $g=e=0$  and  $v=0$ ) and their structural response has been compared.

A priori, it is expected that the following values change with  $f$ :

- 1) the length, hence the stiffness, of the struts. The length increases with  $f$  and thus the stiffness decreases when employing the same cross-section
- 2) the verticality of the struts increases with  $f$ , ie: the inclination of the struts in longitudinal view (Figure 4-1) decreases with  $f$ . In plan view their position does not change, but for SABs they also become more vertical since they are longer.
- 3) the out-of-plane sag of the arch increases with  $f$
- 4) in-plane horizontal forces at abutments and in-plane bending moments are expected to decrease with  $f$  like it happens in planar arch bridges with a straight superior deck.

According to 3, it is expected that the out-of-plane behavior increases with  $f$ . However, according to the increase of out-of-plane verticality with explained in 2, the out-of-plane forces introduced by the struts on the arch should decrease, but the axial forces will change due the increase of the out-of-plane sag (3) and also because the struts are fixed and their stiffness changes according to (1).

<sup>3</sup> Without self-weight or permanent loads

Due to the high influence of out-of-plane forces in this bridge type (Sarmiento-Comesías et al 2012) and that stiffer struts are needed for SABs (Sarmiento-Comesías et al 2012), a priori, lower values of  $f$  are expected to be more favourable for this bridge type. With the  $v$  case study (section 0), it has been observed that the struts verticality is less important than their length. Probably lower values than for planar arch bridges with a straight superior deck.

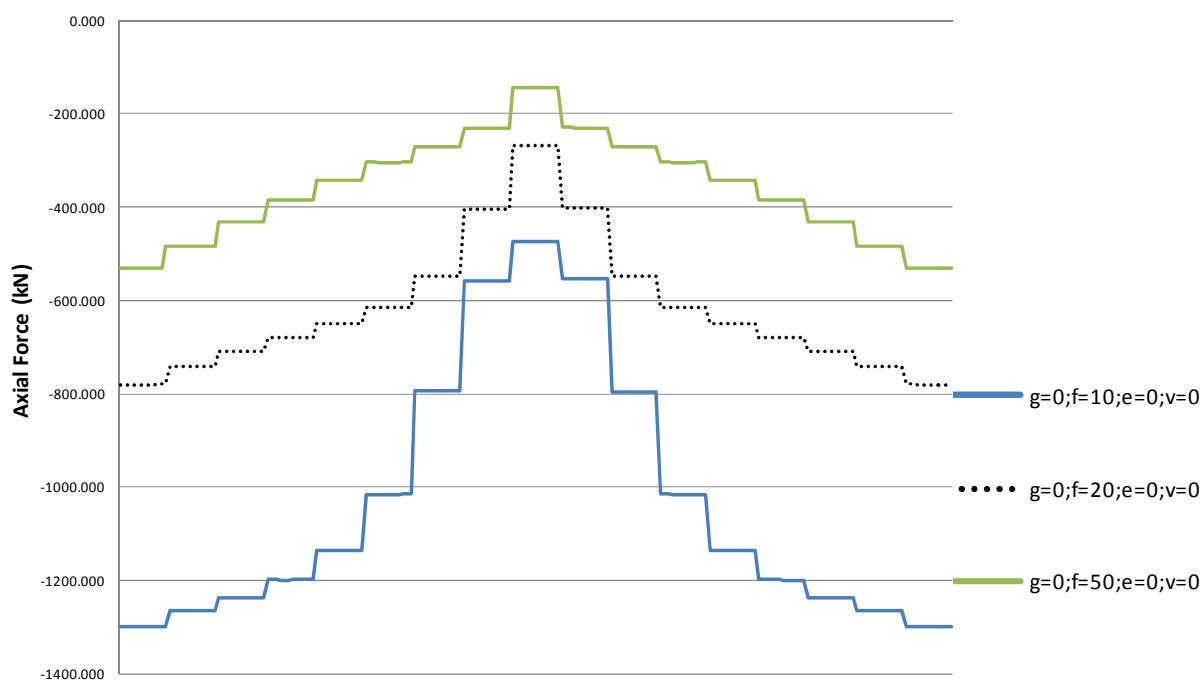
The results are displayed in figures from Figure 4-2 to Figure 4-19 and the following observations should be highlighted:

- Whatever the  $f$  value, the arch and deck total bending and torsional moments at around the key points  $g/1,2$  hardly change (Figure 4-16 and Figure 4-17), since they are controlled with an efficient  $e$  value.
- Total bending moments in the arch slightly decrease with  $f$  at the extremes (Figure 4-8), except at the span center ( $L/3-2L/3$ ). The same happens with in plane bending moments at span center ( $3L/8-5L/8$ ; Figure 4-9), contrary to what was expected and happens for planar arch bridges ( $g=0$ , Figure 4-4). This is explained by the difference in the evolution of axial forces in struts with the variation of  $f$  in SABs and planar arch bridges, which is explained on the following paragraphs.
- Out-of-plane bending moments approximately at  $L/3$  increase with  $f$ . As previously explained out-of-plane bending moments were expected to increase, since the out-of-plane sag of the arch increases with  $f$ . However this effect only takes place in a certain length of the arch, where the axial forces in the struts increase (Figure 4-19).
- When increasing  $f$ , struts become longer and more vertical (Figure 4-1), especially the ones at the extremes. Therefore, the stiffness of struts at extremes decreases more with the increase of  $f$  than the stiffness of central struts. Axial forces for different struts become more similar, since extreme struts take a lower load (Figure 4-6). For low  $f$  values, the axial forces in struts are larger for longer struts near to the abutments (1<sup>st</sup> struts in our model) than for those at span center (8<sup>th</sup> strut in our model). This difference decreases with  $f$  (Figure 4-6 and Figure 4-19).
- For SABs with a vertical planar arch and a superior curved deck, the difference with the contiguous struts is highly increasing. As  $f$  increases the difference between the axial forces in extreme and central struts decreases but between the central struts (8th strut in our model) and their contiguous struts (5<sup>th</sup> and 6<sup>th</sup> in our model), the difference increases. For  $f=50m$  the axial forces in central struts diminish until they are even tensioned (Figure 4-19). This happens because for  $f=50m$ , the arch and deck displacements at span center have opposite sign (upwards and inwards for the arch- Figure 4-12 and Figure 4-13- and downwards and outwards for the deck), whereas for lower  $f$  values ( $f<25m$ ) the displacements at span center are downwards and outwards for both, arch and deck, and the central struts are compressed (Figure 4-19).
- The deck is tensioned for  $f>20$  for  $g=20$  (Figure 4-15) at span center, whereas the deck is always under compression for  $g=0$  (Figure 4-3). For SABs with  $f<25m$  at  $L/3$  there is a



large variation in the axial forces of the deck. Note that the deck internal forces of  $g=20\text{m}$  and  $g=0$  are not really comparable because longitudinal displacements are free in  $g=0$  and they are restrained for  $g=20\text{m}$ , according to the previous section recommendations.

- All in all, the initial intuition that smaller  $f$  values are more adequate for this type of SABs in comparison with conventional planar arch bridges, in terms of the structural response is confirmed, on seeing the increase of the arch bending moments.
- For SABs with a vertical planar arch and a curved superior deck, there are large variations of total arch displacements at span center (Figure 4-14), which decrease with  $f$ . At  $L/8$ , they increase with  $f$ . The lowest displacements are obtained for  $f=20\text{m}=L/5$ . For  $g=0$  the lowest displacements are obtained for  $f=50\text{m}=L/2$
- For  $f=10\text{m}$  in-plane displacements are very high (Figure 4-12), but out-of-plane ones are controlled (Figure 4-13). The opposite happens with  $f=50\text{m}$ .
- For  $10\text{m} < f < 50\text{m}$  in- and out-of-plane arch maximal displacements have approximately the same value (Figure 4-12 and Figure 4-13).



**Figure 4-2: Arch axial forces comparison for different  $f$  values and  $g=0$ . The abscissas are the arch length from 0 to  $L_A$**

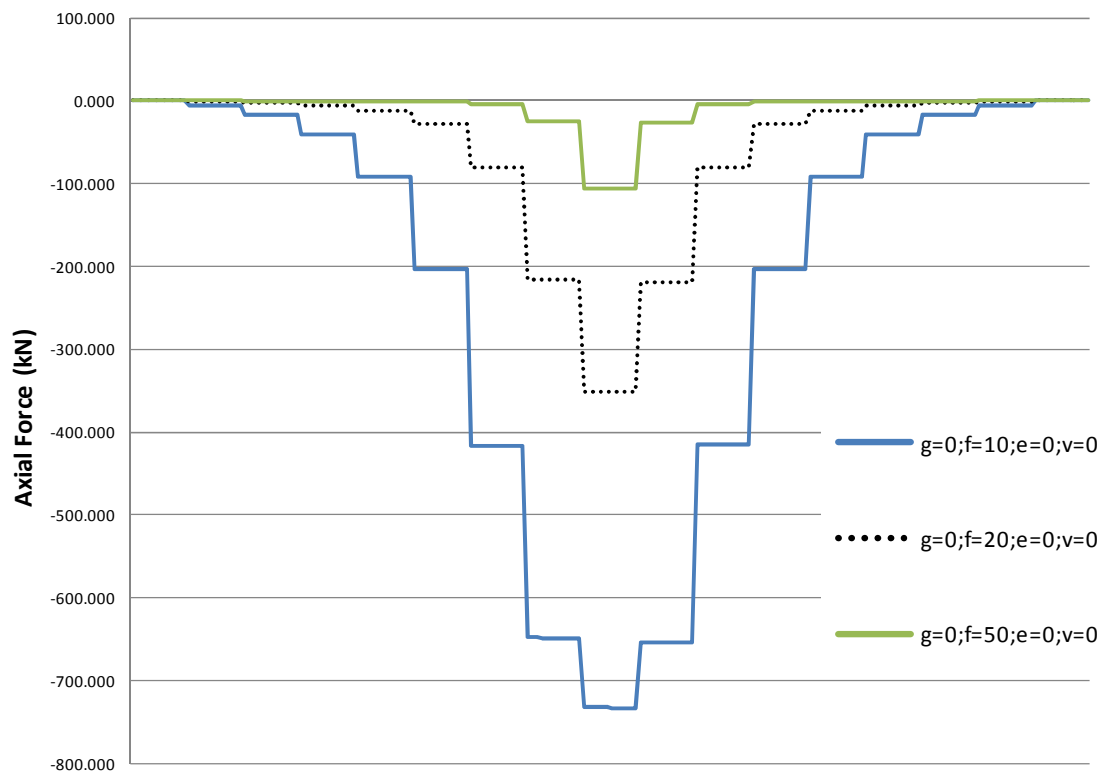


Figure 4-3: Deck axial forces comparison for different  $f$  values and  $g=0$ . The abscissas are the deck length from 0 to  $L_D$

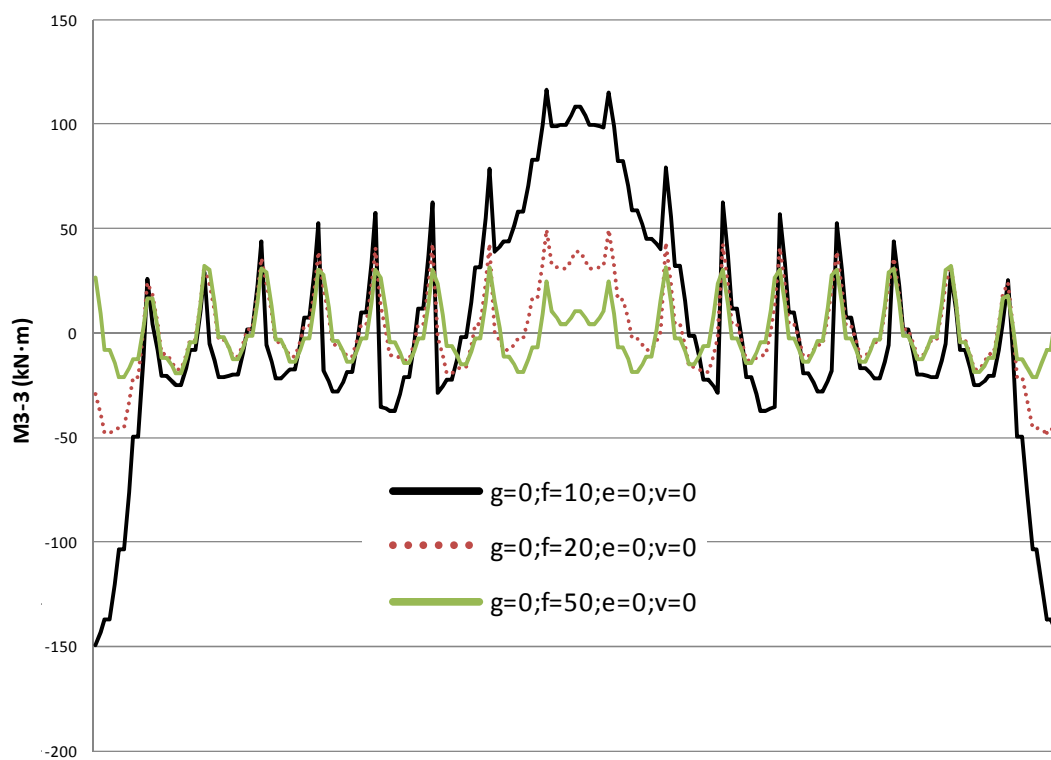


Figure 4-4: Arch bending moments comparison for different  $f$  values and  $g=0$ . The abscissas are the arch length from 0 to  $L_A$

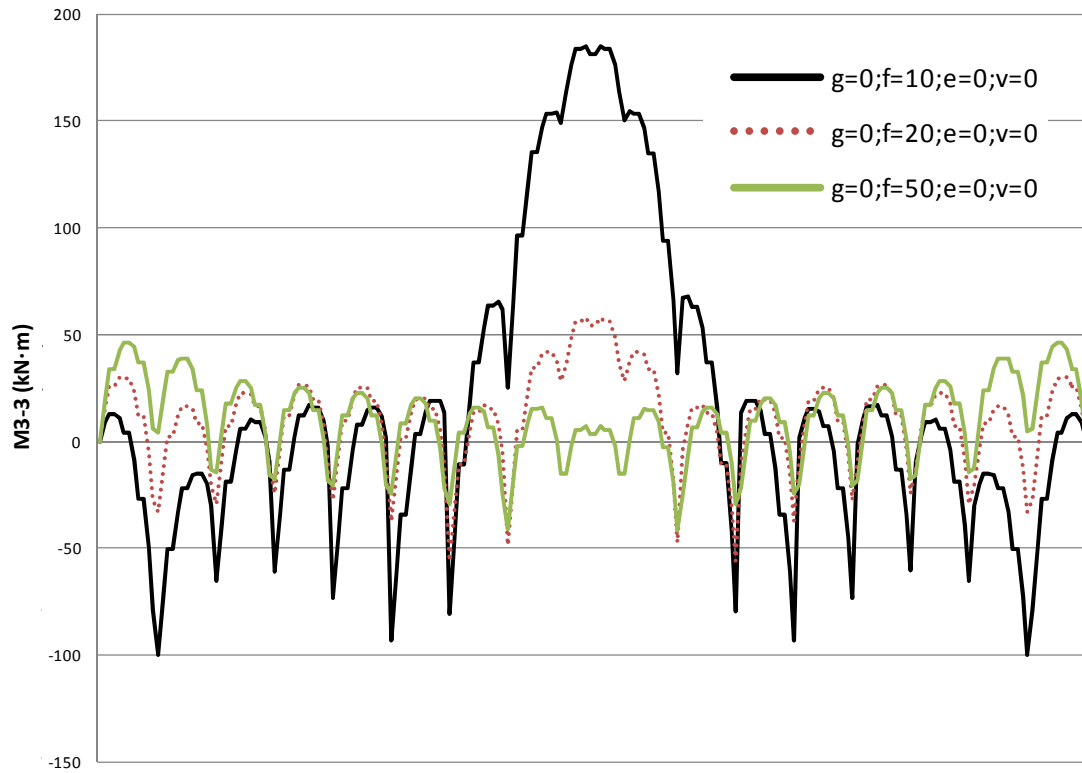


Figure 4-5: Deck bending moments comparison for different  $f$  values and  $g=0$ . The abscissas are the deck length from 0 to  $L_D$

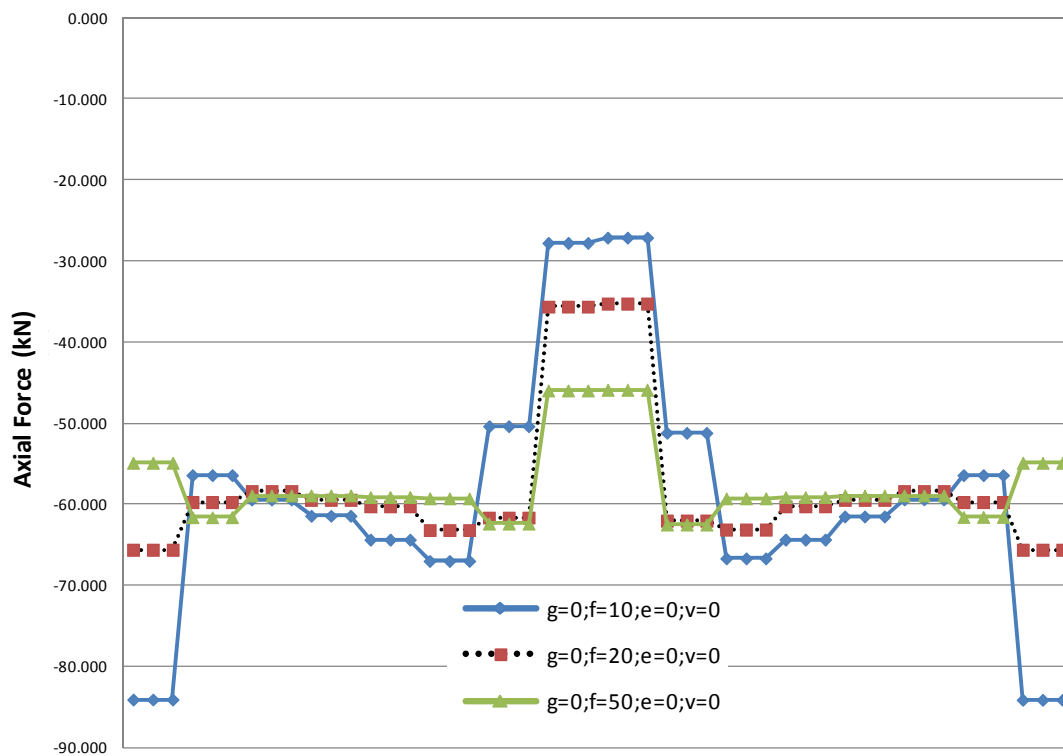


Figure 4-6: Struts axial forces comparison for different  $f$  values and  $g=0$ . The abscissas are the output stations of the different struts (at the bottom, center and the top of their length).

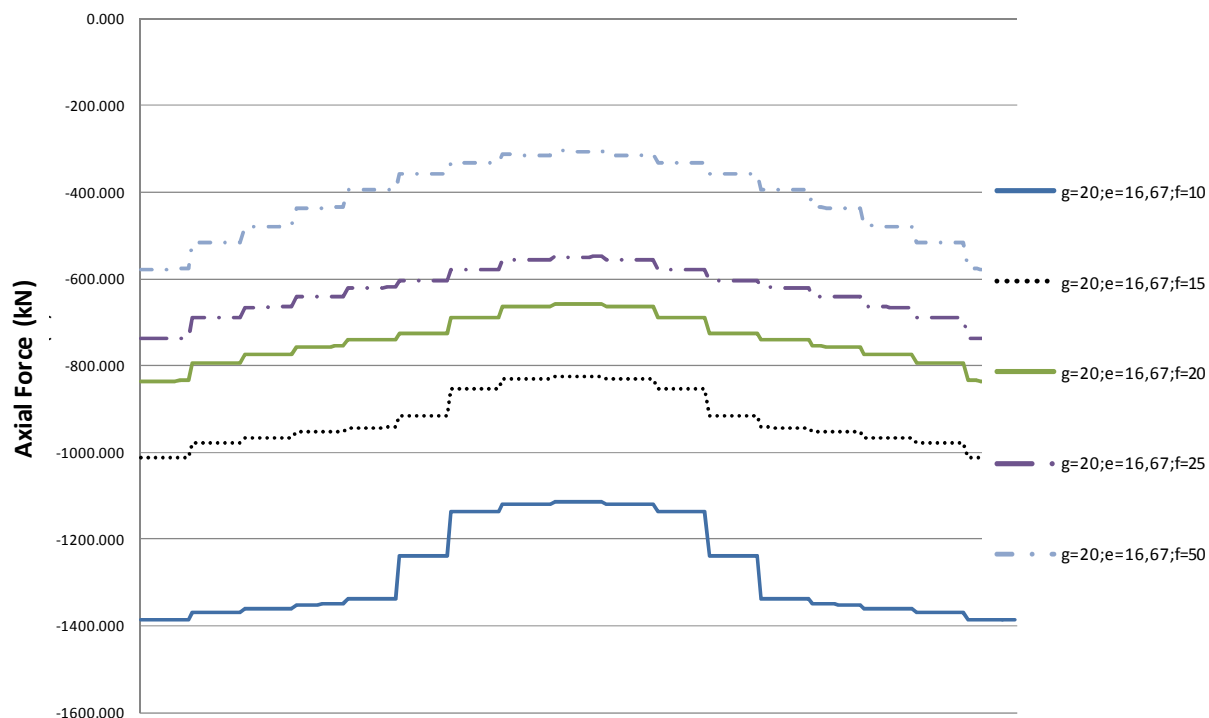


Figure 4-7: Arch axial forces comparison for different  $f$  values and  $g=20$ . The abscissas are the arch length from 0 to  $L_A$

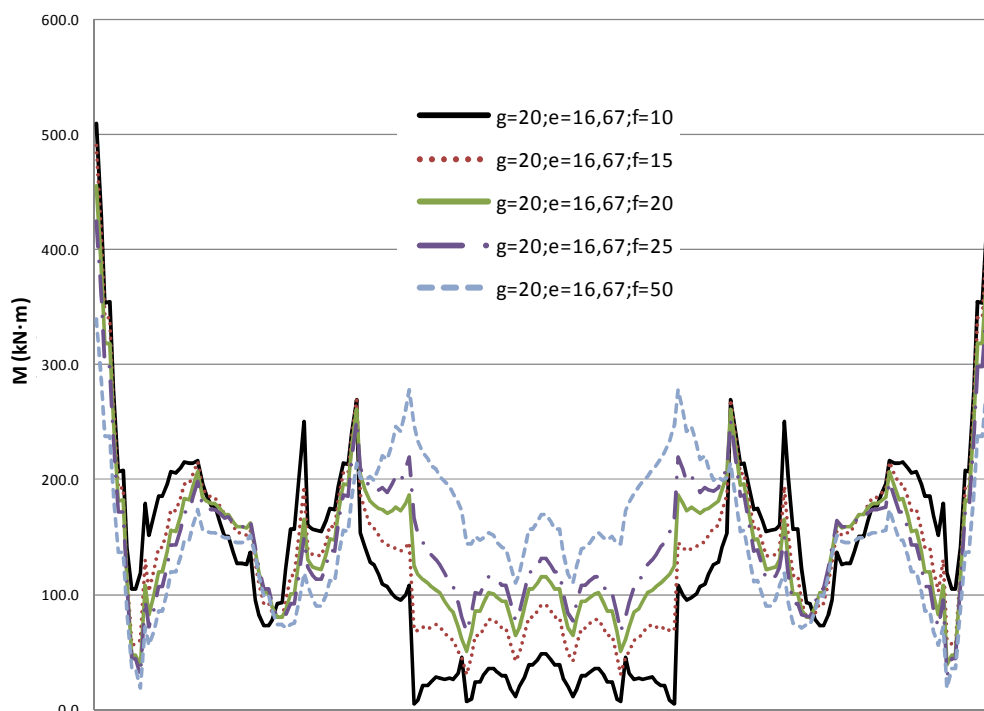


Figure 4-8: Arch total bending moments comparison for different  $f$  values and  $g=20$ . The abscissas are the arch length from 0 to  $L_A$

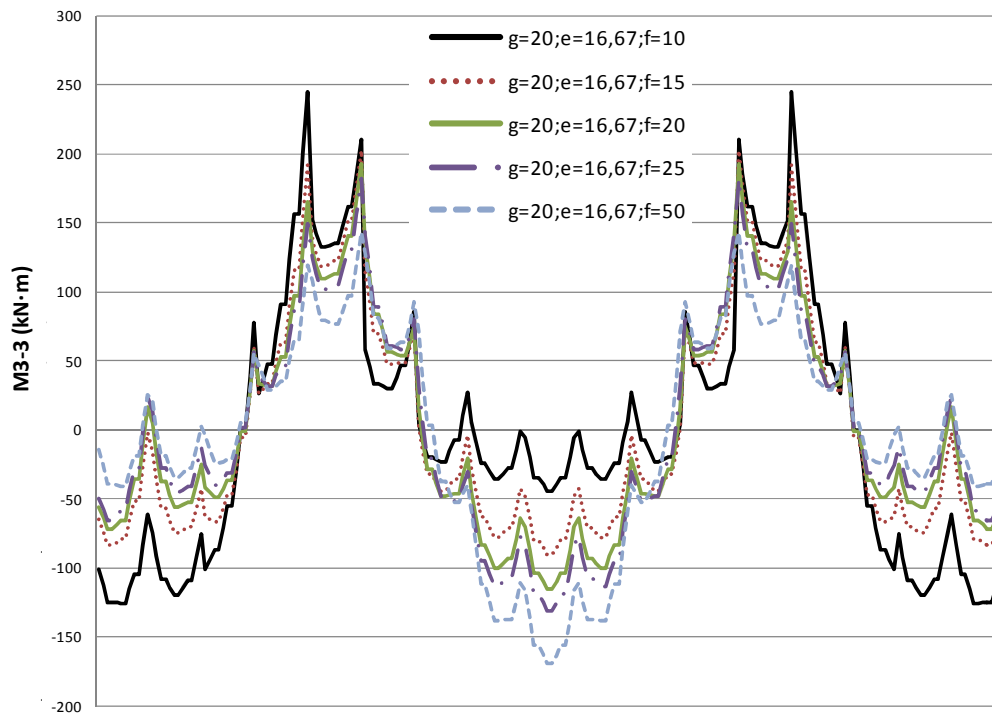


Figure 4-9: Arch in-plane bending moments comparison for different  $f$  values and  $g=20$ . The abscissas are the arch length from 0 to  $L_A$

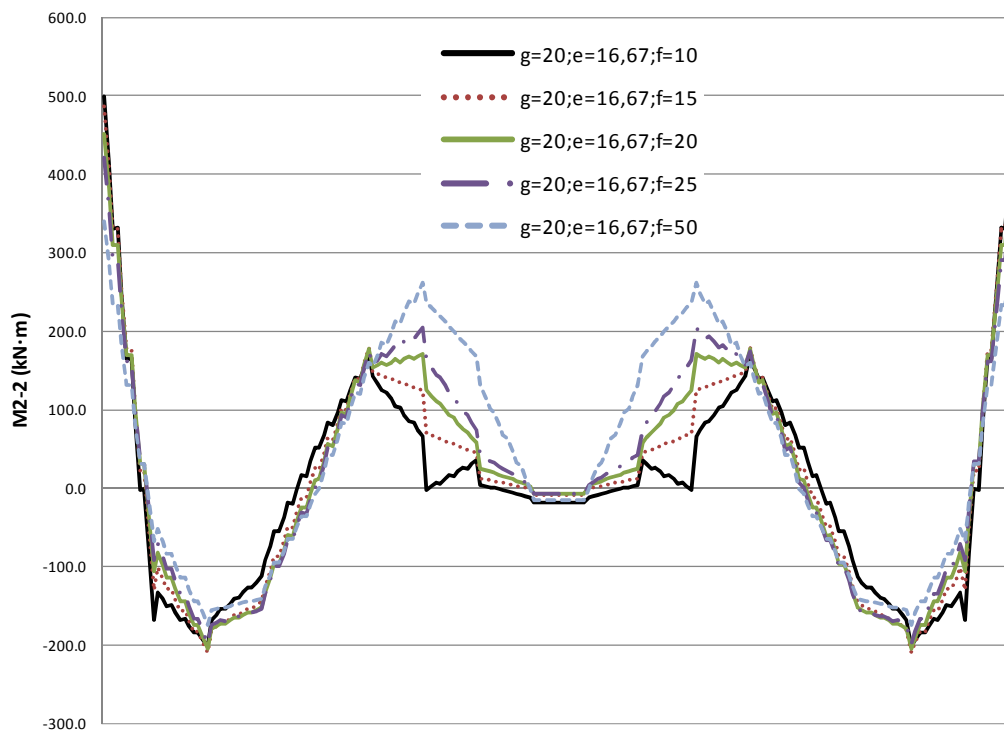
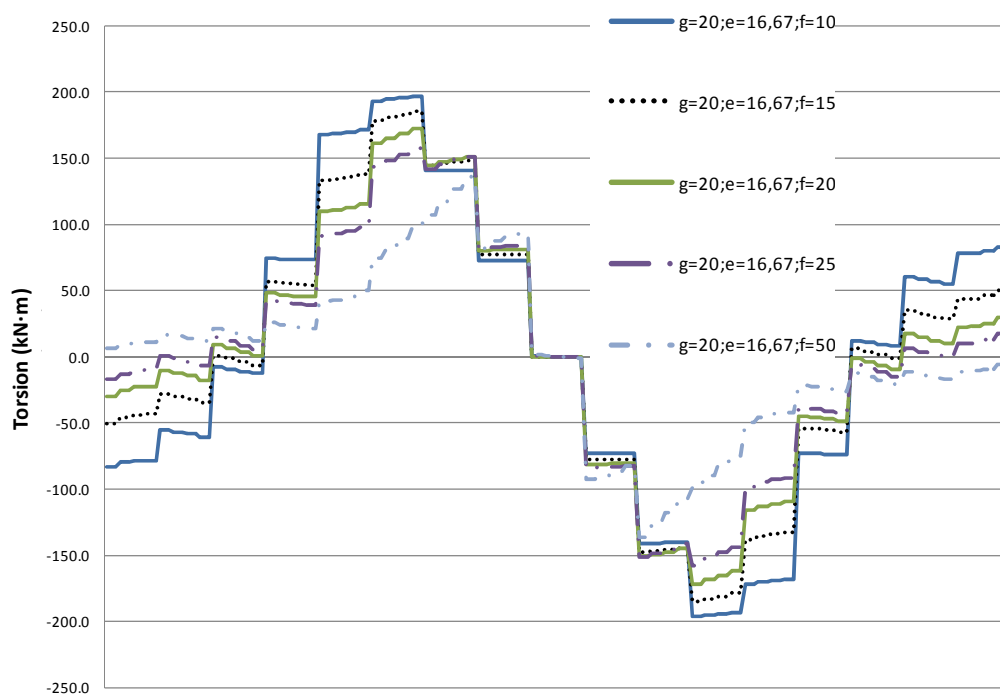
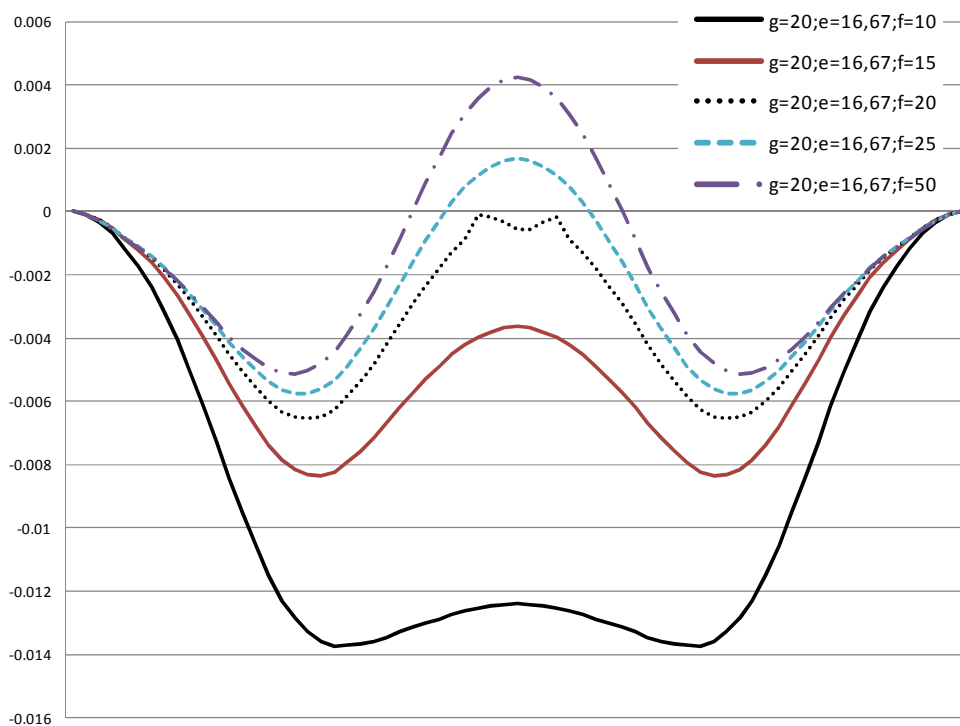


Figure 4-10: Arch out-of-plane bending moments comparison for different  $f$  values and  $g=20$ . The abscissas are the arch length from 0 to  $L_A$



**Figure 4-11:** Arch torsional moments comparison for different  $f$  values and  $g=20$ . The abscissas are the arch length from 0 to  $L_A$



**Figure 4-12:** Arch in-plane displacements comparison for different  $f$  values and  $g=20$ . The abscissas are the arch length from 0 to  $L_A$ . Ordinates: arch displacements in meters.

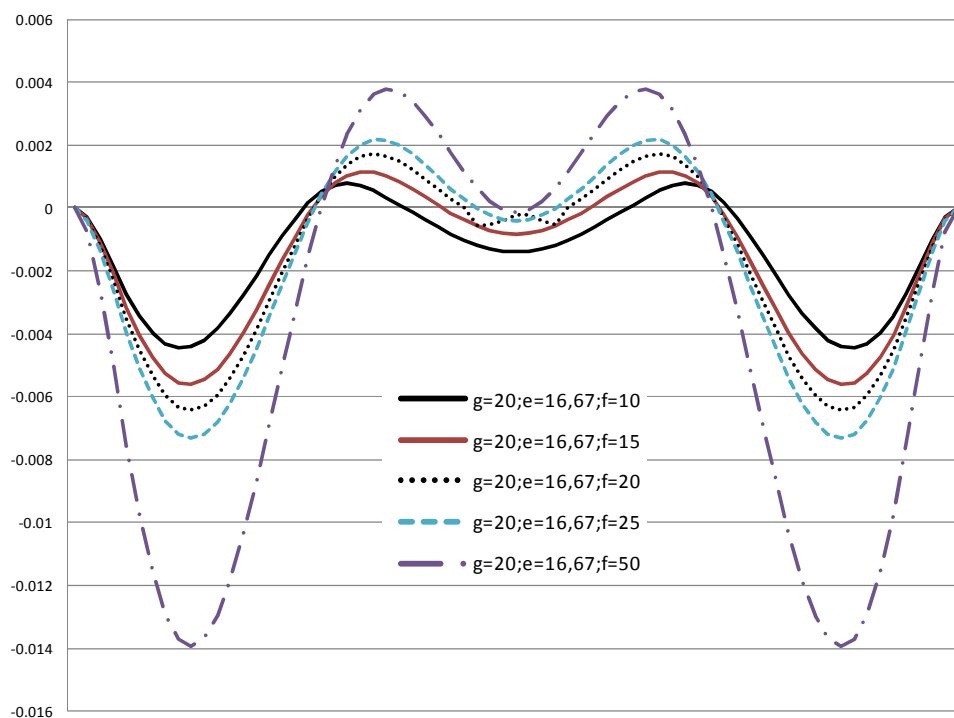


Figure 4-13: Arch out-of-plane displacements comparison for different  $f$  values and  $g=20$ . The abscissas are the arch length from 0 to  $L_A$ . Ordinates: arch displacements in meters.

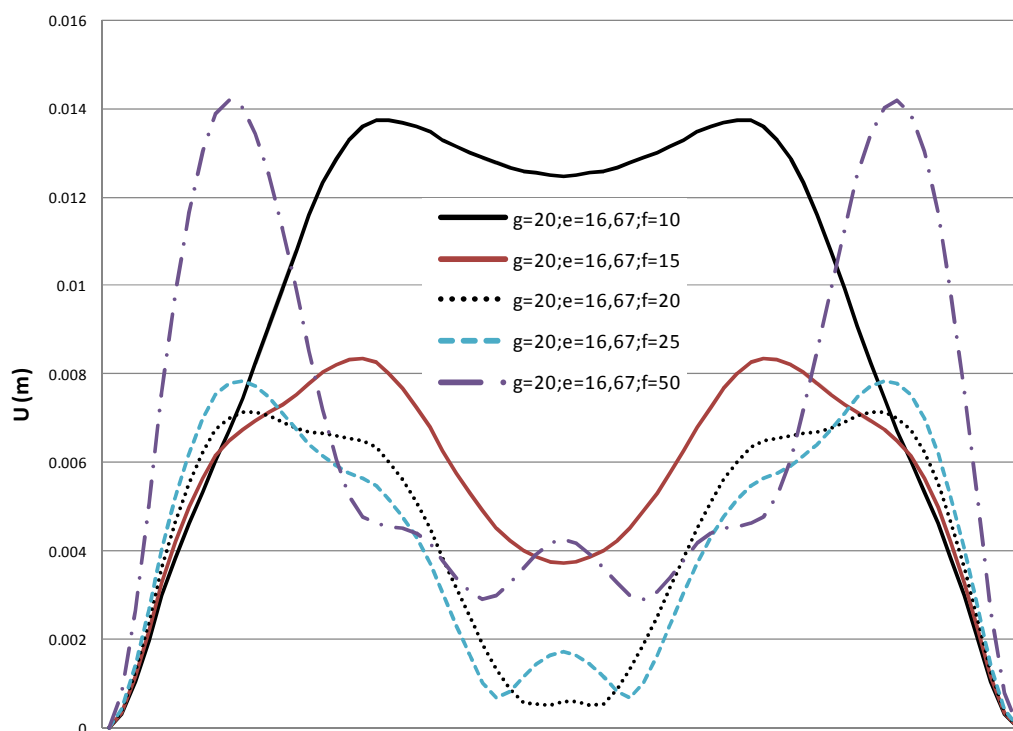


Figure 4-14: Arch total displacements comparison for different  $f$  values and  $g=20$ . The abscissas are the arch length from 0 to  $L_A$ . Arch displacements in meters.

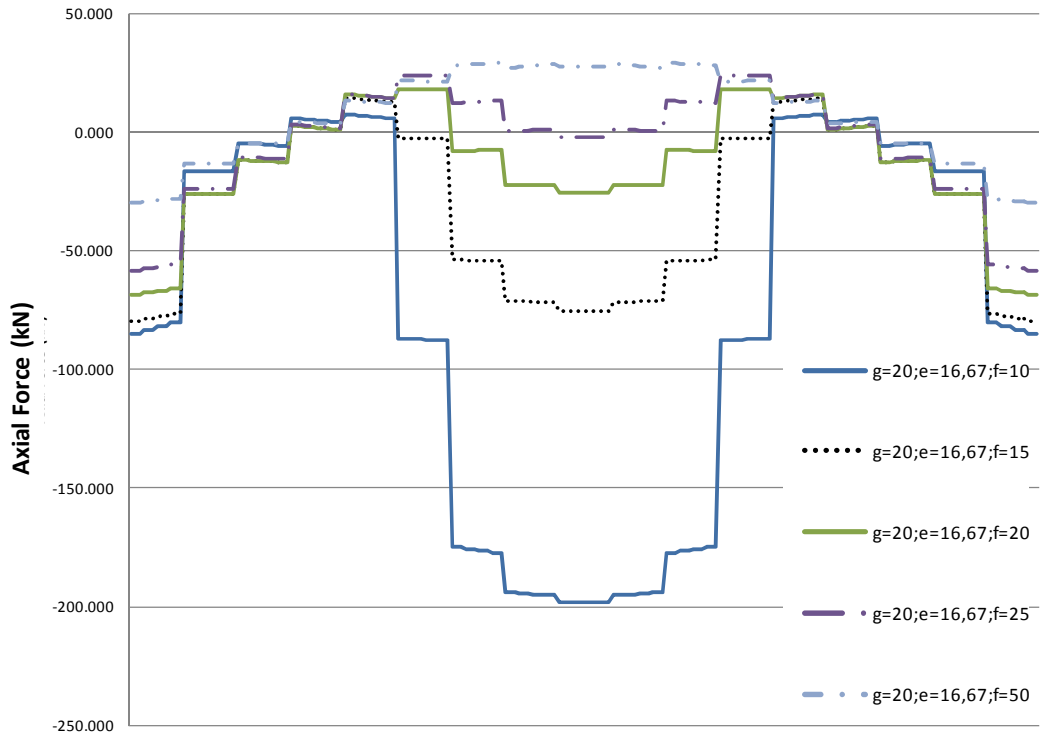


Figure 4-15: Deck axial forces comparison for different  $f$  values and  $g=20$ . The abscissas are the deck length from 0 to  $L_D$

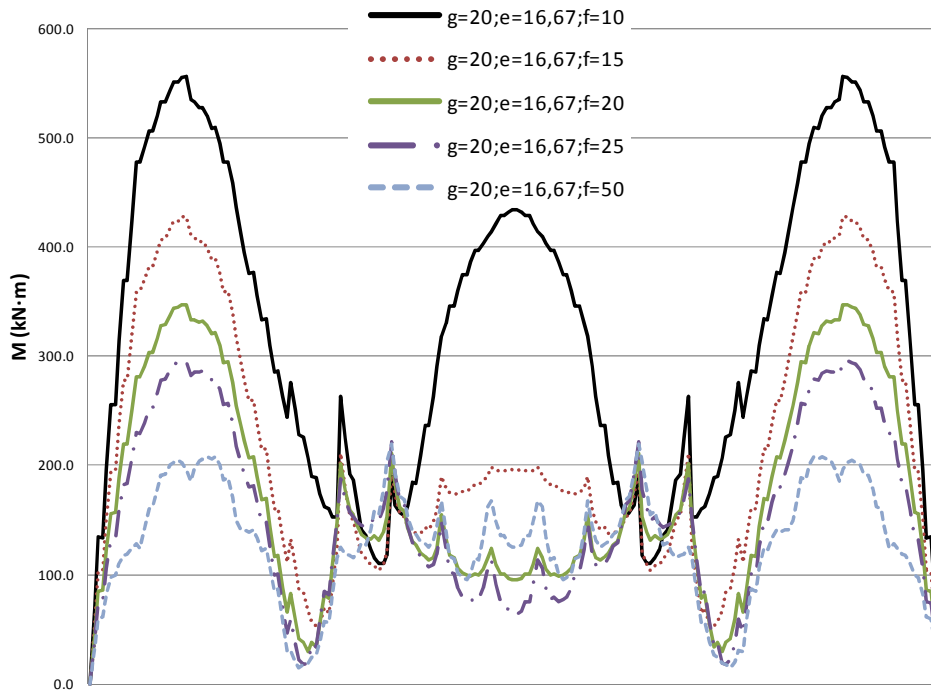


Figure 4-16: Deck total bending moments comparison for different  $f$  values and  $g=20$ . The abscissas are the deck length from 0 to  $L_D$



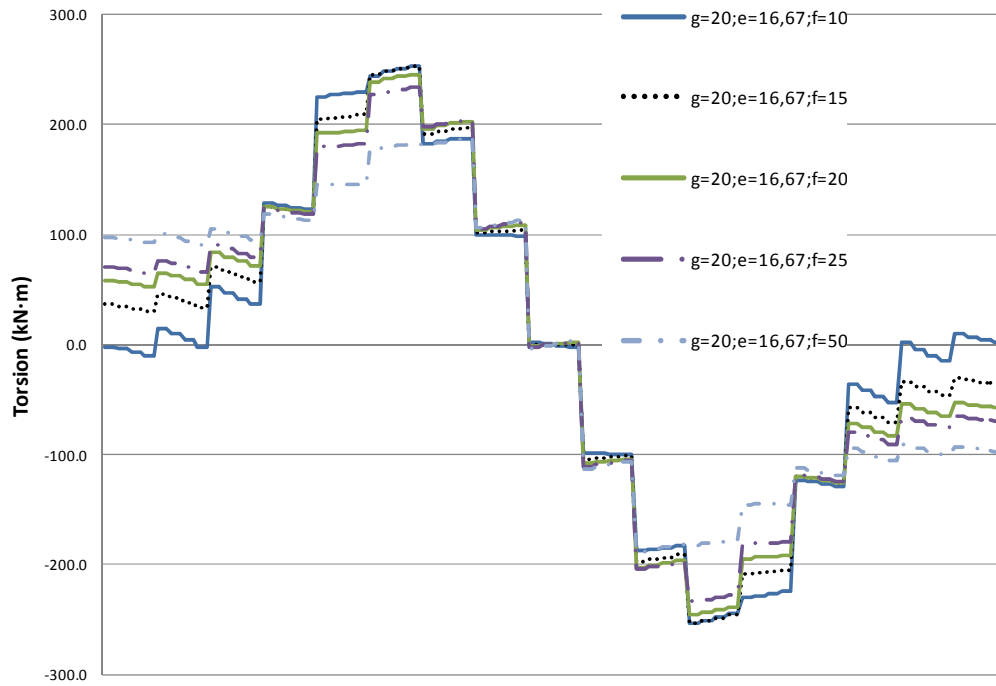


Figure 4-17: Deck torsional moments comparison for different  $f$  values and  $g=20$ . The abscissas are the deck length from 0 to  $L_D$

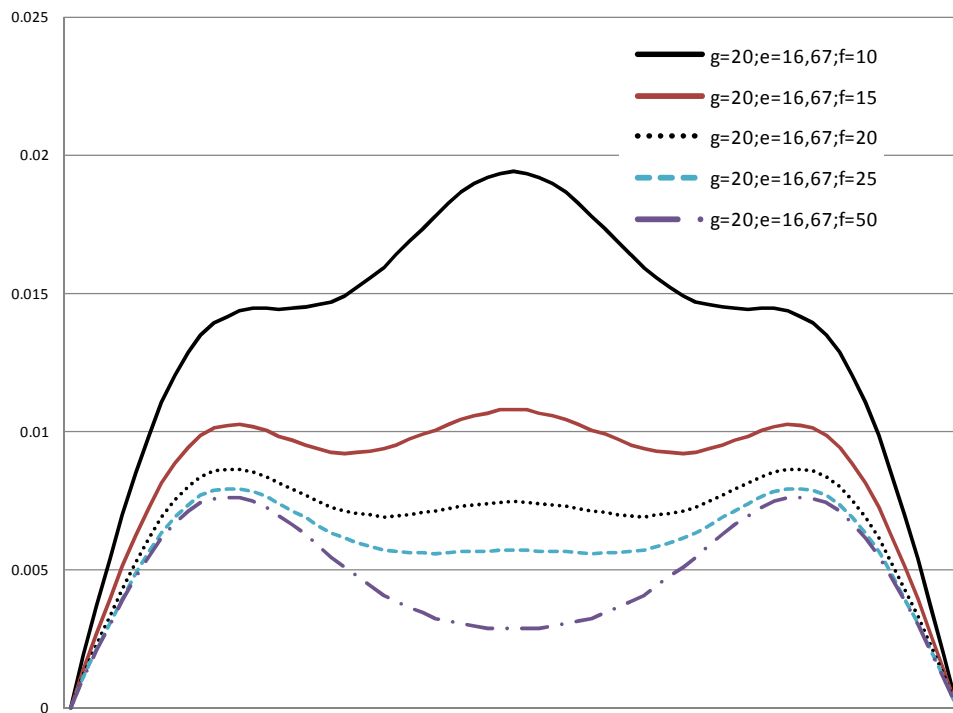
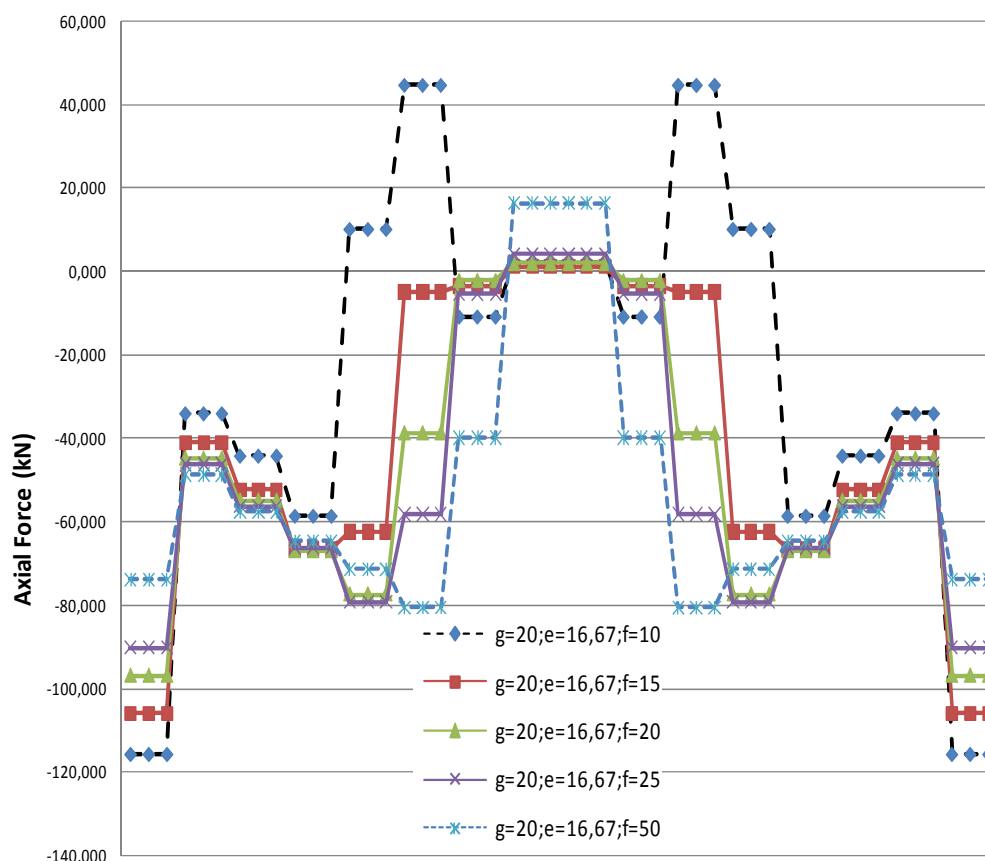


Figure 4-18: Deck total displacements comparison for different  $f$  values and  $g=20$ . The abscissas are the deck length from 0 to  $L_D$ . Displacements in meters.



**Figure 4-19: Struts axial forces comparison for different  $f$  values and  $g=20$ . The abscissas are the output stations of the different struts (at the bottom, center and the top of their length).**

### 4.3 STRESS BEHAVIOUR UNDER $q$ AND DESIGN AND COMPARISON IN ULTIMATE LIMIT STATE

Firstly, in Figure 4-20 the comparison of the arch stresses only under  $q=10\text{kN/m}$  for different  $f$  values, for  $g=0\text{m}$  and the reference model cross-sections (Table 1-1) is shown. For  $g=20\text{m}$  and  $e=16,67\text{m}$ , an equivalent comparison is displayed in Figure 4-21. Stresses in the deck are displayed in Figure 4-22 and Figure 4-23 and in struts for  $g=20\text{m}$  and  $e=16,67\text{m}$  in Figure 4-24.

Secondly, the different loading combinations described in section 1.5.2 and 1.5.3 have also been analysed, obtaining the worst loading cases for the different models. According to these determinant loading cases, the cross-sections of the different models have been designed.

Finally, the main aspects of the results for different models are analysed in this section.

- For conventional vertical arch bridges ( $g=0$ ), whatever the  $f$  value, the maximal stresses in the arch and deck are significantly higher for combination A2, when the loading is applied on half the deck span (section 1.5.2). For  $f=10$  and  $50\text{m}$  the stresses in the struts are also maximal for A2. However, for  $f=20$  the maximal stresses in the central struts take place under A1, but in the rest of the struts also for A2.
- For SABs with a superior curved deck, the critical load case, for stresses in the arch is A2 for the springing and around  $L/4$  and combination A1 for the rest of the arch. For the

aforementioned cross-sections A2 differs only slightly to A1, whereas for  $g=0$  the difference was very large.

- The maximal stresses in the deck are significantly higher for A2, except at span center where maximal stresses are obtained for A1. For  $f \leq 20\text{m}$  the stresses in the struts are all maximal for A2 except the four struts in the span center. Similarly, for  $f > 20\text{m}$  the maximal stresses in the two central struts take place under A1, but in the rest of the struts also for A2.
- For  $g=20\text{m}$ ,  $f=10$  to  $25\text{m}$  and  $e=16,67\text{m}$  when employing the reference model cross-sections (Table 1-1), the worst hypothesis for the arch is A1 except at springing and  $L_A/4$  where A2 is worse, determined by the loading case  $l_a$  (Figure 2-15).
- The importance of asymmetrical loading for stresses in the arch diminishes when increasing the value of  $f$ . The worst loading cases combination for  $g=20\text{m}$ ,  $f=50\text{m}$ ,  $e=g/1,2=16,67\text{m}$  for the reference model cross-sections and for  $g=20\text{m}$ ,  $f=20\text{m}$ ,  $e=16,67\text{m}$  for the SSDS model (Table 1-1) cross-sections is A1.

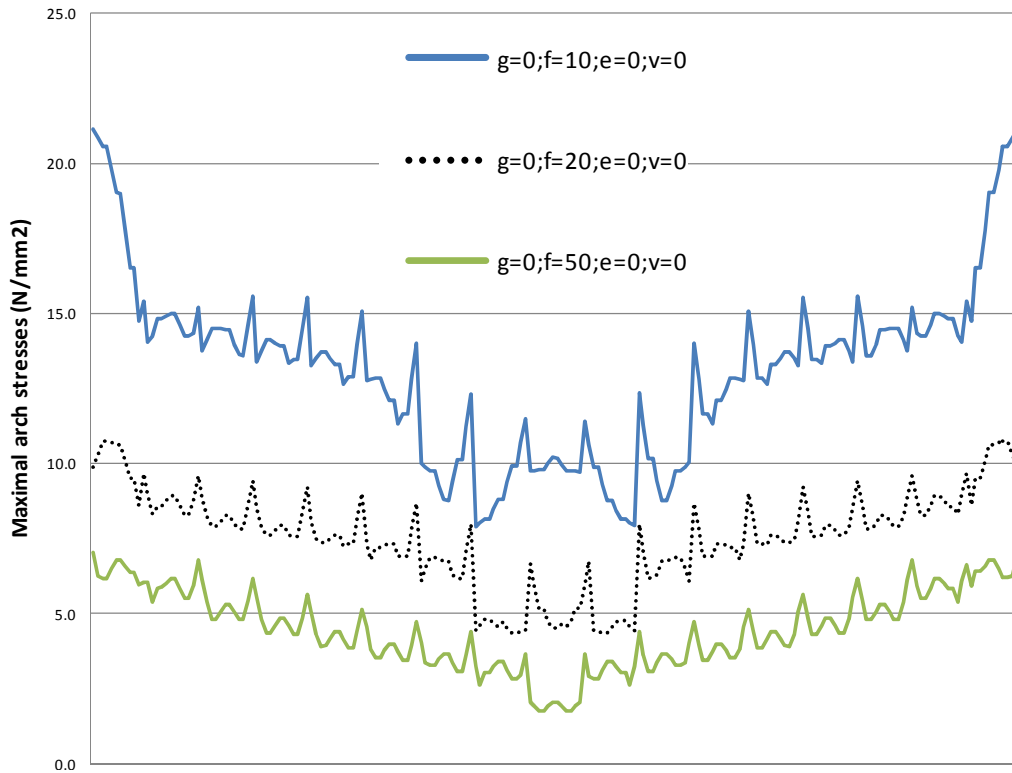


Figure 4-20: Arch stresses comparison only under  $q$  for different  $f$  values and  $g=0$ . The abscissas are the arch length from 0 to  $L_A$

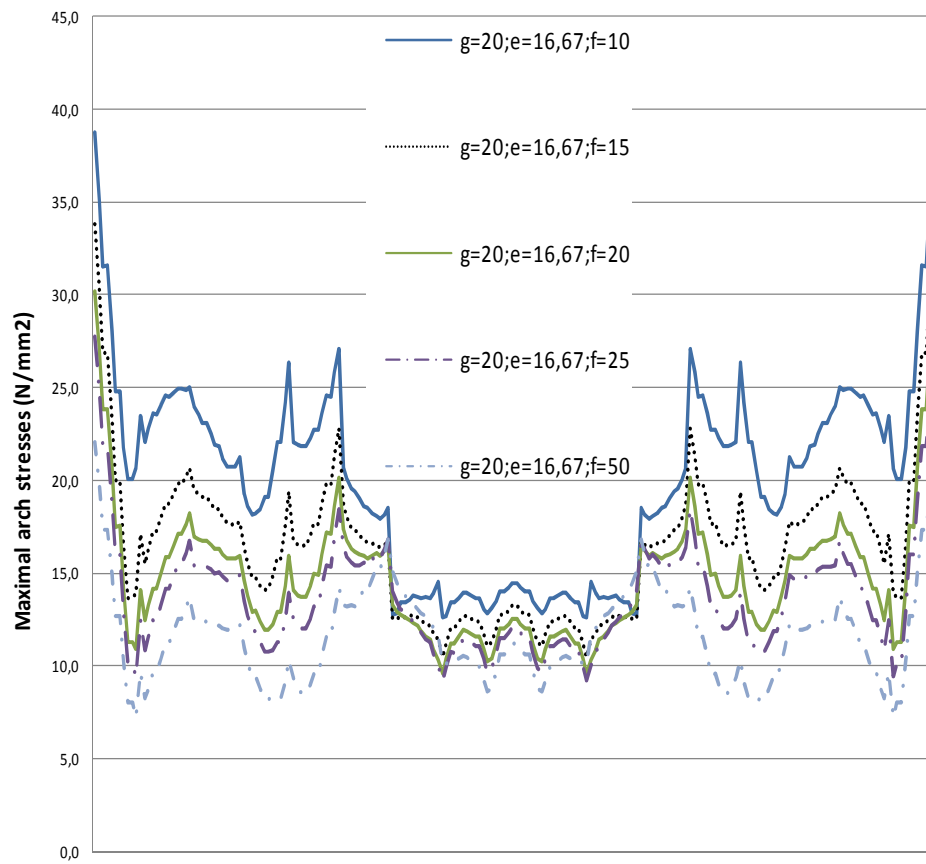


Figure 4-21: Arch stresses comparison only under  $q$  for different  $f$  values and  $g=20$ . The abscissas are the arch length from 0 to  $L_A$

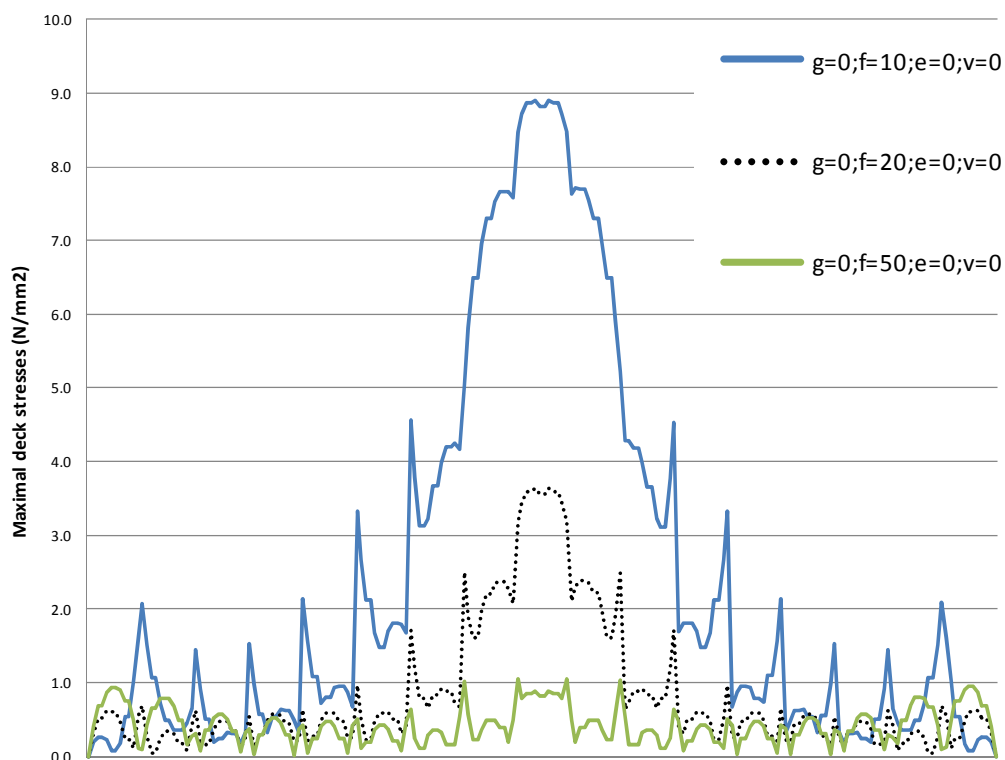


Figure 4-22: Deck stresses comparison only under  $q$  for different  $f$  values and  $g=0$ . The abscissas are the deck length from 0 to  $L_D$

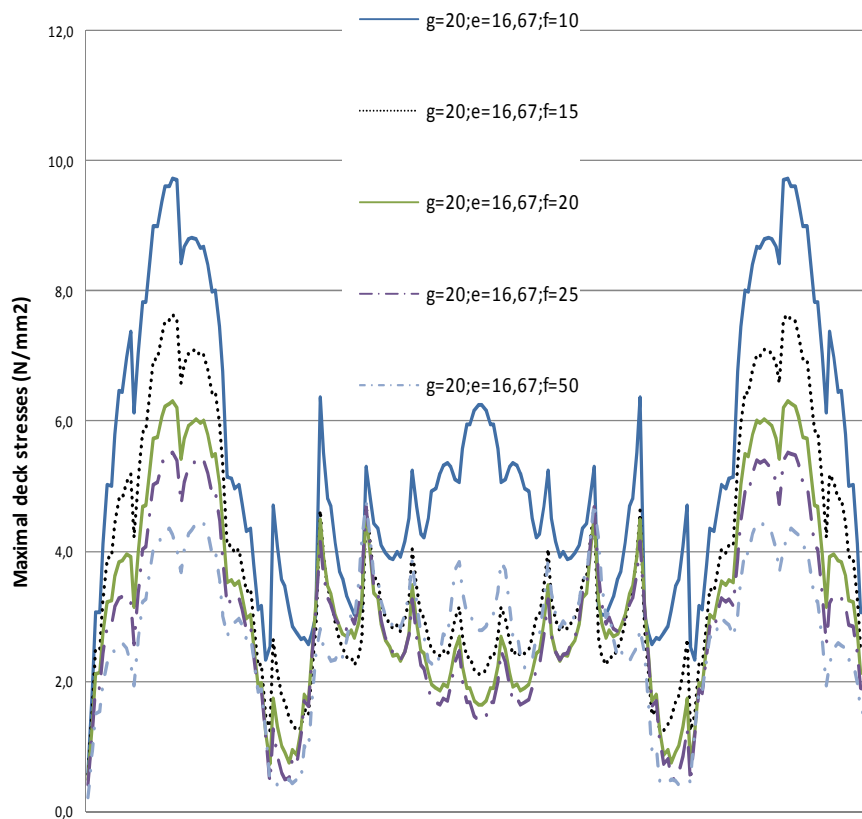
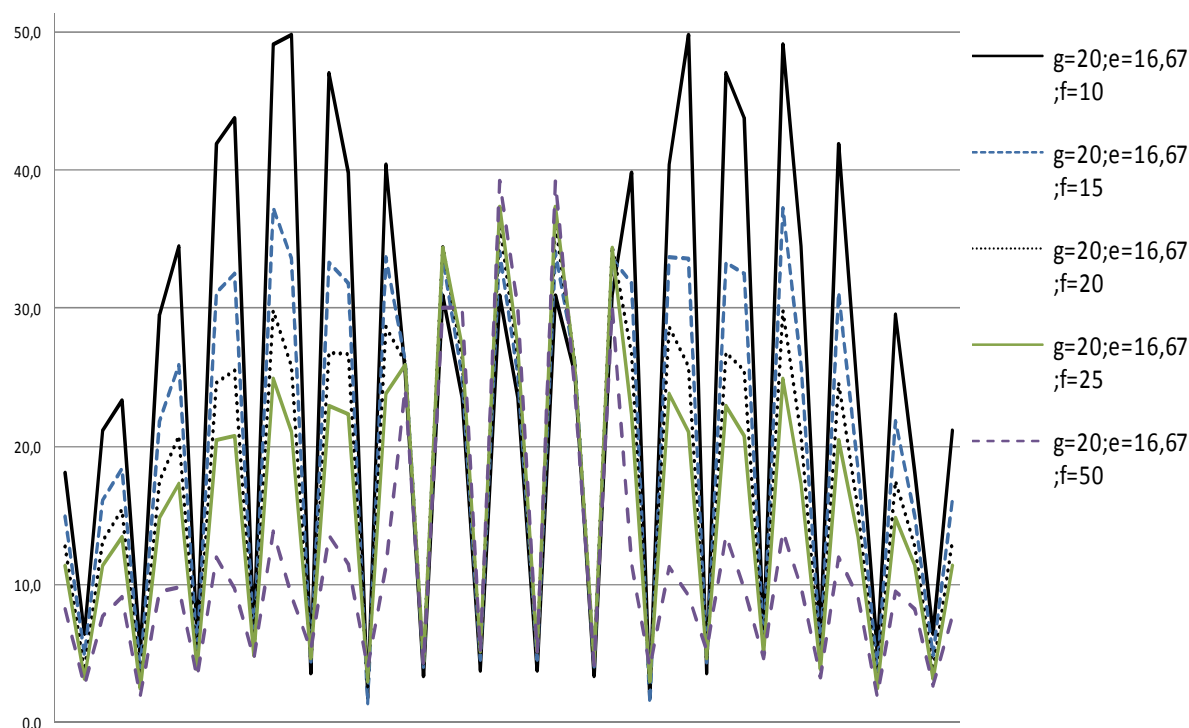


Figure 4-23: Deck stresses comparison only under  $q$  for different  $f$  values and  $g=20$ . The abscissas are the deck length from 0 to  $L_D$



**Figure 4-24: Struts stresses comparison for different  $f$  values and  $g=20$ . The abscissas are the output stations of the different struts (at the bottom, center and the top of their length).**

- As  $f$  increases, stresses in the arch under a uniform loading  $q=10\text{kN/m}$  decrease (Figure 4-20 and Figure 4-21) and stresses in the deck decrease greatly (Figure 4-22 and Figure 4-23). Stresses in struts also decrease with  $f$  except for central struts (Figure 4-24), as also observed for axial forces (Figure 4-19). However, the length of the arch and the struts also increase, so more material will be necessary.

The different elements in the bridge have been dimensioned for the envelope of stresses resulting in:

- Whatever the  $f$  value the deck should be a  $4000 \times 700 \neq 10\text{mm}$  steel box girder. It would be enough with 3mm to resist the stresses considering a compact cross-section. However, 10mm are considered for local bending moments, local instability of compressed plates and durability.

For  $g=20$ , the models with  $f=10, 15, 20, 25$  and  $50\text{m}$  have been dimensioned. The following cross-sections for S 355 steel have been obtained employing a linear analysis.

- The arches are CHS of 750mm diameter and thickness ranging from 10mm to 20mm for  $f=50$ , from 10mm at springings to 25mm at span center for  $f=25\text{m}$ , from 10mm at springings to 30mm at span center for  $f=15$  and  $20\text{m}$ , and from 20mm at extremes to 40mm at springings for  $f=10\text{m}$ .
- The struts are CHS of 300mm diameter and thickness ranging from 15mm at extremes to 45mm at span center for  $f=50$ , from 15mm at extremes to 35mm at span center for  $f=20$  and  $25\text{m}$ , and from 20mm at extremes to 55mm at  $L/3$  approximately for  $f=15\text{m}$ . For

$f=10\text{m}$ , CHS of 300mm struts were not possible and CHS of 350mm struts were employed, with thickness ranging from 15mm at extremes to 50mm at  $L/3$  approximately.

For  $g=0$ , the models with  $f=10, 20$  and  $50\text{m}$  have been dimensioned. The following cross-sections for S 355 steel have been obtained employing a linear analysis.

- The arches are CHS of 750mm diameter and thickness ranging from 10mm to 20mm for  $f=50$ , from 6mm to 25mm at springings center for  $f=20\text{m}$ , and from 8mm to 32mm at springings for  $f=10\text{m}$ .
- The struts are CHS of 300mm diameter and thickness ranging from 6mm at extremes to 12mm at span center for  $f=50$ , from 5mm to 25mm for  $f=20$ , and from 16mm at extremes to 50mm at  $L/3$  approximately for  $f=10\text{m}$ .

#### 4.4 EFFICIENCY CRITERIA

The results of the chosen criteria are shown for the different models which have been studied in tables from Table 4-1 to Table 4-9. In these tables the nomenclature already given in section 1.3 is employed. Please use the bookmark to comfortably interpret the tables, and note whether the length is considered or not, since the nomenclature and units of the criteria are modified. The following values are specifically employed for the tables in this section:

- $f^*$  is the value of  $f$  which minimizes each criteria (m)
- $i=\%$  of difference of B from the most efficient  $f$  value for B ( $f^*$ )

A different  $f^*$  is obtained for each criteria. The results of the efficiency criteria are commented in the following lines:

- The total mass of the struts for  $g=20$  and  $f=10$  does not seem to correspond to a logical evolution with  $f$  of the other  $g=20$  models of the  $f$  comparison case study (Table 4-7). This is due to the fact that a larger diameter had to be employed in comparison with the rest of models. The same diameter is needed in order to do a reliable comparison. Therefore, new mass values have obtained employing the same diameter for all the models.
- Values of  $f$  between  $L/6,67-L/4$  (15-25m) give a negligible difference of the total mass of the bridge (Table 4-2 and Table 4-8), so they can be considered with an equivalent efficiency. Employing a vertical rise  $f>L/4$  for the arch is not recommendable. This is valid whatever the deck curvature. Planar vertical arch bridges with a superior straight deck can use lower  $f$  values with a negligible mass increase (Table 4-2). If a larger diameter is employed instead of increasing the thickness this is also valid for SABs (Table 4-6), since, as proved for other SABs in Chapter IV and also reflected in the present study, what needs to be highly increased in SABs is the flexural rigidity of the cross-section of the struts.
- It must be highlighted that the mass of the bridge can be a misleading criteria in order to choose the most efficient parameters if it is not correctly employed. In order to employ it correctly, the cross-sections of the different elements should be carefully chosen in order to minimise the mass of each specific studied model. For each combination of variables

different design cross-sections can be obtained. There will be a combination of diameter and thickness which gives a minimal mass. Conceptually, can only then be the masses compared, regardless of employing or not the same diameters for the different elements. However, a certain diameter might be fixed also for aesthetical reasons. In the present study we consider a constant diameter as a valid way to compare the efficiency criteria of the different models when varying  $f$ , in correspondence with the internal forces comparison.

- The maximal displacement under permanent loads is the simplest criteria to employ (Table 4-1, Table 4-4 and Table 4-5), equivalent to consider the lowest mass of the bridge depending on  $f$ , since the total mass for  $f=20$  or  $25$ m is approximately the same (Table 4-2 and Table 4-6), the lowest maximal stress or the sum of stresses (in the arch or the whole bridge and whatever the load) considering the length of all the elements (Table 4-1 and Table 4-4). The lowest sum of the total bending moments in the arch under permanent loads (Table 4-4 C) cannot be considered a valid criteria for SABs, but, for planar vertical arch bridges with a superior straight deck, it is a valid criteria (Table 4-1C).
- The way in which the stress criteria is calculated (Criterias 0, 1 and 2, Table 4-2 and Table 4-6) is not relevant, since they all lead to the same result.
- The fact that the displacement criteria gives nearly the same results as the mass criteria confirms that a linear analysis is enough in order to determine which  $f$  value is the most efficient.

Model	Criteria							
	A	B	C	D	E	F	G	H
$g=0;f=10;e=0;v=0$	4320384	6645456	5563495	667131	951012	53969	5278	10193
$g=0;f=20;e=0;v=0$	3583052	5484528	4268285	466714	617553	52463	3268	3080
$g=0;f=50;e=0;v=0$	4841903	7922334	15692357	442889	557447	79747	3410	7885
$f^*$	$f=20$	$f=20$	$f=20$	$f=50$	$f=50$	$f=20$	$f=20$	$f=20$

**Table 4-1: Efficiency criteria for the value of  $f$  for  $g=0$  considering the length of the elements**



Criteria					
Model	Mass of the bridge (kg)	% of mass of the bridge variation with respect to the lowest one	Criteria 0: Stress efficiency average of the bridge*total length of the bridge (m)	Criteria 1: Sum of stress efficiency average of the element (arch, bridge and deck)*length of the element (m)	Criteria 2: Sum of the stress efficiency in each output station*Length of each output station of the bridge (m)
g=0;e=0;f=10;v=0	116767.3	3.3	14573.4	15.5	44.2
g=0;e=0;f=20;v=0	113001.6	0.0	12027.5	12.0	37.9
g=0;e=0;f=50;v=0	122862.9	8.7	17373.5	15.0	55.8
Minimal Value	113001.6		12027.5	12.0	37.9
<i>f</i> *	<b>f=20</b>		f=20	f=20	f=20

**Table 4-2: Efficiency criteria for the value of *f* for g=0 considering the length and the mass of the elements**

Criteria								
Model	Mass of the arch (kg)	% of mass of the arch variation with respect to the lowest one	Mass of the struts (kg)	% of mass of the struts variation with respect to the lowest one	Mass of the deck (kg)	Mass of the arch (kg/m)	Mass of the struts (kg/m)	Mass of the deck (kg/m)
g=0;e=0;f=10;v=0	26798.4	24.2	8966.8	0.0	81002.0	261.2	170.9	734.8
g=0;e=0;f=20;v=0	21569.3	0.0	10430.3	16.3	81002.0	196.4	110.8	734.8
g=0;e=0;f=50;v=0	26860.9	24.5	15000.0	67.3	81002.0	181.6	63.7	734.8
Minimal Mass (kg)	21569.3		8966.8					

**Table 4-3: Mass of the different elements, according to *f* values for g=0**

Criteria								
Model	A	B	C	D	E	F	G	H
g=20;e=16,67;f=10	7582440	12478661	18904808	1250084	1941837	75088	11914	11631
g=20;e=16,67;f=15	6548326	10933656	21166890	1092824	1655958	67918	10996	7465
g=20;e=16,67;f=20	6242197	10436932	24107370	1042618	1564838	65286	10503	6754
g=20;e=16,67;f=25	6222403	10377686	27203488	1035907	1543181	64893	10315	7671
g=20;e=16,67;f=50	7675480	12628244	45902020	1214494	1788309	76580	11303	17638
<i>f</i> *	<i>f</i> =25	<i>f</i> =25	<i>f</i> =10	<i>f</i> =25	<i>f</i> =25	<i>f</i> =25	<i>f</i> =25	<i>f</i> =20

**Table 4-4: Efficiency criteria for the value of *f* for g=20 considering the length of the elements**

Model	Criteria							
	A	B	C	D	E	F	G	H
g=20;e=16,67;f=10	24666	40594	61499	4067	6317	244	39	38
g=20;e=16,67;f=15	20112	33580	65009	3356	5086	209	34	23
g=20;e=16,67;f=20	17958	30026	69354	2999	4502	188	30	19
g=20;e=16,67;f=25	16724	27892	73114	2784	4148	174	28	21
g=20;e=16,67;f=50	14962	24616	89478	2367	3486	149	22	34
<i>f</i> *	<i>f</i> =50	<i>f</i> =50	<i>f</i> =10	<i>f</i> =50	<i>f</i> =50	<i>f</i> =50	<i>f</i> =50	<i>f</i> =20

**Table 4-5: Efficiency criteria for the value of *f* for g=20 not considering the length of the elements**

Model	Mass of the bridge (kg)	% of mass of the bridge variation with respect to the lowest one	Criteria 1: Sum of stress efficiency average of the element (arch, bridge and deck)*length of the element (m)	Criteria 0: Stress efficiency average of the bridge*total length of the bridge (m)	Criteria 2: Sum of the stress efficiency in each output station*Length of each output station of the bridge (m)
g=20;e=16,67;f=10;v=0	133891,4	3.1	77,1	25,8	83,3
g=20;e=16,67;f=15;v=0	132236,0	1.9	67,6	22,3	73,8
g=20;e=16,67;f=20;v=0	130543,5	0.6	64,5	20,9	70,8
g=20;e=16,67;f=25;v=0	129822,7	0.0	64,1	20,5	69,3
g=20;e=16,67;f=50;v=0	141610,3	9.1	78,0	23,2	81,1
Minimal value	129822,7		64,1	20,5	69,3
Minimal value	<i>f</i> =25		<i>f</i> =25	<i>f</i> =25	<i>f</i> =25

**Table 4-6: Efficiency criteria considering the length and the mass of the elements**

Model	Mass of the arch (kg)	% of mass of the arch variation with respect to the lowest one	Mass of the struts (kg)	% of mass of the struts variation with respect to the lowest one	Mass of the deck (kg)	Mass of the arch (kg/lm)	Mass of the struts (kg/lm)	Mass of the deck (kg/lm)
g=20;e=16,67;f=10;v=0	33707.7	17.0	19107.1	0.0	81076.6	328.5	202.3	734.8
g=20;e=16,67;f=15;v=0	29136.9	1.1	22022.6	15.3	81076.6	275.6	200.9	734.8
g=20;e=16,67;f=20;v=0	29065.9	0.9	20401.0	6.8	81076.6	264.7	160.0	734.8
g=20;e=16,67;f=25;v=0	28808.2	0.0	19937.9	4.3	81076.6	251.0	135.7	734.8
g=20;e=16,67;f=50;v=0	34749.1	20.6	25784.6	34.9	81076.6	235.0	101.2	734.8
Minimal Mass (kg)	28808.2		19107.1					

**Table 4-7: Mass of the different elements, according to *f* values for g=20**

Model	Mass of the bridge (kg)	% of mass of the bridge variation with respect to the lowest one	Criteria 1: Sum of stress efficiency average of the element (arch, bridge and deck)*length of the element (m)	Criteria 0: Stress efficiency average of the bridge*total length of the bridge (m)	Criteria 2: Sum of the stress efficiency in each output station*Length of each output station of the bridge (m)
g=20;e=16,67;f=10;v=0	139293.4	7.3	77,1	25,8	83,3
g=20;e=16,67;f=15;v=0	132236,0	1.9	67,6	22,3	73,8
g=20;e=16,67;f=20;v=0	130543,5	0.6	64,5	20,9	70,8
g=20;e=16,67;f=25;v=0	129822,7	0.0	64,1	20,5	69,3
g=20;e=16,67;f=50;v=0	141610,3	9.1	78,0	23,2	81,1
Minimal value	129822,7		64,1	20,5	69,3
Minimal value	<i>f=25</i>		<i>f=25</i>	<i>f=25</i>	<i>f=25</i>

**Table 4-8: Efficiency criteria considering the length and the mass of the elements employing the same diameter for all struts**

Model	Mass of the arch (kg)	% of mass of the arch variation with respect to the lowest one	Mass of the struts (kg)	% of mass of the struts variation with respect to the lowest one	Mass of the deck (kg)	Mass of the arch (kg/lm)	Mass of the struts (kg/lm)	Mass of the deck (kg/lm)
g=20;e=16,67;f=10;v=0	33707.7	17.0	24509.2	22.9	81076.6	328.5	202.3	734.8
g=20;e=16,67;f=15;v=0	29136.9	1.1	22022.6	10.5	81076.6	275.6	200.9	734.8
g=20;e=16,67;f=20;v=0	29065.9	0.9	20401.0	2.3	81076.6	264.7	160.0	734.8
g=20;e=16,67;f=25;v=0	28808.2	0.0	19937.9	0.0	81076.6	251.0	135.7	734.8
g=20;e=16,67;f=50;v=0	34749.1	20.6	25784.6	29.3	81076.6	235.0	101.2	734.8
Minimal Mass (kg)	28808.2		19937.9					

**Table 4-9: Mass of the different elements, according to *f* values for g=20 employing the same diameter for all struts**

## 4.5 PARAMETER DISCUSSION

The parameter discussion has been already exposed in the previous sections. In this section the main conclusions and explanations are exposed:

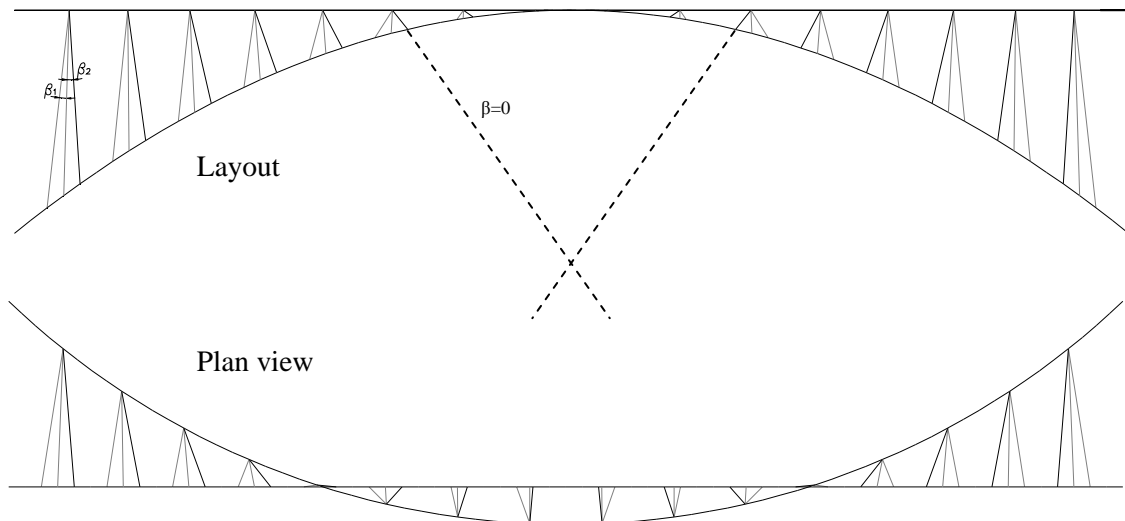
- Displacements give a clear idea of how the behavior of the arch changes with  $f$ : for low  $f$  values the out-of-plane behavior is under control, but not in-plane behavior. Vice versa for large  $f$  values.
  - For  $f=10\text{m}$  in-plane displacements are higher, but out-of-plane ones are controlled. The opposite happens with  $f=50\text{m}$ .
  - For  $10\text{m}<f<50\text{m}$  in- and out-of-plane arch maximal displacements have approximately the same value.
- When increasing  $f$ , the length increases, and thus the stiffness decreases, and the out-of-plane sag of the arch increases, hence increasing the out-of-plane behavior of the arch. Moreover, a longer length is related to higher masses. Due to the high influence of out-of-plane forces in this bridge type and that stiffer struts are needed for SABs, large  $f$  values are not convenient.
- However, the verticality of the struts increases with  $f$ . Low  $f$  values are related to very horizontal struts which do not work as efficiently and low  $f$  values also have a worse in-plane behaviour.
- Therefore, it is logical that the structural behavior of internal forces and stresses and the efficiency criteria lead to the following conclusions:
  - **The range of adequate values of  $f$  for SABs is smaller than for  $g=0$ .**
  - **Efficient values of  $f$  for SABs are in the range  $L/6,67$  and  $L/4$ .**

## 5. INCLINATION OF STRUTS ( $\beta$ ) PARAMETRICAL STUDY

### 5.1 DEFINITION AND EMPLOYED VALUES

#### 5.1.1 Employed values

The reference model employed for the strut distribution is the one obtained from equal divisions of arch and deck. This strut distribution is called a radial system of struts in the present study. Each strut axis elongation converges below the deck with its symmetrical (Figure 5-1). These are taken as the reference orientation, considering  $\beta=0$  for each strut. A more vertical orientation ( $\beta_2$ ) of the struts and a distribution of struts in which each strut axis elongation converges above the deck with its symmetrical ( $\beta_1$ , opposite inclination to the original system) have also been studied (Figure 5-1). The latter distribution is called a convergent system of struts in the present study. For the other parameters the chosen values are the following:  $L=100\text{m}$ ,  $g=0$  and  $20\text{m}$ ,  $e=L/1,2=16,67\text{m}$ , for each case  $f=L/5=20\text{m}$  and  $f=L/4=25\text{m}$ , which are both valid  $f$  values according to the previous case study (section 4.5).



**Figure 5-1: Geometry of  $\beta$  variation for  $L=100\text{m}$ ,  $g=f=L/5=20\text{m}$   $e=g/1,2=16,67\text{m}$ ,  $v=0$**

We have observed in the previous sections that stresses at the arch springings are higher, due to the large axial and out-of-plane bending moments which are maximal also at springings. Total arch displacements for a uniformly distributed load are maximal at approximately  $L_A/4$ . Arch out-of-plane displacements are maximal at approximately  $L_A/6$  and in-plane ones at approximately  $L_A/3$ . Therefore, the struts distribution should help to lower stresses at springings and displacements at the aforementioned points. According to this, convergent struts seem the most convenient distribution. However, changing the orientation of the struts also means changing their length and thus their stiffness. Increasing  $\beta$  increases the length of struts, diminishing their stiffness. Therefore, it is not clear a priori what will have more influence, whether to increase the stiffness of the struts or the orientation with which the loads are introduced on the arch.

We must note that for different  $g$  values the orientation of the reference struts changes already (Figure 5-2). We will be studying the models with  $20\text{m}$ .

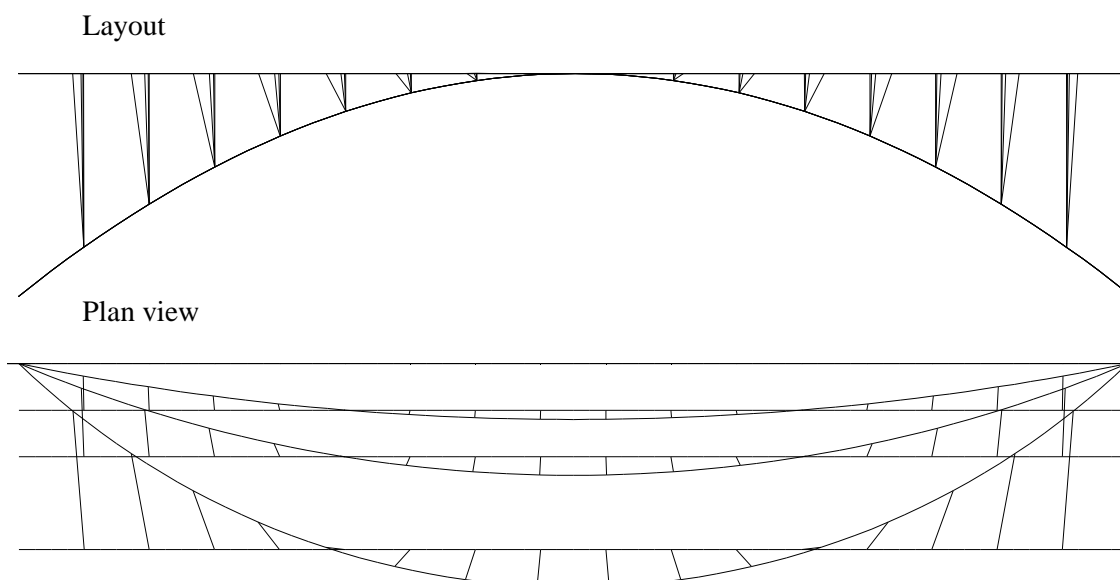


Figure 5-2: Geometry of  $g$  variation for  $L=100\text{m}$ ,  $f=L/5=20\text{m}$ ,  $e=g/1,2$ ,  $v=0$

### 5.1.2 Previous studies

Several studies have been conducted for planar tied arch bridges (Bogaert, 2010 and 2011, and De Zotti et al, 2007).). But the author still does not know any study focused on superior straight deck arch bridges nor SABs.

The inclination of the struts planar vertical arch bridges with an inferior straight deck is studied by Bogaert (2010 and 2011). In the 2010 study it is concluded that an optimum arrangement of sloping hangers with radial distribution (from the deck central zone and sloping radially to the arch) can be found. This is obtained by distributing the hanger nodes in an even manner and concentrating the nodes on the lower chord near to the center. This has also a stabilising effect for buckling in opposition to vertical hangers (Bogaert, 2010). A triangular arrangement of hangers requires less steel than a fan arrangement of hangers concurring at a centre above the arch top (Bogaert, 2011), but fan arrangement can be justified for aesthetical reasons.

De Zotti et al (2007) compare network, fan and vertical arrangements of hangers for inferior straight deck vertical planar arch bridges. They conclude that vertical and fan arrangements lead to minimum values of hanger forces, but higher values of arch and lower chord bending moments.

## 5.2 STRUCTURAL RESPONSE UNDER A UNIFORM VERTICAL LOAD ( $lu$ )

The structural behaviour has been studied for the under a uniform load of  $10\text{kN/m}$  only on the whole deck (Figure 5-1) for  $L=100\text{m}$ ,  $g=20\text{m}$ ,  $f=L/5=20\text{m}$  and  $f=L/4=25\text{m}$ ,  $e=L/1,2=16,67\text{m}$ ,  $v=0$ , with the different values of  $\beta$  and their structural response has been compared.

A distribution of convergent struts ( $\beta_1$ , Figure 5-1) is the most efficient distribution for forces and displacements in the arch for SABWCSD, since they give the minimal values (from Figure 5-3 to Figure 5-9).

The effect of the struts' inclination is most present in the in-plane behaviour of the arch.

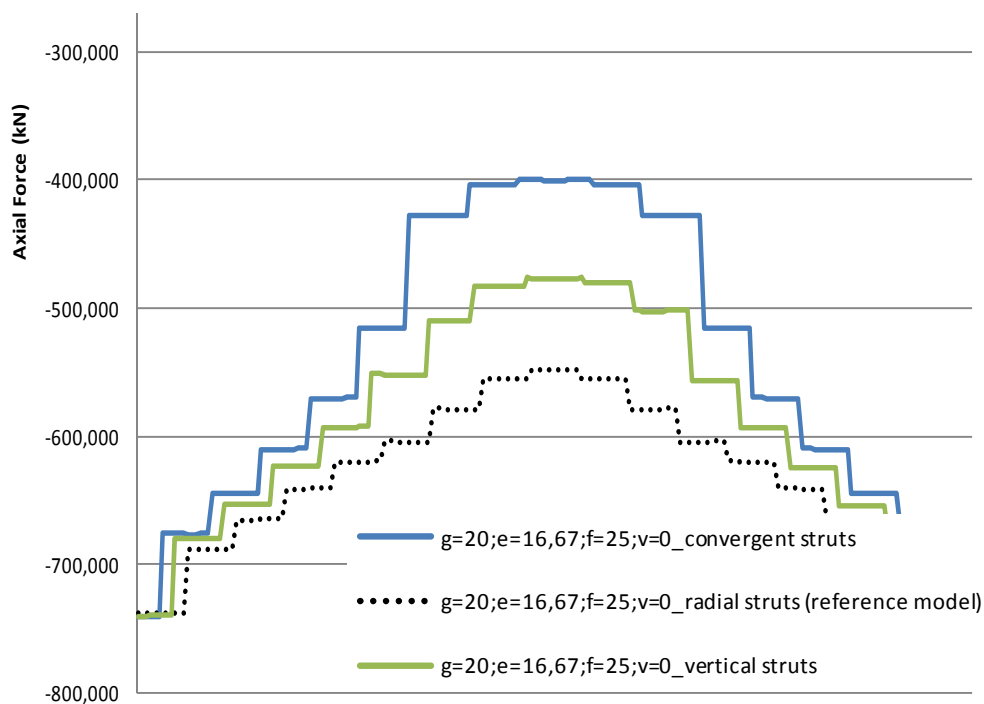


Figure 5-3: Arch axial forces comparison for different  $\beta$  values and  $g=20m$ . The abscissas are the arch length from 0 to  $L_A$

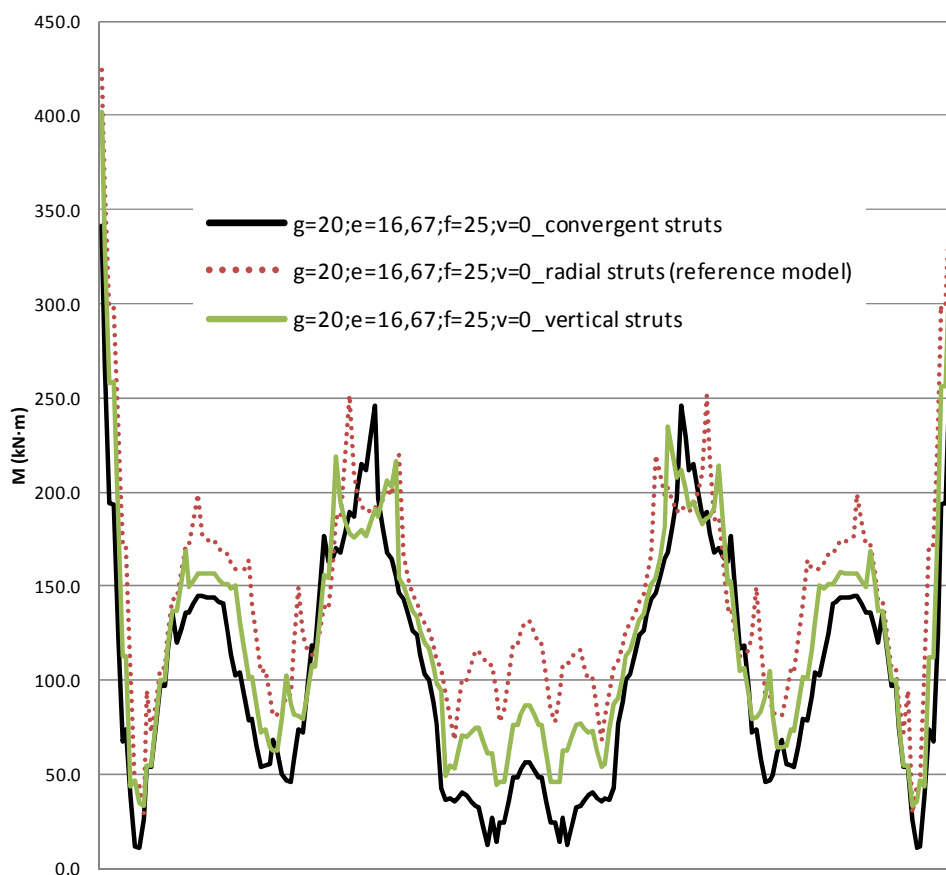


Figure 5-4: Arch total bending moments comparison for different  $\beta$  values and  $g=20m$ . The abscissas are the arch length from 0 to  $L_A$

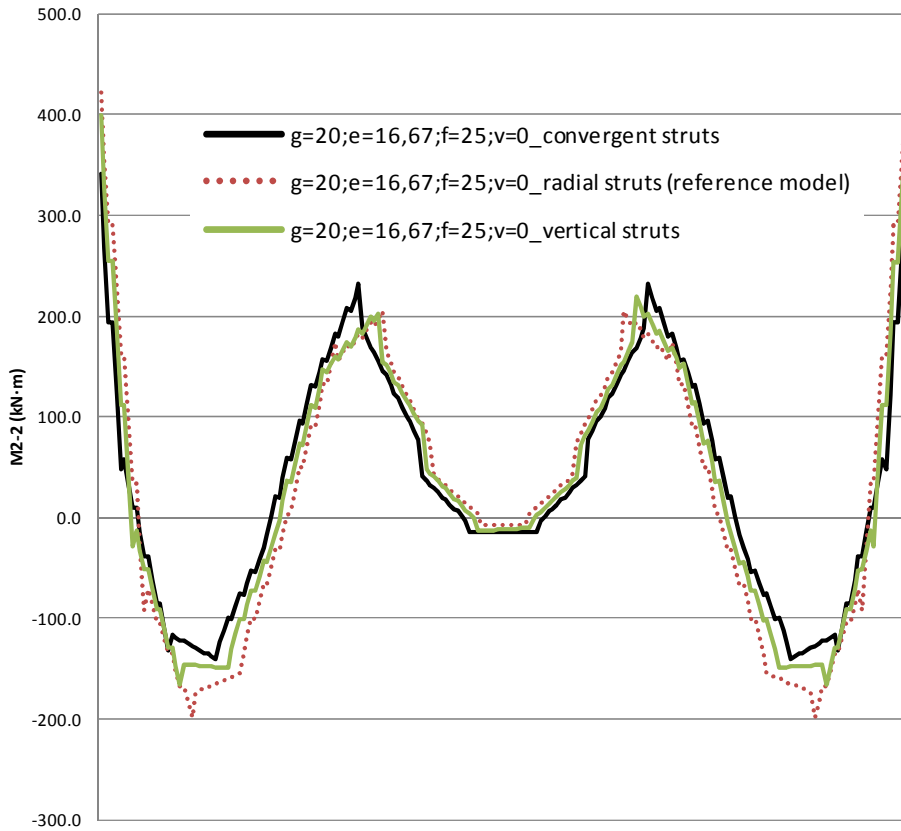


Figure 5-5: Arch out-of-plane bending moments comparison for different  $\beta$  values and  $g=20m$ . The abscissas are the arch length from 0 to  $L_A$

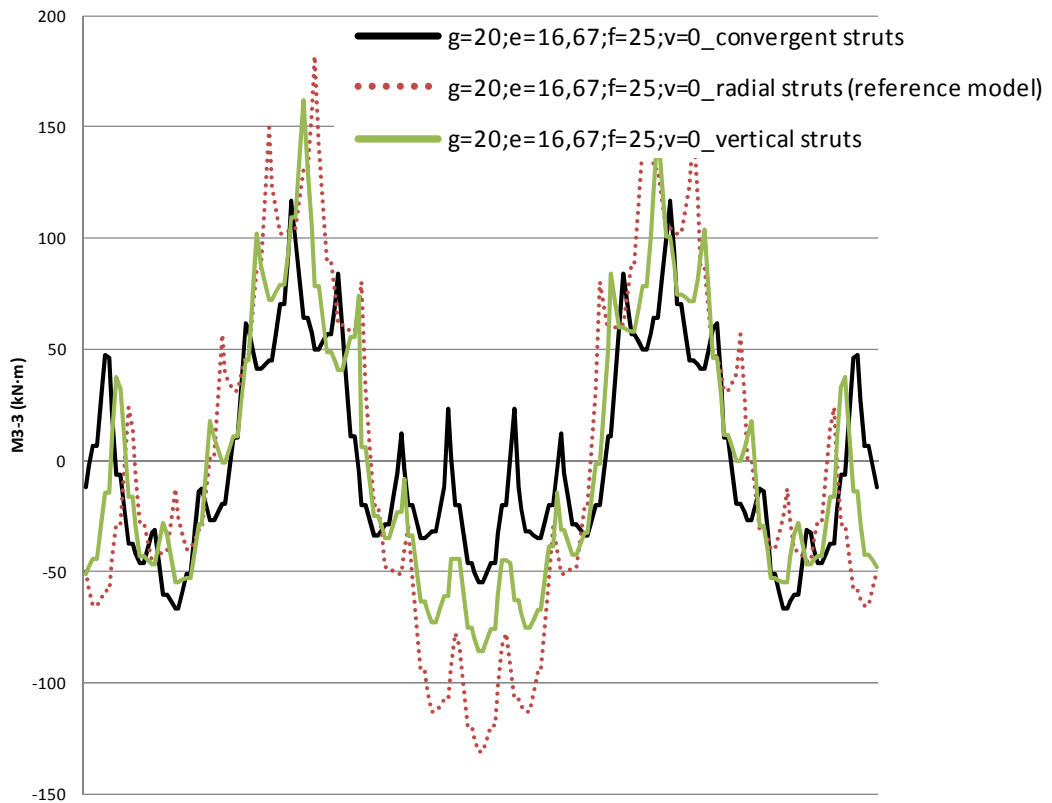
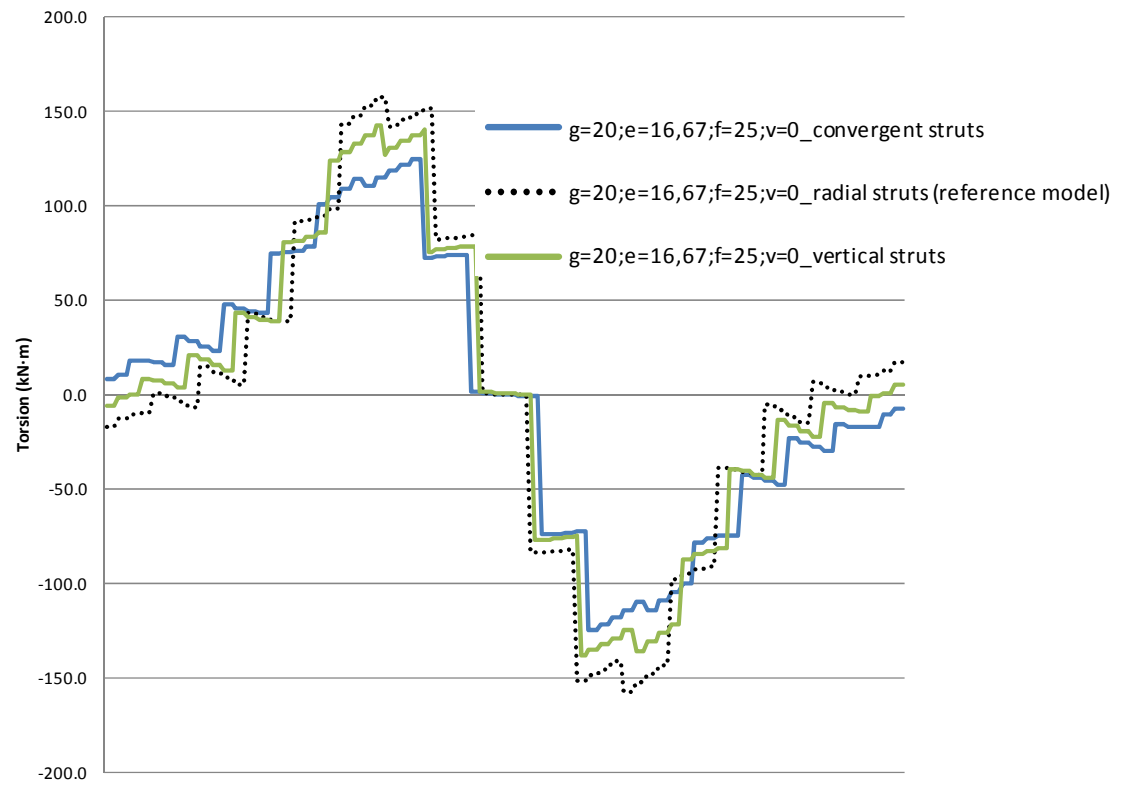
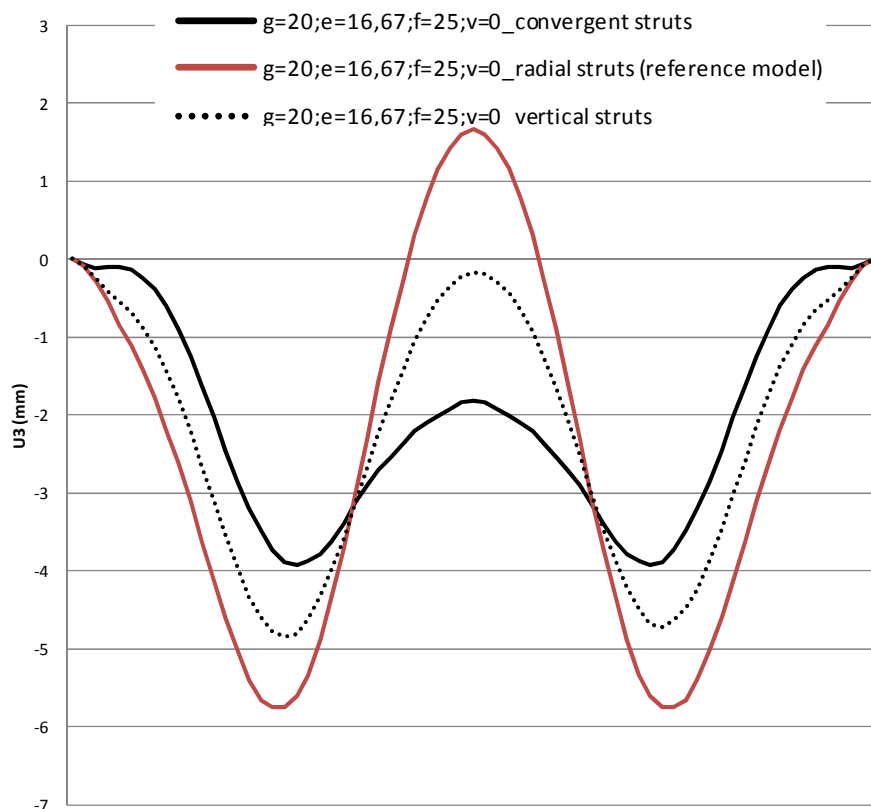


Figure 5-6: Arch in-plane bending moments comparison for different  $\beta$  values and  $g=20m$ . The abscissas are the arch length from 0 to  $L_A$

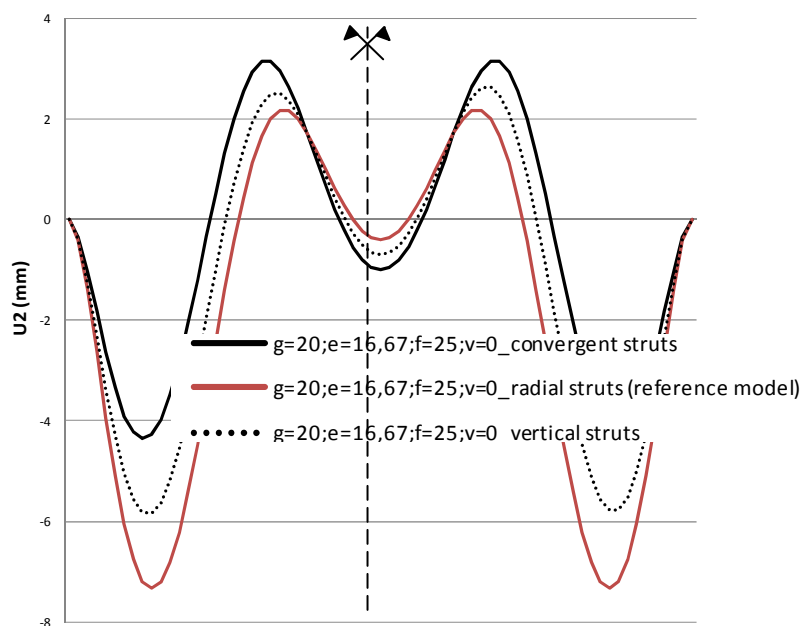




**Figure 5-7: Arch torsional bending moments comparison for different  $\beta$  values and  $g=20\text{m}$ . The abscissas are the arch length from 0 to  $L_A$**



**Figure 5-8: Arch in-plane displacements comparison for different  $\beta$  values and  $g=20m$ . The abscissas are the arch length from 0 to  $L_A$**

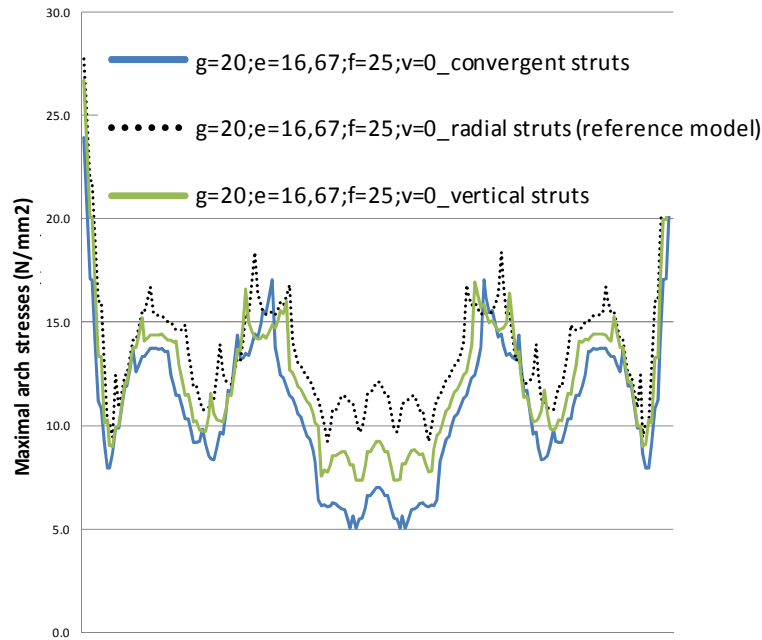


**Figure 5-9: Arch out-of-plane displacements comparison for different  $\beta$  values and  $g=20m$ . The abscissas are the arch length from 0 to  $L_A$**

### 5.3 STRESS BEHAVIOUR UNDER $q$ AND DESIGN AND COMPARISON IN ULTIMATE LIMIT STATE

Employing convergent struts also reduces the stresses in the arch, as a result of the previously observed reduction of internal forces (Figure 5-10).

Whatever the value of  $\beta$ , the most unfavourable load combination is the same one as the one displayed in Figure 2-15. The combination A1 should be employed to dimension the arch except at springing and approximately around  $L_A/3$ .



**Figure 5-10: Arch stresses comparison for different  $\beta$  values and  $g=20m$  under  $q=10kN/m$ . The abscissas are the arch length from 0 to  $L_A$**

For  $g=20m$ ,  $f=20m$  and  $e=16,67m$ , the models with different  $\beta$  values have been dimensioned. The cross-sections for S 355 steel have been obtained employing a linear analysis and are displayed in Table 5-1 with the values of the maximal thickness.

		$g=20m, f=25m$		
		$\beta$ : Radial struts	$\beta$ : Vertical struts	$\beta$ : Convergent struts
ARCH		CHS D=750mm; t=25mm A= 0,0569m <sup>2</sup> I= 0,0037m <sup>4</sup>	CHS D=750mm; t=25mm A= 0,0569m <sup>2</sup> I= 0,0037m <sup>4</sup>	CHS D=750mm; t=20mm A= 0,0459m <sup>2</sup> I= 0,0031m <sup>4</sup>
STRUTS		CHS D=300mm; t=35mm A= 0,0291m <sup>2</sup> I= 0,0003m <sup>4</sup>	CHS D=300mm; t=45mm A= 0,0456m <sup>2</sup> I= 0,0010m <sup>4</sup>	CHS D=300mm; t=35mm A= 0,0291m <sup>2</sup> I= 0,0003m <sup>4</sup>

**Table 5-1: Design cross-section values of the arch and struts for  $g=20m$  and  $f=25m$  with different  $\beta$  values. Note: the values of the thickness are the maximal ones.**

### 5.4 EFFICIENCY CRITERIA

The results of the chosen criteria are shown for the different models which have been studied in tables from Table 5-2 to Table 5-7. In these tables the nomenclature already given in section 1.3 is employed. Please use the bookmark to comfortably interpret the tables, and note whether the

length is considered or not, since the nomenclature and units of the criteria are modified. The following values are specifically employed for the tables in this section:

- $\beta^*$  is the value of  $\beta$  which minimizes each criteria (m)
- $i = \%$  of difference of B from the most efficient  $\beta$  value for B ( $\beta^*$ )

Given the length values shown in Table 5-5, it is necessary to calculate the total mass values for the different models. The design cross-sections obtained in section 5.3 are employed.

A different  $\beta^*$  is obtained for each criteria. The results of the efficiency criteria are commented in the following lines:

It is convenient to employ a convergent distribution of struts ( $\beta_1$ , Figure 5-1) in order to reduce the total material employed for the bridge, in spite of being the longest ones (Table 5-5).

The maximal displacement under permanent loads is the simplest criteria to employ, equivalent to consider the lowest mass of the bridge depending on  $\beta$  (Table 5-3 and Table 5-7), the lowest stresses considering the length of all the elements or not (from Table 5-2 to Table 5-7) and the lowest sum of the total bending moments in the arch under permanent loads (Table 5-2, Table 5-3, Table 5-4 and Table 5-6). The differences are not negligible (Table 5-3 and Table 5-7).

The fact that the displacement criteria gives the same results as the mass criteria confirms that a linear analysis is enough in order to determine which  $\beta$  value is the most efficient.

A small  $\beta$  variation leads to an important mass variation. Therefore,  $\beta$  is a key parameter for the efficiency of SABWCSD.

This conclusion for superior deck arch bridges looks aesthetically different than the one for inferior straight deck planar vertical arch bridges studied by Bogaert (2010). However, in Bogaert’s study the separation of hangers in the deck varied and in our study it is constant. Just as we varied the distance between struts in the arch, we could try and change also in the deck and make them less uniform maybe concentrating the struts in key points. A future research of struts is worth doing since they can influence so much the total mass.

Model	Criteria							
	A	B	C	D	E	F	G	H
$g=20; e=16,67; f=20; v=0$								
radial struts (reference model)	17958	30026	69354	2999	4502	188	30	19
vertical struts	16575	27945	61659	2743	4211	181	29	16
convergent struts	14679	25540	48932	2425	3937	169	26	15
Minimal values	convergent struts	convergent struts	convergent struts	convergent struts	convergent struts	convergent struts	convergent struts	convergent struts

**Table 5-2: Efficiency criteria for  $L=100m, g=20m; e=16,67m; f=20m; v=0$  and different  $\beta$  values, not considering the length of the elements**

Model $g=20;e=16,67;$ $f=20;v=0$	Mass of the bridge (kg)	Criteria 1: Stress efficiency average of the bridge*total length of the bridge (m)	Criteria 2: Sum of the stress efficiency in each output station*Length of each output station of the bridge (m)	Relative Mass Variation (%) in comparison with the Minimal Mass Model
radial struts (reference model)	73862,7	20,9	70,8	38,8
vertical struts	60433,7	16,4	37,6	13,6
convergent struts	53204,0	15,0	33,9	0,0
Minimal Mass (kg)	53204,0			

*Criteria 1=Criteria 2 if calculated separately for arch deck and struts and then added*

**Table 5-3: Efficiency criteria and relative differences for  $L=100m$ ,  $g=20m$ ;  $e=16,67m$ ;  $f=20m$ ;  $v=0$  and different  $\beta$  values, considering the length of the elements**

Model $g=20;e=16,67;$ $f=25;v=0$	Criteria							
	A	B	C	D	E	F	G	H
radial struts (reference model)	16724	27892	73114	2784	4148	174	28	21
vertical struts	15049	25408	62119	2489	3764	175	27	16
convergent struts	13414	23328	51370	2213	3551	157	24	13
Minimal values	convergent struts	convergent struts	convergent struts	convergent struts	convergent struts	convergent struts	convergent struts	convergent struts

**Table 5-4: Efficiency criteria for  $L=100m$ ,  $g=20m$ ;  $e=16,67m$ ;  $f=25m$ ;  $v=0$  and different  $\beta$  values, not considering the length of the elements**

<b>Model</b> <i>g=20;e=16,67;</i> <i>f=25;v=0</i>	<b>Total structure length (m)</b>	<b>L struts (m)</b>
radial struts (reference model)	372,1	147,0
vertical struts	379,0	153, 9
convergent struts	393,1	168,0

**Table 5-5: Total length of the structure and the struts for different  $\beta$  values**

<b>Model</b> <i>g=20;e=16,67;</i> <i>f=25;v=0</i>	<b>Criteria</b>							
	A	B	C	D	E	F	G	H
radial struts (reference model)	6222402,7	10377685,6	27203488,1	1035906,5	1543181,2	64893,3	10315,3	7670,7
vertical struts	5702948,3	9628491,1	23540143,7	943273,6	1426239,9	66190,7	10122,5	6161,3
convergent struts	5273091,5	9170013,7	20193268,3	869854,6	1396016,0	61615,0	9402,9	5264,8
Minimal values	convergent struts	convergent struts	convergent struts	convergent struts	convergent struts	convergent struts	convergent struts	convergent struts

**Table 5-6: Efficiency criteria for  $L=100m, g=20m; e=16,67m;f=25m;v=0$  and different  $\beta$  values, considering the length of the elements**

<b>Model</b> <i>g=20;e=16,67;</i> <i>f=25;v=0</i>	<b>Mass of the bridge (kg)</b>	<b>Criteria 1: Stress efficiency average of the bridge*total length of the bridge (m)</b>	<b>Criteria 2: Sum of the stress efficiency in each output station*Length of each output station of the bridge (m)</b>	<b>Relative Mass Variation (%) in comparison with the Minimal Mass Model</b>
radial struts	73141,9	20,5	69,3	9,6
vertical struts	84025,2	26,0	86,7	25,9
convergent struts	66722,3	17,5	59,1	0,0
Minimal Mass (kg)	66722,3			

*Criteria 1=Criteria 2 if calculated separately for arch deck and struts and then added*

**Table 5-7: Efficiency criteria and relative differences for  $L=100m, g=20m;e=16,67m;f=25m; v=0$  and different  $\beta$  values, considering the length of the elements**

## 5.5 PARAMETER DISCUSSION

The parameter discussion has been already exposed in the previous sections. In this section the main conclusions and explanations are exposed:

- It is convenient to employ a convergent distribution of struts ( $\beta_1$ , Figure 5-1) in order to reduce the total material employed for the bridge, in spite of being the longest ones. Controlling key points proves to be more efficient than verticality or stiffness small variations.
- A small  $\beta$  variation leads to an important mass variation. Therefore,  $\beta$  is a key parameter for the efficiency of SABWCSD.

## 6. DECK HEIGHT ( $z$ ) PARAMETRICAL STUDY

### 6.1 DEFINITION AND EMPLOYED VALUES

The conclusions of section 2 drew attention to the key points at a distance of  $0,28L$  of the springings of the arch, where it is recommendable to obtain the stiffest struts. This conclusion is valid for a superior-deck SAB and close to the one obtained for an inferior-deck SAB specific study with other efficiency criteria (Jorquera 2007, for  $g=10\text{m}$ ). Changing the distance from the deck to the arch, which changes with the value of  $z$ , these points can also be made stiffer. Therefore, the present study analyses the effects of  $z$  variation for different  $f$  values,  $f=10\text{m}$  and  $f=20\text{m}$  and for  $g=20\text{m}$  and  $e=16,67\text{m}$  (most efficient  $e$  value according to section 2).

The studied cases are the following: Superior deck with  $f=z=10\text{m}$  and  $20\text{m}$ , inferior deck with  $f=20\text{m}$  and  $z=0$ , middle deck with  $f=20\text{m}$  and  $z=16,22\text{m}$  and  $z=10\text{m}$  (Figure 6-1 and Figure 6-2).

The value  $z=16,22\text{m}$  is chosen because it is the point where the arch is fixed to the deck at  $g/1,2$  in plan which had been observed as the most efficient to increase the stiffness of the struts at these points.

Models with  $z=f=10\text{m}$  and  $z=f=20\text{m}$  are both analysed to be compared with the model with  $f=20\text{m}$  and  $z=10\text{m}$ . The rest of  $z$  values are all considered for  $f=20\text{m}$  arches. The rest of  $z$  values are all considered for  $f=20\text{m}$  arches.

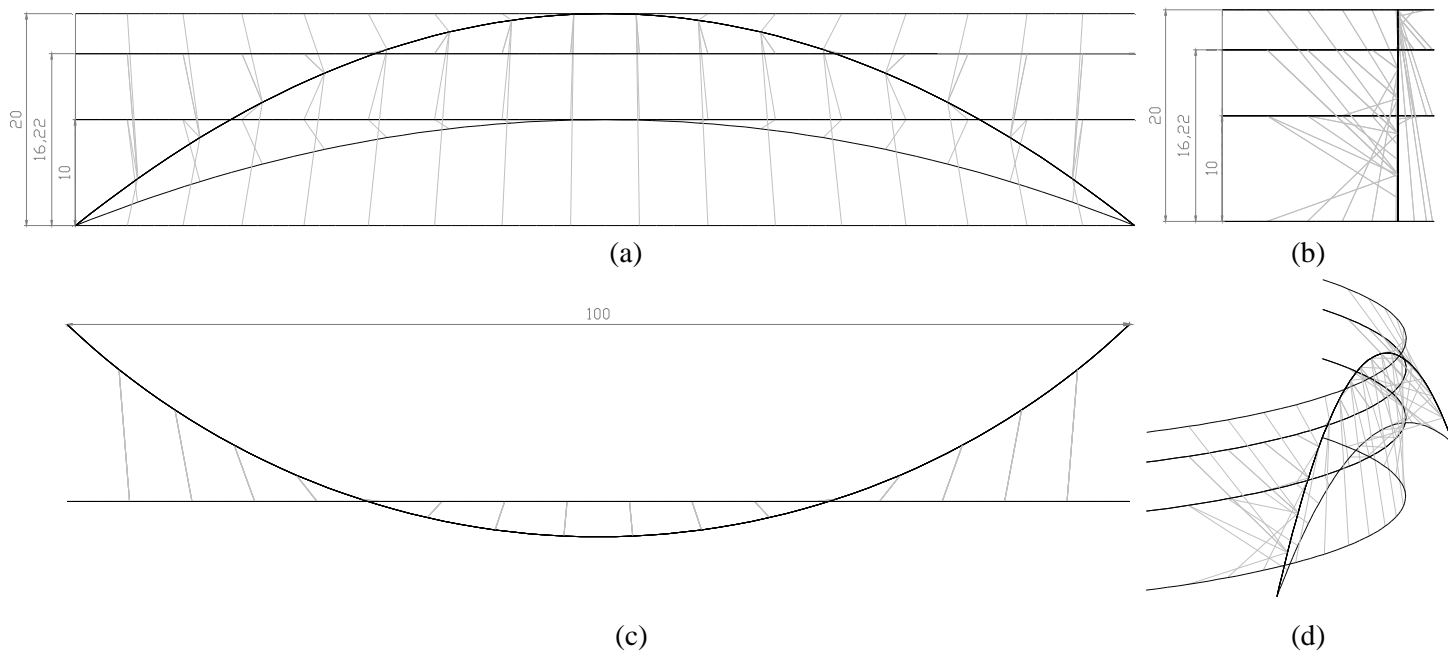


Figure 6-1: Variation of  $z$  (a) Layout. (b) Side view. (c) Plan view (d) Perspective

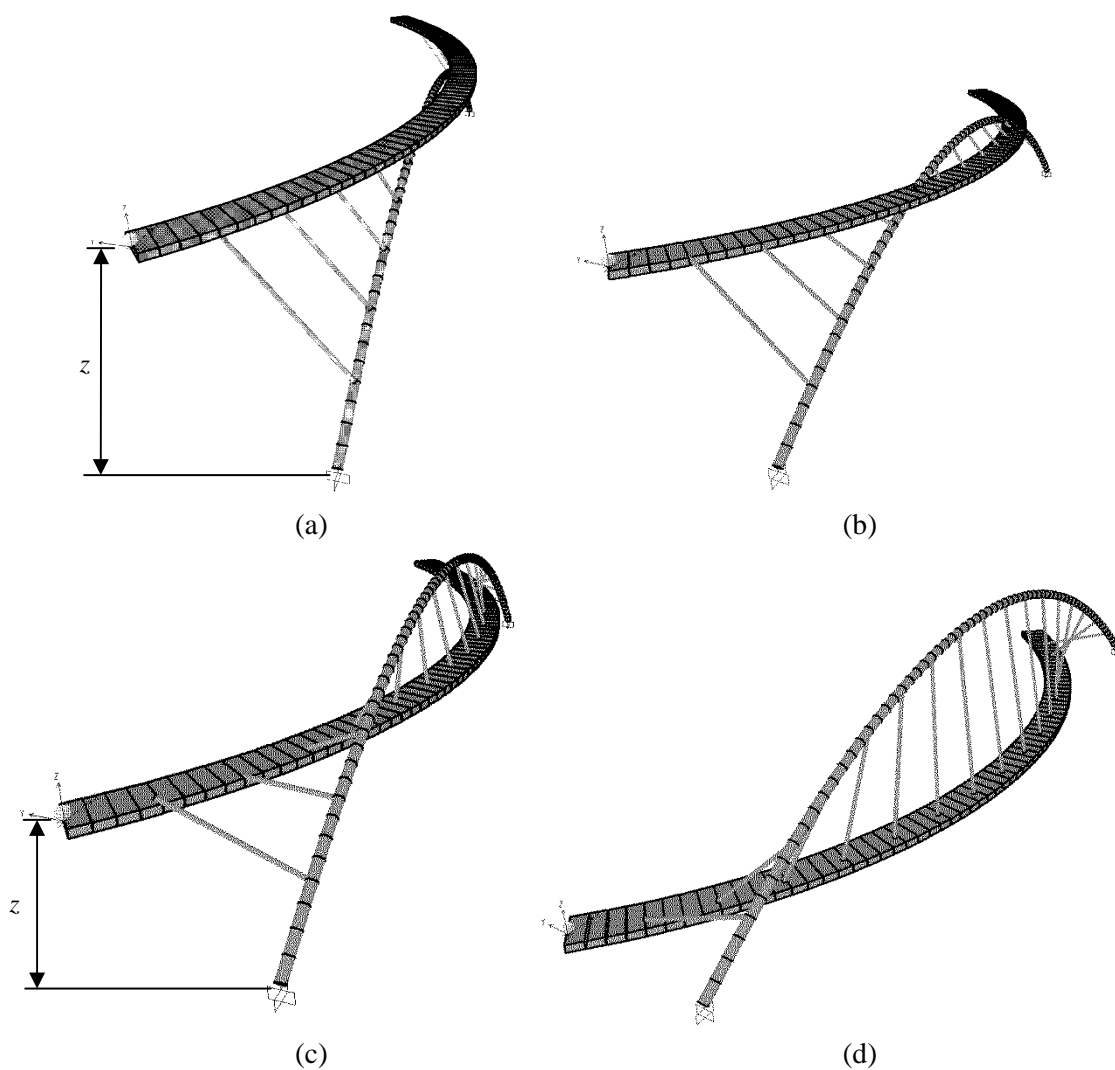


Figure 6-2: Bridge perspectives for different  $z$  values: (a)  $f=z=20\text{m}$ ; (b)  $f=20\text{m}, z=16,22\text{m}$ ; (c)  $f=20\text{m}, z=10\text{m}$ ; (d)  $f=20\text{m}, z=0$



## 6.2 STRUCTURAL RESPONSE UNDER A UNIFORM VERTICAL LOAD ( $lu$ )

The structural behaviour has been studied under a uniform load of 10kN/m on the whole deck<sup>4</sup> (Figure 1-2) for the described models with the different values of  $z$ . Their structural response has been compared. Internal forces are shown from Figure 6-3 to Figure 6-16.

### 6.2.1 Arch internal forces (Figure 6-3 to Figure 6-9)

- Models with  $f=20\text{m}$  employing a superior and inferior deck show similar values of axial forces in the arch. The lowest axial forces are obtained when employing a middle deck with  $z=16,22\text{m}$  (Figure 6-3).
- When employing a superior deck the total bending moments with  $f=10\text{m}$  in the arch are minimal at span center in comparison with the rest of models. This is due to the  $f$  value as observed in section 4.
- When employing  $f=20\text{m}$  at span, center and at  $5*L_A/24$  approximately, the total bending moments are minimal for  $z=16,22\text{m}$ , and for  $z=10$  and  $20\text{m}$ , at springings (Figure 6-4).
- Whatever the  $f$  value, when employing a superior deck the out-of-plane bending moments in the arch are minimal at span center (Figure 6-5). When employing a middle deck with  $z=10$  and inferior deck they increase considerably because the axial forces transmitted by the struts increase (Figure 6-6), since they are more vertical (Figure 6-1a) and transmit a greater part of the vertical load also with a higher out-of-plane component.
- At springings, for  $z=0$  (inferior deck), the out-of-plane bending moments decrease to less than half their value for the other models (Figure 6-5) because the axial forces transmitted by the struts are much lower (Figure 6-6). This is due to the orientation of the struts (Figure 6-1a). Moreover, they should be expected to be tensioned but they are compressed. In a real model they would be tensioned since we would be prestressing the hangers.
- When employing a superior deck the in-plane bending moments with  $f=20\text{m}$  in the arch are maximal at span center, for  $f=10$  they are maximal at  $L/4$  approximately and when employing an inferior deck, at springings (Figure 6-8).
- In general in-plane bending moments are minimal for  $z=16,22\text{m}$ . This improved behaviour in comparison with the rest of models and the moderate out-of-plane behaviour makes this model more efficient than the superior deck in relation to total bending moments as previously observed (Figure 6-4), in spite of having much higher out-of-plane bending moments. In-plane bending moments improvements is achieved by the increase of the struts verticality.
- Arch torsional moments are minimal when employing an inferior deck (Figure 6-9), since, in comparison with the rest of models, hangers have lower axial forces (Figure 6-6) and much lower bending moments (Figure 6-7) which hence transmit smaller torsional moments to the arch and deck.
- The same effect occurs with deck torsional moments (Figure 6-12).

<sup>4</sup> Without self-weight or permanent loads

### 6.2.2 Deck internal forces (Figure 6-10 to Figure 6-20)

- Deck axial forces are minimal when employing an inferior deck, since hangers are more vertical. The deck is compressed at span center and tensioned at its extremes (Figure 6-10).
- Axial forces and total bending moments in the deck are maximal at abutments and span center when employing a superior deck instead of a middle deck for the same  $z$  value ( $f=z=10$  compared to  $f=20, z=10$ , Figure 6-10 and Figure 6-11).
- For a fix  $f$  value, varying the value of  $z$  causes important changes in the deck axial forces, compressions at its center and tensions at  $L/4$  largely increase when employing a middle deck (compare  $z=0$ ;  $z=16,22m$ ;  $z=10m$  and  $z=20m$  for  $f=20m$ , Figure 6-10), whereas deck total bending moments can increase or decrease depending on the  $z$  value (Figure 6-11).
- The solution  $z=16,22m$  would be expected to be nearer to  $z=20m$  than  $z=10m$ , but it is not for axial forces and total bending moments. It does follow an expected gradual change for torsional moments (Figure 6-12), justified by the decrease of struts internal forces (Figure 6-6 and Figure 6-7) as explained in the previous section 6.2.1.
- Deck balcony-beam bending moments are lower when employing a superior deck (Figure 6-13).

### 6.2.3 Arch displacements (Figure 6-14 to Figure 6-16)

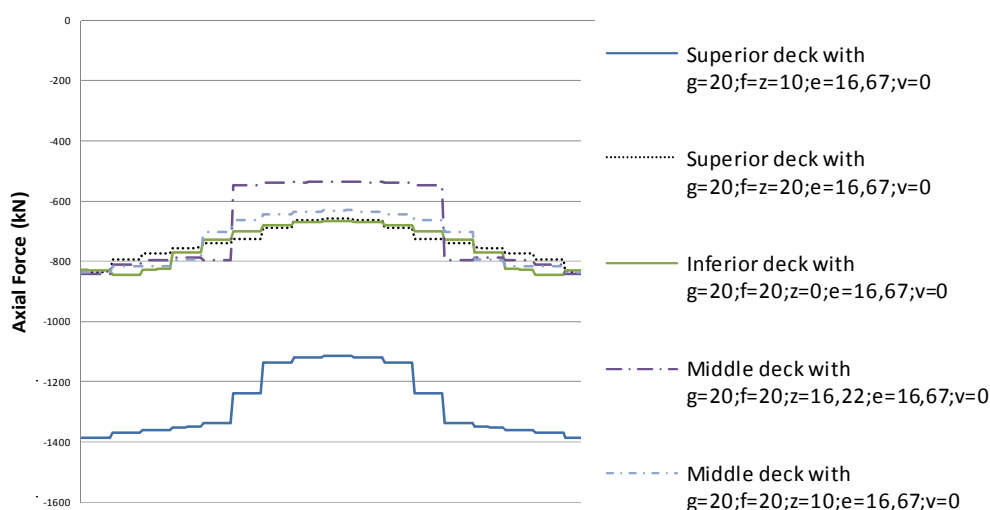
- Employing a superior deck diminishes the out-of-plane displacements of the arch (Figure 6-14).
- A superior deck controls better the out-of-plane behaviour at span center, as observed for out-of-plane bending moments (section 6.2.1, Figure 6-5). A middle deck controls better the arch out-of-plane behaviour at approximately  $L_A/6$ . Employing an inferior deck controls better than a middle deck out-of-plane displacements at span center, due to the lower torsional moments (section 6.2.1, Figure 6-9), but much worse than a superior deck. However, arch out-of-plane displacements at  $L_A/3$  are really high when employing an inferior deck (Figure 6-14).
- Maximal in-plane displacements hardly change with  $z$  for the same  $f$  value (Figure 6-15). At span center they are best controlled by a superior deck, but this bridge type has a worse control at  $L_A/3$ , which is improved when diminishing  $z$ .
- The higher influence of out-of-plane displacements on the total displacements is reflected in Figure 6-16.

### 6.2.4 Deck displacements (Figure 6-17 to Figure 6-18)

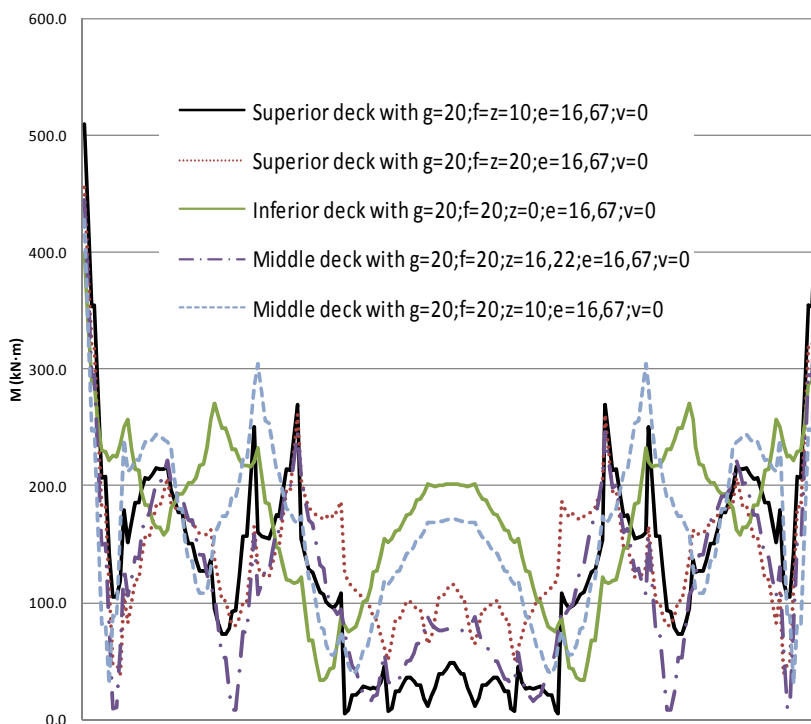
- Apparently the deck displacements do not follow a trend with  $z$  as torsional moments do (Figure 6-17 and Figure 6-18). But they follow the same trend as deck bending moments. The explanation is in the struts structural behavior (Figure 6-6 and Figure 6-7). It is logical that the models employing an inferior or superior deck have the lowest displacements at span center (Figure 6-17 and Figure 6-18). Struts supporting the superior deck are very short (Figure 6-2a) and therefore very stiff (proportional to  $EI/L_{strut}^3$ , ie: the length has a high influence) in spite of being nearly horizontal. When employing an inferior deck (Figure 6-2d), struts are long but very vertical and work mainly with axial

forces which control the deck displacement (the stiffness is proportional to  $EA/L_{strut}$ , ie: the length is not as important as for bending moments).

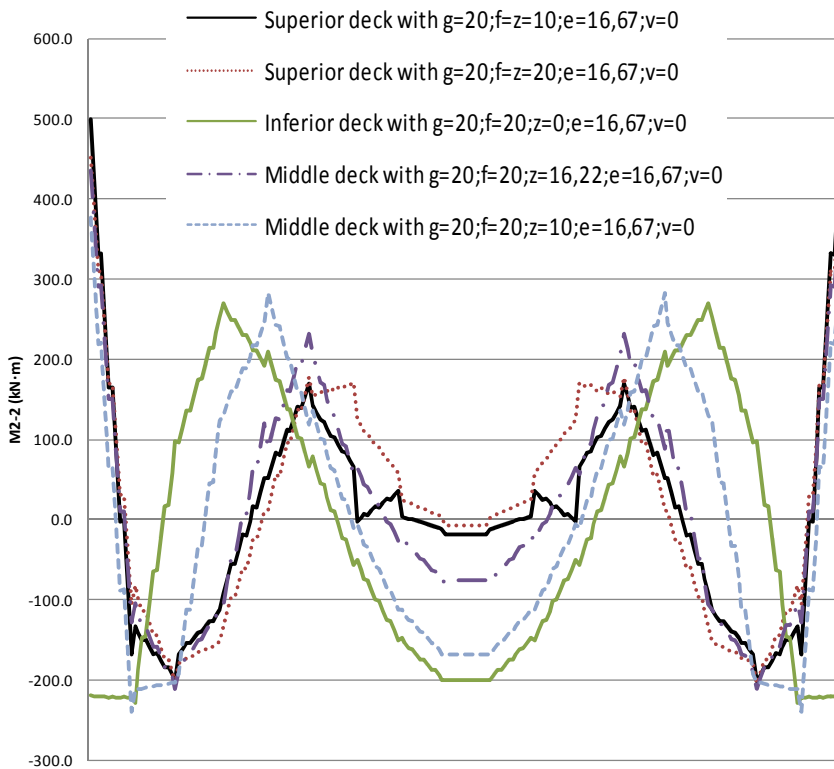
- For a middle deck with  $f=20m$  and  $z=16,22m$  (Figure 6-2b), both vertical and horizontal deck displacements at span center (Figure 6-17 and Figure 6-18) are higher since hangers at span center are not vertical enough to have an efficient axial stiffness, but are too long to have enough bending moment stiffness to control the displacements (Figure 6-2b). With  $f=20m$  and  $z=10m$  deck vertical displacements (Figure 6-17) and total displacements at span center are also high, but horizontal displacements have the lowest values in the whole deck (Figure 6-18), because central hangers are more vertical than for  $z=16,22m$  and vertical axial stiffness increases, whereas horizontal axial stiffness and bending stiffness diminish at span center (Figure 6-2c). Extreme struts are shorter (Figure 6-2c), so bending stiffness increases at extremes. The same as for deck horizontal displacements happens with vertical axis bending moments in the deck, ie: they are minimal for  $f=20m$  and  $z=10m$ .



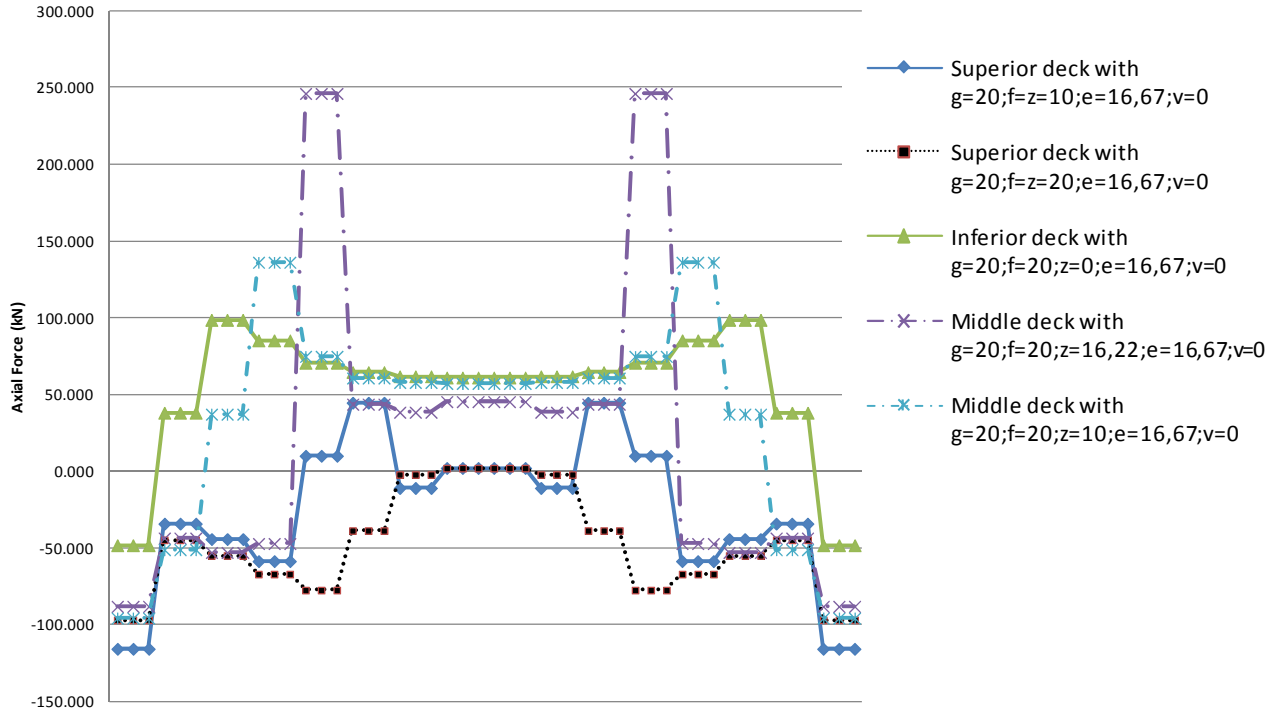
**Figure 6-3: Arch axial forces comparison for different  $z$  values when employing the reference model cross-sections (Table 1-1).. The abscissas are the arch length from 0 to  $L_A$**



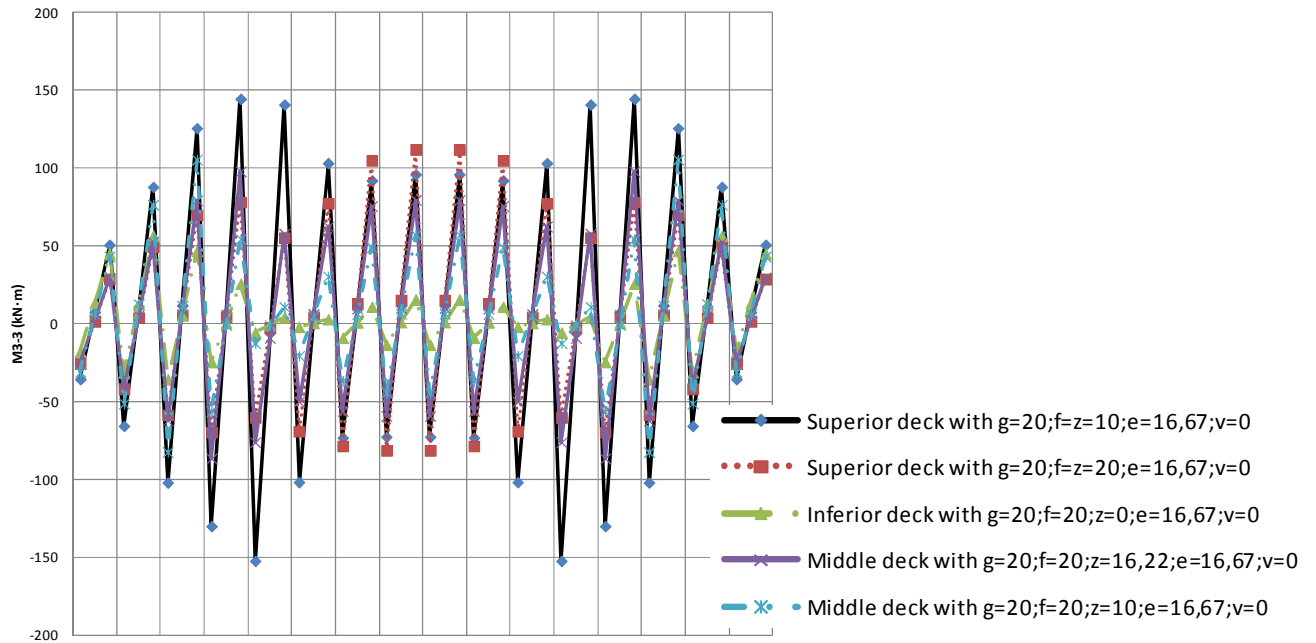
**Figure 6-4:** Arch total bending moments comparison for different  $z$  values when employing the reference model cross-sections (Table 1-1).. *The abscissas are the arch length from 0 to  $L_A$*



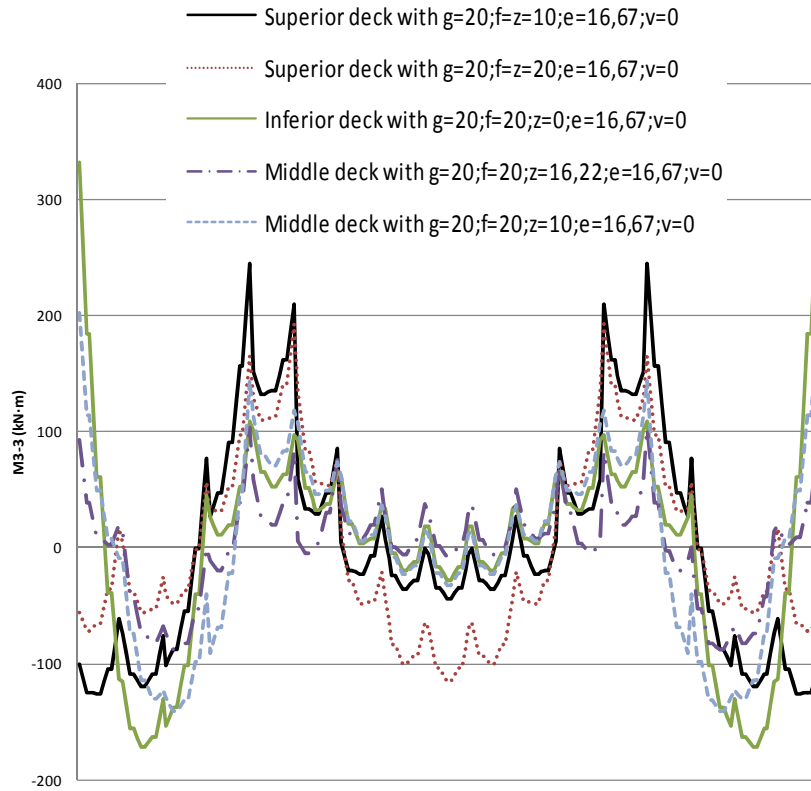
**Figure 6-5:** Arch out-of-plane bending moments comparison for different  $z$  values when employing the reference model cross-sections (Table 1-1).. *The abscissas are the arch length from 0 to  $L_A$*



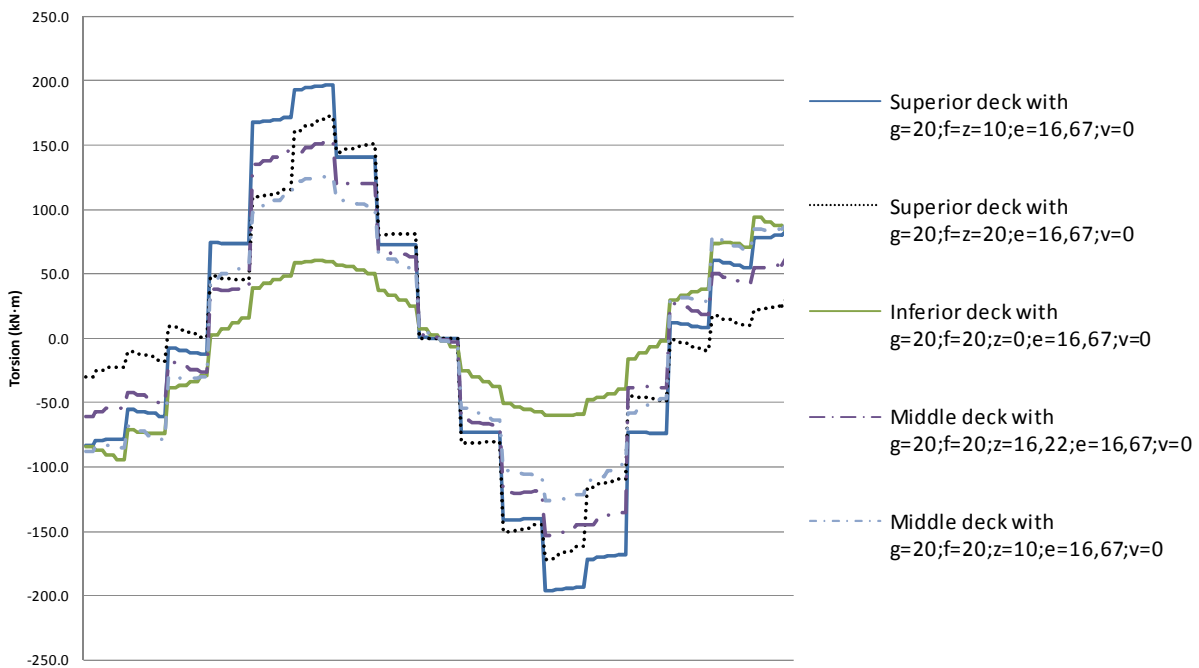
**Figure 6-6:** Struts axial forces comparison for different  $z$  values when employing the reference model cross-sections (Table 1-1).. *The abscissas are the output stations of the different struts (at the bottom, center and the top of their length).*



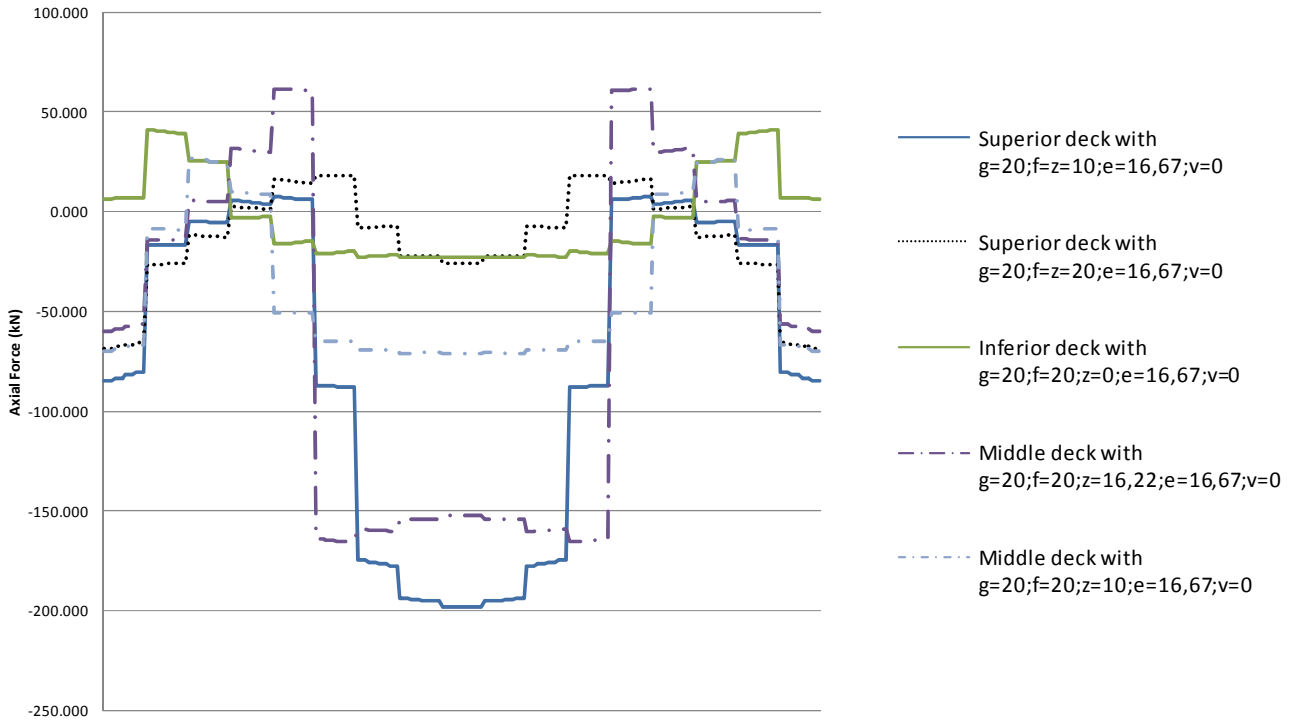
**Figure 6-7:** Struts bending moments comparison for different  $z$  values when employing the reference model cross-sections (Table 1-1).. *The abscissas are the output stations of the different struts (at the bottom, center and the top of their length).*



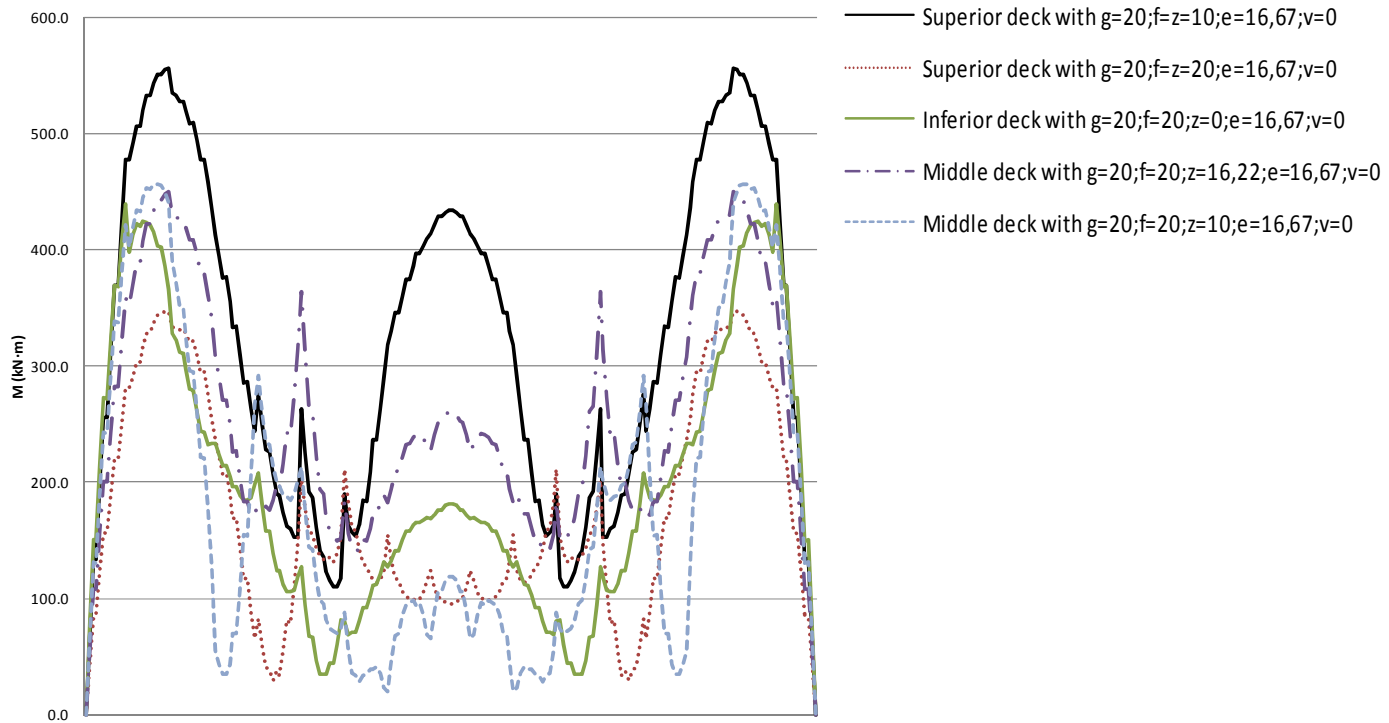
**Figure 6-8:** Arch in-plane bending moments comparison for different  $z$  values when employing the reference model cross-sections (Table 1-1).. *The abscissas are the arch length from 0 to  $L_A$*



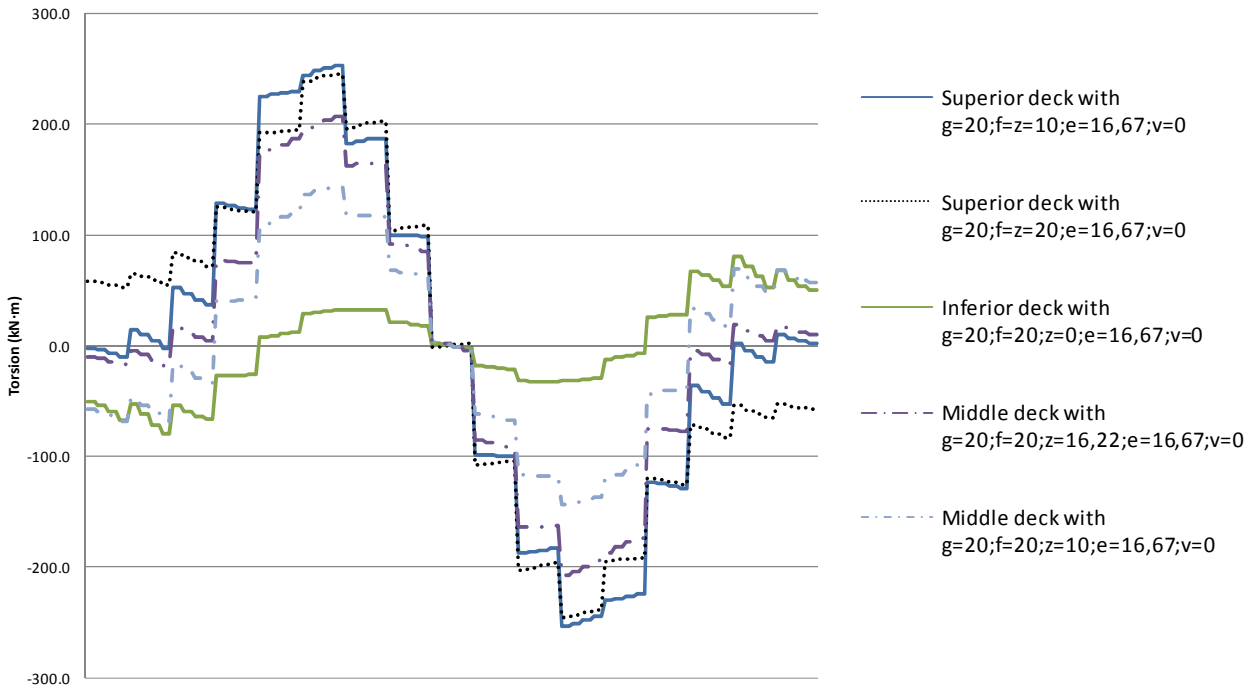
**Figure 6-9:** Arch torsional moments comparison for different  $z$  values when employing the reference model cross-sections (Table 1-1).. *The abscissas are the arch length from 0 to  $L_A$*



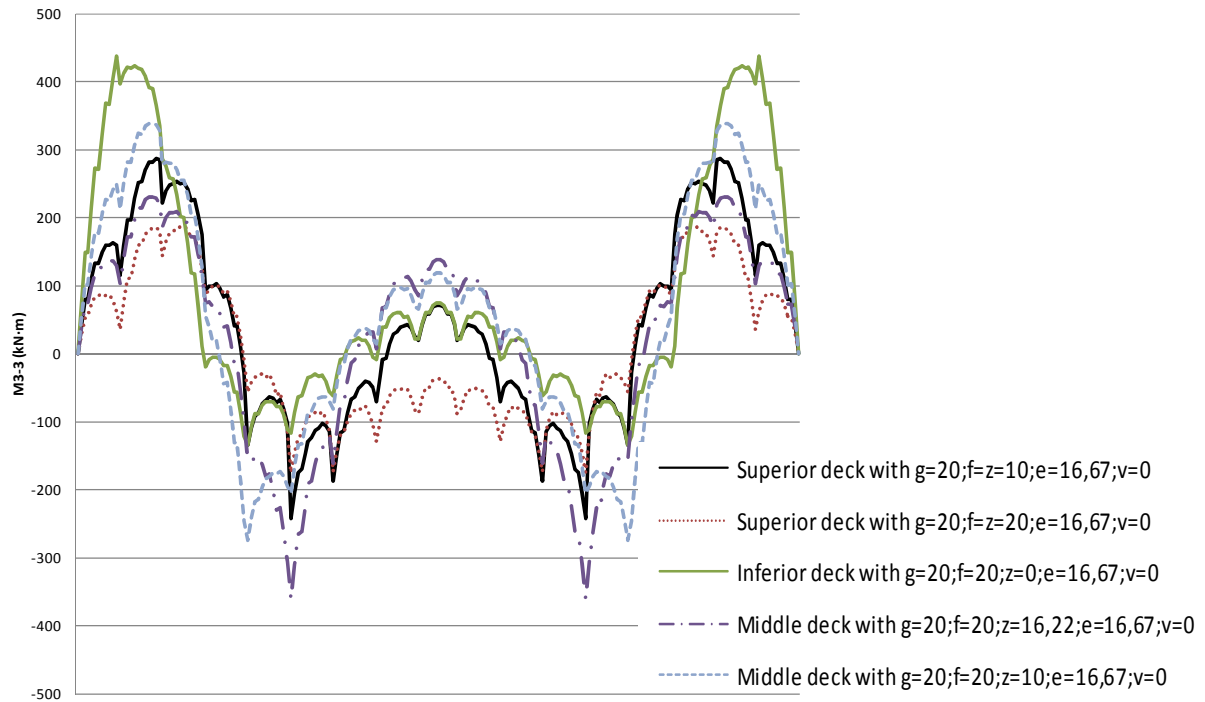
**Figure 6-10: Deck axial forces comparison for different  $z$  values when employing the reference model cross-sections (Table 1-1).. The abscissas are the deck length from 0 to  $L_D$**



**Figure 6-11: Deck total bending moments comparison for different  $z$  values when employing the reference model cross-sections (Table 1-1).. The abscissas are the deck length from 0 to  $L_D$**

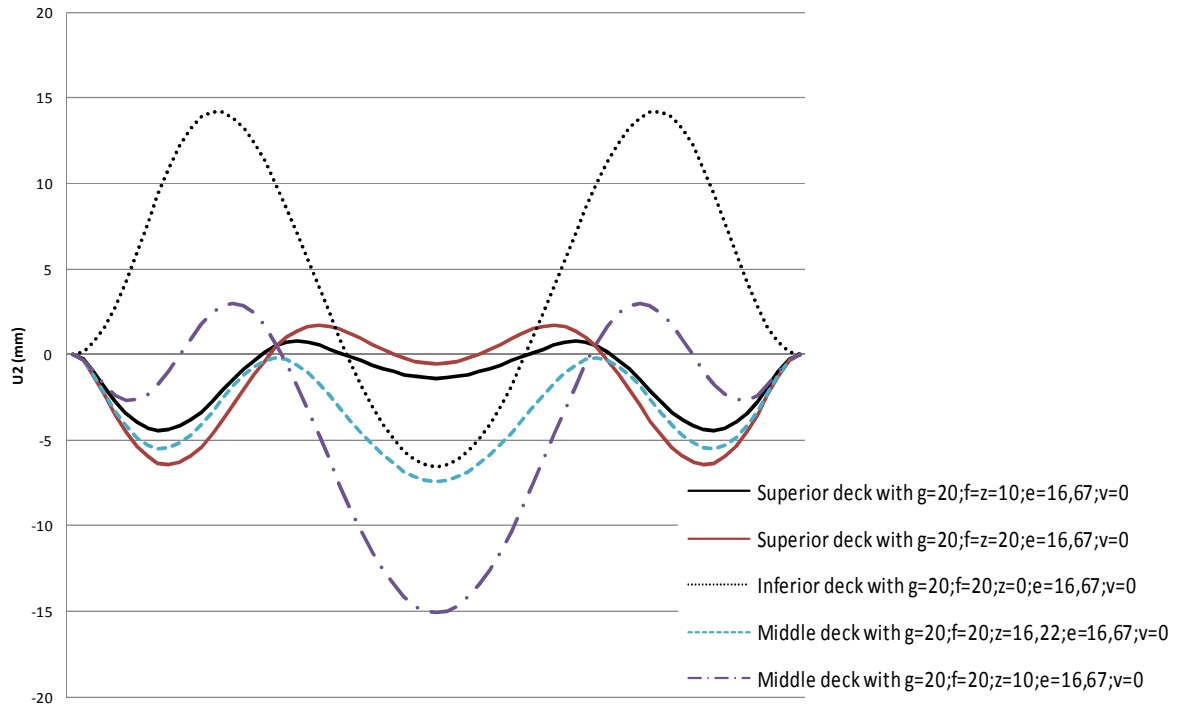


**Figure 6-12: Deck torsional moments comparison for different  $z$  values when employing the reference model cross-sections (Table 1-1).. The abscissas are the deck length from 0 to  $L_D$**

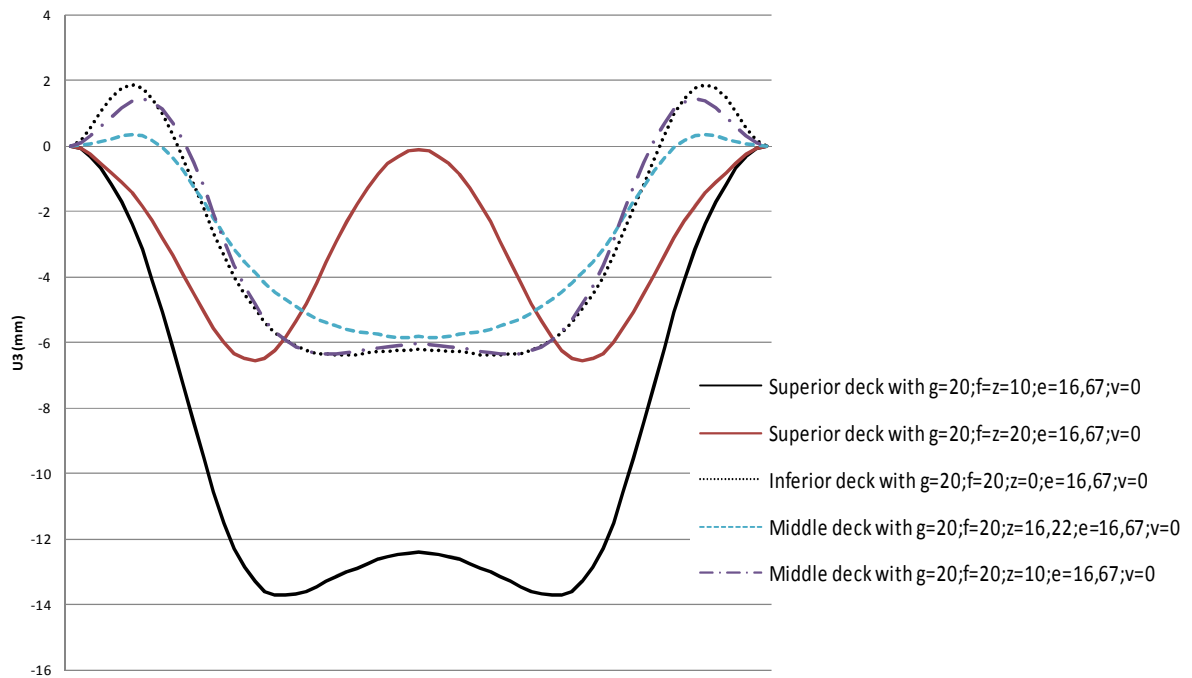


**Figure 6-13: Deck out-of-plane bending moments comparison for different  $z$  values when employing the reference model cross-sections (Table 1-1).. The abscissas are the deck length from 0 to  $L_D$**

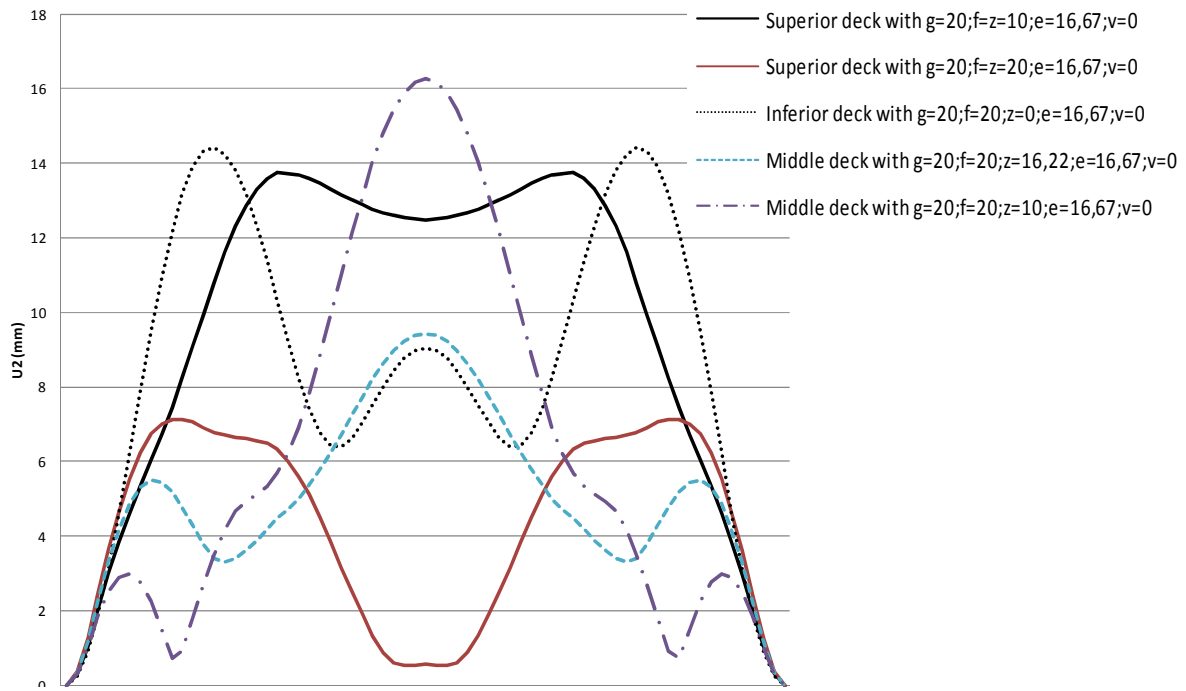




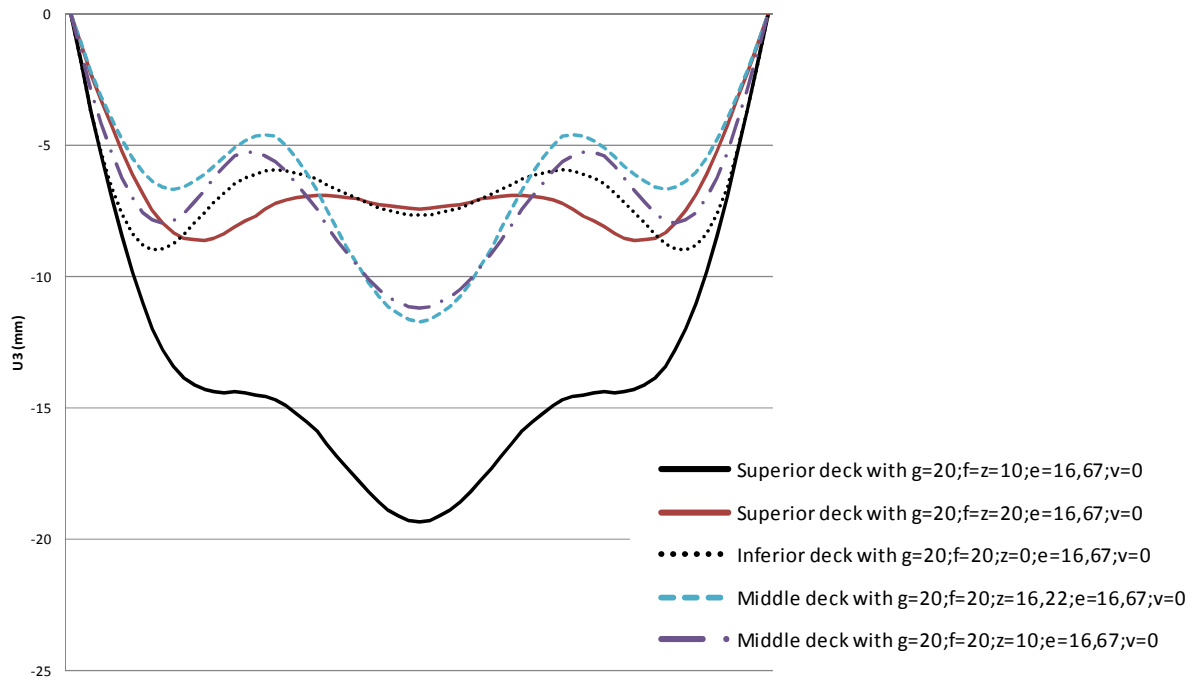
**Figure 6-14: Arch out-of-plane displacements comparison for different  $z$  values when employing the reference model cross-sections (Table 1-1).. The abscissas are the arch length from 0 to  $L_A$**



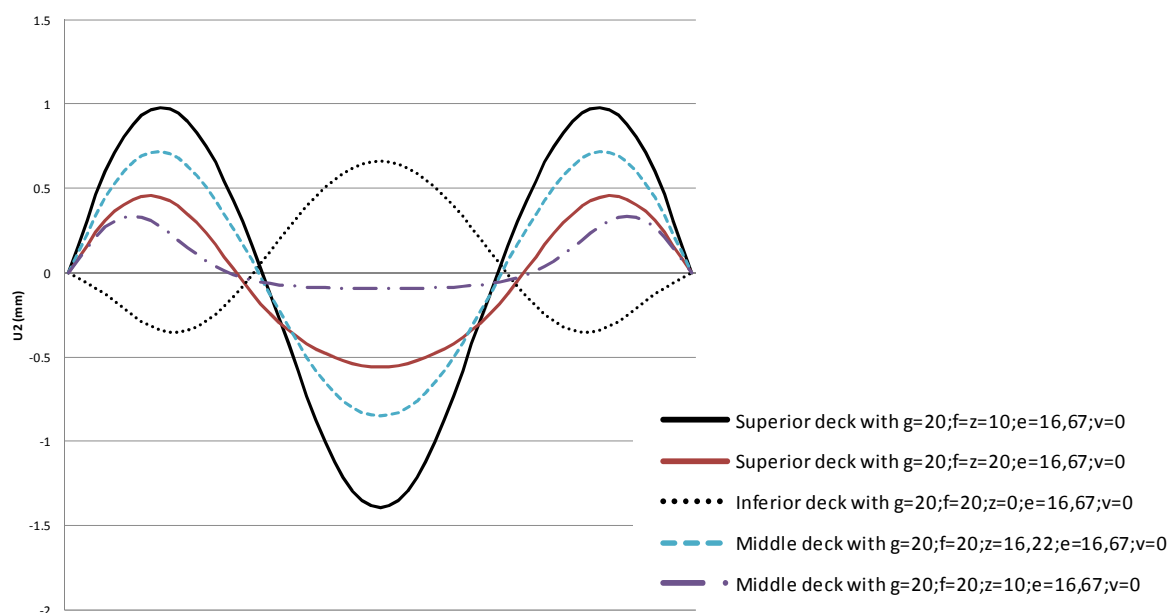
**Figure 6-15: Arch in-plane displacements comparison for different  $z$  values when employing the reference model cross-sections (Table 1-1).. The abscissas are the arch length from 0 to  $L_A$**



**Figure 6-16: Arch total displacements comparison for different  $z$  values when employing the reference model cross-sections (Table 1-1).. The abscissas are the arch length from 0 to  $L_A$**



**Figure 6-17: Deck vertical displacements for different  $z$  values when employing the reference model cross-sections (Table 1-1).. The abscissas are the deck length from 0 to  $L_D$**



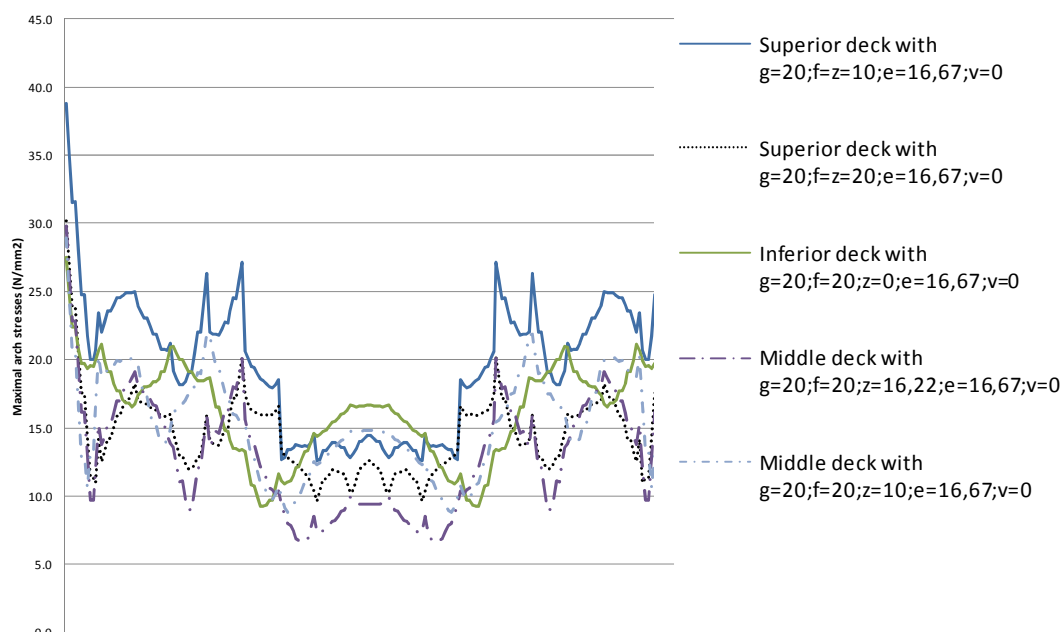
**Figure 6-18: Deck horizontal displacements for different  $z$  values when employing the reference model cross-sections (Table 1-1).. The abscissas are the deck length from 0 to  $L_D$**

### 6.3 STRESS BEHAVIOUR UNDER $q$ AND DESIGN AND COMPARISON IN ULTIMATE LIMIT STATE

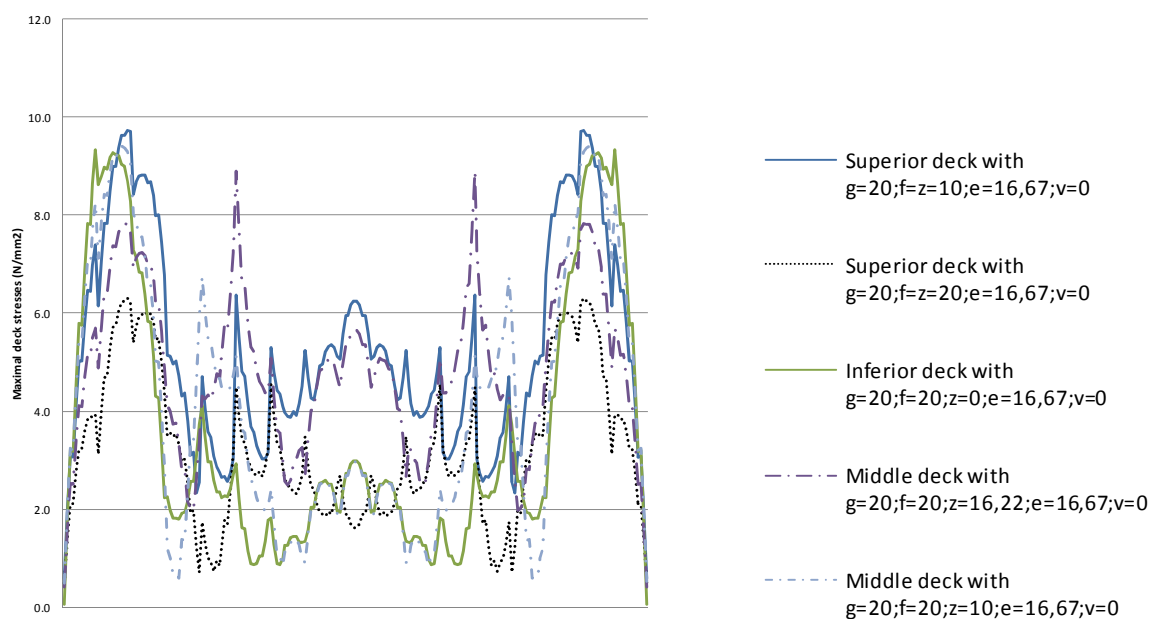
#### 6.3.1 Stresses behaviour under a uniform load $q=10\text{kN/m}$

Stresses in the arch and deck only under a uniform load  $q$  can be observed in Figure 6-19 and Figure 6-20 for the reference cross-sections (Table 1-1):

- Stresses in the arch are minimal for  $z=16,22\text{m}$  (Figure 6-19)
- For the deck the stress distribution is more variable and it is more difficult to determine a priori for which  $z$  value the deck will need less material (Figure 6-20).



**Figure 6-19: Arch stresses comparison for different  $z$  values under  $q=10\text{kN/m}$  when employing the reference model cross-sections (Table 1-1).. The abscissas are the arch length from 0 to  $L_A$**



**Figure 6-20: Deck stresses comparison for different  $z$  values under  $q=10\text{kN/m}$  when employing the reference model cross-sections (Table 1-1).. The abscissas are the deck length from 0 to  $L_D$**

### 6.3.2 Critical loading combinations in ULS

- For SABs with a **superior curved deck** and a planar vertical arch at  $e=g/1,2$ , the critical load case, for stresses in the arch is combination A2 for the springings and around  $L/3$  and combination A1 for the rest of the arch when employing a superior deck (Figure 2-15).
- When employing an **inferior deck**, the critical load case for stresses in the arch is A2 at around  $L/3$  and A1 for the rest of the arch.

- When employing a **middle deck** the difference of the arch stresses caused by A1 and A2 are very low at  $L/3$  and springings, A1 could be considered the most unfavourable load case for the whole arch. At springings the difference between these load cases and combination C (considering both live loads and temperature variation) is also very low, whereas for superior and inferior decks the stresses caused by temperature in the arch are much lower.

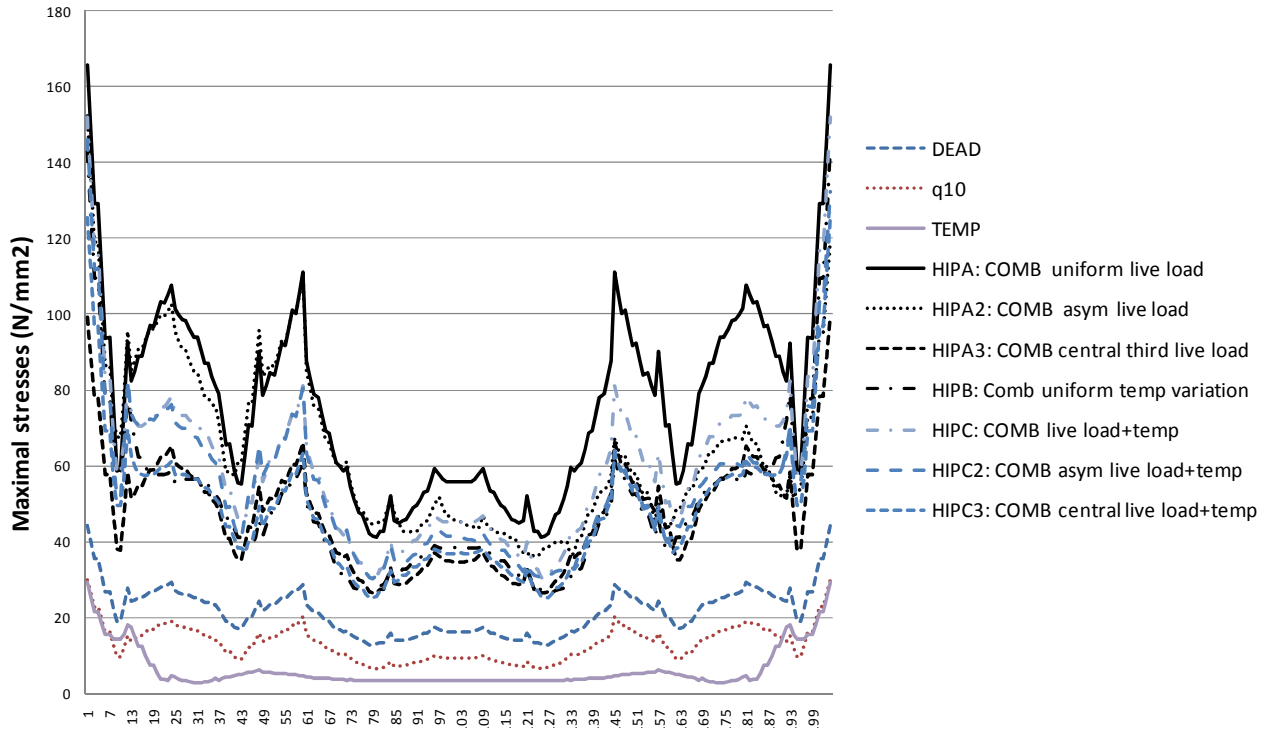


Figure 6-21: Stresses in the arch caused by different loading cases combination for  $g=20\text{m}$ ,  $f=20\text{m}$  and  $e=16,67\text{m}$  when employing the reference model cross-sections (Table 1-1). The abscissas are the arch length from 0 to  $L_A$

### 6.4 EFFICIENCY CRITERIA

Results of the different efficiency criteria (described in section 1.3, see also bookmark) not considering the length of the elements are displayed in Table 6-1 and considering the total length of all the elements of the bridge (Table 6-2) are displayed in Table 6-3. Please use the bookmark to comfortably interpret the tables, and note whether the length is considered or not, since the nomenclature and units of the criteria are modified. The following values are specifically employed for the tables in this section:

- $z^*$  is the value of  $z$  which minimizes each criteria (m)
- $i=\%$  of difference of B criteria (section 1.3 and bookmark) from the most efficient  $z$  value for B ( $z^*$ )

A different  $z^*$  is obtained for each criteria. The results of the efficiency criteria are commented in the following lines:

- If the arch is fixed to the deck at the points  $g/1,2$  in plan where it had been observed that it was efficient to increase the stiffness of the struts (section 0) the total stresses in the bridge, considering the length or not, decrease (B in Table 6-1 and Table 6-3).
- Minimal total stresses in the bridge are coincident with the shortest total bridge length in comparison with the other models with the same  $f$  value (Table 6-2). Therefore, it is already possible to assure that the mass criteria will be equivalent to B criteria.
- Also, the lowest sum of the total bending moments in the arch under permanent loads decreases (C criteria in Table 6-1 and Table 6-3).
- Varying  $z$  has non-negligible effects in the sum of total maximal stresses of the bridge (i in Table 6-3).
- The arch maximal displacement, considering the length of the structure or not, is not minimal for this same value, but for the model with a superior deck with  $f=z=20m$  (H in Table 6-1 and Table 6-3). The fact that the displacement criteria does not give the same results as the stress criteria confirms that a linear analysis is not enough in order to determine which  $z$  value is the most efficient. Therefore the conclusions of this  $z$  parametrical study are not definitive. They must still be verified with a non-linear analysis.

Model	Criteria							
	A	B	C	D	E	F	G	H
Superior deck with $g=20;f=z=10;e=16,67;v=0$	24666	40594	61499	4067	6317	244	39	38
Superior deck with $g=20;f=z=20;e=16,67;v=0$	17958	30026	69354	2999	4502	188	30	19
Inferior deck with $g=20;f=20;z=0;e=16,67;v=0$	21300	30199	87796	3341	4479	181	27	33
Middle deck with $g=20;f=20;z=16,22;e=16,67;v=0$	15660	28240	52776	2685	4531	166	30	23
Middle deck with $g=20;f=20;z=10;e=16,67;v=0$	18745	29752	74080	3162	4670	162	29	40
Minimal values	Middle deck with $z=16,22$	Middle deck with $z=16,22$	Middle deck with $z=16,22$	Middle deck with $z=16,22$	Inferior deck	Middle deck with $z=10$	Inferior deck	Superior deck with $f=z=20$

**Table 6-1: Efficiency criteria for  $z$  values, not considering the length of the elements**

	Total structure length (m)
Superior deck with $g=20;f=z=10;e=16,67;v=0$	307,4
Superior deck with $g=20;f=z=20;e=16,67;v=0$	347,6
Inferior deck with $g=20;f=20; z=0; e=16,67;v=0$	475,7
Middle deck with $g=20;f=20;z=16,22;e=16,67;v=0$	327,6
Middle deck with $g=20;f=20;z=10;e=16,67;v=0$	358,9
Minimal values	Superior deck $f=z=10m$
Minimal values $f=20m$	Middle deck with $z=16,22m$

**Table 6-2: Total length of the bridges of the analysed models**

<b>Criteria</b>									
<b>Model</b>	<b>A</b>	<b>B</b>	<b>C</b>	<b>D</b>	<b>E</b>	<b>F</b>	<b>G</b>	<b>H</b>	<b>i</b>
Superior deck with $g=20;f=z=10;e=16,67;v=0$	7582440	12478661	18904808	1250084	1941837	75088	11914	11631	35
Superior deck with $g=20;f=z=20;e=16,67;v=0$	6242197	10436932	24107370	1042618	1564838	65286	10503	6754	13
Inferior deck with $g=20;f=z=20;e=16,67;v=0$	10131808	14364839	41762243	1589316	2130317	86268	13076	15911	55
Middle deck with $g=20;f=20;z=16,22;e=16,67;v=0$	5129870	9251227	17288632	879489	1484271	54273	9766	7504	0
Middle deck with $g=20;f=20;z=10;e=16,67;v=0$	6728242	10679014	26589666	1134863	1676293	58063	10390	14200	15
Minimal values	Middle deck with $z=16,22$	Middle deck with $z=16,22$	Middle deck with $z=16,22$	Middle deck with $z=16,22$	Middle deck with $z=16,22$	Middle deck with $z=16,22$	Middle deck with $z=16,22$	Middle deck with $z=16,22$	Superior deck with $f=z=20$

**Table 6-3: Efficiency criteria for  $z$  values, considering the length of the elements**

## 6.5 PARAMETER DISCUSSION

The parameter discussion has been already exposed in the previous sections. In this section the main conclusions and explanations are exposed:

- It is convenient to employ an intermediate deck, if the ground is strong enough to bear horizontal loads and the intermediate position helps to stiffen the key points around  $0,28L$ .
- If this intermediate position cannot be obtained and there are no ground limitations, employing a superior deck is more efficient than an inferior one (B in Table 6-1 and Table 6-3).
- The fact that the displacement criteria does not give the same results as the stress criteria confirms that a linear analysis is not enough in order to determine which  $z$  value is the most efficient. A geometrically non-linear analysis should be conducted to prove these conclusions.

## 7. NON-VERTICAL ARCHES. ARCH IN PLAN SAG ( $g_A$ ) PARAMETRICAL STUDY

### 7.1 DEFINITION AND EMPLOYED VALUES

In the previous case studies a planar vertical arch has been considered. However, a previous study (see section V.A) demonstrated that, of different spatial arch bridges with a superior deck, imposed curvature arch bridges ( $g_A=g$ , defined in chapter III.A and Jorquera 2007) or employing an arch with opposite curvature of the deck ( $g_A=-g$ ) showed a better structural behaviour when compared with a planar vertical arch bridge with  $e=0$ . Other studies employ antifunicular arches (Schlaich and Moschner, 1999 and Jorquera 2007) which, if mass criteria and bending moments criteria coincide (which is proved for the previous case studies), would be the optimal solution. For superior deck arch bridges no comparison has been done for different  $g$  and  $e$  values, neither for different arch geometries. Therefore, the present case study is devoted to determine which arch shape is nearer to a more efficient solution, a further step of this case study is purposed in section 0.

The values  $g_A=-20\text{m}$ , for which the arch has an opposite curvature to the superior deck,  $g_A=20\text{m}$ , which is an SDABWIC and  $g_A=0$ , which is a SABWCSD with a vertical planar arch bridge like the ones employed until now in the present chapter.

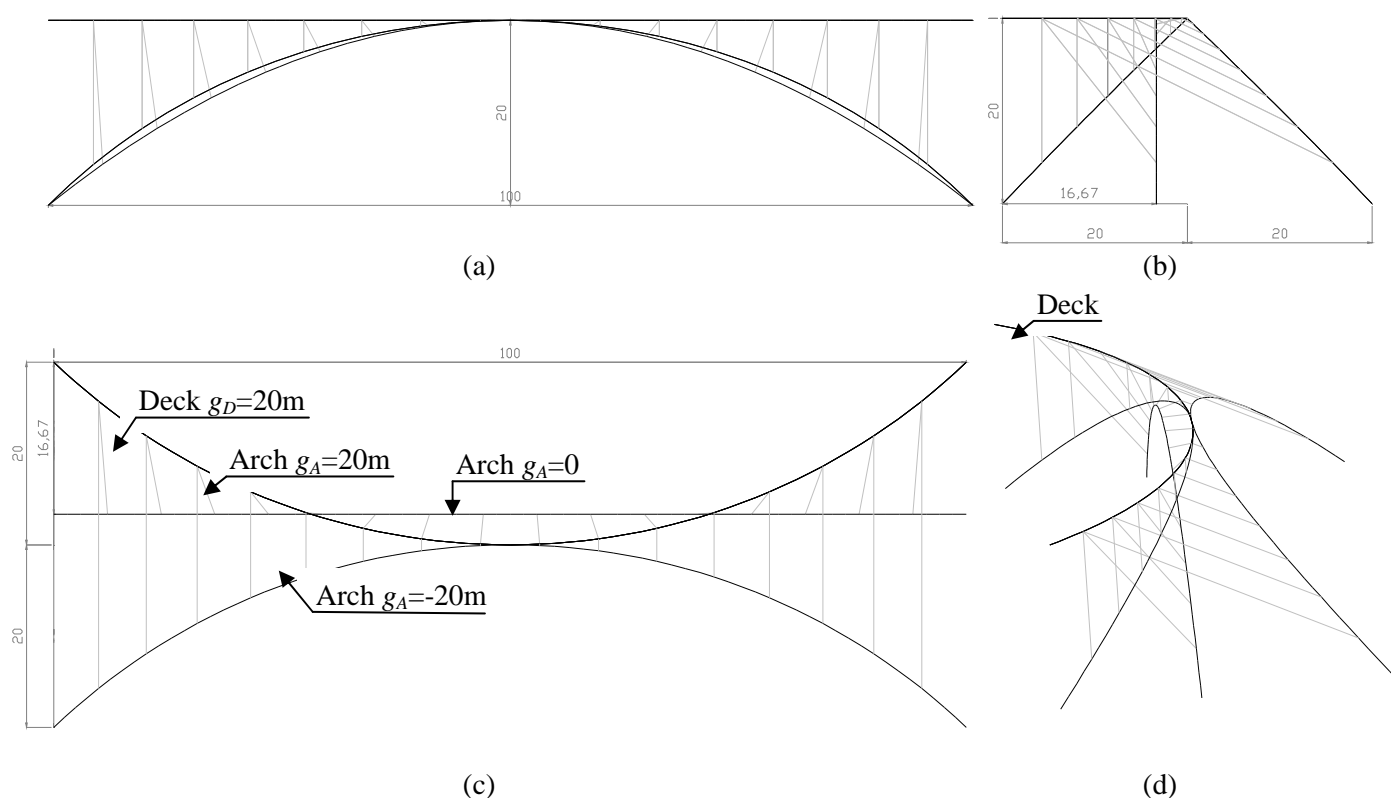


Figure 7-1: Variation of arch  $g_A$  (a) Plan view. (b) Longitudinal view. (c) Side view. (d) Perspective



## 7.2 STRUCTURAL RESPONSE UNDER A UNIFORM VERTICAL LOAD ( $lu$ )

The structural behaviour has been studied under a uniform load of 10kN/m on the whole deck (Figure 1-2) for the described models with the different values of  $g_A$  and their structural response has been compared.

### 7.2.1 Arch internal forces (Figure 7-2 to Figure 7-6)

- $g_A=0$  gives the most uniform axial forces, out-of-plane and total bending moments distribution in the arch, the lowest axial forces and in-plane, out-of-plane and total bending moments in the arch springings, the lowest out-of-plane and total bending moments in the arch span center (from Figure 7-2 to Figure 7-5) and the largest torsional bending moments (Figure 7-6), whereas
- $g_A=g$  gives the lowest axial forces in the arch span center (Figure 7-2) and
- $g_A=-g$ , the lowest torsional bending moments (Figure 7-6).

### 7.2.2 Deck and struts internal forces (Figure 7-7 to Figure 7-10)

- $g_A=0$  gives the lowest axial forces in the deck and struts (Figure 7-7 and Figure 7-10). It also gives the lowest total bending and torsional moments in the deck, since the arch transmits more axial forces to the deck when it is curved in plan view (from Figure 7-7 to Figure 7-9).
- As explained in section V.A the deck is tensioned for  $g_A=g$  and compressed for  $g_A=-g$  (Figure 7-7).

### 7.2.3 Arch displacements (Figure 7-11)

- $g_A=0$  gives the lowest in-plane and out-of-plane and hence total, arch displacements, whereas
- $g_A=-g$ , gives the largest in-plane and out-of-plane and hence total, arch displacements
- this shows that the best way to control the both, in- and out-of-plane behavior of the arch is employing a vertical planar bridge with an efficient  $e$  value.

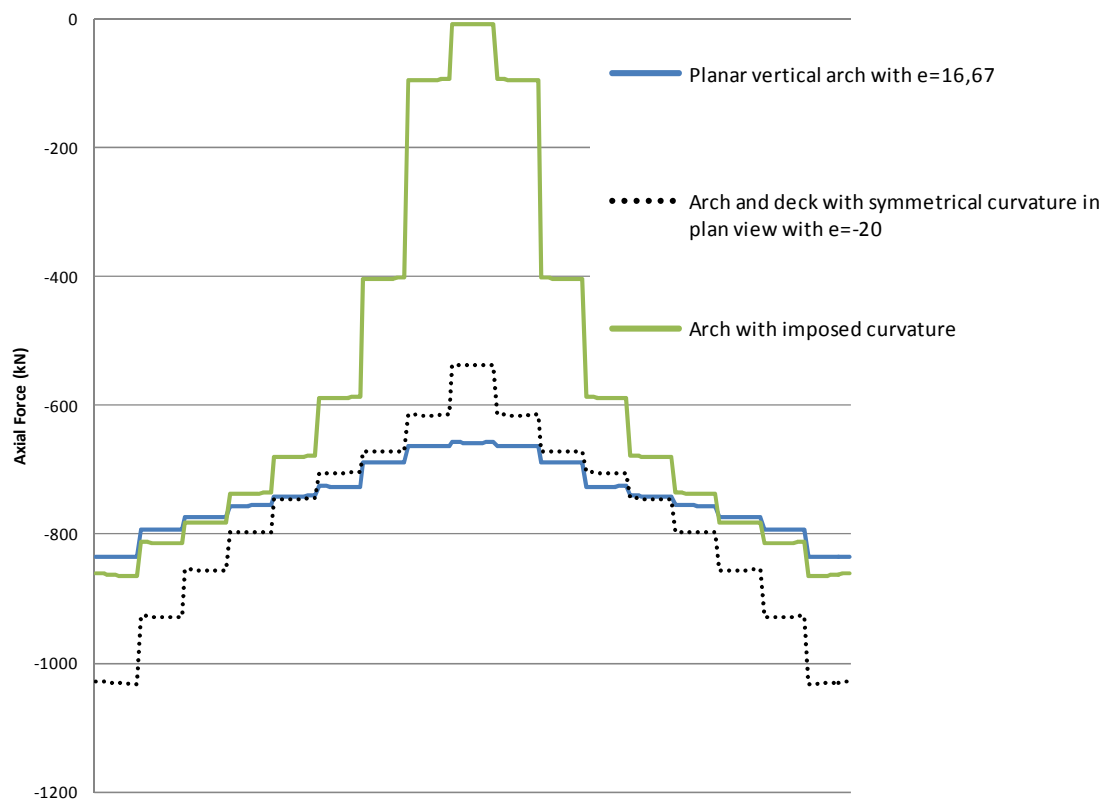


Figure 7-2: Arch axial forces comparison for different  $g_A$  values. The abscissas are the arch length from 0 to  $L_A$

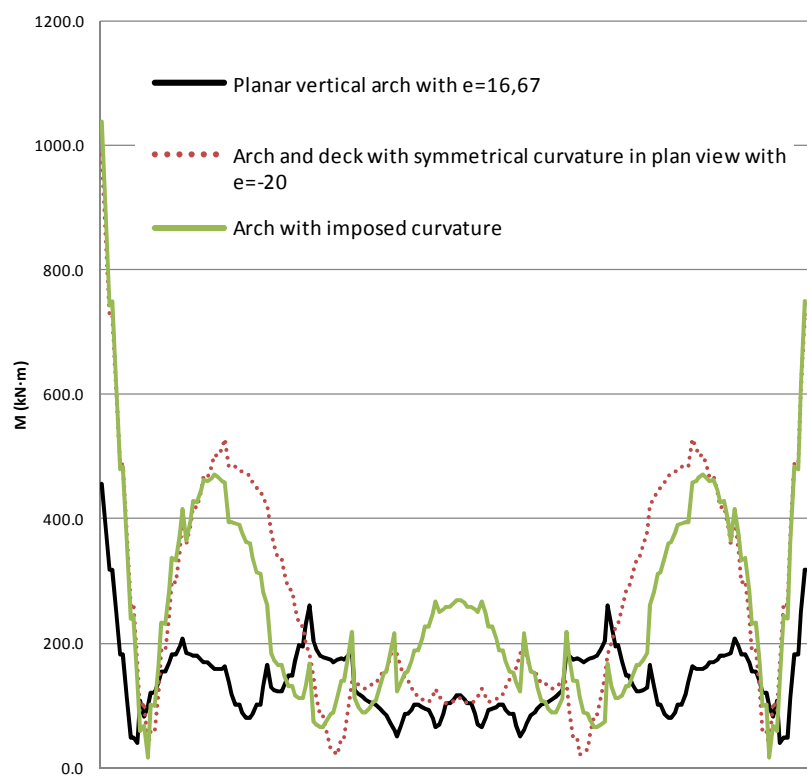


Figure 7-3: Arch total bending moments comparison for different  $g_A$  values. The abscissas are the arch length from 0 to  $L_A$

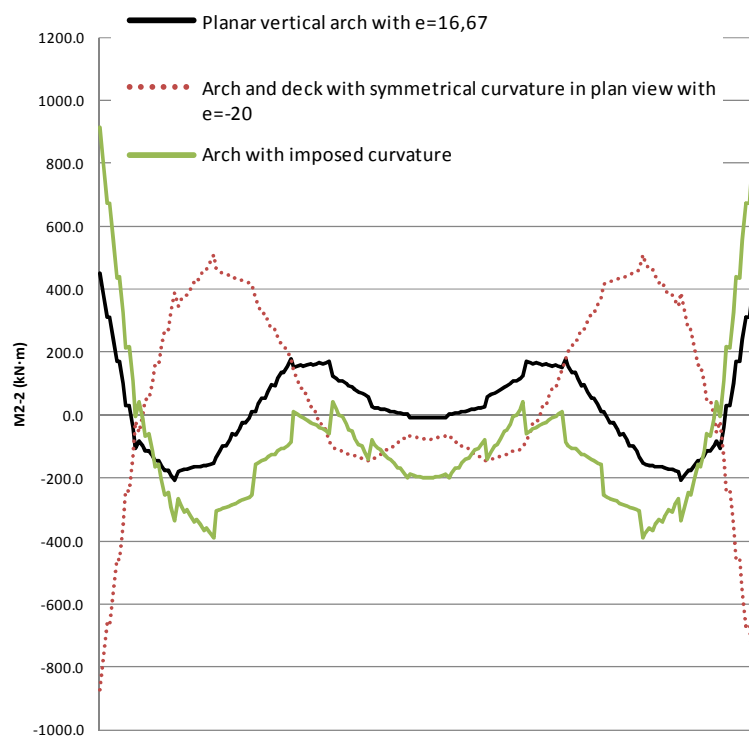


Figure 7-4: Arch out-of-plane bending moments comparison for different  $g_A$  values. *The abscissas are the arch length from 0 to  $L_A$*

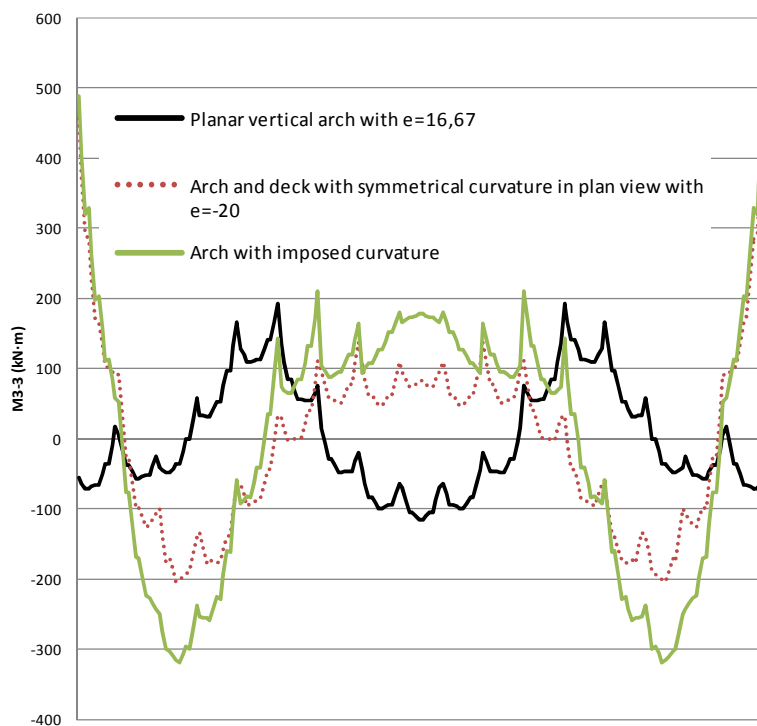
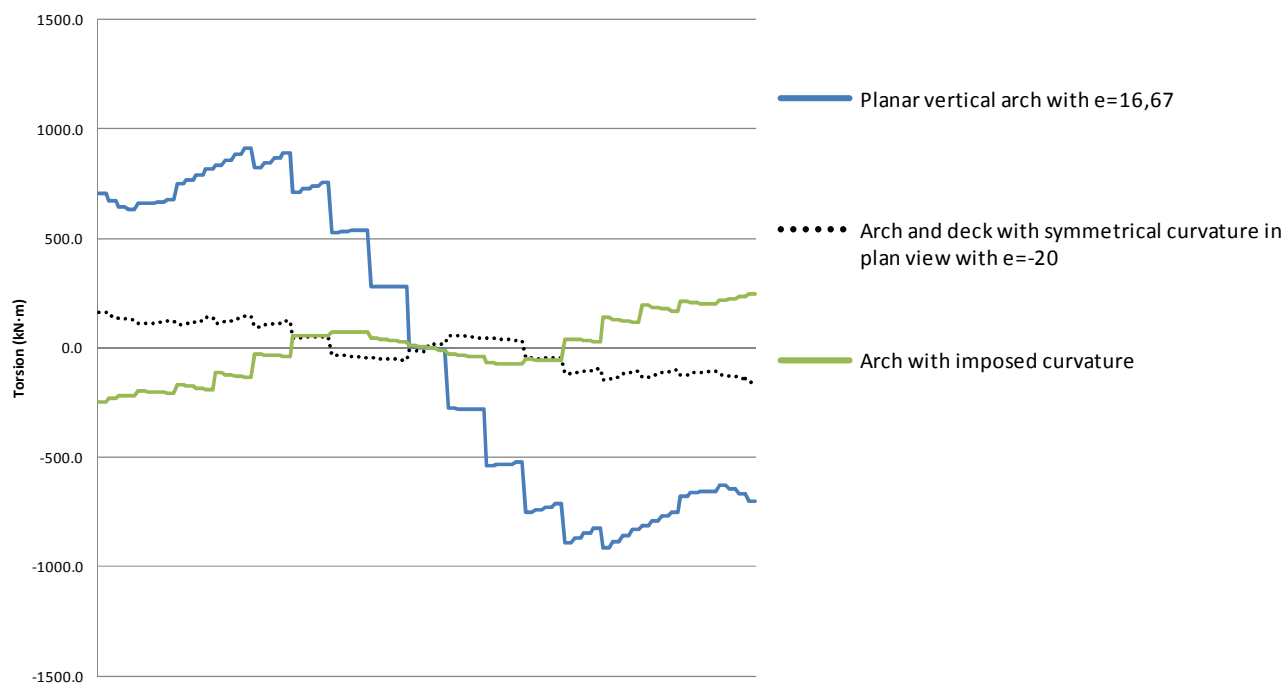
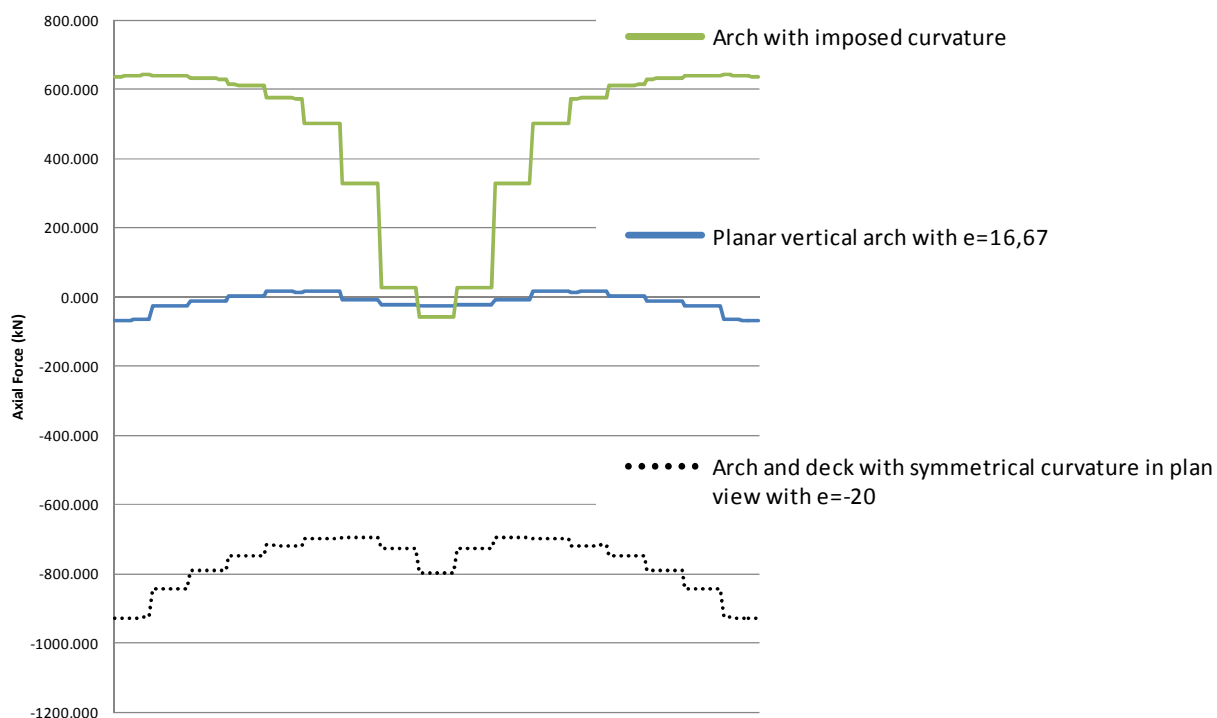


Figure 7-5: Arch in-plane bending moments comparison for different  $g_A$  values. *The abscissas are the arch length from 0 to  $L_A$*



**Figure 7-6:** Arch torsional moments comparison for different  $g_A$  values. *The abscissas are the arch length from 0 to  $L_A$*



**Figure 7-7:** Deck axial forces comparison for different  $g_A$  values. *The abscissas are the deck length from 0 to  $L_D$*

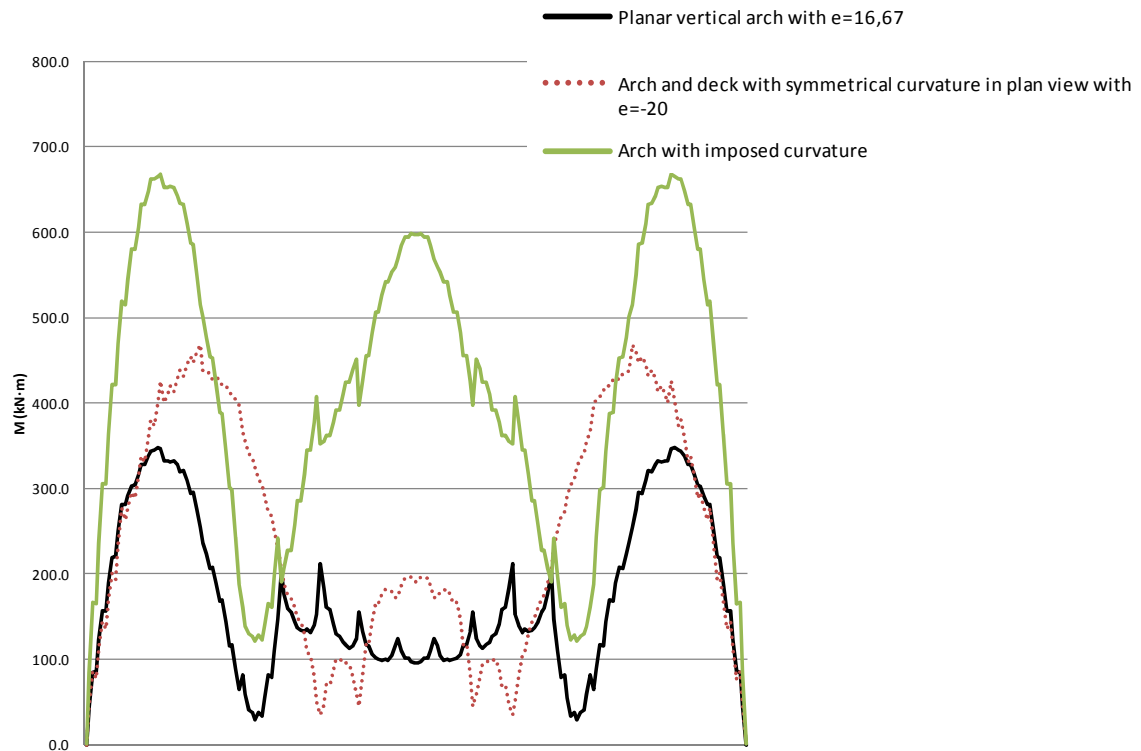


Figure 7-8: Deck total bending moments comparison for different  $g_A$  values. The abscissas are the deck length from 0 to  $L_D$

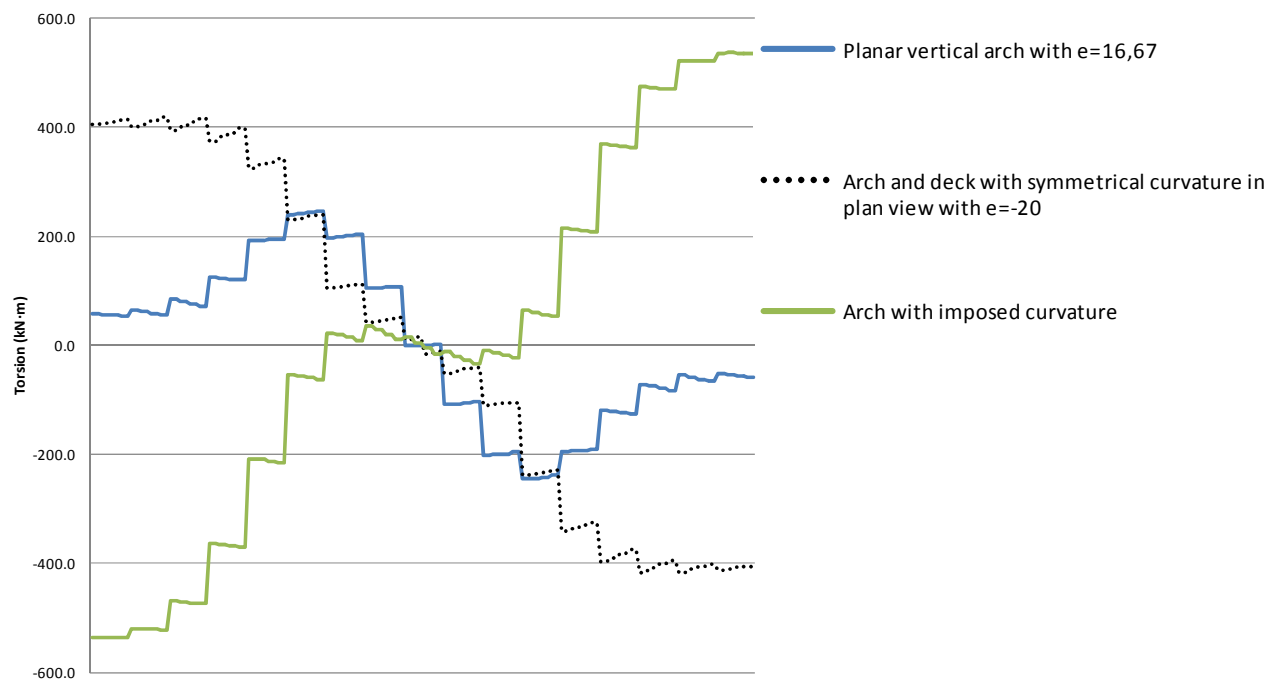
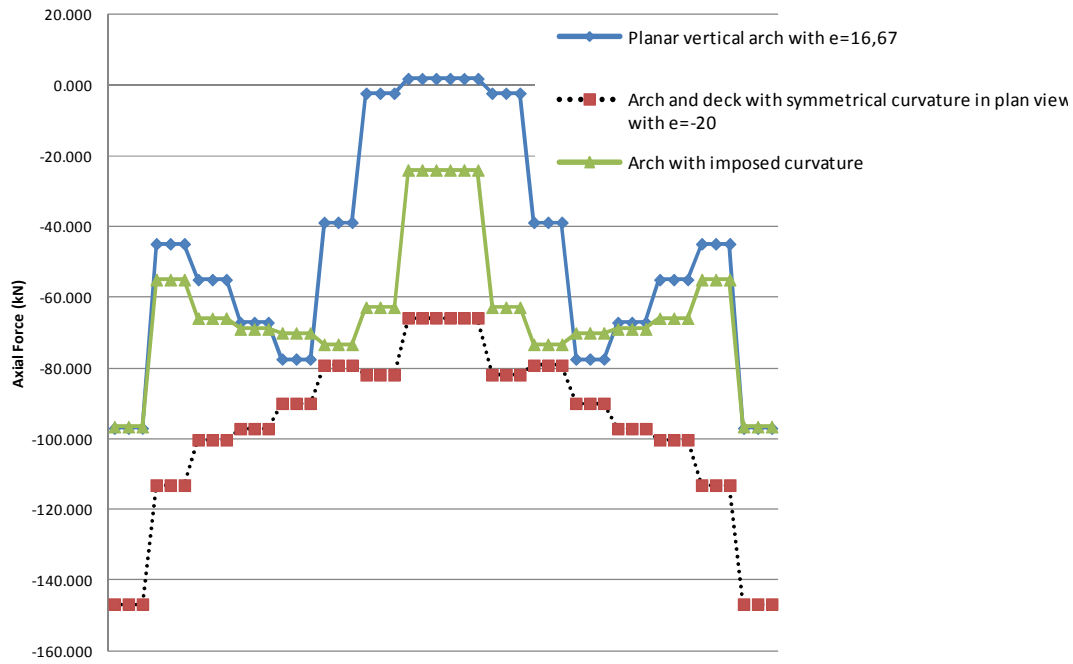
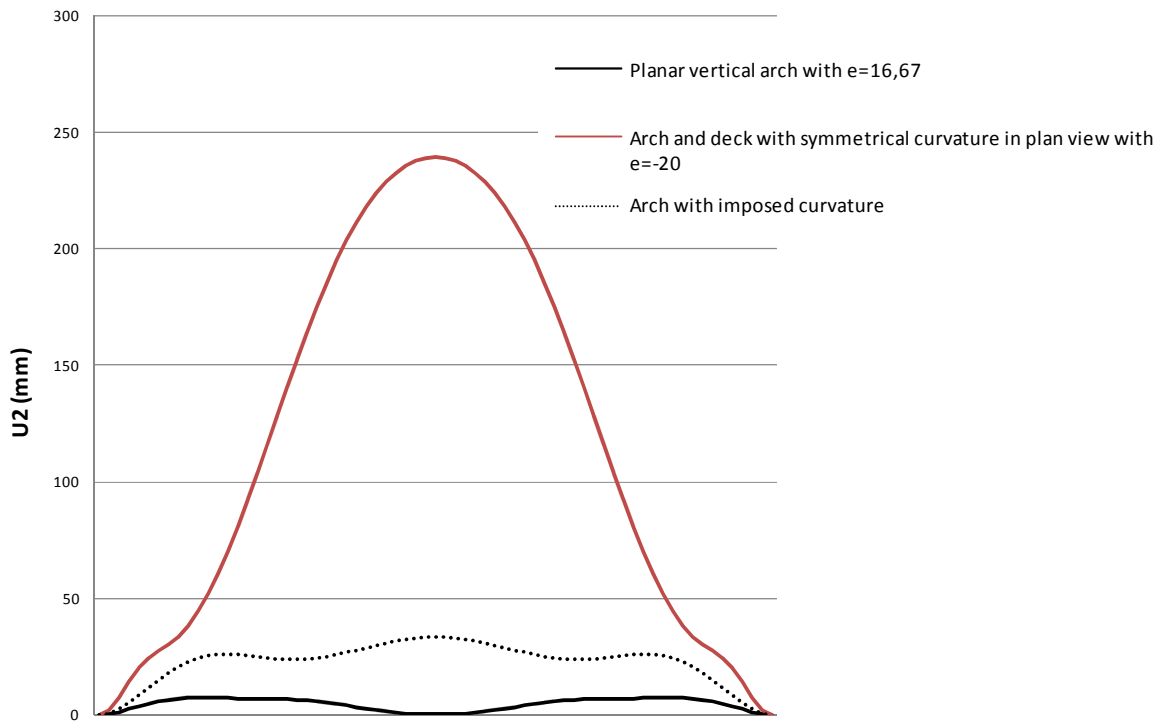


Figure 7-9: Deck torsional moments comparison for different  $g_A$  values. The abscissas are the deck length from 0 to  $L_D$



**Figure 7-10: Struts axial forces comparison for different  $g_A$  values. The abscissas are the output stations of the different struts (at the bottom, center and the top of their length).**



**Figure 7-11: Total Arch displacements for different  $g_A$  values. The abscissas are the arch length from 0 to  $L_A$**

### 7.3 STRESS BEHAVIOUR UNDER $q$ AND DESIGN AND COMPARISON IN ULTIMATE LIMIT STATE

#### 7.3.1 Stresses behaviour under a uniform load $q=10\text{kN/m}$

Stresses in the arch and deck only under a uniform load  $q$  can be observed in Figure 7-12 and Figure 7-13 for the reference values (Table 1-1):

- Stresses in the arch at springings and  $L_A/4$  are minimal when employing a planar vertical arch with  $e=g/1,2$  (Figure 7-12)
- Stresses in the arch at span center are minimal when employing an arch with  $g_A=-g$  (Figure 7-12), but stresses for this case are maximal at approximately  $L_A/4$
- Stresses in the deck are clearly minimal when employing a planar vertical arch with  $e=g/1,2$  (Figure 7-13)

#### 7.3.2 Critical loading combinations in ULS

Stresses in the arch and deck for the reference values (Table 1-1) under different combinations of loading cases can be observed from Figure 7-14 to Figure 7-16. These are the values employed for dimensioning the design cross-sections.

- For SABs with a **superior curved deck** and a planar vertical arch at  $e=g/1,2$ , the critical load case, for stresses in the arch is A2 for the springing and around  $L/4$  and A1 for the rest of the arch when employing a superior deck (Figure 7-14), as observed already in the previous case studies.
- When employing an **arch curved in plan view** the critical loading case in the arch is A1 in all its length (Figure 7-15 and Figure 7-16).

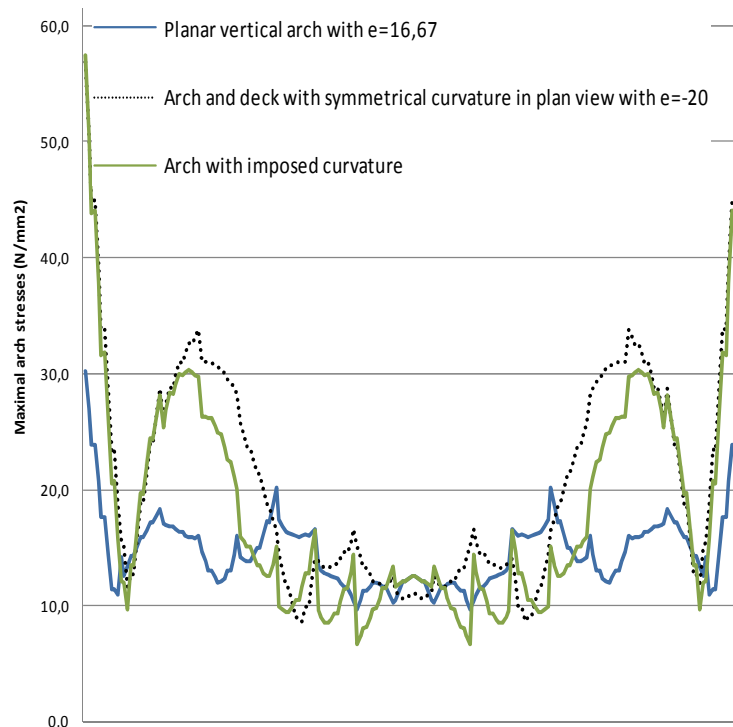


Figure 7-12: Arch stresses comparison for different  $g_A$  values only under  $q=10\text{kN/m}$  for the reference values (Table 1-1). The abscissas are the arch length from 0 to  $L_A$

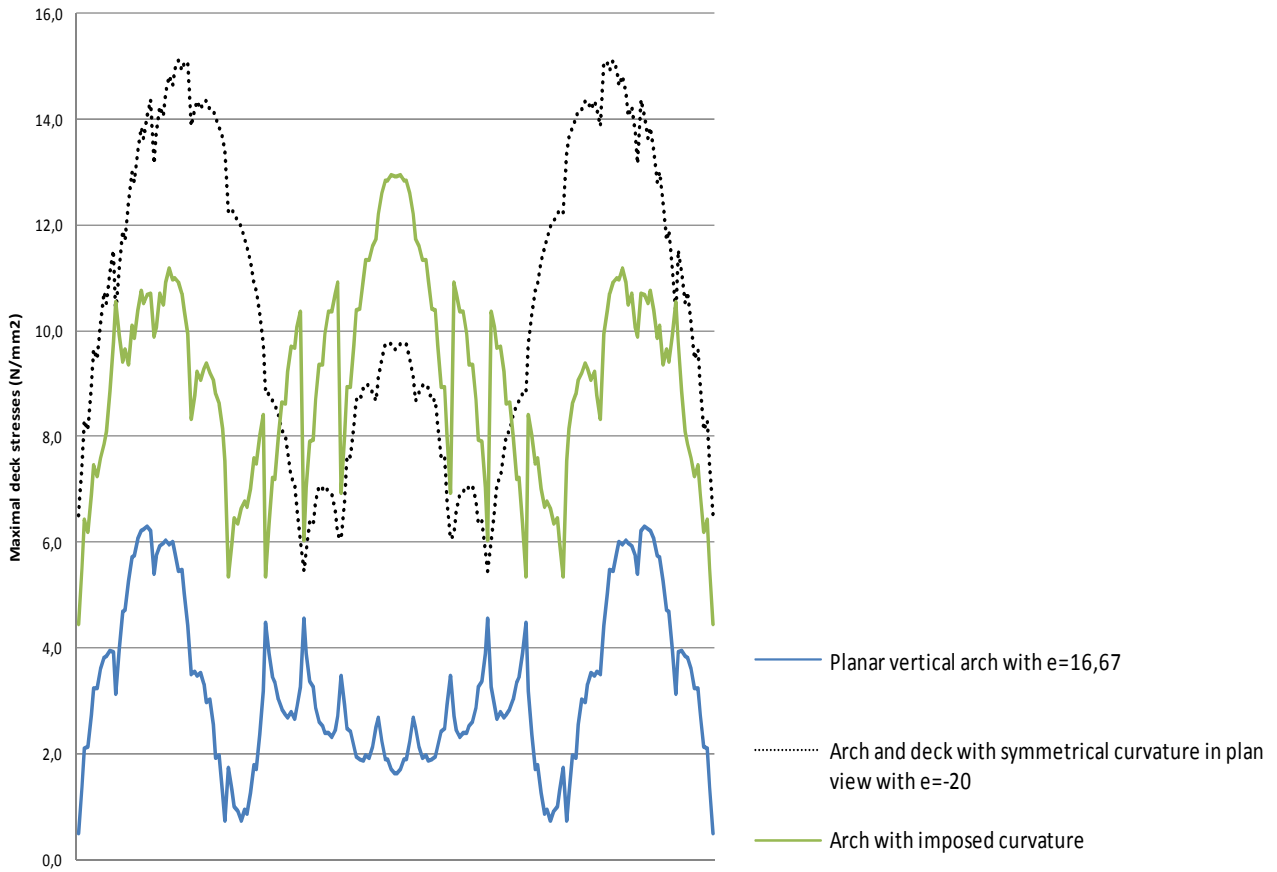


Figure 7-13: Deck stresses comparison for different  $g_A$  values only under  $q=10\text{kN/m}$  for the reference values (Table 1-1). The abscissas are the deck length from 0 to  $L_D$

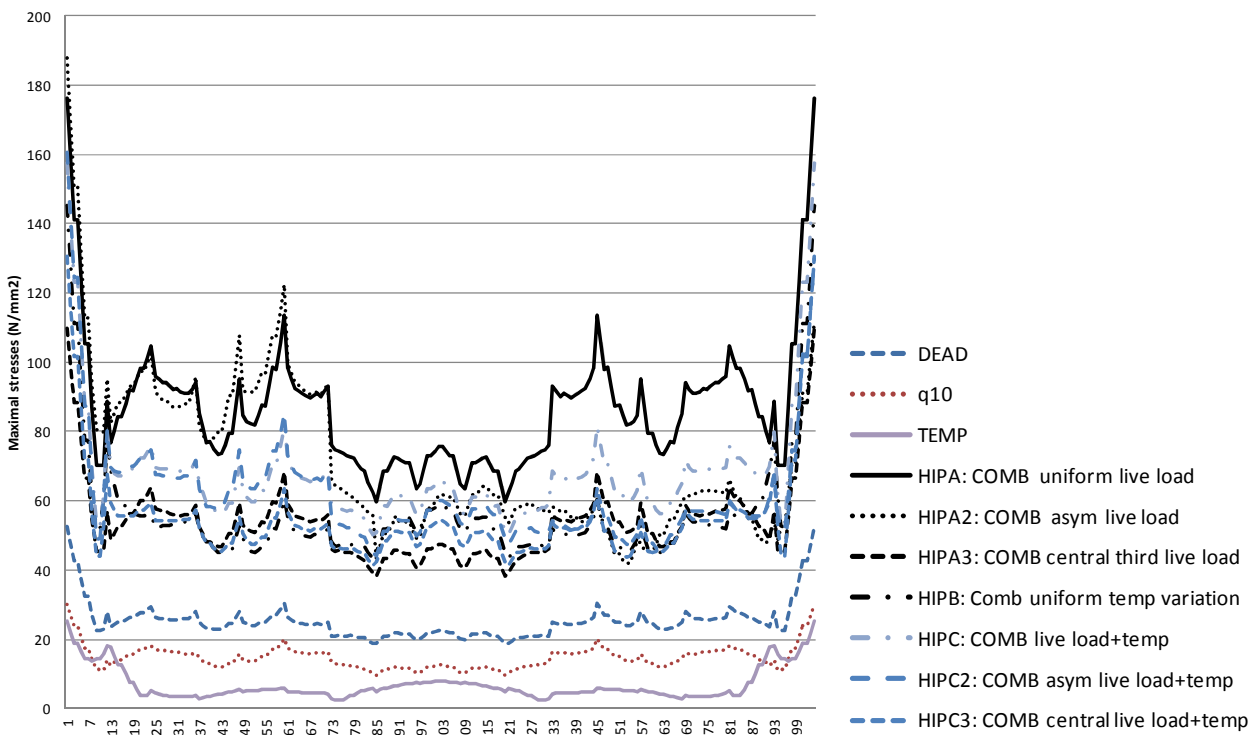


Figure 7-14: Stresses caused by different loading cases combination for  $g=20\text{m}$ ,  $f=20\text{m}$  and  $e=16,67\text{m}$  for the reference values (Table 1-1). The abscissas are the arch length from 0 to  $L_A$



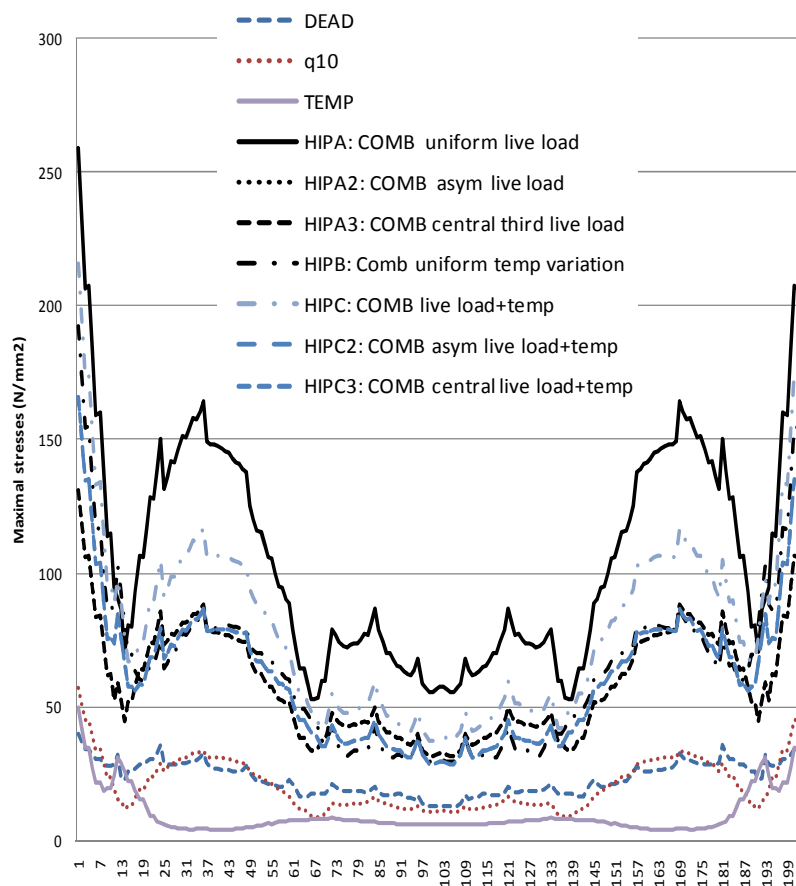


Figure 7-15: Stresses in the arch for different loading combinations for SABs with the arch and deck with symmetrical curvature in plan view with  $e=-20$ ;  $g_A=-g=-20m$  for the reference values (Table 1-1). *The abscissas are the arch length from 0 to  $L_A$*

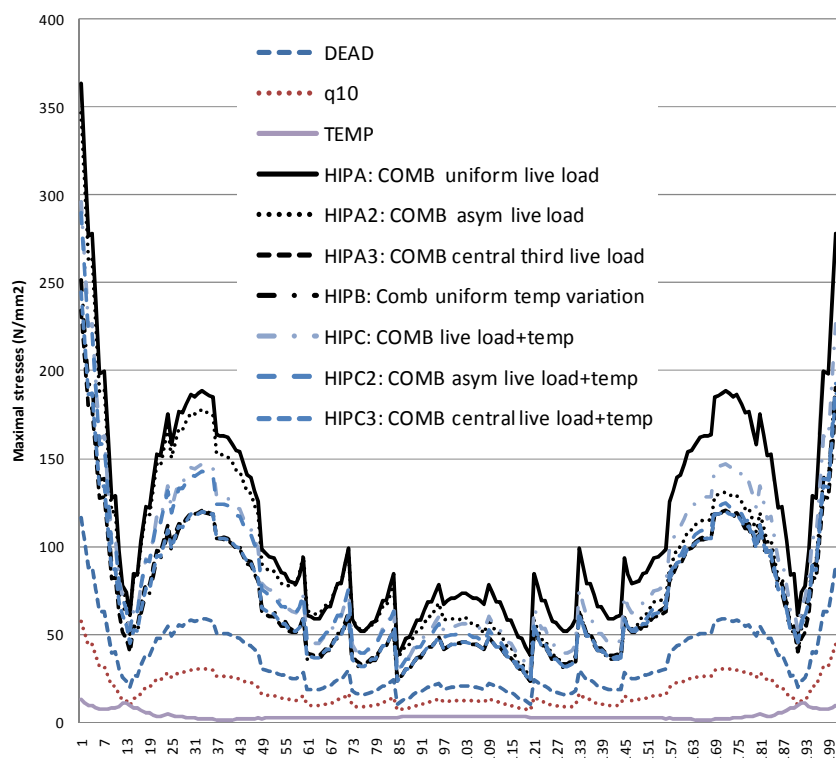


Figure 7-16: Stresses in the arch for different loading combinations for SDABWIC with  $e=0$ ;  $g_A=g=20\text{m}$  for the reference values (Table 1-1). The abscissas are the arch length from 0 to  $L_A$

#### 7.4 EFFICIENCY CRITERIA

Results of the different efficiency criteria not considering the length of the elements are displayed in Table 7-1 and considering the total length of the bridge (Table 7-2) in Table 7-3. Please use the bookmark to comfortably interpret the tables, and note whether the length is considered or not, since the nomenclature and units of the criteria are modified. The following values are specifically employed for the tables in this section:

- The expression “minimal value” refers to the bridge configuration which minimizes each criteria (m)
- $i=\%$  of difference of B from the most efficient configuration for B

The results of the efficiency criteria are commented in the following lines:

- It is convenient to employ a planar vertical arch in order to reduce the total stresses in the bridge.
- The model which presents the shortest length is the one with  $g_A=-g$  (Table 7-2), the model with  $g_A=0$  is 7% longer. However, in the previously studied cases it has been demonstrated that the criteria *sum of total maximal stresses of the bridge\*total bridge length* is always equivalent to the *total mass of the bridge* criteria. Therefore in the present study we will consider this equivalency without proving it for this particular case.
- The maximal displacement under permanent loads is the simplest criteria to employ, equivalent to consider the lowest stresses considering the length of all the elements or not, and the lowest sum of the total bending moments in the arch under permanent loads (Table 7-1 and Table 7-3).

- Varying  $g_A$  has non-negligible effects in the sum of total maximal stresses of the bridge (i in Table 7-3).
- The fact that the displacement criteria gives the same results as the sum of total maximal stresses of the bridge criteria confirms that a linear analysis is enough in order to determine which  $g_A$  value is the most efficient.

Model	Criteria							
	A	B	C	D	E	F	G	H
Planar vertical arch with $e=16,67; g_A=0$	17958	30026	69354	2999	4502	188	30	19
Arch and deck with symmetrical curvature in plan view with $e=-20; g_A=-g$	21794	38565	76166	4299	7370	259	57	41
Arch with imposed curvature; $g_A=g$	23347	43280	154536	3767	6947	363	57	91
Minimal values	Planar vertical arch with $e=16,67$	Planar vertical arch with $e=16,67$	Planar vertical arch with $e=16,67$	Planar vertical arch with $e=16,67$	Planar vertical arch with $e=16,67$	Planar vertical arch with $e=16,67$	Planar vertical arch with $e=16,67$	Planar vertical arch with $e=16,67$

**Table 7-1: Efficiency criteria for different  $g_A$  values, not considering the length of the elements**

	Total structure length (m)
Planar vertical arch with $e=16,67; g_A=0$	347.6
Arch and deck with symmetrical curvature in plan view with $e=-20; g_A=-g$	444.1
Arch with imposed curvature; $g_A=g$	323.8

**Table 7-2: Length of the models with different  $g_A$  values**

Model	Criteria								
	A	B	C	D	E	F	G	H	i
Planar vertical arch with $e=16,67; g_A=0$	6242197	10436932	24107370	1042618	1564838	65286	10503	6754	0
Arch and deck with symmetrical curvature in plan view with $e=-20; g_A=-g$	9678483	17126462	33825062	1908967	3272794	83807	18419	13217	64
Arch with imposed curvature; $g_A=g$	7560372	14014965	50041791	1219960	2249556	161248	25521	40536	34
Minimal values	Planar vertical arch with $e=16,67$	Planar vertical arch with $e=16,67$	Planar vertical arch with $e=16,67$	Planar vertical arch with $e=16,67$	Planar vertical arch with $e=16,67$	Planar vertical arch with $e=16,67$	Planar vertical arch with $e=16,67$	Planar vertical arch with $e=16,67$	Planar vertical arch with $e=16,67$

**Table 7-3: Efficiency criteria for different  $g_A$  values, considering the length of the elements**

## **7.5 PARAMETER DISCUSSION**

The parameter discussion has been already exposed in the previous sections. In this section the main conclusions and explanations are exposed:

- It is convenient to employ a planar vertical arch in order to reduce the total stresses in the bridge and improve both, the in-plane and out-of-plane behavior of the arch.
- Employing an arch with a large curvature in plan view is only interesting when desired to reduced torsional moments in the arch.

## 8. CONCLUSIONS

The most efficient model for spatial arch bridges with a curved superior deck sustained by a planar vertical arch is displayed in Figure 8-1.

The variables are detailed in the previous sections and the bookmark.

The angle  $\beta$  for the strut distribution is measured taking as reference the model obtained from equal divisions of arch and deck (explained in section 5).

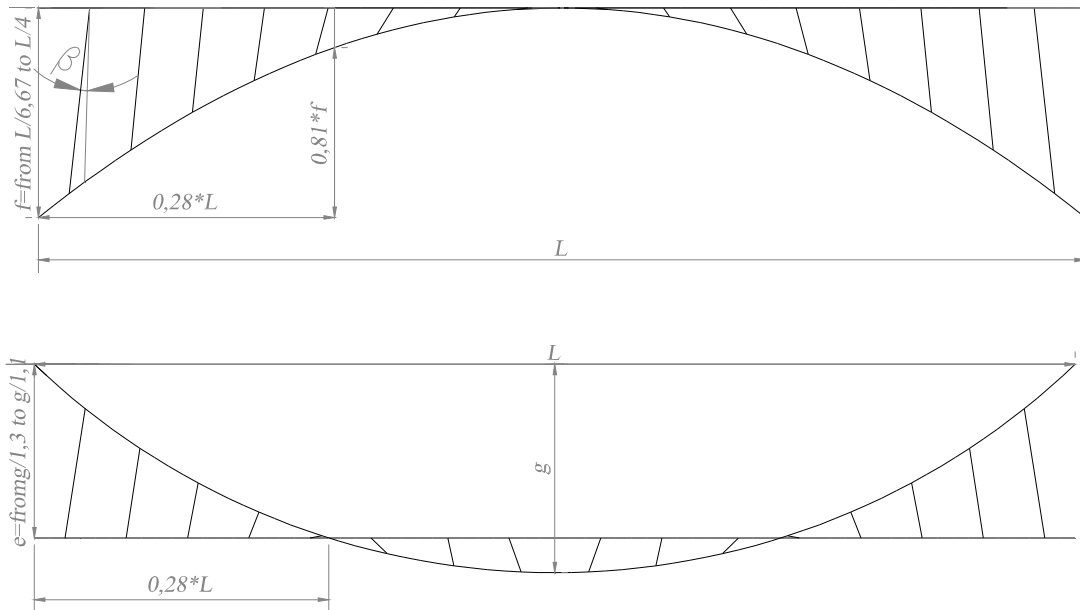


Figure 8-1: Most efficient model for spatial arch bridges with a curved superior deck

### 8.1 Parameter conclusions

$e$  and  $\beta$  are key parameters for spatial arch bridges with a curved superior deck sustained by a planar vertical arch.

Regarding  $e$ , whatever the deck curvature, the value of  $f$ , the stiffness of the strut-deck system or that of the arch:

- Results for all the different indicators are low enough in the range of  $g/1,3 \leq e \leq g/1,1$ , approximately in the range in which there is the same number of hangers at each side of the arch.
- Given a  $g$  value, in the range  $g/1,36 \leq e \leq g/1,2$  the internal forces in the whole bridge are reasonable.
- The value  $e = g/1,2 = 0,83g$  is the most efficient value for the arch/eccentricity in plan view according to all of the studied efficiency indicators. For this value internal torsional moments in the arch and the deck under a uniform deck load are minimal and the maximal in-plane and maximal out-of-plane displacements acquire the same value
- $e = g/1,2 = 0,83g$  is at a distance of approximately  $0,28L$  of length and at  $0,81*f$  of height of the springings of the arch (Figure 2-1), whatever the  $g$  value. It is a key point to control

the arch behaviour, since at this point controlling the out-of-plane behaviour is most critical. Therefore, it is the most efficient  $e$  value because it obtains the stiffest struts at this key point.

- For high  $g$  values, ie: when spatial behaviour increases, the influence of  $e$  is larger.
- The higher the  $f$  value, the higher the importance of choosing an adequate  $e$  value.
- Regarding the stresses in the arch, the influence of employing a stiff strut-deck system is lower for values of  $e$  between  $g/1,30$  and  $g/1,20$ .

Regarding  $v$ :

- Depending on the stiffness of the strut-deck system it might be worth or not adjusting the value of  $e$ .
- $v=0$  is the most convenient value, since it stiffens the struts at key points  $e=g/1,2$ .
- Increasing the verticality of the struts by increasing the vertical distance between the arch crown and the deck mid-span ( $v$ ), decreases the efficiency of the system, since it increases the length of the struts and thus decreases their stiffness.
- For an efficient  $e$  value,  $v$  has a significant influence in the internal forces, stresses and mass of the bridge. However, most important is to control  $e$ .

Regarding  $f$

- Whatever the value of  $g$ , values of  $f$  between  $L/6,67-L/4$  give a negligible difference of the total mass of the bridge, so they can be considered with an equivalent efficiency.
- Employing a vertical rise  $f>L/4$  for the arch is not recommendable.
- The range of adequate values of  $f$  for SABs is smaller than for  $g=0$ .

Regarding  $\beta$

- It is convenient to employ a convergent distribution of struts (ie: a distribution of struts in which each strut axis elongation converges above the deck with its symmetrical), in order to reduce the total material employed for the bridge, in spite of being the longest ones. Controlling key points proves to be more efficient than verticality or stiffness small variations.
- A small  $\beta$  variation leads to an important mass variation. Therefore,  $\beta$  is a key parameter for the efficiency of SABWCSD.

Regarding  $z$ :

- From a structural point of view, it is convenient to employ an intermediate deck crossing the arch at  $0,28L$ , if the ground is strong enough to bear horizontal loads. If this intermediate deck position cannot be obtained and there are no ground limitations, employing a superior deck is more efficient than an inferior one.
- Employing a middle deck improves the in-plane behaviour of the arch, but not the out-of-plane behaviour, causing a displacement increase at span center. This behaviour has been studied with a linear analysis, but a geometrically non-linear parametrical analysis (GNLPA) has not been conducted. The described conclusions should be verified with a

GNLPA due to the described large displacements of the model which has shows a stress reduction..

Regarding  $g_A$ :

- If employing an efficient value of  $e$ , it is convenient to employ a planar vertical arch ( $g_A=0$ ) instead to a curved in plan arch in order to reduce the total stresses in the bridge.

## 8.2 Efficiency criteria conclusions

Regarding the different comparison criteria which have been studied in order to decide the most efficient value of the different parameters:

- It has been demonstrated that, for spatial arch bridges with a curved superior deck, given a certain stiffness of the bridge elements, comparing the maximal displacements of the arch is always equivalent to comparing the total mass of the bridge. Therefore, for this bridge type, reducing the maximal displacement of the arch is equivalent to reducing the total mass of the bridge.
- It is remarkable that for efficient parameters for SABs with a planar vertical arch with a superior curved deck, the out-of-plane maximal arch displacements have a similar value to in-plane maximal arch displacements. This is a simple and representative enough criterion for easily evaluating the efficiency of a model without doing a parametrical study.
- Given an  $f$  and cross-section values of the bridge, reducing the total bending moments of the arch, ie: tending to its antifunicular under permanent loads, is also a valid criterion to reduce the total mass of the bridge.
- When studying the stiffness of the system, the total mass of the bridge must be compared.
- It must be noted that the mass of the bridge can be a misleading criteria in order to choose the most efficient parameters if it is not correctly employed. Two different procedures can be defined to employ this criterion correctly:
  - the cross-sections of the different elements should be carefully chosen in order to minimise the mass of each specific studied model. Only then can the masses be compared, regardless of employing or not the same diameters for the different elements.
  - Fix the diameter (for CHS) or width and depth (for box girders) under an aesthetical criterion and only vary the plate thickness when dimensioning the cross-sections.

In order to obtain the most efficient parameter value, a linear analysis is enough in all the studied cases, except for the  $z$  parameter, where inferior, intermediate and superior deck SABs where compared. For this case study a further geometrically non-linear analysis should be conducted.

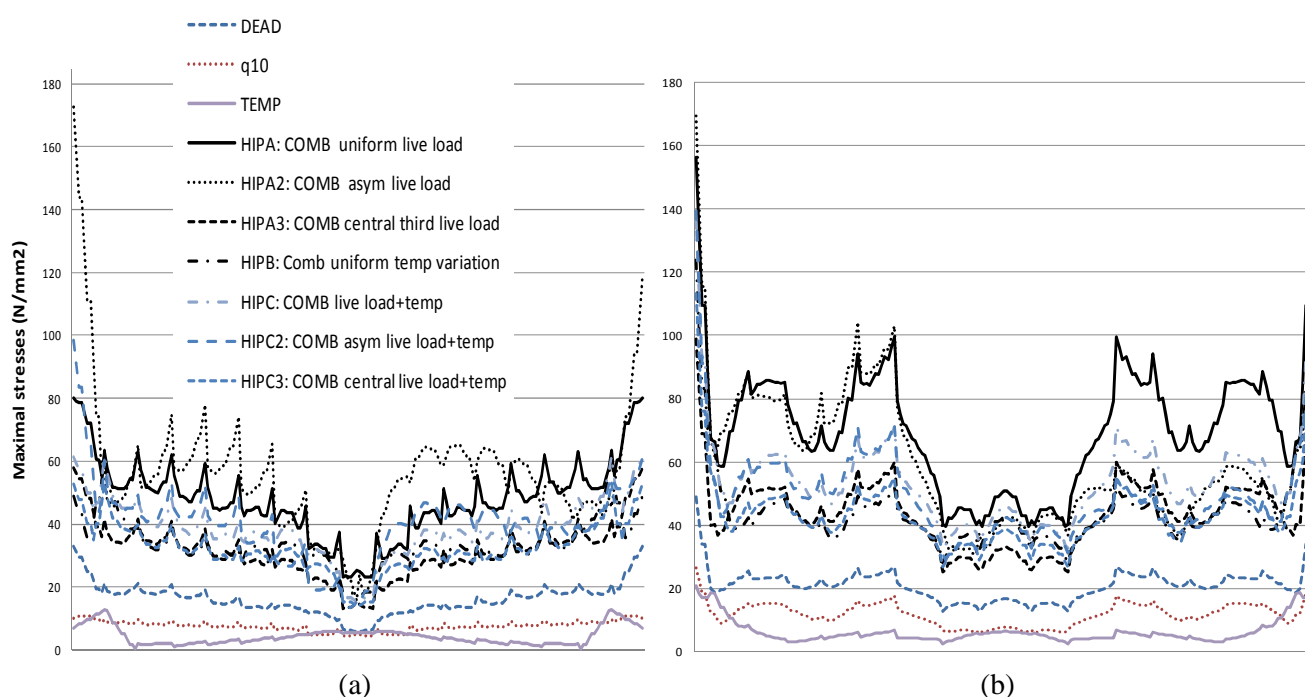
The geometrically non-linear behavior can be observed in Chapter VI. C.

### 8.3 Critical loading combinations conclusions

Regarding the critical loading combinations it has been proved for the different parameters and it can be clearly appreciated in Figure 8-2 that, in comparison with a planar vertical arch with a straight deck (Figure 8-2a), asymmetrical loading in half the deck loses importance for SABs with a superior curved deck (Figure 8-2b).

The higher the importance of the out-of-plane behavior of the arch, the lower the influence of an asymmetrical uniform live loading on half the deck span ( $la$ , Figure 1-2).

The worst loading combination in ULS for the most efficient model described in Figure 8-1 is A1 except at springings and approximately around  $L_A/3$ , where the worst loading case is A2 (Figure 8-2b).



**Figure 8-2: Stresses in the arch caused by different loading cases combination for (a) a vertical planar arch with straight deck, with  $g=0m$  and  $f=20m$  (b) model described in Figure 8-1, with curved superior deck  $g=20m$ ,  $f=20m$ ,  $e=16,67m$  and convergent struts. In both cases the reference model cross-sections (Table 1-1) are employed and the abscissas are the arch length from 0 to  $L_A$**



## 9. FUTURE LINES OF STUDY

The present chapter can be further researched regarding antifunicularity, cross-sections and struts distributions. Several possible lines of study are detailed in the following lines:

- Stiffness analysis distribution with more cross-sections.
- Parametrical analysis of the struts distribution concentrating the struts in the area  $0,28*L$  of the arch and deck.
- Conduct a new the parametrical analysis of  $z$  employing geometrically non-linear analysis
- The present case study is devoted to planar vertical arch bridges with a curved deck. A study of arch in plan view curvature has been conducted, to determine which arch shape is nearer to a more efficient solution (section 7). A next step would be to study the optimal  $e$  value for each shape, determine the antifunicular solution and compare the mass variation of the most efficient solution with the most efficient  $e$  in each case in order to determine whether finding the antifunicular shape is worth the mass variation it implies. However this last step involves developing a software which is not contained in the scope of this thesis since it has been developed in previous works, and it is also not necessary for the objectives of the present thesis since the present case study is enough to understand the structural behaviour and determine easy design criteria.
- It has been proved that for planar arch bridges the most efficient  $e$  value is independent of  $f$ . The relationship of  $e^*$  is always approximately an 80% of the value of  $f$  and  $g$ . If we were working with antifunicular arches the plan view and longitudinal view geometries would be coupled and we would not be able to do the same statement. For future lines of study we recommend first to fix the recommended design criteria for planar vertical bridges in the present and find the antifunicular arch. If the differences o the mass of the dimensioned bridge are negligible, planar arches can be employed and further researches are not necessary. If not, another parametrical study for  $e$  would be necessary, finding the antifunicular arch for each case, since the most adeuqate  $e$  value might change when employing antifunicular arches for a specific  $f$  value.
- The arch maximal displacement, not considering the length of the structure or not, is not minimal for this same value, but for the model with a superior deck with  $f=z=20m$  (H in Table 6-1 and Table 6-3). The fact that the displacement criteria does not give the same results as the stress criteria confirms that a linear analysis is not enough in order to determine which  $z$  value is the most efficient. Therefore this study is not definitively valid its validity must still be verified with a non-linear analysis.

## REFERENCES

- BILLINGTON D. P., “The Role of Science in Engineering.” *Robert Maillart’s Bridges. The Art of Engineering*. Princeton University Press. New Jersey, 1979, pp. 94-105 and 111-112.
- DE ZOTTI, A., PELLEGRINO, C. and MODENA, C.. “A parametric study of the hanger arrangement in arch bridges”. *ARCH '07. Proceedings of the 5th International Conference on Arch Bridges*. Madeira , Portugal September 12-14, 2007. pp. 476-481
- Eurocode 1: Actions on structures — Part 2: Traffic loads on bridges
- Eurocode 2: Design of concrete structures
- Eurocode 3: Design of steel structures
- JORQUERA J. J., “Structural Behaviour of Spatial Arch Bridges”, *Proceedings of the IASS Symposium 2009, Evolution and Trends in Design, Analysis and Construction of Shell and Spatial Structures* (Domingo, A., and Lázaro, C. (Eds)), Valencia, 2009, pp. 2447-2457.
- JORQUERA J. J., *Study of the Structural Behaviour of Spatial Arch Bridges*, PhD Thesis. Supervised by Prof. Manterola, Technical University of Madrid (UPM), 2007 (in Spanish).
- KOLLBRUNNER C. F. and BASLER K.. *Torsion in structures: An engineering approach*. Springer-Verlag, 1969, pp280
- O’CONNOR, C. (1971). “Arches.” *Design of Bridges Superstructures*, John Wiley & Sons, New York, 488–544.
- SARMIENTO-COMESÍAS, M., RUIZ-TERAN, A. and APARICIO, A. C.. “Elastic behaviour of planar vertical arch bridges with a superior curved deck” *Proceedings of the 7th Conference on Arch Bridges “ARCH 2013”*, Split, Croatia, 2013, pp. 1-8 (CD-ROM)
- SCHLAICH, J., and MOSCHNER, T.. “Die Ripshorster Brücke über den Rhein-Herne-Kanal, Oberhausen”, *Bautechnik*, 6(76), 1999pp. 459-462.
- VAN BOGAERT, P., “Bending of Converging Hangers in Steel Tied Arch Bridges.” *Proceedings of the 35th International Symposium on Bridge and Structural Engineering*, jointly organised by IABSE-IASS: ‘Taller, Longer, Lighter’, London, UK, September 20-23, 2011
- VAN BOGAERT, P., “Tied Arch Bridges with Optimised Arrangement of a Limited Number of Hangers.” *Proceedings of the 34th International Symposium on Bridge and Structural Engineering (IABSE): ‘Large Structures and Infrastructures for Environmentally Constrained and Urbanised Areas’*, Venice, Italy, 2010, pp. 1-7 (CD-ROM)

VI. STABILITY ANALYSES OF  
SPATIAL ARCH BRIDGES WITH A  
CURVED DECK



# VI. A) BASIS OF STABILITY ANALYSIS FOR ARCH BRIDGES



## INDEX

1. INTRODUCTION.....	265
2. BUCKLING .....	265
2.1 Codes.....	265
2.2 Research .....	267
2.3 FE software: elastic buckling .....	270
3. IMPERFECTIONS AND GEOMETRICALLY NON-LINEAR ANALYSES.....	271
3.1 Codes.....	271
3.2 Research .....	272
3.3 Built examples of imperfection employed values .....	274
4. CONCLUSIONS AND FUTURE LINES OF STUDY .....	276
REFERENCES.....	277





## 1. INTRODUCTION

There are no existent research studies for the buckling of SABs or geometrically non-linear analyses including imperfections. Only some papers of buckling calculations for specific SABs have been found (Žickis and Cypinas, 2003). Therefore, the state-of-the-art of buckling and equivalent imperfections for planar vertical arch bridges with a straight deck is detailed in the following lines and specific highlights for the differences expected in SABs are commented.

## 2. BUCKLING

SABs have been explained to be submitted to important bending moments (Chapters IV and V). However, lateral torsional buckling due to bending moments is not considered in the present research. It is not likely to take place, since closed cross-sections with enough diaphragms to avoid distortion are employed. Torsional buckling (caused by compression buckling in-plane of the arch with two elements, such as in a double arch, buckling in opposite directions) is also disregarded for the same reason. When employing a stiff cross-section formed by two frame boxes (Table 1-1 of section 1.6 of Chapter V. B), the frames are considered stiff enough for torsional buckling not to take place.

Plates are considered thick enough to avoid local buckling.

Therefore, the present state-of-the-art and research study are devoted exclusively to compression buckling.

### 2.1 Codes

The loading distribution for which  $N_{cr}$  is given in Eurocode 3 (EC3, 2006) Part 2 Annex D3 is not clearly stated, but, according to Figure D.4 in EC3 and to the formulation in Galambos (1988), it is for a uniformly distributed vertical load in the whole deck length.

EC3 Part 2 Annex D3 employs the following formulae to calculate elastic buckling for arches:

#### Arch in-plane buckling

$$N_{cr} = \left( \frac{\pi}{\beta \cdot s} \right)^2 \cdot EI_y \quad \text{Eq1}$$

$N_{cr}$  is the critical buckling axial force at arch springing

$s$  is half the length of the arch

$EI_y$  the in-plane flexural stiffness of the arch

$\beta$  is the buckling length factor

Through the factor  $\beta$  the following characteristics of the bridge are considered:

- Bearing conditions and buckling shape (it must be remarked that there are no coefficients in table D4 of Eurocode 3 Part 2 Annex D3 for fixed bridges and symmetric buckling. Therefore not all the buckling shapes and arch types are covered).

- If the deck behaves as a tension tie and has flexible hangers, it is considered: the number of hangers and arch rise related to the bridge length and arch shape

A factor  $K$  is calculated as a criterion to prevent snap-through.

In the case of SABs with curvature in-plan snap-through should also be verified in the horizontal plane. However, a system controlling out-of-plane forces is always necessary and snap-through is not expected to take place in SABs.

#### Arch out-of-plane buckling

$$N_{cr} = \left(\frac{\pi}{\beta \cdot l}\right)^2 \cdot EI_z \quad \text{Eq2}$$

$N_{cr}$  is the critical buckling axial force at arch springing

$l$  is the arch span (projection length)

$EI_z$  the out-of-plane flexural stiffness of the arch

$\beta$  is the buckling length factor

Through the factor  $\beta$  the following characteristics of the bridge are considered:

- The  $f/L$  relationship
- Arch cross-section flexural rigidity ( $I_z$ ): constant or variable
- Inferior or superior deck and the load taken by the struts or hangers in relation to the total load
- There is a specific value of  $\beta$  if the arch is circular with a radial loading
- Arch bracing is considered if there is more than one arch

The codes do not consider the stiffness of the deck and struts or rigid hangers. It is stated in the codes that the out-of-plane buckling factors are for free standing arches. However, in  $\beta$  it is considered whether the deck is inferior or superior and the load taken by the struts or hangers in relation to the total load as stated above, so the value given by the code is not expected to be exactly for a free standing arch loaded itself with the whole load. It seems that the codes might not be considering a certain arch-deck interaction, but it is not clearly stated and the results in VI. B prove that it is not efficiently considered in some cases.

It must be noted that these formulae are for elastic buckling and this value does not consider residual stresses, load eccentricity variations or imperfections. To consider them for other structures buckling curves can be employed but there are no buckling curves for arches, non-linear analyses should be hence conducted (see section 3).

## 2.2 Research

### *Compressive axial forces buckling*

Earliest arch out-of-plane buckling formulae treat the slenderness of the arch as a straight column under uniform compression with identical cross-section and with the arch length equal to the column length. They consider a free-standing arch, with no influence of the deck and hangers/struts.

Galambos (1988, p578) summarizes in a table the different studies (Austin and Ross, 1976; Kollbrunner 1936 and 1942; Timoshenko and Gere, 1961) to determine the critical in-plane buckling load of parabolic, antifunicular or circular arches under a uniformly distributed loading and with either fixed springings or 2-pinned or 3-pinned arches. Studies for vertical asymmetrical uniform loadings from Chang (1973) and Harrison (1982) are also exposed in Galambos (1988, pp579,583 and584). Galambos also presents the aforementioned formulae employed in the EC3.

Timoshenko and Gere (1961) conducted studies of arch in-plane and out-of-plane buckling for circular arches with radial loading applied directly on the arch, also described in Galambos (1988, p594) and Bergmeister et al (2009, p149).

The arch in-plane buckling is usually controlled by the stiffness of the deck and struts or hangers, so formulae for in-plane buckling of free standing arches are not applicable. The out-of-plane buckling will be influenced by the bearing conditions and the stiffness of the strut-deck or hanger-deck system will also have influence in the out-of-plane buckling of the arch, so these formulae are incomplete.

According to Petersen (1980) it is important to consider the buckling for the asymmetrical loading.

The necessity to include material non-linearities and imperfections to obtain an accurate representation of arches was recognized in Japan by the end of the 1970s. Column curves were proposed by Sakimoto et al (1990) based on experiments (Spoorenberg et al, 2012). Their applicability was limited to arches with square hollow sections and rise-to-span ratios between 0,1 and 0,2 and free-standing arches. Since in these Japanese studies the arch was treated as a straight column under uniform compression with identical cross-section and with the arch length equal to the column length, the rise-to-span ratio of the arch was considered to be of minor importance. However earlier theoretical studies than the described column curves already revealed the importance in arch buckling of arch-to-span ratio. Citing Spoorenberg et al (2012): “This was recognized by Ppangelis and Trahair who performed experiments on arch buckling” (...) “According to Pi and Trahair and Pi and Bradford the arch slenderness was defined as the square root of the ratio between the plastic capacity and out-of-plane elastic buckling load, taking implicitly into account the geometric properties of the arch”.

Östlund (1954), Godden (1954) and Shukla and Ojalvo (1971) conducted studies of out-of-plane buckling for parabolic arches with loading applied on hangers and struts, also described in Galambos (1988, p601) and Bergmeister et al (2009, p150). Another study of arch out-of-plane

buckling, which is more recent and complete, but it is specific for open profiles, is Kang and Yoo (1994), described in Bergmeister et al (2009).

There are several studies for braced arches (Galambos, 1988, p601): Tokarz (1971), Östlund (1954), Almeida (1970), Kuranishi (1961) and Sakimoto and Namita (1971).

Bergmeister et al (2009, p153) consider the transverse stiffness of the deck to calculate the out-of-plane buckling load of planar vertical arches with an inferior straight deck longitudinally pinned (Eq3). Horizontal springs are employed to model the stiffness of the deck and a coefficient (Eq 3) is calculated to modify the out-of-plane buckling load obtained by the Eurocode 3 (Eq 2).

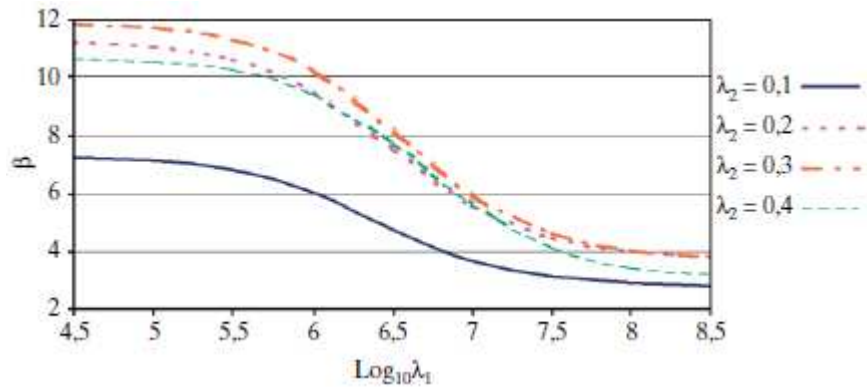
$$q_{cr} = \left( \frac{\pi^2 \cdot EI_{arch}}{L^3} \right) \cdot \beta(\lambda_1, \lambda_2) \quad \text{Eq3}$$

where:

$\beta(\lambda_1, \lambda_2)$  is defined in Figure 2-1

$$\lambda_1 = \frac{L^4}{I_{deck}} \quad \text{Eq4}$$

$$\lambda_2 = \frac{f}{L} \quad \text{Eq5}$$



**Figure 2-1:  $\beta$  values according to Bergmeister et al for Eq3. Figure extracted from Bergmeister et al (2009, p153)**

Considering equations from 3 to 5, the EC3 modified equation is:

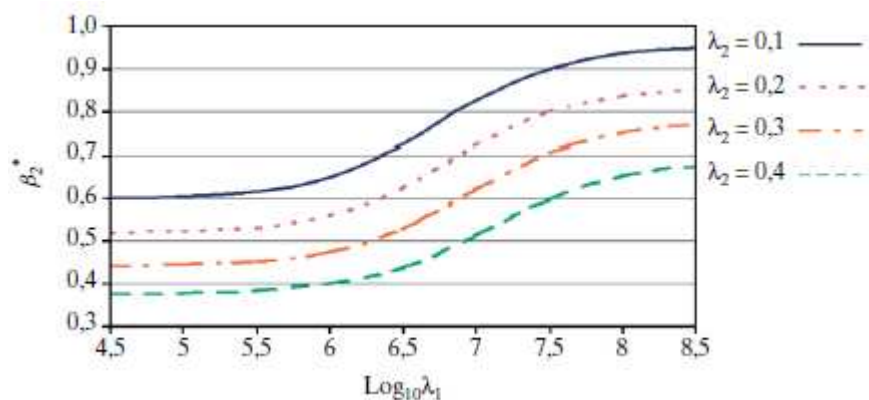
$$N_{cr}^{EC3 \text{ modified}}(\lambda_1, \lambda_2) = \left( \frac{\pi^2 \cdot EI_{arch}}{L^2} \right) \cdot \frac{1}{\beta_1^2} \cdot \frac{1}{\beta_2^{*2}} \quad \text{Eq6}$$

where:

$\beta_1$  is defined in Eurocode 3 Part 2 Annex D3 Table D7

$\beta_2^*(\lambda_1, \lambda_2)$  is defined in Figure 2-2

$\lambda_1$  and  $\lambda_2$  are defined in Eqs 4 and 5, respectively



**Figure 2-2:  $\beta_2^*$  values according to Bergmeister et al for Eq3. Figure extracted from Bergmeister et al (2009, p153)**

Correia (2006) developed a simplified method to consider imperfections and 2<sup>nd</sup> order effects to calculate the out-of-plane buckling load for bow-string braced double arches. The stiffness of the hangers is also considered and the deck is considered “infinitely” stiff.

For a same load SABs stand lower axial forces than vertical planar arch bridges with a straight deck, so compressive axial force buckling is expected to take place for larger load values. However, bending moments increase, so buckling might happen for lower loads. It is therefore not clear whether elastic buckling critical loads will be higher or lower in comparison with equivalent planar arch bridges with a straight with the same span. Elastic buckling of both bridge types will be compared.

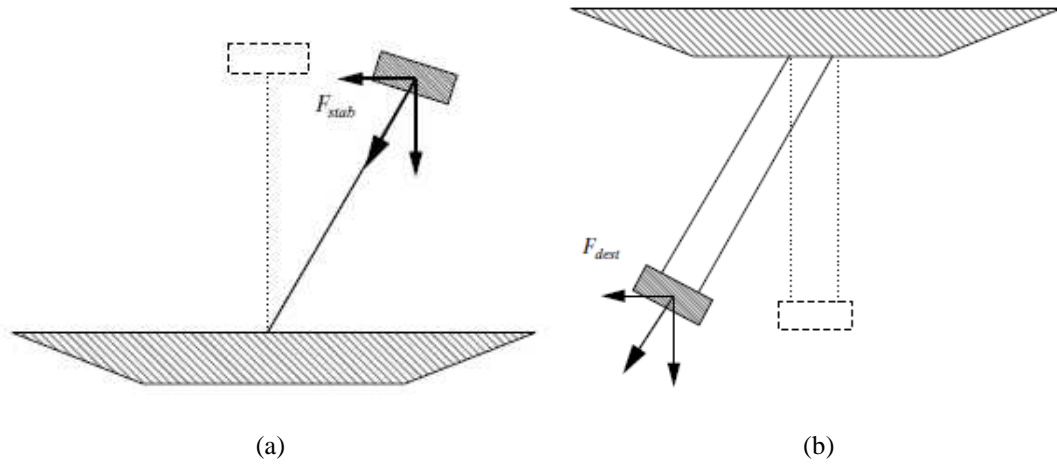
For planar vertical arch bridges with an inferior straight deck a useful simplified formulation would be the one described by Bergmeister et al (2009) to obtain elastic out-of-plane buckling and compared to the elastic buckling results obtained with the buckling analysis of a FE 3D frame model. Eq2 (section 2.1) of EC3 is expected to be more conservative since hangers have a stabilizing effect.

For planar vertical arch bridges with a superior straight deck EC3 formulation (Eq 1 and 2 of section 2.1) will be employed to obtain the simplified load of critical elastic buckling and compared to the elastic buckling results obtained with the buckling analysis of a FE 3D frame model.

According to Petersen (1980, p601) antifunicular arch bridges can already buckle under their self-weight. In 3-pinned arches (pinned at springings and with an articulate joint at span center), the buckling form is symmetrical for  $f/L \leq 0,3$ , and antimmetrical for larger  $f/L$  values.

Petersen separates the loads into two types: those with a “reliable direction” which maintain their direction in spite of the structure deformation and those with a non-reliable direction, which change their direction according to the deformation (Petersen, pp603-604). When considering the whole system instead of the free-standing arch, it is clear that the loading system of the arch changes from having a reliable direction to a non-reliable direction. This means, that not only has the hanger or strut deck system an important influence due to its stiffness contribution but also in the fact that the direction in which the loads are transmitted to the arch changes

according to the deck and struts/ hangers own deformation. Hence the hanger/strut and deck system can have a stabilizing or destabilizing effect on the arch buckling as shown in for inferior and superior deck, respectively (Bergmeister et al, 2009 and Petersen, 1980).



**Figure 2-3: Effect of the deck vertical position on arch buckling (a) Inferior deck stabilizing effect. (b) Superior deck destabilizing effect. Figures extracted from Bergmeister et al (2009, p150)**

### 2.3 FE software: elastic buckling

Only axial forces are considered in a FE software elastic buckling analysis, since the buckling is obtained from the autovalues which make the determinant of the following matrix null:

$$\vec{F} = \{\tilde{K}_0 + \tilde{K}_g\} \cdot \vec{D} \quad \text{Eq7}$$

where:

$\tilde{K}_0$  is the stiffness matrix

$\vec{F}$  is the vector of internal forces

$\vec{D}$  is the vector of displacements

$\tilde{K}_g$  is the geometrical stiffness matrix, which is modified in every iteration when geometrically non-linear effects are considered. It modifies the stiffness of the structure according to the variation of the position where the axial force is applied:

$$\tilde{K}_g = N \cdot \tilde{G} \quad \text{Eq8}$$

where:

N is the axial force value

$\tilde{G}$  is the geometry matrix

However, bending moments also contribute to deform the structure and therefore 2<sup>nd</sup> order effects will be due to both, imperfections and flexural bending moments.

### 3. IMPERFECTIONS AND GEOMETRICALLY NON-LINEAR ANALYSES

Euler buckling accounts for the equilibrium bifurcation and it is meant for “perfect structures”. It is elastic buckling and does not include geometrically non-linear effects, neither plastic, neither local cross-sectional imperfections, off-centered loads, global imperfections, nor residual stresses.

To model these effects, imperfections and residual stresses should be introduced. An equivalent imperfection can also model imperfections and residual stresses. A geometrically non-linear plastic analysis can lead to results which are nearer to reality than elastic buckling. The imperfections will highly influence the geometrically non-linear elastic-plastic behavior.

#### 3.1 Codes

The Eurocode 3 (EC3) Part 1.1 chapter 6.3.1.2 displays buckling curves for compressed members obtained empirically, including imperfections and residual stresses. There are no equivalent buckling curves for arch bridges. Therefore, in order to do an as accurate as possible geometrically non-linear analysis when residual stresses are not modeled, the coded imperfections in EC3 Part 1.1 chapter 5.3.2 should be employed following the first mode of buckling shape as stated in Eurocode 3. These imperfection values are expected to be conservative.

Moreover, this part of the code is specific for buildings. Therefore, the specific values for imperfections in arches in EC3 Annex D.3.5 are also employed to check the sensitivity of SABs to imperfections.

The in-plane imperfections to consider for arches, according to the code EAE 22.3.4 and EC3 Annex D.3.5 Table D.8 are shown in Table 3-1.

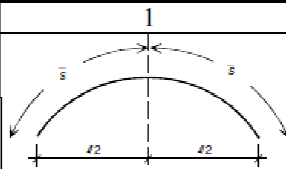
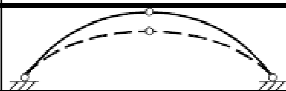
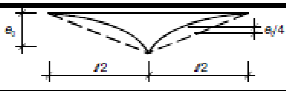

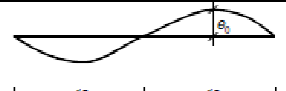
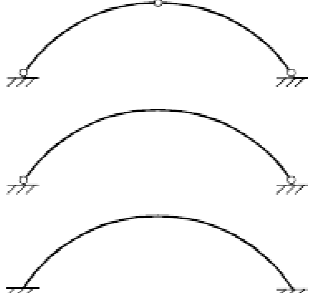
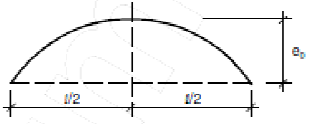
	1	2	3			
			e <sub>0</sub> according to classification of cross section to buckling curve			
		shape of imperfection (sinus or parabola)	a	b	c	d
1			$\frac{s}{300}$	$\frac{s}{250}$	$\frac{s}{200}$	$\frac{s}{150}$
2			$\frac{l}{600}$	$\frac{l}{500}$	$\frac{l}{400}$	$\frac{l}{300}$

Table 3-1: Shape and amplitudes for in-plane buckling of arches. Table extracted from Table D.8 of EC3 Annex D.3.5

The out-of-plane imperfections to consider for arches, according to the code EAE 22.3.4 and EC3 Annex D.3.5 Table D.9 are shown in Table 3-1.

	shape of imperfection (sinus or parabola)	$e_0$ according to classification of cross section to buckling curve				
		a	b	c	d	
		$l \leq 20 \text{ m}$	$\frac{l}{300}$	$\frac{l}{250}$	$\frac{l}{200}$	$\frac{l}{150}$
		$l > 20 \text{ m}$ $l_1 = \sqrt{20} \ell [\text{m}]$	$\frac{l_1}{300}$	$\frac{l_1}{250}$	$\frac{l_1}{200}$	$\frac{l_1}{150}$

**Table 3-2: Shape and amplitudes for out-of-plane buckling of arches. Table extracted from Table D.9 of EC3 Annex D.3.5**

### 3.2 Research

Outtier et al (2007) have developed an analytical method to calculate the equivalent out-of-plane imperfections of a constructed arch bridge. Strains are measured by means of gauges and a detailed analytical model was developed. Comparing the stresses in the model and the ones obtained from the strain measurements an equivalent imperfection was calculated and appeared to be approximately  $L/1000$ , for  $L$  the arch span. In a sequel paper (De Backer et al, 2009) they calculate the buckling loads of different variants of the aforementioned bridge and also four other bridges examples employing the calculated imperfections out-of-plane with a sinusoidal deformed shape. A curve is plotted with the results and it is compared with the buckling curves of EC3 Part 1.1 chapter 6.3.1.2.

Manzanares et al (2011) also plot such curves but for clamped and hinged arches and employing a cosine function for the deformed shape out-of-plane and a maximal imperfection  $L/1000$  additional to residual stresses. Residual stresses are introduced in their model, but the equivalent imperfection to residual stresses is not given. Neither is a relation between stresses caused by the geometrical imperfection and residual stresses given. Obtaining such a value would be interesting. It could then be evaluated which part of the coded imperfections should be considered as residual stresses for different bridge types and cross-sections.

The results from De Backer et al (2009) and Manzanares et al (2011) are all above curve a. It is concluded that the coded buckling curves are conservative for arches, since according to the cross-section, as stated in De Backer et al (2009) curve b should be employed.

For planar vertical arch bridges with a straight inferior deck (bow-tie) and a triangular hanger distribution, De Backer et al (2009) demonstrate that buckling is highly influenced by employing POT or neoprene bearings and the shape and the direction and the direction of the geometrical out-of-plane imperfections.

Manzanares et al (2011) also compare their results with critical stress values of out-of-plane buckling for parabolic arches with uniformly distributed vertical ultimate load obtained by



Sakimoto and Komatsu (1977, referenced in Manzanares et al, 2011), relating the arch cross-section shape factor to the proportion  $q_u/q_p$  (where  $q_u$  is the uniformly distributed vertical ultimate load obtained with a series of non-linear elastic–plastic analyses and  $q_p$  the uniformly distributed vertical load that produces yielding by compression in the extremes of the arch when a first order study is performed). They obtain similar curves. An interaction surface with the parameters  $q_u/q_p$ ,  $L$ , and the shape form for hinged and clamped arches has been adjusted Manzanares et al (2011). It enables the size of the arch to be calculated when considering lateral buckling. An analysis of the “ $L-q_u/q_p$ ” graph indicates that the results are similar to those obtained in EC3 (Part 1.1 chapter 6.3.1.2) for the buckling curves ( $\chi-\lambda_y$ ), although in EC3, the  $\alpha$  imperfection factor influences the results, whilst in Manzanares et al (2011) the results depend upon the shape factor.

According to Manzanares et al, 2011, “*the real ultimate lateral strength of the arches is calculated and confirms that, previous to the final collapse of the structure, a disproportionate increase in the arch centre lateral displacement occurs, which constitutes a clear sign of the breakage by lateral buckling*”.

For planar vertical arch bridges with inferior straight deck a useful simplified formulation would be the one described by Bergmeister et al (2009) to obtain elastic lateral buckling and it should be modified according to the buckling curve  $a$  to consider residual stresses, imperfections and 2<sup>nd</sup> order effects, according to the results of Outtier et al (2007) and Manzanares (2011). This is still expected to be conservative.

In the present research a benchmark has been developed (chapter III. B section 2.5), employing the program SAP2000 v14 which is used for the present research. It confirms that the coded imperfections in EC3 Part 1.1 chapter 5.3.2 are conservative for a straight beam with respect to the buckling curves of EC3 Part 1.1 chapter 6.3.1.2

Since according to Backer et al (2009) buckling curves in EC3 Part 1.1 chapter 6.3.1.2 are also conservative for arches, the imperfection coded in EC3 Part 1.1 chapter 5.3.2 is conservative when developing an equivalent buckling curve, ***EC3 Part 1.1 chapter 5.3.2 calculation method can be safely used for arch bridges and will be considered valid for SABs in the present research.***

Manzanares et al (2011) modeled residual stresses in a FE mode and considered a  $L/1000$  out-of-plane imperfections value. This means that an equivalent imperfection would be larger than  $L/1000$ , value obtained by Outtier et al (2007). Since only one example (for the specific case of a bow-tie hanging of two braced arches with a triangular hanger distribution) was calculated by Outtier et al(2007) and no further equivalent imperfection values calculated to match real measured strains have been found in published researches, it will be considered that the minimal and maximal imperfection values to employ in the present research are:

Min  $e_0 = \{L/1000; e_0 \text{ from EC3 Part 1.1 chapter 5.3.2}; e_0 \text{ from EC3 Annex D.3.5}\}$

Max  $e_0 = \{e_0 \text{ from EC3 Part 1.1 chapter 5.3.2}; e_0 \text{ from EC3 Annex D.3.5}\}$

Considering the state-of-the-art of buckling a geometrically non-linear analyses of arch bridges, the buckling analyses of spatial arch bridges with a curved superior deck and a planar vertical arch have been conducted and a study has been devoted to non-linear analyses of spatial arch bridges with a curved superior deck and a planar vertical arch, employing different imperfection values. The objective is to evaluate the buckling and geometrical non-linear imperfections sensitivity of this bridge type, in comparison to planar vertical arch bridges and in relation to different parameters.

These two research studies are detailed in the following different sections B and C in the present chapter.

### 3.3 Built examples of imperfection employed values

There are hardly no published construction imperfection measures as far as the authors know.

The values of the Dreiländerbrücke spatial arch bridge (Figure 3-1a) have been provided by Leonhardt, Andrä und Partner and reach a value of 83mm for vertical displacements at the arches crowns, considering assembly in workshop and erection values.

This was considered negligible for the bridge structural calculations, in which an in-plane imperfection value of 300mm was employed<sup>1</sup>. However, the 300mm include the equivalent imperfection of residual stresses. If 83mm are considered as constructive imperfections out of 300mm, the off-centered loads and residual stresses have a value of  $(300-83)=217$ mm, which is very large according to usual experience. Therefore, the coded imperfections can be considered conservative. However, the usual comparison which is carried out in the construction control of “*measured imperfection value*” < “*imperfection value employed for calculation*” is not always reliable. This control procedure needs to be coded.

The Dreiländerbrücke consists of a double vertical steel arch and an inclined steel arch braced to the latter. The arches have 229,4m span (L) and a 20m rise (f), which is equal to  $L/11,5$ . The middle deck hangs from the arches 196,2m (span L') by means of a hanger system for each arch anchored to the deck edges (Figure 3-1a). The rise above the deck is  $f'=14$  m, equivalent to  $L'/14$ . The 83mm vertical imperfection value is equal to  $L'/2364 = f'/169 = L/2764 = f/241$ .

---

<sup>1</sup> according to DIN 18800/2, section 6.3 Tables 23 and 24 (values equal to those stated by EC3 Part 1.1 chapter 6.3.1.2 buckling curves, curve b for all the arches). Out-of-plane a 250mm value was employed. Both of these values are based on the span of the deck hanging from the arch (ie: measured in between the points where the deck crosses the arch).

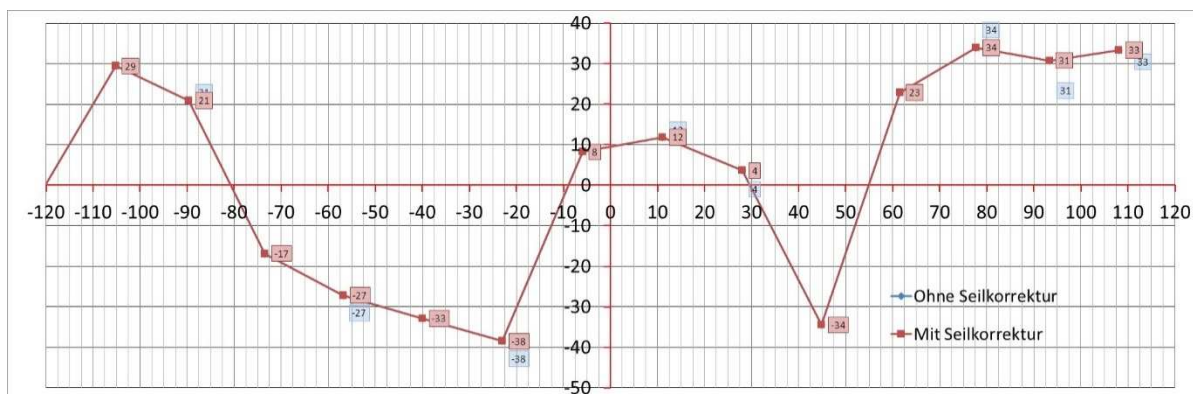


**Figure 3-1: (a) Dreiländer bridge (b) Nijmegen bridge (both images reproduced by kind permission of Hans-Peter Andrä).**

A planar vertical arch bridge example is the Nijmegen bridge (Figure 3-1b). It has a steel arch with 285m span ( $L$ ) and a 60m rise ( $f$ ), which is equal to  $L/4,75$ . The inferior deck hangs from the arch by means of a double hanger system anchored at the deck edges. The hangers of each hangers-system criss-cross once. The maximal construction vertical imperfections of the arch of the Nijmegen bridge have been also provided by Leonhardt, Andrä und Partner. They have a value of 38mm near to the span centre, 34mm at approximately  $L/3$ , 33mm at one of the springings and 10mm at span center (Figure 3-2). The 38mm maximal vertical imperfection value is equivalent to  $L/7500$  and approximately  $f/1580$ .

The EC3 establishes values of a total in-plane imperfection of  $L/500$  for buckling curve b. This would give an imperfection of 570mm for the Nijmegen bridge. If 38mm are considered as constructive imperfections out of 570mm, that would mean that load eccentricity variation and residual stresses have a value of  $(570-38)=532$ mm, which is very large.

Out-of-plane imperfections are often not measured in construction control and no data have been obtained.



**Figure 3-2: Measured imperfection vertical values along the axis of the Nijmegen Bridge (Reproduced by kind permission of Hans-Peter Andrä). Vertical axis in mm, horizontal axis in m, origin at the bridge span center**

#### 4. CONCLUSIONS AND FUTURE LINES OF STUDY

- The hanger/strut and deck system can have a stabilizing or destabilizing effect on the arch buckling
- Codes and research give buckling formulation but the hypothesis under which these formulae are valid are not clearly stated and not all cases for arch bridges are included.
- There are no equivalent European buckling curves for arch bridges. According to several researches, the coded buckling curves in Eurocode 3 Part 1.1 chapter 6.3.1.2 are conservative for arches.
- The values of the imperfections and geometry for arch bridges in order to conduct a geometrically non-linear analyses can be obtained in two different ways according to Eurocode 3 (EC3): as complex structures with the geometry based on the buckling shape (EC3 Part 1.1 chapter 5.3.2) or specifically for arches (EC3 Annex D.3.5). The latter separates in- and out-of-plane imperfections.
  - Buckling curves in EC3 Part 1.1 chapter 6.3.1.2 are conservative for arches (Backer et al, 2009)
  - coded imperfections in EC3 Part 1.1 chapter 5.3.2 are conservative for a straight beam with respect to the buckling curves of EC3 Part 1.1 chapter 6.3.1.2 according to the benchmark developed in the present study.
  - Therefore, *EC3 Part 1.1 chapter 5.3.2 calculation method can be safely used for arch bridges.*
- There are hardly no published construction imperfection measures as far as the authors know.
- When imperfections measured in the construction site are compared to those stated by the codes for the design analyses, the difference should correspond to residual stresses. However the value is very large, coded imperfections might be far too much on side of security. Empirical studies should be conducted.

## REFERENCES

BERGMEISTER K., CAPSONI A., CORRADI L., MENARDO A., “Lateral Elastic Stability of Slender Arches for Bridges including Deck Slenderness”. *Structural Engineering International*, n. 2 v. 19. pp. 149-154(6). May 2009

CORREIA, Antonio A.; VIRTUOSO, Francisco B. E.. “Comportamento nao linear de uma ponte “bow-string” metálica”. *V Congresso de Construcao Metálica e Mista*. Abril 2005 (in portuguese)

DE BACKER H, OUTTIER, A., , and VAN BOGAERT, P. “The effect of using beam buckling curves on stability of steel arch bridges” *Proceedings of the Nordic Steel Construction Conference*, 2009. Available at: <<http://www.nordicsteel2009.se/pdf/43.pdf>>

GALAMBOS, T. V.. *Guide to stability design: Criteria for metal structures*. 4th Ed, pp15-25, pp575-608, pp609-625. New York: John Wiley & Sons, 1988. ISBN: 0-471-09737-3

MANZANARES J. L. and HINOJOSA, I., “Non-linear plastic analysis of steel arches under lateral buckling”. *Journal of Constructional Steel Research*, i. 12, v. 67. pp 1789-1984. December 2011

OUTTIER, A., DE BACKER H, and VAN BOGAERT, P. “Assessment of the out-of-plane imperfections of a steel tied arch bridge” *ARCH '07. Proceedings of the 5th International Conference on Arch Bridges*. Madeira, Portugal September 12-14, 2007. pp. 249-256

PETERSEN C. *Statik und Stabilität der Baukonstruktionen: Elasto- und plasto-statische Berechnungsverfahren druckbeanspruchter Tragwerke: Nachweisformen gegen Knicken, Kippen, Beulen* [Gebundene Ausgabe]. 960pp Verlag: Vieweg Verlagsgesellschaft; Auflage: 2., durchges. Aufl. 1982 (24. Oktober 1982) (in German) ISBN-10: 3528186631 ISBN-13: 978-3528186630

SPOORENBERG, R.C., SNIJDER, H.H., HOENDERKAMP, J.C.D. and BEG, D. “Design rules for out-of-plane stability of roller bent steel arches with FEM”. *Journal of Constructional Steel Research*, 79, 9-21. 2012

TIMOSCHENKO, S.; GERE, J.M.. *Theory of Elastic Stability*. New York: McGraw Hill. 1961

ŽICKIS, D. and CYPINAS, I. “Design and construction of a steel arch bridge in Vilnius over the Neris” *Proceedings of the 25th International Baltic Road Conference*. Vilnius, 2003. Available at: <[http://www.balticroads.org/downloads/25BRC/25brc\\_e1\\_zickis\\_1.pdf](http://www.balticroads.org/downloads/25BRC/25brc_e1_zickis_1.pdf)>



**VI. B) BUCKLING ANALYSES OF  
SPATIAL ARCH BRIDGES WITH A  
CURVED DECK**





## INDEX

1. INTRODUCTION .....	283
1.1 Previous considerations .....	283
1.2 Studied parameters .....	285
1.3 Objectives .....	287
1.4 Loading cases and combinations .....	287
1.5 Research procedure and values .....	288
2. ARCH BRIDGES WITH A SUPERIOR DECK.       BUCKLING RESULTS.....	292
2.1 ARCH RISE ( $f$ ) AND BEARING CONDITIONS INFLUENCE ON BUCKLING	293
2.2 CROSS-SECTION VALUES INFLUENCE ON BUCKLING .....	301
2.3 STRUTS INCLINATION IN LONGITUDINAL VIEW ( $\beta$ ). INFLUENCE ON BUCKLING .....	309
2.4 3D BUCKLING: DECK INFLUENCE ON THE BUCKLING OF SABWSCD .....	316
3. ELASTIC BUCKLING OF INFERIOR DECK ARCH BRIDGES.....	317
3.1 Analyses of the results for reference cross-section values .....	318
3.2 Analyses of the results for a rigid hanger-deck system .....	321
4. COMPARISON OF NUMERICAL RESULTAS VERSUS ANALYTICAL RESULTS OF THE BUCKLING LOADS .....	322
4.1 Planar arch bridges with a superior straight deck. Analytical and numercial results comparison for different bearing conditions .....	322
4.1.1 Considerations .....	322
4.1.2 Analyses of the results.....	323
4.2 Superior deck arch bridges. Analytical and numerical results comparison for different $g$ and $f$ values and for different deck stiffness values.....	325
4.2.1 Considerations .....	325
4.2.2 Analyses of the results.....	325
4.3 Inferior deck arch bridges. Analytical and numerical results comparison for.....	328
5. CONCLUSIONS .....	330
6. FUTURE LINES OF STUDY .....	331
REFERENCES .....	331



## 1. INTRODUCTION

### 1.1 Previous considerations

It is noteworthy that, for the studied bridge type, there is no buckling design criteria and, for arch bridges, there is also a very little number of reliable formulations and not all the cases are covered.

A detailed state-of-the-art of the stability of arches can be read in chapter VI. A section 2.

The formulation of Eurocode 3 (Part 2, 2006) does not consider the hanger or struts' distribution possibilities, nor the arch inclination, nor the deck stiffness, nor the imperfections nor the second order effects, neither the case of non-planar arches.

Recent research studies to obtain the buckling load include the rigidity of the deck (*Bergmeister et al, 2009*) and others the imperfections and second order effects (*A. A. Correia, 2006*). However, they are specific for vertical, planar arch bridges with a straight inferior deck and for certain bearing conditions. A formula which considers those different criteria at the same time has still not been developed and buckling curves have been proved to be too conservative (*De Backer et al, 2009, and Manzanares et al, 2011*). Moreover, the aforementioned formulations are for arches with hangers and for a vertical loading contained in the arch's plane. But SABs undergo out-of-plane effects already for vertical loadings. The hangers or struts might not even be in the plane of the arch and the arch might also not be contained in a plane. For SABs employing a planar arch, buckling is expected a priori to take place in both planes (in-plane and out-of-plane of the arch).

It is expected that buckling has a relationship with the following values:

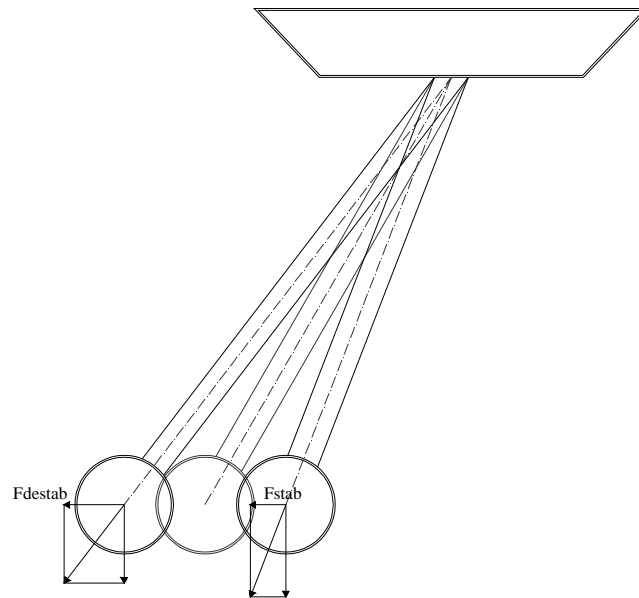
- Axial forces in the arch
- Displacements in the arch and deck
- Arch stiffness
- Deck boundary conditions
- Deck stiffness
- Struts stiffness

They are all related to the geometry of the bridge and the stiffness of the different elements.

A priori it is impossible to determine whether the deck has a stabilising or destabilising effect in SABs because:

- it is not clear whether the arch will buckle in-plane or out-of-plane
- if the hypothesis of out-of-plane buckling is made:
  - The struts have different inclinations in different cross-sections of the bridge and they will have a stabilising effect in one direction of the buckling and a destabilising effect in the other direction. The destabilizing effect is larger due to the increase of the struts' inclination in that direction (Figure 1-1).

- As in the case of  $g=0$ , the stabilising effect cannot be reliably stated, since the deck will move with the arch. Figure 1-1 or the figures shown in chapter VI.A for various researches for  $g=0$  (Bergmeister et al, 2010 and Galambos 1988), are not considering the movement of the deck and its bearing conditions that might change the hypothesis that its effect on the arch when employing a superior deck is destabilising. Fixing the transverse movement of the deck would be expected to have a stabilising effect.



**Figure 1-1: Stabilising or destabilising effects of struts on SABs**

The present study does not pretend to obtain a specific formulation, but to give an idea of the elastic buckling behavior of this bridge type and whether it will be conditioning for the design. Imperfections are not considered in the present chapter. A further research including imperfections is conducted in chapter VI. C.

The elastic buckling loading and shape is obtained for a series of 3D FE frame models with SAP2000. Two of the models have been compared with equivalent models analysed in SOFISTIK and ABAQUS and equivalent results have been obtained.

For spatial arch bridges with superior curved deck (SABWSCD) and a planar vertical arch, a broad study has been conducted. It is based on the results of chapter V. B. The influence different parameters on the buckling shape and loading is analysed.

In order to understand the behaviour of these arches, different frame 3D models have been developed and analyzed with commercial software, as part of a set of thorough parametric analyses (parameters described in section 1.2). As described in the parametric study analyses (chapter V. B), the deck plan curvature is measured as horizontal sag ( $g$ ), the arch rise is called  $f$ , the arch/deck eccentricity in plan view is  $e$ , the distance between arch and deck at span center is  $v$  and the arch and deck spans are  $L_{SA}$  and  $L_{SD}$  respectively and are considered equal ( $L$ ) in all models.  $\beta$  is the longitudinal inclination of the struts in relation to the reference distribution

obtained by dividing the arch and deck uniformly (radial distribution,

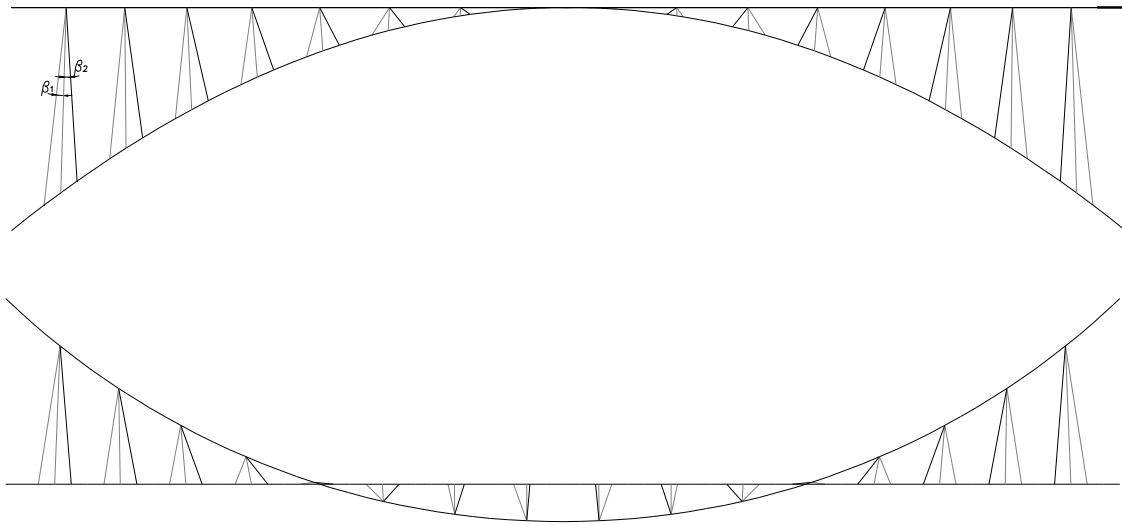


Figure 1-2). Please employ the bookmark to see these parameters in the figure.

In section 4.3, a case study for inferior deck arch bridges with imposed curvature (IDABWIC, defined in chapter IV) is also conducted.

Planar arch bridges are also analysed and the results of the buckling loads are compared with equivalent SABs with the same span ( $L$ ) and the same rise ( $f$ ), with the results obtained for the aforementioned formulations.

As mentioned in section A2.1 of the present chapter VI, the loading distribution for which  $N_{cr}$  is given in Eurocode 3 (EC3) Part 2 Annex D3 is not clearly stated, but, according to Figure D.4 in EC3 and to the formulation in Galambos (1988) (commented in section 2.2 section A of the present chapter), it is for a uniformly distributed vertical load in the whole deck length. Therefore, in the present research the criteria that  $N_{cr}$  is the largest axial force value in the arch under a uniformly distributed vertical loading on the whole deck length has been adopted. The loads are detailed in section 1.4.

## 1.2 Studied parameters

Based on the results of the parametric analyses of chapter V.B, the most efficient  $e$  value (please check the nomenclature of the figure in the bookmark) for the maximal deck curvature  $g=20\text{m}$  is employed for the curved superior deck SAB models of the present buckling study.

The influence of  $f$  on the arch buckling is analysed (Figure 1-3), as well as the influence of employing different cross-sections, ie: influence of the stiffness distribution of arch, deck and struts.

The influence of angle  $\beta$  (

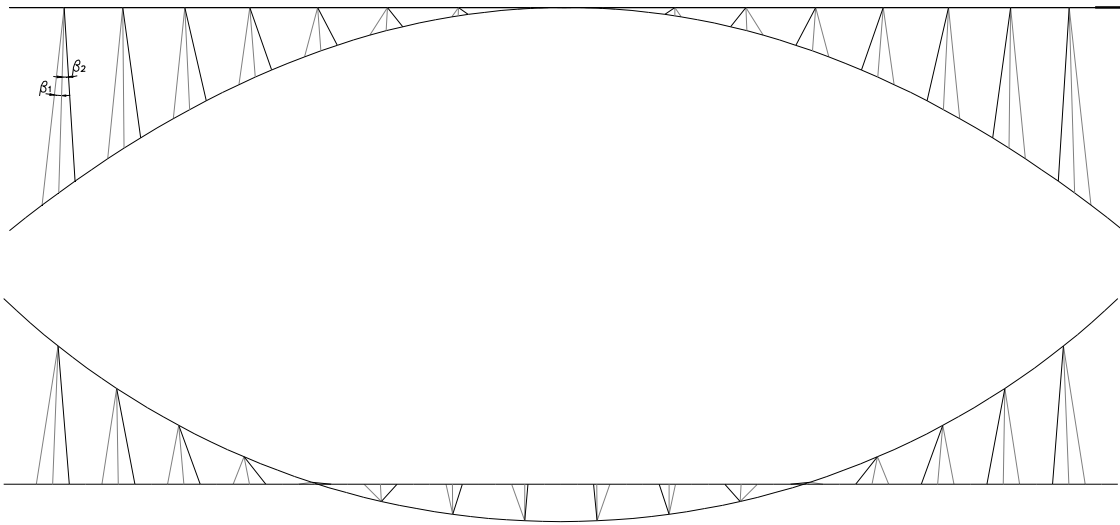


Figure 1-2) on buckling is also analysed. For such a purpose  $f=25\text{m}$  and design cross-sections values with a stiffer deck (Table 1-6) are employed, for SABWSCD with a planar vertical arch with  $g=20\text{m}$  and  $e=16,57\text{m}$ .

The reference model employed for the strut distribution is the one obtained from equal divisions of arch and deck. This strut distribution is called a radial system of struts in the present study. Each strut axis elongation converges below the deck with its symmetrical (

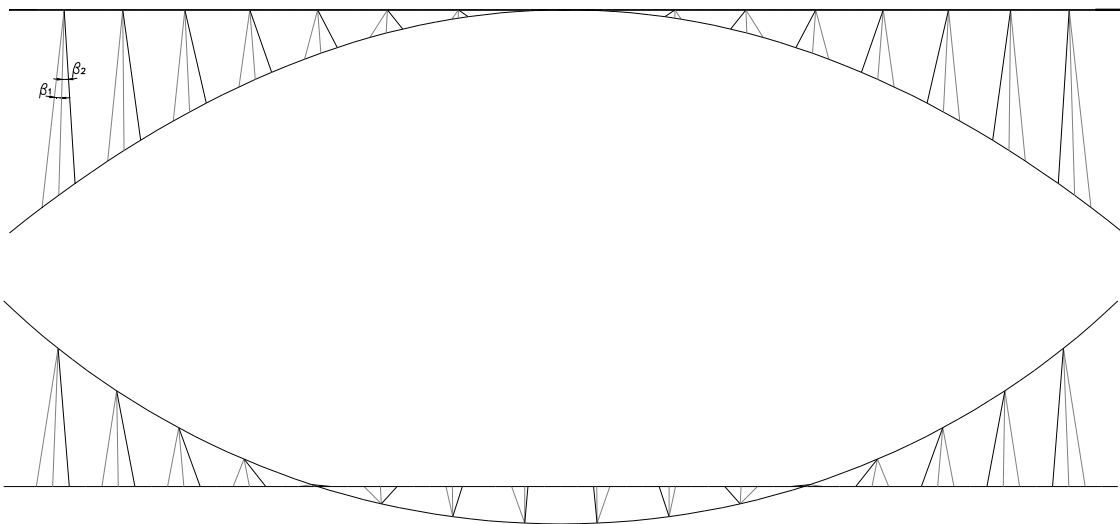


Figure 1-2). These are taken as the reference orientation, considering  $\beta=0$  for each strut. A more vertical orientation ( $\beta_2$ ) of the struts and a distribution of struts in which each strut axis elongation converges above the deck with its symmetrical ( $\beta_1$ , opposite inclination to the original system)

have also been studied (

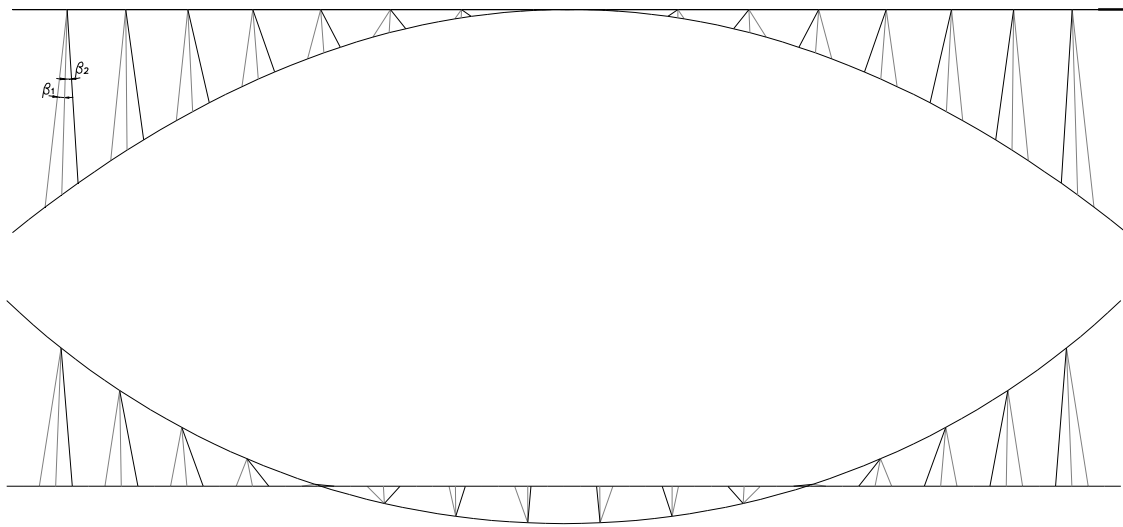


Figure 1-2). The latter distribution is called a convergent system of struts in the present study.

The buckling of IDABWIC with  $g=20\text{m}$  and  $f=20\text{m}$  and reference cross-sections of Table 1-1 is also analysed and compared with a planar vertical arch bridge with straight deck for different cross-section values.

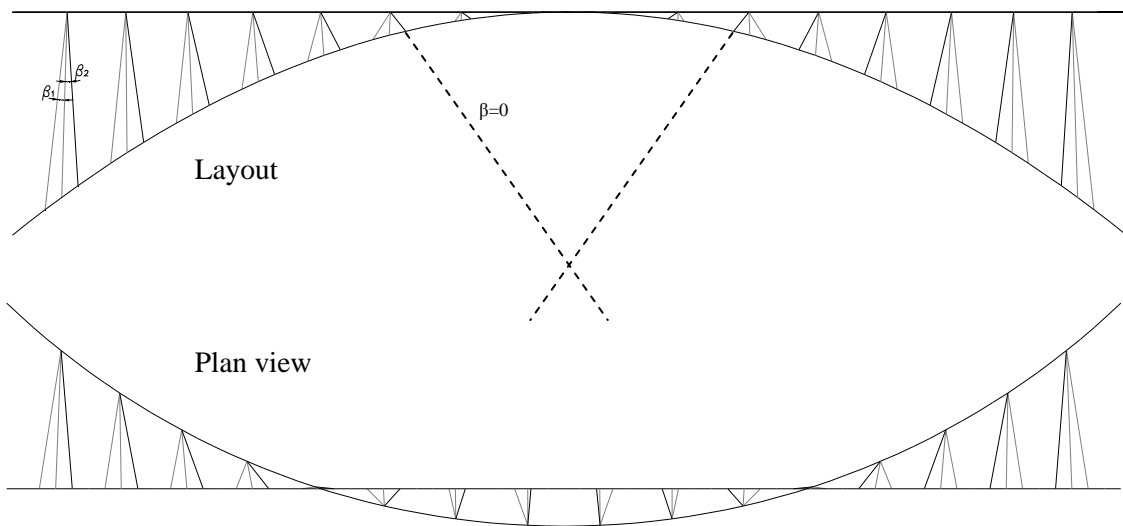


Figure 1-2: Geometry of  $\beta$  variation for  $L=100\text{m}$ ,  $g=f=L/5=20\text{m}$   $e=g/1,2=16,67\text{m}$ ,  $v=0$

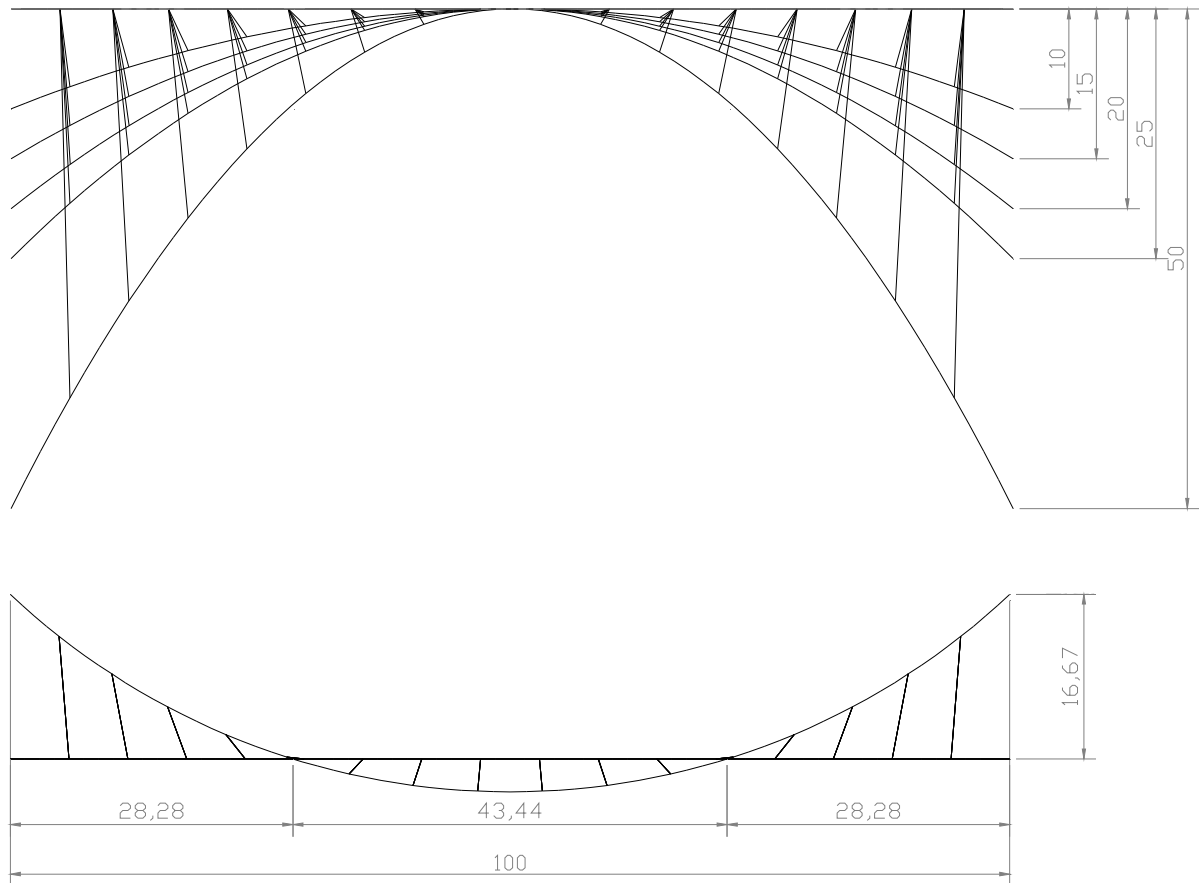


Figure 1-3: Geometry of  $f$  variation ( $f=10, 15, 20, 25$  and  $50\text{m}$ ) for  $L=100\text{m}$ ,  $g=20\text{m}$ ,  $e=L/1,2=16,67\text{m}$ ,  $\nu=0$

### 1.3 Objectives

The purpose of our study is:

- to analyse the influence of different parameters ( $f$ ,  $\beta$ ,  $EI$  and  $GJ$  of arch, struts and deck) on the buckling shape and loading of SABWSCD with a planar vertical arch with  $g=0$  and  $g=20\text{m}$  and  $e=16,57\text{m}$
- to analyse the buckling behaviour of IDABWIC with  $g=20\text{m}$  and  $f=20\text{m}$  and different cross-sections
- to compare the buckling shape and loading of SABs with that of equivalent (ie: with the same arch rise ( $f$ ) and span ( $L$ ) values) planar vertical arch bridges with a straight deck
- to evaluate the validity of different existing formulations for the determination of arch bridge buckling values
- to evaluate the worst live load distribution for SABs buckling



### 1.4 Loading cases and combinations

The loading combinations A1 and A2 are employed for the elastic buckling analyses with SAP2000. These load case combinations have been considered according to the ultimate state response of EC1 Part 2.

Different buckling coefficient values have been obtained:

The buckling coefficient  $\alpha$  corresponds to the live load in the combination A1, ie:

- Combination A1 for elastic buckling:  $1,35 \cdot (w+pl) + \alpha \cdot lu$

The buckling coefficient  $\alpha_1$  corresponds to the combination A1, ie:

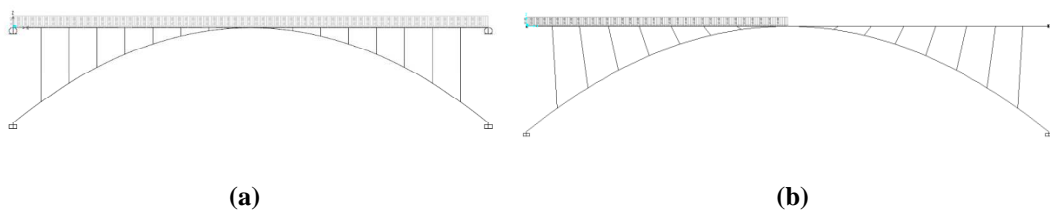
- Combination A1 for elastic buckling:  $\alpha_1 \cdot [1,35 \cdot (w+pl) + 1,5 \cdot lu]$

The buckling coefficient  $\alpha_2$  corresponds to the combination A2, ie:

- Combination A2:  $\alpha_2 \cdot [1,35 \cdot (w+pl) + 1,5 \cdot la]$

In these combinations for the elastic buckling:

- $w$  is the self-weight, with a steel weight of  $76,97 \text{ kN/m}^3$
- $pl$  is the permanent load of  $2,5 \text{ kN/m}^2$ . Considering 4m width:  $pl=10 \text{ kN/m}$
- $lu$  is a uniform live loading on the whole length of the deck (Figure 1-4a) and
- $la$  is an asymmetrical live loading on half the length of the deck (Figure 1-4b)
- Live loads value is of  $5 \text{ kN/m}^2$  according to EC1 Part 2. Section 4.3.5. Considering 3m of usage width, employing the rest of the width for the railings, *the value of live loads is 15kN/m.*
- In the case of  $\alpha$ , the buckling analysis starts after the geometrically non-linear analysis (GNLA) of the permanent load state:  $1,35 \cdot (w+pl)$
- In the case of  $\alpha_1$  and  $\alpha_2$ , the whole analysis is elastic, ie: the elastic buckling analysis starts from an unstressed state.
- The self-weight ( $w$ ) and the permanent load ( $pl$ ) are not scaled by the buckling coefficient  $\alpha$ , but they are by  $\alpha_1$  and  $\alpha_2$ .
- Note that ULS coefficients are included in the loads and are all affected by  $\alpha_1$  and  $\alpha_2$ , but, in the case of coefficient  $\alpha$ , the ULS coefficient of the live load is not included in the load, but in  $\alpha$ .



**Figure 1-4: Load system: 15kN/m (a) on the whole length of the deck ( $lu$ ) and (b) on half the length of the deck ( $la$ )**

### 1.5 Research procedure and values

The values employed in the different frame 3D models are described in the following paragraphs. Please employ the bookmark to see these parameters in the figure.

In all the models a vertical planar arch has been employed.

The arch is fixed at its springings. The struts are fixed to both, arch and deck.

Different bearing conditions have been considered for the deck at abutments:

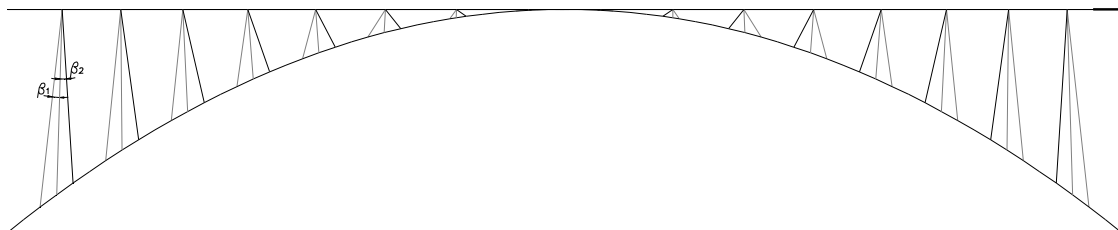
- The deck is always pinned at the abutments.
- Transverse and vertical displacements are always restrained, if not mentioned specifically.
- Longitudinal displacements can be restrained (rtr) or free (ftr).
- Torsional rotations can be restrained (rtr) or free (ftr).

This comparison is conducted since it is the best configuration for internal forces to fix longitudinal displacements for  $g=20\text{m}$  but to free them for  $g=0$ , as indicated in chapter V. A. In order to compare the buckling it makes sense to compare each model at its best, but also to compare them in identical conditions. Torsional rotations would be considered to be restrained in both models in practice, though for a linear analysis for  $g=0$  it is not necessary. The possibility to free torsional rotations has been considered just as a theoretical possibility in order to test its influence on buckling.

For all the studies presented, the following dimensions have been employed:

- $L_{SA}=L_{SD}=L=100\text{m}$ ;
- $g=0$  and  $20\text{m}$
- $e=g/1,2=16,67\text{m}$  for  $g=20\text{m}$  as recommended in chapter V.B
- $f$  varying from  $L/10=10$  to  $L/2=50\text{m}$  (Figure 1-3)
- $\nu=0$

The shape of the arch is always a parabola. 16 struts have been employed in all the models. The inclination of the struts is determined by the uniform division of the deck and the arch for all the models, which leads to a radial distribution. As stated, a study of the influence of the inclination of the struts in longitudinal view ( $\beta$ ) is conducted, considering radial, vertical and convergent struts



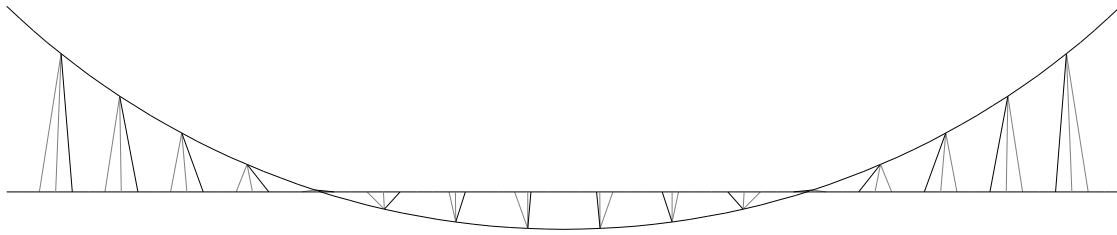


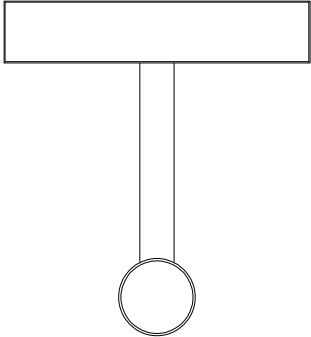
Figure 1-2).

The material employed is steel with a  $2,0 \cdot 10^8$  kN/m<sup>2</sup> modulus of elasticity (E).

A linear buckling analysis has been employed.

Different cross-section values have been considered and compared:

- Reference cross-section values (Table 1-1): the stiffness of the different elements is equal for all the models, so that buckling differences between models are not due to the employed cross-sections, but to the geometry.
- Design cross-section values (Table 1-2, Table 1-3 and Table 1-4): the stiffness of the different elements is different for each model. The comparison of the buckling coefficients is a more realistic value, since bridges which satisfy the ULS are being compared.
- Design arch and struts cross-section values (Table 1-5 and Table 1-6) and a thicker deck: the influence of the stiffness of the deck is being evaluated.
- A less stiff deck (Table 1-7)

Reference model	
	
ARCH	CHS D=1m; t=30mm A= 0,0914m <sup>2</sup> J= 0,0215m <sup>4</sup> I2= 0,0108m <sup>4</sup> I3= 0,0108m <sup>4</sup>
DECK	BOX GIRDER 4000x800mm; t=15mm A= 0,1431m <sup>2</sup> J= 0,0615m <sup>4</sup> I2= 0,2517m <sup>4</sup> I3= 0,0196m <sup>4</sup>
STRUTS	CHS D=451mm;t=22,6mm A= 0,0304m <sup>2</sup> J= 0,0014m <sup>4</sup> I2= 0,0007m <sup>4</sup>

	$I_3 = 0,0007m^4$
--	-------------------

**Table 1-1: Reference cross-sections**

$g=20m$					
	$f=10m$	$f=15m$	$f=20m$	$f=25m$	$f=50m$
ARCH	CHS D=750mm; t=40mm A= 0,0892m <sup>2</sup> J= 0,0113m <sup>4</sup> I= 0,0056m <sup>4</sup>	CHS D=750mm; t=30mm A= 0,0679m <sup>2</sup> J= 0,0088m <sup>4</sup> I= 0,0044m <sup>4</sup>		CHS D=750mm; t=25mm A= 0,0569m <sup>2</sup> J= 0,0075m <sup>4</sup> I= 0,0037m <sup>4</sup>	CHS D=750mm; t=20mm A= 0,0459m <sup>2</sup> J= 0,0061m <sup>4</sup> I= 0,0031m <sup>4</sup>
DECK	BOX GIRDER 4000x700mm; t=10mm A= 0,0936m <sup>2</sup> J= 0,0324m <sup>4</sup> I <sub>2</sub> = 0,1608m <sup>4</sup> I <sub>3</sub> = 0,0100m <sup>4</sup>				
STRUTS	CHS D=300mm;t=60mm A= 0,0452m <sup>2</sup> J= 0,0007m <sup>4</sup> I= 0,0003m <sup>4</sup>	CHS D=300mm;t=55mm A= 0,0423m <sup>2</sup> J= 0,0007m <sup>4</sup> I= 0,0003m <sup>4</sup>	CHS D=300mm;t=35mm A= 0,0291m <sup>2</sup> J= 0,0005m <sup>4</sup> I= 0,0003m <sup>4</sup>		CHS D=300mm;t=45mm A= 0,0360m <sup>2</sup> J= 0,0006m <sup>4</sup> I= 0,0003m <sup>4</sup>

**Table 1-2: Design cross-section values for  $g=20m$**

$g=0$			
	$f=10m$	$f=20m$	$f=50m$
ARCH	CHS D=750mm; t=32mm A= 0,0722m <sup>2</sup> J= 0,0093m <sup>4</sup> I= 0,0047m <sup>4</sup>	CHS D=750mm; t=25mm A= 0,0569m <sup>2</sup> J= 0,0075m <sup>4</sup> I= 0,0037m <sup>4</sup>	CHS D=750mm; t=20mm A= 0,0459m <sup>2</sup> J= 0,0061m <sup>4</sup> I= 0,0031m <sup>4</sup>
DECK	BOX GIRDER 4000x700mm; t=10mm A= 0,0936m <sup>2</sup> J= 0,0324m <sup>4</sup> I <sub>2</sub> = 0,1608m <sup>4</sup> I <sub>3</sub> = 0,0100m <sup>4</sup>		
STRUTS	CHS D=300mm;t=50mm A= 0,0393m <sup>2</sup> J= 0,0006m <sup>4</sup> I= 0,0003m <sup>4</sup>	CHS D=300mm;t=25mm A= 0,0216m <sup>2</sup> J= 0,0004m <sup>4</sup> I= 0,0002m <sup>4</sup>	CHS D=300mm;t=12mm A= 0,0109m <sup>2</sup> J= 0,0002m <sup>4</sup> I= 0,0001m <sup>4</sup>

**Table 1-3: Design cross-section values for  $g=0$**

$g=20m, f=25m$			
	$\beta$ : Radial struts	$\beta$ : Vertical struts	$\beta$ : Convergent struts
ARCH	CHS D=750mm; t=25mm A= 0,0569m <sup>2</sup> I= 0,0037m <sup>4</sup>	CHS D=750mm; t=25mm A= 0,0569m <sup>2</sup> I= 0,0037m <sup>4</sup>	CHS D=750mm; t=20mm A= 0,0459m <sup>2</sup> I= 0,0031m <sup>4</sup>
STRUTS	CHS D=300mm;t=35mm A= 0,0291m <sup>2</sup> I= 0,0003m <sup>4</sup>	CHS D=300mm;t=45mm A= 0,0456m <sup>2</sup> I= 0,0010m <sup>4</sup>	CHS D=300mm;t=35mm A= 0,0291m <sup>2</sup> I= 0,0003m <sup>4</sup>

**Table 1-4: Design cross-section values of the arch and struts for  $g=20m$  and  $f=25m$  with different  $\beta$  values**

$g=20m$					
	$f=10m$	$f=15m$	$f=20m$	$f=25m$	$f=50m$
ARCH	CHS D=750mm; t=40mm A= 0,0892m <sup>2</sup> I= 0,0056m <sup>4</sup>	CHS D=750mm; t=30mm A= 0,0679m <sup>2</sup> I= 0,0044m <sup>4</sup>		CHS D=750mm; t=25mm A= 0,0569m <sup>2</sup> I= 0,0037m <sup>4</sup>	CHS D=750mm; t=20mm A= 0,0459m <sup>2</sup> I= 0,0031m <sup>4</sup>
DECK	BOX GIRDER 4000x700mm; t=20mm A= 0,1864m <sup>2</sup> I2= 0,3179m <sup>4</sup> I3= 0,0195m <sup>4</sup>				
STRUTS	CHS D=300mm;t=60mm A= 0,0452m <sup>2</sup> I= 0,0003m <sup>4</sup>	CHS D=300mm;t=55mm A= 0,0423m <sup>2</sup> I= 0,0003m <sup>4</sup>	CHS D=300mm;t=35mm A= 0,0291m <sup>2</sup> I= 0,0003m <sup>4</sup>		CHS D=300mm;t=45mm A= 0,0360m <sup>2</sup> = 0,0003m <sup>4</sup>

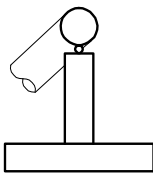
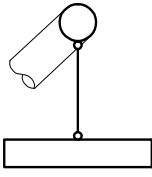
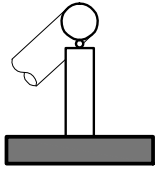
**Table 1-5: Design cross-section values of the arch and struts for  $g=20$  and a stiffer deck**

$g=0$			
	$f=10m$	$f=20m$	$f=50m$
ARCH	CHS D=750mm; t=32mm A= 0,0722m <sup>2</sup> I= 0,0047m <sup>4</sup>	CHS D=750mm; t=25mm A= 0,0569m <sup>2</sup> I= 0,0037m <sup>4</sup>	CHS D=750mm; t=20mm A= 0,0459m <sup>2</sup> I= 0,0031m <sup>4</sup>
DECK	BOX GIRDER 4000x700mm; t=20mm A= 0,1864m <sup>2</sup> I2= 0,3179m <sup>4</sup> I3= 0,0195m <sup>4</sup>		
STRUTS	CHS D=300mm;t=60mm A= 0,0452m <sup>2</sup> I= 0,0003m <sup>4</sup>	CHS D=300mm;t=60mm A= 0,0452m <sup>2</sup> I= 0,0003m <sup>4</sup>	CHS D=300mm;t=60mm A= 0,0452m <sup>2</sup> I= 0,0003m <sup>4</sup>

**Table 1-6: Design cross-section values of the arch and struts for  $g=0$  and a stiffer deck**

BOX GIRDER 4000x700mm; t=3mm A= 0,0282m <sup>2</sup> J= 0,0099m <sup>4</sup> I2= 0,0486m <sup>4</sup> I3= 0,0031m <sup>4</sup>
--------------------------------------------------------------------------------------------------------------------------------------------

**Table 1-7: Deck less stiff cross-section mechanical properties**

	Reference model	Reference model with flexible hangers	Stiff hanger-deck system model
	 <p>Hangers fixed at deck and transversally pinned at arch (M3-3 released at arch)</p>		 <p>Hangers fixed at deck and transversally pinned at arch (M3-3 released at arch)</p>
ARCH	CHS D=1m; t=30mm $A= 0,0914m^2$ $J= 0,0215m^4$ $I_2= 0,0108m^4$ $I_3= 0,0108m^4$	CHS D=1m; t=30mm $A= 0,0914m^2$ $J= 0,0215m^4$ $I_2= 0,0108m^4$ $I_3= 0,0108m^4$	CHS D=1m; t=30mm $A= 0,0914m^2$ $J= 0,0215m^4$ $I_2= 0,0108m^4$ $I_3= 0,0108m^4$
DECK	BOX GIRDER 4000x800mm; t=15mm $A= 0,1431m^2$ $J= 0,0615m^4$ $I_2= 0,2517m^4$ $I_3= 0,0196m^4$	BOX GIRDER 4000x800mm; t=15mm $A= 0,1431m^2$ $J= 0,0615m^4$ $I_2= 0,2517m^4$ $I_3= 0,0196m^4$	$A= 0,1431m^2$ $J= 10m^4$ $I_2= 0,2m^4$ $I_3= 0,2m^4$
STRUTS	CHS D=451mm;t=22,6mm $A= 0,0304m^2$ $J= 0,0014m^4$ $I_2= 0,0007m^4$ $I_3= 0,0007m^4$	<i>Flexible hangers</i> Stay cables $A= 9,8 \cdot 10^{-4} m^2$ $J= 0 m^4$ $I_2= I_3= 0 m^4$	$A= 0,0304m^2$ $J= 0,0011m^4$ $I_2= 7,34m^4$ $I_3= 7,34m^4$

**Table 1-8: Cross-section values for IDABWIC case study**

## 2. ARCH BRIDGES WITH A SUPERIOR DECK. BUCKLING RESULTS

In this section the buckling coefficients for the different loads or load combinations described in section 1.4 are obtained, comparing different bearing combinations for the cases  $g=0$  and  $g=20m$  of deck plan curvature. These buckling coefficient values are shown in Figure 2-1, Figure 2-2 and Figure 2-3. The curves for different  $f$  values are given. A radial distribution of struts, result of dividing the arch and deck in equal lengths between struts, is employed in all cases.

The buckling loads for different  $f$  values with a radial distribution of the struts and no imperfections have been compared employing reference cross-section values (given in Table 1-1) for all the models, so that buckling differences between models are not due to the employed cross-sections, but to the geometry (Figure 2-1, Figure 2-2 and Figure 2-3).

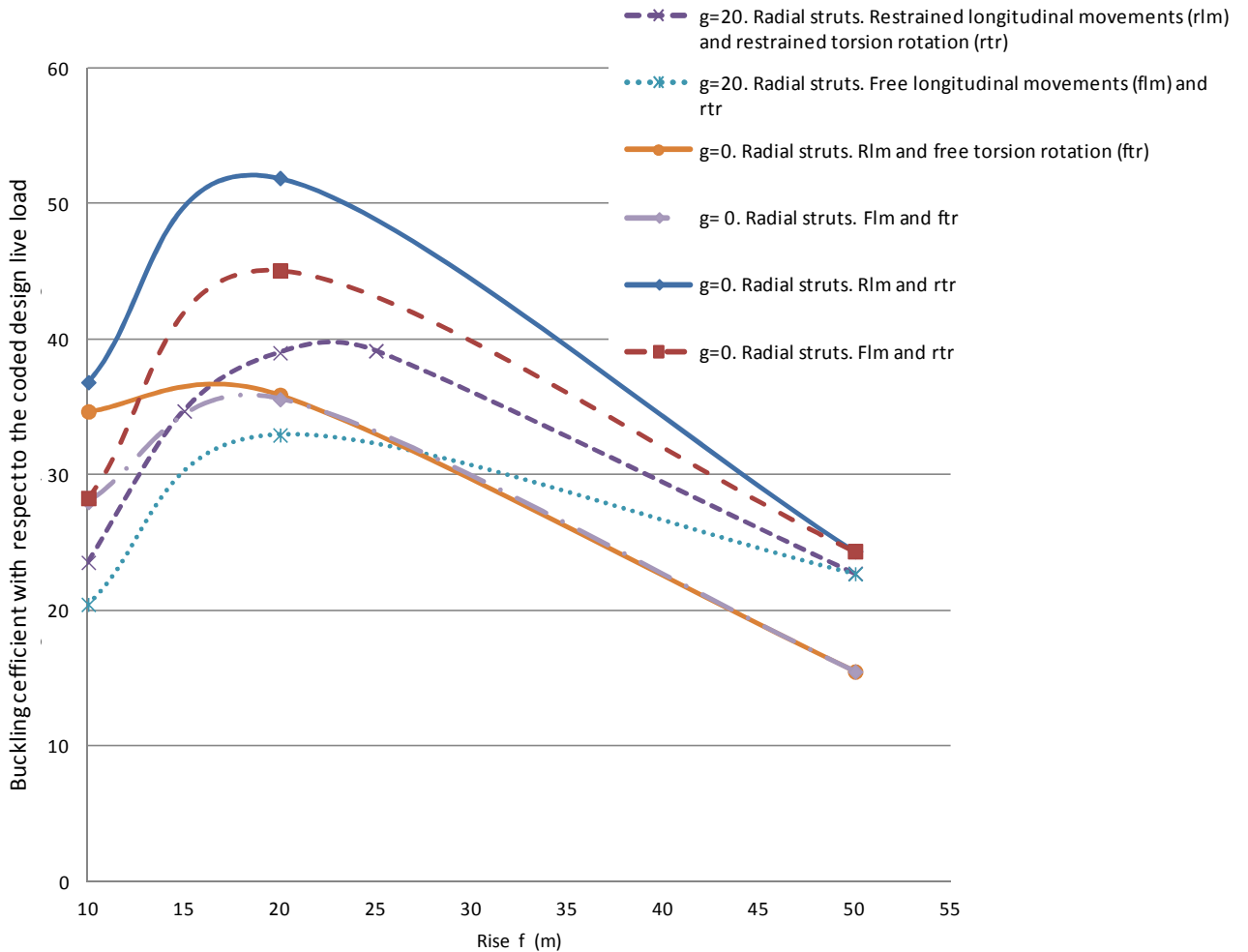
The influence of the struts inclination ( $\beta$ ) is analysed in Figure 2-17 and Figure 2-18 for models with  $g=L/5=20m$  and  $f=L/4=25m$  with different cross-section values.

In Figure 2-10, Figure 2-11 and Figure 2-12 the design cross-section values, obtained in chapter V.B and displayed in Table 1-2 and Table 1-3, are employed. In Figure 2-11 and Figure 2-12 other stiffness distributions are also considered, employing a stiffer deck is also considered (Table 1-5 and Table 1-6).

Considering imperfections or not does not influence the elastic buckling analysis studied in the present chapter, which corresponds to the bifurcation of the equilibrium state.

### 2.1 ARCH RISE ( $f$ ) AND BEARING CONDITIONS INFLUENCE ON BUCKLING

The influence of the arch rise ( $f$ ) and of the bearing conditions on buckling has been studied and the results are summarized in figures from Figure 2-1 to Figure 2-3.



**Figure 2-1: Buckling coefficient  $\alpha$  of the design live load on the whole deck ( $lu$ ) for the bridge already loaded with permanent loads. Comparison of different arch rise ( $f$ ) values and bearing conditions, employing the reference cross-section values of Table 1-1**

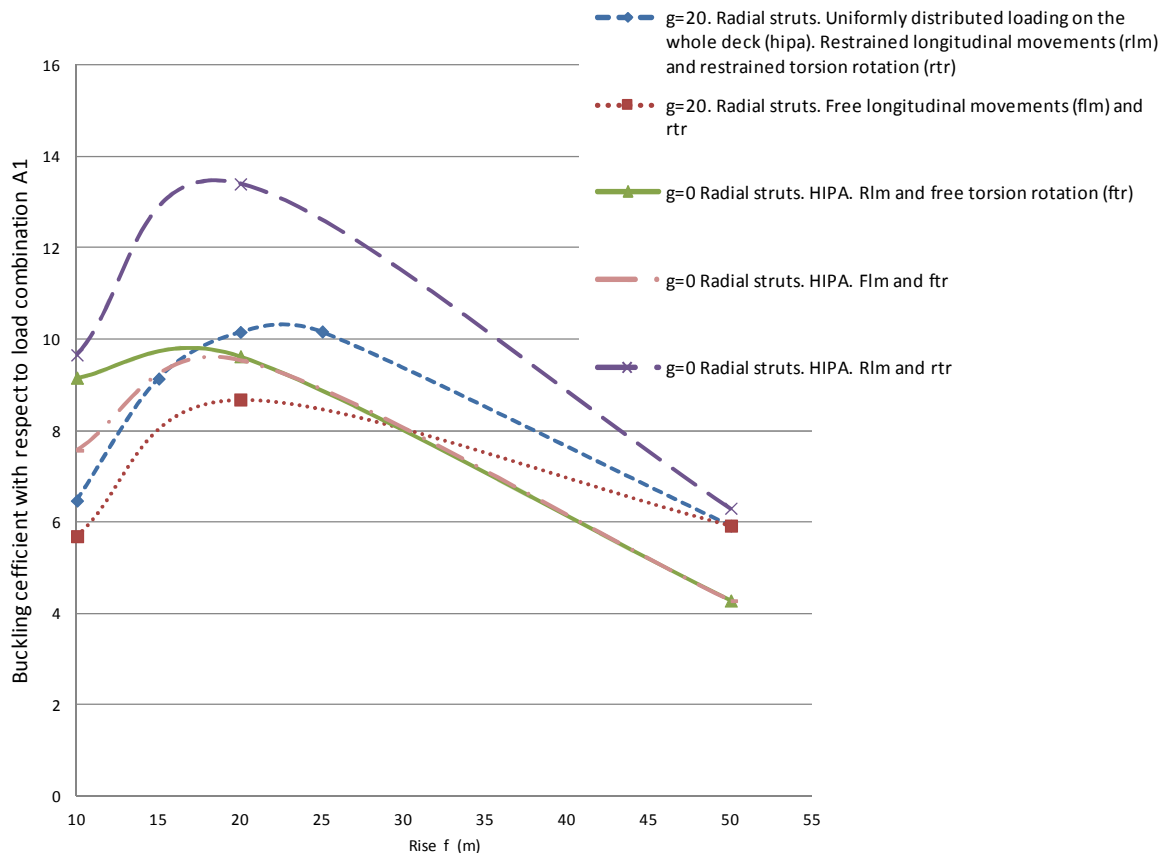


Figure 2-2: Buckling coefficient  $\alpha_1$  of the loading combination A1 for different arch rise ( $f$ ) values and bearing conditions, employing the reference cross-section values of Table 1-1

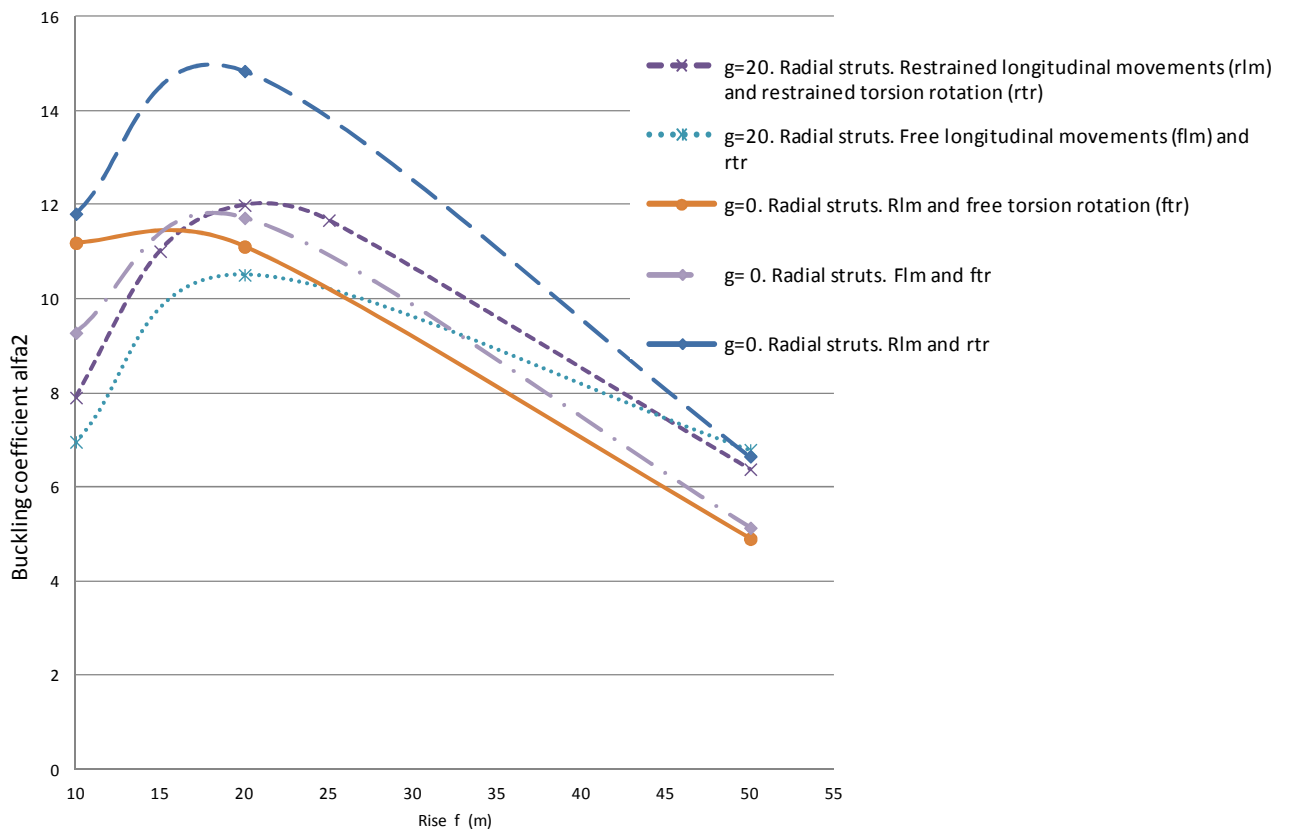


Figure 2-3: Buckling coefficient  $\alpha_2$  of the loading combination A2 for different arch rise ( $f$ ) values and bearing conditions, employing the reference cross-section values of Table 1-1



The following conclusions are drawn of the results:

- Whereas the most efficient  $f$  value regarding both steel mass and stresses is  $25m=L/4$ , other  $f$  values give the highest buckling load, ie:  $f=20=L/5$ , if  $g=20m$  and  $flm$  are employed;  $15m < f < 20m$ , if  $g=0$ , and  $20m < f < 25m$ , if  $g=20m$  and  $rlm$  are employed. For  $f > 25m$  the buckling load diminishes. For  $f=50m$  and  $g=20m$  and both,  $flm$  or  $rlm$ , the structure buckles for a load 23 times the live load specified in EC1 (Figure 2-1). Therefore, unless imperfections and non-linear geometrical forces lead to buckling for a lower load, the buckling load is higher than the coded ULS live load with 1,5 safety factor. However, the employed sections are not the dimensioned ones (see section 2.2).
- Buckling is highly dependent on the bearing conditions of the deck, especially for  $f \leq L/5 = 20m$ . For large  $f$  values, what has more influence is whether deck torsional rotations are restrained at the abutments, this implies larger changes in the buckling critical load than the value of  $g$  (from Figure 2-1 to Figure 2-3).
- Whatever the load case, the relationship of the buckling factor with  $f$  and the bearing conditions follows a similar tendency (compare from Figure 2-1 to Figure 2-3), except for the case of  $g=0$  with free longitudinal movements ( $flm$ ) and torsional rotations ( $fr$ ) which shows an improved behaviour in comparison with other bearing conditions for the live loads in half the length of the deck (Figure 2-3).
- The lowest buckling condition for all cases is obtained for a uniform distributed load (compare from Figure 2-2 to Figure 2-3).
- If the total load on the bridge is calculated for  $\alpha$  and  $\alpha_1$  very similar values are obtained, but the error is non-negligible (approximately 6%). Strictly correct method and most realistic would be to calculate  $\alpha$ , employing  $\alpha_1$  gives insecure (larger) buckling load values.
- When employing  $flm$ ,  $ftm$ ,  $fr$  and pinned hangers the destabilising effect of the deck can be clearly observed (Table 2-1 and Figure 4-1, in spite of what could be expected with a theoretical simplified cross-sectional analysis (Figure 3-5b)). However, when restraining the transverse displacements, when comparing the results to the ones of the free standing arch, it can be concluded that the deck improves the buckling behaviour of the arch (Table 4-1).
- Given a certain loading, it would seem logical that arches working under larger axial forces buckle for a lower load than those under lower axial forces (Figure 2-4 and Figure 2-5). However, it is not always so. This is due to the fact that the shape, length and stiffness have a larger influence on buckling. Observing the buckling shapes helps understanding buckling better.
- For large  $f$  values the arch buckles nearly independently of the deck (Figure 2-6a). This happens because the struts are longer and thus less stiff. However, for low  $f$  values the arch and deck buckle together (Figure 2-6b). This is because the struts for low values of  $f$

are shorter and hence stiffer. Therefore, the arch and deck tend to work as a truss and this improves the buckling behaviour.

- Planar vertical arches with a superior straight deck buckle out-of-plane and symmetrically when restraining longitudinal movements (rlm) if torsional rotations are restrained (rtr):
  - For flm and ftr the bridge also buckles symmetrically out-of-plane whatever the  $f$  value (Figure 2-6 from a to d).
  - For  $f \leq 20\text{m}$  the bridge buckles asymmetrically in-plane for flm and rtr (Figure 2-6e), but has higher  $\alpha$  values, except for  $f=10\text{m}$ . Restraining torsional rotations improves the buckling behaviour, since it diminishes the destabilizing effect of the deck described in chapter VI. A.
- Planar vertical SABs with a planar vertical arch and a superior curved deck buckle in both planes of the arch symmetrically except for low  $f$  values:
  - For  $g=20\text{m}$ ,  $f=10\text{m}$  buckling takes place in both planes but it is asymmetrical (Figure 2-7).
  - For  $f \leq 15\text{m}$  buckling takes place in both planes but mostly in-plane (Figure 2-7). For  $f=20\text{m}$  the buckling shape deforms as much as in-plane as out-of-plane (Figure 2-8).
  - For  $f \geq 25\text{m}$  symmetrical buckling takes place in both planes but mostly out-of-plane (Figure 2-9).
  - The larger the  $f$  value, the larger the out-of-plane component.
  - The buckling shapes are equivalent whatever the value of the cross-sections employed and of the bearing conditions.

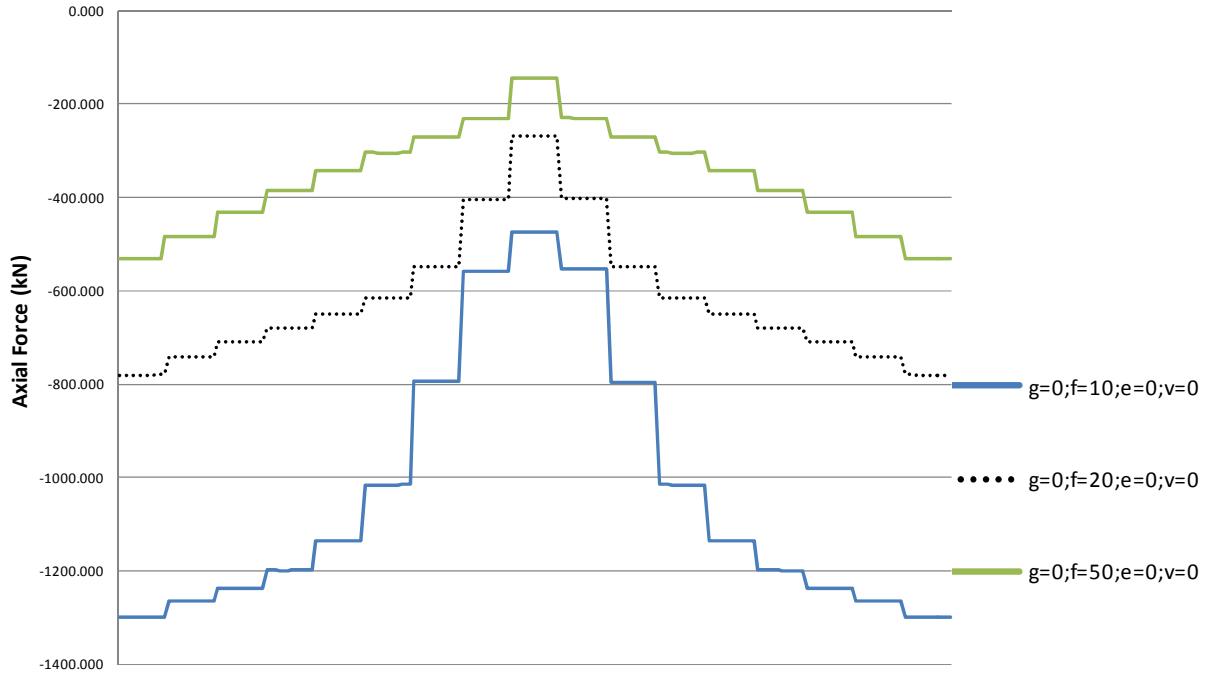


Figure 2-4: Arch axial forces comparison for different  $f$  values and  $g=0$ . The abscissas are the arch length from 0 to  $L_A$

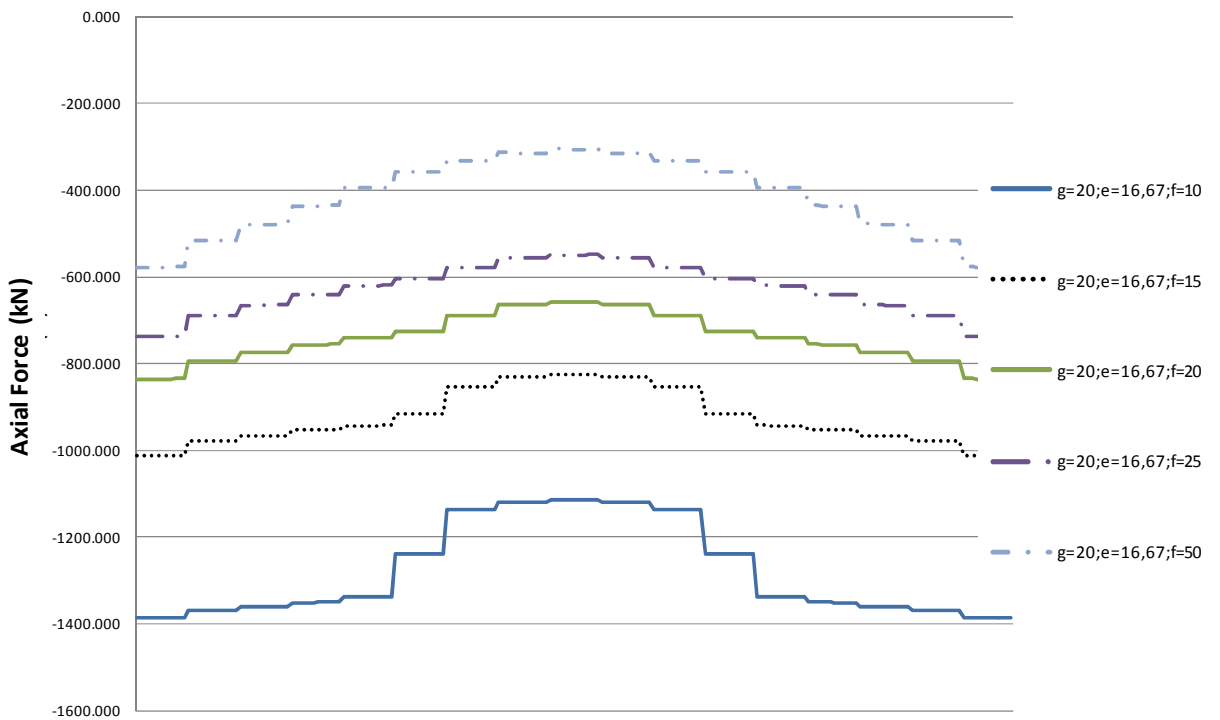
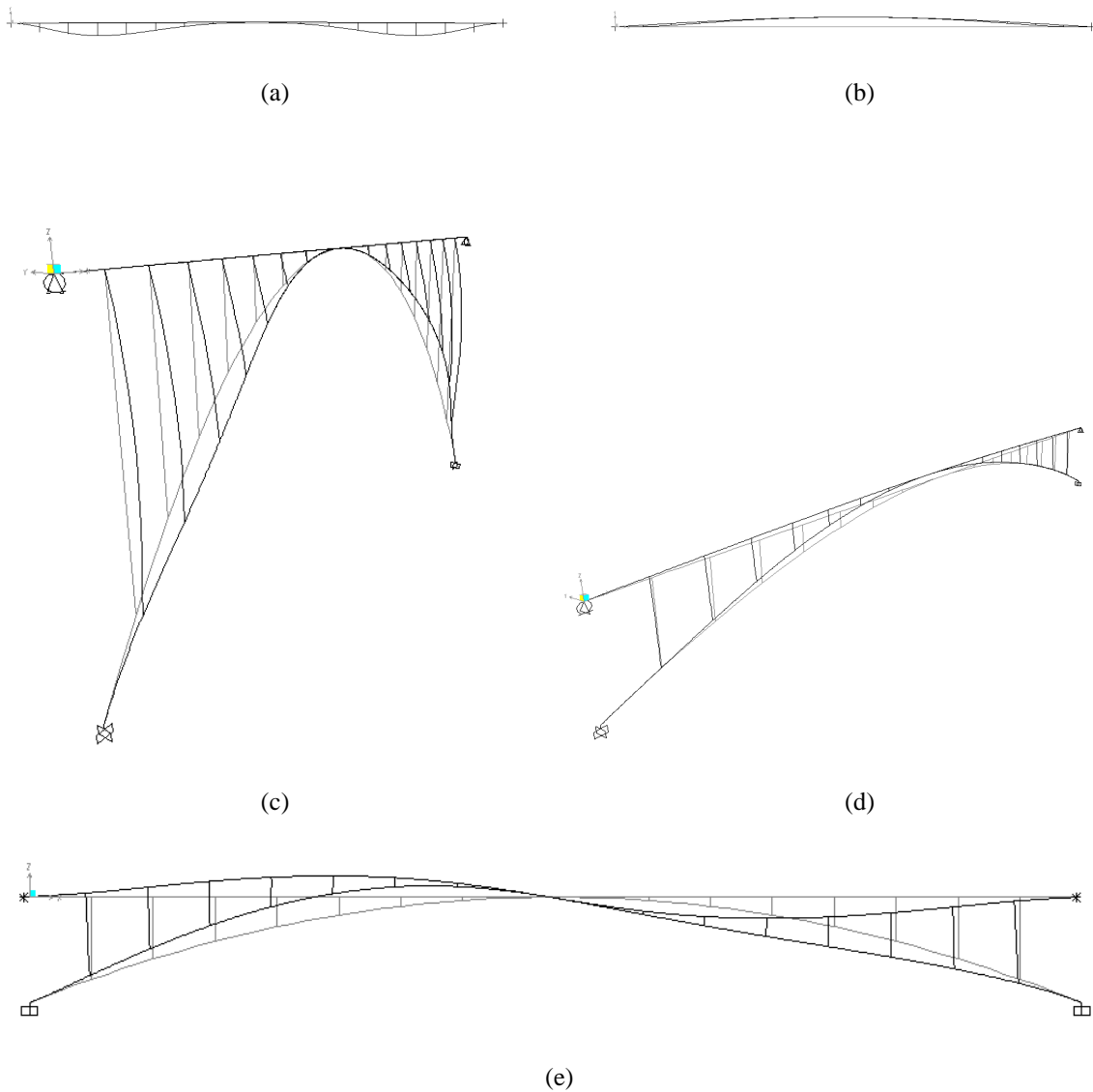
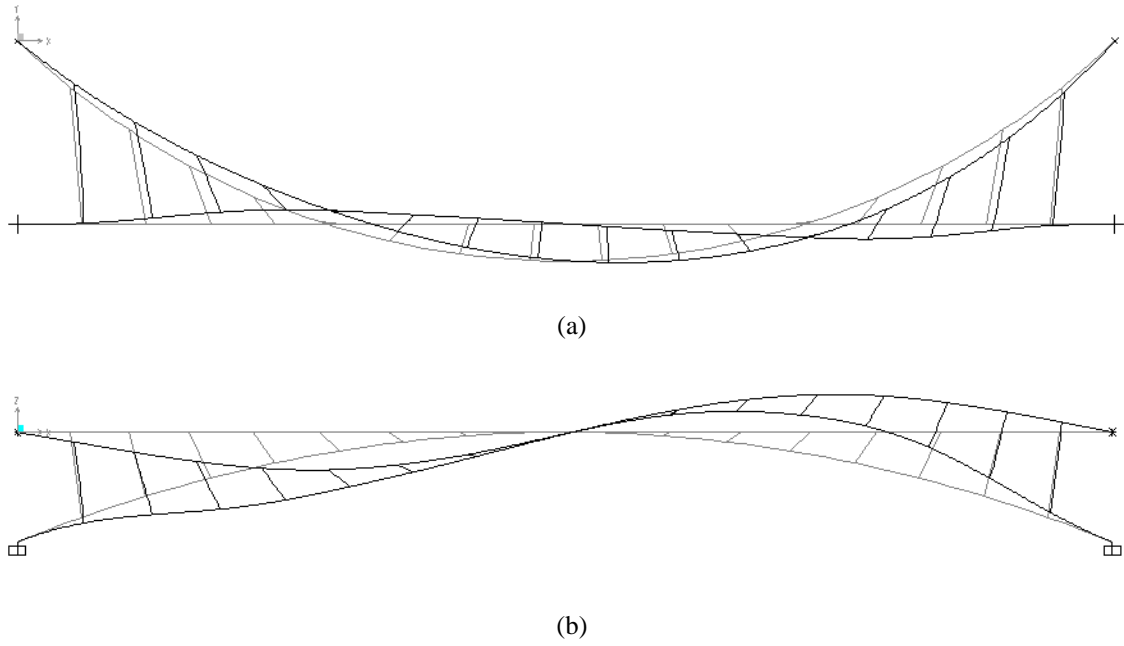


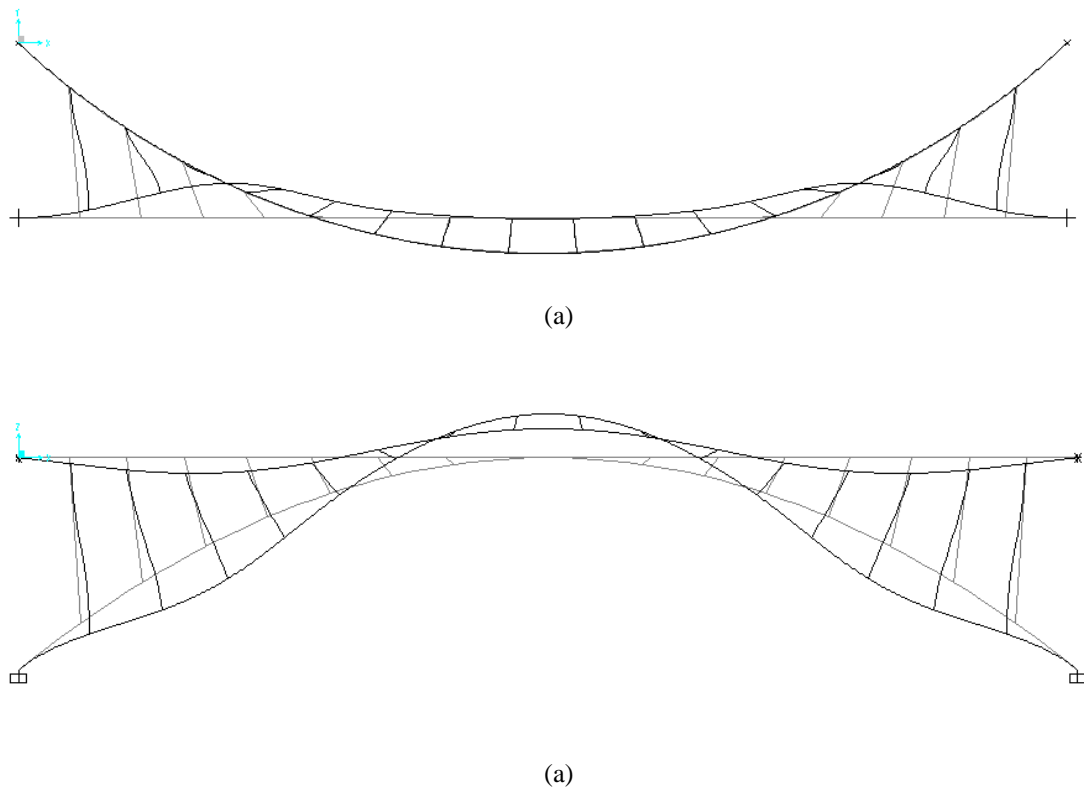
Figure 2-5: Arch axial forces comparison for different  $f$  values and  $g=20$ . The abscissas are the arch length from 0 to  $L_A$



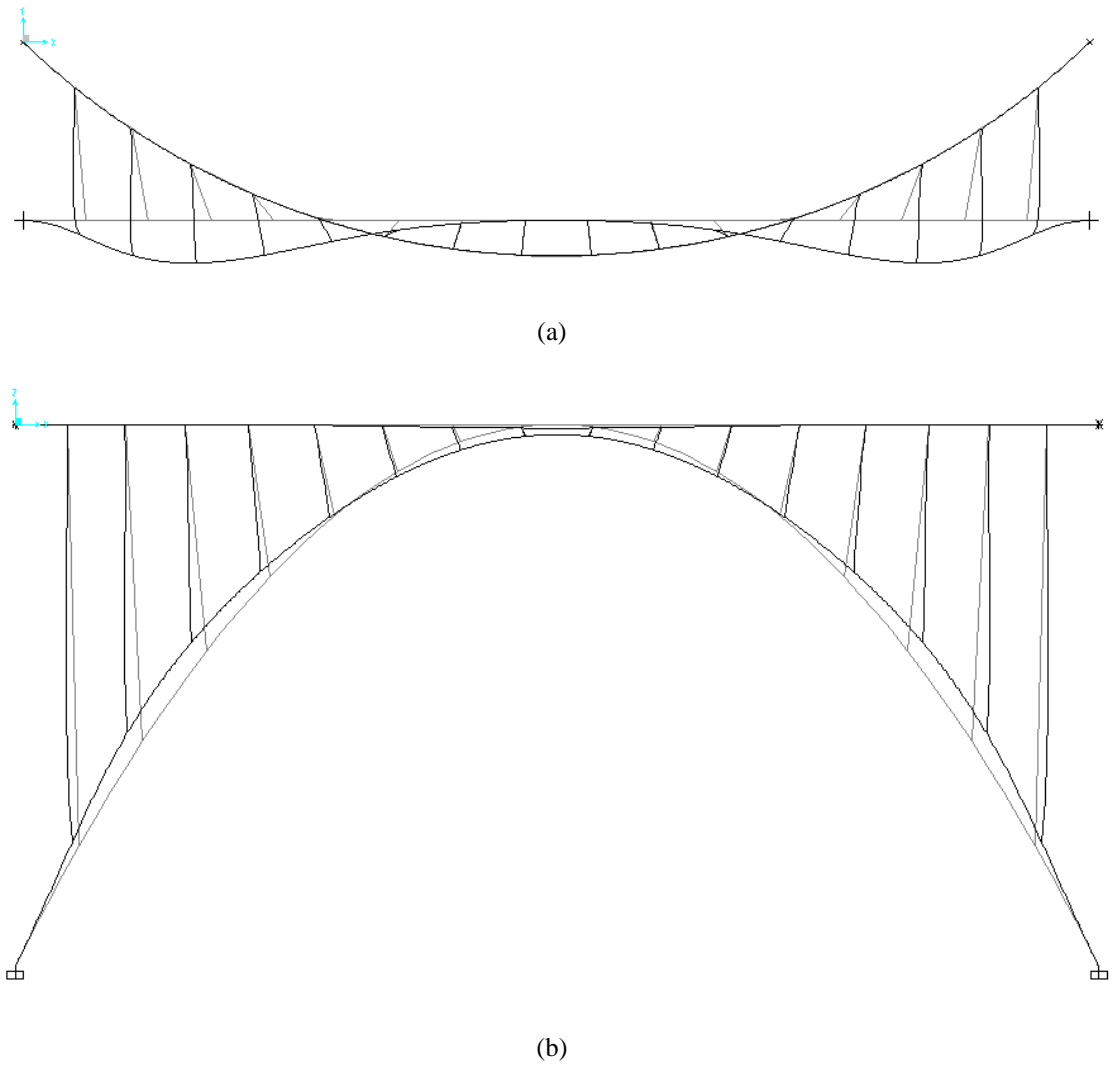
**Figure 2-6: Planar bridge. Buckling shape for  $g=0$ , employing reference cross-sections. Out-of-plane symmetrical buckling: (a) Plan view of the buckling shape of model with flm, ftr,  $f=50\text{m}$  (b) Plan view of the model with flm, ftr,  $f=10\text{m}$ . (c) Perspective of the model with flm, ftr,  $f=50\text{m}$  (d) Perspective of the model with flm, ftr,  $f=10\text{m}$ . In-plane symmetrical buckling: (e) Longitudinal view of the model with rlm, ftr,  $f=10\text{m}$**



**Figure 2-7: SAB asymmetrical buckling shape in both planes for  $g=20\text{m}$ ,  $f=10\text{m}$ , rlm and rtr, employing reference cross-sections (a) Plan view (b) Layout**



**Figure 2-8: SAB symmetrical buckling shape in both planes for  $g=20\text{m}$ ,  $f=20\text{m}$ , rlm and rtr, employing reference cross-sections (a) Plan view (b) Layout**



**Figure 2-9: SAB symmetrical buckling shape in both planes for  $g=20m, f=50m$ , rlm and rtr, employing reference cross-sections (a) Plan view (b) Layout**

$g$ (m)	distribution of struts	Bearing conditions	$f$ (m)	$L$ (m)	Numerical Ncr (kN)	Buckling shape according to the numerical analysis
0	radial (reference model)	flm, ftr	20	100	44833	Out-of-plane
0	radial (reference model)	rlm, rtr	20	100	63310	Out-of-plane
0	radial (reference model)	flm, rtr	20	100	55975	In-plane
0	radial (reference model)	flm, flm, ftr pinned hangers	20	100	3465	Out-of-plane
0	radial (reference model)	free standing arch	20	100	6978	Out-of-plane

**Table 2-1: Results comparison for different bearing and joint conditions employing the reference cross-sections. Influence of the boundary conditions on Ncr**

## 2.2 CROSS-SECTION VALUES INFLUENCE ON BUCKLING

The most efficient  $f$  value for  $g=20\text{m}$ , regarding both steel mass and stresses, is  $25\text{m}=L/4$ , whereas  $f=20=L/5$  gives the highest buckling load, which is nearly 5 times the ULS load (Figure 2-10) for  $g=20\text{m}$  employing design cross-sections (Table 1-2). For higher  $f$  values, the buckling load diminishes. For  $f=50\text{m}$  the structure buckles for a load twice the ULS and 6 times the live load (Figure 2-1) specified in EC1. Therefore, unless imperfections and non-linear geometrical forces lead to buckling before, the buckling load is higher than the coded one with 1,5 safety factor. This means that the most stressed cross-section will plasticize before buckling.

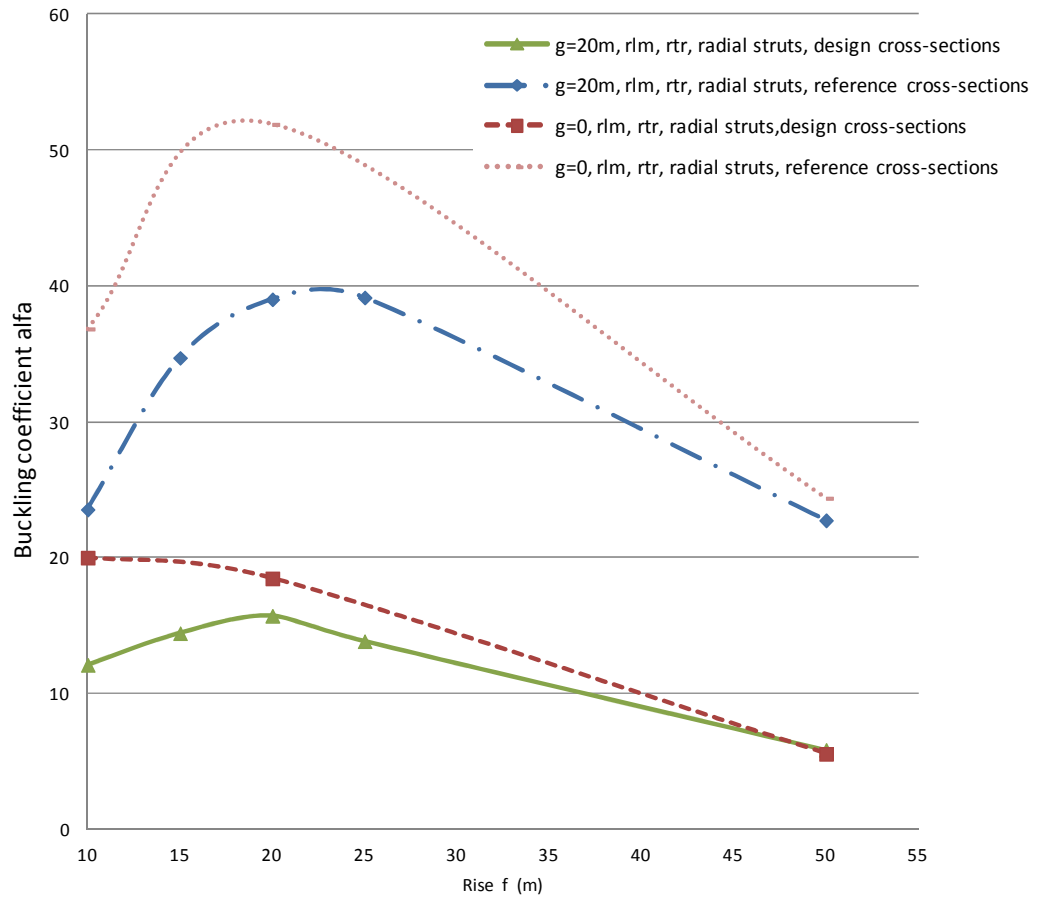
When comparing the buckling of models employing reference cross-sections (Table 1-1) or design cross-section values (Table 1-2 and Table 1-3) a change in the dependence of the buckling coefficient  $\alpha$  on  $f$  and  $g$  can be appreciated (Figure 2-10):

- The buckling coefficients of  $g=0$  and  $g=20\text{m}$  become more similar, especially for  $f>20\text{m}$ . For  $40\leq f\leq 50\text{m}$  the differences can be considered negligible (Figure 2-10). This effect slightly increases when increasing the stiffness of the deck (Figure 2-11 and Figure 2-12).
- For  $f\geq L/2=50\text{m}$ , SABs employing a planar vertical arch with a curved superior deck even buckle later than planar vertical arches with a superior straight deck, when considering the dimensioned cross-sections (Figure 2-10).
- For  $g=0$  the dependence of  $\alpha$  on  $f$  clearly changes for  $f\leq 20\text{m}$ . The model with  $f=10\text{m}$  is the one with the highest buckling coefficient when employing dimensioned cross-sections (Figure 2-10). This happens because a stiffer arch is employed for this model, the relationship  $I_{\text{arch}}/I_{2\text{deck}}$  of design cross-sections decreases with  $f$ . This effect highly increases when increasing the stiffness of the deck (Figure 2-11 and Figure 2-12), but does not take place if the longitudinal movements of the deck are free at abutments

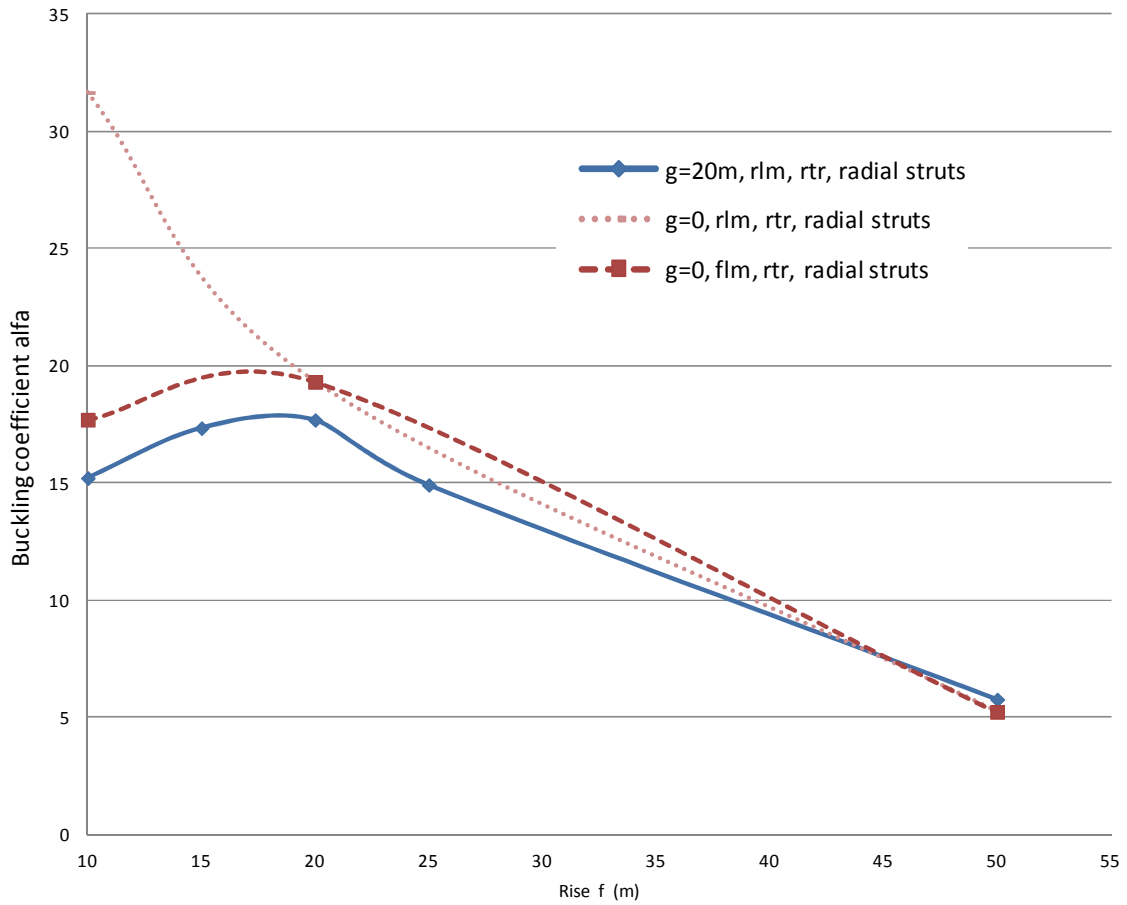
(Figure 2-11), since the arch buckles in-plane. If longitudinal movements are restrained the deck helps stabilizing the arch.

- For  $g=0$  and  $f \geq L/5=20\text{m}$  restraining longitudinal movements or not has no influence, for planar vertical arch models with a superior straight deck ( $g=0$ , Figure 2-11). This is so because when employing a stiffer deck the arch and deck buckle independently (Figure 2-13a). For less stiff decks as the one employed in the previous section the deck still has a stabilizing influence on the arch when torsional rotations are restrained, either buckling in-plane due to the flm (Figure 2-13b) or out-of-plane when rlm (Figure 2-13c).
- Employing a stiffer deck improves the buckling behaviour for  $f$  values below  $L/4=25\text{m}$ , whatever the value of  $g$  and the bearing conditions (Figure 2-11 and Figure 2-12). As expected, for low  $f$  values, the stiffness of the deck has more influence on the buckling of models with  $g=0$  than on SABs (Figure 2-11 and Figure 2-12). For low  $f$  values and  $g=0$  the deck has a stabilizing effect, this happens because the deck buckles with the arch (Figure 2-14) but for  $f > 25\text{m}$  the destabilizing effect of the deck described in chapter VI.A takes place. This is appreciated because the deck does not buckle with the arch (Figure 2-6a and Figure 2-15).
- For  $g=20\text{m}$  the deck has a stabilizing effect, on the contrary of what was expected a priori (Figure 1-1). The axial forces might destabilize the arch but, since struts are fixed to both arch and deck, the shear forces and bending moments, which they produce on the arch, stabilize it (Figure 2-16).
- The buckling shape of the models does not change with the cross-sections, except for the model flm, rtr  $g=0$  in which when increasing the stiffness of the deck the arch buckles out-of-plane and symmetrically instead of in-plane asymmetrically as it occurred for the reference cross-section (section 2.1).

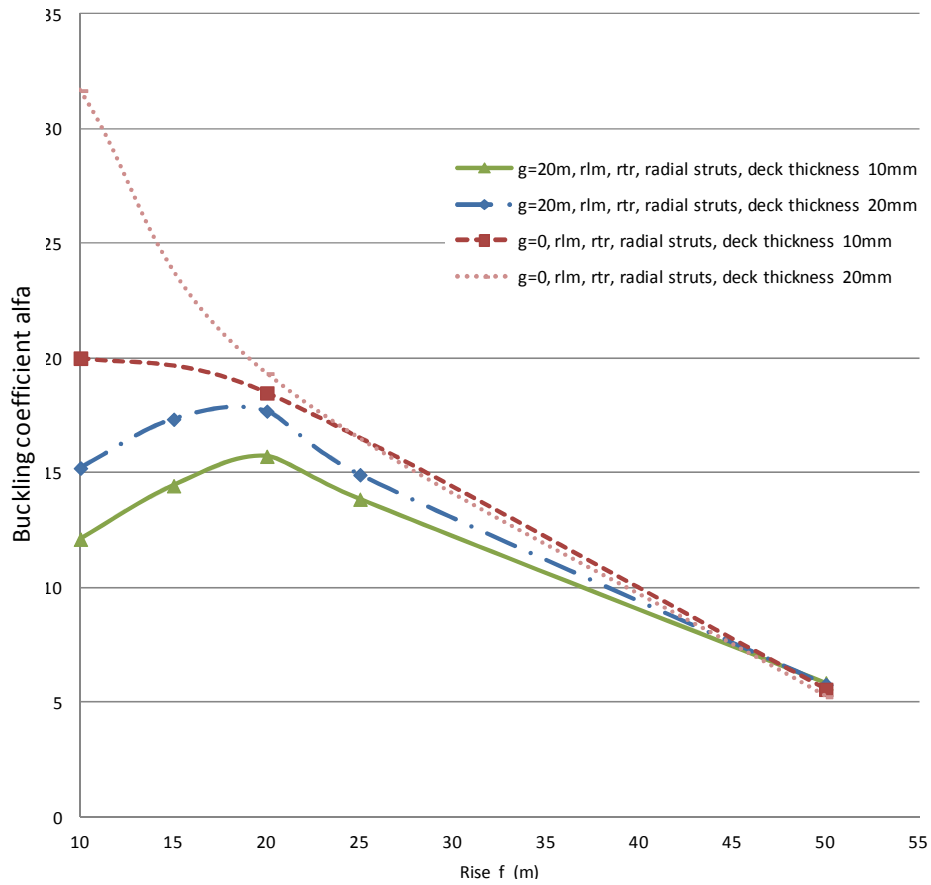




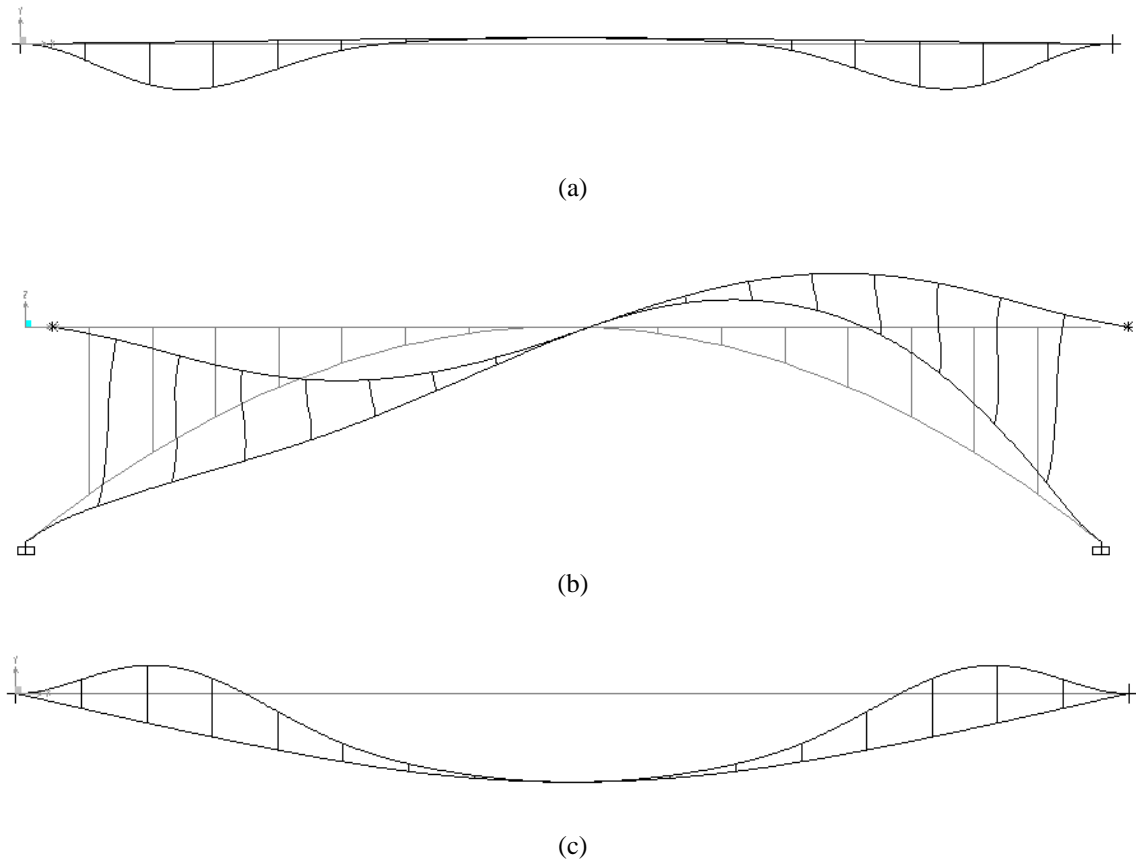
**Figure 2-10: Comparison of different arch rise ( $f$ ) values, employing the design cross-section values for each model or the reference cross-section values for all the models (from Table 1-1 to Table 1-3). Buckling coefficient  $\alpha$  of the design live load on the whole deck ( $lu$ ) for the bridge already loaded with permanent loads.**



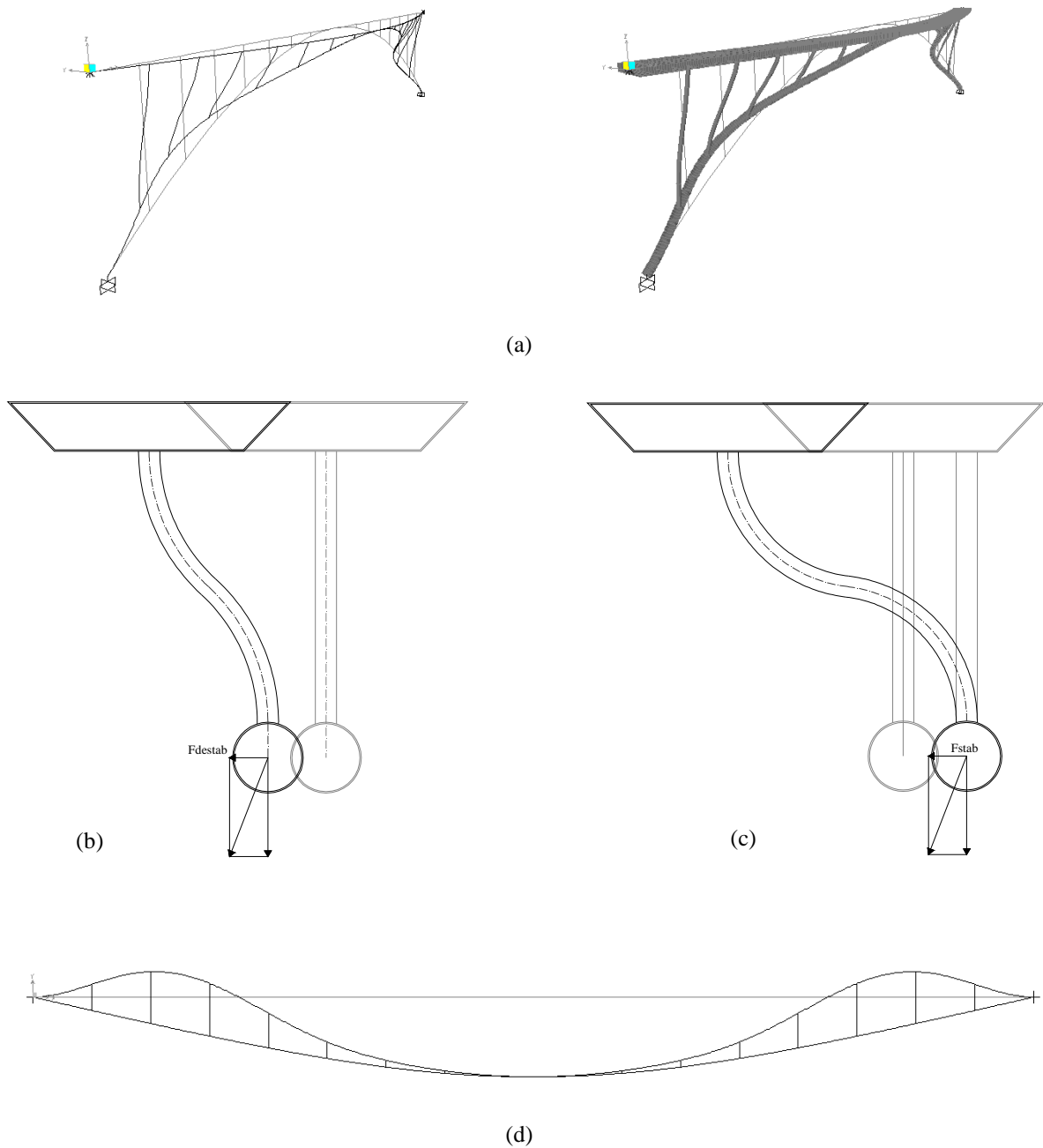
**Figure 2-11: Comparison of different arch rise ( $f$ ) values and bearing conditions, employing the design cross-section values for the arch and struts for each model and a stiffer deck of the same dimensions as the design deck (4000x700mm) but thicker (20mm) (Table 1-5 and Table 1-6). Buckling coefficient  $\alpha$  of the design live load on the whole deck ( $lu$ ) for the bridge already loaded with permanent loads.**



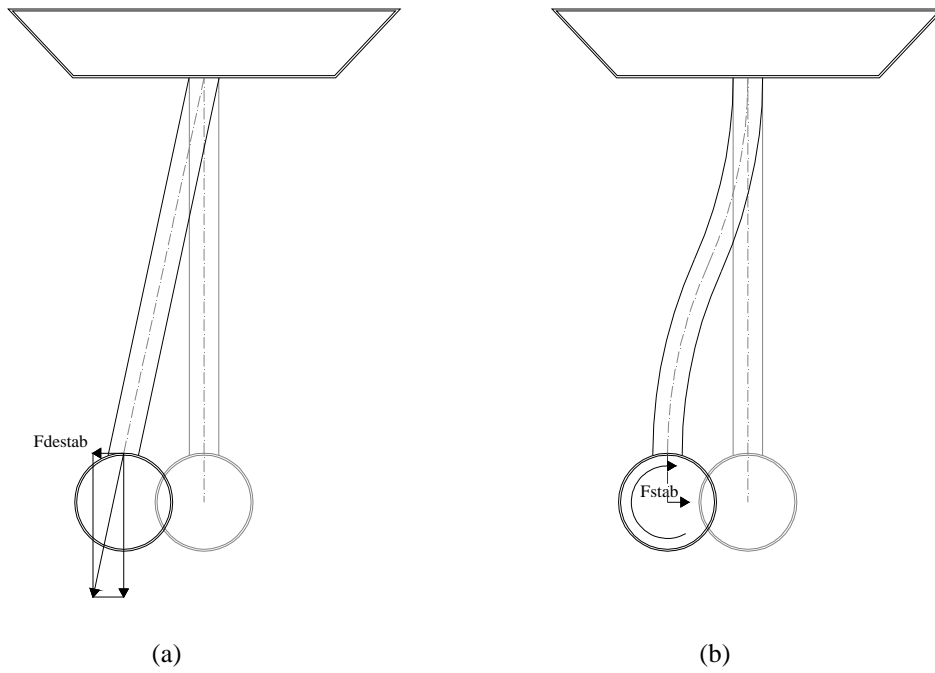
**Figure 2-12: Comparison of different arch rise ( $f$ ) values and deck stiffness (4000x700mm, thickness 10mm versus 20mm, employing the design cross-section values for the arch and struts (from Table 1-2 to Table 1-6). Buckling coefficient  $\alpha$  of the design live load on the whole deck ( $lu$ ) for the bridge already loaded with permanent loads.**



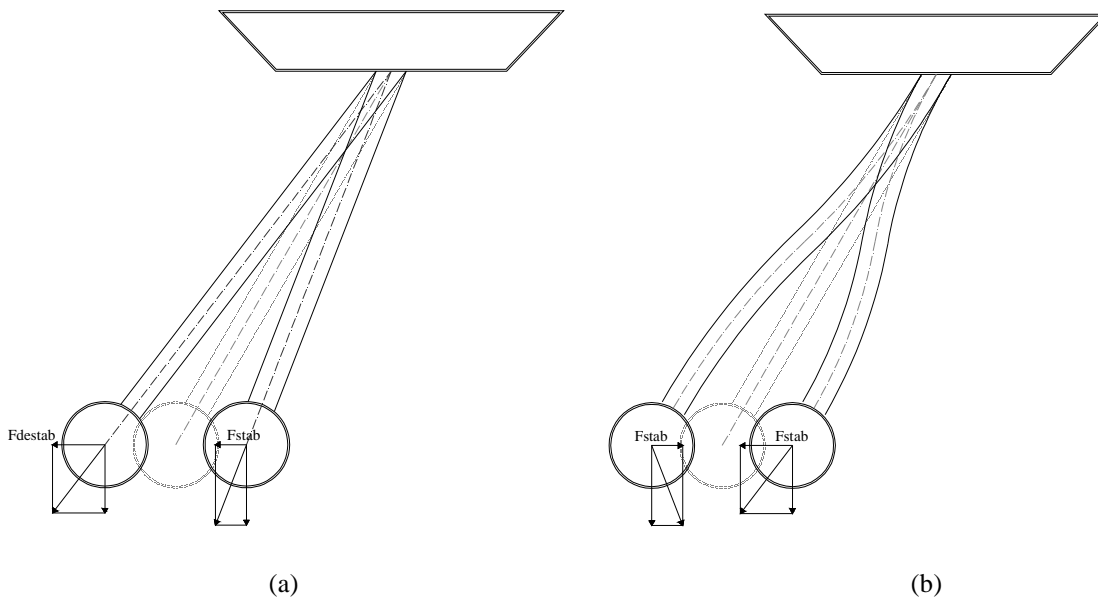
**Figure 2-13: Planar bridges. Buckling shapes for  $g=0$  and  $f=20\text{m}$  models (a) Plan view of the out-of-plane identical buckling shape for both flm and rtr when employing cross-sections in Table 1-6. (b) Longitudinal view of the in-plane buckling shape when employing flm, rtr and reference cross-sections in Table 1-1. (c) Plan view of the out-of-plane buckling shape when employing rlm, rtr and reference cross-sections in Table 1-1.**



**Figure 2-14: Planar bridges. Buckling shape of arch bridge model with  $g=0, f=20\text{m}$ , rlm and rtr (a) Perspective. (b) Cross-section: destabilizing effect caused by both shear and axial forces (c) Cross-section: destabilizing effect caused by axial forces out-of-plane projection and stabilizing effect caused by shear forces (d) Plan view**



**Figure 2-15: (a) Destabilizing effect of struts on arch buckling due to the axial forces; (b) Stabilizing effect of struts on arch buckling when considering shear forces and bending moments**



**Figure 2-16: (a) Stabilizing and destabilizing effect of struts on arch buckling when not considering shear forces due to bending moments; (b) Stabilizing effect of struts on arch buckling when considering shear forces due to bending moments**

### 2.3 STRUTS INCLINATION IN LONGITUDINAL VIEW ( $\beta$ ). INFLUENCE ON BUCKLING

The nomenclature of  $\beta$  is described in section 1.2. As a reminder the inclinations considered are the following and can be seen in

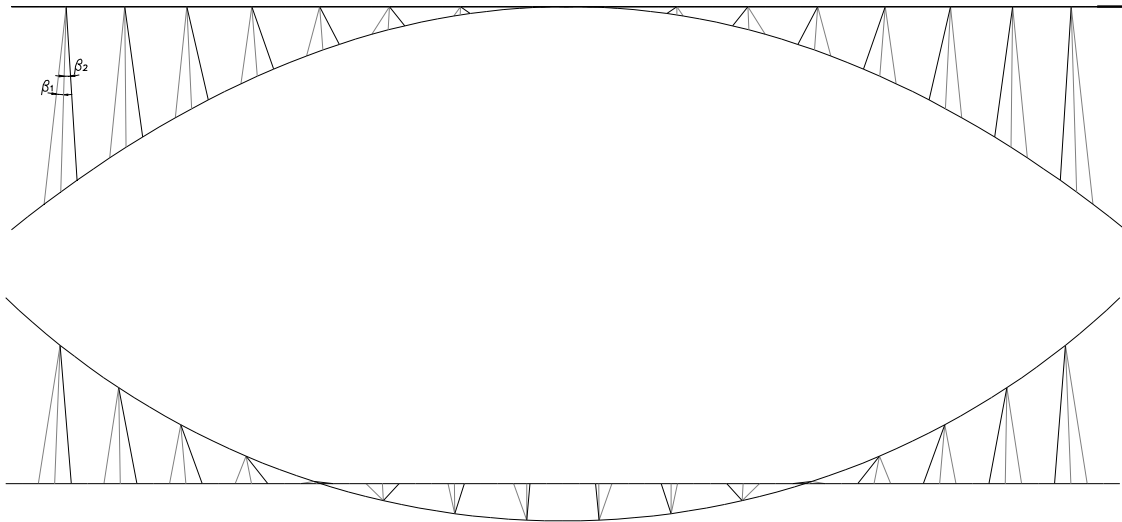


Figure 1-2:

- Radial strut distribution system: each strut axis elongation converges below the deck with its symmetrical.
- A more vertical orientation ( $\beta_2$ ) of the struts and
- Convergent system of struts: each strut axis elongation converges above the deck with its symmetrical ( $\beta_1$ , opposite inclination to the radial system).

The influence of the struts inclination ( $\beta$ ) for models with  $g=L/5=20\text{m}$  and  $f=L/4=25\text{m}$  is analysed in Figure 2-17 and Figure 2-18. In Figure 2-17 the influence of cross-section values is shown. In Figure 2-18 reference cross-sections are employed for all models to check the influence of the of  $\beta$  in buckling for the designed models for both cases uniform loading on half the deck length and on the whole length. The results are displayed with the already analysed models with  $g=0$  and different  $f$  values and bearing conditions, so as to be shown in the comparative context previously commented.

The geometry that best resists buckling, when employing reference cross-section values, is employing convergent struts (Figure 2-17). This is coincident with the fact that for this geometry the arch bears the lowest axial forces and stresses (Figure 2-19 and Figure 2-20). This means that it is not a phenomenon of stabilizing geometry but of the fact that for a same loading lower axial forces are transmitted to the arch and, therefore, it reaches the critical axial buckling load for a larger loading.

However, when employing design cross-section values for the struts and arch (Table 1-4), either with a design cross-section deck of 10mm thickness (Table 1-2) or a stiffer one with 20mm thickness (Table 1-5), the model employing vertical struts shows the best behaviour (Figure 2-17

and Figure 2-18) in spite of the axial forces being lower for the convergent struts (Figure 2-21). This is due to the stiffness distribution in the bridge. It must be also observed that, when employing design cross-sections, arch axial forces of the model employing vertical struts are more similar to the ones of the model employing convergent struts than when employing reference cross-sections (Figure 2-19 and Figure 2-21).

The model with radial struts employing design cross-sections has a stiffer arch, but this does not help increasing the buckling load, since the geometry gives the largest axial forces with an important difference (Figure 2-21).

The model with vertical struts has struts with a larger flexural rigidity (Table 1-4). In spite of being longer than the ones with a radial distribution, they are stiffer and, thus, deform less (as commented in the following paragraphs) so that they produce a stabilizing effect.

When employing a stiffer deck the buckling behaviour improves for the models with a radial or convergent distribution. This means that the deck has a stabilizing effect in this bridge type. The model employing stiffer struts does not improve its buckling behaviour since the struts were already stiff enough.

In all cases, but especially for convergent struts a uniformly distributed loading on the whole deck is more unfavourable than on half the length (Figure 2-18).

Whatever the value of  $\beta$  and the employed cross-sections, the buckling shape is very similar, as shown in Figure 2-22 and Figure 2-23. A slight difference in the struts can be observed:

- When employing reference cross-sections (Table 1-1), the convergent struts have the lowest displacements compared to other  $\beta$  values (Figure 2-22c).
- When employing design cross-sections (Table 1-4), the vertical struts have the lowest displacements compared to other  $\beta$  values (Figure 2-23b). This happens because they are stiffer, as previously observed.
- Radial struts are the ones with the largest displacements whatever the cross-sections employed (Figure 2-22a and Figure 2-23a)



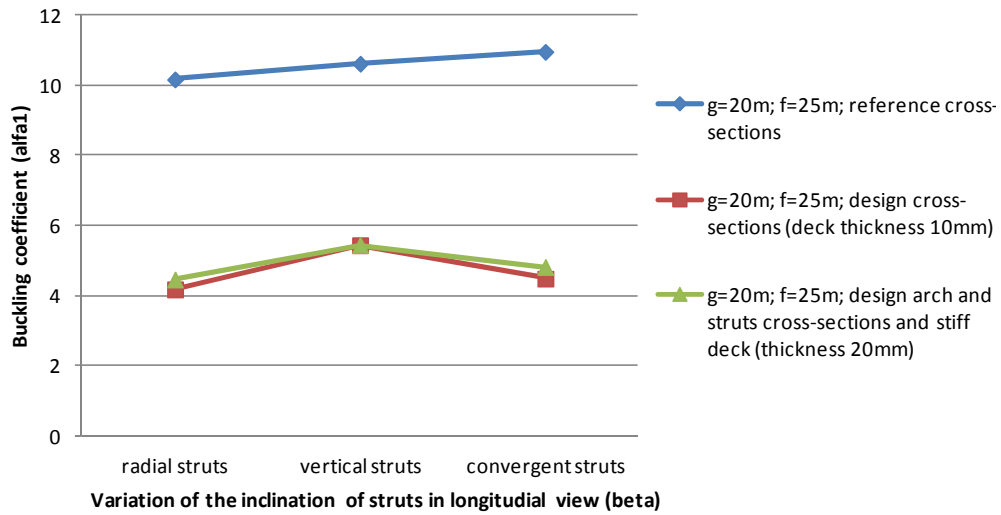
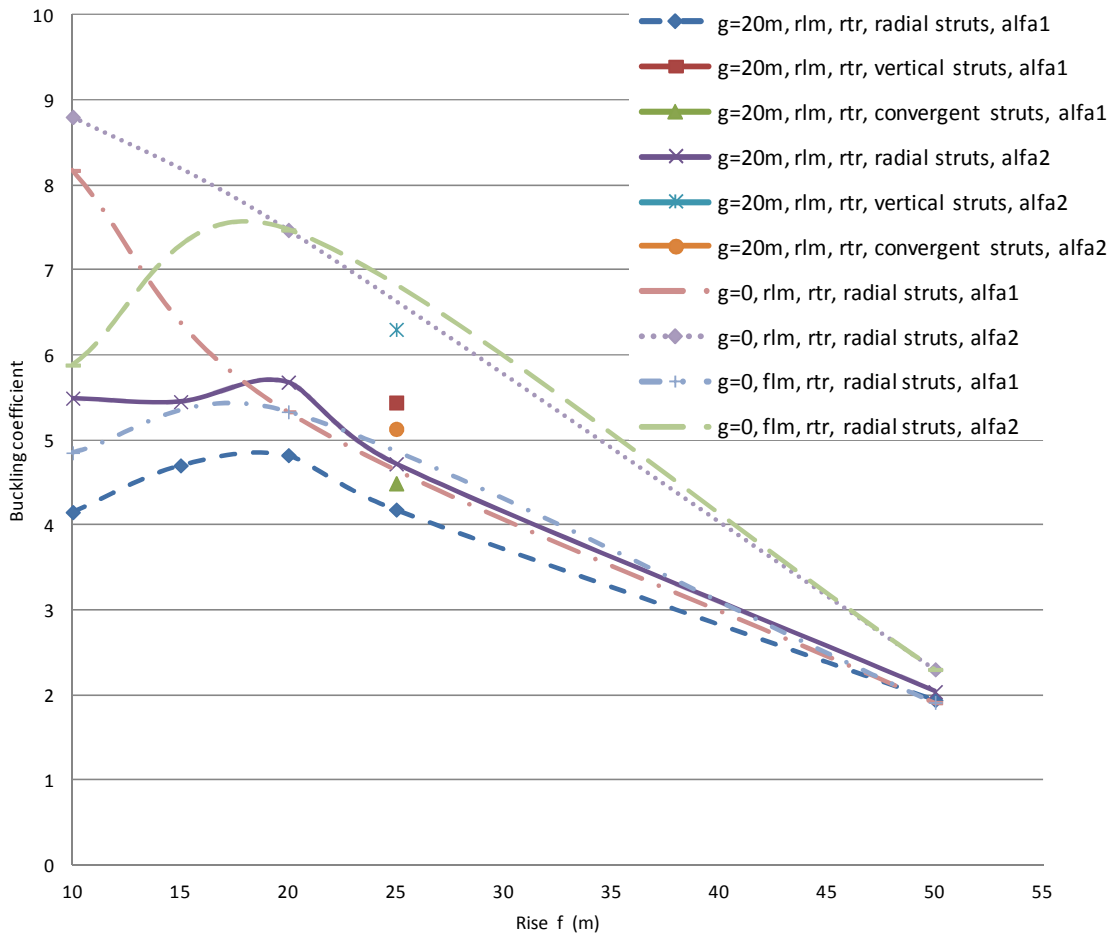
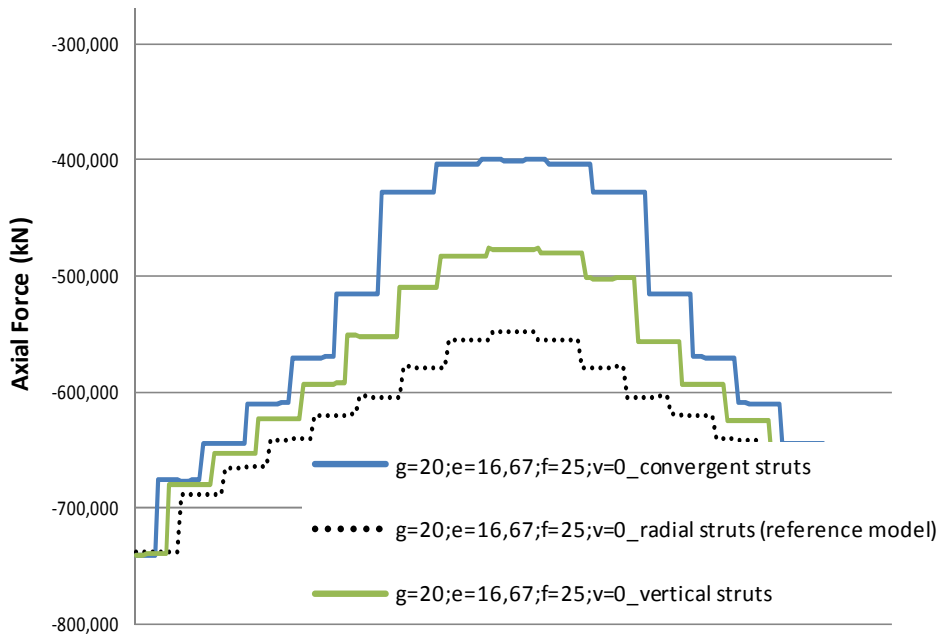


Figure 2-17: Buckling coefficient  $\alpha_1$  ( $\alpha_1$ ) comparison of struts inclination ( $\beta$ ) values when employing different cross-sections (Table 1-1, Table 1-2 and Table 1-5) with  $g=20m$  and  $f=25m$

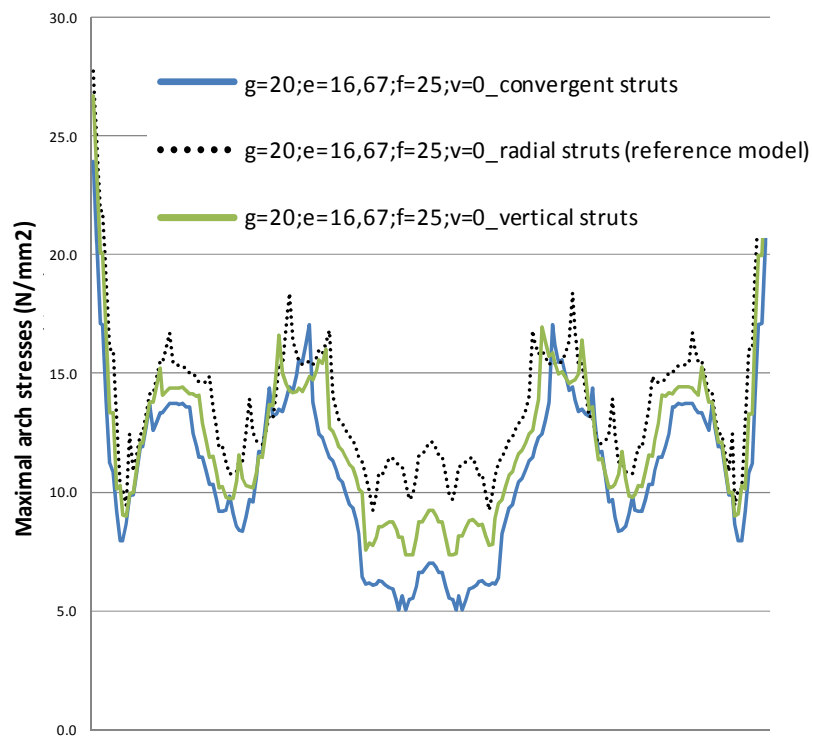


Note: for the cases with vertical and convergent struts only arches with  $f=25m$  have been analysed. Hence there is a single result

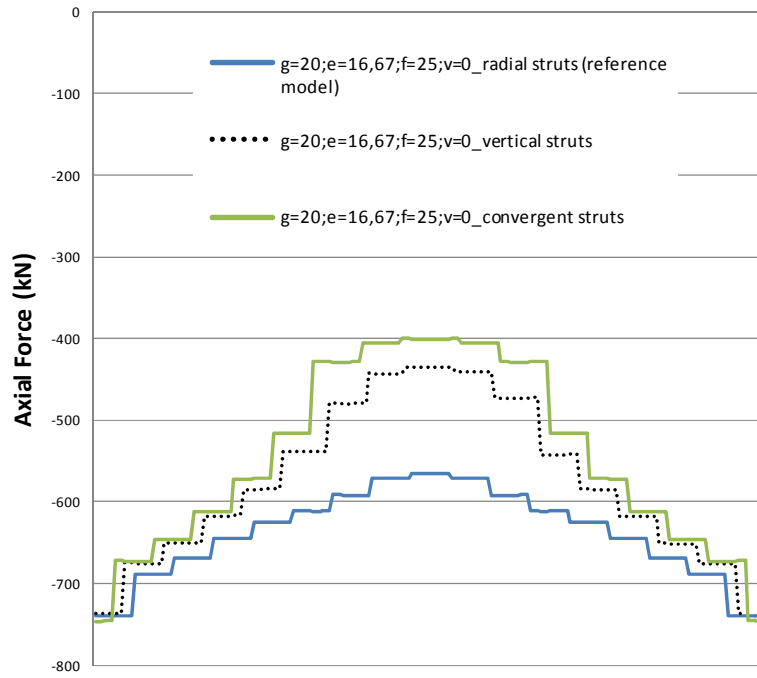
Figure 2-18: Buckling coefficient  $\alpha_1$  ( $\alpha_1$ ) and  $\alpha_2$  ( $\alpha_2$ ) (defined in section 1.4). Comparison of different arch rise ( $f$ ) values, struts inclination ( $\beta$ ) values and bearing conditions. The design cross-section values (Table 1-2 and Table 1-3) are employed for each model. Note that for non-radial struts only the values for  $f=25m$  are given



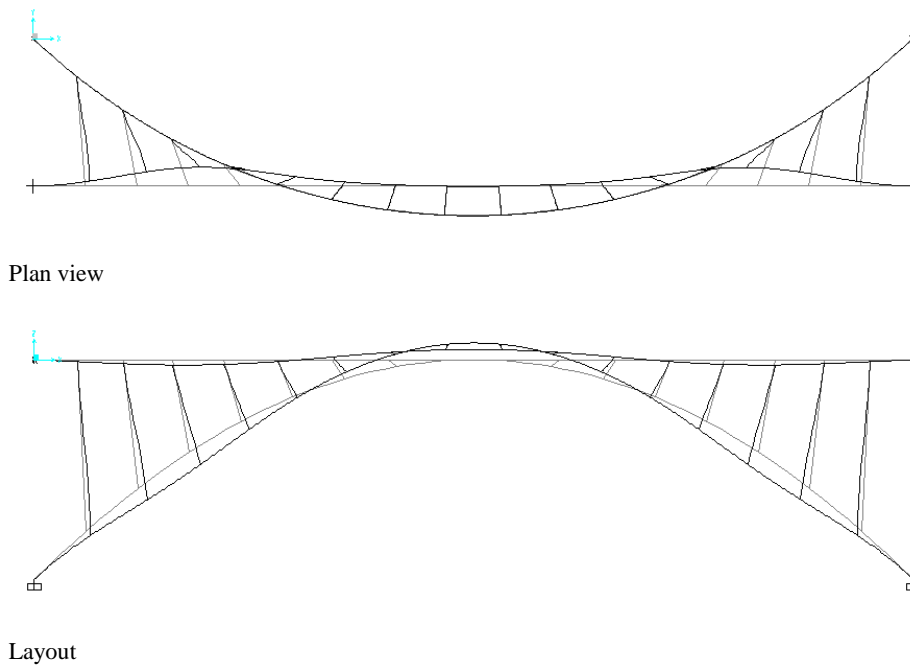
**Figure 2-19:** Arch axial forces comparison for different  $\beta$  values,  $f=25\text{m}$  and  $g=20\text{m}$ , employing reference cross-sections (Table 1-1), under a uniform loading on the whole deck length (self-weight not included, only  $q=10\text{kN/m}$ ). *The abscissas are the arch length from 0 to  $L_A$*



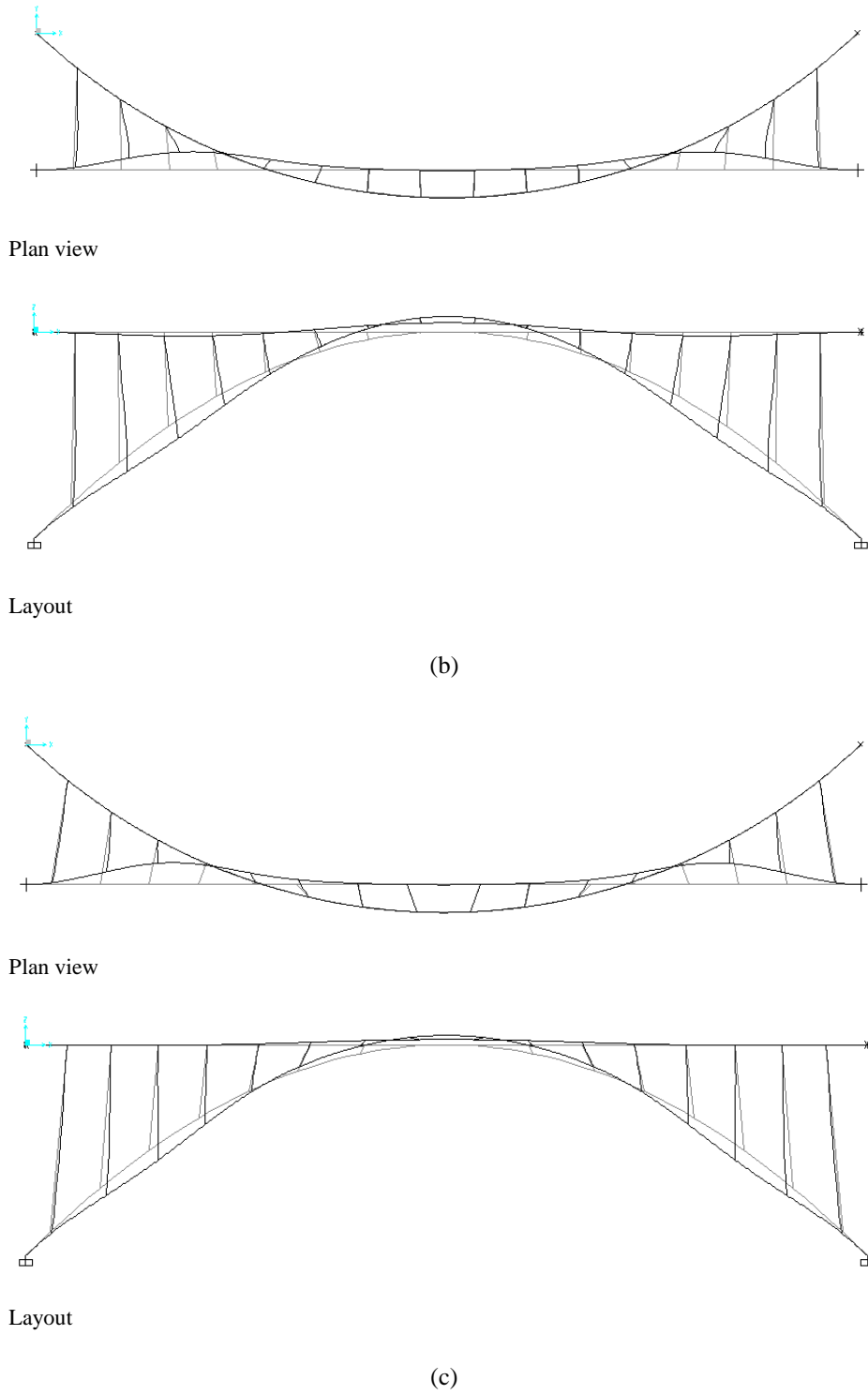
**Figure 2-20:** Arch stresses comparison for different  $\beta$  values,  $f=25\text{m}$  and  $g=20\text{m}$ , employing reference cross-sections (Table 1-1), under a uniform loading on the whole deck length (only  $q=10\text{kN/m}$ ). *The abscissas are the arch length from 0 to  $L_A$*



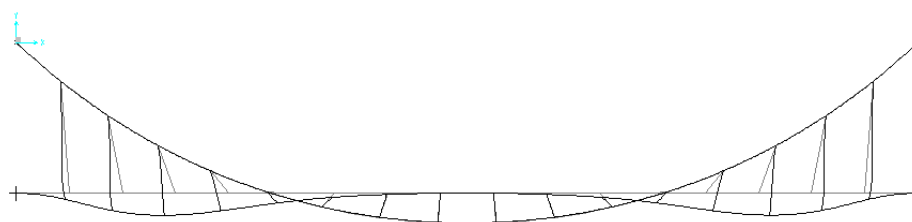
**Figure 2-21: Arch axial forces comparison for different  $\beta$  values,  $f=25\text{m}$  and  $g=20\text{m}$ , employing design cross-sections (Table 1-4), under a uniform loading on the whole deck length (only  $q=10\text{kN/m}$ ). The abscissas are the arch length from 0 to  $L_A$**



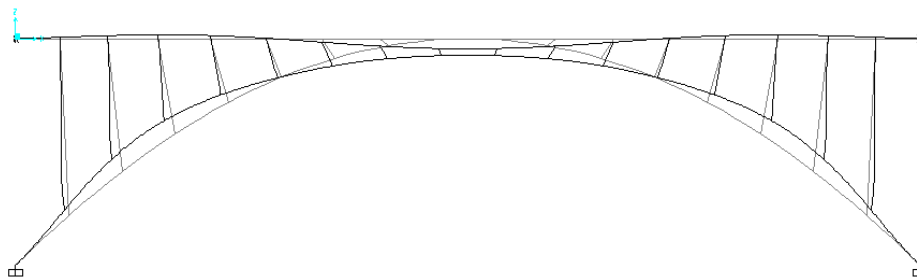
(a)



**Figure 2-22: Buckling shapes for  $g=20m, f=25m$  and different  $\beta$  values employing reference cross-sections. (a) Radial struts (b) Vertical struts (c) Convergent struts**

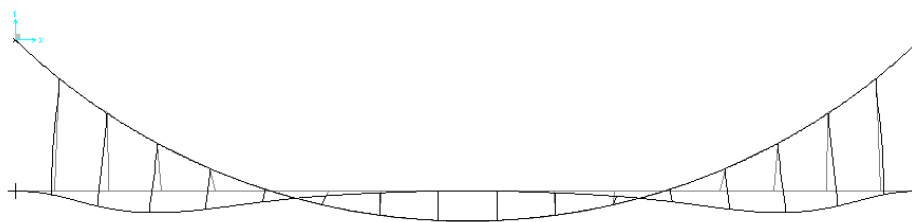


Plan view

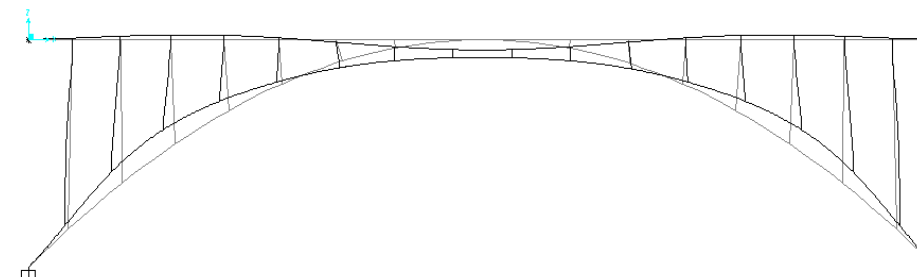


Layout

(a)

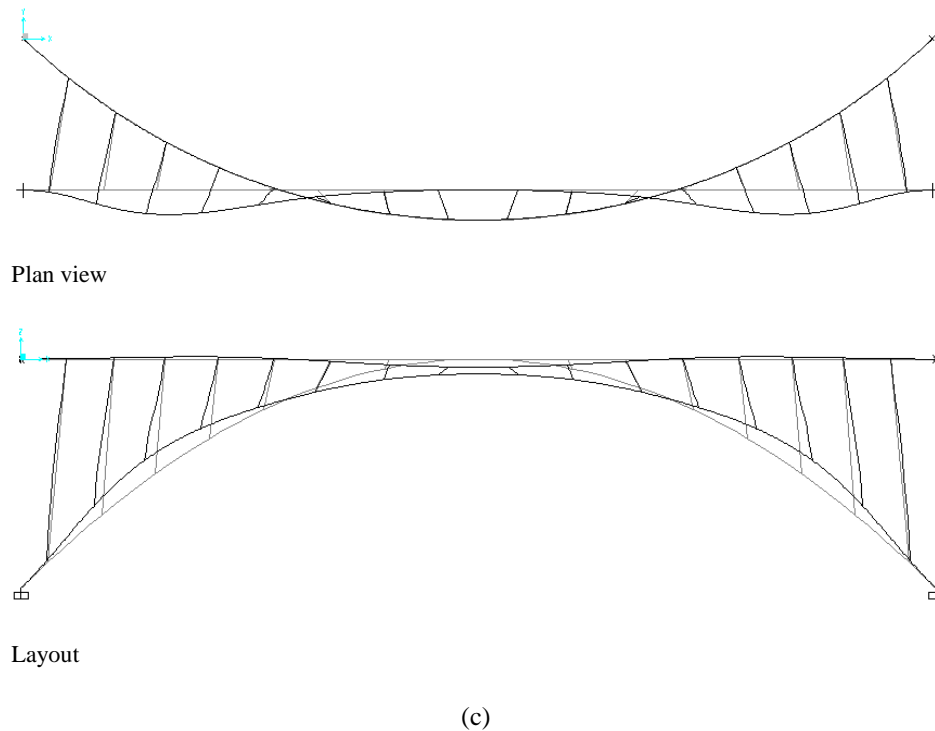


Plan view



Layout

(b)



**Figure 2-23: Buckling shapes for  $g=20\text{m}$ ,  $f=25\text{m}$  and different  $\beta$  values employing design cross-sections. (a) Radial struts (b) Vertical struts (c) Convergent struts**

## 2.4 3D BUCKLING: DECK INFLUENCE ON THE BUCKLING OF SABWSCD

As the results in the previous sections attest, SABs suffer a unique phenomenon in comparison to planar arch bridges with a straight deck: 3D buckling.

The fact that SABs buckle in two planes is something expected a priori due to their own definition which involves an important spaciality character, but it is an important difference with planar arch bridges with a straight deck and does not have an obvious explanation. It may be due to different facts:

- A vertical loading on the deck is introduced by the struts on the arch as in-plane and out-of-plane forces.
- The curved deck has a radial stiffness which could be modelled as out-of-plane springings on the arch.

However, the arch suffers the buckling only due to axial forces and the out-of-plane forces introduced by struts produce bending and torsional moments on the arch, but do not contribute to axial forces. Therefore, 3D buckling must be due to the deck radial stiffness. Nonetheless, planar vertical arch bridges with a straight superior deck and struts fixed to both arch and deck also have the influence of the transverse stiffness of the deck, but only buckle in one plane.

In order to explain 3D buckling and assure it is produced by the shape of the deck and not by the orientation of the struts a model without deck has been analysed. The loads transmitted to the struts by the deck under the load combination A1 (defined in section 1.4) have been introduced

into a model of structure system of the arch with fixed struts and with no superior deck. Buckling elastic analysis has been conducted.

The value of  $\alpha_1$  obtained for the described model with  $f=50\text{m}$  and employing the cross-sections described in Table 1-2 is 0,26. This value versus  $\alpha_1$  obtained for the equivalent model with deck ( $\alpha_1=0,26$ , versus  $\alpha_1=5,92$ ) demonstrates the important stabilising effect of the deck.

The arch buckles out-of-plane and not in-plane. This clearly proves that the arch does not buckle in two planes due to the fact that it is submitted to forces in and out-of-plane under vertical loading of the deck, but due to the curved superior deck. However, 3D buckling is not really due to the deck stiffness, but to the fact that under vertical loadings the deck is acting as an arch in plan view and suffers radial displacements which are transmitted as out-of-plane displacements to the arch. When the arch starts buckling in-plane or out-of-plane the direction of its movements is altered by 3d movements of the deck.

Just as the arch and deck move in 3D under vertical loadings under the buckling load, the arch buckles in both planes.

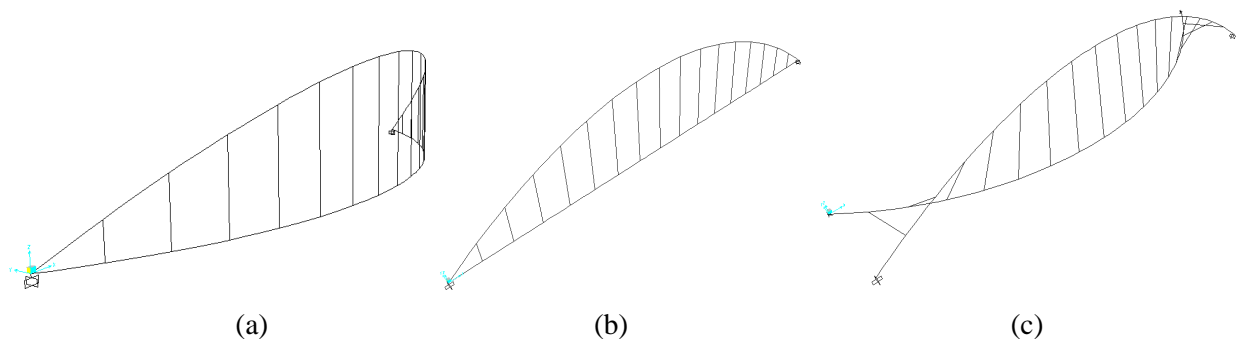
### 3. ELASTIC BUCKLING OF INFERIOR DECK ARCH BRIDGES

Several models of IDABWIC have been analysed in chapter IV. A.

The buckling loads and modes of an IDABWIC with  $L=100\text{m}$ ,  $g=20\text{m}$  and  $f=20\text{m}$  (Figure 3-1a), as studied in chapter IV. A, have been analysed here and compared to those of an equivalent inferior straight deck planar arch bridge with  $g=0$  and  $f=20\text{m}$  (Figure 3-1b). The arch is fixed to the deck which is itself fixed at abutments.

Different cross-sectional properties have been employed (Table 1-8). Rigid hangers fixed to both arch and deck have been employed, as well as flexible pinned hangers.

The elastic buckling of planar vertical arch bridges with an inferior curved deck with the equivalent values to the previously studied superior arch bridges, with  $L=100\text{m}$ ,  $g=20\text{m}$ ,  $e=16,67\text{m}$  and  $f=20\text{m}$  has also been studied for reference cross-section values (Figure 3-1c).



**Figure 3-1. Studied geometries (a) IDABWIC with  $L=100\text{m}$ ,  $g=20\text{m}$  and  $f=20\text{m}$  (b) Planar vertical arch with an inferior straight deck,  $g=0$  and  $f=20\text{m}$  (c) Planar vertical arch with a curved inferior deck with  $L=100\text{m}$ ,  $g=20\text{m}$ ,  $e=16,67\text{m}$  and  $f=20\text{m}$**

### 3.1 Analyses of the results for reference cross-section values

The results are displayed in Table 3-1, Figure 3-2, Figure 3-3 and Figure 3-4 and are commented as follows:

- The critical buckling load for an IDABWIC is much higher than for a planar vertical bridge, because the arch takes lower axial forces (see Chapter IV.A and values of axial forces in Table 3-1). However, for a planar vertical bridge with a curved inferior deck it is interesting to note that the buckling load is very similar to that of a planar vertical arch bridge with an inferior straight deck (Table 3-1), since destabilizing forces take place at span center. At span center the deck has less influence on the arch and there is a longer destabilizing path (Figure 3-4 BB').
- The deck in both cases, planar vertical arch bridges and IDABWIC, acts stabilizing the arch buckling, since the hangers are under tension (Figure 3-5). However, when comparing the results of  $\alpha_1$  with arch bridges employing a superior deck (results for  $f=20\text{m}$  in Figure 2-2 (rlm, rtr) versus Table 3-1), the buckling load for vertical planar arches with a straight or curved inferior deck ( $\alpha_1= 4,4$  and  $5$ , respectively) is lower than with a straight or curved superior deck ( $\alpha_1= 13,5$  and  $10,2$ , respectively). This is so because, in spite of the fact that an inferior deck offers more stabilizing forces, a superior deck controls better the movements of the arch at span center, where the struts are shorter and, thus, stiffer.
- For a planar vertical arch with an inferior straight deck a larger buckling load is obtained when employing rigid, fixed hangers. However, flexible hangers have given higher buckling loads than rigid ones in IDABWIC. This is so because the axial forces in the arch are greatly diminished when employing flexible hangers (ie, no Vierendel effect), but not because the structure has a better buckling behaviour. If the axial forces are compared (Table 3-1) it is clear that, in spite of buckling for a larger load, the arch has a worse buckling behaviour.
- In comparison to planar vertical arch bridges, IDABWICs buckle for a larger load, but as just observed it is due to the fact that, given a loading value, the arch undergoes lower axial forces for IDABWIC.
- The values of critical buckling axial loads are similar for all the models except for the planar vertical arch with an inferior straight deck suspended of flexible hangers which has a lower axial buckling critical load (Table 3-1).
- The IDABWIC model with  $g=20$  and rigid hangers fixed to arch and deck, however, has a different behavior than the rest of the studied examples. Whereas in all cases the arch is under compression in its whole length, for this model the arch is tensioned at springings.
- For all models the axial compressive critical buckling force ( $N_{cr}$ ) takes place at springings is given in Table 3-1, but, for the IDABWIC model with rigid hangers, it takes place at span center. These values are given in Table 3-1.

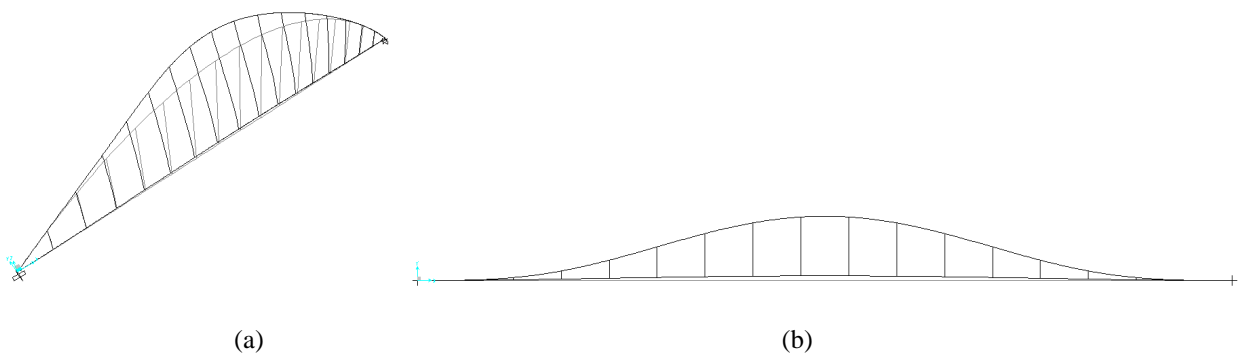


ARCH GEOMETRY	Buckling Mode	$q_{CRITICAL}$	$\alpha_1$	$N_{cr}$	$N_{q_0 \text{ min}}$ (kN)	Buckling Form
ID-ABWIC with $g=20$ and rigid hangers fixed to arch and deck	1	$96,2q_0$	11,85	24748	302	Unsymmetrical In and out of plane Figure 3-3
ID-ABWIC with $g=20$ and flexible hangers	1	$139,2q_0$	17,15	20696	192	Unsymmetrical In and out of plane
Planar vertical arch with inferior curved deck	1	$36,6 q_0$	4,98	22894	-	Symmetrical In and out of plane Figure 3-4
Planar vertical arch with inferior straight deck and rigid hangers fixed to arch and deck	1	$36,6q_0$	4,44	23441	754	Symmetrical Out of plane Figure 3-2
	2	$39,1q_0$				Asymmetrical Out of plane
	3	$82,2q_0$				Symmetrical Out of plane
Planar vertical arch with inferior straight deck and flexible hangers	1	$26,2q_0$	3,18	14818	756	Symmetrical Out of plane

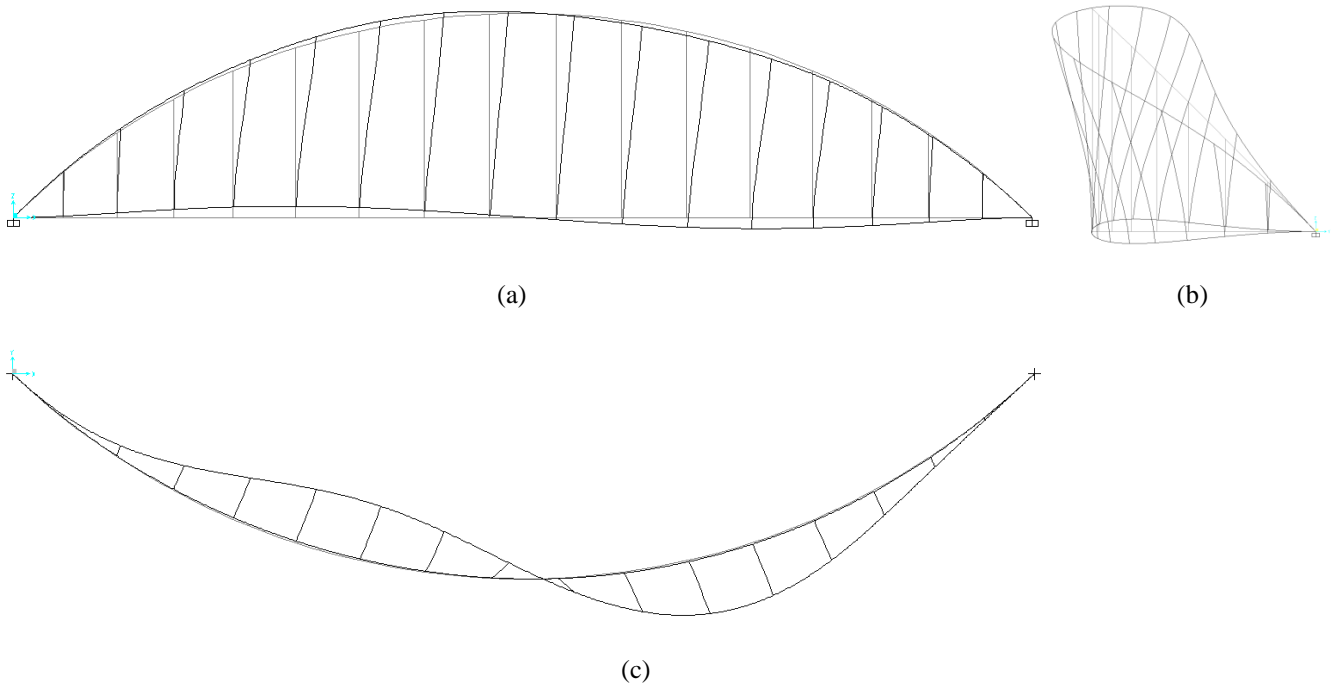
$q_0=10\text{kN/m}$

$N_{q_0 \text{ min}}$ =Minimal axial force in the arch under  $q_0$  uniformly distributed loading on the whole deck

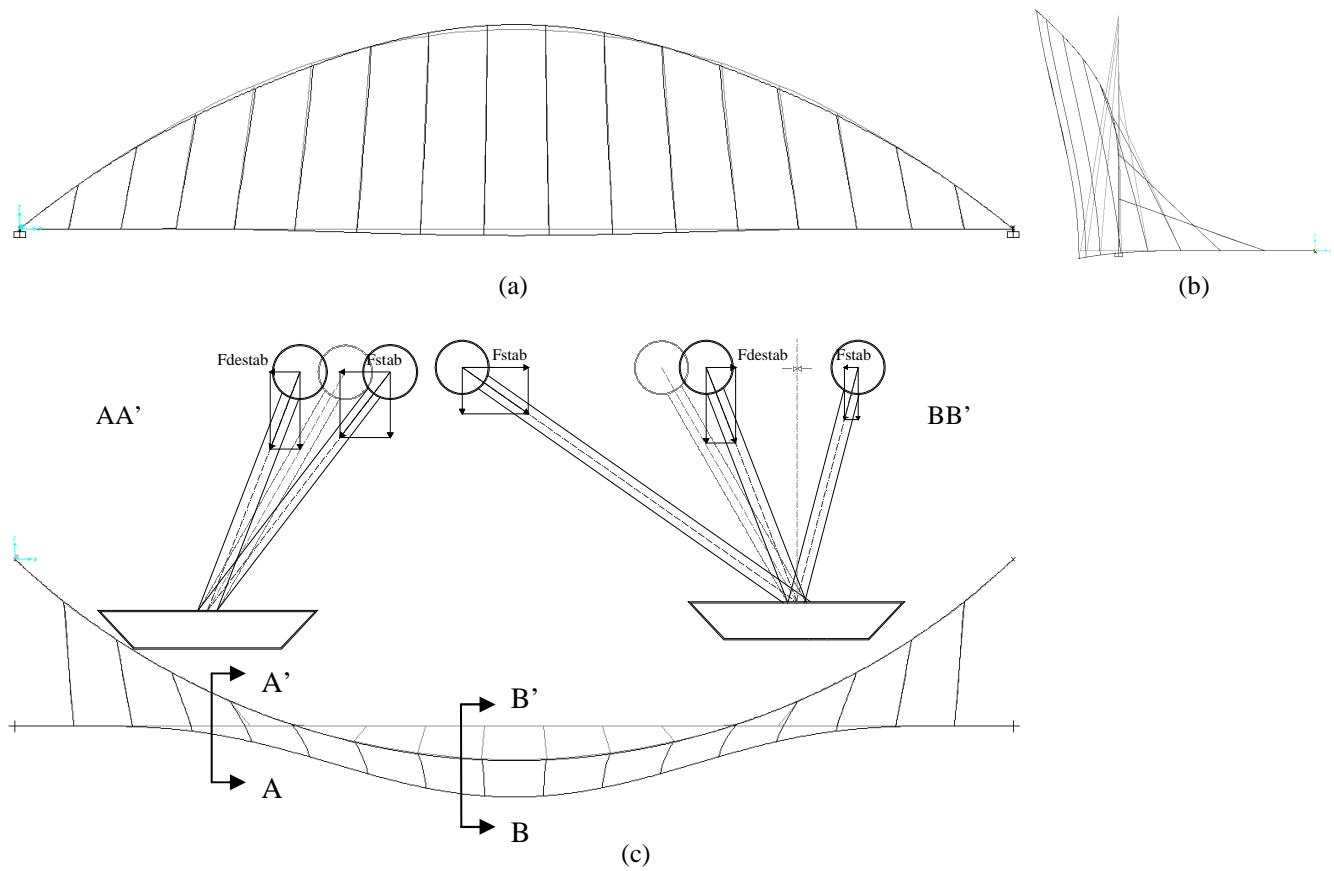
**Table 3-1: Buckling critical loads comparison for the first 3 modes of an IDABWIC and a planar vertical bridge employing reference cross-sections (Table 1-8)**



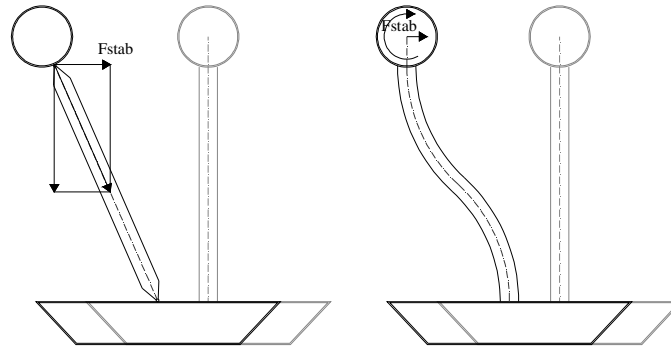
**Figure 3-2: Buckling shape of arch bridge model with  $g=0$  and  $f=20\text{m}$ , employing reference cross-sections (Table 1-8). (a) Perspective (b) Plan view**



**Figure 3-3: Buckling shape of IDABWIC with  $g=20\text{m}$  and  $f=20\text{m}$  employing reference cross-sections (Table 1-8). (a) Longitudinal view (b) Lateral view (c) Plan view**



**Figure 3-4: Buckling shape of planar vertical arch bridge with an inferior curved deck with  $g=20\text{m}$ ,  $e=16,67\text{m}$  and  $f=20\text{m}$ , employing reference cross-sections (Table 1-8). (a) Longitudinal view (b) Lateral view (c) Plan view with cross sections showing stabilizing and destabilizing forces**



**Figure 3-5: Cross-section of buckling shape for both, of the arch bridge model with  $g=0$  and  $f=20m$  and of the IDABWIC with  $g=20m$  and  $f=20m$ , employing reference cross-sections. (a) Stabilizing effect caused by axial forces out-of-plane projection and (b) stabilizing effect caused by shear forces which appear due to fixed hanger joints.**

### 3.2 Analyses of the results for a rigid hanger-deck system

The results of the buckling analyses employing cross-section values for a rigid hanger-deck system (Table 1-8) are displayed in Table 3-2.

- The cross-section values for a radially (or transversally) very stiff hanger-deck system given in Table 1-8 (and employed at the end of chapter IV) are theoretical values, that is why this models give incredibly higher buckling loads in comparison with the reference values. Nonetheless, the buckling forms are equal and IDABWICs still buckle in both planes.
- When the hanger-deck system has a large transversal stiffness, IDABWICs and planar vertical arches with an inferior straight deck buckle nearly for the same vertical uniformly distributed loading (Table 3-2).
- As it happens with the structural behavior of IDABWIC regarding internal forces, it is also much more efficient increasing the hangers radial stiffness than the transverse one-meaning with transverse the orientation perpendicular to the straight imaginary line which would join the abutments, ie: the hangers would all be parallel. Thus, radially stiff hangers give a buckling load more than double than transversally stiff ones (Table 3-2).

ARCH GEOMETRY	$q_{CRITICAL}$	$\alpha 1$	Buckling Form
ID-ABWIC with $g=20$ and with radially stiff hangers	$247,9q_0$	34,0	Unsymmetrical in and out-of-plane
ID-ABWIC with $g=20$ and with transversally stiff hangers	$116,6q_0$	15,5	Unsymmetrical in and out-of-plane
Planar vertical arch with inferior straight deck	$113,3q_0$	15,5	Unsymmetrical in-plane

*$q_0=10kN/m$ ; radially stiff hangers have their largest stiffness oriented radially to the deck curvature, transversally stiff hangers are orientated perpendicularly to the cord of the deck*

**Table 3-2: First mode of buckling critical loads comparison for the first 3 modes of an IDABWIC and a planar vertical bridge employing a stiff hanger-deck system (Table 1-8)**

## 4. COMPARISON OF NUMERICAL RESULTS VERSUS ANALYTICAL RESULTS OF THE BUCKLING LOADS

The comparison of analytical and numerical results is carried out in the present chapter for the following cases:

- Planar arch bridges with a superior straight deck with different bearing conditions
- Superior deck arch bridges with different  $g$  and  $f$  values and with different deck stiffness values.
- Different inferior deck arch bridges

In order to establish if the analytical formulation is good enough it is compared with the numerical results. To compare the results, the error for various parameters is calculated as follows:

$$error = \frac{\text{numerical value} - \text{analytical value}}{\text{numerical value}} \cdot 100$$

As mentioned in section A2.1 of the present chapter, the loading distribution for which  $N_{cr}$  is given in Eurocode 3 (EC3) Part 2 Annex D3 is not clearly stated, but, according to Figure D.4 in EC3 and to the formulation in Galambos (1988) (commented in section 2.2 of section A of the present chapter), it is for a uniformly distributed vertical load in the whole deck length. Therefore, in the present research the criteria that  $N_{cr}$  is the largest axial force value in the arch under a uniformly distributed vertical loading on the whole deck length has been adopted.

An analytical formulation, proposed for inferior deck planar vertical arch bridges in a recent research study (Bergmeister et al, 2009), has also been employed.

### 4.1 Planar arch bridges with a superior straight deck. Analytical and numerical results comparison for different bearing conditions

#### 4.1.1 Considerations

Out-of-plane buckling in the codes is for free standing arches, but the buckling factor is dependent on certain characteristics of the deck. Therefore, it is not clear for which bearing conditions are the code formulae developed. A comparison of different bearing conditions has been therefore carried out (Table 4-1) to validate the codes formulae under different conditions and joints. The following situations for  $g=0$  and  $f=20\text{m}$  have been considered:

- Free longitudinal movements (flm) and free rotations (including free torsional rotations, ftr) at deck abutments. Transverse and vertical displacements are restrained. The arch is fixed at its springings and struts are fixed at both ends, ie: at arch and deck.
- All movements are restrained (including longitudinal movements, rlm), torsional rotations are restrained (rtr) and the rest of rotations at deck abutments are free. The arch is fixed at its springings and struts are fixed at both ends, ie: at arch and deck.
- Free longitudinal movements (flm) and restrained torsional rotations (rtr) at deck abutments. Transverse and vertical displacements are restrained and the rest of rotations

are free. The arch is fixed at its springings and struts are fixed at both ends, ie: at arch and deck.

- Free longitudinal movements (flm), free transverse movements (ftm) and free rotations (including free torsional rotations, ftr) at deck abutments. Vertical displacements are restrained. The arch is fixed at its springings and struts are pinned at both ends, ie: at arch and deck.
- Free standing arch (no deck or struts) fixed at its springings.

Since there are no coefficients in table D4 of Eurocode 3 (EC3) Part 2 Annex D3 for fixed bridges and in-plane symmetric buckling, the buckling case of some examples cannot be handled. Therefore, the coefficients for fixed arches and asymmetric buckling have been employed in all cases.

It must be highlighted that the formula for out-of-plane  $N_{cr}$  of Bergmeister et al (2010) is for inferior-deck planar arch bridges, as explained in Chapter VI. A, so it is only comparable in such a case.

Reference cross-sections have been employed for this study.

#### 4.1.2 *Analyses of the results*

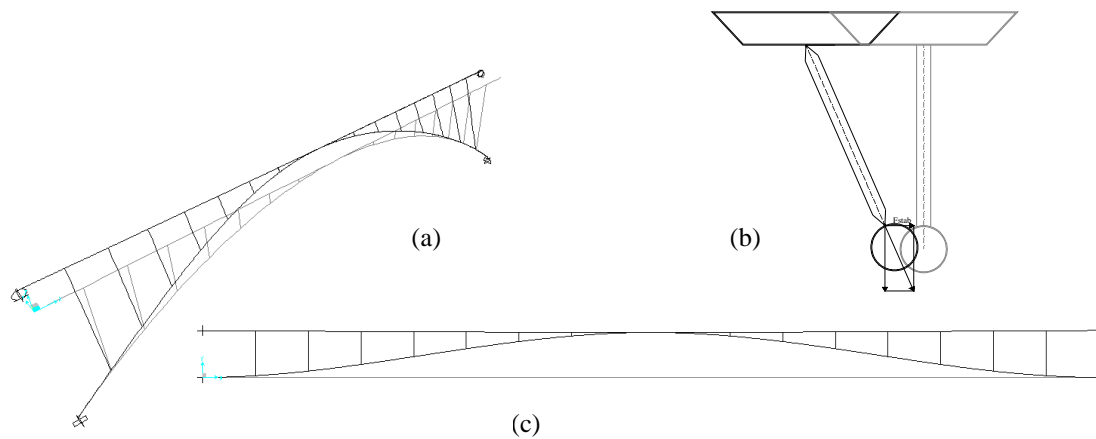
An example of the buckling shape can be observed in Figure 4-1.

The results are summarized in Table 4-1 and are commented as follows:

- It is clear that the out-of-plane formulation is for a free standing arch as the code states, in spite of the deck being considered in the buckling factors of the formulation (Table 4-1). The  $N_{cr}$ , however is more similar to the one obtained at the deck crown:
  - Free standing arch:
    - $N_{cr}$  at springings for the numerical value of the buckling load: 6978kN
    - $N_{cr}$  at crown for the numerical value of the buckling load: 5336kN
    - $N_{cr}$  according to EC3: 5043kN
- The results of EC3 of the simplified formulation do not give a good enough approximation for buckling in arch bridges (minimal error=68%, Table 4-1).
- As already observed in Figure 2-1 and Figure 2-2 the model with rlm and rtr is the one which presents the best behaviour to buckling according to the numerical analyses.
- Whereas according to EC3 the arch would buckle out-of-plane for all cases (Table 4-1), the FE model show that for flm and rtr the buckling takes place in-plane, as already observed in Figure 2-6e.

$g$ (m)	distribution of struts	Bearing conditions	$f$ (m)	$L$ (m)	Numerical $N_{cr}$ (kN)	Buckling shape according to the numerical analysis	Minimal $N_{cr}$ in-plane or out-of-plane according to EC3 (kN)		Error of EC3 simplified formula with respect to $N_{cr}$ numerical results (%)
0	radial (reference model)	flm, ftr	20	100	44833	Out-of-plane	14430.8	Buckling out-of-plane	68
0	radial (reference model)	rlm, rtr	20	100	63310	Out-of-plane	14554.0	Buckling out-of-plane	69
0	radial (reference model)	flm, rtr	20	100	55975	In-plane	14515.4	Buckling out-of-plane	77
0	radial (reference model)	flm, ftm, ftr pinned hangers	20	100	3465	Out-of-plane	10564.1	Buckling out-of-plane	-205
0	radial (reference model)	free standing arch	20	100	6978	Out-of-plane	5043.2	Buckling out-of-plane	28

**Table 4-1: Analytical results comparison for different bearing and joint conditions employing the reference cross-sections**



**Figure 4-1: Buckling shape of arch bridge model with  $g=0, f=20m$ , flm, ftm, ftr and pinned hangers  
(a) Perspective (b) Cross-section: stabilizing effect (c) Plan view**

## 4.2 Superior deck arch bridges. Analytical and numerical results comparison for different $g$ and $f$ values and for different deck stiffness values.

### 4.2.1 Considerations

- The comparison of the numerical results of the axial loads at the arch springings obtained for the critical buckling load, for different  $g$  and  $f$  values, with the ones obtained with simplified formulae detailed in Eqs 1 and 2 in section A2.1 of the present chapter VI are displayed in Table 4-2 and Table 4-3. For both tables, design cross-sections have been employed for the struts and arch (Table 1-2 and Table 1-3).
- In Table 4-3 a stiffer deck than the one needed according to design has been employed (Table 1-6).
- In Table 4-2 a less stiff deck with 3mm thickness (Table 1-7) has been employed.
- Models with  $g=0$  have free longitudinal movements at deck abutments, the rest of the movements are restrained and the rotations are all free (flm, ftr), because these were the bearing conditions with a lower error according to Table 4-1, apart from the free standing arch.
- For models with  $g=20m$ , all the movements and the torsional rotations are restrained at deck abutments, the rest of the rotations are free.
- For  $g=20m$ , these bearing conditions are chosen for the deck because they are the ones which best work for this bridge type, as proved in chapter V.A.

### 4.2.2 Analyses of the results

- A priori, a less stiff deck is expected to have less influence on the buckling of the arch and, therefore, the results would be expected to be nearer to the ones obtained analytically by means of EC3 formulae in the case of  $g=0$ .
  - This is so for  $f \leq 20m$  (errors of EC3 in Table 4-2 compared to Table 4-3). As already commented in section 2.2 these are the values mainly affected by the rigidity of the deck, since arch and deck buckle together.
  - For  $f > 20m$  the error in Table 4-3 and Table 4-2 is the same, since the deck has a lower influence on the buckling of the arch.
- The formulae of EC3 are for free standing arches as demonstrated in section 4.1. Therefore, the error committed for all the analysed models is very high, whatever the  $g$  value.
- Not only need formulae for SABs be developed, but also an improvement of the existing formulae for planar arch bridges with a superior straight deck is required, since existing formulae are very conservative.

$g$ (m)	distribution of struts	$f$ (m)	$L$ (m)	$I_{arch}$ (m <sup>4</sup> )	$I_{deck}$ (m <sup>4</sup> )	Numerical Ncr (kN)	Minimal Ncr in-plane or out-of-plane according to EC3 (kN)		Error of EC3 simplified formula with respect to Ncr numerical results (%)
0	radial (reference model)	10	100	4.66E-03	4.86E-02	14268.80	7532.1	Buckling out-of-plane according to EC3	47
	radial (reference model)	20	100	3.75E-03	4.86E-02	12800.44	4302.9	Buckling out-of-plane according to EC3	66
	radial (reference model)	50	100	3.75E-03	4.86E-02	5038.30	901.6	Buckling out-of-plane according to EC3	82
20	radial (reference model)	10	100	5.64E-03	4.86E-02	19862.81	8937.9	Buckling out-of-plane according to EC3	55
	radial (reference model)	20	100	4.41E-03	4.86E-02	17565.65	5117.1	Buckling out-of-plane according to EC3	71
	radial (reference model)	50	100	3.06E-03	4.86E-02	6452.21	818.1	Buckling out-of-plane according to EC3	87

**Table 4-2: Analytical results comparison for different  $f$  and  $g$  values employing the design cross-sections and a low stiffness deck with a thickness of 3mm, neglecting local buckling**



$g$ (m)	distribution of struts	$f$ (m)	$L$ (m)	$I_{arch}$ (m <sup>4</sup> )	$I_{deck}$ (m <sup>4</sup> )	Numerical $N_{cr}$ (kN)	Minimal $N_{cr}$ in-plane or out-of-plane according to EC3 (kN)		Error of EC3 simplified formula with respect to $N_{cr}$ numerical results (%)
0	radial (reference model)	10	100	4.66E-03	3.18E-01	40477.57	7669.2	Buckling in-plane	81
	radial (reference model)	20	100	3.75E-03	3.18E-01	16427.09	4382.9	Buckling out-of-plane	73
	radial (reference model)	50	100	3.75E-03	3.18E-01	4975.45	907.3	Buckling out-of-plane	82
20	radial (reference model)	10	100	5.64E-03	3.18E-01	41340.86	8617.2	Buckling out-of-plane	79
	radial (reference model)	15	100	4.41E-03	3.18E-01	32063.15	6153.8	Buckling out-of-plane	81
	radial (reference model)	20	100	4.41E-03	3.18E-01	26422.85	4938.1	Buckling out-of-plane	81
	radial (reference model)	25	100	3.75E-03	3.18E-01	20028.60	3359.8	Buckling out-of-plane	83
	radial (reference model)	50	100	3.06E-03	3.18E-01	7690.35	727.4	Buckling out-of-plane	91

**Table 4-3: Analytical results comparison for different  $f$  and  $g$  values employing the design cross-sections with a stiffer deck (Table 1-6).**

### 4.3 Inferior deck arch bridges. Analytical and numerical results comparison for

In section A2.1 of the present chapter VI it has been stated according to the state-of-the-art that for planar vertical arch bridges with inferior straight deck a useful simplified formulation would be the one described by Bergmeister et al (2009) to obtain elastic buckling (Eq 3 and 6 in section A2.1 of the present chapter VI). This is still expected to be conservative. This has been verified with numerical results. Results are shown in Table 4-4.

In all the models, the abutments are fixed to the arch springings, which are themselves fixed to the ground. Rigid hangers are employed and they are fixed to arch and deck.

- When compared to a free standing arch of identical geometry as the one employed for the planar vertical arch bridge, the EC3 results are nearer to numerical ones than when considering the whole bridge, as observed in section 4.1.
- It is clear that the deck and struts have a stabilizing effect, allowing more than thrice the buckling load of a free standing arch.
- IDABWICs have a much higher buckling load, nearly 9 times the buckling load of a free standing arch.
- The larger values of  $q_{cr}$  of IDABWIC in comparison with planar arch bridges, in spite of a smaller  $N_{cr}$ , are due to the structural behavior of the arch bridge in which the arch takes smaller axial forces. This has been already explained for different models in the previous sections.
- As it occurred in the previous analysed cases EC3 values give a very high error.
- Bergmeister et al (2009) formulae give an error which is even higher than the EC3 formula, since the  $q_H/q$  relationship to determine  $\beta_2$  (Table D7 EC3) is not considered.
- Not only need formulae for IDABWICs be developed, but also an improvement of the existing formulae for planar arch bridges with an inferior straight deck is required, since existing formulae are very conservative.

<b>Geometry</b>	<b>Planar vertical arch with inferior straight deck with rigid hangers fixed to arch and deck</b>	<b>IDABWIC with rigid hangers fixed to arch and deck</b>	<b>Free standing arch</b>
<b>g (m)</b>	0	20	0
<b>f (m)</b>	20	20	20
<b>L (m)</b>	100	100	100
<b>Iarch (m4)</b>	0,0108	0,0108	0,0108
<b>Ideck (m4)</b>	0,2517	0,2517	-
<b>Numerical Ncr (kN) (1)</b>	23441	24748	19320
	Symmetrical. Out-of-plane	Antymmetrical In and out of plane	Symmetrical. Out-of-plane
<b>Numerical qcr (kN/m)</b>	304	801	90
<b>Minimal Ncr in-plane or out-of-plane according to EC3 (kN) (2)</b>	5369	5213	5043
	Buckling in-plane according to EC3	Buckling out-of-plane according to EC3	Buckling out-of-plane according to EC3
<b>Error of EC3 simplified formula with respect to Ncr numerical results (%)</b> $\frac{(1) - (2)}{(1)} \cdot 100$	77	79	27
<b>Ncr out-of-plane according to EC3 (kN)</b>	9100	5213	5043
<b>Error of EC3 out-of-plane simplified formula with respect to Ncr numerical results (%)</b>	61	79	27
<b>Ncr out-of-plane buckling according to Bergmeister et al EC3 formula modification (kN)</b>	6980	6980	-
<b>Error of Bergmeister et al EC3 formula modification with respect to Ncr numerical results (%)</b>	70	72	-
<b>qcr out-of-plane buckling according to Bergmeister et al formula (kN/m)</b>	81	81	-
<b>Error of Bergmeister et al simplified formula with respect to qcr numerical results (%)</b>	73	90	-

Table 4-4: Analytical results comparison for arch bridges with an inferior deck with different *g* values and *f*=20m (Figure 3-1), employing the reference cross-sections

## 5. CONCLUSIONS

- SABs with a curved deck buckle in- and out-of-plane at the same time, even if a planar vertical arch is employed. This is so because, for a vertical loading, the deck undergoes horizontal and vertical displacements due to spatial the geometry of SABs.
- Critical buckling loads for a uniform distributed load on the whole deck length ( $lu$ ) are lower than for a uniformly distributed loading on half the deck length ( $la$ ) as expected, since  $lu$  causes larger axial forces in the arch than  $la$ .
- Geometries which give lower critical buckling loads usually coincide with geometries which bear larger axial forces in the arch. However,  $f$  values approximately in the range  $L/6 \leq f \leq L/4$  buckle for a larger load than  $f > L/4$ , in spite of undergoing larger axial forces.
- For large  $f$  values the arch buckles nearly independently of the deck because the struts are longer and thus less stiff.
- For low  $f$  values the arch and deck buckle together because arch and deck tend to work as a truss.
- For planar vertical arches with a superior straight deck, restraining torsional rotations improves the buckling behaviour, since it diminishes the destabilizing effect of the deck.
- Planar vertical SABs with a planar vertical arch and a superior curved deck buckle in both planes of the arch symmetrically except for low  $f$  values:
- The larger the  $f$  value, the larger the out-of-plane component.
- The buckling shapes are equivalent whatever the value of the cross-sections employed and of the bearing conditions.
- The geometry that best resists buckling is employing convergent struts, since for this geometry the arch bears the lowest axial forces and stresses. As expected, this is coincident with the most efficient model for spatial arch bridges with a curved superior deck sustained by a planar vertical arch regarding the minimum mass criteria employing design cross-sections as concluded in chapter V. B.
- However, when employing the design cross-sections to analyse the buckling, not only the geometry has influence, but also the stiffness distribution in the bridge. Since models employing vertical struts need stiffer struts, employing vertical struts happens to be more favourable for avoiding buckling in practice.
- Employing a stiffer deck or struts improves the buckling behaviour of the arch, since the deck has a stabilizing effect. This is more efficient than increasing the arch stiffness.
- Not only need formulae for SABs be developed, but also an improvement of the existing formulae for planar arch bridges with a straight deck is required, since the existing formulae are very conservative.

- If the total load on the bridge is calculated for the buckling coefficient  $\alpha$  under the load case  $(1,35 \cdot (w+pl) + \alpha \cdot lu)$  and  $\alpha_1$  ( $\alpha_1 \cdot [1,35 \cdot (w+pl) + 1,5 \cdot lu]$ ) very similar values are obtained, but the error of employing  $\alpha_1$  instead of  $\alpha$  is non-negligible (approximately 6%). Strictly correct method and most realistic would be to calculate  $\alpha$ , employing  $\alpha_1$  gives insecure (larger) buckling load values.

## 6. FUTURE LINES OF STUDY

- Development of analytical formulae for the critical buckling load of SABs
- Improvement of the existing formulae for the critical buckling load of planar arch bridges with a straight deck, since existing formulae are very conservative.

## REFERENCES

BERGMEISTER K., CAPSONI A., CORRADI L., MENARDO A., “Lateral Elastic Stability of Slender Arches for Bridges including Deck Slenderness”. *Structural Engineering International*, n. 2 v. 19. pp. 149-154(6). May 2009

CORREIA, Antonio A.; VIRTUOSO, Francisco B. E.. “Comportamento nao linear de uma ponte “bow-string” metálica”. *V Congresso de Construcao Metálica e Mista*. Abril 2005 (in portuguese)

DE BACKER H, OUTTIER, A., , and VAN BOGAERT, P. “The effect of using beam buckling curves on stability of steel arch bridges” *Proceedings of the Nordic Steel Construction Conference*, 2009. Available at: <<http://www.nordicsteel2009.se/pdf/43.pdf>>

MANZANARES J. L. and HINOJOSA, I., “Non-linear plastic analysis of steel arches under lateral buckling”. *Journal of Constructional Steel Research*, i. 12, v. 67. pp 1789-1984. December 2011

GALAMBOS, T. V.. *Guide to stability design: Criteria for metal structures*. 4th Ed, pp15-25, pp575-608, pp609-625. New York: John Wiley & Sons, 1988. ISBN: 0-471-09737-3



VI. C) GEOMETRICALLY NON-  
LINEAR ANALYSES OF SPATIAL  
ARCH BRIDGES WITH A CURVED  
SUPERIOR DECK AND A PLANAR  
VERTICAL ARCH





## INDEX

1. INTRODUCTION.....	337
1.1 Previous studies.....	337
1.2 Objectives.....	337
1.3 Loading cases and combinations.....	338
1.4 Research procedure and values.....	339
1.4.1 <b>Model values</b> .....	339
1.4.2 <b>Analyses method</b> .....	341
1.4.3 <b>Imperfection values</b> .....	341
2. ANALYSES OF THE RESULTS.....	342
2.1 STRUCTURAL RESPONSE UNDER DESIGN LOADING.....	342
2.1.1 SOFISTIK and SAP2000 results comparison.....	342
2.1.2 Linear and geometrically non-linear analyses comparison.....	345
2.2 STRUCTURAL RESPONSE OF THE ARCH UNDER STEP LOADING.....	348
2.2.1 First buckling mode imperfections direction sign.....	349
3. CONCLUSIONS.....	354
4. FUTURE LINES OF STUDY.....	354
REFERENCES.....	354



## 1. INTRODUCTION

Spatial arch bridges might undergo important geometrical non-linearities. Therefore, their behavior should be checked conducting a geometrically non-linear analysis and obtaining the ultimate load.

For the present study it is considered that the ultimate load is reached when the first fibre of the cross-section bearing the largest stresses plasticizes.

### 1.1 Previous studies

There are no equivalent European buckling curves for arch bridges. Therefore, the coded imperfections will be employed following the first mode of buckling shape as stated in Eurocode 3 (EC3 Part 1.1 Chapter 5.3.2). The specific values for arches in EC3 (Annex D.3.5) will also be employed. These imperfection values are expected to be conservative, as confirmed in the benchmark for the program SAP2000 v14 presented in Chapter III. B.

These tables are for planar vertical arch bridges with a straight deck and are not meant for composing both imperfections, but for evaluating each buckling mode independently. There is no reason while in this bridge type the imperfection should be larger than the maximal usual value for arches. However, since the imperfection according to EC3 Part 1.1 chapter 5.3.2 will also be employed and the sensitivity to imperfections is being evaluated, the composition of in-plane and out-of-plane imperfections will be employed.

In Manzanares et al (2011) the value  $L/1000$  has been employed for out-of-plane imperfections as additional to residual stresses for a planar arch bridge with a straight deck and the same value has been used by Outtier et al (2007) for modelling imperfections, together with eccentricity variations and residual stresses.

### 1.2 Objectives

The purpose of our study is to:

- compare the effects of geometrical non-linearities on planar arch bridges with a straight deck and on SABs with a superior curved deck.
- compare the effects of geometrical non-linearities on SABs with a superior curved deck with different  $f$  values.
- evaluate the sensitivity of SABs with a superior curved deck to the values of imperfections stated in EC3
- evaluate whether the design cross-sections obtained from a linear analysis (LA) are still valid when considering geometrical non-linearities

### 1.3 Loading cases and combinations

LA-GNLA comparison of the model with the cross-section already designed for LA is conducted under:

- Combination A1 and Combination A2 (defined in chapter V. B section 1.5.3 and bookmark), since most of the forces of the stress envelope of the arch come from Combination A1 with small differences with Combination A2 but it is interesting to see what happens with Combination A2
- Combination B and Combination A2 (defined in chapter V. B section 1.5.3 and bookmark), since most of the forces of the stress envelope of the deck come from these hypothesis
- Combination A1 and Combination A2, since most of the forces of the stress envelope of the struts come from these hypothesis

The cross-section design is obtained from the loading combinations envelope which gives the highest stresses when conducting a LA, as described in Chapter V. B.

The loading combination A1 (Chapter V. B section 1.5.3), with a UDL on the whole arch, is employed as basis for the geometrically non-linear step-loading analyses with SAP2000 (combination A1' defined in the following lines). This load case combination has been chosen, since it was the more critical loading distribution for buckling (previous section B of the present chapter) and proved to be the loading combination which gave the largest arch stresses in the results obtained in chapter V. B.

Based on the aforementioned combination a step loading ( $\Delta q$ ) has been conducted in order to obtain a live load coefficient ( $\alpha$ ) for the beginning of the plasticization for each model, ie: for a certain  $\Delta q$  plasticization starts for an  $\alpha$  value that satisfies  $\Delta q = \alpha \cdot lu$

The load under which the bridge is analysed is Combination A1':  $1,35 \cdot (w + pl) + \Delta \cdot q$ , where:

- $w$  is the self-weight, with a steel specific weight of  $76,97 \text{ kN/m}^3$
- $pl$  is the permanent load of  $2,5 \text{ kN/m}^2$ . Considering 4m width:  $pl = 10 \text{ kN/m}$
- $lu$  is a uniform live loading on the whole length of the deck. The live load value is of  $5 \text{ kN/m}^2$  according to EC1 Part 2. Section 4.3.5 for footbridges. Considering 3m of usage width, employing the rest of the width for the railings, *the value of live loads is 15 kN/m.*
- The step loading analysis starts after the geometrically non-linear analysis (GNLA) of the permanent load state  $1,35 \cdot (w + pl)$  has been performed

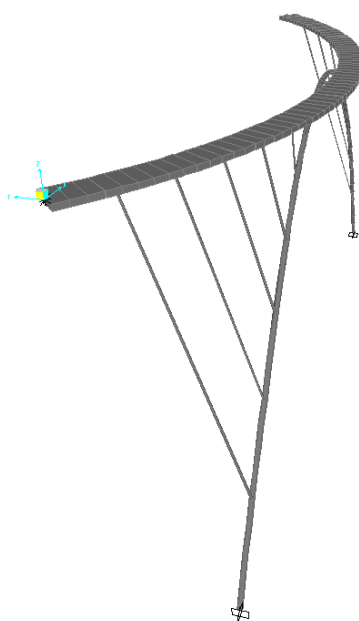
## 1.4 Research procedure and values

### 1.4.1 Model values

In order to understand the behaviour of these arches, different frame 3D models have been developed and analysed with commercial software. As in the previous studies, the arch and deck plan curvature are measured as horizontal sag ( $g_A$  and  $g_D$  respectively), the arch rise is called  $f$ , the arch/deck eccentricity in plan view is  $e$ , the distance between arch and deck at span center is  $v$  and the arch and deck spans are  $L_{SA}$  and  $L_{SD}$  respectively and are considered equal ( $L$ ) in all models (see Figure 1-1 for a particular model as an example).

The parameters are closely detailed in Chapter V.B section 1.2. Please refer to the aforementioned chapter or employ the bookmark.

The imperfection value considered at the arch point with maximal displacement in the deformed buckling shaped is named  $e\theta$ .



**Figure 1-1: Frame 3D model for  $g=20\text{m}$ ,  $f=20\text{m}$  and maximal spatial imperfection  $e\theta = 224\text{mm}$**

For all the studies presented, the following dimensions have been employed:

- $L_{SA}=L_{SD}=L=100\text{m}$ ;
- $g_A=0$ ;  $g=g_D= 0$  and  $20\text{m}$
- $e=g/1,2=16,67\text{m}$  for  $g=20\text{m}$  as recommended in chapter V.B
- $f=L/5=20\text{m}$  as recommended in chapter V.B and section VI.B of the present chapter and  $f=L/2=50\text{m}$ , since it gave the lowest buckling load in section VI.B of the present chapter
- $v=0$

The shape of the arch is always a parabola. 16 struts have been employed in all the models. The inclination of the struts is determined by the uniform division of the deck and the arch for all the models, which leads to a radial distribution.

The material employed is steel S355 with a  $2,0 \cdot 10^8 \text{ kN/m}^2$  modulus of elasticity (E) and resistance  $f_y=355\text{MPa}$ .

The studied arches in each of the considered models are fixed at the springings. The deck is pinned at abutments and tangential longitudinal displacements are restrained for SABs and free for  $g=0$ , as recommended in Chapter V.A. The radial displacements are restrained.

The struts are completely fixed to arch and deck.

For stresses and axial forces values  $>0$  are tensions and  $<0$ , compressions.

A GNLA has been conducted for the reference cross-section values (Table 1-1) and also for the design cross-sections for arch, deck and struts (Table 1-2 and Table 1-3) obtained in Chapter V.B.

ARCH	CHS D=1m; t=30mm A= 0,0914m <sup>2</sup> J= 0,0215m <sup>4</sup> I2= 0,0108m <sup>4</sup> I3= 0,0108m <sup>4</sup>
DECK	BOX GIRDER 4000x800mm; t=15mm A= 0,1431m <sup>2</sup> J= 0,0615m <sup>4</sup> I2= 0,2517m <sup>4</sup> I3= 0,0196m <sup>4</sup>
STRUTS	CHS D=451mm; t=22,6mm A= 0,0304m <sup>2</sup> J= 0,0014m <sup>4</sup> I2= 0,0007m <sup>4</sup> I3= 0,0007m <sup>4</sup>

**Table 1-1: Reference cross-section values**

		g=20m	
		f=20m	f=50m
ARCH	CHS D=750mm; t=30mm A= 0,0679m <sup>2</sup> J= 0,0088m <sup>4</sup> I= 0,0044m <sup>4</sup>	CHS D=750mm; t=20mm A= 0,0459m <sup>2</sup> J= 0,00061m <sup>4</sup> I= 0,0031m <sup>4</sup>	
DECK	BOX GIRDER 4000x700mm; t=20mm A= 0,1864m <sup>2</sup> J= 0,0629m <sup>4</sup> I2= 0,3179m <sup>4</sup> I3= 0,0095m <sup>4</sup>		
STRUTS	CHS D=300mm; t=35mm A= 0,0291m <sup>2</sup> J= 0,00052m <sup>4</sup> I= 0,0003m <sup>4</sup>	CHS D=300mm; t=45mm A= 0,0360m <sup>2</sup> J= 0,0006m <sup>4</sup> I= 0,0003m <sup>4</sup>	

**Table 1-2: Design cross-section values for g=20m**

$g=0$	
$f=20m$	
ARCH	CHS D=750mm; t=25mm $A= 0,0569m^2$ $J= 0,0075m^4$ $I= 0,0037m^4$
DECK	BOX GIRDER 4000x700mm; t=20mm $A= 0,1864m^2$ $J= 0,0629m^4$ $I_2= 0,3179m^4$ $I_3= 0,0095m^4$
STRUTS	CHS D=300mm;t=60mm $A= 0,0452m^2$ $J= 0,00069m^4$ $I= 0,0003m^4$

**Table 1-3: Design cross-section values for  $g=0$**

### 1.4.2 Analyses method

A step loading and geometrically non-linear analysis (GNLA) with SAP2000 v14 has been developed for the 3D frame models with values described in section 1.4.1. The P-delta+large displacements method (as recommended in the benchmark in chapter III. B) has been employed. An example of one of these frame models can be observed in Figure 1-1. Various models with different number of FE have been analysed. An analysis with SOFISTIK has also been conducted for the model with  $g=20m$  and  $f=50m$ .

A previous benchmark has been done with both softwares (chapter III. B). Whereas SAP2000 gave better results. Hence, SAP2000 is used for the step loading analysis (section 2.2). However, introducing the imperfections based on the 1<sup>st</sup> mode buckling shape is quicker with SOFISTIK. Therefore, SOFISTIK is employed to obtain the imperfection geometry and for section 2.1 in this chapter. Employing both softwares in a SAB example and comparing the results (section 2.1.1), shows the equivalency of employing one software or another for this section.

Analyses have been conducted with both displacement and load control for one of the models. Both methodologies have shown identical results and load control has been applied for all the models.

An elastic analysis has been employed and it is considered valid until the yielding of the most stressed cross-section of the structure. For the step-loading analyses this gives a loading coefficient value  $\alpha$  described in section 1.3.

### 1.4.3 Imperfection values

As already explained in section 1.1 and the state-of-the-art in the present chapter V.A, there are no equivalent European buckling curves for arch bridges. Therefore, the coded imperfections will be employed following the first mode of buckling shape as stated in EC3 Part 1.1 Chapter 5.3.2. Two different imperfection values have been employed for each model according to EC3 Part 1.1 Chapter 5.3.2 and EC3 (Annex D.3.5)

These imperfection values are conservative, as demonstrated with a benchmark for the program SAP2000 v14 in chapter III.B and Outtier et al (2007a).

According to EC3 (Annex D.3.5) imperfections of arches are only given in one plane, either in-plane or out-of-plane of the arch. However spatial arch bridges buckle in both planes as demonstrated in Chapter III.B. Therefore the buckling shape is employed and as imperfection value it seems logical to consider the maximal value either in-plane or out-of-plane given by the standards, since imperfections should not expected to be bigger as in a planar arch. However, on the side of security and in order to see the influence of large imperfections, the vector of both in-plane and out-of-plane imperfections given in EC3 (Annex D.3.5) have been employed.

The imperfection values obtained for each model and according to both, EC3 (Annex D.3.5) and specific for arch bridges (EC3 Annex D.3.5 Tables D.8 and 9, shown in section A of the present chapter) are displayed in Table 1-4.

<b>L (m)</b>	<b>g (m)</b>	<b>f (m)</b>	<b>e0(mm) according to imperfections for complex structures</b>	<b>e0(mm) according to imperfections for arch bridges (EC3 Annex D.3.5)</b>
100	20	20	23	224
100	20	50	44	224
100	0	20	29	149

**Table 1-4: Arch imperfection values according to different chapters of EC3**

L/1000 is employed as the maximal out-of-plane imperfection by Manzanares et al (2011), a much larger value than the measured imperfections, but it is not really comparable since these were in-plane imperfections in the vertical direction. Outtier et al (2007) employ L/1000 for out-of-plane imperfections, but including the residual stresses.

## **2. ANALYSES OF THE RESULTS**

### **2.1 STRUCTURAL RESPONSE UNDER DESIGN LOADING**

A first study has been conducted for g=20m and f=50m, based on the results of Chapter V. B.

On the one hand, the validity of both, the SAP2000 software and SOFISTIK is controlled by comparing the results obtained with each software. Both softwares will be combined since certain features are easier in one or another (section 1.4.2).

On the other hand, the bridge behavior and stresses under the design load obtained by means of a first order analysis and a GNLA have been compared, in order to see the influence of non-linearities in this bridge type on a first approach. No imperfections have been introduced for this first approach.

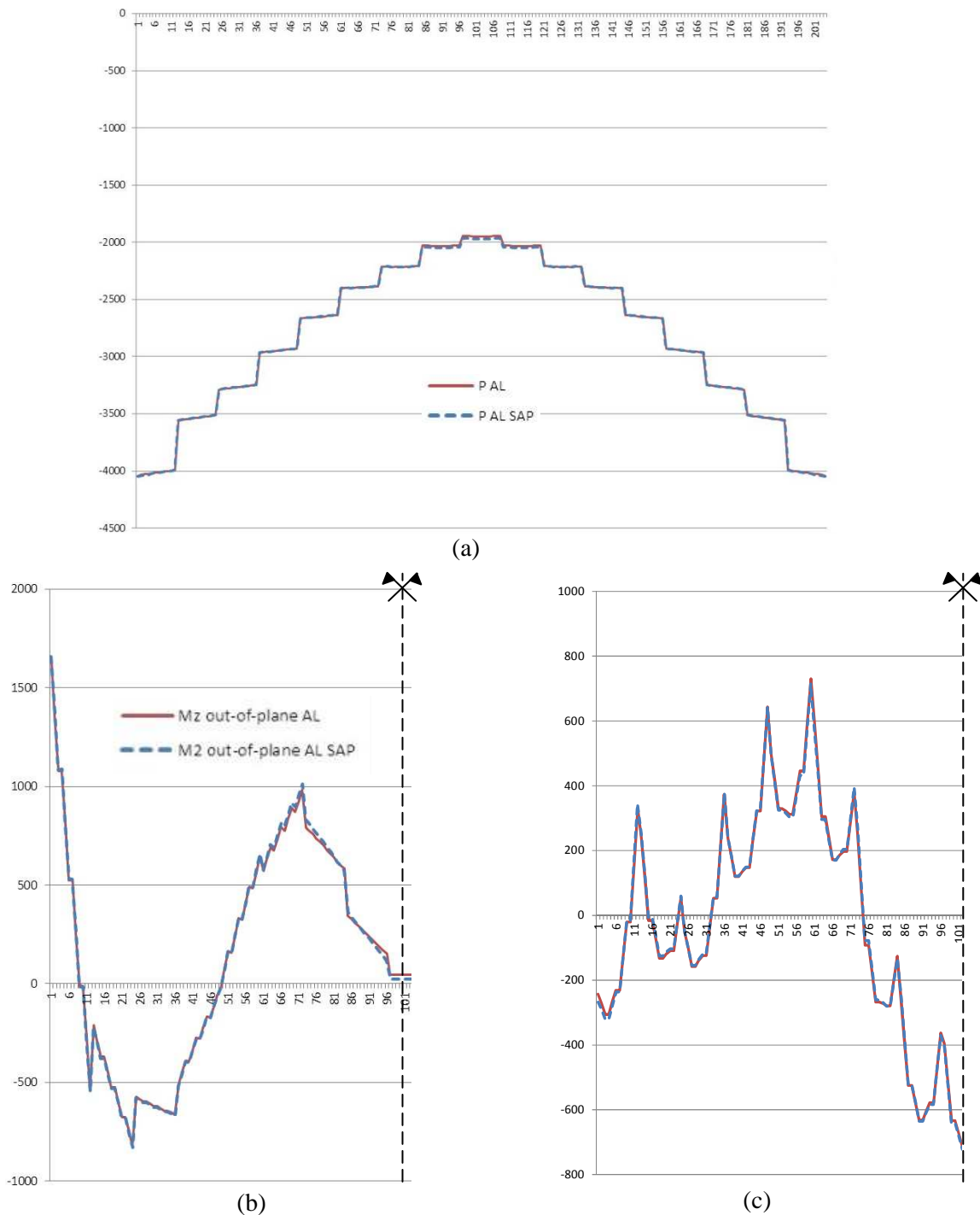
#### **2.1.1 SOFISTIK and SAP2000 results comparison**

A SAB model with planar vertical arch, g=20m and f=50m and a superior curved deck with e=16,67 has been analysed with SAP2000 and SOFISTIK. Reference cross-sections have been employed.

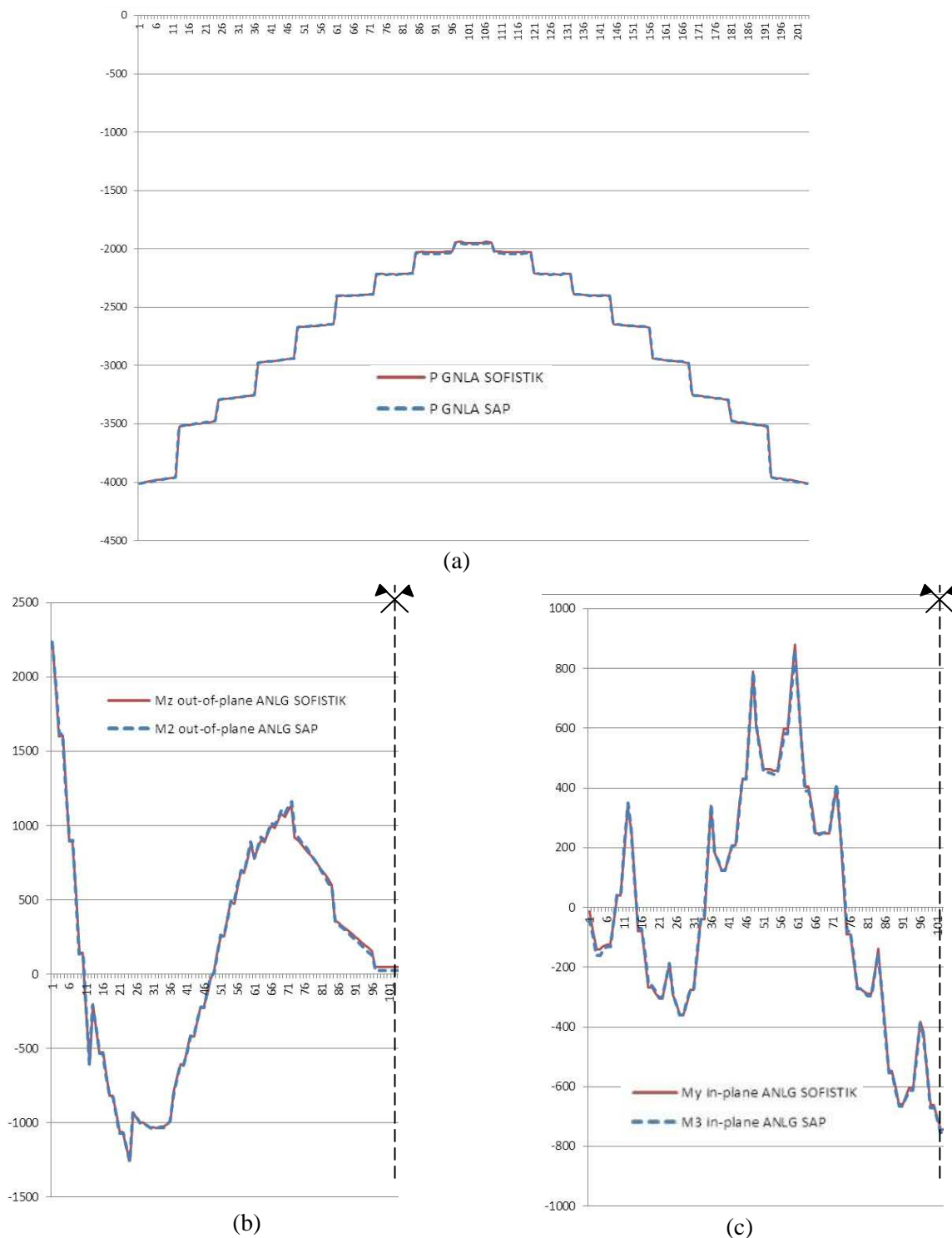
Both LA and GNLA have been carried out with each software and compared. The arch structural forces response comparison under Combination A1 is displayed in Figure 2-1 and Figure 2-2.



The same forces have been obtained with both softwares employed for the analysis, the differences are negligible. Both, in the case of linear and geometrically non-linear analysis.



**Figure 2-1: Internal forces under Combination A1 LA for  $g=20$  and  $f=50m$ . SAP2000 and SOFISTIK LA comparison. (a) Arch axial forces (kN); (b) Arch out of plane bending moments (M2-2, kN·m); (c) Arch in-plane bending moments (M3-3, kN·m) The abscissas are the arch length from 0 to  $L_A$  (or from 0 to  $L_A/2$  in cases b and c, the symmetry dashed line marks  $L_A/2$ , the numbers indicate the station of the FE analysis numeration)**

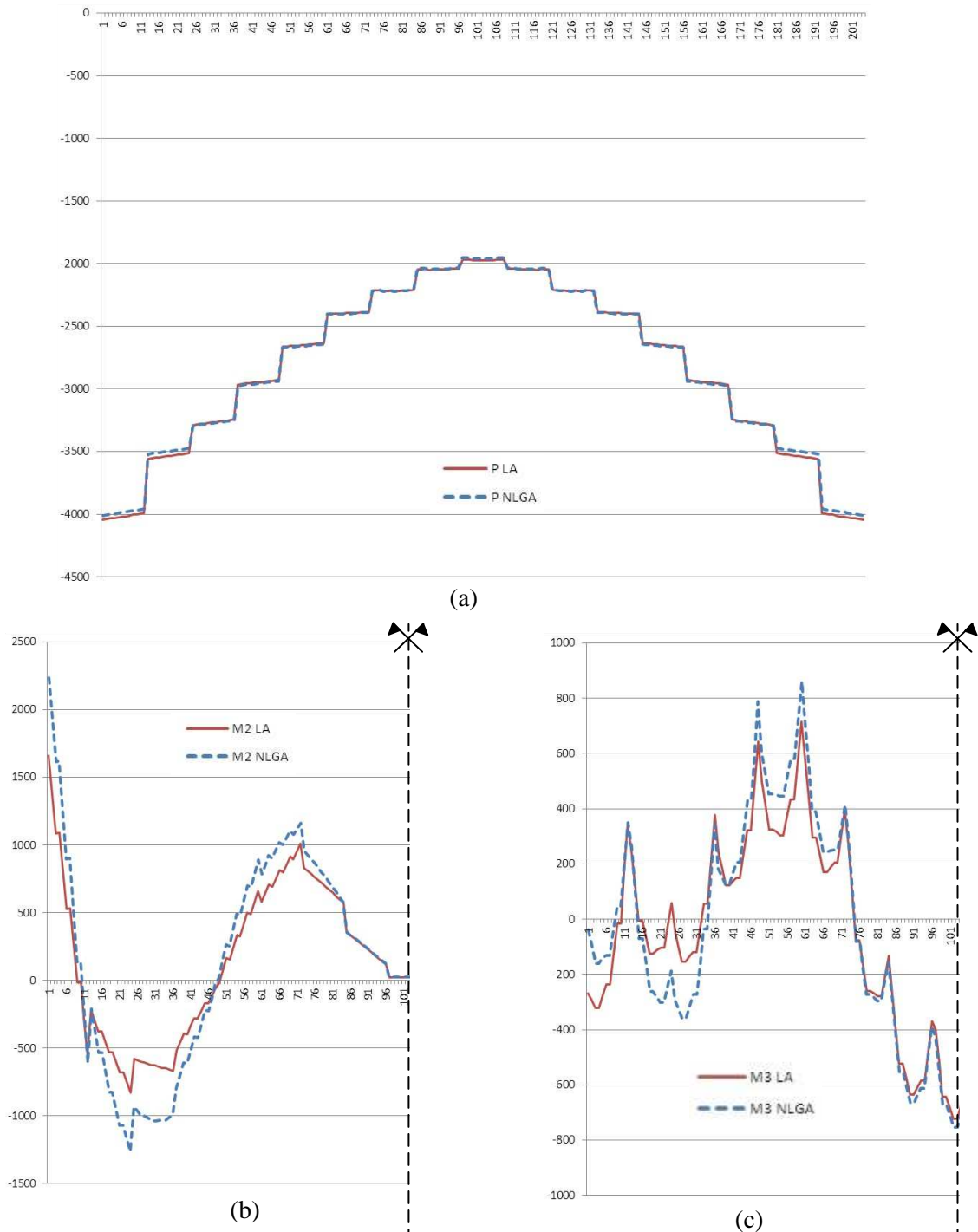


**Figure 2-2: Internal forces under Combination A1 GNLA for  $g=20$  and  $f=50$ m. SAP2000 and SOFISTIK GNLA comparison. (a) Arch axial forces (kN); (b) Arch out of plane bending moments (M2-2,  $kN \cdot m$ ); (c) Arch in-plane bending moments (M3-3,  $kN \cdot m$ ) The abscissas are the arch length from 0 to  $L_A$  (or from 0 to  $L_A/2$  in cases b and c, the symmetry dashed line marks  $L_A/2$ , the numbers indicate the station of the FE analysis numeration)**

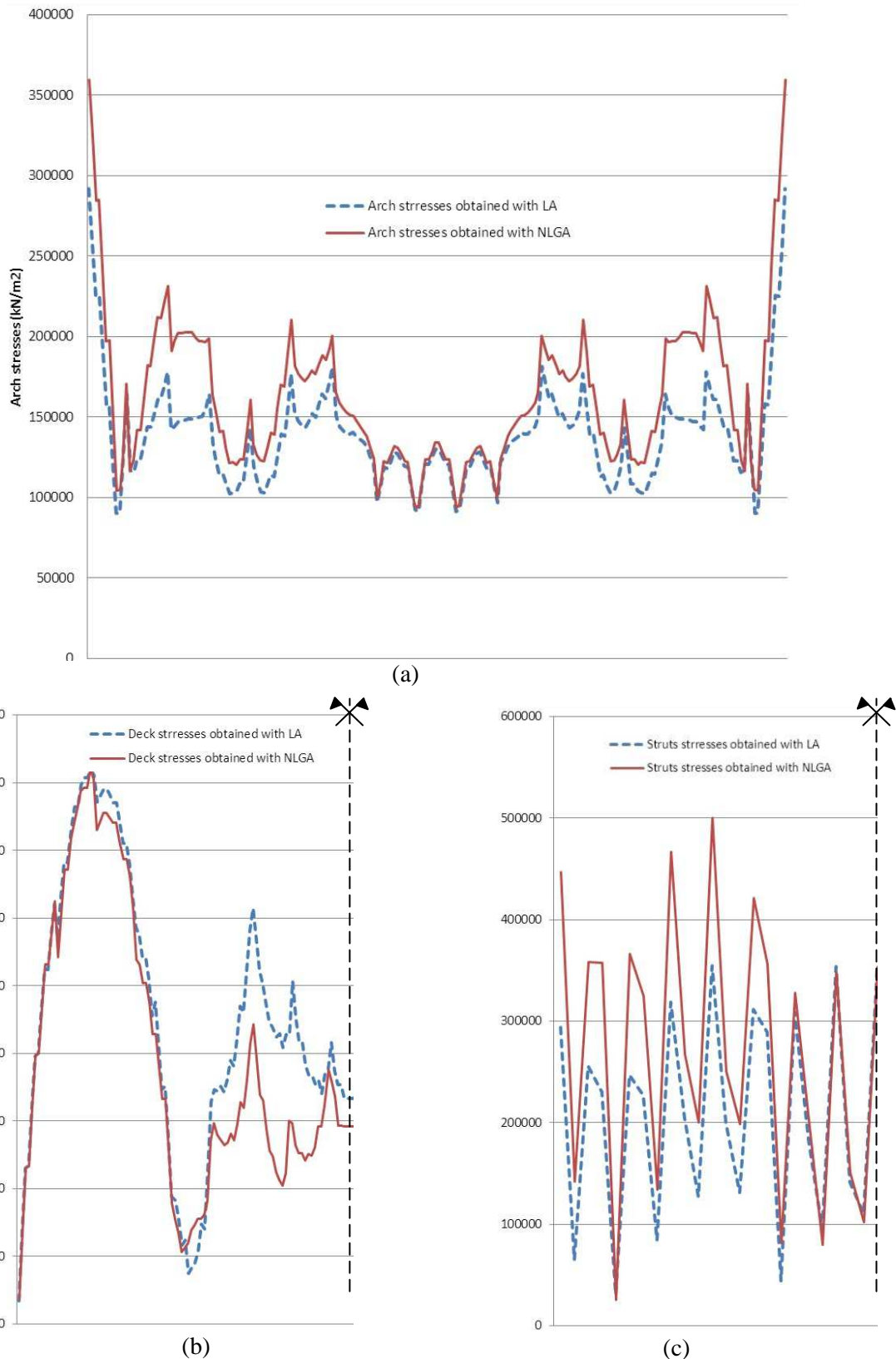
### 2.1.2 Linear and geometrically non-linear analyses comparison

A SAB model with planar vertical arch,  $g=20\text{m}$  and  $f=50\text{m}$  and a superior curved deck with  $e=16,67$  has been analysed with SAP2000 performing a LA and a GNLA. Reference cross-sections have been employed.

Internal forces in the arch and stresses in the bridge under Combination A1 obtained by both, LA and GNLA, have been compared (Figure 2-3 and Figure 2-4, respectively).



**Figure 2-3: Internal forces under Combination A1 for  $g=20$  and  $f=50\text{m}$ . LA and GNLA comparison. (a) Arch axial forces (kN); (b) Arch out of plane bending moments (M2-2, kN·m); (c) Arch in-plane bending moments (M3-3, kN·m) The abscissas are the arch length from 0 to  $L_A$  (or from 0 to  $L_A/2$  in cases b and c, the symmetry dashed line marks  $L_A/2$ , the numbers indicate the station of the FE analysis numeration)**



**Figure 2-4: Stresses ( $\text{kN/m}^2$ ) under Combination A1 for  $g=20$  and  $f=50\text{m}$ . LA and GNLA comparison. (a) Stresses along the arch. The abscissas are the arch length from 0 to  $L_A$ ; (b) Stresses along the deck. The abscissas are the deck length from 0 to  $L_D/2$ ; (c) Stresses in struts. The abscissas are half the struts from the closest to the springings to the nearest at span center**

### Arch

From the arch internal forces point of view the geometrical non-linearity is highly significant for bending and torsional moments.

- Out-of-plane bending moments (Figure 2-3b) nearly double at  $L/8$  (40% maximal relative error), torsional moments nearly double at the arch springings (30% maximal relative error).
- In-plane bending moments (Figure 2-3c) more than double themselves at  $L/8$  (40% maximal relative error) and have also high differences at  $L/3$ .
- This is because the deformations increase the eccentricities with respect to the pressure line of the arch.
- However, this effect is hardly significant in the axial forces (Figure 2-3a), which only diminish slightly at the arch springings and crown (1% maximal relative error).

The stresses in the arch highly increase with respect to the ones obtained from a linear analysis (Figure 2-4a), When considering the geometrical non-linear effects.

- The maximal relative error is 37% and takes place at  $L/8$ .
- The highest effects of geometrical non-linearity take place at springings,  $L/8$  and  $L/3$  of the arch. This corresponds to the cross-sections where the main increase in bending moments takes place.
- Local buckling establishes a minimal thickness for the cross-sections. Only near to the springings are they dependent on the internal forces.
- Considering the geometrical non-linearities the arch cross-sections would plastify at springings when dimensioned with a linear analysis. There is a 27% stress maximal variation at springings
- When considering the geometrical non-linearities the live load which the structure can bear before the first fiber in the arch cross-section plastifies is nearly half than when geometrical non-linearities are not considered.

### Deck

From the internal forces point of view the geometrical non-linearity is very important for bending moments and also quite significant for shear forces.

- The shape of the distribution of  $M_2$  is completely different. The location of the maximal bending moments changes when considering geometrical non-linearities.

From stresses standpoint the geometrical non-linear has a non-negligible influence; with a maximal error of 68% (Figure 2-4b).

- The highest effects of geometrical non-linearity take place in the central third of the deck.
- The design of the cross-sections does not change when considering geometrical non-linearities, since the deck is overdimensioned for the design loads because the given 10mm thickness is needed for local bending moments, local instability of compressed plates and durability.

When considering geometrical non-linearity, the displacements become completely unbearable. Hence, a dynamic analysis is carried out in Chapter VII

### Struts

Stiffer cross-sections are needed when considering geometrical non-linearities, in comparison with the ones designed to resist the forces obtained with a linear analysis.

When considering the geometrical non-linear effects, the stresses in the struts can even double themselves with respect to the ones obtained from a linear analysis (maximal relative error 120%, Figure 2-4c).

All in all, it is necessary to consider geometrical non-linearity in this bridge type.

## **2.2 STRUCTURAL RESPONSE OF THE ARCH UNDER STEP LOADING**

The different models described in 1.4.1 have been analysed under Combination A1' (section 1.3). The design cross-section values detailed in Table 1-2 and Table 1-3 have been employed.

The largest stresses in the arch take place at springings for all models (Figure 2-5), as stated in section 2.1.

The results of the axial forces and total bending moments at the arch springings under LA and GNLA with and without imperfections and with the different imperfection values described in 1.4.3 have been plotted for the different steps of loading<sup>1</sup>. This gives the interaction diagram for the most critical cross-section of the arch (from Figure 2-5 to Figure 2-8).

When comparing planar arch bridges with a superior straight deck with SABs with a curved superior deck and a planar vertical arch (Figure 2-6), the following conclusions can be drawn:

- NLG effects have a high influence on the behavior of arch bridges, as expected.
- For SABs, results obtained with a LA are nearer to the GNLA than for planar arch bridges with a superior straight deck. This is so because important bending moments are already obtained for SABs with LA due to their geometry and structural behavior described in Chapter V.B.

When comparing SABs with a curved superior deck and a planar vertical arch with different rise and imperfection values (Figure 2-7), the following conclusions can be drawn:

---

<sup>1</sup> In all the cases the yielding load is under a 50% of the buckling load. Hence the results are considered to be reliable according to the benchmark in chapter III. B section 2.4

- NLG effects have a high influence on the behavior of SABs. A GNLA must be conducted for this bridge type, since the design obtained with LA can give values which will not resist ULS when considering GNL effects.
- The influence of NLG effects is larger for arches with large rise values than when employing  $f$  values recommended in Chapter V.B.
- The value of imperfections has a lower influence for arches with large rise values than when employing  $f$  values recommended in Chapter V.B

Slightly stiffer cross-sections are needed when considering geometrical non-linearities, in comparison with the ones designed to resist the forces obtained with a linear analysis.

The  $f=50$  model has been analysed with a D750t20 arch, a D300t45 struts and a 700x4000t20 deck cross-sections with and without imperfections.

- Whereas a security factor of 2,2 for live loads is obtained with a linear analysis without imperfections, a 1,4 security factor is obtained with a GNLA of the model without imperfections (Figure 2-6).
- This value is below the security factor of 1,5 for live loads established by the spanish code IAP2011 and the EC1 Part2.
- With imperfections according to EC3 Part 1.1 Chapter 5.3.2, the security factor can fall to 1,2.

Note that for  $f=50$ m, when employing very large imperfection values the arch first plasticizes for a larger load than when analyzing the model with no imperfections. This happens because it bears lower axial forces and similar bending moments (Figure 2-8). However it is clear, that for larger loads, if the material had not failed, the geometrically non-linear effects are more important when employing large imperfections. It must be, though, highlighted, that values above the plasticization load are not valid anymore, since material non-linearities have not been considered.

### 2.2.1 First buckling mode imperfections direction sign

The buckling shape obtained by means of the FE Model has two directions, positive or negative. Due to the asymmetry of SABs with a curved deck, both directions should be analysed.

Since the objective of the present study was not the bridge design, but evaluating the influence of geometrical non-linearity on this bridge type and such influence has been already proved by employing the buckling shape in one direction, the negative direction will not be considered.

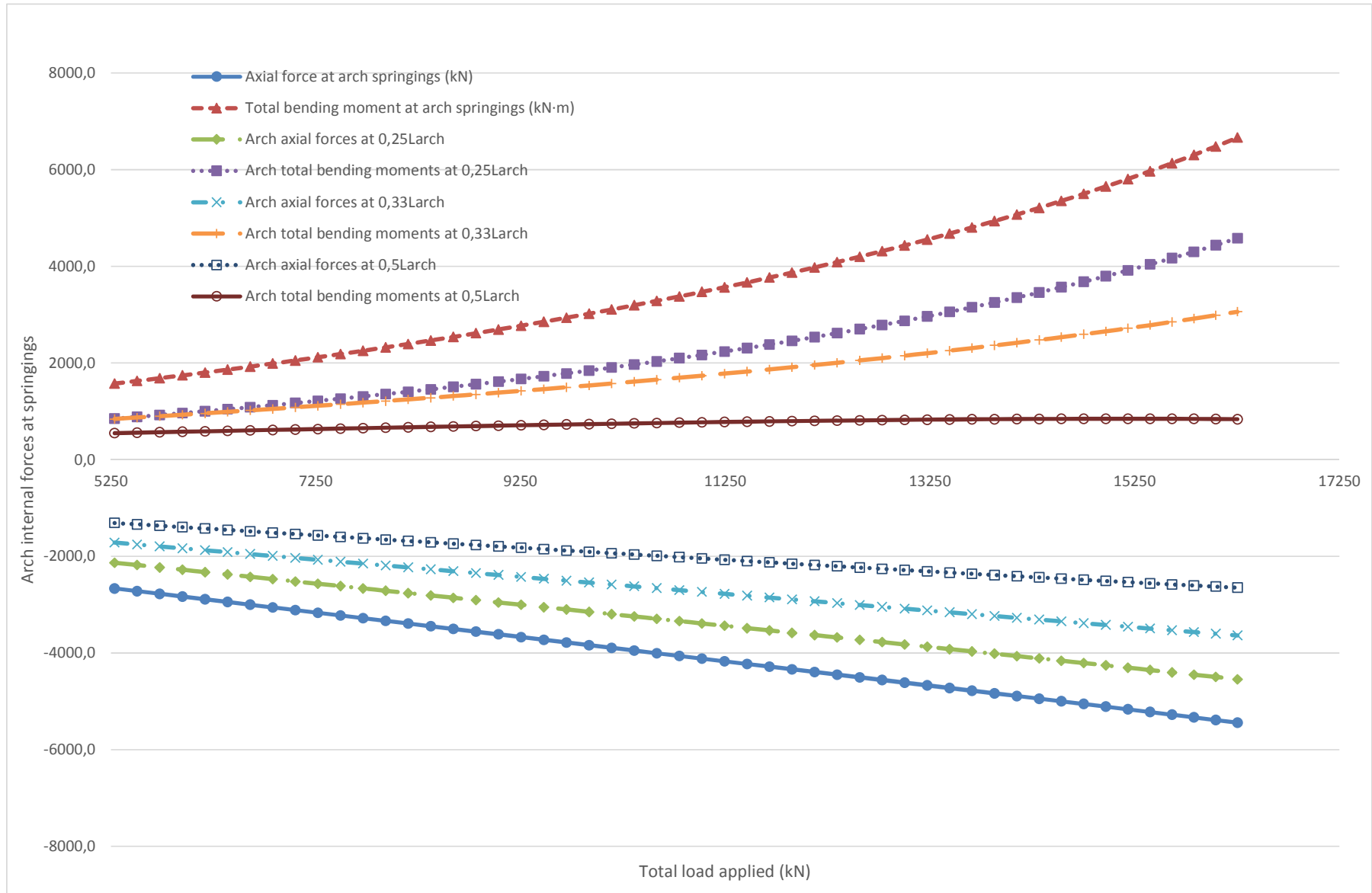


Figure 2-5: Step loading GNLA results. Axial and bending moments at different arch sections for SABs with  $f=50\text{m}$  with 224mm imperfections



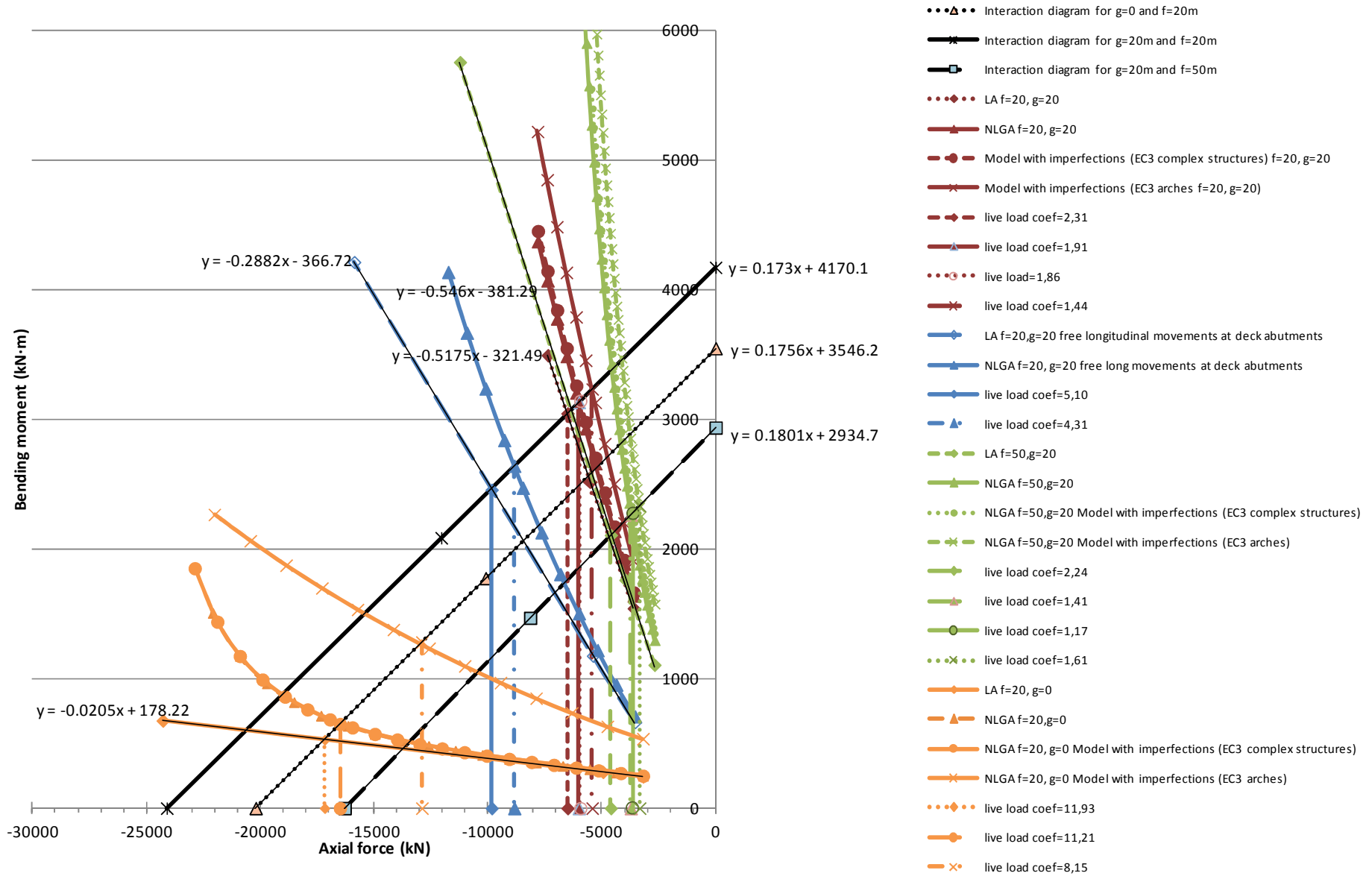


Figure 2-6: Step loading diagram for different models with different imperfection values and with the corresponding interaction diagrams

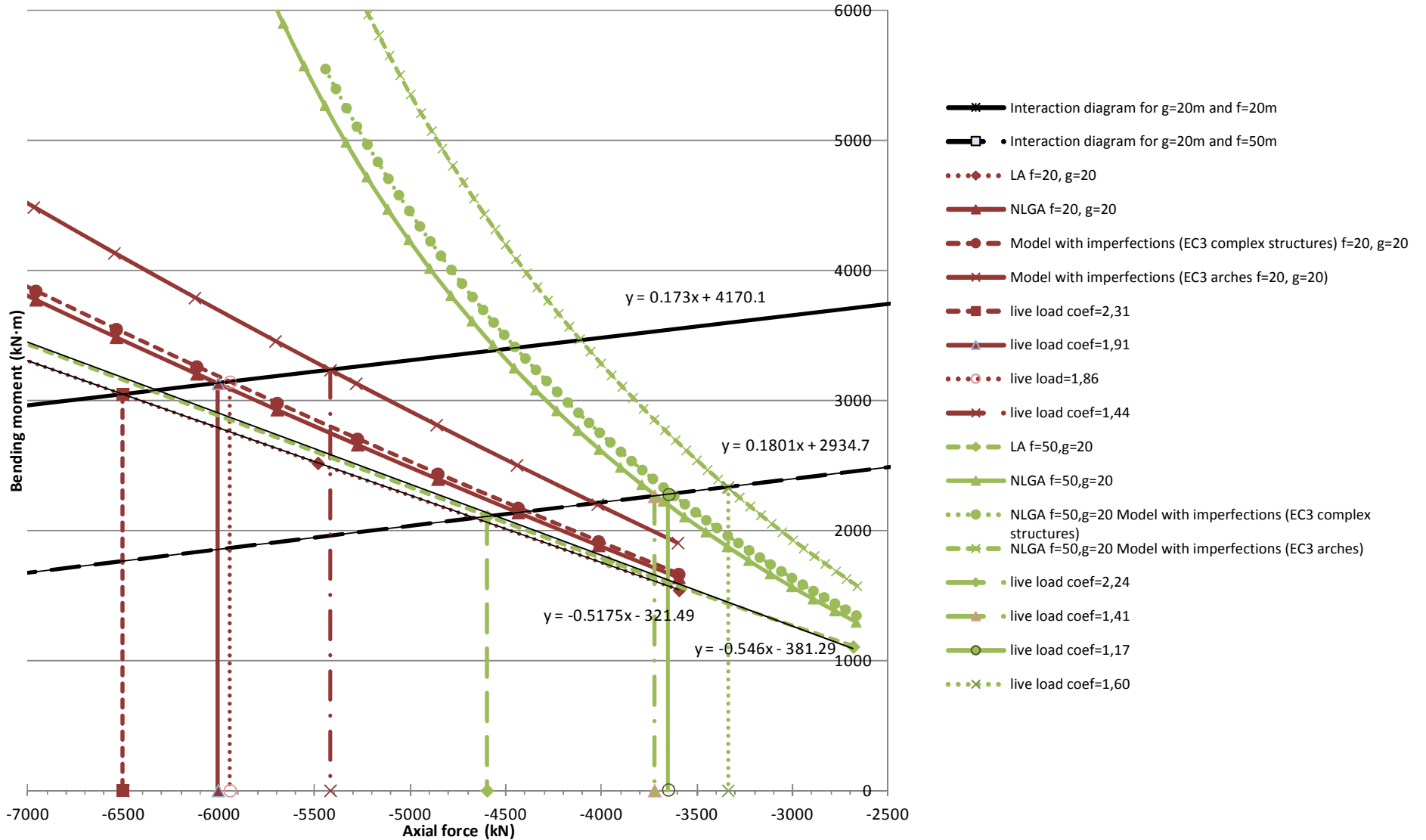


Figure 2-7: Step loading diagram for SAB models with different imperfection values and with the corresponding interaction diagrams. Movements restrained at deck abutments. Yielding steps detail

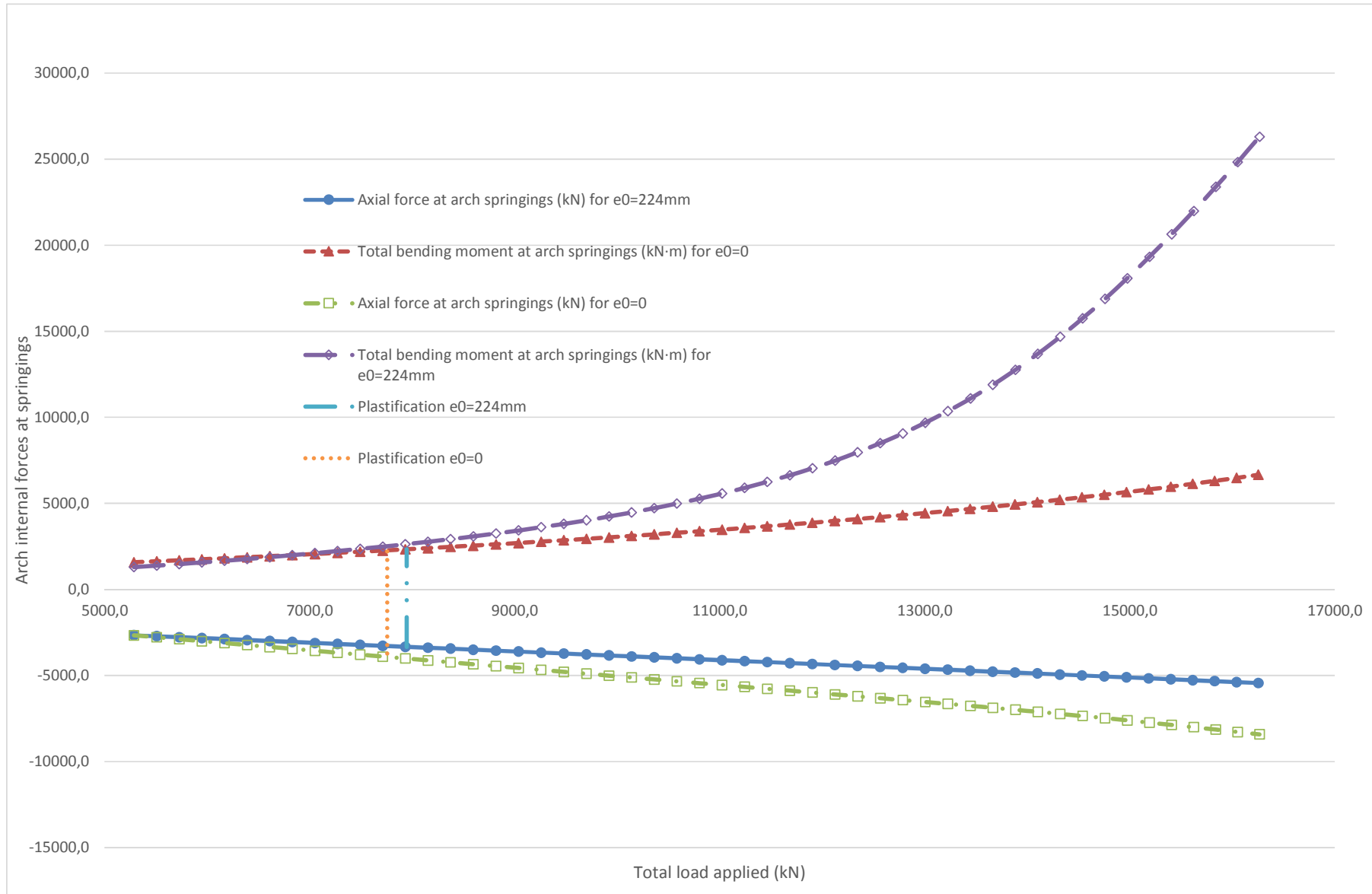


Figure 2-8: Step loading GNLA results. Axial and bending moments at arch springings for SABs with f=50m without imperfections and with 224mm imperfections

### 3. CONCLUSIONS

- NLG effects have a high influence on the behavior of SABs with a superior curved deck. A GNLA must be conducted for this bridge type, since the design obtained with LA can give values which will not resist ULS when considering GNL effects and elastic material failure.
- For SABs, results obtained with a LA are nearer to the GNLA than for planar arch bridges with a superior straight deck. This is so because important bending moments are already obtained for SABs with LA due to their geometry and structural behavior.
- The influence of NLG effects is lower when employing  $f$  values  $L/5=20\text{m}$  (recommended in Chapter V.B) than for arches with larger rise values.
- The value of imperfections has a lower influence for arches with large rise values than when employing  $f$  values recommended in Chapter V.B.

### 4. FUTURE LINES OF STUDY

- Compare the behavior of different imperfection shapes obtained by the positive and negative buckling deformed shapes, by conducting a GNLA.
- Consider material non-linearity as well as geometrical non-linearity, in order to observe the formation of hinges and the bearing capacity margin of these structures with respect to the material linear analysis.

### REFERENCES

MANZANARES J. L. and HINOJOSA, I., "Non-linear plastic analysis of steel arches under lateral buckling". *Journal of Constructional Steel Research*, i. 12, v. 67. pp 1789-1984. December 2011

OUTTIER, A., DE BACKER H, and VAN BOGAERT, P. "Assessment of the out-of-plane imperfections of a steel tied arch bridge" *ARCH '07. Proceedings of the 5th International Conference on Arch Bridges*. Madeira, Portugal September 12-14, 2007a. pp. 249-256

OUTTIER, A., DE BACKER H, and VAN BOGAERT, P. "Numerical approach to the lateral buckling of steel tied-arch bridges" *ARCH '07. Proceedings of the 5th International Conference on Arch Bridges*. Madeira, Portugal September 12-14, 2007b. pp. 484-490

VII. DYNAMIC BEHAVIOUR OF  
SPATIAL ARCH BRIDGES WITH A  
CURVED SUPERIOR DECK AND A  
PLANAR VERTICAL ARCH



## INDEX

1. INTRODUCTION AND OBJECTIVES.....	359
2. BASIS OF ANALYSIS AND DESIGN.....	360
<b>2.1 Codes and research.....</b>	<b>360</b>
<b>2.2 Examples of dynamic behaviour .....</b>	<b>369</b>
<b>2.2.1 Dynamic response of the Millenium Bridge. Quantification of the locking effect .....</b>	<b>369</b>
<b>2.2.2 Highlights on SABs.....</b>	<b>370</b>
3. STUDIED PARAMETERS AND GEOMETRIES.....	371
4. NATURAL FREQUENCIES AND NEED OF CONDUCTING A DYNAMIC ANALYSIS.....	372
5. LOAD CASES .....	380
<b>5.1 Crowd dynamic load cases according to Sétra Guidelines (2006).....</b>	<b>380</b>
<b>5.2 Vertical loading of a single pedestrian and a small pedestrian group crossing the bridge 382</b>	
6. DISCUSSION OF RESULTS .....	383
<b>6.1 Crowd dynamic load cases according to Sétra Guidelines (2006) results.....</b>	<b>383</b>
<b>6.2 Small pedestrian group and single pedestrian dynamic load results.....</b>	<b>389</b>
7. CONCLUSIONS .....	393
8. FUTURE LINES OF STUDY .....	393
REFERENCES .....	394





## 1. INTRODUCTION AND OBJECTIVES

For footbridges with more than 50 m span, more than 3m walkway or non-conventional bridge types, a dynamic analysis is necessary (IAP 2011, Ruiz-Teran and Aparicio, 2009). SABs in the present study satisfy all those characteristics, so whatever the frequencies would be, a dynamic analysis is necessary.

Moreover, the natural frequencies of the studied SABs in the previous chapters are in the critical range for vibrations.

Therefore, the conclusions of the study are not complete without conducting a dynamic analysis, since dynamic behaviour can be critical in this bridge type design.

The present chapter does not pretend to draw conclusions on dynamic behaviour of this bridge type, which could be a subject for future lines of study. It merely pretends to check the dynamic behavior of the geometry concluded in previous chapters as most efficient for SABs with a planar vertical arch with a superior curved deck. Its dynamic behaviour is also compared with that of a planar vertical arch with straight deck with an equivalent span and rise.

The necessity to conduct a dynamic analysis is evaluated according to the natural frequency of each structure under criteria stated by both, the IAP 2011 and the Sétra Guidelines (2006), which are discussed in the basis of analyses and design.

The load cases are defined following the Sétra Guidelines (2006). These guidelines and the reasons for employing them and not others are discussed in the basis of analyses and design.

The aim of the present study is giving a first approach of the dynamic behaviour of a type of SABs. It is therefore interesting to analyse its behaviour under design dynamic loads of one of the present codes or guidelines and also the behaviour under the dynamic load case of a single pedestrian and of a small group.

## 2. BASIS OF ANALYSIS AND DESIGN

### 2.1 Codes and research

#### Dynamic analysis necessity research

According to Ruiz-Teran and Aparicio, 2009: *“The correlation between deflections and accelerations (proposed by Smith and accepted by several codes) only exists for systems with a single degree of freedom (or for systems in which one mode dominates the dynamic response). No correlation between both approaches can be established for real structures with multiple degrees of freedom.*

*“Consequently, conducting a full dynamic analysis is required in order to verify the SLS vibrations.”* In the aforementioned paper the acceleration-based approach is proposed for the appropriate verification of the SLS of vibrations, since for non-conventional bridges, also with small spans, the deflection-based approach might be unsafe for some cases and too conservative for other cases of non-conventional bridges, leading to an over-design.

#### Eurocode 1

The EC1 Part2 section 5 on actions on footways, cycle tracks and footbridges states that appropriate dynamic models of pedestrian loads and comfort criteria should be defined. The dynamic models of pedestrian loads and associated comfort criteria may be defined in the National Annex or for the individual project. Therefore, the dynamic analyses is not defined for the EC, leaving the criteria of this analysis to the designers.

#### Eurocode 1 UK National Annex

In general, for road and railway bridges, the Eurocode 1 UK National Annex NA.2.50 (2003) states that determining whether a dynamic analysis is required (in addition to static analysis) is based on a series of requirements in which, firstly, it must be differentiated between simple and complex structures. According to EC1 UK NA (2003):

*“Simple structures which exhibit longitudinal line beam behaviour with insignificant contributions from other dynamic modes will generally comprise of deck type structures of slab, beam and slab or box and slab construction where the tracks are located over the webs of longitudinal spanning elements and where the deck/floor elements are not required to directly distribute axle/wheel load effects to the longitudinal elements by transverse bending”.*

*“Complex structures require deck/floor elements to distribute axle/wheel loads to primary longitudinal elements. Complex structures will typically include through/half through structures with primary transverse spanning deck/floors, as well as deck type structures of beam and slab (or box and slab) construction where the deck/floor elements are required to distribute loads to the longitudinal elements in bending”.*

Once classified into simple or complex, the need of a dynamic analysis depends on the maximum speed at the bridge and the span length and the first natural bending frequency of the bridge loaded by permanent actions.

For footbridges, dynamic models are defined in NA.2.44 and they are associated to comfort criteria. Two analyses are required:

- The maximal vertical deck acceleration
- The likelihood of large synchronized lateral responses.

We would like to highlight, that the EC1 UK NA (2003) already takes into account the lock-in of a pedestrian crowd, but reliable test measurements on which the code is based are only available for footbridges with lateral frequencies in the range of 0,5 and 1,1Hz. If out of this range, or if out of the lock-in stability boundaries, the EC1 UK NA does not define a lateral dynamic loading to conduct an analysis.

As for vertical acceleration dynamic loading analysis, the EC1 UK NA establishes no limits to decide whether it should be checked or not. It directly considers the necessity of defining a vertical dynamic loading.

Bridges are categorized into bridge classes by their usage to determine the appropriate actions due to pedestrians. Group sizes for each bridge class and densities should be applied as given in Table 2-1.

According to NA.2.44.2 “Depending on the expected bridge usage, it may be determined that jogging cases given in Table NA.7 can be neglected for individual projects”.

Bridge class	Bridge usage	Group size (walking)	Group size (jogging)	Crowd density $\rho$ (persons/m <sup>2</sup> ) (walking)
A	Rural locations seldom used and in sparsely populated areas.	N = 2	N = 0	0
B	Suburban location likely to experience slight variations in pedestrian loading intensity on an occasional basis.	N = 4	N = 1	0.4
C	Urban routes subject to significant variation in daily usage (e.g. structures serving access to offices or schools).	N = 8	N = 2	0.8
D	Primary access to major public assembly facilities such as sports stadia or major public transportation facilities.	N = 16	N = 4	1.5

**Table 2-1: Recommended densities for design (Source: EC1 UK NA Table NA.7)**

According to NA.2.44.3:

“In calculating the peak vertical deck accelerations account should be taken of the following.

- The load models provided should be applied in order to determine the maximum vertical acceleration at the most unfavourable location on the footbridge deck.
- The calculated vertical responses should include the effect of torsional or other motions.
- Modes other than the fundamental mode may need to be taken into account in order to calculate the maximum responses.
- When the vertical deck modes are not well separated, consideration should be given to the use of more sophisticated methods of analysis, in order to determine combined mode

*responses. In all cases, it is conservative to use the vector sum of the peak accelerations for those modes that need such combination.”*

The design maximum vertical accelerations that result from single pedestrians or pedestrian groups should be calculated by assuming that these are represented by the application of a vertical pulsating force ( $F$ , sinusoidal time history function), moving across the span of the bridge at a constant speed:

$$F = F_0 \cdot k(f_v) \cdot \sqrt{1 + g \cdot (N - 1)} \cdot \sin(2\pi \cdot f_v \cdot t)$$

The natural frequency of the bridge is employed to define the time history function.

The reference load of a pedestrian and walking speed is defined in Table 2-2.

Several factors are employed in order to consider:

- the effects of a more realistic pedestrian population,
- the harmonic responses
- the pedestrian sensitivity to response
- the unsynchronized combination of actions in a pedestrian group, depending on damping and effective span
- the mode shape.

**Parameters to be used in the calculation of pedestrian response**

Load parameters	Walking	Jogging
Reference load, $F_0$ (N)	280	910
Pedestrian crossing speed, $v_t$ (m/sec)	1,7	3

*$F_0$  is the reference amplitude of the applied fluctuating force  $F$*

**Table 2-2: Parameters to be used in the calculation of pedestrian response (Source: ECI UK NA Table NA.8)**

The design maximum vertical accelerations that result from pedestrians in crowded conditions may be calculated by assuming that these are represented by a vertical pulsating distributed load, applied to the deck for a sufficient time so that steady state conditions are achieved.

A sinusoidal time history function with the natural frequency of the bridge is employed.

The crowd is limited to 1.0 persons/m<sup>2</sup>. This is because crowd densities greater than this value produce less vertical response as the forward motion slows.

In addition to the previously mentioned factors to define the single pedestrians or pedestrian groups load, other factors are employed in order to define the crowd load:

- Factor to allow for the unsynchronized combination of actions in a crowd.
- The effective number of pedestrians when loading from only part of the span contributes to the mode of interest.

NA.2.44.6 defines a limit acceleration which depends on:

- the site usage

- the route redundancy (ie: if there other routes available)
- the height of structure

Note that the two latter are not considered in other codes or guidelines summarized in the present document.

Finally, the EC1 UK NA also considers the importance of avoiding lateral responses due to crowd loading in NA.2.44.7:

- “Structures should be designed to avoid unintended unstable lateral responses.
- *If there are no significant lateral modes with frequencies below 1,5Hz it may be assumed that unstable lateral responses will not occur”.*

For all other situations, the pedestrian mass damping parameter and the mode frequency should be compared with a stability boundary defined in the code (*Lateral lock-in stability boundaries*, Figure NA.11, EC1 UK NA, 2003)

The pedestrian mass damping parameter depends on:

- the mass per unit length of the bridge
- the mass per unit length of pedestrians for the relevant crowd density
- the structural damping

**Instrucción de Acciones en Puentes (IAP 2011, Spanish bridge action code)**

According to IAP (2011), in general, apart from the exceptions indicated on the following lines, the SLS of vibrations in footbridges will be considered under control if their natural frequencies are outside the two ranges below:

- Critical range for vertical and longitudinal vibrations: from 1.25 to 4.60 Hz
- Critical range for lateral vibrations: from 0.50 to 1.20 Hz

In those gateways whose natural frequencies are within these ranges shall be required specific dynamic studies to ensure comfort requirements of pedestrians.

In any case, regardless of the value of the natural frequencies, also be checked by dynamic studies proper vibrational response of the walkways when any of the following circumstances:

- Span greater than 50 m
- Platform width greater than 3.0 m
- Special structural type or new materials
- Location in urban areas where heavy pedestrian traffic is expected or with a risk of concentration of people on the footbridge itself

The comfort level according to the acceleration is also defined in this code (see **Table 2-3**).

<i>Comfort level</i>	<i>Vertical acceleration</i>	<i>Lateral acceleration</i>
Maximum	< 0,50 m/s <sup>2</sup>	< 0,10 m/s <sup>2</sup>
Middle	From 0,50 to 1,00 m/s <sup>2</sup>	From 0,10 to 0,30 m/s <sup>2</sup>
Minimum	From 1,00 to 2,50 m/s <sup>2</sup>	From 0,30 to 0,80 m/s <sup>2</sup>
Unacceptable	>2,50 m/s <sup>2</sup>	> 0,80 m/s <sup>2</sup>

**Table 2-3: Comfort level for different acceleration ranges according to IAP2011**

In this code no specific loading is given to conduct the dynamic analyses.

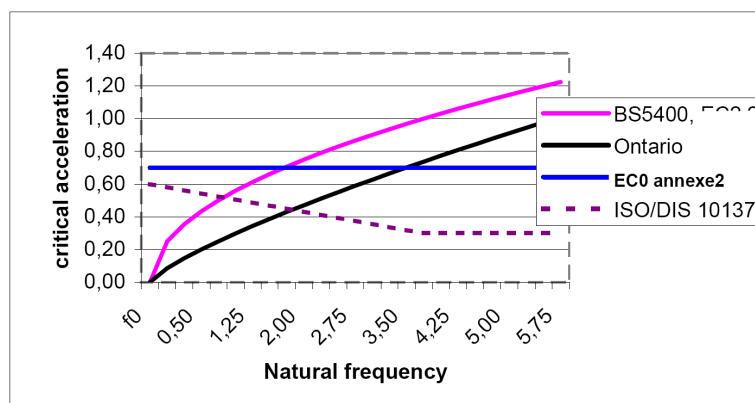
### Sétra Guidelines

The Sétra guidelines (2006) take into account the lock-in of a pedestrian crowd studied by Fujino et al (1993), the theory formulated for the Millenium footbridge, the Solferino footbridge and also performed laboratory tests on a platform. The analysis of these studies lead to the conclusion that the concept of critical acceleration seems more relevant than that of a critical number of pedestrians. It is thus the critical acceleration threshold, which is mainly discussed in the Sétra guidelines.

The Sétra recommendations offer a summary of the risk frequencies for vertical vibrations in current regulations (*Table 2-4*) and critical accelerations given a natural frequency (*Figure 2-1*).

Eurocode 2 ( Ref. [4] )	1.6 Hz and 2.4 Hz and, where specified, between 2.5 Hz and 5 Hz.
Eurocode 5 ( Ref. [5] )	Between 0 and 5 Hz
Appendix 2 of Eurocode 0	<5 Hz
BS 5400 ( Ref. [6] )	<5 Hz
Regulations in Japan ( Ref. [30] )	1.5 Hz – 2.3 Hz
ISO/DIS standard 10137 ( Ref. [28] )	1.7 Hz – 2.3 Hz
CEB 209 Bulletin	1.65 – 2.35 Hz
Bachmann ( Ref. [59] )	1.6 – 2.4 Hz

**Table 2-4: Risk frequencies in current regulations (Source: Sétra, 2006)**



**Figure 2-1: Vertical critical accelerations in  $m/s^2$  as a function of the natural frequency for various regulations (Source: Sétra, 2006)**

The Sétra guidelines themselves establish the acceleration ranges for different comfort levels (*Figure 2-2*). Accelerations in Range 1 corresponds to the maximum comfort level, 3 to the minimum and 4 to uncomfortable acceleration levels that are not acceptable.

The horizontal acceleration is limited in any case to  $0,10m/s^2$  to avoid “lock-in” effect (*Figure 2-2b*).

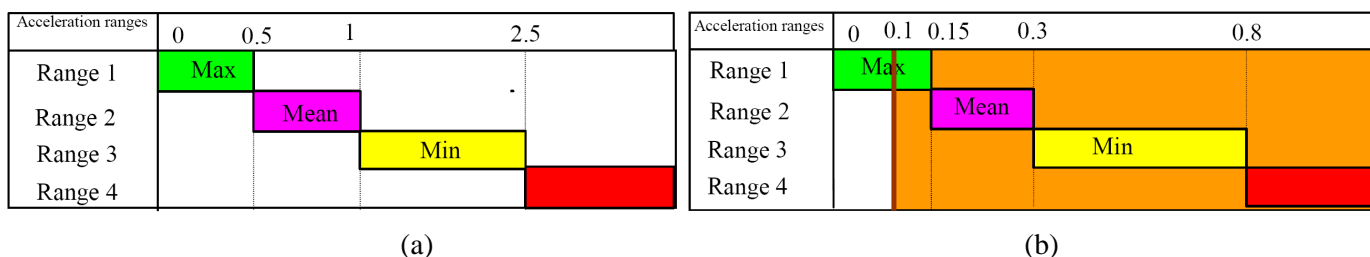


Figure 2-2: Acceleration ranges in  $m/s^2$  for (a) vertical and (b) horizontal vibrations (Sétra, 2006)

The risk of resonance is classified in different ranges for different frequencies (Figure 2-3) with 2 mass assumptions: empty footbridge and loaded throughout its bearing area, to the tune of one 700N pedestrian per square meter.

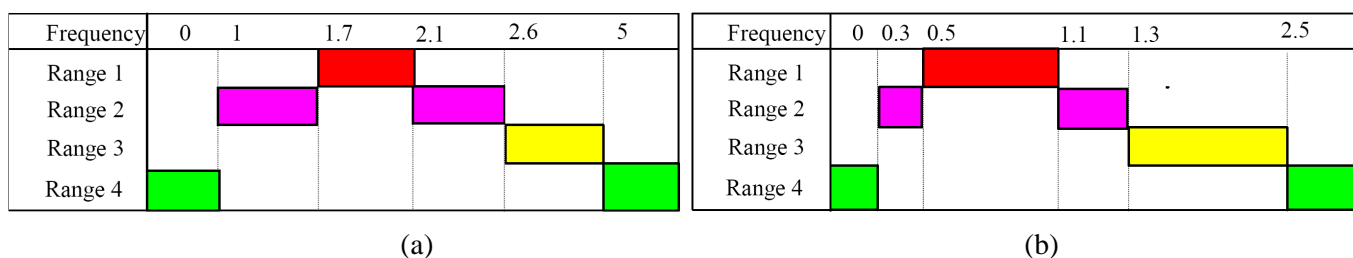


Figure 2-3: Risk of resonance. Frequency ranges in Hz for (a) vertical and (b) horizontal vibrations (Source: Sétra, 2006)

The necessity of the dynamic calculation is decided according to the natural frequency range (from range 1 with a maximum risk of resonance to 3 minimum, being the risk negligible for frequencies in the range 4). The natural frequency range and the bridge class gives the dynamic load cases for which it must be conducted (Figure 2-4). The class depends on the bridge usage. For very light bridges Sétra advises to consider at least class III to ensure a minimum amount of risk control.

		Load cases to select for acceleration checks		
Traffic	Class	Natural frequency range		
		1	2	3
Sparse	III	Case 1	Nil	Nil
	II		Case 1	Case 3
Very dense	I	Case 2	Case 2	Case 3

Case No. 1: Sparse and dense crowd  
Case No. 2: Very dense crowd

Case No. 3: Crowd complement (2nd harmonic)

Figure 2-4: Verifications. Load case under consideration of the natural frequency and class of the footbridge (Source: Sétra, 2006)

The loading adopted for the dynamic analyses establishes the density of the crowd ( $d$ ) for the different cases. Given the total area of the footbridge, the density gives the number of pedestrians involved. This is transformed into an equivalent number of pedestrians

**Case 1:**

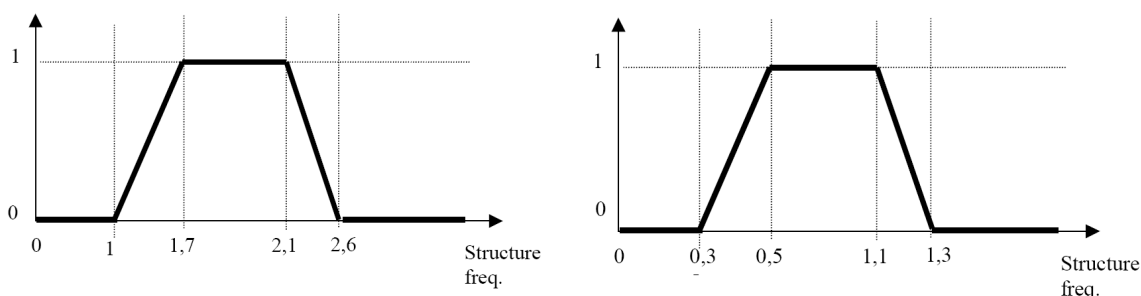
The details of this case are given as an example and will be used to calculate the loading for the present study (section 5). Summarising and citing Sétra (2006):

“The density  $d$  of the pedestrian crowd is to be considered according to the class of the footbridge” (Table 2-5).

Class	Density $d$ of the crowd
III	0.5 pedestrians/m <sup>2</sup>
II	0.8 pedestrians/m <sup>2</sup>

**Table 2-5: Density  $d$  of the pedestrian crowd according to the class of the footbridge (Source: Sétra, 2006)**

“The load that is to be taken into account is modified by a minus factor  $\phi$  which makes allowance for the fact that the risk of resonance in a footbridge becomes less likely the further away from the range 1.7 Hz – 2.1 Hz for vertical accelerations, and 0.5 Hz – 1.1 Hz for horizontal accelerations”. The values which this factor adopts for different frequencies are shown in Figure 2-5.



**Figure 2-5: Factor  $\phi$  in the case of walking, for vertical and longitudinal vibrations on the left, and for lateral vibrations on the right. (Source: Sétra, 2006)**

Table 2-6 “summarises the load per unit area to be applied for each direction of vibration, for any random crowd” (Sétra, 2006).

- $\xi$  represents the critical damping ratio (no unit), and  $n$  the number of pedestrians on the footbridge ( $d \times S$ ).
- These loads are to be applied until the maximum acceleration of the resonance is obtained.
- These load cases are not to be applied simultaneously. The vertical load case is applied for each vertical mode at risk, and the longitudinal load case for each longitudinal mode at risk, adjusting on each occasion the frequency of the load to the natural frequency concerned.



Direction	Load per m <sup>2</sup>
Vertical (v)	$d \times (280N) \times \cos(2\pi f_v t) \times 10.8 \times (\xi/n)^{1/2} \times \psi$
Longitudinal (l)	$d \times (140N) \times \cos(2\pi f_l t) \times 10.8 \times (\xi/n)^{1/2} \times \psi$
Transversal (t)	$d \times (35N) \times \cos(2\pi f_t t) \times 10.8 \times (\xi/n)^{1/2} \times \psi$

Table 2-6: Load per unit area to be applied for each direction of vibration (Source: Sétra, 2006)

Cases 2 and 3 are obtained by the same process but with other values.

The load direction should follow the sign of the mode shape as shown in Figure 2-6.

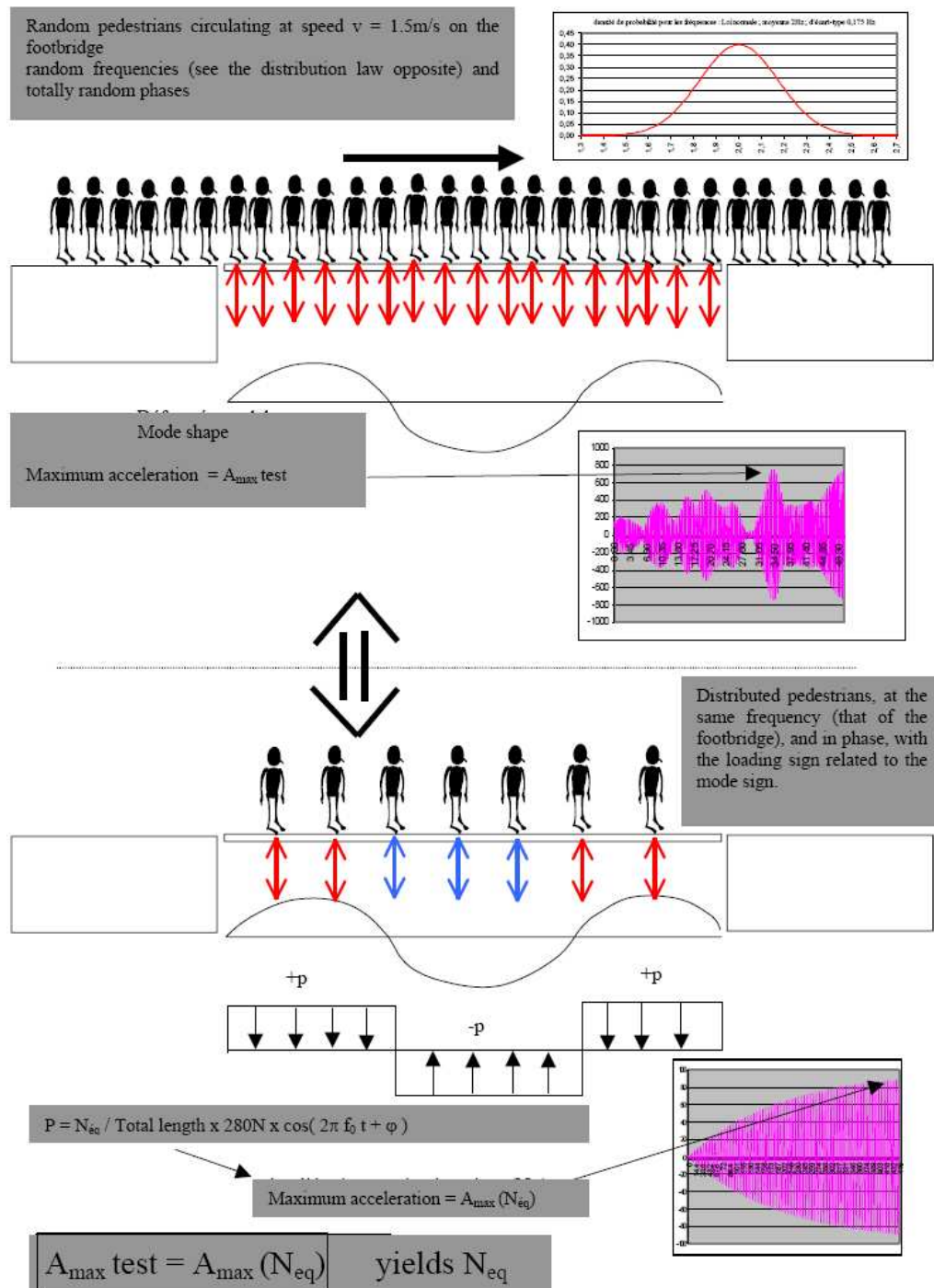


Figure 2-6: Calculation methodology for the equivalent number of pedestrians  $N_{eq}$  (Source: Sétra, 2006)

**“Design of floor structures for human induced vibrations” (JRC European Commission)**

Feldmann et al (2009) have developed a report under the JRC-ECCS cooperation agreement for the evolution of Eurocode 3. This report gives a procedure for the determination and assessment of floor responses to walking of pedestrians and leads to easy-to-use design charts, taking account of the complexity of the mechanical vibrations problem.

The phases of walking are described. The duration of the pace and the distribution of the weight on the floor during time depend exclusively on the frequency of the pedestrian. A statistical study of the dynamic loading normalized to the weight and according to the frequency is described in this report. This leads to a polynomial function which describes the contact force due walking along the time (Figure 2-7a). Another polynomial function describes the duration of the pace as a function of the frequency (Figure 2-7b).

Polynomial function for the contact force due to a single step:			
$\frac{F(t)}{G} = K_1t + K_2t^2 + K_3t^3 + K_4t^4 + K_5t^5 + K_6t^6 + K_7t^7 + K_8t^8$			
Coefficient	step frequency ranges		
	$f_s \leq 1.75$ Hz	$1.75 < f_s < 2$ Hz	$f_s \geq 2$ Hz
$K_1$	$-8 \times f_s + 38$	$24 \times f_s - 18$	$75 \times f_s - 120$
$K_2$	$376 \times f_s - 844$	$-404 \times f_s + 521$	$-1720 \times f_s + 3153$
$K_3$	$-2804 \times f_s + 6025$	$4224 \times f_s - 6274$	$17055 \times f_s - 31936$
$K_4$	$6308 \times f_s - 16573$	$-29144 \times f_s + 45468$	$-94265 \times f_s + 175710$
$K_5$	$1732 \times f_s + 13619$	$109976 \times f_s - 175808$	$298940 \times f_s - 553736$
$K_6$	$-24648 \times f_s + 16045$	$-217424 \times f_s + 353403$	$-529390 \times f_s + 977335$
$K_7$	$31836 \times f_s - 33614$	$212776 \times f_s - 350259$	$481665 \times f_s - 888037$
$K_8$	$-12948 \times f_s + 15532$	$-81572 \times f_s + 135624$	$-174265 \times f_s + 321008$

(a)

$$T_s = 2.6606 - 1.757 f_s + 0.3844 f_s^2$$

(b)

**Figure 2-7: (a) Contact force due walking along the time. (b) Duration of the pace as a function of the frequency**

The weight of the pedestrian and the frequency are independent variables.

In order to obtain a time history of the dynamic loads due to several people walking on the structure:

- 1)  $n$  pace frequencies of pace and  $n$  pedestrian masses are chosen randomly.
- 2) Frequencies and masses are paired randomly.
- 3) A time history of each pair of data is generated, ie for each pedestrian a time history is generated with the aforementioned polynomial function
- 4) All the time histories obtained are added

This method leads to establish a time history, enabling a dynamic loading analysis which will give an acceleration. The comfort degree can then be obtained with the comfort degrees given by different codes for footbridges, such as the aforementioned IAP 2011 or the Sétra Guidelines.

## 2.2 Examples of dynamic behaviour

### 2.2.1 Dynamic response of the Millenium Bridge. Quantification of the locking effect

An example worth mentioning, that set out different tests and researches, which added to previous ones, set nowadays codes, is the London Millenium Bridge, a suspension footbridge.

Citing Dallard et al (2001): *“During design of the London Millenium Bridge, a modified BS 5400 approach was used for assessment of the response to vertical pedestrian excitation, using a higher input force than is recommended in the code”. “To take into account the effects resulting from the inclined cables, including the coupling of lateral and torsional movements, the lateral and torsional response to eccentrically applied vertical loads was also assessed”.*

*“It is estimated that between 80 000 and 100 000 people crossed the bridge during the opening day. Analysis of video footage showed a maximum of 2000 people on the deck at any one time, resulting in a maximum density of between 1.3 and 1.5 people per square metre” (Dallard et al 2001).* Unexpected excessive lateral vibrations of the bridge occurred. The movements took place mainly at a frequency of around 0.8Hz and at frequencies of just under 0.5Hz and 1.0Hz (different values for different spans that were not the most critical ones of the aforementioned analysis).

*“Excessive vibration did not occur continuously, but built up when a large number of pedestrians were on the affected spans of the bridge and died down if the number of people on the bridge reduced, or if the people stopped walking “(Dallard et al 2001).*

*“From visual estimation of the amplitude of the movements on the south and central span, the maximum lateral acceleration experienced on the bridge was between 200 and 250 milli.-Agt”.* The strong lateral response of the Millennium Bridge was caused by resonance.

Until the research lead as a result of the incident of the excessive vibration of the London Milenium bridge the phenomenon of *synchronous lateral excitation was explained in a few reports, but none of them gave any reliable quantification of the lateral force due to the pedestrians, or any relationship between the force exerted and the movement of the deck surface (Dallard et al 2001).* Research was conducted through laboratory tests and crowd tests on the Millennium Bridge itself. Useful results were obtained, which enabled the design of the retrofit to be progressed.

## 2.2.2 Highlights on SABs

Some examples of SABs with a vertical inclined arch and a straight deck are the Merchants Bridge and the York Millenium Bridge (Figure 2-8) and the Dreiländer bridge with a straight deck suspended of a vertical arch braced to an inclined arch (Figure 2-9).



(a) (b)  
**Figure 2-8: (a) Merchants Bridge. (b) York Millenium Bridge**

Tuned mass dampers were installed within the deck of the Merchants Bridge (Mairs, 2001). The York Millenium Bridge did not require the use of dampers. An analysis was conducted with an average of 2 people per square meter of main span each applying a peak dynamic load of 25N. This generates a horizontal acceleration of  $0,4\text{m/s}^2$  (Mairs, 2001).

### *Dreiländer bridge*



**Figure 2-9: Dreiländer bridge (reproduced by kind permission of Hans-Peter Andrä)**

The natural frequency of the bridge is 0,9Hz according to a modal analysis (Strobl et al, 2007). This is in the range of pedestrian lateral frequency. A dynamic analysis was conducted according to Fujino et al (1990 and 2005). According to this analysis, walking crowds with a density higher than  $0,24\text{pers/m}^2$  would destabilize the bridge and the use of 10T mass damper at midspan would be needed.

However, practical dynamic tests were performed on the bridge, giving a natural frequency a 10% higher (1,01Hz). For  $0,24\text{pers/m}^2$  the frequency of the pedestrian pace was below 1Hz. Bringing the pace near to the bridge frequency, an acceleration of  $1,5\text{m/s}^2$  was reached. It was decided to use no dampers and there have been no problems up to date in spite of the large pedestrian density during the bridge inauguration and celebrations (Strobl et al, 2007, and LAP internal reports, 2015).

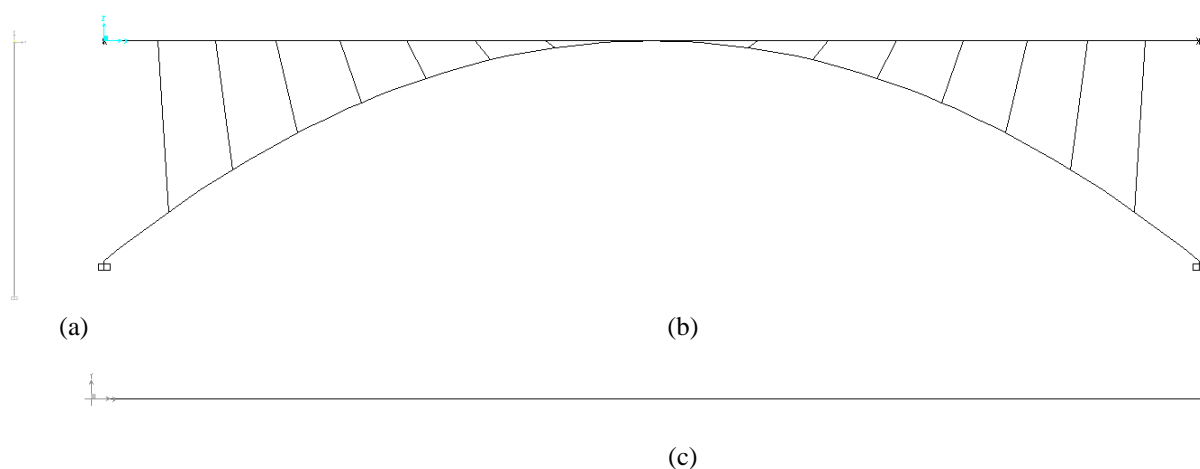
### 3. STUDIED PARAMETERS AND GEOMETRIES

A dynamic analysis has been conducted for vertical planar arch bridges with a straight superior deck and spatial arch bridges with a vertical planar arch and a superior curved deck with  $g=20\text{m}$  (see *Figure 3-1*, *Figure 3-2* and bookmark) and the values  $e=16,67\text{m}$  and  $f=20\text{m}$ , concluded to be the most efficient in Chapter V.

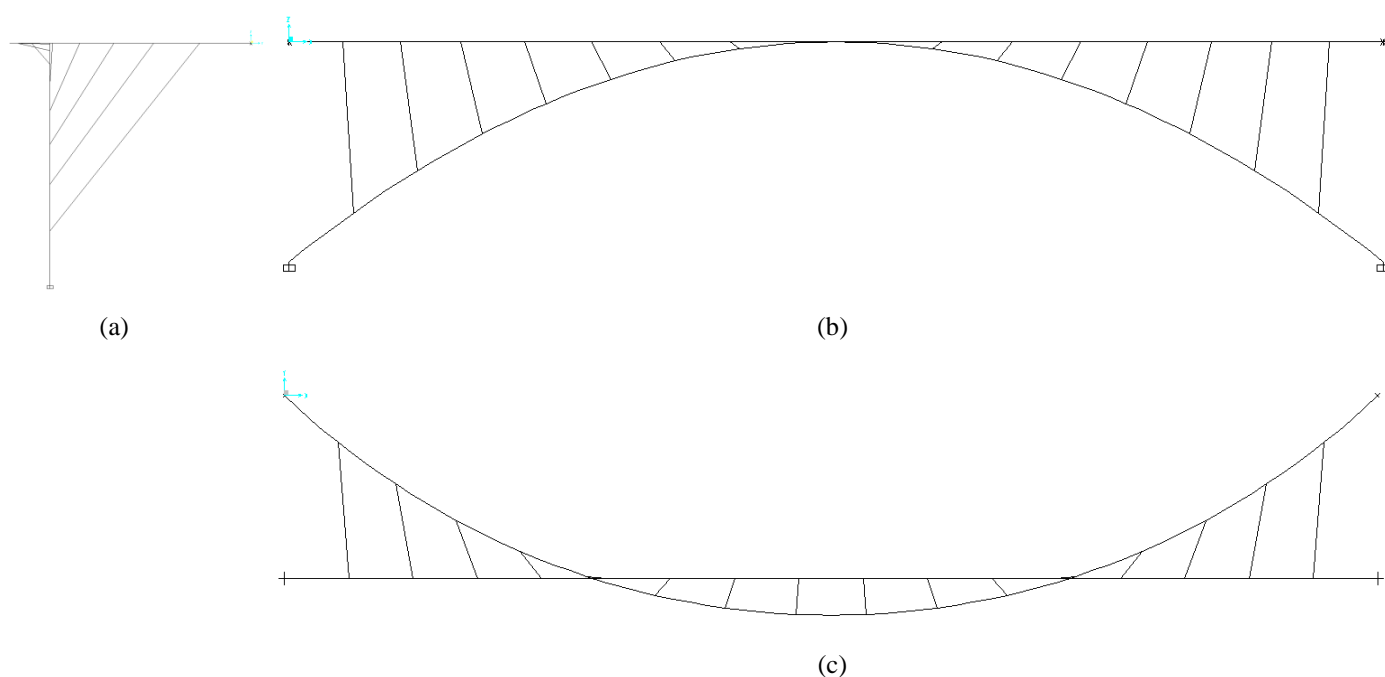
The cross-sections employed are detailed in *Table 4-4*.

The damping coefficient employed, considering that it is a steel structure is 0,4%

The arch in both bridges is fixed at its springings. The torsional rotations are restrained at the deck abutments (rtr), other rotations are free and vertical and transverse/radial movements are restrained. Longitudinal movements are restrained (rlm) at the deck abutments for SABs and are free (flm) for the planar vertical arch with straight deck.



**Figure 3-1: Geometry of arch bridge with  $g=0$  and  $f=20\text{m}$ . (a) Lateral view (yz); (b) Layout (xz); (c) Plan view (xy)**



**Figure 3-2: Geometry of arch bridge with  $g=20\text{m}$  and  $f=20\text{m}$ . (a) Lateral view (yz); (b) Layout (xz); (c) Plan view (xy)**

g	e	f	Struts	Arch	Deck	Movements at deck abutments**
0	0	20	D300t25. Reference distribution*	D750t25	B4000H700t20→Sec1	flm,rtr
20	16,67	20	D300t35. radial (Reference*)	D750t30	B4000H700t20→Sec1	rlm,rtr
20	16,67	20	D300t35. radial (Reference*)	D750t30	B4000H700t12→Sec2	rlm,rtr

\*See chapter V.B    \*\* See chapter V.A or bookmark

**Table 3-1: Characteristics of the analysed models**

#### 4. NATURAL FREQUENCIES AND NEED OF CONDUCTING A DYNAMIC ANALYSIS

A modal analysis has been conducted prior to the determination of the loads for the dynamic analyses.

The modes observed are shown from Figure 4-1 to Figure 4-5. For bridges with a straight deck  $g=0$ , the bridge deforms in the different directions for separate modes, whereas for bridges with a curved deck (Figure 4-5), the 1st mode is already in all directions x, y and z. The bridge with a curved deck has clearly a spatial behaviour.

The first mode of the model with a straight deck (Figure 4-5) gives the natural frequency in y direction. The 2<sup>nd</sup> mode (Figure 4-2) gives the frequency in z direction. This mode shape is non-symmetrical. The next mode also gives a natural frequency in z direction, but it is symmetrical (Figure 4-5). The bridge with a curved deck also shows a non-symmetrical deformed shape for the first mode and symmetrical for the second mode.

Since for the bridges with a curved deck, the first mode already causes deformations in all three directions (**Figure 4-5**), we might wonder whether the aforementioned comment in Sétra “These load cases are not to be applied simultaneously. The vertical load case is applied for each vertical mode at risk, and the longitudinal load case for each longitudinal mode at risk, adjusting on each occasion the frequency of the load to the natural frequency concerned” (section 2.1) should be applied here or not. It seems logical studying the dynamic behaviour with the load cases in all three directions at the same time (see section 5). Before doing so, the participating mass ratios are observed (see tables from Table 4-1 to Table 4-3).

The frequencies obtained in each case are detailed in Table 4-4. The necessity to perform a dynamic load case calculation is determined according to the natural frequency of the bridge. This evaluation has been done based on both, IAP 2011 and Sétra Guidelines (2006) (Table 4-4), as described in section 2.1

The EC1 UK NA does not establish frequency ranges which define the need of a dynamic analyses.

In some cases the lateral response is out of the range of frequencies of the test measurements on which EC1 UK NA is based. Hence, this code has not been employed to evaluate the necessity of checking lateral stability.

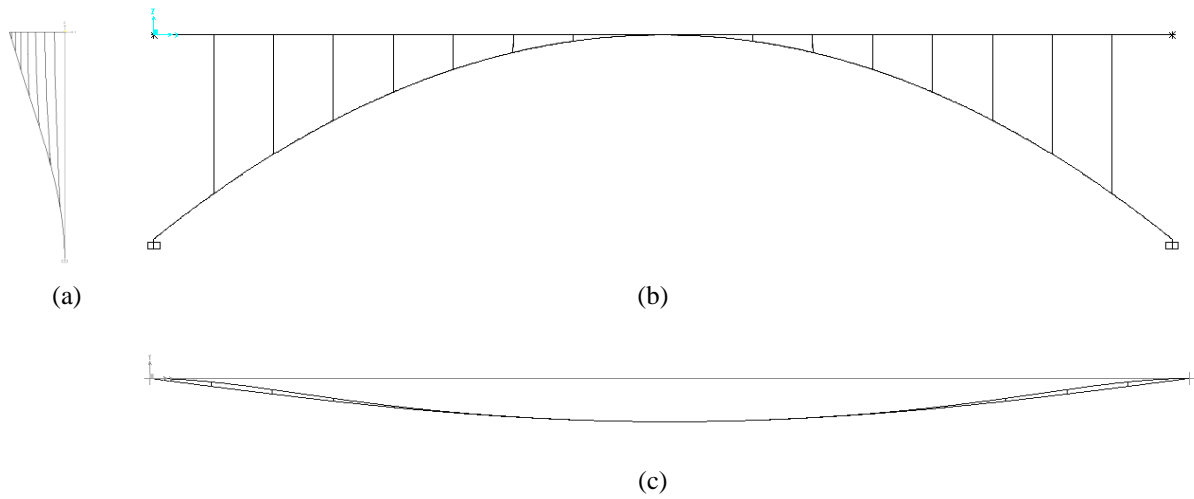


Figure 4-1: 1st mode  $g=0m$ ;  $f=20m$  (Table 3-1). (a) Lateral view; (b) Layout; (c) Plan view

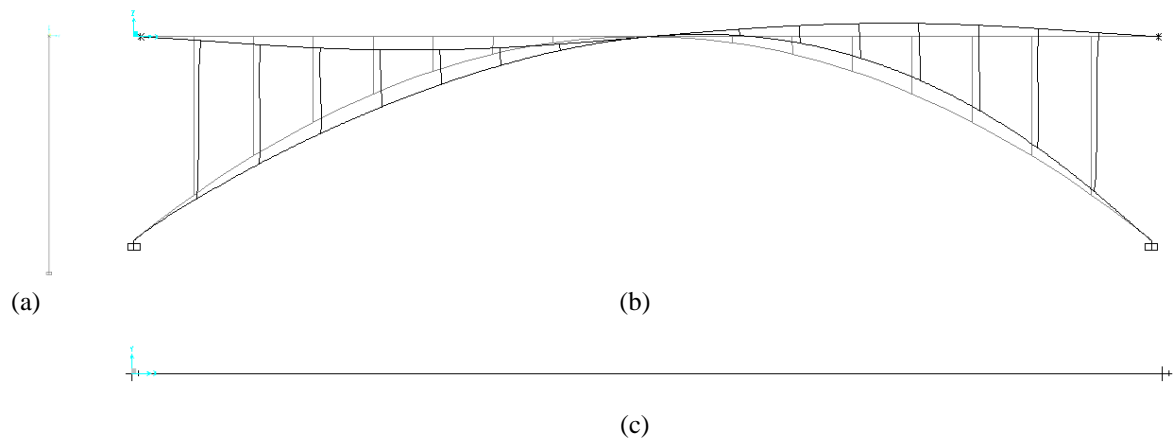


Figure 4-2: 2nd mode  $g=0m$ ;  $f=20m$  (Table 3-1). (a) Lateral view; (b) Layout; (c) Plan view

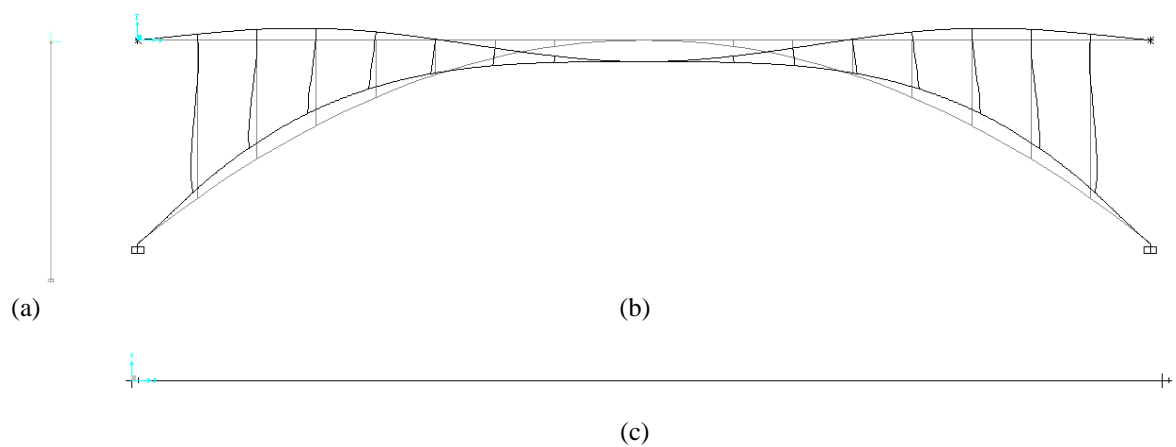


Figure 4-3: 3rd mode  $g=0m$ ;  $f=20m$  (Table 3-1). (a) Lateral view; (b) Layout; (c) Plan view

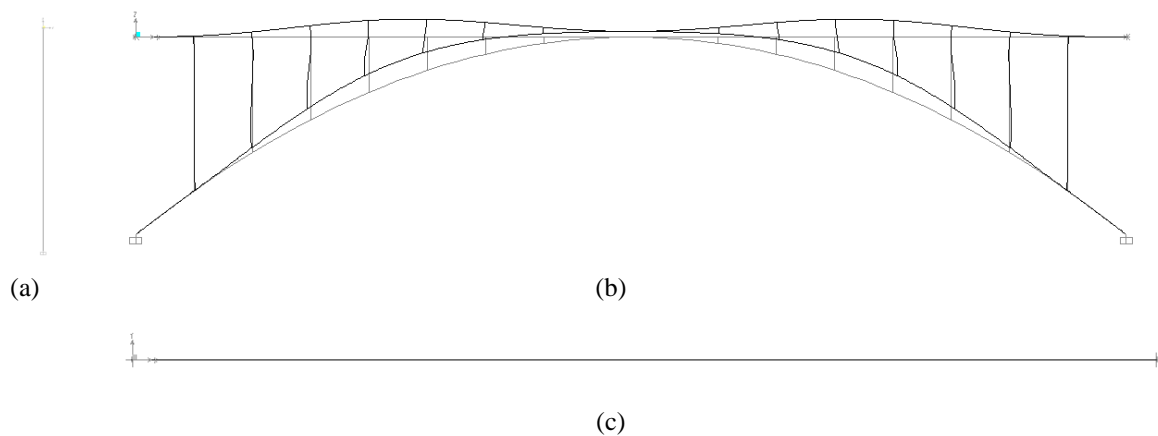


Figure 4-4: 8th mode  $g=0m$ ;  $f=20m$  (Table 3-1). (a) Lateral view; (b) Layout; (c) Plan view

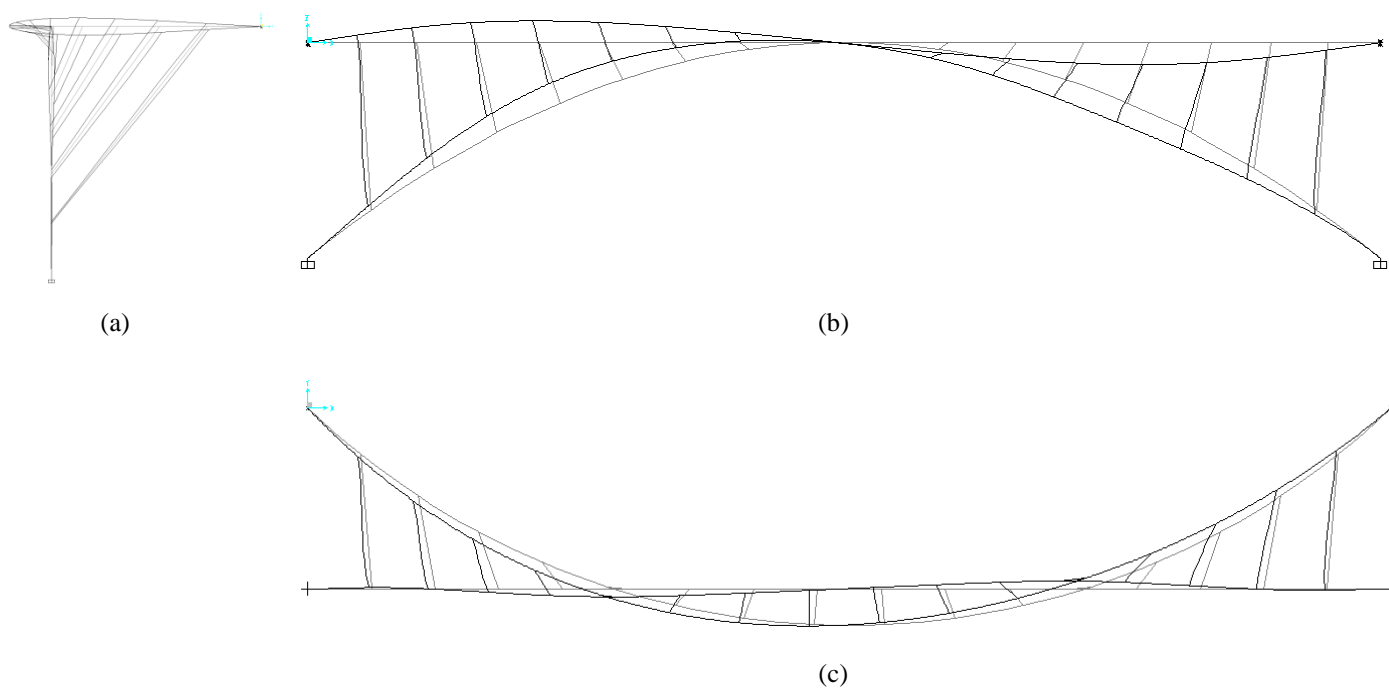
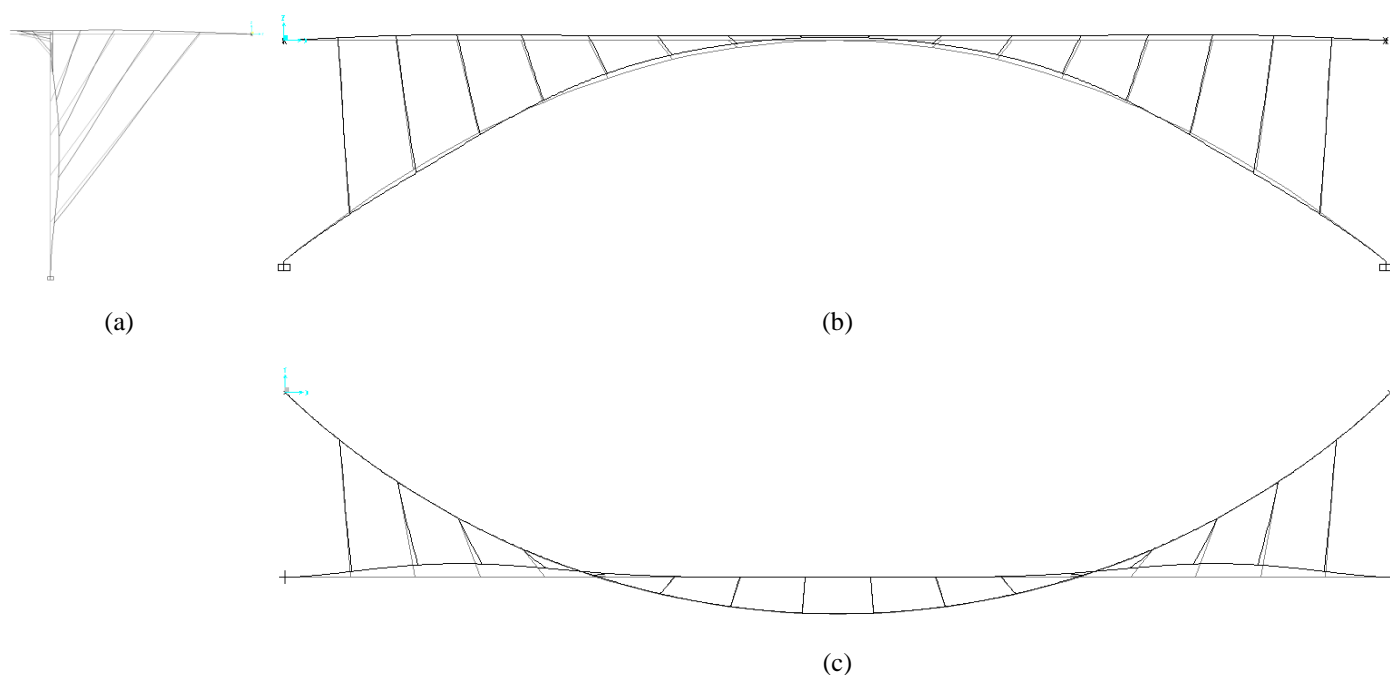


Figure 4-5: 1st mode  $g=20m$ ;  $f=20m$  and deck with Sec1 and Sec2 (Table 3-1). (a) Lateral view; (b) Longitudinal view; (c) Plan view





**Figure 4-6: 3rd mode  $g=20m$ ;  $f=20m$  and deck with Sec1 and 4<sup>th</sup> mode with Sec2 (Table 3-1). (a) Lateral view; (b) Longitudinal view; (c) Plan view**

The participating mass ratio of the structure modal output must be near to 1 for each direction when adding the mass ratios participating in each direction in the different modes. In order to obtain such a value the first 20 modes are analysed for the case of a vertical planar arch with a straight deck ( $g=0$ , geometry shown in *Figure 3-1* and participating mass ratios in *Table 4-1*). For the SAB models (*Figure 3-2*) the first 30 modes are analysed to obtain values of participating mass near to one (*Table 4-2* and *Table 4-3*).

Whereas planar vertical arch bridges with a straight deck mobilise masses only in one direction for each natural mode (*Table 4-1*), SABs mobilise masses in different directions for the same natural mode (*Table 4-2* and *Table 4-3*).

The modes which will be studied and the participating mass ratio are marked in each table.

Modal Participating Mass Ratios									
		Period	Frequency	UX	UY	UZ	SumUX	SumUY	SumUZ
		Sec	Cyc/sec	Unitless	Unitless	Unitless	Unitless	Unitless	Unitless
Mode	1	1.349	0.74	0.000	0.801	0.000	0.000	0.801	0.000
Mode	2	1.221	0.82	0.343	0.000	0.000	0.343	0.801	0.000
Mode	3	0.549	1.82	0.000	0.000	0.000	0.343	0.801	0.000
Mode	4	0.372	2.69	0.000	0.000	0.000	0.343	0.801	0.000
Mode	5	0.326	3.07	0.000	0.028	0.000	0.343	0.828	0.000
Mode	6	0.305	3.28	0.001	0.000	0.000	0.343	0.828	0.000
Mode	7	0.279	3.59	0.000	0.000	0.000	0.343	0.828	0.000
Mode	8	0.249	4.01	0.000	0.000	0.720	0.343	0.828	0.720
Mode	9	0.199	5.04	0.000	0.000	0.189	0.343	0.828	0.910
Mode	10	0.160	6.26	0.365	0.000	0.000	0.709	0.828	0.910
Mode	11	0.150	6.67	0.000	0.023	0.000	0.709	0.851	0.910
Mode	12	0.145	6.89	0.000	0.064	0.000	0.709	0.914	0.910
Mode	13	0.138	7.27	0.000	0.000	0.000	0.709	0.914	0.910
Mode	14	0.131	7.61	0.245	0.000	0.000	0.954	0.914	0.910
Mode	15	0.108	9.25	0.000	0.000	0.028	0.954	0.914	0.937
Mode	16	0.089	11.23	0.000	0.000	0.000	0.954	0.914	0.937
Mode	17	0.085	11.79	0.002	0.000	0.000	0.956	0.914	0.937
Mode	18	0.084	11.93	0.000	0.003	0.000	0.956	0.917	0.937
Mode	19	0.076	13.09	0.000	0.000	0.000	0.956	0.917	0.937
Mode	20	0.068	14.66	0.000	0.000	0.010	0.956	0.917	0.947

**Table 4-1: Participating mass ratios in each mode for planar vertical arch bridge with superior straight deck (g=0, see Figure 3-1 and Table 3-1)**

Modal Participating Mass Ratios									
		Period	Frequency	UX	UY	UZ	SumUX	SumUY	SumUZ
		Sec	Cyc/sec	Unitless	Unitless	Unitless	Unitless	Unitless	Unitless
Mode	1	0.789	1.267	0.108	0.000	0.000	0.108	0.000	0.000
Mode	2	0.668	1.497	0.000	0.000	0.005	0.108	0.000	0.005
Mode	3	0.419	2.386	0.000	0.045	0.472	0.108	0.045	0.476
Mode	4	0.411	2.433	0.056	0.000	0.000	0.164	0.045	0.476
Mode	5	0.354	2.825	0.032	0.000	0.000	0.195	0.045	0.476
Mode	6	0.332	3.011	0.000	0.068	0.267	0.195	0.113	0.743
Mode	7	0.248	4.025	0.110	0.000	0.000	0.305	0.113	0.743
Mode	8	0.246	4.061	0.000	0.002	0.051	0.305	0.115	0.794
Mode	9	0.221	4.522	0.000	0.109	0.005	0.305	0.225	0.799
Mode	10	0.173	5.772	0.002	0.000	0.000	0.308	0.225	0.799
Mode	11	0.151	6.624	0.000	0.016	0.025	0.308	0.241	0.824
Mode	12	0.148	6.744	0.033	0.000	0.000	0.341	0.241	0.824
Mode	13	0.130	7.696	0.000	0.002	0.033	0.341	0.244	0.858
Mode	14	0.125	7.989	0.000	0.574	0.011	0.341	0.817	0.869
Mode	15	0.113	8.855	0.045	0.000	0.000	0.386	0.817	0.869
Mode	16	0.109	9.200	0.000	0.011	0.063	0.386	0.829	0.932
Mode	17	0.103	9.743	0.000	0.000	0.000	0.386	0.829	0.932
Mode	18	0.088	11.409	0.003	0.000	0.000	0.389	0.829	0.932
Mode	19	0.084	11.926	0.000	0.001	0.002	0.389	0.829	0.934
Mode	20	0.081	12.372	0.000	0.000	0.012	0.389	0.830	0.946
Mode	21	0.071	14.105	0.001	0.000	0.000	0.390	0.830	0.946
Mode	22	0.069	14.497	0.000	0.020	0.000	0.390	0.850	0.946
Mode	23	0.068	14.786	0.002	0.000	0.000	0.392	0.850	0.946
Mode	24	0.060	16.710	0.000	0.001	0.000	0.392	0.851	0.946
Mode	25	0.057	17.588	0.000	0.000	0.007	0.392	0.851	0.953
Mode	26	0.055	18.071	0.441	0.000	0.000	0.833	0.851	0.953
Mode	27	0.053	18.719	0.001	0.000	0.000	0.834	0.851	0.953
Mode	28	0.050	20.172	0.021	0.000	0.000	0.855	0.851	0.953
Mode	29	0.049	20.512	0.000	0.000	0.000	0.855	0.851	0.953
Mode	30	0.047	21.390	0.000	0.000	0.001	0.855	0.852	0.954

**Table 4-2: Participating mass ratios in each mode for planar vertical arch bridge with superior curved deck (g=20m, Sec1, see Figure 3-2 and Table 3-1)**

<b>TABLE: Modal Participating Mass Ratios</b>									
		<b>Period</b>	<b>Frequency</b>	<b>UX</b>	<b>UY</b>	<b>UZ</b>	<b>SumUX</b>	<b>SumUY</b>	<b>SumUZ</b>
		Sec	Cyc/Sec	Unitless	Unitless	Unitless	Unitless	Unitless	Unitless
Mode 1	1	0,848	1,180	0,135	0,000	0,000	0,135	0,000	0,000
Mode 2	2	0,698	1,432	0,000	0,001	0,009	0,135	0,001	0,009
Mode 3	3	0,432	2,315	0,023	0,000	0,000	0,159	0,001	0,009
Mode 4	4	0,406	2,463	0,000	0,106	0,210	0,159	0,107	0,219
Mode 5	5	0,357	2,798	0,032	0,000	0,000	0,190	0,107	0,219
Mode 6	6	0,337	2,964	0,000	0,040	0,476	0,190	0,147	0,695
Mode 7	7	0,263	3,802	0,000	0,017	0,037	0,190	0,164	0,732
Mode 8	8	0,253	3,955	0,000	0,095	0,018	0,190	0,259	0,750
Mode 9	9	0,246	4,066	0,096	0,000	0,000	0,286	0,259	0,750
Mode 10	10	0,184	5,440	0,007	0,000	0,000	0,293	0,259	0,750
Mode 11	11	0,159	6,295	0,000	0,071	0,015	0,293	0,330	0,765
Mode 12	12	0,153	6,523	0,049	0,000	0,000	0,342	0,330	0,765
Mode 13	13	0,141	7,081	0,000	0,425	0,000	0,342	0,755	0,765
Mode 14	14	0,136	7,365	0,000	0,074	0,078	0,342	0,830	0,843
Mode 15	15	0,127	7,903	0,027	0,000	0,000	0,370	0,830	0,843
Mode 16	16	0,111	9,011	0,001	0,000	0,000	0,370	0,830	0,843
Mode 17	17	0,111	9,035	0,000	0,006	0,082	0,370	0,835	0,926
Mode 18	18	0,091	10,956	0,000	0,001	0,005	0,370	0,836	0,930
Mode 19	19	0,089	11,196	0,000	0,000	0,000	0,370	0,836	0,930
Mode 20	20	0,084	11,915	0,000	0,003	0,009	0,370	0,839	0,939
Mode 21	21	0,076	13,133	0,000	0,015	0,001	0,370	0,854	0,940
Mode 22	22	0,076	13,232	0,000	0,000	0,000	0,371	0,854	0,940
Mode 23	23	0,070	14,300	0,008	0,000	0,000	0,379	0,854	0,940
Mode 24	24	0,064	15,662	0,000	0,000	0,004	0,379	0,855	0,944
Mode 25	25	0,062	16,045	0,414	0,000	0,000	0,793	0,855	0,944
Mode 26	26	0,059	17,007	0,000	0,001	0,004	0,793	0,855	0,947
Mode 27	27	0,057	17,539	0,023	0,000	0,000	0,816	0,855	0,947
Mode 28	28	0,055	18,204	0,008	0,000	0,000	0,824	0,855	0,947
Mode 29	29	0,051	19,484	0,000	0,000	0,000	0,824	0,855	0,947
Mode 30	30	0,049	20,553	0,000	0,000	0,004	0,824	0,855	0,951

**Table 4-3: Participating mass ratios in each mode for planar vertical arch bridge with superior curved deck (g=20m, Sec2, see Figure 3-2 and Table 3-1)**

Models with a superior curved deck, which differ in the cross-section employed for the deck (*Table 3-1*) have very similar values of natural frequencies which need be analysed. Since the model with a slightly stiffer deck (Sec1) has more frequency values to be analysed, the dynamic analysis will be further carried out for this model, but not for the one employing Sec2 (shaded in *Table 4-4*). The same deck is employed for the model with a planar vertical arch with a straight deck. Therefore, the deck for both for which the dynamic analysis will be carried out differs only in its geometry and its influence can be hence compared.

		fx (Hz)	Need of dynamic analysis		fy (Hz)	Need of dynamic analysis		fz (Hz)	Need of dynamic analysis	
			According to IAP2011	According to Sétra 2006		According to IAP2011	According to Sétra 2006		According to IAP2011	According to Sétra 2006
g=0	Sec1	0,82 Mode 2	out of pedestrian load range	Range 4: negligible risk of resonance	0,74 Mode 1	<b>need of dynamic analysis</b>	<b>Range 1: maximum risk of resonance</b>	4.01 Mode 8	<b>need of dynamic analysis</b>	Range 3: low risk of resonance for standard loading situations
		6,26	out of pedestrian load range	Range 4: negligible risk of resonance	-					
g=20m	Sec1	1,27 Mode 1	<b>need of dynamic analysis</b>	Range 2: medium risk of resonance	2.39 Mode 3	<b>need of dynamic analysis</b>	Range 3: low risk of resonance for standard loading situations	2.39 Mode 3	<b>need of dynamic analysis</b>	Range 2: medium risk of resonance
		4,02 Mode 7	<b>need of dynamic analysis</b>	Range 3: low risk of resonance for standard loading situations	3,01 Mode 6	out of pedestrian load range	Range 4: negligible risk of resonance	3,01 Mode 6	<b>need of dynamic analysis</b>	Range 3: low risk of resonance for standard loading situations
		18,07 Mode 26	out of pedestrian load range	Range 4: negligible risk of resonance	4,52 Mode 9	out of pedestrian load range	Range 4: negligible risk of resonance	4,52 Mode 9	<b>need of dynamic analysis</b>	Range 3: low risk of resonance for standard loading situations
		-			7,99 Mode 14	out of pedestrian load range	Range 4: negligible risk of resonance	7,99	out of pedestrian load range	Range 4: negligible risk of resonance
	Sec2	1,18 Mode 1	out of pedestrian load range	Range 2: medium risk of resonance	2,46 Mode 4	out of pedestrian load range	Range 3: low risk of resonance for standard loading situations	2,46 Mode 4	<b>need of dynamic analysis</b>	Range 2: medium risk of resonance
		16,05 Mode 25	out of pedestrian load range	Range 4: negligible risk of resonance	2,96 Mode 6	out of pedestrian load range	Range 4: negligible risk of resonance	2,96 Mode 6	<b>need of dynamic analysis</b>	Range 3: low risk of resonance for standard loading situations
		-			7,08 Mode 13	out of pedestrian load range	Range 4: negligible risk of resonance	-		

**Table 4-4: Frequency values for the 1<sup>st</sup> modes and necessity of dynamic analysis**

## 5. LOAD CASES

Sétra Guidelines and UK National Annex to EC1 have been followed to establish the load cases for the dynamic analysis.

The Sétra Guidelines have been employed to obtain the crowd load case, as discussed in section **Fehler! Verweisquelle konnte nicht gefunden werden.** Since a single pedestrian is not considered in this guidelines, the EC1 UK NA has been employed to define the dynamic load case of a single pedestrian and of a small group, but employing another time history function that allows tracking the different pedestrian locations.

The following values and criteria have been employed:

- The time given is the time required by a pedestrian to cross the bridge and reach a maximal acceleration in the dynamic load case of a crowd. Additionally such an extra time lapse has been employed that, once the crowd has crossed the bridge, there is enough time for the free oscillation until the movement is damped. This gives the number of cycles.
- The damping coefficient employed, considering that it is a steel structure is 0,4%
- The usage width of the bridge is 3m.

### 5.1 Crowd dynamic load cases according to Sétra Guidelines (2006)

According to Sétra (2006), as described in section 2.1, the following values and criteria have been employed:

- Class III with sparse traffic has been considered. This gives a crowd density of 0,5pedestrians/m<sup>2</sup>.
- The Sétra minorisation factor has been employed. The load per area to be applied for each direction of vibration is summarized in **Table 5-1**.
- The load is applied for the different vibration modes (**Table 4-4** and from **Figure 4-1** to **Figure 4-5**).
- The dynamic load cases are defined as modal time history cosines functions with the corresponding period (**Table 5-1**).

According to EC1 UK NA, the equivalent class to III of Sétra is class B. The crowd density is then 0,4persons/m<sup>2</sup>, only slightly lower than the one indicated by Sétra. It has been decided to employ Sétra Guidelines for the crowd loading.

$g$	Tz (s) vertical	Vertical load (N/m)/cos(2*pi*fz*t)	Ty (s) transversal, radial	Transverse load (N/m2)/cos(2*pi*fy*t)	Tx (s) longitudinal, tangential	Longitudinal load (N/m2)/cos(2*pi*fy*t)
g=0	0.249	0	1.349	39.207	1.2	0
	-	-	-	-	0.16	0
g=20m, Sec1 (Table 3-1)	0.221	0	0.221	0		-
	0.332	0	0.332	0	0.055	0
	0.125	0	0.125	0	0.248	0
	0.419	130.594	0.419	0	0.789	58.458

**Table 5-1: Dynamic loads simulating crowds on the bridge following the Sétra Guidelines**

The loads in the different directions should not be applied simultaneously according to Sétra Guidelines (2006).

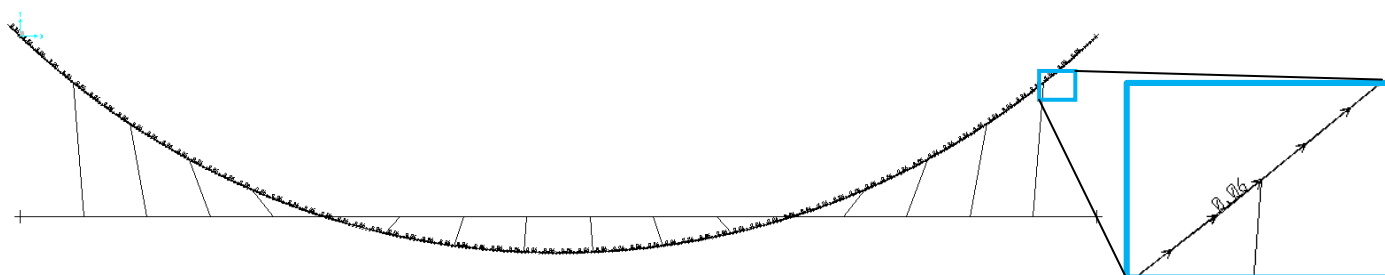
However, pedestrians cause the loads in all the different directions when walking. They are concomitant actions.

The reasons for which this is so are not specified in the Guidelines, but according to the Authors, it is due to:

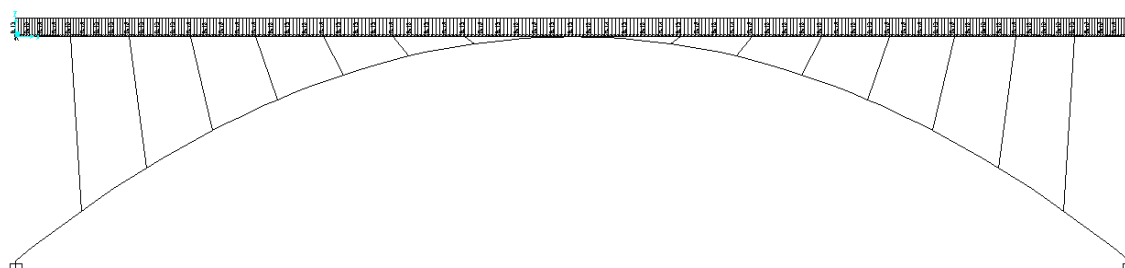
- The load cases which cause dynamic effects in one direction, do not contribute in the dynamic effects of other vibrations, so they not need to be applied simultaneously.
- The lock-in effect has not been proved to take place in different directions at the same time.

This makes sense for planar arch bridges with a straight deck, which have deformations in each direction for different modes.

However, for SABs with a planar arch bridge and a curved deck, which have shown to have a spatial behaviour, it makes sense to load the bridge in the three directions simultaneously.



**Figure 5-1:  $g=20$ , Sec1 (Table 3-1) Longitudinal pedestrian loading, amplitude for the time history longitudinal function**



**Figure 5-2:  $g=20$ , Sec1 (Table 3-1) Vertical pedestrian loading, amplitude for the time history longitudinal function**

Torsional vibration occurs with vertical loads. It has not been considered in the present study, since this analysis is only a first approach and many effects are mixed in the spatial model. Therefore, it is better to understand the behaviour of separate effects. If the bridge is already sensitive to vertical or transverse vibrations, it already points out the need of further research and the torsional dynamics should also be included in such a research. If not, the torsional vibration will be studied in a next section.

## 5.2 Vertical loading of a single pedestrian and a small pedestrian group crossing the bridge

Sétra Guidelines design footbridges with crowd loads, but do not consider the necessity to study a single pedestrian or small group. However, as already explained in section 2.1, EC1 UK NA considers group loads.

For the present example class B has been employed. According to EC1 UK NA a group size of 4 pedestrians walking should be considered.

Depending on the bridge usage, 1 jogging pedestrian should also be considered for class B, but EC1 UK NA establishes that this can be neglected. It is not considered in the present analysis.

The code does not indicate how to distribute the load. Therefore, instead of employing the code, a reasonable common used methodology has been employed.

The EC1 UK National Annex states the dynamic analysis should be conducted with pedestrian loads matching the natural frequency of the bridge. Nonetheless, it also states the speed of a pedestrian walking of 1,7m/s should be employed (*Table 2-2*). Hence, for the group load, two different pedestrian walking frequencies have been employed.

To see the bridge behaviour under small groups, the vertical loading of a single walking pedestrian and a small group of 4 pedestrians, walking in 2 rows of 2, has been analysed according to usual walking speed values.

This loading has been studied only for the SAB model with a superior curved deck ( $g=20m$ , *Figure 3-2*) and employing a slightly stiffer deck (Sec1, *Table 3-1*).

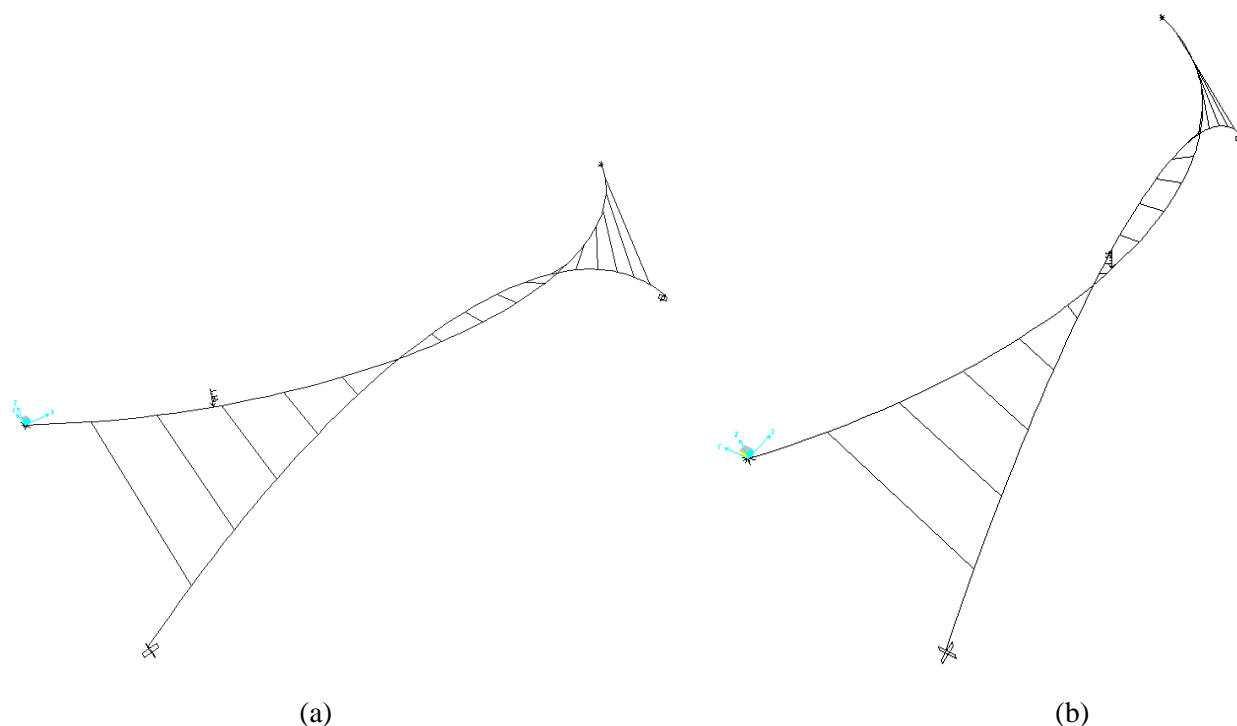
The following values and criteria have been employed:

- Time history functions are defined as triangular periodic functions in SAP2000 v14. They simulate the increase and fall of a step linearly in the time the step takes place and reaching its peak value at the midpoint of the time lapse.
- To match the natural frequency of the bridge, as a pedestrian walks at a 0,82m/s. Therefore the arrival time of pedestrians has been set to 0,98s for vertical loads. The peak of the function corresponds with this value.
- As a pedestrian walks at a 1,7m/s, according to EC1 UK NA, the arrival time of pedestrians has been set to 0,48s for vertical loads. The peak of the function corresponds with this value.
- To achieve the rise and fall of the amplitude caused by a single pedestrian ( $0,7kN\pm 0,28kN$ ) or group(2 groups of 2, ie:  $1,4kN\pm 0,146kN$ ) every 0,98s or 0,48s, respectively, are given to the periodic time history function.
- The loading has been calculated employing minus factor values as defined in EC1 UK National Annex. Results are given in *Table 5-2*.
- A series of 98 point loads are defined as static loads in SAP2000 v14. These static loads define the position (approximately every meter) and value of the loads. Their values correspond to the loading results of *Table 5-2*.
- All these static loads are combined with the time history function, each taking place at successive arrival times, simulating the pedestrian or group of 4 pedestrians crossing the whole bridge length (*Figure 5-3*). A last time lapse is added with no loading in order to observe the bridge damping.



	N walking (table NA.7)	Pedestrian mass (kg)	Minus factor k walking (Fig NA.8)	Minus factor gamma (pedestrian Fig NA.9)	Vertical load (N/m <sup>2</sup> )
g=20m, Sec1 (Table 3-1)	1	70.00	1.00	1.00	280.0
	4	280.00	0.52	1.00	291.2

**Table 5-2: Dynamic loads according to EC1 UK National Annex**



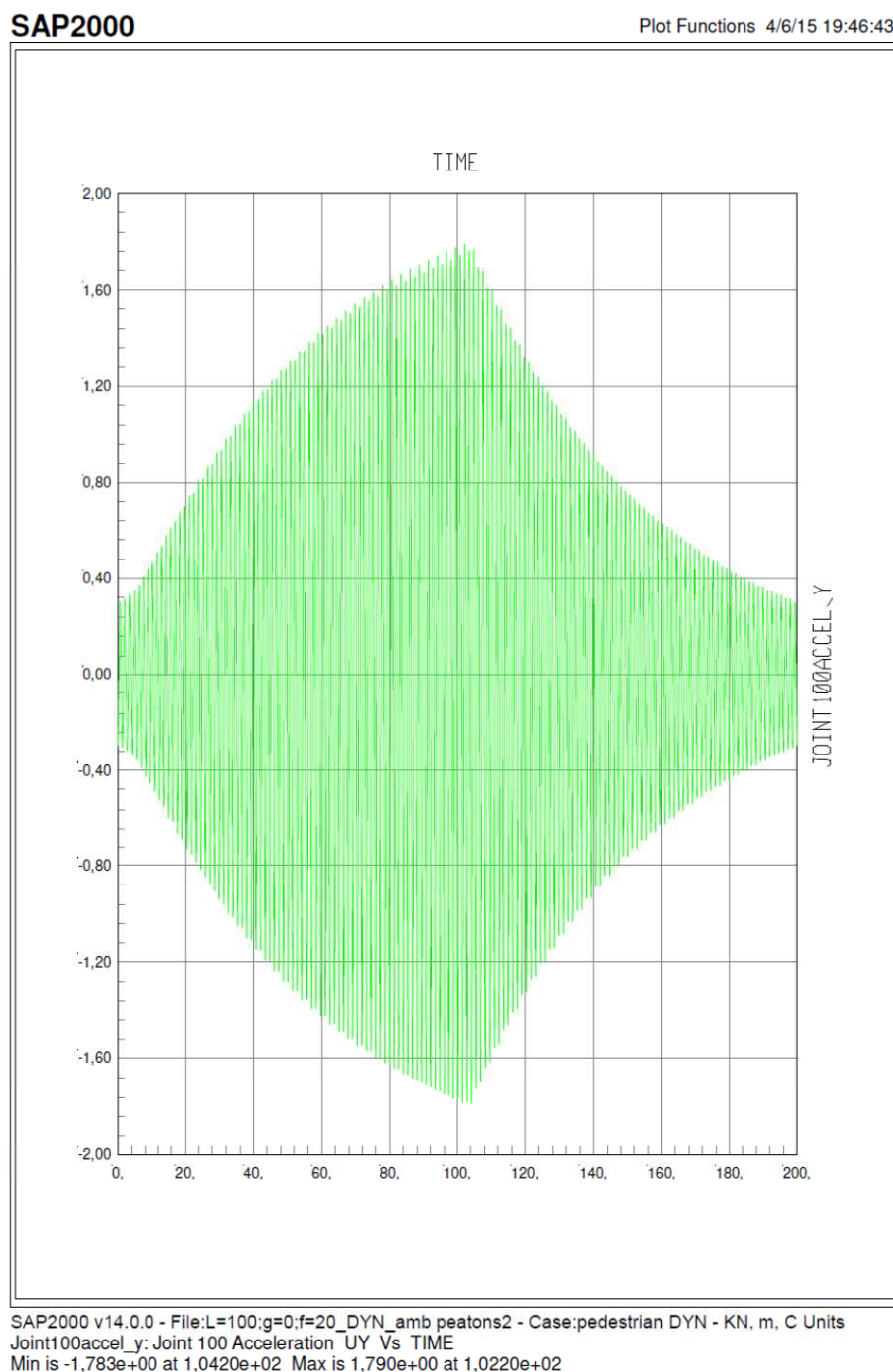
**Figure 5-3: Examples of static point loads defining the pedestrian load in different positions. Each position is associated for an arrival time. They all have the same load value**

## 6. DISCUSSION OF RESULTS

### 6.1 Crowd dynamic load cases according to Sétra Guidelines (2006) results

The evolution of accelerations with time for the different models, as the crowd described by Sétra Guidelines (see section 5.1) crosses the bridge, is shown in figures from *Figure 6-1* to *Figure 6-4*. In all cases and directions it can be observed that:

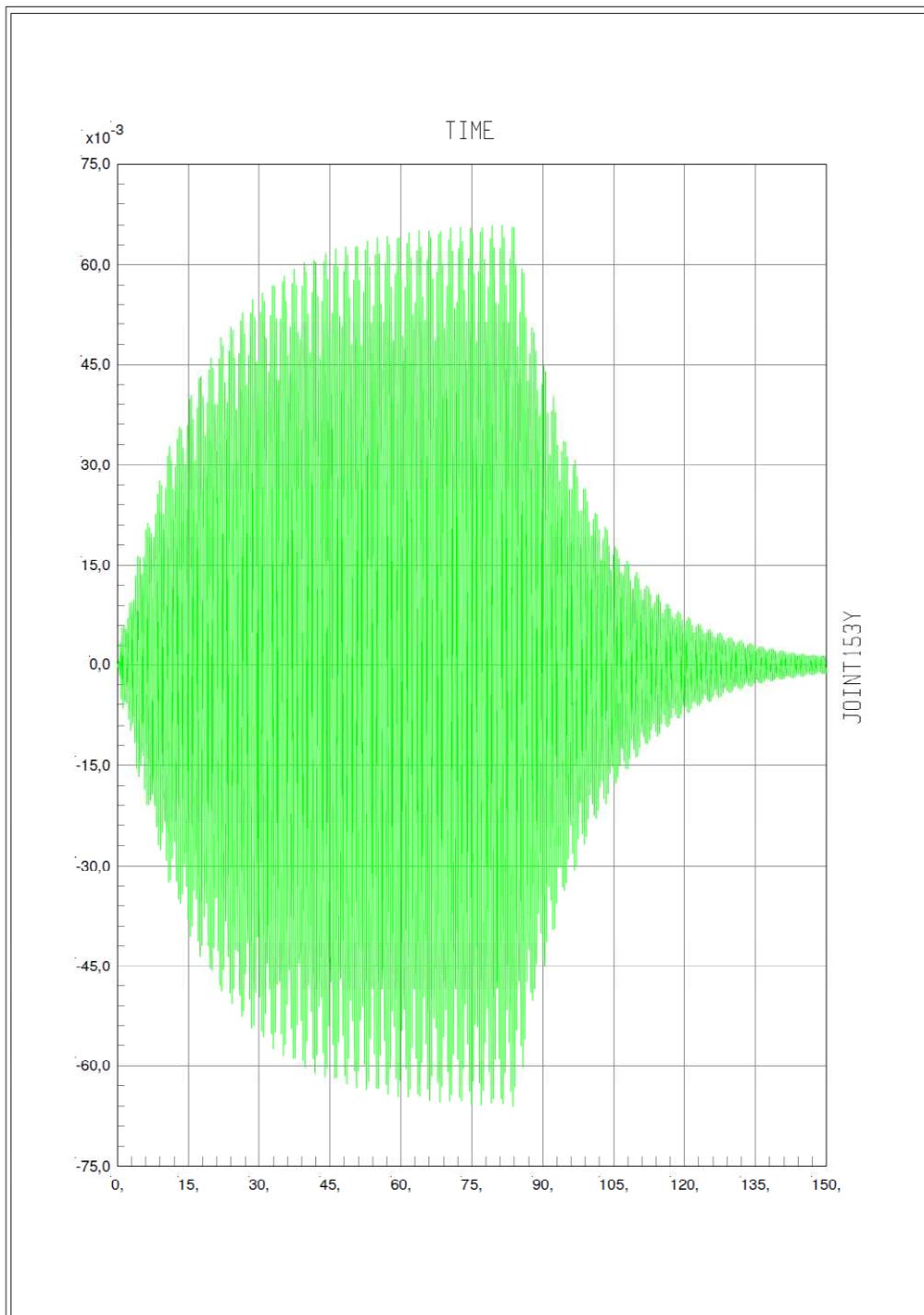
- The accelerations increase as the crowd crosses the bridge.
- When the crowd has already crossed the bridge accelerations decrease due to the damping effect.



**Figure 6-1: Transverse acceleration ( $m/s^2$ , ordinates) versus time at midspan (s, abscissae) for the model with a straight deck ( $g=0$  and Sec1, Table 3-1) under transverse dynamic loading**

SAP2000

Plot Functions 3/30/15 20:20:45

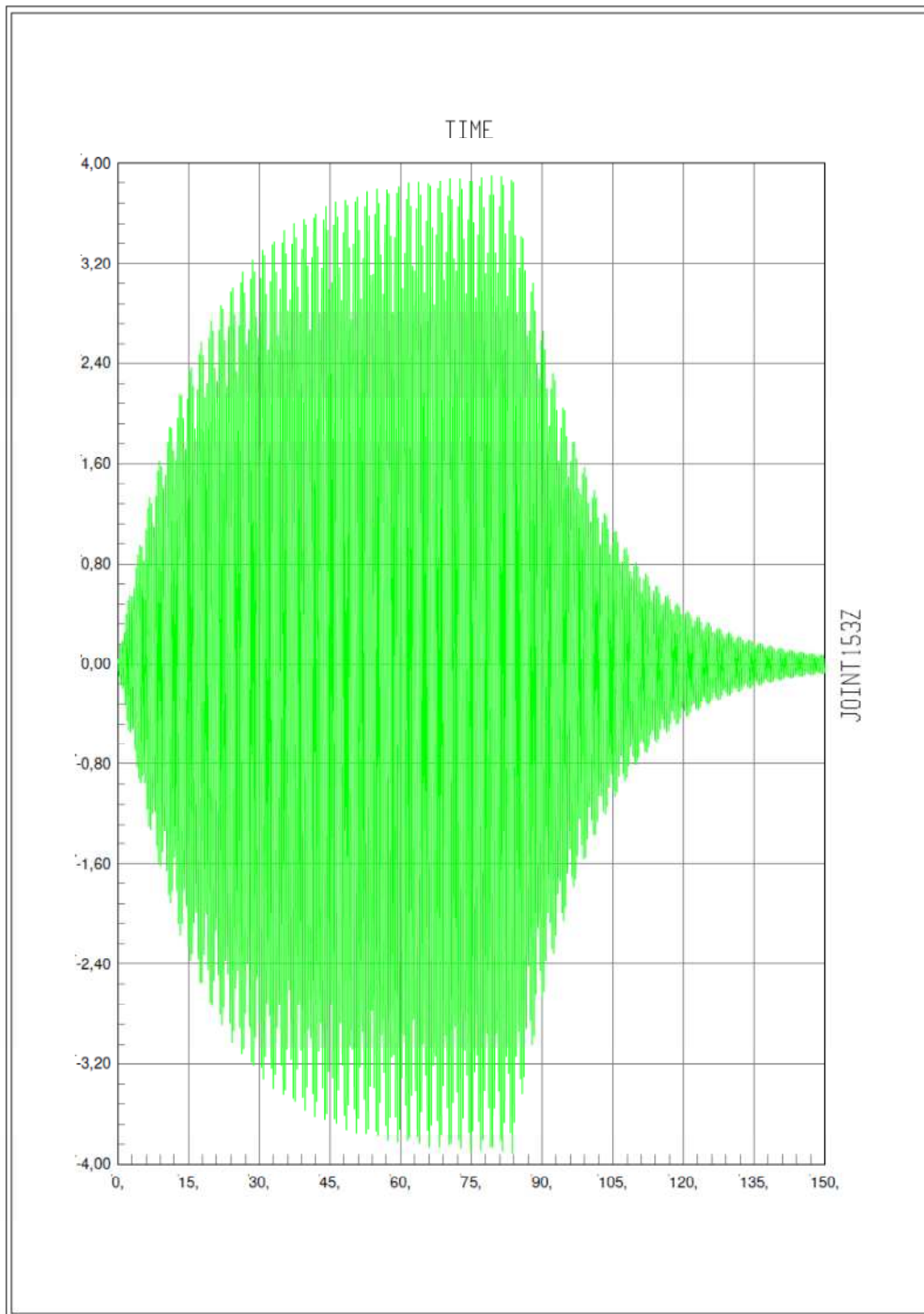


SAP2000 v14.0.0 - File:L=100;g=20;f=20\_ARCO VERT\_TABL CURV\_e=16.67\_v=0\_dyn\_amb peatons2 V14 - Case:Setra  
Joint153y: Joint 153 Acceleration UY Vs TIME  
Min is -6,603e-02 at 8,3700e+01 Max is 6,595e-02 at 8,1400e+01

**Figure 6-2: Transverse acceleration ( $m/s^2$ , ordinates) versus time at  $0,25L$  (s, abscissae) for the model with a straight deck ( $g=20$  and Sec1, Table 3-1) under vertical dynamic loading**

SAP2000

Plot Functions 3/30/15 19:33:21

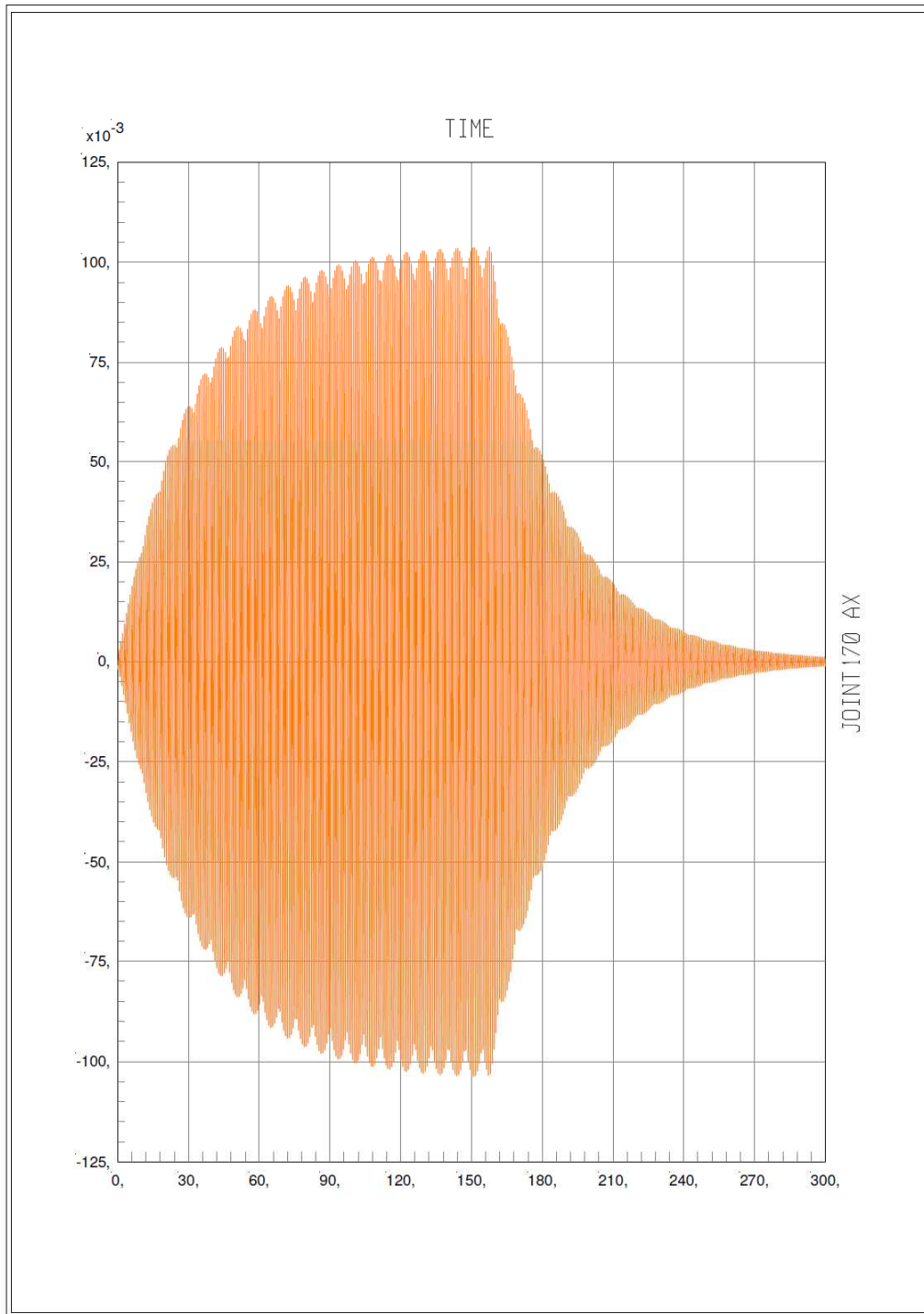


SAP2000 v14.0.0 - File:L=100;g=20;f=20\_ARCO VERT\_TABL CURV\_e=16,67\_v=0\_dyn\_amb peatons2 V14 - Case:Setri  
Joint153z: Joint 153 Acceleration UZ Vs TIME  
Min is -3,907e+00 at 8,3700e+01 Max is 3,900e+00 at 7,9300e+01

Figure 6-3: Vertical acceleration ( $m/s^2$ , ordinates) versus time at  $L/4$  (s, abscissae) for the model with curved deck ( $g=20m$  and Sec1, Table 3-1) under vertical dynamic loading

SAP2000

Plot Functions 4/7/15 0:07:47



SAP2000 v14.0.0 - File:L=100;g=20;f=20\_ARCO VERT\_TABL CURV\_e=16,67\_v=0\_dyn\_amb peatons2 V14 - Case:Setr:  
Joint170 ax: Joint 170 Acceleration UX Vs TIME  
Min is -1,038e-01 at 1,5090e+02 Max is 1,037e-01 at 1,5760e+02

**Figure 6-4: Longitudinal acceleration ( $m/s^2$ , ordinates) versus time at midspan (s, abscissae) for the model with curved deck ( $g=20m$  and Sec1, Table 3-1) under longitudinal dynamic loading**

The maximal acceleration results for the model with a **straight deck** ( $g=0$ , Sec1, see Table 3-1 and Figure 3-1), for the analysed time history function (see section 5.1) are summarised in Table 6-1.

- Dynamic loading in the transverse direction only causes acceleration in the transverse direction.
- The transverse acceleration of  $1,8\text{m/s}^2$ , is above the comfortable and admissible level range (Range 4, Figure 2-2b). A possible solution is to install dampers in order to change the natural frequency of the bridge and assure that lock-in does not happen.

The maximal acceleration results for the model with a **curved deck** ( $g=20\text{m}$ , Sec1, see Table 3-1 and Figure 3-2), for each of the analysed time history functions (see section 5.1) are summarised in Table 6-2.

- Dynamic loading in one direction causes acceleration in all directions.
- The maximal transverse acceleration of  $0,07\text{m/s}^2$ , is within the maximal comfort level range (Range 1, Figure 2-2b) and below the  $0,1\text{m/s}^2$  threshold, so the lock-in effect does not take place.
- The maximal transverse acceleration is caused by the vertical dynamic loading.
- The maximal vertical acceleration of  $3,9\text{m/s}^2$ , is extremely large, well above the  $0,8\text{m/s}^2$  threshold, which defines uncomfortable acceleration levels that are not acceptable (Range 4, Figure 2-2a)
- A possible solution is to install dampers in order to change the natural frequency of the bridge and assure that the vertical acceleration is within the required range of comfort.

	Cosine function with $T=1,349\text{s}$ (transverse loading)
Maximal $a_x$ ( $\text{m/s}^2$ )	0
Maximal $a_y$ ( $\text{m/s}^2$ )	1,8 at midspan
Maximal $a_z$ ( $\text{m/s}^2$ )	0

**Table 6-1: Maximal acceleration results for the model  $g=0$ , Sec1 (see Figure 3-1 and Table 3-1)**

	Cosine function with $T=0,419\text{s}$ (vertical loading)	Cosine function with $T=0,789\text{s}$ (longitudinal loading)
Maximal $a_x$ ( $\text{m/s}^2$ )	0,004 at L/4	0,10 at midspan
Maximal $a_y$ ( $\text{m/s}^2$ )	0,066 at L/4	0,017 at L/4
Maximal $a_z$ ( $\text{m/s}^2$ )	3,9 at L/4	0,043 at L/4

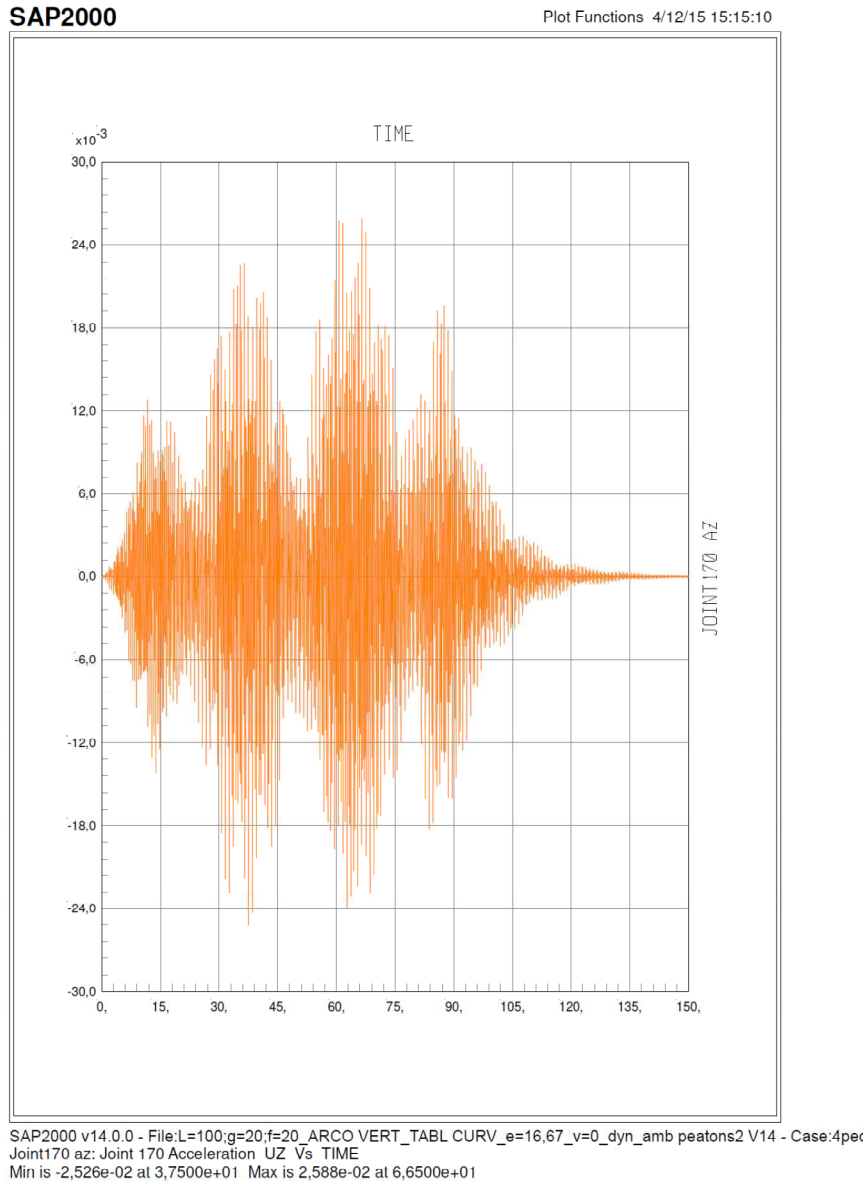
**Table 6-2: Maximal acceleration results for the model  $g=20\text{m}$ , Sec1 (see Figure 3-2 and Table 3-1)**

In relation to SABs spatial behaviour and different modes the statement in EC1 UK NA (“When the vertical deck modes are not well separated, consideration should be given to the use of more sophisticated methods of analysis, in order to determine combined mode responses. In all cases, it is conservative to use the vector sum of the peak accelerations for those modes that need such combination”) should be observed and further defined.

## 6.2 Small pedestrian group and single pedestrian dynamic load results

The results of the vertical acceleration for the analysed SAB under dynamic loads are shown in *Figure 6-5* and *Figure 6-7*. The following conclusions can be drawn:

- The acceleration increases remarkably when the pedestrians reach certain locations.
- These locations are the same for a small pedestrian group of 4 people crossing the group in two rows (*Figure 6-5*) and for a single pedestrian (*Figure 6-7*), ie: they do not depend on the load.
- They are also the same for the pedestrians walking at different speeds, ie: they do not depend on the pedestrian frequency.
- These vertical dynamic load locations, which give relative maximal vertical acceleration values, correspond with the ones shown in **Fehler! Verweisquelle konnte nicht gefunden werden.** and their longitudinally symmetricals, ie: approximately  $L/6$  and  $L/3$ .
- The maximal vertical acceleration for the pedestrian group is  $0,025\text{m/s}^2$
- The maximal vertical acceleration for the single pedestrian is  $0,013\text{m/s}^2$

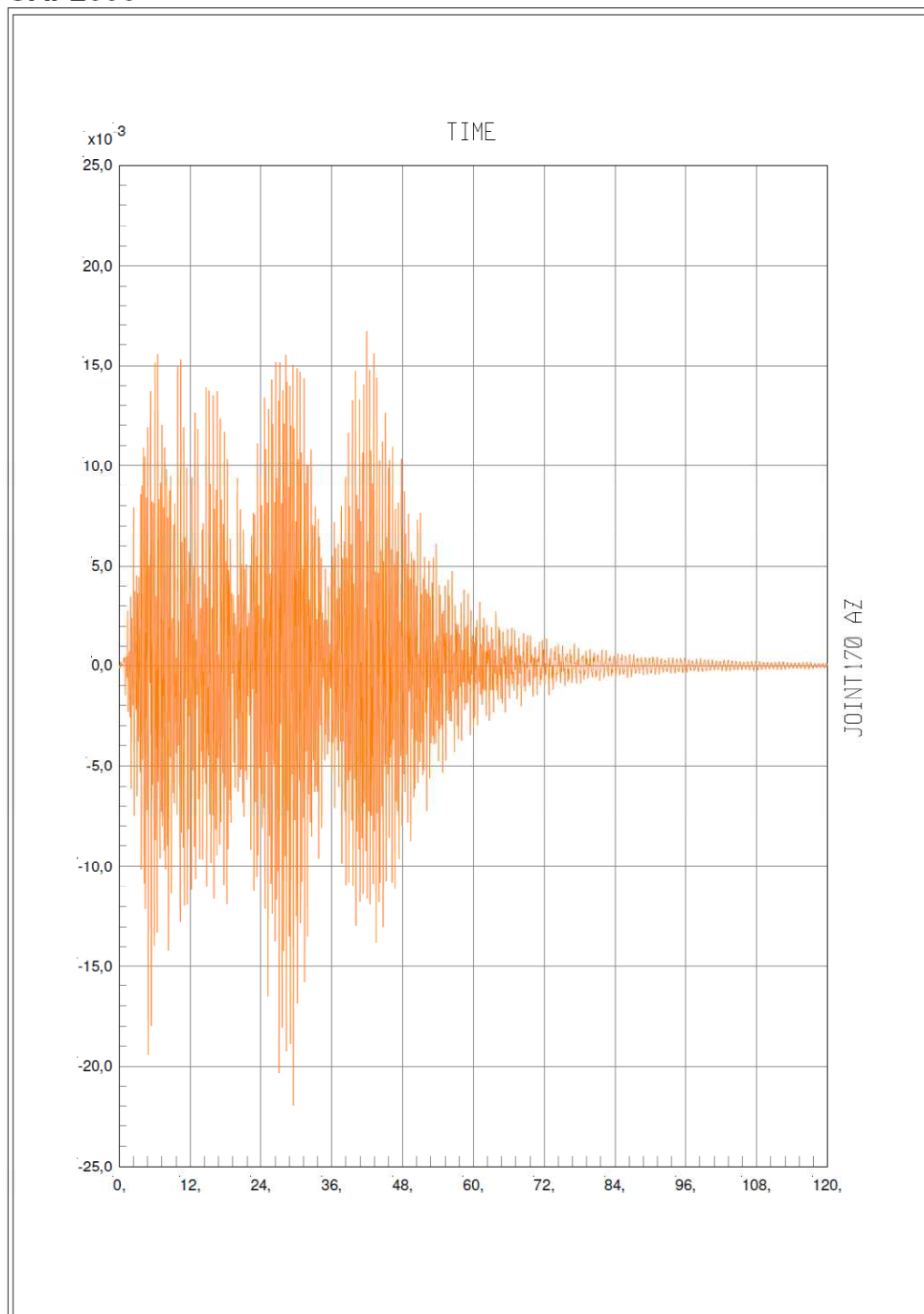


**Figure 6-5: Vertical acceleration ( $m/s^2$ , ordinates) depending on the time (s, abscissae) for a SAB (Figure 3-2) under the dynamic load of a group of 4 pedestrians walking at the natural frequency of the bridge**



SAP2000

Plot Functions 4/18/15 17:56:48

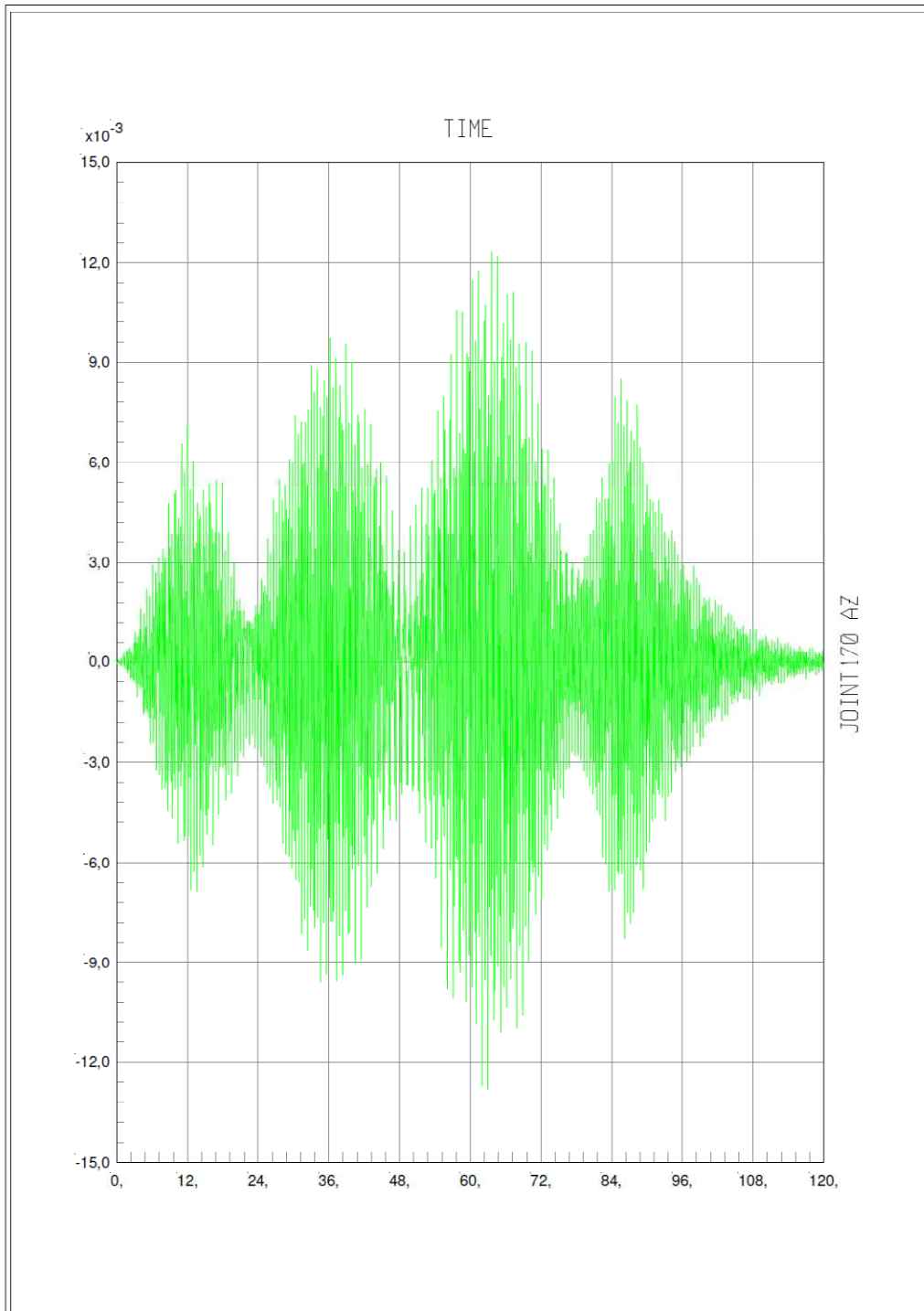


SAP2000 v14.0.0 - File:L=100;g=20;f=20\_ARCO VERT\_TABL CURV\_e=16,67\_v=0\_dyn\_amb peatons2 V14 - Case:4pe  
Joint170 az: Joint 170 Acceleration UZ Vs TIME  
Min is -2,196e-02 at 2,9500e+01 Max is 1,669e-02 at 4,1900e+01

**Figure 6-6: Vertical acceleration ( $m/s^2$ , ordinates) depending on the time (s, abscissae) for a SAB (Figure 3-2) under the dynamic load of a group of 4 pedestrians walking at 1,7m/s**

SAP2000

Plot Functions 4/7/15 0:44:18



SAP2000 v14.0.0 - File:L=100;g=20;f=20\_ARCO VERT\_TABL CURV\_e=16,67\_v=0\_dyn\_amb peatons2 V14 - Case:1pe  
Joint170 az: Joint 170 Acceleration UZ Vs TIME  
Min is -1,282e-02 at 6,3000e+01 Max is 1,231e-02 at 6,3600e+01

**Figure 6-7: Vertical acceleration ( $m/s^2$ , ordinates) depending on the time (s, abscissae) for a SAB (Figure 3-2) under the dynamic load of a single pedestrian walking at the natural frequency of the bridge**

## 7. CONCLUSIONS

The results obtained in the present chapter lead to the following conclusions:

- When comparing the dynamic behaviour of a planar vertical arch with a straight superior deck with an equivalent planar vertical arch with a curved superior deck, the first one shows to be sensitive to transverse accelerations, but not to vertical ones, whereas the SAB is highly sensitive to vertical dynamic loads but not to transverse ones.
- Whereas planar vertical arch bridges with a straight deck mobilise masses only in one direction for each natural mode, SABs mobilise masses in different directions for the same natural mode. Some guidelines (Sétra, 2006) state not to apply dynamic loads in different directions simultaneously. This criteria should be revised for SABs.
- For SABs with a planar vertical arch with a superior curved deck, dynamic loading in one direction causes acceleration in all directions, whereas for planar vertical arch bridges with a superior straight deck, dynamic loading in one direction only causes acceleration in that same direction.
- Existing codes or guidelines do not consider the spatial effects of arch bridges with a curved deck, in which dynamic loading in one direction causes acceleration in all directions.
- The studied planar vertical arch with a straight superior deck presents a too large transverse acceleration, which surpasses the threshold that assures comfort. Mass or viscous dampers must be employed for the studied model.
- Arch bridges with a curved deck reach very high vertical accelerations for the geometry (very large deck curvature,  $f=g$ ) and cross-sections employed in the present research, but undergo low transverse accelerations. Mass or viscous dampers must be employed for the studied model.
- The acceleration increases remarkably when the pedestrians reach certain locations.
- These locations do not depend on the load or on the pedestrian frequency.
- These vertical dynamic load locations, which give relative maximal vertical acceleration values, correspond with the ones shown are approximately  $L/6$  and  $L/3$ .

## 8. FUTURE LINES OF STUDY

- Dynamic loading in existing codes and guidelines should be revised for SABs.
- The high vertical accelerations of SABs, together with the fact that dynamic loading in one direction causes acceleration in all directions in this bridge type, highlight the need of a deep research of the dynamic behaviour of this bridge type.
- In relation to SABs spatial behaviour and different modes the statement in EC1 UK NA (“*When the vertical deck modes are not well separated, consideration should be given to the use of more sophisticated methods of analysis, in order to determine combined mode responses. In all cases, it is conservative to use the vector sum of the peak accelerations for those modes that need such combination*”) should be observed and further defined.

- Torsional vibration occurs with vertical loads. Given that the bridge is already sensitive to vertical or transverse vibrations, it is important to include the torsional dynamics study in a further research.
- Influence of the stiffness of different elements on the dynamic behaviour of different SAB bridge types.
- In the present research it is established which parameters are determinant for an efficient behaviour of SABs with a curved under static loading. Conducting an equivalent parametric study under dynamic loading is recommended.
- Studying possible solutions for diminishing the large vertical accelerations of SABs under dynamic loading of pedestrian crowds is necessary.
- Study for SABs if the locations where the pedestrians cause the largest accelerations are coincident with the load position which causes the largest deformation

## REFERENCES

DALLARD, P. and FITZPATRICK, A. J. “The London Millennium Footbridge”. *The Structural Engineer*, November 2001, v79n22, pp17-33

ESPAÑA. MINISTERIO DE FOMENTO. Dirección general de carreteras. Puentes de carretera. Normas técnicas. *Instrucción sobre las acciones a considerar en el proyecto de puentes de carretera (IAP, 2011)*. Madrid: Ministerio de Fomento. Centro de Publicaciones, 2011 (in Spanish)

Eurocode 1 (EC1): Actions on structures –Part 2: Traffic loads on bridges.

FELDMANN, M., HEINEMEYER, C., BUTZ, C., CAETANO, E., CUNHA, A., GALANTI, F., GOLDACK, A., HECHLER, O., HICKS, S., KEIL, A., LUKIC, M., OBIALA, R., SCHLAICH, M., SEDLACEK G., SMITH, A. and WAARTS, P.. *Design of floor structures for human induced vibrations. Background document in support to the implementation, harmonization and further development of the Eurocodes*. JRC European Commission. 2009

Footbridges-Assessment of vibrational behavior of footbridges under pedestrian loading-Practical Guidelines. Sétra, 2006

MAIRS, D. „York Millenium Bridge- A Footbridge with an Inclined Arch, UK. “Recent Structures”. *Structural Engineering International*. 3/2001, pp172-174

RUIZ-TERAN, A. M. and APARICIO, A. C.. “Verification criteria of the SLS of vibrations for road bridges with slender prestressed concrete decks”. *International FIB Symposium 2009, Concrete: 21st Century Superhero*. London, UK, 2009

STROBL, W., KOVACS, I., ANDRÄ, H. P. and HÄBERLE, U.. „Eine Fußgängerbrücke mit einer Spannweite von 230m“. *Stahlbau*, Berlin, 2007. n76v12. (in German)

UK National Annex to Eurocode 1: Actions on structures –Part 2: Traffic loads on bridges. 2003

# VIII. CONCLUSIONS

## VIII. CONCLUSIONS

## **VIII. CONCLUSIONS**

The present doctoral thesis presents an extensive state-of-the-art of Spatial Arch Bridges (SABs), gives a clear and compact definition of this bridge type as well as a classification. This state-of-the-art makes clear the necessity of developing a research of this bridge type, due to the increasing number of built examples and the scarce number of systematic research studies on the subject.

A very scarce number of published papers deals with the behavior of some examples this bridge type and there are no design criteria recommendations and no studies of their stability or dynamic behavior. However, there are several papers dealing with antifunicularity obtention methodologies for this bridge type.

The present thesis research achieves to extend the present knowledge of SABs, since this thesis:

- Gives a clear definition for this bridge type and classification.
- Explains the structural behavior of SABs of the type of inferior deck arch bridges with imposed curvature (defined in chapter III.A) and SABs with a superior curved deck, especially those supported by a planar vertical arch, for which a thorough parametrical study has been conducted.
- Develops conceptual models and simplified formulations, which help clearly understanding the behavior, before undergoing the linear numerical analysis for which various series of models are analysed.
- Clarifies several aspects of the behavior of SABs, for which an answer was not given on previous research studies.
- Compares the structural behaviour of SABs with a curved deck, with planar, vertical arch bridges with a straight deck, given a bridge span and an arch vertical rise employing the same cross-sections. SABs, in general, present lower axial forces, larger bending moments (both in- and out-of-plane) and torsional bending moments.
- To control the structural behavior and the amount of steel needed for the SABs structures, it is important to control the out-of-plane behavior of this bridge type. Given a plan curvature, this can be achieved by:
  - carefully selecting the key geometrical parameters, namely the vertical rise and the arch/deck eccentricity,
  - keeping the arch cross-section to the strictly necessary dimensions in order to mainly stand in-plane forces, and employing a stiff hanger/struts-deck system.
  - Creative ways to control the out-of-plane behavior, such as employing secondary hangers system lead to interesting solutions.

- To control the structural behavior of SABs with a curved deck under both, vertical loads and temperature variations, it is recommended to restrain displacements in all directions and torsional rotations at the deck abutments and to fix the deck/struts or deck/hangers joints connections.
- Instability of this bridge type has also been studied with buckling and geometrically non-linear analyses. A state-of-the-art of arch bridge instability has been presented and formulation in the codes and research is compared with the numerical results in the studied bridge models.
- The dynamic behavior of an example of SABs has also been checked and demonstrates that SABs present accelerations in all directions under dynamic vertical loads, with far too large vertical acceleration values.
- The research of the aforementioned SAB types leads to design criteria recommendations.
- Following the design criteria recommendations given in this thesis, employing a SAB instead of a traditional planar vertical arch with a straight deck implies a significant but not important steel mass increase. As an order of magnitude, for a 100m bridge span, employing a steel planar vertical arch with a curved superior with a 20m ( $L/5$ ) horizontal sag, increases the total mass of the bridge a 15% when compared with a steel vertical planar bridge with a straight deck of the same span. When employing another geometry but with the same cross-sections main dimensions, the mass could be about 5 times more than for a steel vertical planar bridge with a straight deck of the same span.

All in all, it can be concluded that SABs not only prove to be architecturally interesting, but also present a bearable structural behaviour when employing a geometry that enhances the arch/deck interaction and the correspondent adequate boundary conditions.

The conclusions derived of this document are summarized and grouped for each chapter and at the end a series of design criteria are summarised.

### **Chapter III:**

In this chapter spatial arch bridges have been fully defined and classified, and the variables that define both the geometrical and structural configuration have been presented.

- Under the global concept of “spatial arch bridges” (SABs) we understand both, bridges supported by *arch ribs* and by *shells*.
- *SABs employing arch ribs* are arch bridges in which vertical deck loads produce bending moments and shear forces not contained in the arch plane due to their geometrical and structural configuration. Moreover, the arch itself may not be contained in a plane.
- Their definition can be developed further: “*true spatial arch rib bridges*” are those in which vertical deck loads centred on the deck induce internal forces not contained in the arch plane,



due to their geometrical and structural configuration.

- *Shell arch bridges* have a completely different configuration and structural behaviour. In such bridges the main bearing element is an arch consisting of a shell with double curvature
- A type of *true spatial arch rib bridges* are *Arch Bridges With Imposed Curvature (ABWIC)*. In these SABs, the arches are forced to have the same curvature in plan as the deck. Therefore, the arch and deck centroid lines are contained in the same vertical cylinder. They can have an inferior or superior deck (IDABWIC and SDABWIC). ABWIC can have either planar (inclined arch) or non-planar.
- The spatial arch bridge type has its origins in some of Maillart's bridges built at the beginning of the 19th century, whose rationale was based on functional considerations. Its use has reached its peak in the 1990s and until nowadays, becoming increasingly popular in urban areas as a means of creating city landmarks.

**Chapter IV and corresponding annexes:**

In the context of the study conducted in chapter IV for inferior deck arch bridges with imposed curvature (ID-ABWIC), we can conclude:

- Non-planar arches with imposed curvature can be approximated by inclined planar arches with imposed curvature with the same rise, with an error for internal forces inferior to 1,3% for uniform distributed loading applied on the whole deck span and to 2% for uniform distributed loading applied on half the length of the deck span, in both cases for  $f/g \leq 1$ .
- The minimal total bending moment in the arch, when employing a deck cross-section with large torsional rigidity, is obtained with M3-3 fixed at hanger/deck joints. By fixing M3-3 at hanger/deck joints, when employing a stiff to torsion deck and stiff hangers, the total bending moments can be reduced 6 times the crown of the arch and 9 times at the arch springings, the maximal torsional bending moments, 32 times, whereas the axial force compression increases 6 times in the arch crown and changes from being tensioned at springings to compressions slightly larger as in the arch crown.
- If the hangers most stiff direction is oriented radially to the arch plan curve the behaviour of total bending moments and axial forces improves at springings (83% decrease and 12% increase, respectively).
- There is a value for the out-of-plane arch rigidity for which the distribution of axial forces along the arch changes, tending to concentrate either at mid-span or at springings, and also a bound for which the internal forces and deflections converge. Increasing the balcony beam rigidity above this bound has no advantage at all.
- Given a vertical rise of the arch, and employing pinned hangers, the higher the plan curvature, the lower the axial forces and the higher both, the out-of-plane and in-plane, bending moments in the arch.

## VIII. CONCLUSIONS

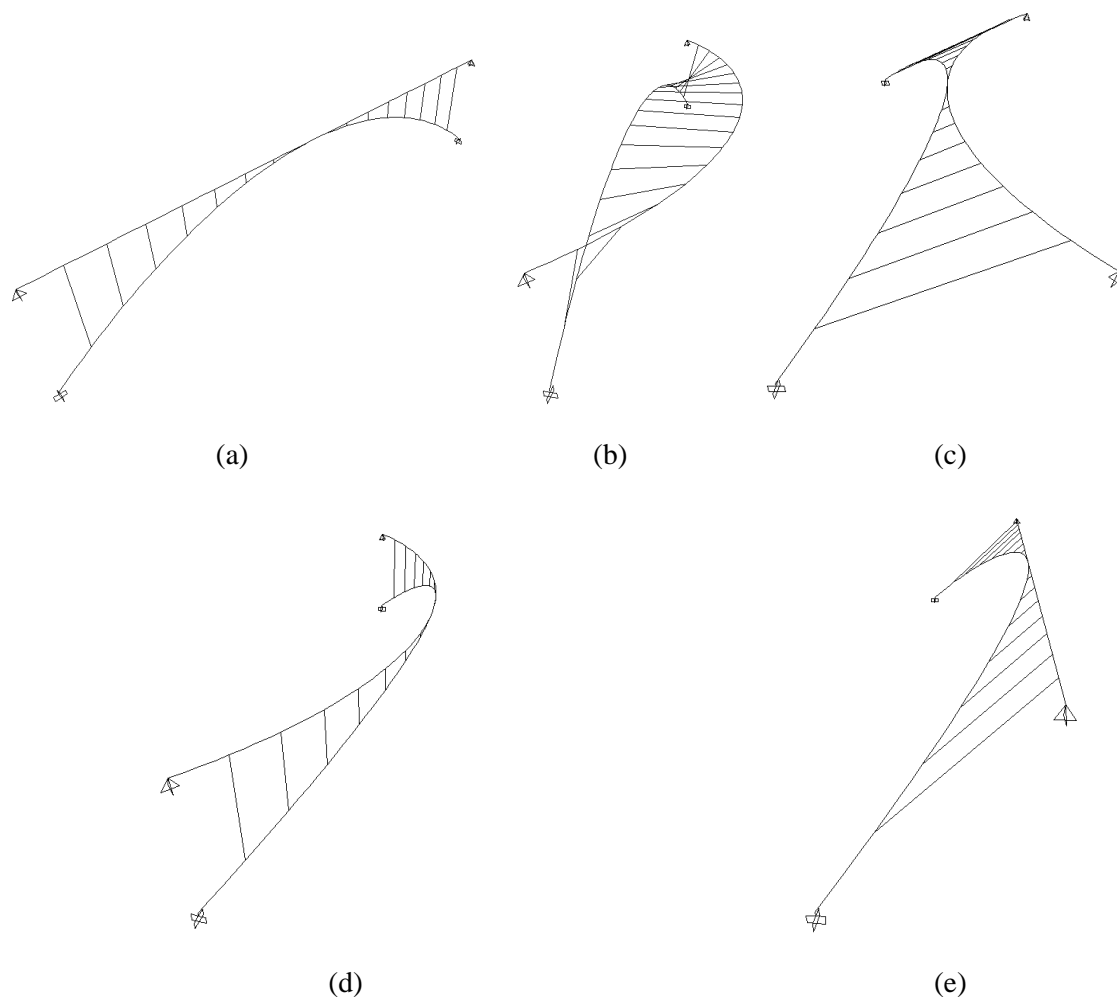
- To enhance the arch behaviour in an ID-ABWIC, employing a rigid hanger-deck system (a deck with high torsional rigidity and hangers with high transverse flexural rigidity) and an arch with low flexural rigidity is more efficient than increasing the rigidity of the arch<sup>1</sup>. This ‘ideal configuration’ is the simplest way to make the arch tend toward its anti-funicular form.
- For ID-ABWIC with a large  $g/f$  ratio, the critical live load case is obtained when the uniform distributed loading is applied on the whole deck span, whereas for a conventional vertical arch bridge ( $g=0$ ) the maximal arch shear forces, bending moments and deflections are higher for a uniform distributed loading applied on half the deck span.
- Employing a compensatory hanger system with an adequate distribution increases the axial forces compressions in the arch (160% in the arch crown and 95% at springings for the studied models), because it increases the in-plane behaviour of the arch, and diminishes the out-of-plane and total bending moments (40% in the arch crown, 65% at  $L/3$  and 22% at springings for the studied models), because it controls the out-of-plane behaviour of the arch.
- These conclusions are valid for a linear behaviour of ID-ABWIC.

---

<sup>1</sup> As a quantitative example: giving the arch cross-section an out-of-plane rigidity equal to the deck vertical rigidity-ie 20 larger as the arch in-plane rigidity-, the out-of-plane bending moments of the arch are multiplied by 10 and the in-plane bending moments are doubled in comparison with an arch with the same in-plane and out-of-plane rigidity 20 times lower than that of the deck

**Chapter V. A:**

From the analyses of the results of the studied cases of SABs with a superior deck (Figure 1), the following conclusions can be inferred:



**Figure 1: Studied bridge geometries.** (a) Vertical planar arch bridge with superior straight deck (reference model); (b) Vertical planar arch with superior curved deck; (c) Arch and deck with symmetrical curvature in plan; (d) Arch and deck with coincident curvature in plan (imposed curvature); (e) Arch curved in plan with superior straight deck (both contained in the same plane)

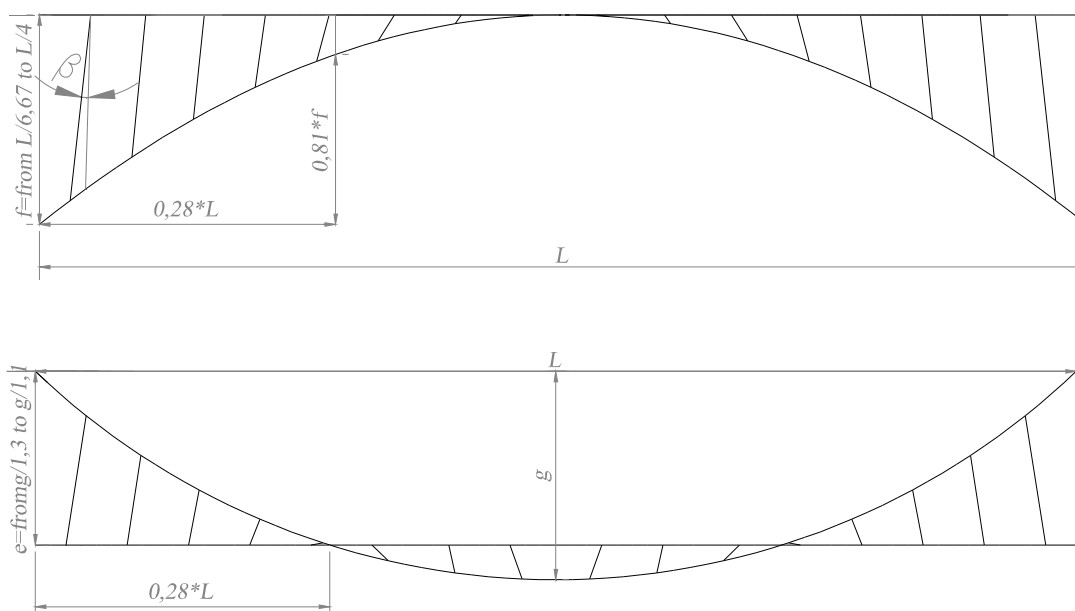
- The highest total ( $M = \sqrt{M_{22}^2 + M_{33}^2}$ ) and out of plane (M2-2) bending moments in L/4 of the arch and in the arch springings under a vertical uniform loading are obtained for model (b). M3-3 bending moments are very high too (about fifty times larger than for model (a) in the deck and a hundred times in the arch).
- The highest total and out of plane bending moments in the mid-span of the arch under a vertical uniform loading are obtained for model (e).
- Models (c) and (d) show the best structural behavior if the longitudinal displacements of the deck abutments are restrained.

## VIII. CONCLUSIONS

- Spatial arch bridges have an improved structural behaviour under temperature increments with respect to conventional vertical arch bridges (model (a)) when restraining the longitudinal displacements of the deck abutments. Axial forces in the deck decrease, *e.g.*: for model (c) with r.l.d. the axial forces in the deck are nearly a hundred times smaller than those for model (a). In exchange, significant M2-2 bending moments appear in the deck, but they are resisted by the deck's width, which is its highest dimension.
- For models with a curved deck (models (b), (c) and (d)), it is convenient to restrain longitudinal displacements of the deck abutments under both vertical and temperature increments. This is a very important difference with conventional vertical arch bridges.
- For models with a straight deck (models (a) and (d)) it is obviously better to release longitudinal displacements of the deck abutments under temperature increments.
- In general, the restriction of the twisting rotations at the support sections on the abutments does not have a significant impact on the structural response

### Chapter V. B:

- The most efficient model for spatial arch bridges with a curved superior deck sustained by a planar vertical arch is displayed in Figure 2.
  - The angle  $\beta$  for the strut distribution is measured taking as reference the model obtained from equal divisions of arch and deck.



**Figure 2: Most efficient model for spatial arch bridges with a curved superior deck**

***Parameter conclusions***

$e$  and  $\beta$  (Figure 3) are key parameters for spatial arch bridges with a curved superior deck sustained by a planar vertical arch.

Regarding  $e$  (the arch/deck eccentricity in plan view, Figure 3):

Whatever the deck curvature, the value of  $f$  (Figure 3), the stiffness of the strut-deck system or that of the arch:

- Results for all the different indicators are low enough in the range of  $g/1,3 \leq e \leq g/1,1$ , approximately in the range in which there is the same number of hangers at each side of the arch.
- Given a  $g$  value, in the range  $g/1,36 \leq e \leq g/1,2$  the internal forces in the whole bridge are reasonable.
- The value  $e=g/1,2=0,83g$  is the most efficient value for the arch/eccentricity in plan view according to all of the studied efficiency indicators. For this value internal torsional moments in the arch and the deck under a uniform deck load are minimal and the maximal in-plane and maximal out-of-plane displacements acquire the same value
- $e=g/1,2=0,83g$  is at a distance of approximately  $0,28L$  of length and at  $0,81*f$  of height of the springings of the arch (Figure 2), whatever the  $g$  value. It is a key point to control the arch behaviour, since at this point controlling the out-of-plane behaviour is most critical. Therefore, it is the most efficient  $e$  value because it obtains the stiffest struts at this key point.
- For high  $g$  values, ie: when spatial behaviour increases, the influence of  $e$  is larger.
- The higher the  $f$  value, the higher the importance of choosing an adequate  $e$  value.
- Regarding the stresses in the arch, the influence of employing a stiff strut-deck system is lower for values of  $e$  between  $g/1,30$  and  $g/1,20$ .
- Given a  $g$  and  $f$  values, choosing the adequate  $e$  value can mean a decrease of between 242 and 307% of the sum of stresses in the bridge, depending on the cross-sections employed.
- Given a  $g$  and bridge cross-sections, choosing the adequate  $e$  value can mean a decrease of between 216 and 652% of the sum of stresses in the bridge, depending on the  $f$  values employed.

Regarding  $v$  (the vertical distance between the arch crown and the deck mid-span, Figure 3):

- Depending on the stiffness of the strut-deck system it might be worth or not adjusting the value of  $e$ .
- $v=0$  is the most convenient value, since it stiffens the struts at key points  $e=g/1,2$ .
- Increasing the verticality of the struts by increasing the vertical distance between the arch crown and the deck mid-span ( $v$ ), decreases the efficiency of the system, since it increase the length of the struts and thus decreases their stiffness.
- For an efficient  $e$  value,  $v$  has a significant influence in the internal forces, stresses and mass of the bridge. However, most important is to control  $e$ .

## VIII. CONCLUSIONS

- Given a  $g$  and bridge cross-sections, and given adequate  $e$  and  $f$  values choosing the adequate  $v$  value can mean a decrease of 12% of the sum of stresses in the bridge.

### Regarding $f$ (the rise of the arch, Figure 3):

- Whatever the value of  $g$ , values of  $f$  between  $L/6,67-L/4$  give a negligible difference of the total mass of the bridge, so they can be considered with an equivalent efficiency.
- Employing a vertical rise  $f > L/4$  for the arch is not recommendable.
- The range of adequate values of  $f$  for SABs is smaller than for  $g=0$ .
- For  $g=0$ , choosing the adequate  $f$  value can mean a decrease of 8,7% in the total mass of the bridge. If  $g=20\text{m}$  is employed together with adequate  $e$  and  $v$  values, a similar influence is obtained: 9,1% variation in the total mass of the bridge.

### Regarding $\beta$ (the inclination of the struts in longitudinal view):

- It is convenient to employ a convergent distribution of struts (ie: a distribution of struts in which each strut axis elongation converges above the deck with its symmetrical), in order to reduce the total material employed for the bridge, in spite of being the longest ones. Controlling key points proves to be more efficient than verticality or stiffness small variations.
- A small  $\beta$  variation leads to an important mass variation (39% given  $g$  and adequate  $e$ ,  $v$  and  $f$  values). Therefore,  $\beta$  is a key parameter for the efficiency of SABWCSD.

### Regarding $z$ (deck height, Figure 3):

- From a structural point of view, it is convenient to employ an intermediate deck crossing the arch at  $0,28L$  of its abutments (in plan view, ie coincident  $0,81f$  height), if the ground is strong enough to bear horizontal loads. If this intermediate deck position cannot be obtained and there are no ground limitations, employing a superior deck is more efficient than an inferior one.
- Employing a middle deck improves the in-plane behaviour of the arch, but not the out-of-plane behaviour, causing a displacement increase at span center. This behaviour has been studied with a linear analysis, but a geometrically non-linear parametrical analysis (GNLPA) has not been conducted. The described conclusions should be verified with a GNLPA due to the described large displacements of the model which has shows a stress reduction.
- Given a  $g$  and bridge cross-sections, and given adequate  $e$ ,  $v$  and  $f$  values choosing the adequate  $z$  value can mean a decrease of 35% of the sum of stresses in the bridge.

### Regarding $g_A$ (curvature of the arch in plan measured by its sag):

- If employing an efficient value of  $e$ , it is convenient to employ a planar vertical arch ( $g_A=0$ ) instead to a curved in plan arch in order to reduce the total stresses in the bridge.

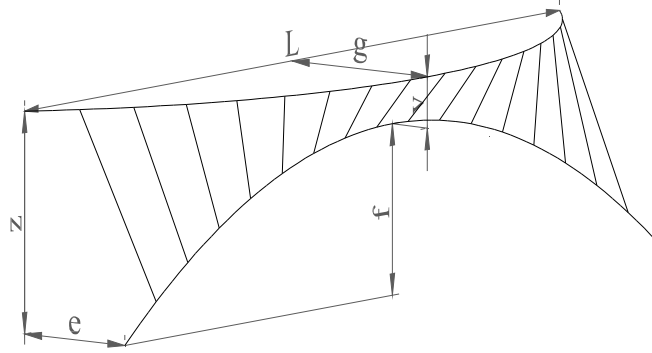


Figure 3: Nomenclature of variables

### *Efficiency criteria conclusions*

Regarding the different comparison criteria which have been studied in order to decide the most efficient value of the different parameters:

- It has been demonstrated that, for spatial arch bridges with a curved superior deck, given a certain stiffness of the bridge elements, comparing the maximal displacements of the arch under permanent loads is always equivalent to comparing the total mass of the bridge. Therefore, reducing the maximal displacement of the arch is equivalent to reducing the total mass of the bridge.
- It is remarkable that for efficient parameters for SABs with a planar vertical arch with a superior curved deck, the out-of-plane maximal arch displacements have a similar value to in-plane maximal arch displacements. This is a simple and representative enough criterion for easily evaluating the efficiency of a model without doing a parametrical study.
- Given an  $f$  and cross-section values of the bridge, reducing the total bending moments of the arch, ie: tending to its antifunicular under permanent loads, is also a valid criterion to reduce the total mass of the bridge.
- When studying the stiffness of the system, the total mass of the bridge must be compared.
- It must be noted that the mass of the bridge can be a misleading criteria in order to choose the most efficient parameters if it is not correctly employed. Two different procedures can be defined to employ this criterion correctly:
  - the cross-sections of the different elements should be carefully chosen in order to minimise the mass of each specific studied model. Only then can the masses be compared, regardless of employing or not the same diameters for the different elements.
  - Fix the diameter (for CHS) or width and depth (for box girders) under an aesthetical criterion and only vary the plate thickness when dimensioning the cross-sections.

In order to obtain the most efficient parameter value, a linear analysis is enough in all the studied cases, except for the  $z$  parameter, where inferior, intermediate and superior deck SABs were compared. For this case study a further geometrically non-linear analysis should be conducted.

### ***Critical loading combinations conclusions***

Regarding the critical loading combinations it has been proved for the different parameters that, in comparison with a planar vertical arch with a straight deck, asymmetrical loading in half the deck loses importance for SABs with a superior curved deck.

The higher the importance of the out-of-plane behavior of the arch, the lower the influence of an asymmetrical uniform live loading on half the deck span.

The worst loading combination in ULS for the most efficient model described in Figure 2 is A1 (see definition in the bookmark) except at springings and approximately around  $L_A/3$ , where the worst loading case is A2 (see the bookmark).

### **Chapter VI. A:**

- The hanger/strut and deck system can have a stabilizing or destabilizing effect on the arch buckling
- Codes and research give buckling formulation but the hypothesis under which these formulae are valid are not clearly stated and not all cases for arch bridges are included.
- There are no equivalent European buckling curves for arch bridges. According to several researches, the coded buckling curves in Eurocode 3 Part 1.1 chapter 6.3.1.2 are conservative for arches.
- The values of the imperfections and geometry for arch bridges in order to conduct a geometrically non-linear analyses can be obtained in two different ways according to Eurocode 3 (EC3): as complex structures with the geometry based on the buckling shape (EC3 Part 1.1 chapter 5.3.2) or specifically for arches (EC3 Annex D.3.5). The latter separates in- and out-of-plane imperfections.
  - Buckling curves in EC3 Part 1.1 chapter 6.3.1.2 are conservative for arches (Backer et al, 2009)
  - coded imperfections in EC3 Part 1.1 chapter 5.3.2 are conservative for a straight beam with respect to the buckling curves of EC3 Part 1.1 chapter 6.3.1.2 according to the benchmark developed in the present study.
  - Therefore, ***EC3 Part 1.1 chapter 5.3.2 calculation method can be safely used for arch bridges.***
- There are hardly no published construction imperfection measures as far as the authors know.



## VIII. CONCLUSIONS

- When imperfections measured in the construction site are compared to those stated by the codes for the design analyses, the difference should correspond to residual stresses. However the value is very large, coded imperfections might be far too much on side of security. Empirical studies should be conducted.

### **Chapter VI. B:**

- SABs with a curved deck buckle in- and out-of-plane at the same time, even if a planar vertical arch is employed. This is so because, for a vertical loading, the deck undergoes horizontal and vertical displacements due to spatial the geometry of SABs.
- Critical buckling loads for a uniform distributed load on the whole deck length ( $lu$ ) are lower than for a uniformly distributed loading on half the deck length ( $la$ ) as expected, since  $lu$  causes larger axial forces in the arch than  $la$ .
- Geometries which give lower critical buckling loads usually coincide with geometries which bear larger axial forces in the arch. However,  $f$  values approximately in the range  $L/6 \leq f \leq L/4$  buckle for a larger load than  $f > L/4$ , in spite of undergoing larger axial forces.
- For large  $f$  values the arch buckles nearly independently of the deck because the struts are longer and thus less stiff.
- For low  $f$  values the arch and deck buckle together because arch and deck tend to work as a truss.
- For planar vertical arches with a superior straight deck, restraining torsional rotations improves the buckling behaviour, since it diminishes the destabilizing effect of the deck.
- SABs with a planar vertical arch and a superior curved deck buckle in both planes of the arch symmetrically except for low  $f$  values:
- The larger the  $f$  value, the larger the out-of-plane component.
- The buckling shapes are equivalent whatever the value of the cross-sections employed and of the bearing conditions.
- The geometry that best resists buckling is employing convergent struts (ie: each strut axis elongation converges above the deck with its symmetrical), since for this geometry the arch bears the lowest axial forces and stresses. As expected, this is coincident with the most efficient model for spatial arch bridges with a curved superior deck sustained by a planar vertical arch regarding the minimum mass criteria employing design cross-sections as concluded in chapter V. B chapter.
- However, when employing the design cross-sections to analyse the buckling, not only the geometry has influence, but also the stiffness distribution in the bridge. Since models employing vertical struts need stiffer struts, employing vertical struts happens to be more favourable for avoiding buckling.

## VIII. CONCLUSIONS

- Employing a stiffer deck or struts improves the buckling behaviour of the arch, since the deck has a stabilizing effect. This is more efficient than increasing the arch stiffness.
- Not only need formulae for SABs be developed, but also an improvement of the existing formulae for planar arch bridges with a straight deck is required, since the existing formulae are very conservative.
- If the total load on the bridge is calculated for the buckling coefficient  $\alpha$  under the load case  $(1,35 \cdot (w+pl) + \alpha \cdot lu)$  and  $\alpha 1$  ( $\alpha 1 \cdot [1,35 \cdot (w+pl) + 1,5 \cdot lu]$ ) very similar values are obtained, but the error of employing  $\alpha 1$  instead of  $\alpha$  is non-negligible (approximately 6%). Strictly correct method and most realistic would be to calculate  $\alpha$ , employing  $\alpha 1$  gives insecure (larger) buckling load values.

### Chapter VI. C:

- NLG effects have a high influence on the behavior of SABs with a superior curved deck. A NLGA must be conducted for this bridge type, since the design obtained with LA can give values which will not resist ULS when considering GNL effects and elastic material failure.
- For SABs, results obtained with a LA are nearer to the NLGA than for planar arch bridges with a superior straight deck. This is so because important bending moments are already obtained for SABs with LA due to their geometry and structural behavior.
- The influence of NLG effects is lower when employing  $f$  values  $L/5=20\text{m}$  (recommended in chapter V.B) than for arches with larger rise values.
- The value of imperfections has a lower influence for arches with large rise values than when employing  $f$  values recommended in chapter V.B.

These conclusions are quantified in Table 1 and \*For bending moments:  $\frac{M_{NLGA} - M_{LA}}{M_{LA}} \cdot 100$ , similar for other internal forces or stresses

**Table 2**, which summarise some results obtained in this thesis research study. The % influence refers to the ultimate live load variation due to considering geometrical non-linearities (with or without imperfections) with respect to a linear analysis.

g (m)	0	20	20
f(m)	20	20	50
% influence of geometrical non-linearities without imperfections	6,04	17,32	37,05
% influence of geometrical non-linearities with EC3 complex structures imperfections	6,04	19,48	47,77
% influence of geometrical non-linearities with EC3 arch bridges imperfections	31,68	37,66	28,13

**Table 1: Influence of geometrical non-linearities and imperfections for models with different g and f values for a 100m span, e=g/1,2 (see Figure 3) and employing design cross-sections**

Arch internal force/ Stress	Out-of-plane bending moments	In-plane bending moments	Torsional moments	Axial forces	Stresses
Maximal variation due to to geometrically non-linear effects without imperfections* and place of the arch where it takes place	40% at L/8	40% at L/8	30% at arch springings	-1% at arch springings and crown	37% at L/8

\*For bending moments:  $\frac{M_{NGLA} - M_{LA}}{M_{LA}} \cdot 100$ , similar for other internal forces or stresses

**Table 2: Influence of geometrical non-linearities on the arch internal forces and stresses of a SAB with superior curved deck and L=100m, g=20m, f=20m, g=e/1,2 and employing reference cross-sections****Chapter VII:**

- When comparing the dynamic behaviour of a planar vertical arch with a straight superior deck with an equivalent planar vertical arch with a curved superior deck, the first one shows to be sensitive to transverse accelerations, but not to vertical ones, whereas the SAB is highly sensitive to vertical dynamic loads but not to transverse ones. Under a transverse crowd loading according to Sétra Guidelines a planar vertical arch with a superior straight deck of 100m span and a 20m rise suffers  $1,8\text{m/s}^2$  transverse accelerations, whereas a SAB with a superior curved deck and a planar vertical arch with the same rise and span and  $e=16,67\text{m}$  undergoes  $0,066\text{m/s}^2$  transverse accelerations but  $3,9\text{m/s}^2$  vertical accelerations.
- Whereas planar vertical arch bridges with a straight deck mobilise masses only in one direction for each natural mode, SABs mobilise masses in different directions for the same natural mode. Some guidelines (Sétra, 2006) state not to apply dynamic loads in different directions simultaneously. This criteria should be revised for SABs.
- For SABs with a planar vertical arch with a superior curved deck, dynamic loading in one direction causes acceleration in all directions, whereas for planar vertical arch bridges with a superior straight deck, dynamic loading in one direction only causes acceleration in that same direction.
- Existing codes or guidelines do not consider the spatial effects of arch bridges with a curved deck, in which dynamic loading in one direction causes acceleration in all directions.
- The studied planar vertical arch with a straight superior deck presents a too large transverse acceleration ( $1,8\text{m/s}^2$ ) under transverse dynamic loading, which surpasses the threshold that assures comfort. Mass or viscous dampers must be employed for the studied model.
- Arch bridges with a curved deck under vertical dynamic loading reach very high vertical accelerations ( $3,9\text{m/s}^2$ ) for the geometry (very large deck curvature,  $f=g$ ) and cross-sections employed in the present research, but undergo low transverse accelerations within the maximal comfort range ( $0,066\text{m/s}^2$ ). Mass or viscous dampers must be employed for the studied model.

## VIII. CONCLUSIONS

- The acceleration increases remarkably when the pedestrians reach certain locations.
- These locations do not depend on the load or on the pedestrian frequency.
- These vertical dynamic load locations, which give relative maximal vertical acceleration values, correspond with the ones shown are approximately  $L/6$  and  $L/3$ .

**IX. DESIGN CRITERIA  
RECOMMENDATIONS**



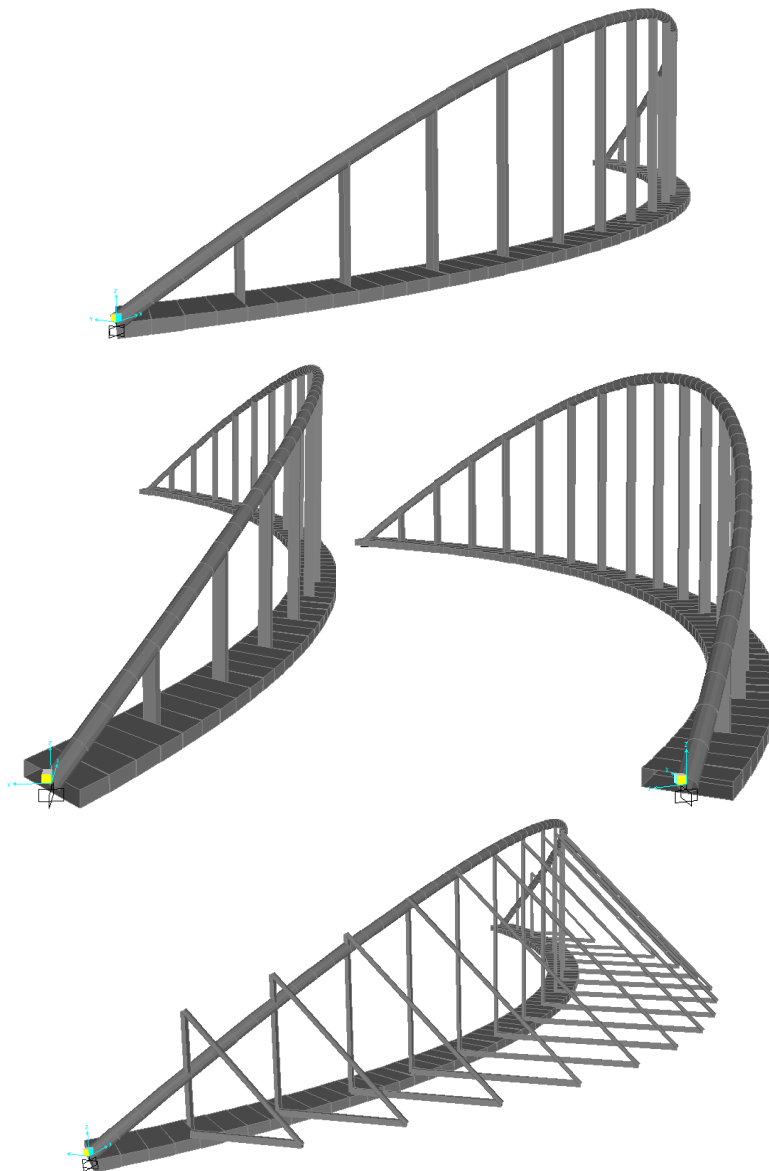
## **IX. DESIGN CRITERIA RECOMMENDATIONS.**

### **Inferior deck arch bridges with imposed curvature:**

For this bridge type the main conclusions for an efficient design are the following:

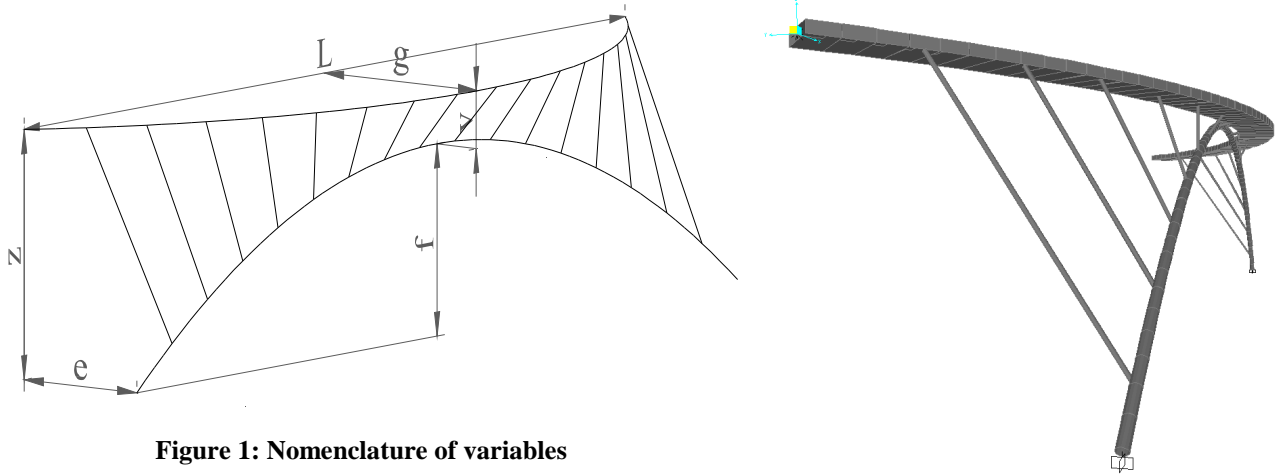
- Stiff hanger-deck system:
  - deck cross-section with a high torsional and flexural rigidity
  - hangers cross-sections with a high flexural rigidity in the radial direction of the deck curvature. Employing a secondary hanger system is an interesting solution to supply stiffness in this direction.
- Slender arch, with low flexural rigidity
- It is important to keep the dynamic behavior of this bridge type under control when employed as a footbridge, since they can reach large vertical accelerations. The use of tuned mass dampers is probably necessary.

In the following figures the aforementioned recommendations can be appreciated:



**Spatial arch bridges with a planar vertical arch and a curved superior deck:**

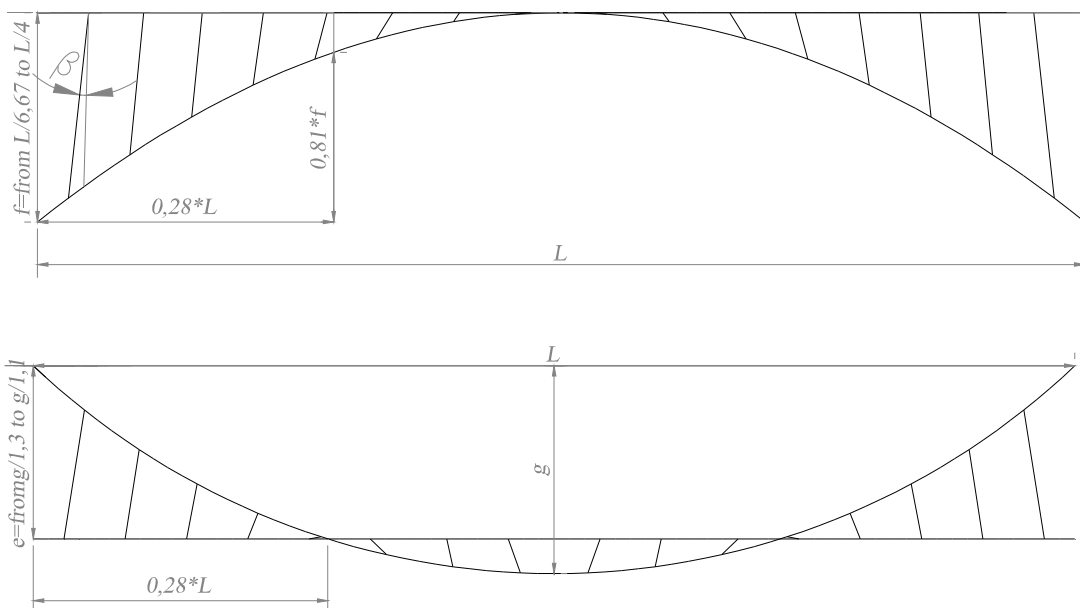
Given a deck with a span  $L$  and a horizontal sag  $g$  supported by a planar vertical arch, it is recommendable to employ the following values for the parameters in **Fehler! Verweisquelle konnte nicht gefunden werden.:**



**Figure 1: Nomenclature of variables**

- $e=g/1,2=0,83g$  is the most efficient value for the arch/eccentricity
- $v=0$
- $L/6,67 \leq f \leq L/4$
- It is convenient to employ a convergent distribution of struts (ie: a distribution of struts in which each strut axis elongation converges above the deck with its symmetrical)
- Torsional rotations and displacements restrained at deck abutments.
- Fixed arch springings.
- Struts fixed to arch and deck

It is important to keep the dynamic behavior of this bridge type under control when employed as a footbridge, since they can reach large vertical accelerations. The use of tuned mass dampers is probably necessary.





## **X. FUTURE LINES OF STUDY**

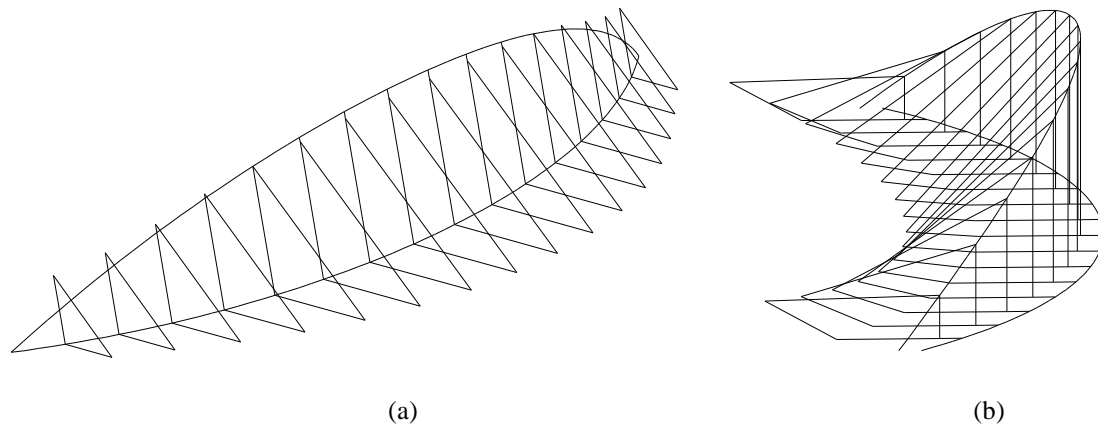
## X. FUTURE LINES OF STUDY

## **IX. FUTURE LINES OF STUDY**

In the following lines we recommend a series of lines of study to extend the research study conducted in this thesis about Spatial Arch Bridges (SABs).

Regarding Inferior Deck Arch Bridges With Imposed Curvature:

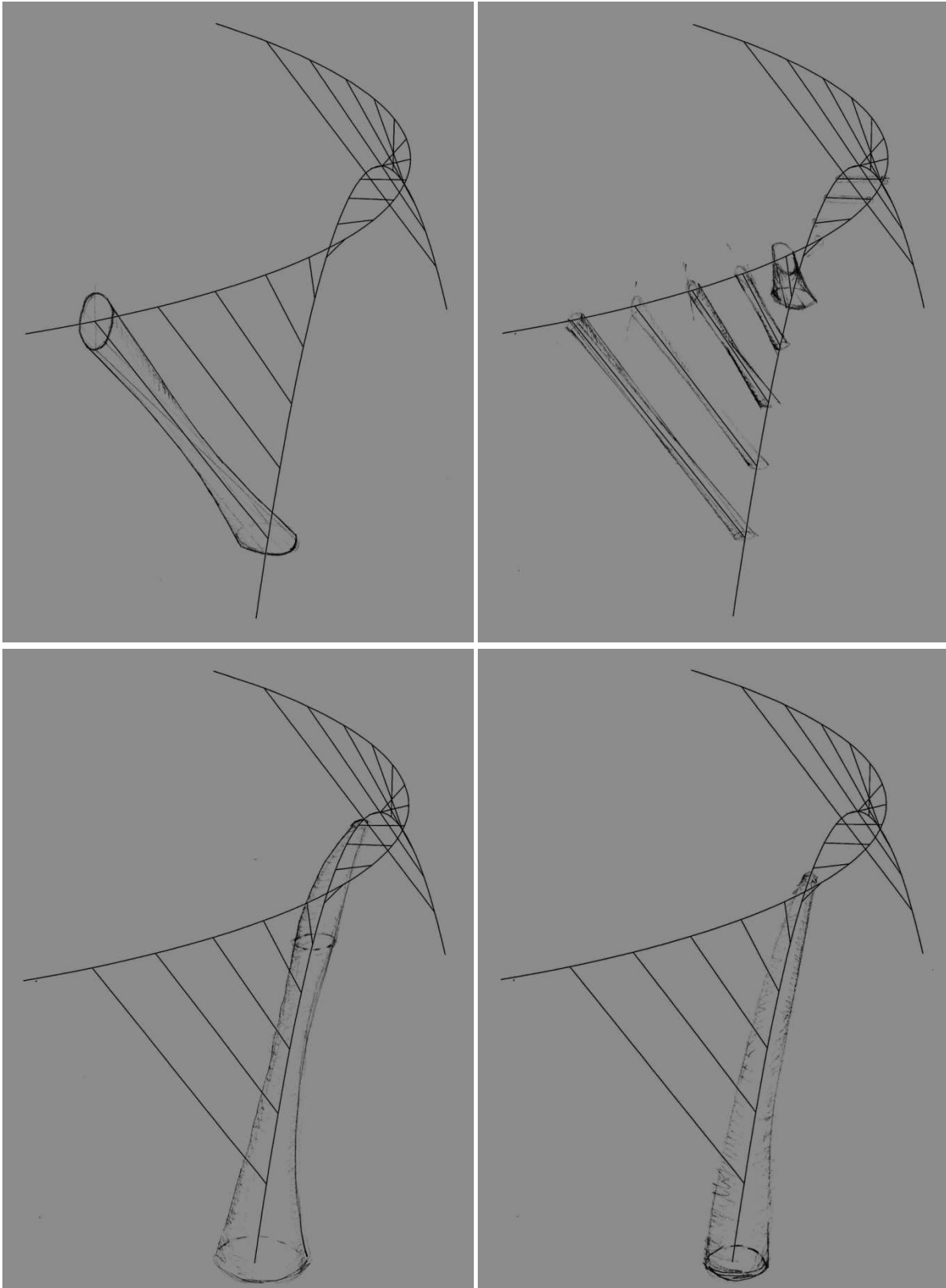
- In a future research the Inferior Deck Arch Bridges With Imposed Curvature (ID-ABWIC) study could be widened for more cross-sections, employing real cross-section values to quantify the improvement of increasing the stiffness.
- A parametrical relationship of the horizontal sag and the torsional and flexural stiffness of arch, hangers and deck could be found.
- The study of second hanger systems could be broadened. A comparison between model (a) (Figure 1) studied in chapter IV and the bridge over the Galindo river (Figure 1b) employing the same cross-section values would be interesting.



**Figure 1: Frame models for IDABWIC employing a secondary hanger system. (a) Model purposed in chapter IV. (b) Galindo bridge**

Regarding SABs with a superior curved deck:

- Considering the importance of the point at  $0,28*L$  for controlling the structural behavior of SABs with a superior curved deck supported by a planar vertical arch, it would be interesting:
  - Conducting a parametrical analysis of the struts distribution concentrating the struts in the area  $0,28*L$  of the arch and deck.
  - Consider varying the stiffness of the different struts along the bridge, varying the stiffness within each strut and along the arch (Figure 2).

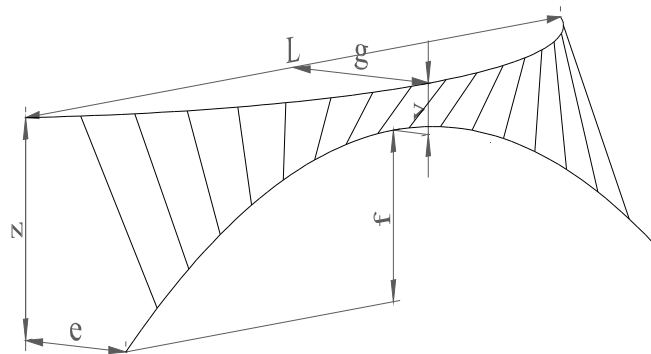


**Figure 2: Variable stiffness possibilities for arch and struts**

## X. FUTURE LINES OF STUDY

- Conduct a new the parametrical analysis of  $z$  employing geometrically non-linear analysis (Figure 3).
- The case study of chapter V.B is devoted to planar vertical arch bridges with a curved deck. A study of arch in plan view curvature has been conducted in chapter V.A and V.B section 7, to determine which arch shape is nearer to a more efficient solution. A next step would be to study the optimal  $e$  value for each shape, determine the antifunicular solution and compare the mass variation of the most efficient solution with the most efficient  $e$  (Figure 3) in each case in order to determine whether finding the antifunicular shape is worth the mass variation it implies.

This last step involves developing a software which is not contained in the scope of this thesis since it has been developed in previous works (Jorquera 2007, Lachauer 2014 and Todisco 2014). It is also not necessary for the objectives of the present thesis since the present case study is enough to understand the structural behaviour and determine easy design criteria. However, due to the considerable number of researches developing antifunicularity-finding-software, it would be interesting to determine whether the improvement structural efficiency due to antifunicularity is valuable or not. If the differences of the mass of the dimensioned bridge are negligible, planar arches can be employed and further researches are not necessary.



**Figure 3: Nomenclature of variables**

Regarding instability analysis of SABs:

- Development of analytical formulae for the critical buckling load of SABs
- Improvement of the existing formulae for the critical buckling load of planar arch bridges with a straight deck, since existing formulae are very conservative.
- Codes and research give buckling formulation, but the hypothesis under which these formulae are valid are not clearly stated and not all cases for arch bridges are included. In an improved formulation this should be clearly stated.

## X. FUTURE LINES OF STUDY

- Model the studied bridge types with sectional FE shells model in order to introduce residual stresses, transverse bracings and diaphragms and sectional changes that might cause load eccentricities.
- Obtainment of construction site imperfection measures and tolerances and comparison with those stated by the codes for the design analyses. The difference should correspond to residual stresses. Compare this value with residual stresses introduced in analytical models and their equivalent imperfection. On such a basis new code imperfection values could be set.
- Development of a series of curves for arch bridges based on empirical values equivalent to the European buckling curves in EC3.
- Compare the behavior of different imperfection shapes obtained by the positive and negative buckling deformed shapes, by conducting a NLGA. In the present study only the imperfection shape for one sign of the buckling shape has been employed.
- Consider material non-linearity as well as geometrical non-linearity, in order to observe the formation of hinges and the bearing capacity margin of these structures with respect to the material linear analysis.

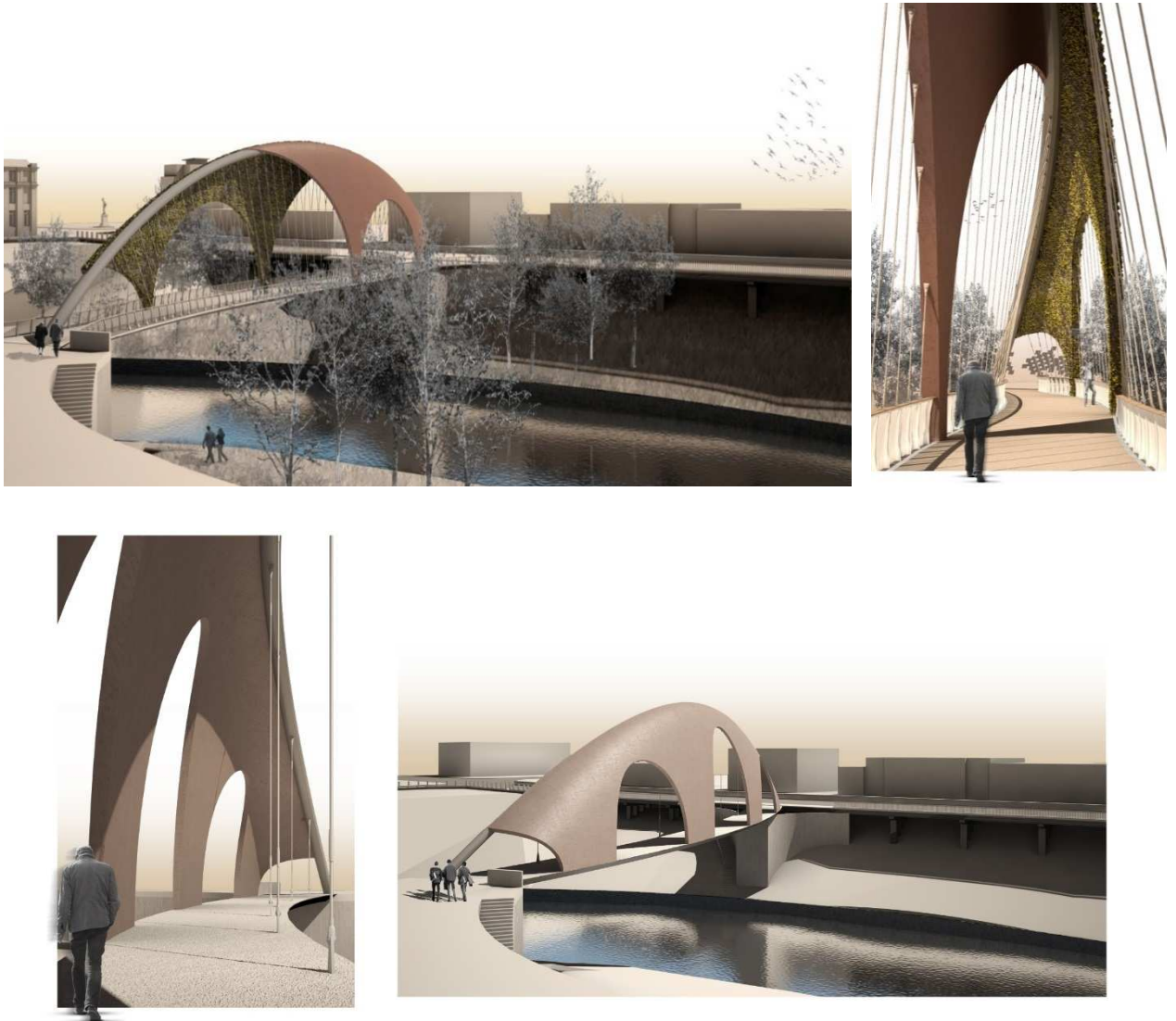
Regarding the dynamic behaviour of spatial arch footbridges:

- Dynamic loading in existing codes and guidelines should be revised for SABs.
- The high vertical accelerations of SABs, together with the fact that dynamic loading in one direction causes acceleration in all directions in this bridge type, highlight the need of a deep research of the dynamic behaviour of this bridge type.
- In relation to SABs spatial behaviour and different modes the statement in EC1 UK NA (*“When the vertical deck modes are not well separated, consideration should be given to the use of more sophisticated methods of analysis, in order to determine combined mode responses. In all cases, it is conservative to use the vector sum of the peak accelerations for those modes that need such combination”*) should be observed and further defined.

The arches have been considered to have rigid boundary conditions, with fixed springings. Of course the flexibility of the foundations will change the boundary conditions of the arches. A study of the flexibility of the foundations and its influence on the bridge behaviour should be conducted.

## X. FUTURE LINES OF STUDY

A specific in depth study of shell SABs could be also a very interesting field of research, due to the scarce number of built examples and research studies. A proposal of research study line would be continuing the already published studies and design proposal published in Sarmiento-Comesías et al, 2013 and 2014 (see Figure 4).



**Figure 4: Shell arch solutions for (a) Salford Meadows Bridge. S-shape in plan IDABWIC (b) C-curved in plan IDABWIC**

## X. FUTURE LINES OF STUDY



# REFERENCES



## REFERENCES

Allied Arts Foundation. The Leonardo bridge project.

Available at: <http://www.leonardobridgeproject.org/> 2001. Accessed 19/02/2012

ALMEIDA, P. A. O., STUCCHI, F.R., RODRIGUES, J. F. S., WAINBERG, M. and BERGER, D.. “Retronanalysis of the tests of the 3rd Bridge over the South Lake in Brasilia (Retroanálise dos ensaios na 3ª Ponte sobre o Lago Sul de Brasília)”. *V Simpósio EPUSP sobre Estruturas de Concreto*, São Paulo, 2003 (in Portuguese)

ARCH '07. Proceedings of the 5th International Arch Bridge Conference. Funchal, Madeira, Portugal, 12-14 September, 2007

ARCH '10. Proceedings of the sixth International Arch Bridge Conference. Fuzhou, China. 11-13 October, 2010

ARCH '04. Arch Bridges IV. Advances in Assessment, Structural Design and Construction. Proceedings of the 4th International Conference on Arch Bridges. Barcelona, 17-19 November, 2004

ARCH '95. Arch bridges: proceedings of the First International Conference on Arch Bridges. Bolton, UK on 3-6 September 1995. 690p. ISBN 0-7277-2048-1

ARENAS DE PABLO, J. J. “Quality in Engineering: Innovation and Maturity (Calidad en la ingeniería: innovación y madurez)”. In: *AEC Proceedings 2005 (The life of bridges: Asociación Española de la Carretera. 2005)*. San Sebastián. 27-29 April 2005. p341 and 343 (in Spanish)

BERGMEISTER K., CAPSONI A., CORRADI L., MENARDO A., “Lateral Elastic Stability of Slender Arches for Bridges including Deck Slenderness”. *Structural Engineering International*, n. 2 v. 19. pp. 149-154(6). May 2009

BILLINGTON D. P., “The Role of Science in Engineering.” *Robert Maillart's Bridges. The Art of Engineering*. Princeton University Press. New Jersey, 1979, pp. 94-105 and 111-112.

BILLINGTON, D. P. *Robert Maillart. Builder, Designer, and Artist*. Cambridge University Press, 1997, pp. 146-149 and pp. 174-182.

BUTTERWORTH, K., CARR D. and KASSABIAN, P.. “Gateshead Millenium Bridge, UK: fabrication, assembly and erection”. *Proceedings of ICE. Civil Engineering 156*. Paper 12826. March 2003, pp. 11-19

CHENG, K. M., KETCHUM, M. A., and DROUILLARD, F.. “Nanning Butterfly Tied Arch Bridge over the Yong River in China”, *Structural Engineering International*, 20 (3). 2010, pp. 308-311

CORREIA, Antonio A.; VIRTUOSO, Francisco B. E.. “Comportamento nao linear de uma ponte “bow-string” metálica”. *V Congresso de Construcao Metálica e Mista*. Abril 2005 (in Portuguese)

CORRES PEIRETTI, H.; SÁNCHEZ DELGADO, J. and SANZ MANZANEDO, C.. “Pasarelas cáscara sobre el río Manzanares en Madrid”. *Proceedings of V Congreso ACHE*. Barcelona, 2011 (in Spanish).

CORRES PEIRETTI, H.; SEIJO VEIGUELA, C.; GARCÍA ESPINEL, J.D.; CALVO HERRERA, I.; GRÁVALOS MORENO, J.; CHOZAS LIGERO, V.; LAMPE CARRERAS, R. and VIÑOLO ALBIOLE, A.. “Aplicación de tecnologías avanzadas del hormigón en las pasarelas en cáscara sobre el río Manzanares para el proyecto de Madrid Río”. *Revista Obras Públicas (ROP)*; 2010, nº 3.515, pp7-18. ISSN: 0034-8619 (in Spanish).

CURRAN, P. “Gateshead Millenium Bridge, UK”, *Structural Engineering International*, November 2003, 13 (4)

DALLARD, P. and FITZPATRICK, A. J. “The London Millennium Footbridge”. *The Structural Engineer*, November 2001, v79n22, pp17-33

DATRY, J.-B.. “The Europe Bridge in Orléans (France): Lessons Learnt”. *ARCH '01. Proceedings of the Third International Arch Bridge Conference*. Paris, 19-21 September 2001. pp735-743 (in French)

DE BACKER H, OUTTIER, A., , and VAN BOGAERT, P. “The effect of using beam buckling curves on stability of steel arch bridges” *Proceedings of the Nordic Steel Construction Conference*, 2009. Available at: <<http://www.nordicsteel2009.se/pdf/43.pdf>>

DE LUCCHI, M.. “The bridge of peace. A monument to Tbilisi's different identities.” *Proceedings of the 34th International Symposium on Bridge and Structural Engineering, IABSE*, Venice, Italy, 2010, pp. 1-8 (CD-ROM)

DE ZOTTI, A., PELLEGRINO, C. and MODENA, C.. “A parametric study of the hanger arrangement in arch bridges”. *ARCH '07. Proceedings of the 5th International Conference on Arch Bridges*. Madeira , Portugal September 12-14, 2007. pp. 476-481

ECCS No. 22. Manual on stability of steel structures; 1976.

MINISTERIO DE FOMENTO. Dirección general de carreteras. Puentes de carretera. Normas técnicas. *Instrucción sobre las acciones a considerar en el proyecto de puentes de carretera (IAP, 2011)*. Madrid: Ministerio de Fomento. Centro de Publicaciones, 2011 (in Spanish)

MINISTERIO DE FOMENTO. *Instrucción EAE de Acero Estructural*. Madrid: Ministerio de Fomento. Centro de Publicaciones, 2011. Artículos 22, 23, 24 y 35

Eurocode 1 (EC1): Actions on structures –Part 2: Traffic loads on bridges.

Eurocode 2 (EC2): Design of concrete structures

Eurocode 3 (EC3): Design of steel structures

FELDMANN, M., HEINEMEYER, C., BUTZ, C., CAETANO, E., CUNHA, A., GALANTI, F., GOLDACK, A., HECHLER, O., HICKS, S., KEIL, A., LUKIC, M., OBIALA, R., SCHLAICH, M., SEDLACEK G., SMITH, A. and WAARTS, P.. *Design of floor structures for human induced vibrations. Background document in support to the implementation, harmonization and further development of the Eurocodes*. JRC European Commission. 2009

FIRTH, I. P. T. and KASSABIAN, P. E.. “The Ribble Way: Characteristics of a three-way arch”. ARCH '01. Proceedings of the Third International Arch Bridge Conference. Paris, 19-21. September 2001. Pp807-812

FLAGA, K. and JANUSZKIEWICZ, K.. “On the aesthetics and technical efficiency of current arched footbridges”. *4th International Conference. Footbridge 2011*. Wroclaw, 6-8 July, 2011

*Footbridges-Assessment of vibrational behavior of footbridges under pedestrian loading-Practical Guidelines*. Sétra, 2006

GALAMBOS, T. V.. *Guide to stability design: Criteria for metal structures*. 4th Ed, pp15-25, pp575-608, pp609-625. New York: John Wiley & Sons, 1988. ISBN: 0-471-09737-3

HOECKMAN, W.. “The Europe Bridge in Orléans (France): Construction Phases”. ARCH '01. *Proceedings of the Third International Arch Bridge Conference*. Paris, 19-21 September 2001. pp745-750

HUSSAIN, N. and WILSON, I.. “The Hulme Arch Bridge, Manchester”. *ICE Proceedings, Civil Engineering* 132. February 1999. pp 2–13

JOHNSON, J. and CURRAN, P.. “Gateshead Millenium Bridge- an eye-opener for engineering”. *Proceedings of ICE. Civil Engineering* 156. Paper 12885. February 2003, pp. 16-24

JORQUERA, J. J., “Structural Behaviour of Spatial Arch Bridges”, *Proceedings of the IASS Symposium 2009, Evolution and Trends in Design, Analysis and Construction of Shell and Spatial Structures* (Domingo, A., and Lázaro, C. (Eds)), Valencia, 2009, pp. 2447-2457.

JORQUERA, J. J., *Study of the Structural Behaviour of Spatial Arch Bridges*, PhD Thesis. Supervised by Prof. Manterola, Technical University of Madrid (UPM), 2007 (in Spanish).

KOLLBRUNNER C. F. and BASLER K.. *Torsion in structures: An engineering approach*. Springer-Verlag, 1969, pp280

LACHAUER, L., JUNGJOHANN, H. and KOTNIK, T. “Interactive Parametric Tools for Structural Design” Proceedings of the 35th International. *Symposium on Bridge and Structural Engineering, jointly organised by IABSE-IASS: ‘Taller, Longer, Lighter’*, London, UK, September 20-23, 2011, pp. 1-8 (CD-ROM)

LAFFRANCHI, M. and MARTI, P.. “Robert’s Maillart’s concrete arch bridges”, *Journal of structural engineering*, 123(10), 1997, pp. 1280-1286.

- LIAGHAT, D., POWELL-WILLIAMS, K. and CAPASSO, M.. “Ponte della Musica: An Urban Bridge in Rome”. *Footbridge 2011. Proceedings of the 4th International Conference Footbridge*. Wrocław, Poland 6 – 8 July 2011
- MAIRS, D. „York Millenium Bridge- A Footbridge with an Inclined Arch, UK. “Recent Structures”. *Structural Engineering International*. 3/2001, pp172-174
- MANTEROLA, J. “Cálculo de tableros de puente por el método del emparrillado”, *Hormigón y acero* n122, pp93-149, ATEP, Madrid, 1977
- MANTEROLA, J. “Composite arch bridges”. *ARCH '01. Proceedings of the Third International Arch Bridge Conference*. Paris, 19-21 September 2001. pp779-785
- MANTEROLA, J., GIL, M. Á., and MUÑOZ-ROJAS, J., “Arch spatial Bridges over the Galindo and Bidasoa Rivers”, *Structural Engineering International*, 21 (1). 2011, pp114-121
- MANTEROLA, J., GIL, M. Á., and MUÑOZ-ROJAS, J., “Arch spatial Bridges over the Galindo and Bidasoa Rivers”, *Cauce 2000: Revista de ingeniería civil*, 147. 2009, pp. 20-29, (in Spanish).
- MANTEROLA, J., MUÑOZ-ROJAS, J., LÓPEZ, A. and FERNÁNDEZ, J.. “Guadalentín river and San Cristobal urban area Project in the city of Lorca (Actuación sobre el río Guadalentín y espacio urbano del barrio de San Cristóbal en la ciudad de Lorca)”. *ACHE Proceedings 2005 (Comunicaciones al III congreso ACHE de puentes y estructuras)*. Zaragoza. 2005. pp1802-1811 (in Spanish)
- MANZANARES JAPÓN, J. L. and HINOJOSA SÁNCHEZ-BARBUDO, I, “Non-linear plastic analysis of steel arches under lateral buckling”, *Journal of Constructional Steel Research*, n. 12 v. 67, December 2011, doi:10.1016/j.jcsr.2011.05.008, pp1850-1863
- Michele De Lucchi Archive (aMDL). Ponte della Pace, Tbilisi (Georgia), 2009-2010. Available at: <http://www.archive.amdl.it/en/index.asp>. Last accessed 2<sup>nd</sup> April 2012
- NICOLETTI, M.. *Sergio Musmeci: organicità di forme e forze nello spazio*. Testo & Immagine, Torino, 1999
- O’CONNOR, C.. “Chapter 10: Arches.” *Design of Bridges Superstructures*, John Wiley and Sons, New York, USA, 1971, pp88-544.
- OUTTIER, A., DE BACKER H, and VAN BOGAERT, P. “Assessment of the out-of-plane imperfections of a steel tied arch bridge” *ARCH '07. Proceedings of the 5th International Conference on Arch Bridges*. Madeira, Portugal September 12-14, 2007a. pp. 249-256
- OUTTIER, A., DE BACKER H, and VAN BOGAERT, P. “Numerical approach to the lateral buckling of steel tied-arch bridges” *ARCH '07. Proceedings of the 5th International Conference on Arch Bridges*. Madeira, Portugal September 12-14, 2007b. pp. 484-490
- PETERSEN C. *Statik und Stabilität der Baukonstruktionen: Elasto- und plasto-statische Berechnungsverfahren druckbeanspruchter Tragwerke: Nachweisformen gegen Knicken*,

Kippen, Beulen [Gebundene Ausgabe]. 960pp Verlag: Vieweg Verlagsgesellschaft; Auflage: 2., durchges. Aufl. 1982 (24. Oktober 1982) (in German) ISBN-10: 3528186631 ISBN-13: 978-3528186630

ARCH '98. *Proceedings of the Second International Arch Bridge Conference*. (Venice, 6-9 Octubre 1998). [s.l.]: Taylor & Francis, 1998. 439p. ISBN 9058090124, 9789058090126.

ROBERTSON, L. "A life in Structural Engineering". In: Nordenson, Guy. *Seven Structural Engineers: The Felix Candela Lectures*. New York: The Museum of Modern Art, 2008. pp83-84

RUIZ-TERAN, A. M. and APARICIO, A. C.. "Verification criteria of the SLS of vibrations for road bridges with slender prestressed concrete decks". *International FIB Symposium 2009, Concrete: 21st Century Superhero*. London, UK, 2009

SARMIENTO, M., RUIZ-TERAN, A. and APARICIO, A. C.. "Structural response of spatial arches with imposed Curvature." Proc., 34th Int. Symp. on Bridge and Structural Engineering, IABSE, Venice, Italy, 2010

SARMIENTO-COMESÍAS M., "Non-linear behaviour and design criteria for spatial arch bridges" MPhil-PhD Transfer report. Jointly supervised by Prof. Aparicio (Director of studies) and Dr Ruiz-Teran, Technical University of Catalonia (UPC), Barcelona, 2009 (in Spanish).

SARMIENTO-COMESÍAS, M., MPhil-PhD Transfer report. Jointly supervised by A. C. Aparicio and A. Ruiz-Teran, Technical University of Catalonia (UPC), Barcelona, Spain 2009 (in Spanish)

SARMIENTO-COMESÍAS, M., RUIZ-TERAN, A. and APARICIO, A. C.. "Elastic behaviour of planar vertical arch bridges with a superior curved deck" *Proceedings of the 7th Conference on Arch Bridges "ARCH 2013"*, Split, Croatia, 2013, pp. 1-8 (CD-ROM)

SARMIENTO-COMESÍAS, M., RUIZ-TERAN, A. and APARICIO, A. C.. "State-of-the-art of spatial arch bridges." Special Issue on Arch bridge of the *Bridge Engineering Journal* of the Institution of Civil Engineering, Vol. 166, Issue 3, April 2013 pp163–176. Published on-line 2011. DOI: [10.1680/bren.11.00010](https://doi.org/10.1680/bren.11.00010)

SARMIENTO-COMESÍAS, M., RUIZ-TERAN, A. AND APARICIO, A. C.. "Superior deck spatial arch bridges." *Proceedings of the 35th International Symposium on Bridge and Structural Engineering, jointly organised by IABSE-IASS: 'Taller, Longer, Lighter'*, London, UK, September 20-23, 2011

SCHLAICH, J., and MOSCHNER, T.. "Die Ripshorster Brücke über den Rhein-Herne-Kanal, Oberhausen", *Bautechnik*, 6(76), 1999pp. 459-462.

SPOORENBERG, R.C., SNIJDER, H.H., HOENDERKAMP, J.C.D. and BEG, D. "Design rules for out-of-plane stability of roller bent steel arches with FEM". *Journal of Constructional Steel Research*, 79, 9-21. 2012

STRÁSKÝ, J and HUSTY, I. "Arch bridge crossing the Brno-Vienna expressway". *Composite constructive – conventional and innovative. International conference*. Innsbrück, 16-18

September 1997. pp.870-871.

STRÁSKÝ, J. “Bridges designed by Strasky, Husty & Partner”. In: AEC Proceedings 2005 (The life of bridges: Asociación Española de la Carretera. 2005). San Sebastián. 27 -29 April 2005. p255-312

STRÁSKÝ, J. and KALAB, P. “Model Test of the Prestressed Concrete Membrane”. *IASS 2007 Conference - Shell and Spatial Structures. Structural Architecture - Towards the future looking to the past*, Venice, Italy, 2007, pp. 1-8 (CD-ROM)

STRÁSKÝ, J., KALAB, P., NECAS, R. and TERZIJSKI, I. “Development of Membrane Roofs from Prestressed Concrete. Structural Concrete in the Czech Republic 2006-2009”. *3rd fib Congress*, Washington, 2010.

STRÁSKÝ, J.. “Bridges Utilizing High-strength concrete”. *30<sup>th</sup> Conference of Slovenian Structural Engineers*. Bled, 2008, pp. 1-18.

STROBL, W., KOVACS, I., ANDRÄ, H. P. and HÄBERLE, U.. „Eine Fußgängerbrücke mit einer Spannweite von 230m“. *Stahlbau*, Berlin, 2007. n76v12. (in German)

TERZIJSKI, I. “Optimization of UHPC for the Model of a Pedestrian Bridge in: Ultra High Performance Concrete (UHPC)”. *Ultra high performance concrete (UHPC): proceedings of the Second International Symposium on Ultra High Performance Concrete*. (Fehling E., Schmidt, M. and Stürwald S. (eds)). Kassel, Germany, March 5-7, 2008, pp. 707-716

THOMAS, G. E. “The Blythe Park Bridge”. In: Martínez, J. (Dir y Ed). *Proceedings of Composite Bridges 2001*. Madrid: Ediciones del Colegio de Ingenieros de Caminos, CC y PP. 2001. Madrid, 22-26 January, 2001. pp 131-144 (in Spanish)

TIMOSCHENKO, S.; GERE, J.M.. *Theory of Elastic Stability*. New York: McGraw Hill. 1961

TIMOSHENKO, S., *Resistencia de materiales. Primera Parte*, Espasa-Calpe S.A., Madrid 1957, p234 (in Spanish)

UK National Annex to Eurocode 1: Actions on structures –Part 2: Traffic loads on bridges. 2003

VAN BOGAERT, P., “Bending of Converging Hangers in Steel Tied Arch Bridges.” *Proceedings of the 35th International Symposium on Bridge and Structural Engineering*, jointly organised by IABSE-IASS: ‘Taller, Longer, Lighter’, London, UK, September 20-23, 2011

VAN BOGAERT, P., “Tied Arch Bridges with Optimised Arrangement of a Limited Number of Hangers.” *Proceedings of the 34th International Symposium on Bridge and Structural Engineering (IABSE): ‘Large Structures and Infrastructures for Environmentally Constrained and Urbanised Areas’*, Venice, Italy, 2010, pp. 1-7 (CD-ROM)

VERLAIN, D., HARDY, D., SCHMIT, C., JORIS C., DUCHÊNE, Y. and DE CATERS, P.. “Bowstring bridge with curved deck”. *ARCH '01. Proceedings of the Third International Arch Bridge Conference*. Paris, 19-21 September 2001. pp715-722 (in French)



VON BUELOW, P., FALK, A. and TURRIN, M. "Optimization of structural form using a genetic algorithm to search associative parametric geometry" *Proceedings of the International Conference on Structures & Architecture (ICSA) 2010*, Guimarães, Portugal. 8p

ŽICKIS, D. and CYPINAS, I. "Design and construction of a steel arch bridge in Vilnius over the Neris" *Proceedings of the 25th International Baltic Road Conference*. Vilnius, 2003. Available at: <[http://www.balticroads.org/downloads/25BRC/25brc\\_e1\\_zickis\\_1.pdf](http://www.balticroads.org/downloads/25BRC/25brc_e1_zickis_1.pdf)>

